Shock Wave and
High Pressure Phenomena

Dennis Grady

Fragmentation of Rings and Shells

The Legacy of N. F. Mott

Springer

Shock Wave and High Pressure Phenomena

Shock Wave and High Pressure Phenomena

L.L. Altgilbers, M.D.J. Brown, I. Grishnaev, B.M. Novac, I.R. Smith, I. Tkach, and Y. Tkach : Magnetocumulative Generators

T. Antoun, D.R. Curran, G.I. Kanel, S.V. Razorenov, and A.V. Utkin : Spall Fracture

J. Asay and M. Shahinpoor (Eds.) : High-Pressure Shock Compression of Solids

S.S. Batsanov : Effects of Explosion on Materials: Modification and Synthesis Under High-Pressure Shock Compression

R. Cherét : Detonation of Condensed Explosives

L. Davison, D. Grady, and M. Shahinpoor (Eds.) : High-Pressure Shock Compression of Solids II

L. Davison, Y. Horie, and T. Sekine (Eds.) : High-Pressure Shock Compression of Solids V

L. Davison, Y. Horie, and M. Shahinpoor (Eds.) : High-Pressure Shock Compression of Solids IV

L. Davison and M. Shahinpoor (Eds.) : High-Pressure Shock Compression of Solids III

A.N. Dremin : Toward Detonation Theory

Y. Horie, L. Davison, and N.N. Thadhani (Eds.) : High-Pressure Shock Compression of Solids VI

R. Graham : Solids Under High-Pressure Shock Compression

J.N. Johnson and R. Cherét (Eds.) : Classic Papers in Shock Compression Science

V.F. Nesterenko : Dynamics of Heterogeneous Materials

M. Sućeska : Test Methods of Explosives

J.A. Zukas and W.P. Walters (Eds.) : Explosive Effects and Applications

G.I. Kanel, S. V. Razorenov, and V.E. Fortov : Shock-Wave Phenomena and the Properties of Condensed Matter

V.E. Fortov, L.V. Altshuler, R.F. Trunin, and A.I. Funtikov : High-Pressure Shock Compression of Solids VII

L.C. Chhabildas, L. Davison, and Y. Horie (Eds.) : High-Pressure Shock Compression of Solids VIII

D. Grady : Fragmentation of Rings and Shells

R.P. Drake : High-Energy-Density Physics

Dennis Grady

Fragmentation of Rings and Shells

The Legacy of N.F. Mott

With 192 Figures

Springer

Dr. Dennis Grady
Applied Research Associates Inc.
4300, San Mateo Blvd. NE
Albuquerque, New Mexico 87110, USA
Email: dgrady@ara.com

Editors-in-Chief:

Dr. Lee Davison
39 Cañoncito Vista Road
Tijeras, NM 87059, USA
Email: leedavison@aol.com

Dr. Yasuyuki Horie
AFRL/MNME Munitions Directorate
2306 Perimeter Road
Eglin AFB, FL 32542, USA
Email: yasuyuki.horie@eglin.af.mil

Library of Congress Control Number: 2004110191

ISBN-10 3-540-27144-9 Springer Berlin Heidelberg New York
ISBN-13 978-3-540-27144-4 Springer Berlin Heidelberg New York

Springer is a part of Springer Science+Business Media

springer.com

Printed in Germany

Typesetting: by the author and techbooks using a Springer LaTeX macro package
Cover design: *design & production* GmbH, Heidelberg

Printed on acid-free paper 54/3100/tb 5 4 3 2 1 0

Preface

My personal interest in the physics of fragmentation of materials predates considerably my introduction to the seminal war years efforts of Sir Nevill F. Mott on the subject. While pursuing my doctoral thesis topic at Washington State University on the effects of shock waves on ferrimagnetic material, I became concerned with the distribution and size of magnetic domains persisting after passage of a shock wave. I found an article by the eminent solid-state physicist Charles Kittel (1949) in which he demonstrated that magnetic domains form in order to reduce the self-magnetic energy of the ferrimagnetic material. Kittel showed that through a balance of this magnetic energy and the domain wall interface energy, he could provide a sensible estimate of the size of domains. I applied these methods to magnetic domain formation under shock in ferrimagnetic materials in my thesis work.

My interest in fragmentation returned in the middle 1970s when substantial efforts at the Department of Energy National Laboratories turned toward the nation's pressing requirements for energy and other natural resources at that time. One specific project undertaken at Sandia National Laboratories was that of finding methods for preparing oil shale deposits for the extraction of their oil bearing content while still underground. Our group at Sandia explored novel methods of explosively fragmenting the oil bearing rock in preparation for the retorting process used to recover the oil, and undertook various experimental, theoretical and computational studies of the processes of explosion-induced fracture and fragmentation. Concepts from my thesis work found direct application to this study. At that time, we benefited mostly from earlier and concurrent work in the petroleum and rock mechanics community.

It was sometime later in the 1980s when we at Sandia attempted to apply some of the earlier theoretical and computational fragmentation methods to the explosive disruption of nuclear weapons systems that we became aware of the vast amount of research that had been performed on the fragmentation of conventional munitions. We began to hear repeated references to the famous Mott distribution (well known to the munitions community), and finally

managed to get nearly illegible copies of Mott's war years reports from the database at Southwest Research Institute.

My first reading of Mott's internal reports and 1947 open literature paper was painful and it was only after several readings over several years that I started to grow the deep appreciation for the incisive physical thinking and strong mathematical talent that this scientist brought to bear on the subject. This appreciation is greatly enhanced when one reflects on the events of the war years during which this scientific study was carried out.

Over the past nine years while with Applied Research Associates I have had the opportunity to work on various programs in which the dynamic fragmentation of materials was a central issue. Each time I would find that some specific aspect of Mott's earlier studies had particular relevance to the problems at hand. In each instance I would find myself expending an undue amount of time pursuing the physics, the mathematics, and the intent of Mott's theories and analyses. I would frequently propose and solve parallel problems in an effort to gain a better understanding of Mott's work.

During the past two years I decided to collect together these past efforts, and the present text is the result of that endeavor.

Toward the end of this undertaking I located and read Mott's autobiography [Sir Nevill Mott: A Life in Science, Taylor & Francis, 1986]. One chapter dwells on his experiences of the war years, and offers some thoughtful insight into the mood and temperament of the times in which he carried out this research.

I would like to thank Lee Davison and Yasuyuki Horie for their assistance in interfacing with Springer Publishing. One consideration was whether or not to include the unpublished reports of Nevill Mott on fragmentation theory in the present text. It was decided to include them as it is difficult to acquire legible copies. Those furnished are best available copies of the original reports with some minor computational cleanup for which I thank Craig Doolittle at Applied Research Associates. Springer Publishing made the decision to also transcribe the Mott reports. The serviceability of the present book is markedly enhanced through their efforts, and I express my appreciation for their undertaking of this task. In editing the transcribed reports I have attempted to maintain a faithful reproduction of the originals.

Permission to include Mott's reports was required, and I am grateful to Professor Neil Bourne for putting me in touch with Samuel Ellis of the UK Defense Ordnance Safety Group in which archives the original reports of Mott reside. I am in turn indebted to Samuel Ellis for not only obtaining the necessary permission, but also providing best available copies of Mott's original reports including the retyping of the two difficult-to-read pages.

During this process two further fragmentation reports by Nevill Mott of which I was not aware surfaced. These latter two reports are also included.

One report is particularly interesting in that Mott speaks quite disparagingly of the fragment distribution that has been the hallmark of fragmentation arena testing for the past sixty years.

Albuquerque, New Mexico *D.E. Grady*
July, 2005

Acknowledgments

The present manuscript is the culmination of fairly intense efforts over the past several years while interacting closely with Lawrence Livermore National Laboratory, Sandia National Laboratories, and the Naval Surface Warfare Center, Dahlgren, on applications where explosive fragmentation of metal shells was of central interest. These interactions have all been carried out with the support and encouragement of Applied Research Associates mamagement and staff. The manuscript also represents the more sporadic reflections, ruminations, and both effective and ineffective analysis on the same topic over the past several decades. I owe special thanks to a number of individuals, especially within the more recent several years, for providing incentives, ideas, and constructive criticism as the various pieces of the present document came together.

I wish to thank Ted Orzechowski, Omar Hurricane, Rich Becker, Dana Goto, James Belak, Juan Moreno, Keith Bradley, and Alan Wan of Lawrence Livermore National Laboratory for their continuing interest and valuable feedback during our several years of programmatic work relating to the present topic. Special thanks is offered to Margaret Olsen who provided the opportunity for collaboration and joint publication on her expanding ring fracture and fragmentation studies on U6Nb.

I wish also to thank Lalit Chhabildas and Tracy Vogler at Sandia National Laboratories for the continuing constructive interaction on the present topics through applications initiated within the joint DOD/DOE Memorandum of Understanding.

Thanks are also due to Leonard Wilson, Donna Reedal and Michael Hopson at Naval Surface Warfare Center, Dahlgren for their encouragements and insights during our study of scaling in the fragmentation of exploding cylinders. Section 7 documents much of that effort.

At Applied Research Associates, Craig Doolittle and Nancy Winfree have provided continuing support and valuable feedback for which I am grateful.

Marlin Kipp has been a longstanding friend and hiking companion. Our numerous cooperative studies of dynamic fracture and fragmentation permiate

much of what is presented here, and I am deeply appreciative of our extended interaction.

Special thanks are due Professor William Proud of Cavendish Laboratory, Cambridge, Professor Neil Bourne of Cranfield University, and Mr. Samual Ellis of DSOG, who kindly invested considerable effort in searching out and provided copies of Mott's reports from the original Ministry of Supply sources.

Lastly, I have reserved special gratitude to Megan Allen who has been my companion and source of inspiration throughout the time the present manuscript has come together.

Contents

Part I

1

Introduction

For a brief period during the latter part of World War II, N. F. Mott, then professor of physics at the University of Bristol (later knighted and a Nobel laureate), undertook an effort to theoretically describe the statistical fragmentation of bodies subjected to intense impulsive loads. Specifically, he focused on fragmentation resulting from the explosive rupture of cylindrical bombs (referred to by Mott as H.E. shells or shell cases). Over a period of about six months in 1943, three internal UK Ministry of Supply reports emerged, which provided the core of his theoretical efforts (Mott and Linfoot, 1943; Mott, 1943a,b). In late 1943 through 1944 three further internal reports (Mott, 1943c; Mott, 1944; Mott et al., 1944) undertook critical examination and experimental testing of his seminal theory of fragmentation. Sometime later he more formally prepared selected portions of these efforts for open literature publication (Mott, 1947). Finally, apparently under stimulus from an earlier conference on fracture in metals held at Cambridge University, Mott (1948) published an extended note titled by him "Fracture of Metals: Some Theoretical Considerations." Some of his most forward-thinking thoughts on the micromechanical and molecular aspects of fracture are included in this last publication.

For scientists and engineers concerned with the dynamic fracture and fragmentation of solid bodies subject to the intense transient loads imparted by explosive detonation or high velocity impact, Mott's original publications contain the seminal theoretical concepts from which numerous later modeling efforts and engineering formulae emerged. The original physical ideas conceived by Mott and the accompanying mathematical analysis pursued are unique and fascinating. They clearly reflect the unusual insight and scientific accomplishment of this individual.

Mott's theoretical results, as put forth in the original internal reports and the later open literature publication have, unfortunately, not been fully appreciated in work by later authors and, in some cases, not fully understood. The presentation by Mott is terse, leaving much for the reader to fill in.

Considerable reflection, with pencil in hand, is required to begin to appreciate the richness and insight offered in these works.

The present book surveys the theoretical analysis put forth by Mott with particular focus on his efforts to characterize the size and distribution of fragments resulting from a dynamic fragmentation event. This book also pursues additional new theoretical analysis. The intent of this analysis, however, is to delve further into the physical ideas and unfinished analysis implicit in Mott's original study. The thesis being that with further time and inclination, those are avenues that Mott himself might have pursued. These additional efforts fall short of exhausting the fruitful thoughts put forth by Mott in his original reports.

Mott pursued several approaches, as his thoughts on the nature of statistical fragmentation matured. Early on he was influenced by the theoretical efforts of Lineau (1936) who, a few years before him, examined in depth the statistical distribution of fragment lengths resulting from the random partitioning of a one-dimensional body (a line). This Lineau distribution was intriguingly close in form to experimental fragment mass distribution data on exploding metal shells available to him at the time. This led Mott, along with Linfoot, in his first report to pursue in some detail the fragment size distributions resulting from the random geometric partitioning of two- and three-dimensional bodies. These efforts, in fact, led to the familiar Mott distribution in which the log of the cumulative fragment number is proportional to the square root of the fragment mass. This Mott distribution continues today as the most common means of representing fragmenting munitions data. Further, the geometric fragmentation problems explored early on by Mott have in the intervening years, provided the source for a large amount of analysis.

Mott became disenchanted with the random geometric approach to the dynamic fragmentation problem as his scientific investigation progressed. He noted the likelihood that both nonuniqueness of the statistical algorithms used, and the lack of statistical homogeneity in the experimental fragmentation event, could easily negate applicability of predicted distributions from the geometric theory. He then embarked on an entirely different, and more physically-based, theoretical study of the statistical fragmentation problem.

In this second exploration of dynamic fragmentation of rapidly expanding shells, concepts emerge concerning the statistical activation of fractures and the interplay among an ensemble of fractures as the propagation of stress release waves ensue. The instructive analysis in which an elementary momentum solution leads to the diffusive nature of tensile stress release from fracture sites is illustrative of this latter effort. This latter approach leads to a coupled physical and statistical theory of fragmentation in which the physical properties governing the fragment size and distribution length scales emerge.

Mott's approach to dynamic fragmentation has been objected to by some more recent workers in the field as too phenomenological in form. A closer look at Mott's efforts, however, reveal extraordinary and successful attempts by him to relate phenomenological parameters from his statistical theory to

the underlying microscopic and atomic physics. Mott was, in fact, an advocate of multiscale physics long before this topic gained its current fashionability.

References

Lineau, C.C. (1936), Random Fracture of a Brittle Solid, *J. Franklin Inst.*, 221, 485–494, 674–686, 769–787.

Mott, N.F. and Linfoot, E.H. (1943), A Theory of Fragmentation, *Ministry of Supply*, AC3348, January.

Mott, N.F. (1943a), Fragmentation of H.E. Shells: A Theoretical Formula for the Distribution of Weights of Fragments, *Ministry of Supply*, AC3642, March.

Mott, N.F. (1943b), A Theory of the Fragmentation of Shells and Bombs, *Ministry of Supply*, AC4035, May.

Mott, N.F. (1943c), Fragmentation of Shell Casings and the Theory of Rupture in Metals, *Ministry of Supply*, AC4613, August.

Mott, N.F. (1944), A Theory of Fragmentation. Application to Wire Wound Bombs such as the American 20 lb. F., *Ministry of Supply*, AC6338, May.

Mott, N.F., Wilkinson, J.H., and Wise, T.H. (1944), Fragmentation of Service Projectiles, *Ministry of Supply*, AC6338, December.

Mott, N.F. (1947), Fragmentation of Shell Cases, *Proc. Royal Soc.*, A189, 300–308, January.

Mott, N.F. (1948), Fracture of Metals: Theoretical Considerations, *Engineering*, 165, 16–18.

2

Geometric Fragmentation Statistics

The statistical issues governing the fragmentation of a body are not well in hand even to this day. Perhaps foremost in the list of objectives is the prediction of the distribution in the size of fragments resulting from a fragmentation event. One intriguing approach to this problem has simply been to investigate the statistically most random way of partitioning a given topology into a number of discrete entities. This approach to statistical fragmentation has been commonly identified as geometric fragmentation.

As noted in the introduction, Mott was initially led in pursuit of a theoretical description of the distribution in fragments from a fragmenting cylinder event by then recent work of Lineau (1936). Fragmenting munitions data available to Mott at the time appeared consistent with the exponential expression resulting from Lineau's one-dimensional model. Thus, his early efforts focused on extending the same geometric statistics approach to the topology of a naturally fragmenting cylinder.

In the present section we pursue some of the approaches to obtaining representations of fragment size distributions using the methods of geometric fragmentation statistics. In particular the well-known Mott distribution will be developed and examined.

2.1 Lineau Distribution

Fundamental to geometric fragmentation are the theoretical efforts of Lineau (1936). He considered the elementary problem of an extended body such as a glass rod or a stretching wire subjected to forces resulting in the multiple fracturing of that body. If any point on the body is as likely as another to fracture the problem is statistically well posed. The problem is modeled as that of an infinite one-dimensional body, or line, in which breaks are introduced with equal probability at any point on that line, as is illustrated in Fig. 2.1.

Thus, as stated, the random geometric fragmentation of a one-dimensional body appears decidedly unambiguous. An analytic solution requires only a

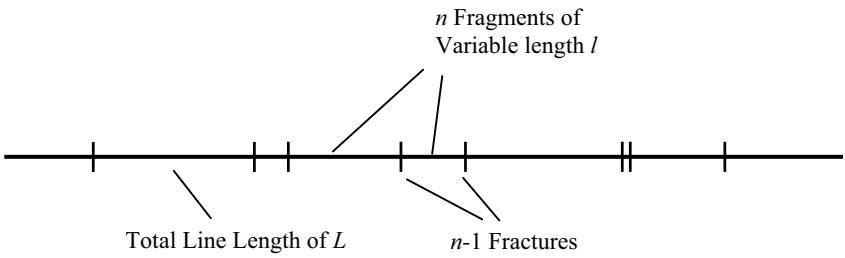

Fig. 2.1. Line of total length L broken at random into fragments of variable length l by $n-1$ fractures

proper probabilistic description of the random breaks, and the lengths of the segments delineated by these breaks. We shall show later that even this prescription for the statistical fragmentation of a one-dimensional body is arguable. At this point, however, we proceed with the solution leading to the one-dimensional Lineau fragment size distribution.

Consider a line of length L in which breaks on the line are introduced at random [Grady, 1990]. Since we are initially interested in partitioning the line into a large number of fragments (the average length is very small compared to the total length L) the finite length of the line is not of consequence and can effectively be considered infinite (Fig. 2.1). The average spacing between breaks λ or equivalently the frequency of breaks per unit length $h_o = 1/\lambda$ characterizes the statistical distribution. The random distribution of points on a line is described by Poisson statistics.

If an arbitrary length l of the line is examined then the probability of finding n points (fractures) within the length l is given by,

$$P\left(n,l\right) = \frac{\left(l/\lambda\right)^n e^{-l/\lambda}}{n!} \; . \tag{2.1}$$

The most probable distribution in fragment lengths is determined by observing that the probability of finding no fractures within the length l is,

$$P\left(0,l\right) = e^{-l/\lambda} \; , \tag{2.2}$$

while the probability of finding one fracture within the subsequent length increment dl is

$$P\left(1,dl\right) = \left(1/\lambda\right) dl \; . \tag{2.3}$$

The probability of occurrence of fragments of length l within a tolerance of increment dl is then,

$$f\left(l\right) dl = P\left(0,l\right) P\left(1,dl\right) = \left(1/\lambda\right) e^{-l/\lambda} dl \; , \tag{2.4}$$

where,

$$f\left(l\right) = \left(1/\lambda\right) e^{-l/\lambda} \; , \tag{2.5}$$

is the fragment length probability density distribution while the integral of $f(l)$,

$$F(l) = 1 - e^{-l/\lambda} , \tag{2.6}$$

is the cumulative fragment distribution.

If a distribution of N_o fragments satisfies the present statistical premises, then the analytic expression,

$$N(l) = N_o e^{-l/\lambda} , \tag{2.7}$$

characterizes the cumulative number distribution of fragments larger than length l. Assigning a density per unit length of the one-dimensional body it is readily shown that the cumulative mass fraction of fragments is given by,

$$M(l) = 1 - (1 + l/\lambda) e^{-l/\lambda} . \tag{2.8}$$

The latter is commonly a more tractable experimental description.

Equation (2.7) can be written in the differential form,

$$\frac{dN}{N} = -\frac{1}{\lambda} dl , \tag{2.9}$$

providing a useful form for generalizing to fragmentation events in which the distribution is biased toward specific fragment sizes. This is accomplished through a dependence of the distribution length scale $\lambda = \lambda(l)$ on the fragment size.

2.1.1 Binomial Distribution

When the number of breaks within the body length L is few then the fragment size probability distribution will depend on the body length. Here probabilistic aspects of the problem are governed by the binomial probability function,

$$P_{j,k}(p) = \frac{k!}{j!(k-j)!} p^j (1-p)^{k-j} , \tag{2.10}$$

when, $P_{j,k}(p)$ is the probability of j successes in k attempts while p is the probability of a single success.

Consider then a one-dimensional body of length L in which $n-1$ randomly distributed breaks partition the body into n fragments.

Consider further a region of length, $l < L$ within the domain of L. The probability of a single fracture occurring within the region is the ratio $p = l/L$. Thus, from the binomial probability function, the probability that none of the $n-1$ fractures occurs within the region l is just,

$$\begin{aligned} P_{0,n-1}(l/L) &= \frac{(n-1)!}{0!(n-1)!} \left(\frac{l}{L}\right)^0 \left(1 - \frac{l}{L}\right)^{n-1} , \\ &= (1 - l/L)^{n-1} . \end{aligned} \tag{2.11}$$

Given that the $n-1$ fractures are outside of the region l the probability that a single fracture occurs within the interval dl is the ratio $p = dl/(L-l)$. Again, from (2.10).

$$P_{1,n-1}\left(\frac{dl}{L-1}\right) = \frac{(n-1)!}{1!\,(n-2)!}\left(\frac{dl}{L-l}\right)^1\left(1-\frac{dl}{L-l}\right)^{n-2}, \quad (2.12)$$
$$\cong \frac{n-1}{L}\left(\frac{dl}{1-l/L}\right).$$

The probability of finding a fragment of length l within an interval dl is then the product of (2.11) and (2.12), or

$$f(l)\,dl = \frac{n-1}{L}\left(1-\frac{l}{L}\right)^{n-2} dl\,, \quad (2.13)$$

where $f(l)$ is the fragment length probability density distribution. The cumulative probability distribution is then,

$$F(l) = 1-(1-l/L)^{n-1}\,. \quad (2.14)$$

With the probability density function from (2.13) the expected value for the fragment length is found to be $\lambda = L/n$. Equation (2.14) can then be written,

$$F(l) = 1-e^{-(1-L/\lambda)ln(1-l/L)}\,, \quad (2.15)$$

which, in the limit $\lambda \ll L$ and $l \ll L$ yields the cumulative fragment probability distribution for a Poisson process on an infinite line in (2.6).

Probability density curves for number of fragments equal to $n = 2$, 3, 4, and 5 are illustrated in Fig. 2.2, along with the Poisson approximation to the $n = 5$ fragments case.

2.2 Mott-Linfoot Fragment Distribution

Mott and Linfoot (1943) referenced the earlier work of Lineau (1936) and furthered his random geometric fragmentation ideas in pursuit of a sensible fragment size distribution relation for the description of fragmenting munitions. Their acceptance of the Lineau approach was bolstered by fragmenting munitions data available to them at the time which were found to plot reasonably linear in a log number versus cube root of the fragment mass representation. Since $m^{1/3}$ is proportional to a length measure of the fragment they reasoned that the same random variable considered in the Lineau one-dimensional development applied in the multidimensional fragmentation event. Further, in examining fragments from the available data, they observed that a substantial portion retained inner and outer surfaces of the original munitions case. This suggested that the fragmentation of a plate or areal region in which event

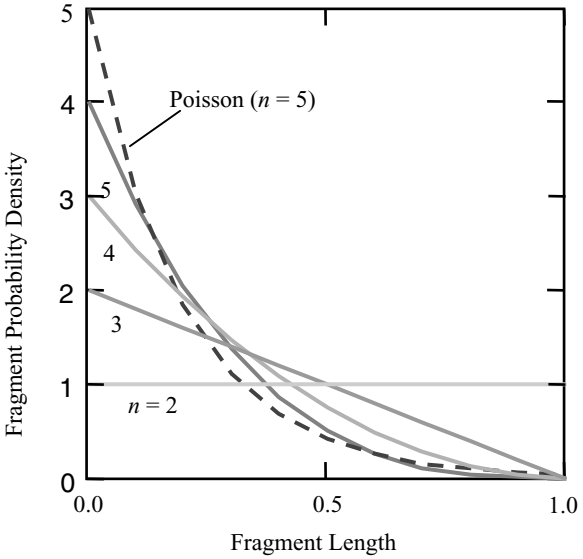

Fig. 2.2. Illustrates fragment probability distributions for fragmentation of unit length body into $n = 2$, 3, 4 and 5 fragments. *Dashed line* shows the Poisson distribution approximation to the $n = 5$ fragments case

the appropriate length scale would be proportional to $m^{1/2}$. Thus, a plot of log number versus $m^{1/2}$ should, by the reasoning given, provide a better fit to the fragment distribution data. In notation consistent with the development of the Lineau distribution in the preceding section, the fragment cumulative probability distribution proposed by Mott and Linfoot (1943) would be,

$$F(m) = 1 - e^{-(m/\mu)^{1/2}} , \tag{2.16}$$

where the characteristic mass μ is the distribution scale parameter. The corresponding probability density distribution is then,

$$f(m) = \frac{1}{2\mu} \left(\frac{m}{\mu} \right)^{-1/2} e^{-(m/\mu)^{1/2}} . \tag{2.17}$$

This distribution in various forms has been successfully used by numerous researchers over the past six decades to organize and compare vast amounts of exploding munitions fragmentation data. Mott expended considerable subsequent effort in a quest to justify the functional form assumed in (2.16) and (2.17).

2.2.1 Random Lines Fragmentation

In these initial efforts to justify their distribution Mott and Linfoot (1943) pursued a very reasonable geometric model. They considered the statistical

partitioning of a surface by the random disposition of vertical and horizontal lines. The spacing of lines in the two orientations was assumed to be independently governed by the Lineau distribution. Thus,

$$f_x(x) = \frac{1}{x_o} e^{-x/x_o} , \tag{2.18}$$

and

$$f_y(y) = \frac{1}{y_o} e^{-y/y_o} , \tag{2.19}$$

where the average spacing or frequency of lines in the vertical and horizontal direction was allowed to differ. It is not difficult to see that this geometric model might sensibly replicate the statistical behavior of an exploding munition. The random lines correlate with observed longitudinal and transverse fractures, while the ratio x_o/y_o simulate the elongated nature or aspect ratio of exploding munitions fragments as illustrated in Fig. 2.3a.

We will subsequently show, as did Mott, that this distribution does not correspond well with the distribution in (2.16) and (2.17) (the Mott distribution) arrived at intuitively by Mott and Linfoot. In a later section, however, it will be shown that this geometric algorithm, when effectively generalized,

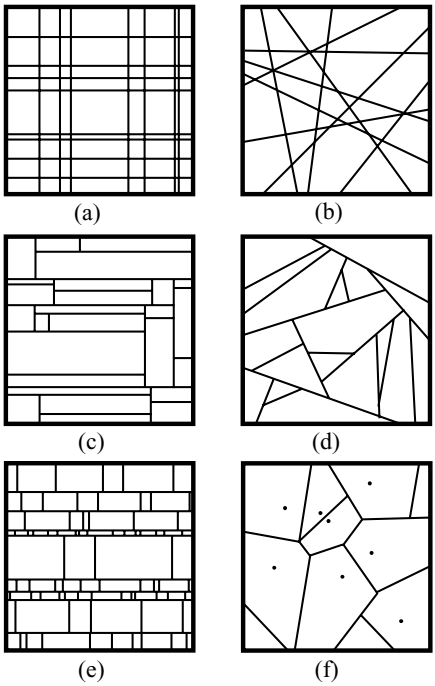

Fig. 2.3. Various geometric random fragmentation algorithms explored by Mott and others

quite nicely approximates the statistical representation of the biaxial fragmentation of expanding shells.

The probability density distribution over fragment length and width is then provided by a juxtaposition of (2.18) and (2.19),

$$f(x,y) = \frac{1}{x_o y_o} e^{-x/x_o - y/y_o} \ . \tag{2.20}$$

Mott and Linfoot (1943) then proceeded to solve for the distribution in fragment size through the following approach: Let $z = \sqrt{xy}$, where xy is the fragment area, provide a measure of the fragment size. The cumulative distribution for fragments of size larger than z is then provided by the integral expression,

$$1 - F(z) = \iint\limits_{xy>z^2} \frac{1}{x_o y_o} e^{-x/x_o - y/y_o} dx dy \ . \tag{2.21}$$

The double integral over area is written,

$$\frac{1}{x_o y_o} \int\limits_0^\infty e^{-x/x_o} \left[\int\limits_{z^2/x}^\infty e^{-y/y_o} dy \right] dx \ , \tag{2.22}$$

which readily reduces to,

$$\frac{1}{x_o} \int\limits_0^\infty e^{-\frac{1}{x_o}\left(x + \frac{x_o}{y_o}\frac{z^2}{x}\right)} dx \ . \tag{2.23}$$

With the change of variable,

$$x = z\sqrt{\frac{x_o}{y_o}}\eta \ , \tag{2.24}$$

the integral becomes,

$$\frac{z}{\sqrt{x_o y_o}} \int\limits_0^\infty e^{-\frac{z}{\sqrt{x_o y_o}}\left(\eta + \frac{1}{\eta}\right)} d\eta \ . \tag{2.25}$$

Introducing the characteristic length $z_o = \sqrt{x_o y_o}$ and making the further change of variable $\eta = e^\theta$ yields,

$$\frac{z}{z_o} \int\limits_{-\infty}^\infty e^{-\frac{z}{z_o}\left(e^\theta + e^{-\theta}\right)} e^\theta d\theta \ , \tag{2.26}$$

which in turn transforms to the integral of the hyperbolic function,

$$2\frac{z}{z_o}\int_0^\infty e^{-2\frac{z}{z_o}\cosh\theta}\cosh\theta d\theta \ . \tag{2.27}$$

The solution of the integral was recognized by Mott and Linfoot as a modified Bessel function. Integral solutions for modified Bessel functions of integer order (Abramowitz and Stegun, 1954) provides,

$$K_n(u) = \int_0^\infty e^{-u\cosh\theta}\cosh n\theta d\theta \ , \tag{2.28}$$

for the modified Bessel function of order n. Thus, we arrive at the cumulative probability distribution over fragment size z,

$$F(z) = 1 - 2\frac{z}{z_o}K_1(2z/z_o) \ . \tag{2.29}$$

The probability density distribution follows directly from $dF(z)/dz = f(z)$ and the modified Bessel function relation (Abramowitz and Stegun, 1954),

$$\frac{d}{du}(uK_1(u)) = -uK_o(u) \ , \tag{2.30}$$

or,

$$f(z) = 4\frac{z}{z_o^2}K_o(2z/z_o) \ . \tag{2.31}$$

An alternative solution method is instructive. Again, start with (2.20) for the probability density distribution over fragment length and width. A transformation to a probability distribution $g(a,r)$ over the fragment area,

$$a = xy \ , \tag{2.32}$$

and the fragment aspect ratio,

$$r = x/y \ , \tag{2.33}$$

is sought.

The differential invariant,

$$f(x,y)\,dxdy = g(a,r)\,dadr \ ,$$

leads to

$$dxdy = \left|\frac{\partial(x,y)}{\partial(a,r)}\right| dadr \ ,$$

for the differential element through the transformation Jacobian (Buck, 1965). The transformed probability density function is then,

$$g(a,r) = f(x(a,r), y(a,r))\left|\frac{\partial(x,y)}{\partial(a,r)}\right| \ . \tag{2.34}$$

Calculating the Jacobian through (2.32) and (2.33),

$$\left|\frac{\partial\,(x,y)}{\partial\,(a,r)}\right| = \frac{1}{2}r^{-1}\ , \tag{2.35}$$

yields,

$$g\,(a,r) = \frac{1}{2x_o y_o}\frac{1}{r}e^{-\left(\frac{1}{x_o}\sqrt{ar}+\frac{1}{y_o}\sqrt{a/r}\right)}\ , \tag{2.36}$$

for the probability density distribution in fragment area and aspect ratio.

To obtain the probability density distribution over area $h(a)$, irrespective of aspect ratio, integrate over all r,

$$h\,(a) = \frac{1}{2x_o y_o}\int_0^\infty \frac{1}{r}e^{-\left(\frac{1}{x_o}\sqrt{ar}+\frac{1}{y_o}\sqrt{a/r}\right)}dr\ . \tag{2.37}$$

Changing the integration variable through $r = (x_o/y_o)e^{2\eta}$ gives,

$$h\,(a) = \frac{2}{a_o}\int_0^\infty e^{-2\sqrt{\frac{a}{a_o}}\cosh\eta}d\eta\ , \tag{2.38}$$

where $a_o = x_o y_o$. The general integral relation for the modified Bessel function of (2.28) yields,

$$h\,(a) = \frac{2}{a_o}K_o\left(2\sqrt{a/a_o}\right)\ . \tag{2.39}$$

The present distribution function over fragment area is equivalent to that of Mott and Linfoot in (2.31) if the transformation $a = z^2$ is performed.

The cumulative distribution over fragment area $H\,(a)$ is readily obtained through the integration of (2.39) and the relation $K_1'\,(u) = -K_o\,(u)$ (Abramowitz and Stegun, 1954),

$$H\,(a) = 1 - 2\sqrt{a/a_o}K_1\left(2\sqrt{a/a_o}\right)\ . \tag{2.40}$$

The density distribution in (2.36) can be pursued further to provide the probability density function over aspect ratio $k\,(r)$ irrespective of fragment size. The integral over fragment area,

$$k\,(r) = \frac{1}{2x_o y_o}\int_0^\infty \frac{1}{r}e^{-\left(\frac{\sqrt{r}}{x_o}+\frac{1}{y_o\sqrt{r}}\right)\sqrt{a}}da\ , \tag{2.41}$$

through the transformation,

$$\xi = \left(\frac{\sqrt{r}}{x_o}+\frac{1}{(y_o\sqrt{r})}\right)\sqrt{a}\ ,$$

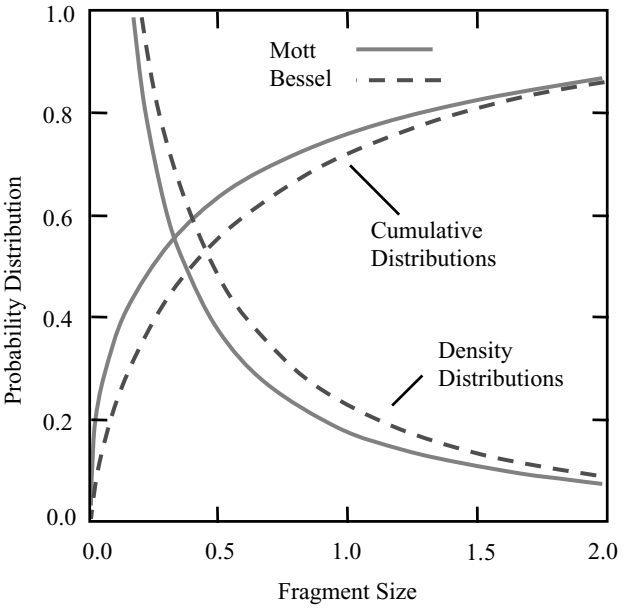

Fig. 2.4. A comparison of the Mott distribution and the Bessel fragment size (area) distribution resulting from the random Lineau placement of vertical and horizontal lines on the surface

yields,

$$k\left(r\right) = \frac{1}{r_o} \frac{1}{\left(1 + r/r_o\right)^2} \int_0^\infty \xi e^{-\xi} d\xi \ , \tag{2.42}$$

where $r_o = x_o/y_o$. Thus,

$$k\left(r\right) = \frac{1}{r_o} \frac{1}{\left(1 + r/r_o\right)^2} \ , \tag{2.43}$$

provides the probability density distribution over fragment aspect ratio.

The probability distribution (both density and cumulative) for the random orthogonal lines geometric fragmentation problem is compared with the Mott distribution in Fig. 2.4 with both distributions normalized to unity. This latter distribution is discussed further in a subsequent chapter. The comparison reveals differences, as was noted by Mott and Linfoot, which failed to provide the justification sought by them. A calculated distribution variance (second moment about the mean) of five for the Mott distribution (2.17) significantly exceeds a variance of three calculated for the Bessel distribution in (2.39). The Mott distribution would predict a larger number of both small and large fragments.

Mott and Linfoot then pursued the geometric fragmentation problem in which orientation as well as placement of lines on the area was a random

variable as illustrated in Fig. 2.3b. They were unable, however, to determine the size distribution for this fragmentation algorithm except in the small fragment limit, which did agree with the proposed dependence of fragment number proportional to the square root of fragment area. Computer solutions of this geometric fragmentation algorithm [Grady and Kipp, 1985] suggest reasonable agreement with the Mott distribution over the full range of fragment sizes.

By considering the geometric problem of randomly oriented vertical and horizontal lines, and then the extension to randomly oriented lines as shown in Fig. 2.3b, Mott and Linfoot tacitly observe that the generated fragment size distribution would probably depend on the algorithm chosen to randomly partition the area. This algorithm dependence of geometric fragmentation methods will be pursued later.

2.2.2 Cylindrical Segmentation Fragmentation

First, however, it is of interest to outline the final geometric fragmentation algorithm pursued by Mott before this line of study was dropped by him. If the fragment size distribution generated in a random geometric fragmentation process is dependent on the fragmentation algorithm, as is becoming apparent, then an algorithm which most closely replicates the event of interest might be expected to better approximate the statistical features sought. Indeed, the present algorithm reasonably approximates the longitudinal fractures and subsequent circumferential breakup observed in a munition fragmentation event. This proximity to the problem of concern most likely guided Mott in selecting this final geometric fragmentation process for study.

This final algorithm is illustrated in Fig. 2.3e. The method consists of first inscribing randomly positioned horizontal lines, and then segmenting each horizontal strip with randomly positioned vertical lines where the average spacing within any strip is proportional to the width of that strip. In pursuing the size distribution solution to this problem, Mott also changed the functional form governing the random placement of horizontal lines and vertical line segments. We will here, however, proceed one step at a time and assume that the Lineau distribution governs the placement of the line and line segments as in the preceding exercise.

It is found in carrying through the solution for the fragment size distribution for this geometric algorithm, with a Lineau distribution of vertical lines and horizontal line segments, that the analysis is not tractable and that the resulting distribution does not converge. Mott must have also observed this difficulty and the observation may have motivated his selection of a distribution function different than the Lineau form. It is also possible that this selection was not arbitrary, but was motivated by physical ideas emerging from the more physically-based theories he was starting to pursue.

In any case, in pursuing the solution to this alternative geometric fragmentation algorithm posed by Mott, it becomes apparent that the probability density distribution for fragments over the areal region cannot simply be

obtained by a juxtaposition of the two linear distributions as was done in the previous analysis. It will initially be necessary to work with number distributions because of difficulties in normalizing the probability distribution. Note first that given a probability density distribution in fragment lengths $f(x)$, the total length dL of fragments of length x within increment dx is just,

$$dL = xdN = N_o x f(x)\, dx \;, \tag{2.44}$$

or

$$L = N_o \int_0^\infty x f(x)\, dx = N_o \langle x \rangle \;, \tag{2.45}$$

where $\langle x \rangle$ is the expected value of x and N_o is the total fragment number. For the Lineau distribution as written in (2.18) the expected value is just $\langle x \rangle = L/N_o = x_o$.

In the geometric fragmentation algorithm illustrated in Fig. 2.3e the region is assumed to be of equal height and width L. Consider one strip of width y. The number of segments (fragments) within this one strip of length x, within increment dx, is just,

$$dN_x = N_{xo} \frac{1}{x_o} e^{-x/x_o} dx = \frac{L}{x_o^2} e^{-x/x_o} dx \;, \tag{2.46}$$

where the Lineau distribution in fragment lengths is assumed. Correspondingly, the number of strips of width, y within increment dy is

$$dN_y = \frac{L}{y_o^2} e^{-y/y_o} dy \;. \tag{2.47}$$

Thus, the number of fragments of length x and width y per unit area (setting $L^2 = 1$) is just the product,

$$dN = dN_x dN_y = \frac{1}{x_o^2 y_o^2} e^{-x/x_o - y/y_o} dx dy \;. \tag{2.48}$$

At this point Mott supplemented the geometric fragmentation algorithm with the assumption that within a strip of width y the average fragment length was proportional to y or,

$$x_o = py \;. \tag{2.49}$$

Mott suggested that the constant p was approximately 5 based on munitions fragments that he had the opportunity to inspect. The present assumption was clearly motivated by observation of fragments from a cylindrical munition fragmentation event in which the nature of the breakup leads to an abundance of elongated fragments.

The resulting fragment number distribution is accordingly,

$$dN = \frac{1}{p^2 y_o^2 y^2} e^{-y/y_o - x/py} dx dy \;. \tag{2.50}$$

We again introduce the change of variables,

$$a = xy, \quad r = x/y \ , \tag{2.51}$$

with Jacobian,

$$\left| \frac{\partial (x, y)}{\partial (a, r)} \right| = 1/2r \ , \tag{2.52}$$

leading to the number distribution,

$$dN = \frac{1}{2p^2 y_o^2} \frac{1}{a} e^{-\sqrt{\frac{a}{ry_o^2}} - r/p} da \ dr \ , \tag{2.53}$$

over fragment area a and aspect ratio r. The number distribution over fragment area is then the integral,

$$\frac{dN}{da} = n(a) = \frac{1}{2p^2 y_o^2} \frac{1}{a} \int_0^\infty e^{-\sqrt{\frac{a}{ry_o^2}} - r/p} dr \ , \tag{2.54}$$

or, with the variable change $r = p\eta$,

$$n(a) = \frac{1}{2py_o^2} \frac{1}{a} \int_0^\infty e^{-\sqrt{\frac{a}{py_o^2}} \frac{1}{\sqrt{\eta}} - \eta} d\eta \ . \tag{2.55}$$

Unfortunately, the integral within (2.55) is not finite. Cursory examination of the distribution shows an unbounded number density distribution as both area a and aspect ratio r become small. Thus, this very natural statistical fragmentation geometry, when combined with the Lineau (Poisson) placement of the fractures, leads to an ill-defined fragment distribution. Although not explicitly discussed in his reports Mott must have tread this path and encountered the same difficulty. Undaunted, he proposed a novel solution resulting in an analytically regular fragment size distribution for the geometric fragmentation problem addressed above. Some further background is necessary, however, to fully appreciate the approach he pursued. Mott's treatment of this final geometric fragmentation algorithm will be revisited in Sect. 2.5.

2.3 Poisson Fragment Distribution and Statistical Heterogeneity

Mott and Linfoot proposed a representation for the statistical distribution of fragment sizes resulting from a munitions fragmentation event which was independent of any specific fragmentation process, geometric or otherwise. Namely, that a measure of the fragment size (proportional to the square root of the fragment area) was distributed over fragment number according to

the Poisson process put forth by Lineau (1936). They then pursued analytic methods to justify the assumed fragment distribution, an approach that served Mott well throughout the course of his theoretical career. As illustrated in the previous section, the statistical geometric methods were not fully successful in validating the proposed distribution.

Others have pursued alternative statistical assumptions regarding the distribution of fragment sizes and have similarly undertaken efforts to justify their assumptions. Here we consider the approach of Grady and Kipp (1985) as it parallels the fragmentation assumptions and geometric statistics justification attempts of Mott and Linfoot (1943). The comparison more starkly brings out features and weaknesses of the approach.

2.3.1 Grady–Kipp Postulate

Within the intervening years since the seminal study of Mott, considerable opportunity has risen to test the distribution of Mott and Linfoot. Although the linear dependence of the logarithm of fragment number against the square root of fragment mass proposed by Mott and Linfoot has in many comparisons been quite satisfactory, there have also been examples of obvious discrepancy. For example, munitions fragment data have been obtained which plot linear in log number versus cube root of fragment mass. This dependence has of course been suggested to apply to thick-walled munitions in which the preponderance of fragments are of size smaller than the wall thickness, as is tacit in the initial development of Mott and Linfoot. Other disparities between the Mott-Linfoot distribution and munitions fragmentation data have also been observed.

Grady and Kipp (1985) have offered an alternative development and explanation for the distributions in fragment sizes observed in munitions fragmentation. They first suggest that if such fragmentation can be represented by mechanism-independent statistical descriptions that perhaps fragment mass, as opposed to fragment size (either $m^{1/2}$ or $m^{1/3}$ in the Mott-Linfoot development), is the more appropriate random variable. They then propose that the mass of the fragment is distributed over fragment number according to a Poisson (or binomial if the fragment number is small) process, which parallels the development of Lineau in Sect. 2.1.

Thus, if the fragment mass is viewed as a random scalar variable, then the random fragmentation of the mass is analogous to the one-dimensional Lineau problem. Fragmentation is determined by breaks distributed randomly over the scalar measure of mass. The breaks determine a Poisson variate and lead to a cumulative fragment probability distribution,

$$F(m) = 1 - e^{-m/\mu} \,, \tag{2.56}$$

and density distribution,

$$f(m) = \frac{1}{\mu} e^{-m/\mu} \,. \tag{2.57}$$

In contrast to the Mott distribution, the present distribution keeps the same linear exponential functional form for both area and volume fragmentation.

2.3.2 Sequential Segmentation

Grady and Kipp (1985) also pursued justification of their fragment distribution relations through geometric fragmentation methods. With the availability of computational resources they were not restricted to geometries with analytic solutions. The algorithms pursued by them are illustrated in Figs. 2.3c and 2.3d. The method is as follows: A point was selected at random on the unit area. Then a random vertical or horizontal direction in Fig. 2.3c or random arbitrary direction in Fig. 2.3d was determined and a line drawn through the point and terminated at the area boundary. A second point was randomly selected and a random line again drawn bisecting the sub area within which the point fell. This process was sequentially repeated until the desired intensity of fragmentation was achieved.

It was found that distributions from both the horizontal and vertical lines, and randomly oriented lines, sequential segmentation geometric processes converged to the linear-exponential distributions in (2.56) and (2.57) with sufficient numbers of fragments for the geometric fragmentation of an area. With some reflection, it is recognized that this geometric algorithm is replicating the Poisson partitioning of a scalar area or volume. Thus, the agreement is expected.

The linear exponential (Poisson) density and cumulative distribution is shown in Fig. 2.5 and differs markedly from the Mott distribution. The much broader Mott distribution has a variance a factor of five larger than the Poisson distribution.

2.3.3 Statistical Heterogeneity

Considering the substantial difference between the exponential distribution and the Mott distribution in Fig. 2.5, and the historic success of the latter in describing munitions fragment distribution data, one may question how the exponential distribution can be offered as a viable representation. Grady and Kipp (1985) provide the following argument in support of the exponential distribution.

In the statistical fragmentation problems considered up to this point, statistical homogeneity over the fragmented region was tacitly assumed. Namely, the average fragment size did not vary from point to point within the region of consideration. In application, uniform or homogeneous fragmentation is usually not achieved. Normally, due to complexity of the device geometry and dynamic loading, the intensity of fracture will vary throughout the body and, correspondingly, the average fragment size will also be a function of position. A uniformly expanding ring or the uniform expansion of a spherical shell are unique experimental geometries in which nearly homogeneous fragmentation

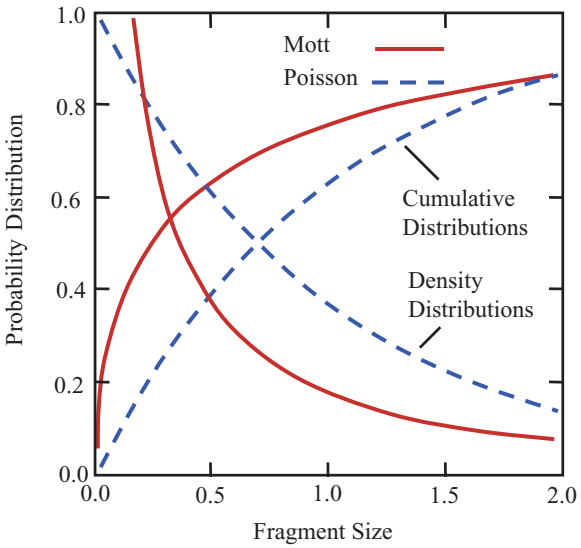

Fig. 2.5. A comparison of the Mott distribution and the Exponential, or Poisson, fragment size (area) distribution resulting from the random segmentation of the surface

is achieved. Most experimental geometries will lead to statistically inhomogeneous fragmentation. This concept was considered by Lineau (1936), but was not pursued.

Additionally, there is some evidence that fracture mechanisms may markedly differ for different parts of the fragment size distribution. This was briefly suggested by Mott for the fragmentation of exploding cylinders and has been pursued in more detail by Odintsov (1992). This possibility will be considered further later in this section.

The linear exponential distribution based on a Poisson process over a scalar mass region,

$$f(m) = \frac{1}{\mu} e^{-m/\mu} \,, \tag{2.58}$$

proposed by Grady and Kipp (1985), assumed statistical homogeneity with average mass μ constant over the region of interest. A second distribution with a different average fragment size could be described equally well with a distribution of the form of (2.58). A mixing of the two distributions would not be characterized by a linear exponential distribution. The distribution would, rather, be represented by the bi-linear form,

$$f\,(m) = \frac{g_1}{\mu_1} e^{-m/\mu_1} + \frac{g_2}{\mu_2} e^{-m/\mu_2} \,, \tag{2.59}$$

where g_1 and g_2 are the number fractions of the respective homogeneous distributions, while μ_1 and μ_2 are the corresponding average fragment masses.

More generally, any statistically inhomogeneous distribution could be approximated with a Poisson mixture [Puri and Goldie, 1979],

$$f(m) = \sum_{1}^{n} \frac{g_i}{\mu_i} e^{-m/\mu_i} \ . \tag{2.60}$$

It can be shown that any Poisson mixture representation of a fragment distribution will have a larger variance than a statistically homogeneous linear exponential representation of that same distribution. It is instructive to compare, for example, the bi-linear distribution from (2.59) with the Mott distribution. Normalizing the Mott distribution to the average fragment mass $x = m/\mu$,

$$f(x) = \frac{1}{\sqrt{2x}} e^{-\sqrt{2x}} \ , \tag{2.61}$$

and similarly the bi-linear distribution with $x = m/\mu$ and $\mu = g_1\mu_1 + g_2\mu_2$,

$$f(x) = \frac{g_1}{\alpha_1} e^{-x/\alpha_1} + \frac{g_2}{\alpha_2} e^{-x/\alpha_2} \ , \tag{2.62}$$

where $\alpha_1 = \mu_1/\mu$ and $\alpha_2 = \mu_2/\mu$.

Constrain the integral of the distribution and the first moment to unity in (2.62),

$$g_1 + g_2 = 1 \ , \tag{2.63}$$

$$\alpha_1 g_1 + \alpha_2 g_2 = 1 \ . \tag{2.64}$$

The second and third distribution moments (equivalently the distribution variance and skewness) can also be equated to the corresponding moments for the Mott distribution yielding,

$$2\left(g_1\alpha_1^2 + g_2\alpha_2^2\right) = 6 \ , \tag{2.65}$$

$$6\left(g_1\alpha_1^3 + g_2\alpha_2^3\right) = 90 \ , \tag{2.66}$$

uniquely constraining the four constants in the bi-linear distribution. A comparison of the Mott and bi-linear distributions (actually complementary cumulative distributions) with identical distribution moments is shown in Fig. 2.6. Although significant visual differences are observed, the bi-linear distribution does start to capture the important features of the Mott distribution. The distributions are compared in a semi-logarithmic representation in which a single exponential (Poisson) distribution plots linear. Better agreement can, of course, be achieved as more terms are included in the Poisson mixture representation.

A mixture of Weibull distributions (referred to as a hyper Weibull distribution) has been proposed by Odintsov (1992) of the form

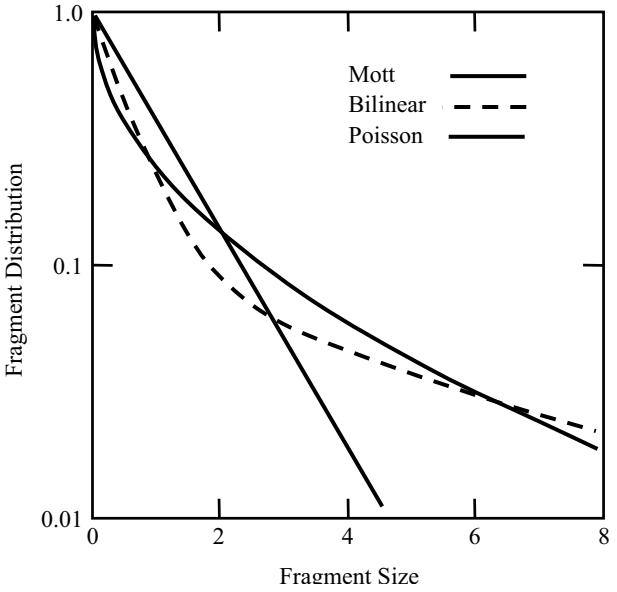

Fig. 2.6. Comparison of the Mott and Poisson fragment size complementary cumulative distribution with a bilinear (Poisson mixture) distribution approximation

$$f\,(m) = \sum_{1}^{n} g_i \frac{n_i}{\mu_i} \left(\frac{m}{\mu_i}\right)^{n_i - 1} e^{-(m/\mu_i)^{n_i}} \,, \tag{2.67}$$

with mean fragment size,

$$\mu = \sum_{1}^{n} g_i \mu_i \Gamma(1 + 1/n_i) \,. \tag{2.68}$$

This distribution, of course, reduces to the Poisson (hyper exponential) mixture provided in (2.60) when the n_i for each distribution component is set to unity. The latter specialized mixture was pursued in some detail be Odintsov.

The issue emphasized in the present section, however, is the statistically inhomogeneous character of experimental fragment distributions. Attempts to represent such distributions with analytic forms developed from homogeneous statistical fragmentation models will be at best approximate. Also, the theoretical logical inconsistencies are not fully satisfying. The introduction of Poisson mixtures to describe statistically inhomogeneous distributions is inherently reasonable. Acceptance of a Poisson (linear exponential) distribution as the homogeneous basis function as has been proposed [Grady and Kipp, 1985; Odintsov, 1992], has not been fully justified, and is open to criticism as later developments will illustrate.

2.3.4 Multimodal Distributions

The power of the mixture distribution representation is illustrated in the description of multimodal fragment distributions as emphasized by Odintsov (1992). Commonly the mass spectra of fragments over size is desired and is obtained from the probability distribution through,

$$dM = mdN = mN_o f(m)dm \; . \tag{2.69}$$

Let $\varphi(m) = dM/dm$ so that,

$$\varphi(m) = \frac{1}{\mu} m f(m) \; , \tag{2.70}$$

for the distribution of the mass of the fragment over the fragment size (or weight) m and with $\mu = 1/N_o$.

For a bilinear Poisson mixture normalized to a fragment size scale of $\mu = 1$ as in (2.62), the mass distribution in (2.70) becomes,

$$\varphi(x) = x \left(\frac{g_1}{\alpha_1} e^{-x/\alpha_1} + \frac{g_2}{\alpha_2} e^{-x/\alpha_2} \right) \; . \tag{2.71}$$

Two distributions are plotted from (2.71) and are shown in Fig. 2.7 for different values of the distribution parameters. In both distributions the number ratio is the same at $g_1/g_2 = 1$. When the size ratio is not large ($\alpha_1/\alpha_2 = 4$

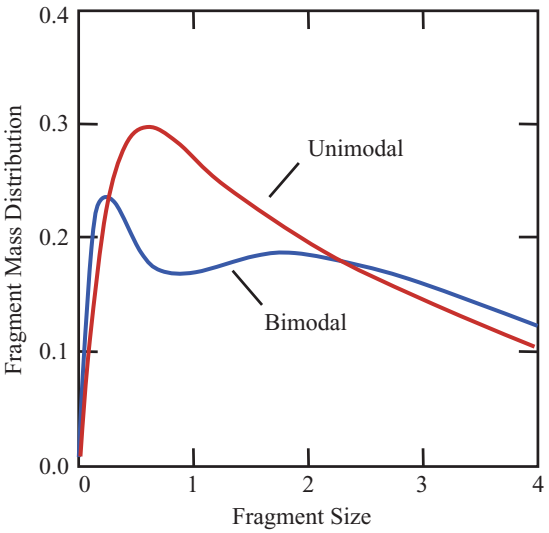

Fig. 2.7. Mass distribution for bilinear Poisson fragment distribution mixtures for selected distribution parameters illustrating both unimodal and bimodel character

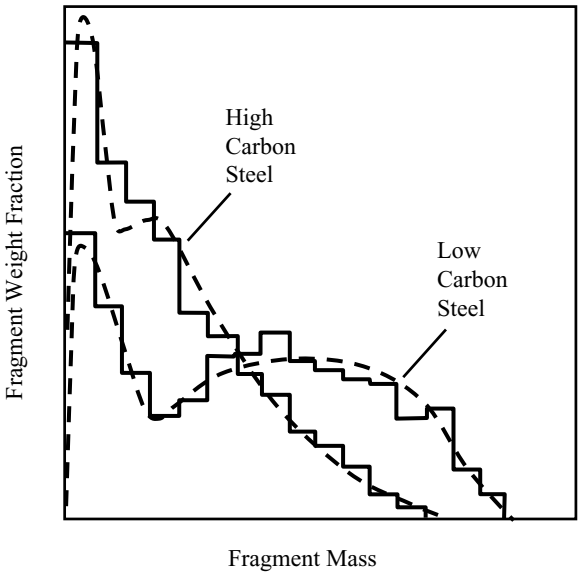

Fig. 2.8. Fragment mass distributions for explosive fragmentation of low carbon and high carbon content steel cylinders and associated bilinear exponential distribution fit in uncalibrated units [Odintsov, 1992]

in Fig. 2.7) the distribution is unimodal. As the size ratio increases (or correspondingly decreases), however, a mode separation is observed in the distribution yielding a distinct bimodal distribution ($\alpha_1/\alpha_2 = 10$ in Fig. 2.7).

Odintsov (1992) has reported detailed fragment distribution properties from explosion-induced natural fragmentation experiments on low-carbon and high-carbon steel cylinders. Histogram distributions for one low-carbon and one high-carbon steel tests are plotted in Fig. 2.8 in uncalibrated units. Bilinear curve fits to the data by Odintsov are also shown. The distribution for the low-carbon steel is distinctly bimodal where as that of high-carbon steel is nearly unimodal.

Odintsov attributes the bimodal character of the distributions to two distinct populations of fragments with possibly distinct fracture mechanisms. The first population is composed of the larger fragments created by through-the-thickness fractures, which retain sections of both the inner and outer surfaces of the original cylinder. The second population is composed of the smaller angular shards created by fracture intersections, near either the inner surface (shear fracture dominated) or the outer surface (tensile fracture dominated). These failure modes were also noted by Mott.

The more brittle high-carbon steel is dominated by fragments from the second population and consequently is nearly unimodal in character. The more ductile low-carbon steel has sensible contributions from both fragment populations leading to the observed bimodal nature of the distribution.

2.4 Voronoi-Dirichlet Fragment Distribution

The present discussions of random geometric fragmentation would be remiss without consideration of the Voronoi-Dirichlet construction [*e.g.*, Boots and Murdoch, 1983]. This method for the random partitioning of space has received by far the lion's share of attention in a much broader spectrum of literature. The resulting distributions have been proposed for such applications as the distribution of galactic matter throughout the universe [Kiang, 1966] and the formation of geologic columnar structures such as the Giant's Causeway in Northern Ireland [Weaire and Rivier, 1984] to name but a few.

The construction algorithm in two dimensions is illustrated in Fig. 2.3f. As in the Grady-Kipp construction, the method begins with a random (statistically homogeneous) distribution of points on the surface (or within the volume if three-dimensional space is considered). Space is then randomly partitioned by construction of perpendicular bisecting lines (or surfaces) as illustrated. On a regular (periodic) lattice of points the same process creates the Wigner-Seitz cells used, for example, in the construction of Brillouin zones in solid state physics [Kittel, 1971]. The space is also randomly partitioned through the reciprocal, or dual, Delauney construction [Watson, 1981] created through the joining, with lines (or surfaces), the points in each Voronoi-Dirichlet cell.

Analytic relations for the fragment size distributions resulting from the Voronoi-Dirichlet construction have not been directly determined. A computational determination of the resulting fragment size distributions has been widely pursued, however [e.g., Crain, 1978], and an analytic expression which successfully reproduce the computational distributions has been arrived at by intuitive means [Kiang, 1966].

Both the analytic distributions and the process of developing them are of interest to the present pursuit of statistical fracture through geometric means. First Kiang (1966) considered the one-dimensional Voronoi-Dirichlet construction, where points are distributed at random on a line (a Poisson process), and then the degenerate perpendicular bisector (the midpoint) of each point pair is determined. Thus, the Voronoi-Dirichlet distribution on a line is the dual of the Lineau distribution considered earlier (or the degenerate Delauney distribution). Whereas, in the Lineau distribution random points on the line were considered as breaks or fractures, in the present Voronoi-Dirichlet distribution these same random points constitute in some sense the centroid of fragments with fractures occurring at the bisector points.

2.4.1 One-Dimensional Voronoi–Dirichlet Distribution

The fragment size distribution for the one-dimensional Voronoi-Dirichlet distribution can be determined directly as follows. The probability of finding a length l between a Poisson point pair is given by the Lineau distribution,

$$f(l)dl = \frac{1}{\lambda} e^{-l/\lambda} \ . \tag{2.72}$$

The probability of finding a point pair of length l_1 adjacent to a point pair of length l_2 is then the product,

$$f(l_1)f(l_2)dl_1dl_2 = \frac{1}{\lambda^2}e^{-(l_1+l_2)/\lambda}dl_1dl_2 \ . \tag{2.73}$$

Implementing the transformation,

$$L = (l_1 + l_2)/2 \ , \tag{2.74}$$

$$\xi = (l_1 - l_2)/2 \ , \tag{2.75}$$

leads to the distribution,

$$f(L) = \frac{1}{\lambda^2}\int_{-L}^{L} e^{-2L/\lambda}d\xi \ , \tag{2.76}$$

where L is the length between midpoints of the point pairs. Integration provide the Voronoi-Dirichlet distribution of fragments on a line,

$$f(L) = \frac{2}{\lambda}\left(\frac{2L}{\lambda}\right)e^{-2L/\lambda} \ . \tag{2.77}$$

Comparison of the one-dimensional Voronoi distribution (2.77) and the Lineau, or Poisson, distribution is provided in Fig. 2.9.

2.4.2 Two and Three Dimensional Analytic Distributions

The distribution in (2.77) is a gamma function of order $n = 2$. Kiang (1966) offered without proof that symmetrically higher order gamma functions would provide analytic fragment distributions for Voronoi-Dirichlet partitioning of an area or a volume. Following Kiang we will write the general expression for the fragment distribution over mass,

$$f(m) = \frac{1}{\mu}\frac{n}{\Gamma(n)}\left(\frac{nm}{\mu}\right)^{n-1} e^{-nm/\mu} \ , \tag{2.78}$$

where $n = 2, 4$ or 6 for a line, surface or volume fragmentation, respectively.

Computational distributions from Voronoi-Dirichlet constructions on an area performed by Kiang (1966) were in acceptable agreement with (2.78) for $n = 4$. A degree of controversy was generated by Kiang's proposal among subsequent authors as to the adequacy of (2.78); both for and against. Apparently the construction of computer algorithms to generate Voronoi-Dirichlet fragment distributions is not a trivial exercise. In any case, for the present geometric fragmentation investigations, (2.78) is an adequate analytic representation of Voronoi-Dirichlet distributions in line and area fragmentation.

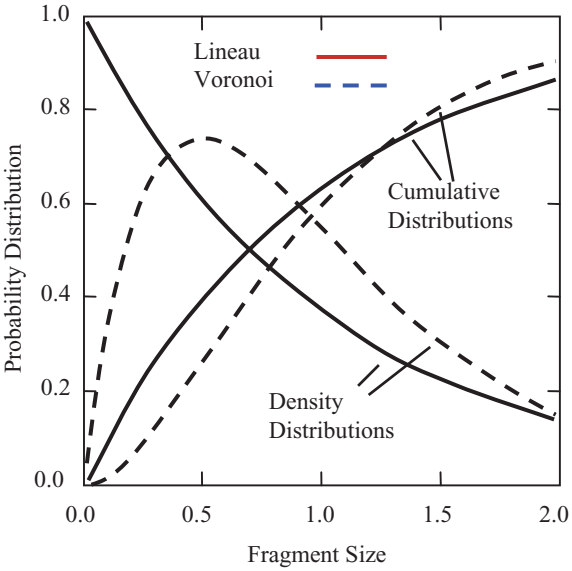

Fig. 2.9. A comparison of the one-dimensional Voronoi distribution and the Lineau, or Poisson, fragment length distribution resulting from the random segmentation of the line according to the respective algorithms

Fragment size (area) distributions resulting from both the Voronoi algorithm and the sequential segmentation algorithm (Poisson distribution) are compared with the Mott distribution from (2.17) in Fig. 2.10. The three density distributions are normalized to unit expected value. The comparisons reveal the stark differences resulting from differing randomization algorithms and differ markedly from the proposed distribution of Mott.

2.5 Mott Cylinder Segmentation Algorithm

Mott undertook one final attempt at justifying through geometric methods the proposed $m^{1/2}$ distribution. The approach was explored earlier in Sect. 2.2. From the elongated and sliver-shaped fragments recovered from exploding munitions tests Mott surmised that fracture in an end-detonated metal shell with cylindrical symmetry would occur through longitudinal running cracks with occasional crack branching and crack intersection resulting in the observed fragments. Thus he proposed the statistical algorithm illustrated in Fig. 2.3e and analyzed earlier with the Lineau distribution of the lines and line segments. To randomly distribute the longitudinal and transverse line features on the plane he made the interesting selection of the one-dimensional Voronoi-Dirichlet distribution discussed in the previous section rather than the Lineau distribution used in his earlier geometric pursuits. He may have made this

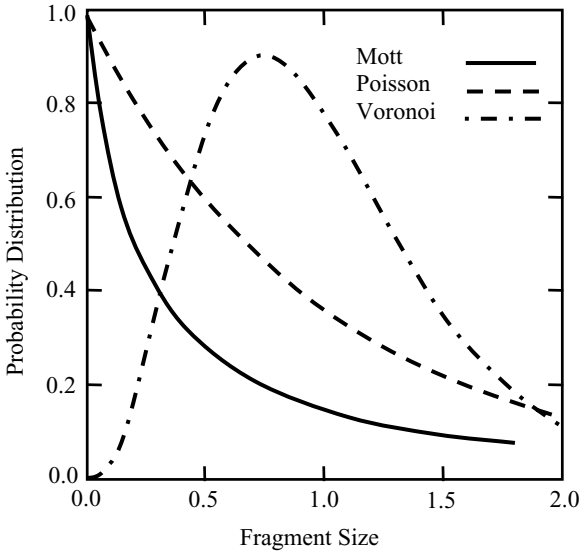

Fig. 2.10. Comparison of the Mott, Poisson and Voronoi distributions for the random fragmentation of an area

choice for one of two reasons. It is possible that he carried through the analysis using the Lineau distribution, as was attempted earlier in this chapter, and found (as was shown in the earlier section) that a solution could not be obtained. Alternatively, ideas to emerge in his later work, and to be discussed in the next chapter, may have influenced this selection: namely, that the physics of fracture interaction precludes the close proximity of parallel fracture, and thus limits the number of smaller fragments. The Voronoi-Dirichlet distribution is observed to better provide a statistical constraint limiting the number of the close parallel fractures and hence the number of smaller fragments.

Following the methods outlined previously, but using the Voronoi-Dirichlet distribution from (2.77) to determine the random placement of longitudinal lines and transverse line segments, the following size distribution over fragment area is obtained,

$$f(a) = \frac{2}{a_o} \frac{1}{\sqrt{4a/a_o}} \int_0^\infty \left(\xi \sqrt{4a/a_o} - 1 \right) \left(1 + 1/\xi^2 \right) e^{-\xi \sqrt{4a/a_o} - 1/\xi^2} d\xi \ . \quad (2.79)$$

This relation corresponds to the distribution provided by Mott and differs only in the distribution variable $\lambda = \sqrt{a/a_o}$ used by him where $a_o = py_o^2$. The corresponding cumulative distribution is then,

$$F(a) = \sqrt{4a/a_o} \int_0^\infty \left(1 + 1/\xi^2 \right) e^{-\xi \sqrt{4a/a_o} - 1/\xi^2} d\xi \ . \quad (2.80)$$

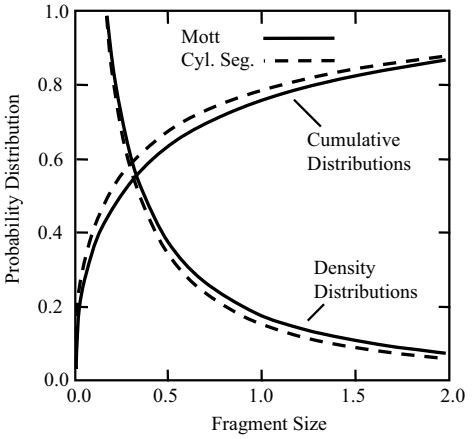

Fig. 2.11. A comparison of the cumulative and density fragment size distributions from the Mott distribution and the geometric cylinder segmentation distribution

The plot in Fig. 2.11 compares the Mott distribution with the cylindrical segmentation algorithm proposed by Mott using the Voronoi algorithm for randomly distributing the partitioning lines and line segments. This figure corresponds to Fig. 2.4 in which the Mott distribution is compared with the random vertical and horizontal lines algorithm. A final comparison is shown in Fig. 2.12 in which the density distributions resulting from both algorithms considered by Mott are compared with the Mott distribution over a wider

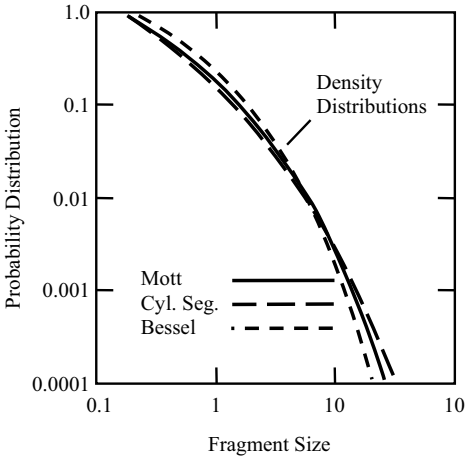

Fig. 2.12. A comparison of the probability density fragment distributions from the Mott distribution, the geometric cylinder segmentation distribution, and the geometric random horizontal and vertical lines (Bessel) distribution. Approximately 95% of the fragment area (mass) is included in the range of the plotted distributions

spectrum of fragment sizes. It is interesting that the distributions from the two algorithms tend to straddle the Mott-Linfoot proposed distribution, each with respectively larger and smaller variance. It is unlikely that anything else can be said.

At this point a degree of healthy suspicion as to the applicability of random geometric fragmentation algorithms to actual physical fragmentation phenomena should be embraced. Later, it will be shown that some utility of these methods can be made use of in modeling the statistical fragmentation phenomena, but they should be employed only with a sensible understanding of the underlying physics.

References

Abramowitz, M. and Stegun, I.A. eds. (1954), Handbook of Mathematical Function, No. 55, *National Bureau of Standards Applied Mathematics Series*, U.S. Government Printing Office.

Boots, B.N. and Murdoch, D.J. (1983), The Spatial Arrangement of Random Voronoi Polygons, *Computers and Geosciences*, 9, 351–365.

Buck, R.C. (1965), *Advanced Calculus*, McGraw-Hill, New York.

Crain, I.K. (1978), The Monte-Carlo Generation of Random Polygons, *Computers and Geosciences*, 4, 131–141.

Grady, D.E. (1990), Particle Size Statistics in Dynamic Fragmentation, *J. Appl. Phys.* 68, 12, 6099–6105.

Grady, D.E. and Kipp, M.E. (1985), Geometric Statistics and Dynamic Fragmentation, *J. Appl. Phys.*, 58, 3, 1210–1222.

Kittel, C. (1971), *Introduction to Solid State Physics*, John Wiley & Sons, New York.

Kiang, T. (1966), Mass Distributions of Asteroids, Stars and Galaxies, *Zeitschrift für Astrophysik*, 64, 426–432.

Lineau, C.C. (1936), Random Fracture of a Brittle Solid, *J. Franklin Inst.*, 221, 485–494, 674–686, 769–787.

Mott, N.F. and Linfoot, E.H. (1943), A Theory of Fragmentation, *Ministry of Supply* AC3348.

Odintsov, V.A. (1992), Hyperexponential Spectra of Exponential Fracture, *Mechanics of Solids*, (Meckhanika Tverdogo Tela), 27, 5, 42–48.

Puri, P.S. and Goldie, C.M. (1979), Poisson Mixtures and Quasi-Infinite Divisibility of Distributions, *J. Appl. Prob.*, 16, 138–153.

Watson, D.F. (1981), Computation the n-Dimensional Delaunay Tessellation with Application to Voronoi Polytopes, *The Computer Journal*, 24, 167–172.

Weaire, D. and Rivier, N. (1984), Soap, Cells and Statistics – Random Patterns in Two Dimensions, *Contemp. Phys.*, 25, 1, 59–99.

3

Physics-Based Statistical Methods

Mott reached closure in his exploration of geometric fragmentation statistics early in his third internal report. In the remainder of this report he undertook a seminal investigation of the fragmentation of exploding shells, and developed a statistical theory of dynamic fragmentation elegant in its formulation and insightful in the physics explored. His theoretical effort has been noted in numerous subsequent studies in dynamic fragmentation but has received little in-depth study. Consequently, the fragmentation theory of Mott now over 60 years in the literature has been neither validated nor refuted. Efforts in the present section attempt to assess and broaden the physical principles of dynamic fragmentation first proposed by Mott. The efforts go beyond the initial analysis of Mott, however, both in the range of fracture processes, as well as in the analytic development.

3.1 Statistical Theory of Mott

The dynamic fracture analysis pursued by Mott is decidedly one-dimensional. It is best visualized as that of a uniformly stretching rod or expanding ring such as illustrated in Fig. 3.1. The model can be usefully abstracted to fragmentation applications, such as a rapidly expanding cylinder in which the circumferential stretching rate substantially exceeds the axial, or a one-dimensional spall event within a body experiencing increasing tension within a region of uniform axial velocity gradient. Here, for clarity, the model exploration will focus on a stretching filament of material of unit cross section as depicted by the expanding ring in Fig. 3.1. Prior to fracture, the body is uniformly stretched to an axial strain ε which is increasing at a constant strain rate $\dot{\varepsilon}$.

Mott considered the body to be rigid perfectly plastic and straining in tension under a constant flow stress Y. The Mott kinematic conditions will be referred to as plastic fracture. Tensile loading in which the body remains elastic up to the point of fracture will also be considered (elastic fracture). Here

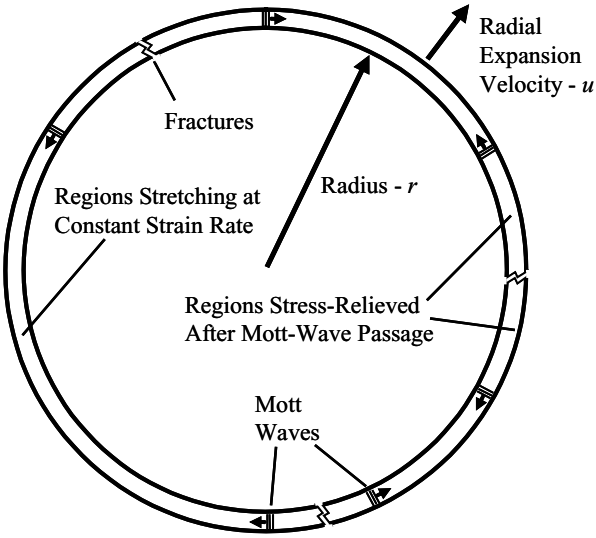

Fig. 3.1. The one-dimensional Mott problem. A one-dimensional ring of material undergoes outward expansion at constant velocity, u. Prior to fracture response of the body is uniform tensile stretching at a strain rate $\dot{\varepsilon} = u/r$. Instantaneous fracture occurs at random sites and waves originate at points of fracture which propagate at finite speeds, relieving tensile stress and further stretching. Strain-dependent fracture continues only in regions not yet encompasses by the stress-relieved waves

tensile stress is related to strain and strain rate according to $\sigma = E\varepsilon = E\dot{\varepsilon}t$ where E is the appropriate elastic modulus.

At onset of breakup fractures are considered to occur at random in both time (or equivalently strain) and in spatial location on the stretching body as illustrated in Fig. 3.1. Following Mott it is assumed that fractures occur instantaneously relieving the tensile stress at the point of fracture to zero. Thus fracture resistance at the point of breakage and corresponding fracture energy during the breakage process is ignored.

Mott argued that the fracture energy was not significant. Rather, he proposed that the statistical nature of the fracture process determined both the characteristic fragment size, as well as the distribution in fragment sizes.

Mott's assumption of both instantaneous fracture and the insignificance of fracture energy can, and should, be examined further. This issue will be investigated in some detail in a later section.

Mott used observations of fracture in notched-bar specimens of steels to support the theoretical approach. He noted that the reduction in the cross-sectional area (the strain) before fracture was not the same from test to test. Scatter in the strain to fracture of a few percent over a number of tests was observed. He then proposed that strain to fracture was a random variable in

the stretching body, and that fracture when the circumferential strain achieved some critical level was governed by probabilistic causes.

Following fracture at a point, waves propagate away from the fracture relieving the tensile stress and subsequent stretching within the regions encompassed by the waves. For plastic fracture, in which waves are propagating into media stretching plastically at a constant flow stress Y these waves are diffusive (Mott waves) and the distance traveled depends on time and physical properties according to,

$$x = \sqrt{2Yt/\rho\dot{\varepsilon}} \; . \tag{3.1}$$

If fracture is elastic, release waves propagate according to,

$$x = \sqrt{E/\rho}t \; , \tag{3.2}$$

where $c = \sqrt{E/\rho}$ is the elastic wave speed.

Fracture physics in either the plastic or the elastic model is governed by the competition of waves of release emanating from existing fractures, with continuing fracture occurring within regions of the body not yet subsumed by these waves.

3.2 Mott Wave Propagation

Equation (3.1) describes the time-dependent propagation of tensile stress release from points of fracture, and is representative of the insightful physics introduced by Mott in pursuing an understanding of the dynamic fracture process.

3.2.1 Mott Rigid Plastic Solution

To pursue his analysis of the distribution of the fracture spacing resulting in the dynamic fracture of an expanding cylindrical shell, it was necessary to establish the speed at which waves, signaling the drop in tensile stress, propagated outward from points of fracture. Accordingly, Mott considered a one-dimensional rod of unit cross section stretching plastically under a tensile stress Y and uniformly at a constant stretching rate, $\dot{\varepsilon}$. Fracture was initiated by setting the tensile stress to zero at time $t = 0$ at some Lagrangian position, say $h = 0$. Regions of the rod experiencing tensile stress less than Y were considered rigid. Mott then realized that a boundary (herein called a Mott wave) separated rod material stretching uniformly at stress Y in front of the boundary from rigid material moving at the same uniform velocity behind the boundary. This boundary (Mott wave) propagates away from the point of fracture at $h = 0$. Features of the stress and velocity associated with the Mott wave at some time $t > 0$ are illustrated in Fig. 3.2. Location of the Mott wave is identified by $x(t)$, while crack opening displacement is given by $y(t)$. The velocity field is then,

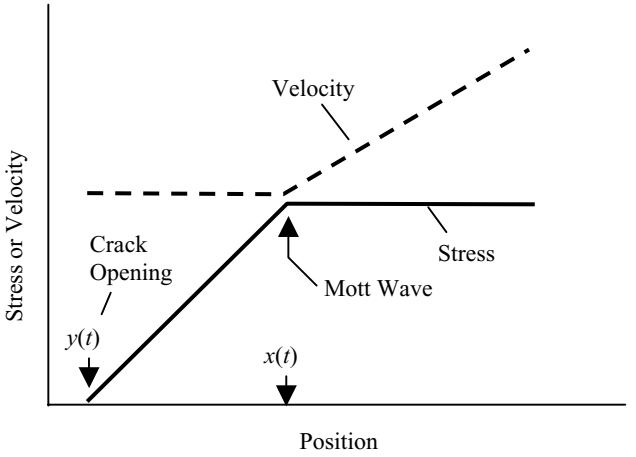

Fig. 3.2. Stress and velocity field at time t after fracture at position $h = 0$ drops tensile stress from Y to zero

$$u\,(h,t) = \begin{cases} \dot{\varepsilon} x\,(t) & 0 \le h < x\,(t) \\ \dot{\varepsilon} h & x\,(t) \le h \le h_o \end{cases} , \tag{3.3}$$

where, h_o is some arbitrary distance.

The corresponding stress field is equally apparent. The total momentum of the rod within the region $0 \le h \le h_o$ is just,

$$\rho\dot{\varepsilon}x^2 + \int_x^{h_o} \rho\dot{\varepsilon}h dh = \frac{1}{2}\rho\dot{\varepsilon}(x^2 + h_o^2)\,. \tag{3.4}$$

Equating the time rate of change of momentum to the imbalance in tensile stress yields the differential equation,

$$\rho\dot{\varepsilon}x\frac{dx}{dt} = Y\,, \tag{3.5}$$

for the position $x(t)$ of the Mott wave at time t. Integration readily yields,

$$x\,(t) = \sqrt{\frac{2Yt}{\rho\dot{\varepsilon}}}\,. \tag{3.6}$$

Thus, fractures occurring in the stretching body lead to the propagation of waves, away from these points of fracture, which unload the tensile stress. The time dependent motions of these Mott waves are governed by both material properties and kinematic conditions according to the relation above. Within regions subsumed by Mott waves, further fracture will not occur. Subsequent fracture will only occur in regions, not yet reached by the unloading Mott waves, which continue to stretch unimpeded at a rate $\dot{\varepsilon}$ and flow stress Y.

Mott recognized that excessively high velocities of the interface $x(t)$, at early times, was a consequence of the rigid-plastic assumption and inconsistent with a more rigorous elastic-plastic treatment of the problem. He acknowledges an analysis due to E. H. Lee, which was published some years later [Lee, 1967]. Lee considered the same initial and boundary conditions posed by Mott, but treated material response behind the interface as elastic. It is shown that the initial drop in stress from $\sigma = Y$ to $\sigma = 0$ at the origin $h = 0$ propagates as a decaying shock discontinuity in stress and particle velocity at an elastic wave speed c. This shock discontinuity decays to zero at a distance of,

$$h = \frac{2Y}{\rho c \dot{\varepsilon}} = \lambda \,, \tag{3.7}$$

and at a time of,

$$\tau = \lambda / c \,. \tag{3.8}$$

Subsequent reflected elastic waves and the interface $x(t)$ are acceleration discontinuities (discontinuities in the slopes of stress and particle velocities). Continued solution reveals that the interface $x(t)$ is a polygon in the h vs. t domain with vertices,

$$h = n\lambda \,, \quad t = n^2 \lambda / c \,, \quad n = 1, 2, 3, \ldots \tag{3.9}$$

where each segment propagates at a velocity of,

$$c_n = \frac{c}{2n - 1} \,. \tag{3.10}$$

The rigid-plastic solution of Mott (1947) and the elastic-plastic solution of Lee (1967) are compared in Fig. 3.3. The former is found to envelop the elastic-plastic solution touching at the vertices. Within several characteristic distances λ the rigid-plastic solution is found to be a very good approximation to both the position of the interface, and to the stress and velocity field behind the interface.

3.2.2 The Diffusion Solution

It is the simplicity of Mott's analysis which so vividly reveals the underlying physics. It is readily apparent that Mott's solution is intended to apply at the point at which hardening in the stretching rod saturates, and the tension versus strain loses its hyperbolic character. At this point of stationary tension, the governing equations become parabolic, and the diffusive nature implicit in the motion of the Mott wave is expected.

The diffusive character of the stress release process can in fact be readily demonstrated by writing the linear diffusion relation,

$$\frac{\partial^2 \sigma}{\partial h^2} - \frac{1}{\kappa} \frac{\partial \sigma}{\partial t} = 0 \,, \tag{3.11}$$

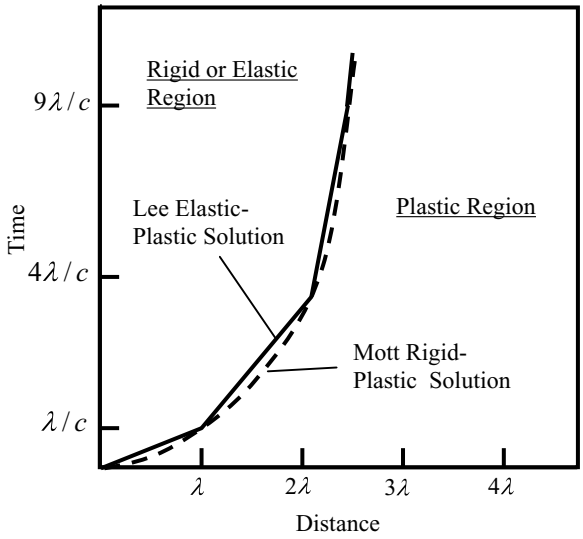

Fig. 3.3. Comparisons of interface $x(t)$ separating plastic region and rigid plastic region according to solutions of Mott (1947) and Lee (1967)

with the diffusion constant,

$$\kappa = Y/2\rho\dot{\varepsilon} \ . \tag{3.12}$$

Consider the same problem treated by Mott in which fracture at $t = 0$ and $h = 0$ instantly decreases the tensile stress from $\sigma = Y$ to $\sigma = 0$. This classic solution [e.g., Matthews and Walker, 1964] can be immediately written down for the stress,

$$\sigma/Y = erf\,(\xi) \ , \tag{3.13}$$

and the velocity,

$$\frac{u}{\dot{\varepsilon}\sqrt{4\kappa t}} = \sqrt{\frac{4}{\pi}}\exp\left(-\xi^2\right) + 2\xi erf\,(\xi) - \xi \ . \tag{3.14}$$

In (3.13) and (3.14) the similarity parameter,

$$\xi = h/\sqrt{4\kappa t} \ , \tag{3.15}$$

has been introduced. The present diffusion equation solution and the rigid-plastic solution of Mott are compared in Fig. 3.4.

The rigid-plastic solution of Mott, the elastic-plastic solution of Lee, and the solution to the diffusion equation are, of course, only models of the actual processes of fracture and stress unloading occurring in the rupture of a rapidly stretching ductile shell. Which model most accurately depicts reality probably cannot be answered. All, however, reveal physics of the fracture process and point to the decidedly diffusive nature of stress wave propagation.

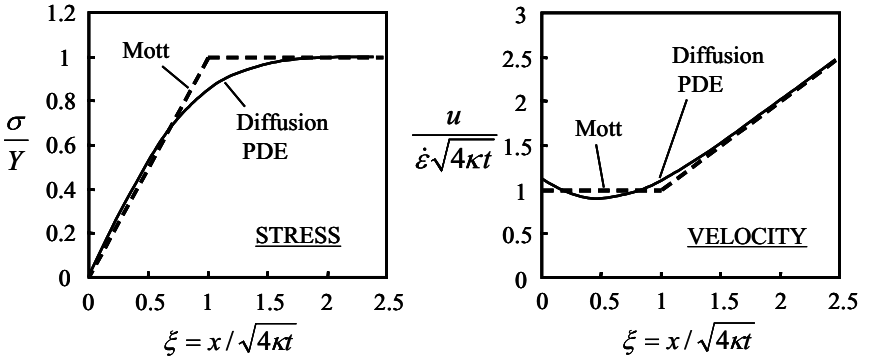

Fig. 3.4. Comparisons of solutions for Mott's rigid-plastic model and a linear stress-diffusion model of fracture in a stretching plastic rod

3.2.3 Fracture Energy Solution

One further extension of the fracture wave analysis developed by Mott is of interest. Mott was convinced at the time of development of the rigid-plastic fracture release wave solution that energy dissipated at the point of fracture was inconsequential and could be ignored. Hence, the assumption of instantaneous stress drop at the point and time of fracture was inherently sensible. The solution method is readily amenable to considerations of fracture when the fracture energy is not inconsequential, [Grady et al., 1984; Kipp and Grady, 1985].

From (3.4), which equates the rate of change of momentum of the circumferential strip of stretching case material $0 \leq h \leq h_o$, adjacent to a fracture initiated at $h = 0$ and at time $t = 0$, to the misbalance in tensile stress at opposite ends of that strip, obtain,

$$\rho\dot{\varepsilon}x\frac{dx}{dt} = \sigma\left(h_o\right) - \sigma\left(0\right). \tag{3.16}$$

The boundary condition in Mott's solution method sets $\sigma(0) = 0$ at $t = 0$ corresponding to instantaneous stress release at the moment of fracture. It is reasonable, however, to consider a model in which the tensile stress is reduced gradually over time from $\sigma(0) = Y$ to $\sigma(0) = 0$ as the crack opens. This model would replicate a fracture resisting crack opening and thus, dissipate energy in the crack-opening process. As illustrated in Fig. 3.5, a coordinate $y(t)$ identifies the crack-open displacement, while $x(t)$ determines the position of the rigid-plastic boundary. A fracture resistance is proposed in which the boundary tensile stress reduces linearly to zero at $y = y_c$. (Other possible models for the boundary resistance are considered in Chap. 4.) An energy of fracture is then given by $\Gamma = Yy_c/2$, the area under the stress-displacement curve. The concepts are quite analogous to crack-opening-displacement models of Dugdale (1960) and Barenblatt (1962) in the treatment of quasistatic fracture

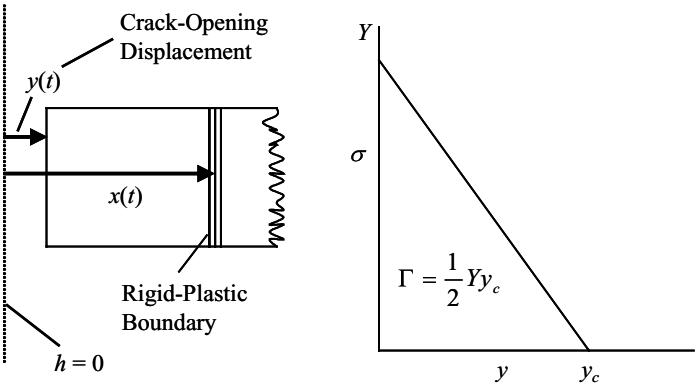

Fig. 3.5. The sketch on the left illustrates crack-opening displacement y due to motion of the rigid section of the strip. On the right the resisting tensile stress as a function of crack-opening displacement is shown which dissipates an energy Γ when displacement achieves a value y_c

resistance. Equation (3.16) then gives the momentum balance relation,

$$\rho\dot{\varepsilon}x\frac{dx}{dt} = \frac{Y^2}{2\Gamma}y \,, \tag{3.17}$$

while motion of the crack-opening displacement provides,

$$\frac{dy}{dt} = \dot{\varepsilon}x \,. \tag{3.18}$$

The coupled (3.17) and (3.18) are readily solved yielding,

$$x\,(t) = \frac{1}{12}\frac{Y^2}{\rho\Gamma}t^2 \,, \tag{3.19}$$

for motion of the rigid-plastic boundary during the crack-opening displacement $0 \le y \le y_c$. The solution for crack-opening displacement is in turn given by,

$$y\,(t) = \frac{1}{36}\frac{\dot{\varepsilon}Y^2}{\rho\Gamma}t^3 \,. \tag{3.20}$$

When y exceeds y_c (completion of fracture) the original solution of Mott applies.

Setting $y = y_c$ in (3.20) and using the expression for fracture energy, $\Gamma = Yy_c/2$, the time t_f at which fracture is complete can be calculated,

$$t_f = \left(\frac{72\rho\Gamma^2}{Y^3\dot{\varepsilon}}\right)^{1/3} \,. \tag{3.21}$$

Correspondingly, the distance x_f traveled by the rigid-plastic boundary during the time of fracture completion from (3.19) is,

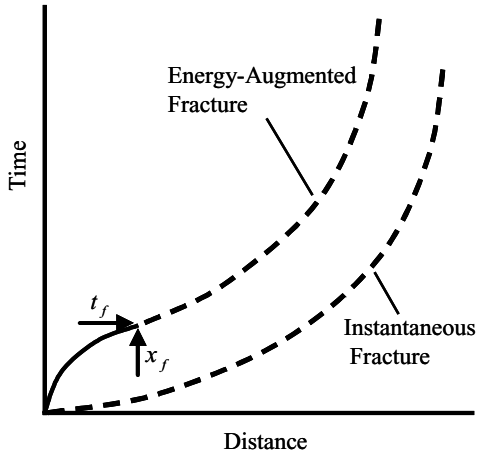

Fig. 3.6. Motion of the rigid-plastic boundary with a resisting fracture energy model is compared with original instantaneous-fracture solution of Mott

$$x_f = \left(\frac{3\Gamma}{\rho\dot{\varepsilon}^2}\right)^{1/3} . \tag{3.22}$$

The motion of the rigid-plastic boundary with the present resisting fracture energy model is compared with Mott's original instantaneous-fracture solution in Fig. 3.6. Equation (3.19) governs the motion until the fracture time t_f at a distance x_f is achieved. Subsequent motion is governed by the same free-boundary conditions as that of instantaneous fracture. The principal effect is to cause a delay in the boundary motion compared to the motion of instantaneous fracture.

It is apparent that if two fractures initiate within a time t_f and with spacing between them of less than $2x_f$ they will interfere with each other before the fracture growth process is complete. Such interactions have been studied and have shown under certain criteria that one or the other of the two fractures will arrest growth and not complete the fracture process [Kipp and Grady, 1985]. Out of this study a nominal fracture spacing of twice x_f or,

$$x_o = \left(\frac{24\Gamma}{\rho\dot{\varepsilon}^2}\right)^{1/3} , \tag{3.23}$$

has been proposed when conditions in the fracture process favor sufficient fracture initiation sites such that fracture interaction and competition processes governed by energy requirements determines the breakup intensity.

Thus, like Lee's elastic-plastic solution places a lower bound on the distance of interface propagation before Mott's rigid-plastic solution is adequate, the present analysis places a lower bound on fracture spacing governing Mott's instantaneous fracture assumption.

The above analysis, of course, opens further questions. What, for example, would be the effect on the calculated fracture properties if crack-opening resistance models other than linear softening were pursued? Also, to what extent are fracture properties sensitive to the scale of initial perturbations responsible for fracture onset? These extended issues detract, however, from the pursuit of Mott's fracture theory, but have been included in a section of the next chapter.

3.3 Statistical Fundamentals

Mott proposed that the occurrence of fracture in a stretching body is governed by a fracture frequency probability function $\lambda(\varepsilon)$ of the strain ε. The expression $\lambda(\varepsilon)d\varepsilon dl$ is the chance that a fracture will occur in a length dl at a strain ε within an interval $d\varepsilon$. Dimensionally it can be considered the random frequency of fracture per unit strain and length of the stretching body. It is useful for both later developments, and for the present conceptualization to consider an expanding ring composed of a large number N_o of equal length segments. Imagine further each of these segments stretching independently, but at the same rate. For the moment it is also convenient to consider segments of unit initial length. Then at a strain ε,

$$\frac{dN}{N} = -\lambda\left(\varepsilon\right) d\varepsilon \ , \tag{3.24}$$

is the fraction of the surviving segments N that fracture as the strain is increased from ε to $\varepsilon + d\varepsilon$. Equation (3.24) is integrated to provide the surviving number of segments as a function of strain,

$$N = N_o e^{-\int \lambda(\varepsilon) d\varepsilon} \ . \tag{3.25}$$

Equation (3.25) readily provides the cumulative probability distribution for fracture within a body of unity length at or before a strain ε is achieved,

$$F\left(\varepsilon\right) = 1 - e^{-\int \lambda(\varepsilon) d\varepsilon} \ . \tag{3.26}$$

The probability of a unit length surviving when strain ε is achieved is, of course,

$$1 - F\left(\varepsilon\right) = e^{-\int \lambda(\varepsilon) d\varepsilon} \ . \tag{3.27}$$

The complementary cumulative probability density function for a unit length surviving to strain ε and fracturing within the subsequent unit strain interval is,

$$f\left(\varepsilon\right) = \frac{dF\left(\varepsilon\right)}{d\varepsilon} = \lambda\left(\varepsilon\right) e^{-\int \lambda(\varepsilon) d\varepsilon} = \left(1 - F\right) \lambda\left(\varepsilon\right) \ . \tag{3.28}$$

In the statistical theory of reliability or life testing the function $\lambda(\varepsilon)$ is commonly known as the hazard function or the conditional failure (mortality)

function [Hahn and Shapiro, 1967] and is more generally identified as $h(\varepsilon)$ in later analysis. Typically time rather than strain is the random variable. However, in the present development time and strain are related through a constant strain rate $\varepsilon = \dot{\varepsilon}t$, and the two random variables are synonymous.

Mott (1943) proposed three functional forms for the fracture frequency function $\lambda(\varepsilon)$. They are

$$\lambda(\varepsilon) = \lambda_o, \quad \text{a constant} , \tag{3.29}$$

$$\lambda(\varepsilon) = \frac{n}{\sigma}\left(\frac{\varepsilon}{\sigma}\right)^{n-1}, \ (n \geq 1) , \tag{3.30}$$

$$\lambda(\varepsilon) = Ae^{\gamma\varepsilon} . \tag{3.31}$$

The first is, of course, a special case of the second power law representation for $n = 1$ leading to a constant or uniform fracture frequency. Mott suggested that the first two expressions could be zero up to some $\varepsilon = \varepsilon_o$ taking their functional representation thereafter. This is not of consequence. Much of Mott's attention attended to the later exponential representation for $\lambda(\varepsilon)$ in (3.31).

The three fracture frequency functions are illustrated in Fig. 3.7. Although, diversely different in this representation, it was shown by Mott that their consequences on fragment size and distribution were not dramatically different.

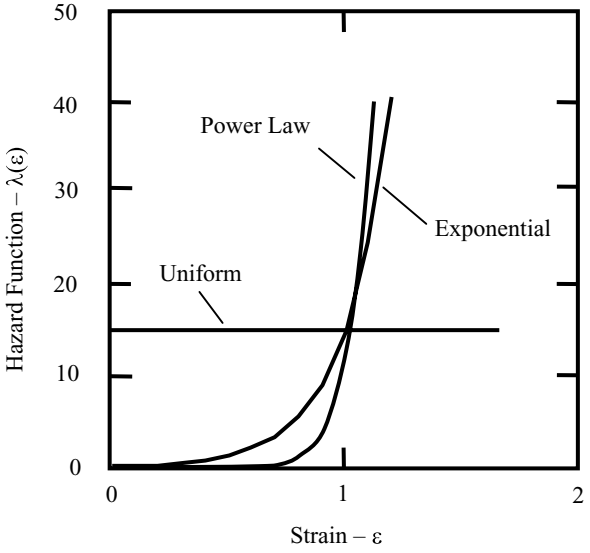

Fig. 3.7. The fracture frequency hazard functions for strain-to-fracture proposed by Mott are compared. The parameters are for the uniform function, $\lambda_o = 15$; the power-law function, $\sigma = 1, n = 12$: and the exponential function, $A = 0.1, \gamma = 5$

Their functional forms have been explored extensively in treatise on statistics [e.g., Hahn and Shapiro, 1967]. The first constant hazard function leads to the familiar exponential probability distribution used, for example, in radioactive decay. The second power-law hazard function leads to the Weibull distribution commonly used in the breaking strength of materials. This distribution reduces to the exponential distribution for $n = 1$ and the Rayleigh distribution for $n = 2$. The third hazard function is a form of asymptotic or extreme-value probability distribution and leads to the Gumbel extreme value distribution [Hahn and Shapiro, 1967].

We will principally pursue the consequences of a power law function and the resulting Weibull distribution for the statistical fragmentation of a one-dimensional stretching body. It has, in the intervening years, become the common statistical representation for strength of solids. Doremus (1983) has pointed out, however, that in spite of popularity of the Weibull distribution, the normal distribution, and the Gumbel distribution, can in some applications better characterize strength data in solids. He points out that Weibull selected the power law form for mathematical convenience and that there was no theoretical basis. There are important differences between the two distributions for the present fragmentation application, which will be pointed out after details of the distributions are discussed.

The Weibull probability density function for fracture within a unit circumferential length of the cylinder is,

$$f(\varepsilon) = \frac{n}{\sigma}\left(\frac{\varepsilon}{\sigma}\right)^{n-1} e^{-(\varepsilon/\sigma)^n} , \tag{3.32}$$

while the cumulative distribution function is,

$$F(\varepsilon) = 1 - e^{-(\varepsilon/\sigma)^n} . \tag{3.33}$$

Shape and scale parameters of the distributions are n and σ, respectively. Both probability-density and cumulative probability distribution functions are shown in Fig. 3.8. Curves illustrate the tendency for the fracture to center about a fixed strain to failure with increasing shape parameter n. The expected value for strain to failure is given by,

$$\sigma\, \Gamma\left(1 + \frac{1}{n}\right) , \tag{3.34}$$

where $\Gamma(\ )$ is the gamma function. The standard deviation about the mean is provided by,

$$\sigma\left[\Gamma\left(1+\frac{2}{n}\right) - \left(\Gamma\left(1+\frac{1}{n}\right)\right)^2\right]^{1/2} \cong 1.28\frac{\sigma}{n} . \tag{3.35}$$

The asymptotic limit as $n \to \infty$ for the standard deviation is shown in (3.35) and is a reasonable estimate over much of the range of n. The functional

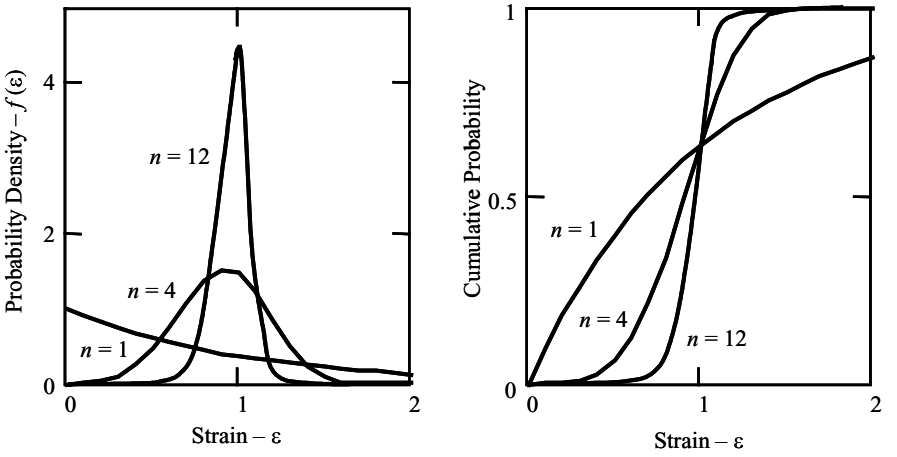

Fig. 3.8. Probability density and cumulative probability distributions for power-law fracture frequency function (Weibull distribution) with selected values of shape parameter n. The scale parameter is $\sigma = 1$

form of these statistical properties for the Weibull distribution is illustrated in Fig. 3.9.

For a body of arbitrary length l the hazard function $\lambda(\varepsilon)$ is replaced by $l\lambda(\varepsilon)$ in previous relations. It is readily shown that σ in (3.34) and (3.35) is

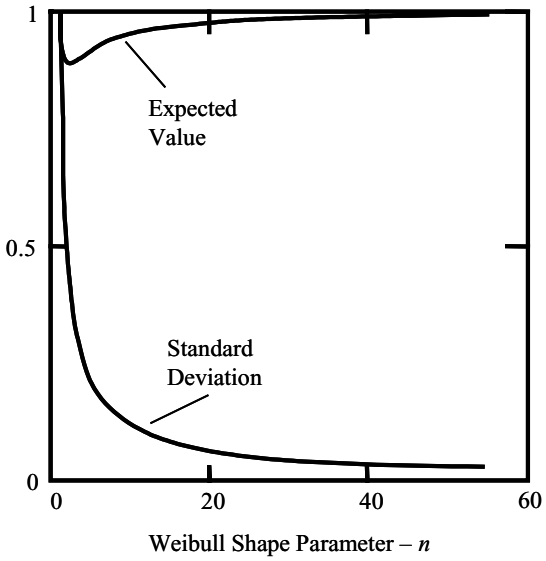

Fig. 3.9. Expected value and standard deviation for strain-to-fracture with increasing values of the Weibull shape parameter n. The scale parameter is $\sigma = 1$

then replaced by $\sigma/l^{1/n}$ illustrating the size dependence of fracture strength common to Weibull statistics.

With reasonably high values of n the power-law hazard function and Weibull distribution quite adequately describe the several percent scatter in failure strain observed in metal tensile specimens. This analytic distribution thus provides a reasonable statistical representation for describing the multiple fragmentation process in rapidly stretching bodies such as the expanding ring illustrated in Fig. 3.1.

In contrast, the strain-to-fracture exponential hazard function $\lambda(\varepsilon) = A\exp(\gamma\varepsilon)$ and the resulting fracture distribution function chosen by Mott for study is, like the power law hazard function and Weibull distribution function, a form of extreme value distribution. More specifically it is commonly known as the Gumbel extreme value distribution [Hahn and Shapiro, 1967]. Characteristics of the distribution are more transparent rewriting the hazard function in the form,

$$\lambda(\varepsilon) = \frac{1}{\sigma} e^{(\varepsilon-\mu)/\sigma} , \tag{3.36}$$

where the correspondence $\sigma = 1/\gamma$ and $(1/\sigma)\exp(-\mu/\sigma) = A$ is made with the relation of Mott. The probability density function for strain-to-fracture is then,

$$f(\varepsilon) = \frac{1}{\sigma}\exp\left(\frac{1}{\sigma}(\varepsilon-\mu) - e^{(1/\sigma)(\varepsilon-\mu)}\right) . \tag{3.37}$$

Both hazard function and probability density function for Gumbel distribution are illustrated in Fig. 3.10. The parameter μ is seen to be the distribution mode and location parameter, while the expected strain to fracture is,

$$\mu - n_e\sigma , \tag{3.38}$$

where $n_e = 0.577$ is the Euler number. The distribution standard deviation is,

$$1.283\sigma . \tag{3.39}$$

Thus, not unlike the Weibull distribution, as σ approaches zero the expected value approaches the mode μ and the distribution converges to a delta function.

It is important at this juncture to point out a very significant difference between the Gumbel extreme value distribution (selected by Mott for application to fragmentation statistics) and the Weibull distribution. Whereas the latter has both a distribution scale and shape parameter, the Gumbel distribution parameters determine only the scale and the location of the distribution but are lacking a shape parameter. This difference will be shown to have an important influence on the theoretically predicted dependence of fragment size on the strain rate. The Gumbel distribution will yield a unique inverse first power dependence on strain rate. Over physically reasonable values of the shape parameter n the Weibull distribution predicts a strain rate dependence

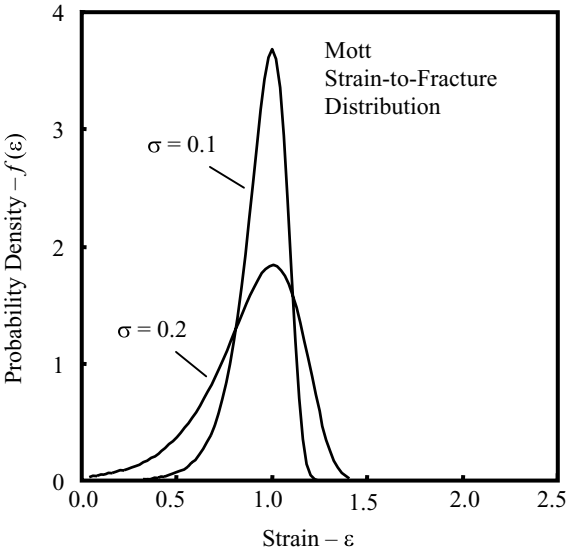

Fig. 3.10. Illustrates the Mott strain-to-failure distribution (Gumbel extreme value distribution) with distribution location parameter $\mu = 1$ and several values of the scale parameter σ

ranging between an inverse first power and an inverse two-thirds power. Mott commented on these differences but did not provide strong justification for selection of the Gumbel distribution.

3.4 The Mott Distribution

The physical and statistical principles just outlined were then used by Mott to determine a distribution in fragment lengths (or fracture spacing) resulting from the plastic fracture of the expanding Mott ring. It should be emphasized that this one-dimensional distribution bears no relationship to the earlier two-dimensional Mott distribution arrived at intuitively by Mott and Linfoot from Lineau's theoretical efforts.

Mott noted that he was not able to develop an analytic solution and proceeded with a graphical method which is described below. It seems likely that with a modest amount of additional time to reflect on his theory Mott would have developed an analytic solution, which was his nature. It is interesting that nearly concurrently other workers [Johnson and Mehl, 1939] were pursuing transformation reaction kinetics in metals and developed analytic tools ideally suited to Mott's statistical fragmentation theory. This sensible extension to the Mott development will also be described here.

The graphical solution to the statistical fragment size distribution derived by Mott proceeds as follows: A parameter D is defined, which is a function of

time t (or strain) such that $0 \leq D(t) \leq 1$. At any time $D(t)$ is the fraction of the stretching body (Fig. 3.1) which has been subsumed by the Mott release wavelets propagating from the points of fracture. Since further fractures are assumed to occur only in the fraction of the body not yet encompassed by these release wavelets $1 - D$, clearly the probable number of fractures which will appear in the time increment t to $t + dt$ is,

$$dN = (1 - D)\,\lambda(\dot{\varepsilon}t)\,\dot{\varepsilon}dt\ . \tag{3.40}$$

As previously pointed out, Mott chose to explore the fracture frequency relation $\lambda(\dot{\varepsilon}t) = A\exp(\gamma\dot{\varepsilon}t)$.

The release fraction $D(t)$ of the plastic stretching body considered by Mott is determined by the collective Mott waves emanating from fractures initiating prior to time t. Each Mott wave propagates according to,

$$x_i = \sqrt{2Y/\rho\dot{\varepsilon}}\,(t - t_i)^{1/2}\ , \tag{3.41}$$

where t_i is the initiation time of the ith fracture. Introducing a dimensionless time through,

$$\xi = \gamma\varepsilon = \gamma\dot{\varepsilon}t\ , \tag{3.42}$$

Equation (3.41) becomes,

$$x_i = \sqrt{2Y/\rho\dot{\varepsilon}^2\gamma}\,(\xi - \xi_i)^{1/2}\ , \tag{3.43}$$

where Mott recognizes the radical expression on the right of (3.43) as the normalizing length scale (proportional to the average fragment length) for the distribution in fragment lengths.

To determine the fragment distribution Mott worked with (3.40) and (3.43). A graphical solution was carried out whereby he introduced fractures at random at successive times determined by (3.40), and computed the collective release fraction of the body $D(t)$ with (3.43). Performing this task a number of times provided a credible histogram of the distribution in fragment lengths. The resulting distribution obtained by Mott as both a density distribution and a complementary cumulative distribution is shown in Fig. 3.11. The normalizing length, L_o is that identified in (3.43). From the graphical distribution Mott noted that the average fragment size was about 1.5 L_o. Again this distribution bears no relation to the Mott distribution inferred by Mott and Linfoot from Lineau's theoretical efforts, and that is commonly used to represent munitions fragmentation data.

This author is aware of only one effort to duplicate the statistical size distribution analysis performed by Mott. Wesenberg and Sagartz (1977) performed fragmentation experiments through magnetic inductive expansion of aluminum cylindrical shells (see Chap. 8). Using computer methods and an appropriate random number generator, they produced fragment size distributions by solving the same pair of equations as Mott (3.40) and (3.43). Distribution results were compared with their fragmentation data.

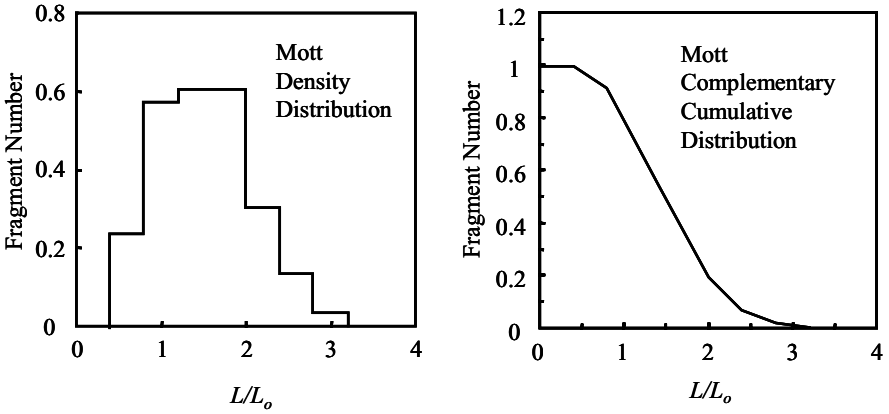

Fig. 3.11. The fractional number density distribution (*left*) and fractional complementary cumulative number distribution (*right*) determined by Mott (1947) for the fragmentation of a uniformly stretching plastic body. Normalizing length scale L_o is identified in the text

Wesenberg and Sagartz displayed their calculated distributions as the average of the individual results of 10 rings, 100 rings, and 1000 rings, respectively, and concluded that a reasonably large number of calculations was required to achieve sensible convergence. Their distribution resulting from the average of 1000 rings is shown in Fig. 3.12 and compared with the distribution of Mott.

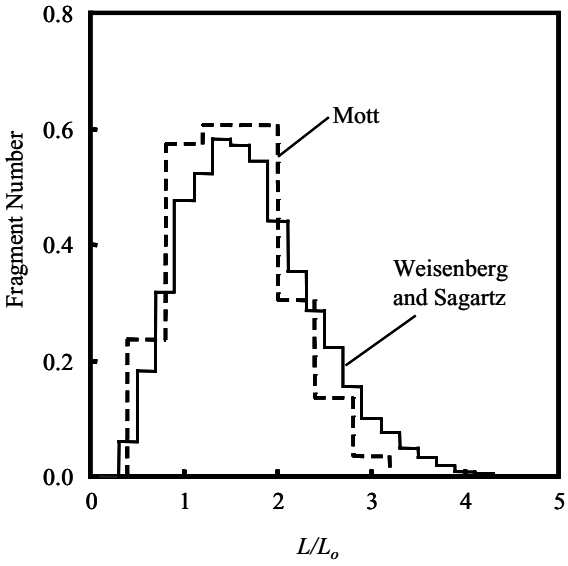

Fig. 3.12. Comparisons of fragment distributions calculated by Mott (1947) and by Weisenberg and Sagartz (1977)

3.5 Dynamic Fracture as a Statistical Transformation Process

In the present and subsequent subsections the essential ideas proposed by Mott on statistical fracture and fragmentation will be pursued further. The analytic statistical methods to be described will not necessarily provide improved predictive capabilities. They will, however, provide alternative points of view and provide analytic relations which are potentially amenable to generalization to more complex fragmentation problems. These methods also help to clarify scaling features in the predicted fragment sizes and distributions.

The processes of dynamic fracture and fragmentation involve spatially and temporally random nucleation and growth of fractures that have similarities to other nucleation and growth phenomena (melting, recrystallization, detonation reaction, etc.). In fracture, as in some of the other phenomena, nucleation and growth of a single fracture can be treated in substantial detail. It is the impingement or influence of one fracture, or region of growth, on others which compounds the complexity of the total nucleation and growth process.

To treat problems of nucleation and growth, Johnson and Mehl (1939) and Avrami (1939) introduced the concept of an extended volume fraction D_x. The factor D_x is defined as the volume fraction of the body transformed disregarding further transformation nucleation in previously transformed material (exclusion), and disregarding the overlap of growing transformation regions (impingement). The extended volume fraction will exceed unity.

The actual transformed volume fraction D of the body is determined from the ratio in the change of the extended and the actual transformed volume fraction, namely,

$$dD/dD_x = 1 - D \,, \tag{3.44}$$

which integrates to,

$$D = 1 - e^{-D_x} \,. \tag{3.45}$$

In the present context the quantities D_x and D will apply to the stress-relieved portion of the stretching ring (Fig. 3.1) during dynamic fracture. The Johnson–Mehl–Avrami (JMA) relation is applicable to two-dimensional bodies or areas, as well as to one-dimensional bodies or lines. Further discussion of the statistical relationship between D and D_x is addressed in Chap. 4.

Although the work of Johnson and Mehl (1939) and Avrami (1939) was focused on phase transformations in materials, their results have more general application. Their result (the JMA relation) is based on the statistics of survival, in this case, survival at any time of the, as yet, untransformed volume. The concept is independent of the physics involved and is applicable to any nucleation and growth process which is random in nature. The JMA relation allows initial attention to focus on the physics of the nucleation and growth process at a single site. Equation (3.45) will then account for the coalescence of multiple transforming regions.

Consequently, analogous to Mott's (3.40), an expression for the number of fractures per unit length which occur at a past time τ within interval $d\tau$, ignoring the stress-released regions, is

$$dN_x = \lambda(\eta)\, d\eta \,. \tag{3.46}$$

In (3.46) $\eta = \dot{\varepsilon}\tau$ is identified as a non-dimensional time or, equivalently, as the strain at past time τ. Release waves from fractures at past time τ (or η) will have propagated a distance,

$$x = g(\varepsilon - \eta) \;, \tag{3.47}$$

at the present time t (or $\varepsilon = \dot{\varepsilon}t$). The function, $g(\varepsilon)$ accounts for either elastic wave speed in elastic fracture or Mott's diffusive wave speed for plastic fracture provided previously in (3.1) and (3.2). Therefore, the increment in extended stress release region due to the earlier fracture is,

$$dD_x = 2g(\varepsilon - \eta)\, dN_x = 2g(\varepsilon - \eta)\, \lambda(\eta)\, d\eta \,, \tag{3.48}$$

where the factor of 2 accounts for right and left facing release waves from each fracture. Integrating over past time to the present yields,

$$D_x = 2\int_0^{\varepsilon} g(\varepsilon - \eta)\, \lambda(\eta)\, d\eta \,. \tag{3.49}$$

Equation (3.45) then provides,

$$D(\varepsilon) = 1 - e^{-D_x(\varepsilon)} \,, \tag{3.50}$$

the fractional stress-relieved region at any time in the dynamic fracture process.

3.6 Fragment Size in the Mott Fracture Process

Perhaps most basic to a dynamic fragmentation event is the characteristic size of the fragments produced. An experiment, such as the rapidly expanding ring shown in Fig. 3.1, results in a number of fragments that can be counted. This number can be divided by the circumferential length of the ring to determine an average fragment length. Additional testing reveals that the number of fractures produced is dependent on both the mechanical properties of the test material as well as the dynamic conditions achieved. This dependence is readily illustrated in Fig. 3.13 in which fragment numbers from similar tests on rapidly expanding aluminum and copper rings are plotted against the radial expansion velocity imparted to the ring at fracture [Grady and Benson, 1983].

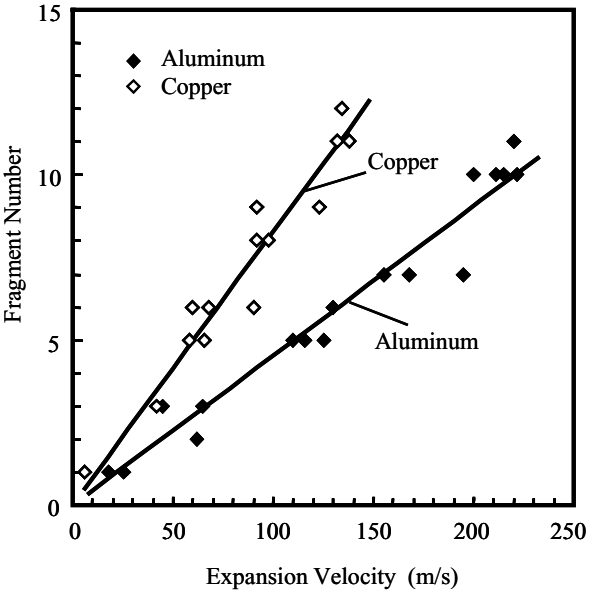

Fig. 3.13. Representative tests showing fragment number versus expansion velocity for fragmenting aluminum and copper ring experiments [Grady and Benson, 1983]

3.6.1 Analysis of Elastic Fracture

In pursuing further the extended statistical approach initiated in the previous section in treating the dynamic fracture model posed by Mott, the power-law fracture frequency function (which results in Weibull extreme value statistics) will be used. Consider first, elastic fracture in which fracture release waves travel at a constant elastic wave velocity. Salient features of the analysis are readily illustrated by the elastic fracture case, while the mathematics are modestly simpler. Accordingly, the power-law fracture frequency from (3.30) and the elastic wave speed (3.2) yield through (3.49),

$$D_x = 2\frac{c}{\dot{\varepsilon}}\frac{n}{\sigma^n}\int_0^{\varepsilon}(\varepsilon-\eta)\,\eta^{n-1}d\eta\,, \tag{3.51}$$

where the elastic wave speed $c=\sqrt{E/\rho}$ has been introduced. The substitution $y=\eta/\varepsilon$ yields,

$$D_x = 2\frac{c}{\dot{\varepsilon}}\frac{n}{\sigma^n}\varepsilon^{n+1}\int_0^{1}(1-y)\,y^{n-1}dy\,, \tag{3.52}$$

where the integral has the solution in terms of the gamma function,

$$\frac{\Gamma(n)\,\Gamma(2)}{\Gamma(n+2)} = \frac{1}{n(n+1)}\,. \tag{3.53}$$

Consequently,

$$D_x = \frac{2c}{(n+1)\,\dot{\varepsilon}\sigma^n}\varepsilon^{n+1}\ , \tag{3.54}$$

and, through (3.50),

$$D = 1 - e^{-\frac{2c}{(n+1)\dot{\varepsilon}\sigma^n}\varepsilon^{n+1}}\ . \tag{3.55}$$

Fracture activation within the unrelieved portion of the stretching body is then calculated through,

$$dN = (1-D)\,\lambda\,(\varepsilon)\,d\varepsilon\ . \tag{3.56}$$

Substituting the appropriate relations, the number of fractures per unit length occurring in the fragmentation process is obtained from the integral over all time,

$$N = \frac{n}{\sigma^n}\int_0^\infty \varepsilon^{n-1}e^{-(a\varepsilon)^{n+1}}d\varepsilon\ , \tag{3.57}$$

where the notation has been simplified through,

$$a^{n+1} = \frac{2c}{(n+1)\,\dot{\varepsilon}\sigma^n}\ . \tag{3.58}$$

Substitute $y = (a\varepsilon)^{n+1}$ in (3.57) yields,

$$N = \frac{1}{(a\sigma)^n}\frac{n}{n+1}\int_0^\infty y^{\frac{n}{n+1}-1}e^{-y}dy\ , \tag{3.59}$$

where the integral is the complete gamma function $\Gamma(n/(n\,+\,1))$. In the original notation, the fracture number per unit length is arrived at,

$$N = \left(\frac{n}{n+1}\right)^{\frac{1}{n+1}}\Gamma\left(\frac{n}{n+1}\right)\left(\frac{\dot{\varepsilon}n}{2c\sigma}\right)^{\frac{n}{n+1}}\ . \tag{3.60}$$

For the special case of $n = 1$,

$$N = \frac{1}{2}\sqrt{\frac{\pi\dot{\varepsilon}}{c\sigma}}\ , \tag{3.61}$$

while for large n approximately,

$$N = \frac{\dot{\varepsilon}n}{2c\sigma}\ . \tag{3.62}$$

3.6.2 Analysis of Plastic Fracture

A solution for the plastic fracture problem considered by Mott follows similar analysis. Using instead the relation for the diffusive propagation of Mott waves (3.1) the expression for the extended fracture release region corresponding to (3.51) becomes,

$$D_x = 2\sqrt{\frac{2Y}{\rho\dot{\varepsilon}^2}}\frac{n}{\sigma^n}\int_0^{\varepsilon}(\varepsilon-\eta)^{1/2}\eta^{n-1}d\eta\ , \tag{3.63}$$

or with $y = \eta/\varepsilon$,

$$D_x = 2\sqrt{\frac{2Y}{\rho\dot{\varepsilon}^2}}\frac{n}{\sigma^n}\varepsilon^{n+1/2}\int_0^{1}(1-y)^{1/2}y^{n-1}dy\ . \tag{3.64}$$

Solving for the integral,

$$\frac{\sqrt{\pi}}{2n+1}\frac{\Gamma(n)}{\Gamma(n+1/2)}\ , \tag{3.65}$$

yields,

$$D_x = \sqrt{\pi}\frac{n}{n+1/2}\frac{\Gamma(n)}{\Gamma(n+1/2)}\sqrt{\frac{2Y}{\rho\dot{\varepsilon}^2}}\frac{\varepsilon^{n+1/2}}{\sigma^n}\ . \tag{3.66}$$

The total number of fractures is calculated similarly through the simplification,

$$D_x = (a\varepsilon)^{n+1/2}\ , \tag{3.67}$$

leading to the integral expression for the fragment number,

$$N = \frac{1}{(a\sigma)^n}\frac{n}{n+1/2}\int_0^{\infty} y^{\frac{n}{n+1/2}-1}e^{-y}dy\ , \tag{3.68}$$

and yielding,

$$N = \frac{1}{(a\sigma)^n}\frac{n}{n+1/2}\Gamma\left(\frac{n}{n+1/2}\right)\ . \tag{3.69}$$

The fragment number per unit length in the original notation for plastic fracture in the Mott model becomes,

$$N = \beta_n\left(\frac{\rho\dot{\varepsilon}^2}{2\pi Y}\frac{n}{\sigma}\right)^{\frac{n}{2n+1}}\ , \tag{3.70}$$

where,

$$\beta_n = \left(\frac{2n}{2n+1}\right)^{\frac{1}{2n+1}}\left(\frac{1}{\sqrt{n}}\frac{\Gamma(n+1/2)}{\Gamma(n)}\right)^{\frac{2n}{2n+1}}\Gamma\left(\frac{2n}{2n+1}\right)\ . \tag{3.71}$$

Again the special cases yield for $n = 1$,

$$N = \Gamma\left(\frac{2}{3}\right)\left(\frac{\rho\dot{\varepsilon}^2}{12Y\sigma}\right)^{1/3} , \tag{3.72}$$

while for large n approximately,

$$N = \sqrt{\frac{\rho\dot{\varepsilon}^2}{2\pi Y}\frac{n}{\sigma}} . \tag{3.73}$$

Comparing standard deviation for the power-law fracture frequency ($\simeq 1.28\sigma/n$) with that for extreme-value function explored by Mott ($\simeq 1.28/\gamma$) we find from (3.73) that an average fragment length of $1/N$ gives,

$$\sqrt{\pi}\sqrt{\frac{2Y}{\rho\dot{\varepsilon}^2}\frac{\sigma}{n}} = \sqrt{\pi}L_o , \tag{3.74}$$

where L_o is the same distribution length scale determined by Mott ((3.43) and Fig. 3.11). Mott determined graphically that an average fragment length was approximately 1.5 L_o, close indeed to the analytic result in (3.74).

3.6.3 Analysis with the Mott Fracture Hazard Function

The same analysis can be carried through with the strain-to-fracture activation function assumed by Mott, namely, the Gumbel extreme value distribution provided by (3.37) and displayed in Fig. 3.10. Using the release propagation function,

$$g(\varepsilon - \eta) = \sqrt{\frac{2Y}{\rho\dot{\varepsilon}^2}}(\varepsilon - \eta)^{1/2} , \tag{3.75}$$

and the activation function,

$$\lambda(\eta) = \frac{1}{\sigma}e^{(\eta-\mu)/\sigma} , \tag{3.76}$$

the extended fracture release region corresponding to (3.63) becomes,

$$D_x = \frac{2}{\sigma}\sqrt{\frac{2Y}{\rho\dot{\varepsilon}^2}}\int_0^{\varepsilon}(\varepsilon - \eta)^{1/2}e^{(\eta-\mu)/\sigma}d\eta . \tag{3.77}$$

The Gumbel distribution has the awkward feature of providing finite values for negative ε. For realistic values of σ and μ, however, this contribution is vanishing small and the integral in (3.77) over the interval $[-\infty, \varepsilon]$ can be assumed providing, after the substitution $y = \varepsilon - \eta$,

$$D_x = \frac{2}{\sigma}\sqrt{\frac{2Y}{\rho\dot{\varepsilon}^2}}e^{(\varepsilon-\mu)/\sigma}\int_0^\infty y^{1/2}e^{-y/\sigma}dy\ , \tag{3.78}$$

or,

$$D_x = 2\Gamma\left(2/3\right)\sqrt{\frac{2Y\sigma}{\rho\dot{\varepsilon}^2}}e^{(\varepsilon-\mu)/\sigma}\ . \tag{3.79}$$

Using the relation between D and D_x from (3.45) and,

$$N = \int_0^\infty (1-D)\lambda\left(\varepsilon\right)d\varepsilon\ ,$$

results in,

$$N = \frac{1}{\sigma}\int_0^\infty e^{(\varepsilon-\mu)/\sigma}e^{-be^{(\varepsilon-\mu)/\sigma}}d\varepsilon\ , \tag{3.80}$$

where b is the pre-exponential term in (3.79). The substitution $y = \exp(\varepsilon-\eta)/\sigma$, and recognizing that the lower limit is approximately zero for $\mu/\sigma \gg 1$, yields,

$$N = \frac{1}{\sqrt{\pi}}\sqrt{\frac{\rho\dot{\varepsilon}^2}{2Y\sigma}}\ . \tag{3.81}$$

Accounting for the differing definitions of σ in the power-law and exponential hazard functions, (3.81) and (3.73) are identical. Recall that Mott used $\gamma = 1/\sigma$ in his application of the Gumbel distribution.

Again, it is emphasized that the lack of a shape parameter in the Gumbel extreme value distribution leads to a unique first power dependence of fragment number on strain rate (3.81). In contrast, strain rate dependence based on the Weibull extreme value statistics depends on the distribution shape parameter n (3.70).

3.7 Size Distribution in the Mott Fracture Process

The statistical analysis developed in the last several sections can be further pursued to provide analytic solutions for the distributions in fragment size. These analytic distribution solutions correspond to the graphic distribution determined in the original analysis of Mott shown in Fig. 3.11. The solution method is somewhat more detailed in that it is necessary to assess statistically when fracture release waves initiate and when they arrest, thus determining the unbroken distance spanned by the wave. The process is illustrated in Fig. 3.14 in which release waves originating from two separate fractures propagate distances l_1 and l_2, respectively, before colliding and arresting. The

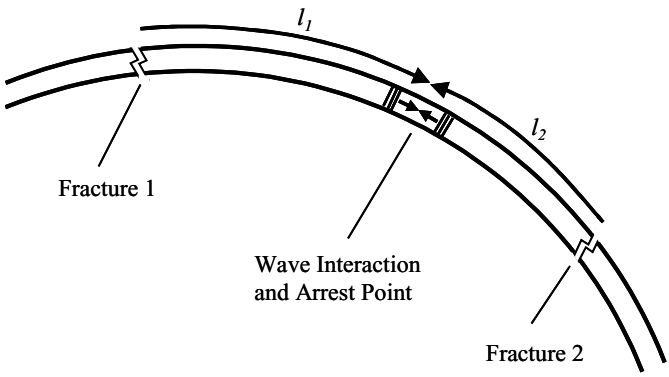

Fig. 3.14. Release waves originating from fracture 1 and fracture 2 travel distances l_1 and l_2, respectively, before arresting. The distance $l_1 + l_2$ constitutes the length of one fragment

distance, $l_1 + l_2$ constitutes the length of one fragment. The statistical fragment size distribution is then the probability function for the expectation of fragments of this specified length.

The solution is carried out for both elastic and plastic (Mott) fracture in the present subsection. The solution method is also presented in general terms in a later chapter, providing a clearer display of the solution methodology.

3.7.1 Analysis of Elastic Fracture

The solution will again be pursued first for that of elastic fracture in which fracture release waves travel at the constant speed $c = \sqrt{E/\rho}$. Also a power-law fracture frequency expression continues to be assumed. The analysis will start with the solution for the extended length fraction of stress relieved region from (3.54),

$$D_x = \frac{2c}{(n+1)\,\dot{\varepsilon}\sigma^n}\varepsilon^{n+1} = (a\varepsilon)^{n+1} \quad , \tag{3.82}$$

where,

$$D = 1 - e^{-D_x} = 1 - e^{-(a\varepsilon)^{n+1}} \quad . \tag{3.83}$$

Calculate first the number of activated release waves N_x without regard for exclusion (activation within previous stress relieved region) or impingement (collision and arrest of opposing release waves). The symbols N_x and N refer here to the number of Mott waves and not the number of fractures as in previous sections. The rate of activation of release waves I_x is,

$$I_x = 2\lambda\,(\varepsilon) = 2\frac{n}{\sigma}\left(\frac{\varepsilon}{\sigma}\right)^{n-1} \quad , \tag{3.84}$$

where the factor of 2 accounts for both a right and left facing wave emanating from each fracture point. N_x is then simply,

$$N_x = \int_0^{\varepsilon} I_x d\varepsilon = 2\left(\frac{\varepsilon}{\sigma}\right)^n . \tag{3.85}$$

But at any time (or strain) a fraction D of the length of the body has been stress relieved. The actual number of active release waves is,

$$N = N_x\,(1-D) = 2\left(\frac{\varepsilon}{\sigma}\right)^n e^{-(a\varepsilon)^{n+1}} , \tag{3.86}$$

accounting for both exclusion and impingement.

The rate of change of N is then,

$$\frac{dN}{d\varepsilon} = \frac{2n}{\sigma^n}\varepsilon^{n-1}e^{-(a\varepsilon)^{n+1}} - \frac{2\,(n+1)\,a^{n+1}}{\sigma^n}\varepsilon^{2n}e^{-(a\varepsilon)^{n+1}} . \tag{3.87}$$

From (3.87) we identify the rate of activation of release waves,

$$I^+ = \frac{2n}{\sigma^n}\varepsilon^{n-1}e^{-(ae)^{n+1}} , \tag{3.88}$$

and the rate of arrest of release waves,

$$I^- = -\frac{2\,(n+1)\,a^{n+1}}{\sigma^n}\varepsilon^{2n}e^{-(a\varepsilon)^{n+1}} . \tag{3.89}$$

The activation rate I^+ can also be calculated from the extended activation rate I_x by accounting for exclusion,

$$I^+ = I_x\,(1-D) = \frac{2n}{\sigma^n}\varepsilon^{n-1}e^{-(a\varepsilon)^{n+1}} . \tag{3.90}$$

Also, note that the arrest rate may be written,

$$I^- = -\,(n+1)\,a^{n+1}\varepsilon^n N . \tag{3.91}$$

With the above relations, we will now proceed to calculate the number of waves which activated at an earlier time η and arrested at a later time ε. The unbroken distance l spanned by these waves will all be the same (Fig. 3.14).

Accordingly, the number δN of release waves activated at time η within increment $\delta\eta$ is, from (3.88),

$$\delta N = \frac{2n}{\sigma^n}\eta^{n-1}e^{-(a\eta)^{n+1}}\delta\eta . \tag{3.92}$$

The fraction of δN arrested at later time ε is, from (3.91),

$$d\,(\delta N) = -\,(n+1)\,a^{n+1}\varepsilon^n\,(\delta N)\,d\varepsilon . \tag{3.93}$$

Equation (3.93) can be separated and integrated to obtain,

$$\delta N = Ae^{-(a\varepsilon)^{n+1}} \ , \tag{3.94}$$

where A is a constant of integration. Setting ε equal to the early time η in (3.94) the constant of integration is seen from (3.92) to be,

$$A = \frac{2n}{\sigma^n}\eta^{n-1}\delta\eta \ , \tag{3.95}$$

and consequently, (3.94) becomes,

$$\delta N = \frac{2n}{\sigma^n}\eta^{n-1}e^{-(a\varepsilon)^{n+1}}\delta\eta \ . \tag{3.96}$$

Substituting the results of (3.96) into the right side of (3.93) yields,

$$d\left(\delta N\right) = -\frac{2n\left(n+1\right)a^{n+1}}{\sigma^n}\varepsilon^n\eta^{n-1}e^{-(a\varepsilon)^{n+1}}\delta\eta d\varepsilon \ . \tag{3.97}$$

We now make the variable change,

$$x = \frac{c}{\dot{\varepsilon}}\left(\varepsilon - \eta\right) \ , \tag{3.98}$$

where x is the distance traveled by the release wave over the time interval $\varepsilon - \eta$.

At the same time switching the incremental order on the left hand side (3.97) results in,

$$\delta\left(dN\right) = -\frac{2n\left(n+1\right)a^{n+1}}{\sigma^n}\frac{\dot{\varepsilon}}{c}dx\left(\eta + \frac{\dot{\varepsilon}}{c}x\right)^n \eta^{n-1}e^{-a^{n+1}\left(\eta+\frac{\dot{\varepsilon}}{c}x\right)^{n+1}}\delta\eta \ . \tag{3.99}$$

Integrating over all past time η provides,

$$dN = -\frac{2n\left(n+1\right)a^{n+1}}{\sigma^n}\frac{\dot{\varepsilon}}{c}dx\int_0^\infty\left(\eta + \frac{\dot{\varepsilon}}{c}x\right)^n \eta^{n-1}e^{-a^{n+1}\left(\eta+\frac{\dot{\varepsilon}}{c}x\right)^{n+1}}\delta\eta \ . \tag{3.100}$$

Substituting y for the exponential exponent simplifies the integral to,

$$\frac{dN}{dx} = -\frac{2n}{\sigma^n}\frac{\dot{\varepsilon}}{c}\left(\frac{\dot{\varepsilon}x}{c}\right)^{n-1}\int_b^\infty\left[\left(y/b\right)^{1/(n+1)} - 1\right]^{n-1}e^{-y}dy \ , \tag{3.101}$$

where,

$$b = \frac{2}{n+1}\left(\frac{\dot{\varepsilon}}{c\sigma}\right)^n x^{n+1} \ . \tag{3.102}$$

Equation (3.101), when normalized, provides the probability distribution in lengths of unbroken release wave segments, such as l_1 and l_2 in Fig. 3.14. It does not, however, provide the distribution in fragment length as release wave

segments combined in pairs to constitute fragments (i.e., l_1 and l_2 in Fig. 3.14 combine to make a fragment of length, $l = l_1 + l_2$).

Thus, the distribution in fragment lengths is,

$$f(l)\,dl = \int\limits_{l=l_1+l_2} p(l_1)\,p(l_2)\,dl_i dl_2 \;, \tag{3.103}$$

where $p(l_i)$ is the normalized distribution in release wave segments and the integral is over all release wave segment length l_1 and l_2 which sum to l.

Equation (3.101) is not analytically tractable for arbitrary values of n. It is readily solved for $n = 1$, however, and this solution is provided here. Recall that $n = 1$ corresponds to a statistically uniform rate of fracture activation following onset of the first fracture. For $n = 1$ (3.101) reduces to,

$$\frac{dN}{dx} = -\frac{2}{\sigma}\frac{\dot{\varepsilon}}{c}\int\limits_{b}^{\infty} e^{-y}dy \;, \tag{3.104}$$

or,

$$\frac{dN}{dx} = \frac{2\dot{\varepsilon}}{\sigma c}e^{-\frac{\dot{\varepsilon}}{\sigma c}x^2} \;. \tag{3.105}$$

Integrating (3.105) provides the normalizing factor and the probability distribution in release wave segments,

$$p(x) = 2\sqrt{\frac{\dot{\varepsilon}}{\pi\sigma c}}e^{-\frac{\dot{\varepsilon}}{\sigma c}x^2} \;. \tag{3.106}$$

or, after introducing a length scale,

$$l_o = \sqrt{\frac{2\sigma c}{\dot{\varepsilon}}} \;, \tag{3.107}$$

Equation (3.103) provides the integral,

$$f(l)\,dl = \frac{8}{\pi l_o^2}\int\limits_{l=l_1+l_2} e^{-2\left(l_1^2+l_2^2\right)/l_o^2}dl_1 dl_2 \;. \tag{3.108}$$

The integral is completed through,

$$l = l_1 + l_2,\; \xi = l_1 - l_2,$$

$$dl_1 dl_2 = \left[\partial(l_1, l_2)/\partial(l, \xi)\right] dl d\xi \;,$$

yielding,

$$f(l) = \frac{4}{\pi l_o^2}e^{-(l/l_o)^2}\int\limits_{-l}^{l} e^{-(\xi/l_o)^2}d\xi \;, \tag{3.109}$$

and finally,

$$f(l) = \frac{4}{\sqrt{\pi}} \frac{1}{l_o} e^{-(l/l_o)^2} \operatorname{erf}(l/l_o) \ , \tag{3.110}$$

where erf( ) is the error function. The cumulative distribution is provided by,

$$F(l) = \int_0^l f(l)\, dl \ , \tag{3.111}$$

while the expected value of l is,

$$\langle l \rangle = \int_0^\infty l f(l) dl = \sqrt{\frac{2}{\pi}} l_o \ , \tag{3.112}$$

identically equal to $\langle l \rangle = 1/N$ for the predicted fragment number per unit length from (3.61). Both the probability density and complementary cumulative distributions for fragment length based on elastic fracture are shown in Fig. 3.15.

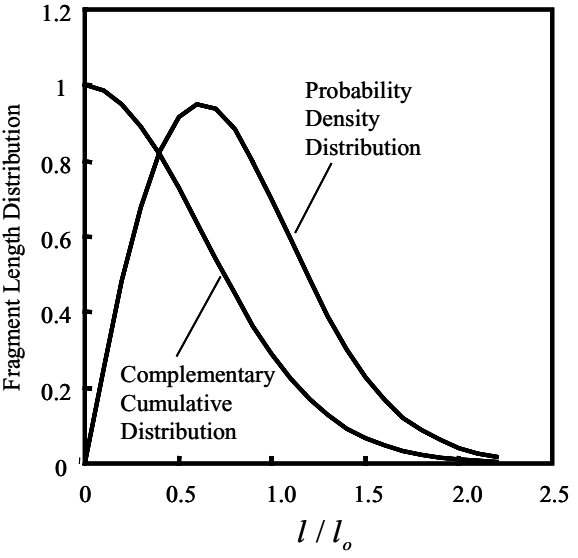

Fig. 3.15. Calculated probability density and complementary cumulative distributions in fragment lengths based on the Mott theoretical model for elastic fracture

3.7.2 Analysis of Plastic Fracture

The similar solution for the plastic fracture process pursued by Mott follows identical steps. A plastic wave speed, $c = \sqrt{2Y/\rho}$, introduced into the

relation for the diffusive propagation of Mott waves yields (3.66) for the extended length fraction of stress-relieved region. Assuming as before, a power-law relation for the rate of fracture activation, the probability distribution in lengths of unbroken release wave segments corresponding to (3.101) is,

$$\frac{1}{x}\frac{dN}{dx} = -\frac{4n}{\sigma^n}\left(\frac{\dot{\varepsilon}}{c}\right)^2\left(\frac{\dot{\varepsilon}x}{c}\right)^{2(n-1)}\int_b^\infty\left[(y/b)^{2/(2n+1)}-1\right]^{n-1}e^{-y}dy\ , \quad (3.113)$$

where,

$$b = \frac{2\sqrt{\pi}n}{2n+1}\frac{\Gamma(n)}{\Gamma(n+1/2)}\left(\frac{\dot{\varepsilon}}{c}\right)^{2n}\frac{x^{2n+1}}{\sigma^n}\ . \quad (3.114)$$

As before, the analytic solution cannot be pursued further for arbitrary values of n. For the special case of $n = 1$ (3.113) reduces to,

$$\frac{1}{x}\frac{dN}{dx} = -\frac{4}{\sigma}\left(\frac{\dot{\varepsilon}}{c}\right)^2\int_b^\infty e^{-y}dy\ , \quad (3.115)$$

with,

$$b = \frac{4}{3}\sigma\left(\frac{\dot{\varepsilon}}{c}\right)^2 x^3\ , \quad (3.116)$$

yielding,

$$\frac{dN}{dx} = \frac{4}{\sigma}\left(\frac{\dot{\varepsilon}}{c}\right)^2 xe^{-\frac{4}{3}\frac{1}{\sigma}\left(\frac{\dot{\varepsilon}}{c}\right)^2 x^3}\ . \quad (3.117)$$

Introducing the length scale,

$$l_o = \left(\frac{3\sigma}{4}\left(\frac{c}{\dot{\varepsilon}}\right)^2\right)^{1/3}\ , \quad (3.118)$$

and normalizing, (3.117) leads to,

$$p(x) = \beta\frac{x}{l_o^2}e^{-(x/l_o)^3}dx\ , \quad (3.119)$$

for the probability density distribution of segment lengths corresponding to (3.106) for elastic fracture and where $\beta = 3/\Gamma(2/3)$.

Combining segment lengths in pairs as discussed in the paragraphs leading to (3.103) provides the fragment size distribution for plastic fracture,

$$f(l) = \frac{\beta^2}{4}\frac{1}{l_o}\left(\frac{l}{l_o}\right)^3 e^{-\frac{1}{4}(l/l_o)^3}\int_0^1\left(1-y^2\right)e^{-\frac{3}{4}(l/l_o)^3y^2}dy\ . \quad (3.120)$$

The integral in (3.120) can be manipulated into an error function expression if desired, although, it is readily computed with most available math software.

The expected fragment size is calculated from the integral,

$$\langle s \rangle = \int_0^\infty l f(l)\, dl \ . \tag{3.121}$$

Performed numerically the integral yields $\langle s \rangle \simeq 1.48 l_o$ with l_o provided from (3.118). This calculation agrees, as it should, with the previous calculation for the total fragment number per unit length in (3.72).

It is also of interest to compare the present analytic distribution with that generated graphically by Mott (1947). Comparisons for both probability density and complementary cumulative probability distributions are shown in Fig. 3.16. Recall, however, that the assumed laws governing the statistical fracture frequency differ markedly in the two calculations. Mott assumed an exponentially escalating rate of fracture activation (3.31). A power law fracture frequency (3.30) was assumed in the analytic derivation which, for the sake of analytic tractability, was reduced to a uniform rate of fracture activation (3.29) corresponding to $n = 1$ in the power law expression. Influence of the differing fracture frequency laws on the statistical distribution in fragment lengths is not known.

Mott's graphical distribution and the present analytic distribution agree quite well as the comparison in Fig. 3.16 shows. Modest differences are perhaps best revealed in the comparison of the complementary cumulative distributions. The present distribution for plastic fracture differs from that of elastic fracture as comparison with the plot in Fig. 3.17 reveals. The comparisons indicate that the law governing the propagation of release waves from the point of fracture (diffusive Mott waves versus elastic waves) is the first order effect in governing the distribution shape. The fracture frequency law, on the other hand, appears to have a smaller influence on the shape of the distribution.

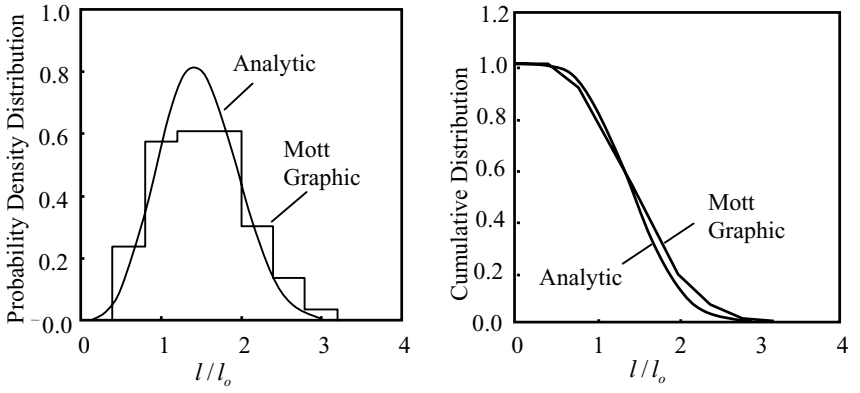

Fig. 3.16. Comparison of the present analytic distribution in fragment lengths for plastic fracture with the graphical distribution of Mott

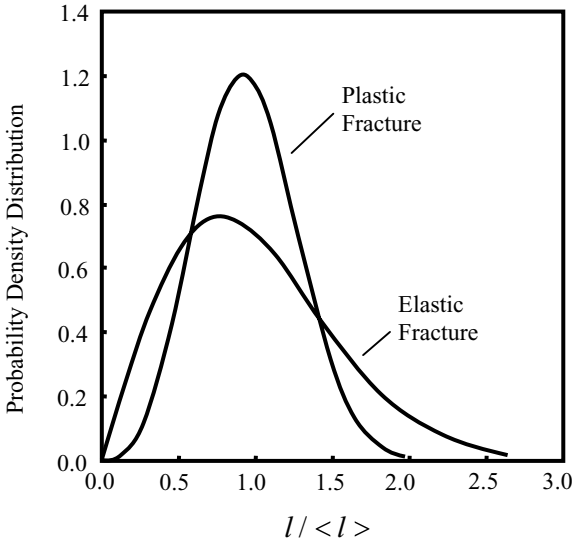

Fig. 3.17. Analytic length distributions for models of elastic and plastic fracture based on Mott statistical fragmentation

The normalizing length scale l_o for the two distributions in Fig. 3.16 are,

$$l_o = \sqrt{2Y/\rho\dot{\varepsilon}^2\gamma}\,,$$

from the Mott (1947) analysis and,

$$l_o = \left[(3\sigma/4)\left(2Y/\rho\dot{\varepsilon}^2\right)\right]^{1/3}\,,$$

from the analytic solution. The separate derivations are based on markedly different assumed fracture frequency laws. That the two distributions successfully overlay without adjustment of the independent length scales seems remarkable.

References

Avrami, M. (1939) *J. Chem. Phys.*, 7, 1103.

Barenblatt (1962), *Adv. Appl. Mech.* 7, 55.

Doremus, R. H. (1983), Fracture Statistics: A Comparison of the Normal, Weibull and Type I Extreme Value Distributions, *J. Appl. Phys.*, 54, 193–198.

Dugdale (1960), *J. Mech. Phys. Solids*, 8, 100.

Grady, D. E. and Benson, D. A. (1983), Fragmentation of Metal Rings by Electromagnetic Loading, *Experimental Mechanics* 23 (4), 393–400.

Grady, D. E., Kipp, M. E. and Benson, D. A. (1984), Energy and Statistical Effects in the Dynamic Fragmentation of Metal Rings, *Proceedings of the Conference of the Mechanical Properties of High Rates of Strain*, Oxford, 1984, Inst. Phys. Conf. Ser. No. 70, 315–320.

Hahn, G. J. and Shapiro, S. S. (1967), *Statistical Models in Engineering*, John Wiley & Sons, New York.

Johnson, W. A. and Mehl, R. F. (1939), Reaction Kinetics in Processes of Nucleation and Growth, *Trans. AIMME*, 135, 414–458.

Kipp, M. E. and Grady, D. E. (1985), Dynamic Fracture Growth and Interaction in One Dimension, *J. Mech. Phys. Solids* 33 (4), 399–415.

Lee, E. H. (1967), The Continuum Mechanics Aspect of Material Properties Determination, *Energetics III*, W. Mueller and M. Shaw, eds., pp. 85–122, Gordon and Breach, New York.

Matthews, J. and Walker, R. L. (1964), *Mathematical Methods of Physics*, W. A. Benjamin, Inc., New York, pp. 228–234.

Mott, N. F. (1947), Fragmentation of Shell Cases, *Proc. Royal Soc.*, A189, 300–308, January.

Wesenberg, D. L. and Sagartz, M. J. (1977), Dynamic Fracture of 6061-T6 Aluminum Cylinders, *J. Appl. Mech.*, 44, 643–646.

4

Further Features of the Mott Statistical Theory

In this chapter some of the theoretical issues introduced by Mott are expanded on and discussed in further detail. Additionally, several issues inspired by Mott's ideas are introduced. First, the statistical development of Mott uses facets of classical survival (or hazard) statistics. Survival statistics methods are pursued here in an alternative way to directly develop statistical fragment size distributions. Next, the statistical treatment of the interaction of multiple fractures was not treated in the original work of Mott (1947). This part of the theory was applied to both the one- and two-dimensional fragmentation problem and is considered in further detail in this chapter. Further, the analytic determination of statistical fragment size distributions from the statistical theory has been performed in the previous chapter for specific Mott fracture activation and growth laws. This development involves analytic details, which are not readily transparent. Here, a more general development of the size distribution relations is developed, which provides a clearer outline of the procedures. After completion of fracture, continued expansion of the fragments also results in a statistical distribution of opening cracks and the associated crack-opening displacement. An analysis is presented which provides an analytic statistical description of the crack-opening displacement for the one-dimensional expanding Mott cylinder. The solution provided earlier for Mott fracture including fracture resistance was restricted to a linear decreasing fracture resistance with crack opening displacement. Here the solution is extended to a power law crack-opening resistance which provides for discussion of fracture resistance ranging from brittle to ductile in character. Lastly, the Mott γ parameter integral to the Mott fragment size prediction is examined further.

4.1 Mott Theory and Survival Statistics

Mott's thoughts on the statistical distribution of fragment sizes from a fragmentation event were initially stimulated by the one-dimensional geometric

theory of Lineau (1936). Through deeper consideration of the physics and statistics of dynamic fragmentation his theoretical efforts developed into the analytic approaches pursued in detail in the previous chapter. Equipped with this theoretical progression, an enlightening approach to the development of appropriate statistical fragment size distribution relations can be pursued by returning to the original ideas of Lineau.

4.1.1 The Survival Statistics Approach to Fragment Size Distributions

To avoid the one-dimensional fragmentation model constraint imposed by Lineau, the following consideration of the fragment size distribution data will be embraced: Consider a collection of N_o fragments which are the consequence of a particular fragmentation event. Arbitrarily select one fragment at a time, weigh the fragment, and consecutively mark a point on a line a distance from the previous fragment point equal to the mass measure m of the fragment. The length of the line is equal to the total mass $M = \Sigma m_i$ of the distribution. The model is now conceptually that of Lineau accept that fragmentation in one (line), two (area) or three (volume) dimensions are equally viable.

Now, starting at any break (the start, or origin, of the line is as good as any) define a function $h(m)$, where $h(m)\,dm$ is the chance that a break will be encountered. Then, according to the tenets of survival statistics, the probability of finding a fragment of size m within interval dm is just the product of finding no breaks within the interval 0 to m, and one break within the interval m to $m + dm$, or,

$$f(m)\,dm = e^{-\int_0^m h(m)dm}\, h(m)\,dm\,. \tag{4.1}$$

Thus the fragment probability density distribution is just,

$$f(m) = h(m)\, e^{-\int_0^m h(m)dm}\,, \tag{4.2}$$

and the cumulative fragment distribution is,

$$F(m) = 1 - e^{-\int_0^m h(m)dm}\,. \tag{4.3}$$

This derivation of the fragment distribution is fully rigorous. The unknown of course is the functional form of the hazard function $h(m)$. This function is determined either by exploring physics specific to the fragmentation process of interest, or else by hypothesizing a functional form and validating through experiment.

For example, given no additional insight into the fragmentation process there is little reason to assume a bias of $h(m)$ toward either the large or the

small masses and the simplest assumption is $h(m) = h_o$, a constant (a Poisson process). Thus $f(m)$ in (4.2) is,

$$f(m) = h_o e^{-h_o m} , \tag{4.4}$$

and the cumulative fragment number distribution is,

$$F(m) = 1 - e^{-m/\mu} , \tag{4.5}$$

where $\mu = 1/h_o$ is the distribution scale parameter and the average fragment mass. Applicability of this distribution to dynamic fragmentation was suggested by Grady and Kipp (1985) and is discussed in Chap. 2.

Mott and Linfoot (1943), following the theoretical work of Lineau (1936) and inspection of some exploding munitions fragmentation data were led to assume that a linear size measure, x of the fragment dimension was a random variable and hence $h_o dx$ provided the chance of fracture determining a fragment of mass m. Mott was interested in the breakup of thin-walled cylinders where fragment dimensions were large compared to wall thickness. Hence, $x \sim m^{1/2}$ and $dx \sim m^{-1/2} dm/2$. Thus, an appropriate hazard function for the Mott and Linfoot distribution is,

$$h(m) = \frac{1}{2\mu} \left(\frac{m}{\mu} \right)^{-1/2} , \tag{4.6}$$

and (4.2) becomes,

$$f(m) = \frac{1}{2\mu} \left(\frac{m}{\mu} \right)^{-1/2} e^{-(m/\mu)^{1/2}} , \tag{4.7}$$

with the corresponding cumulative fragment distribution,

$$F(m) = 1 - e^{-(m/\mu)^{1/2}} , \tag{4.8}$$

familiar to munitions fragmentation analysts.

It is reasonable to consider extending the functional dependence of $h(m)$ to,

$$h(m) = \frac{\beta}{\mu} \left(\frac{m}{\mu} \right)^{\beta - 1} , \tag{4.9}$$

which leads to the cumulative fragment size distribution relation of the Weibull form,

$$F(m) = 1 - e^{-(m/\mu)^{\beta}} . \tag{4.10}$$

This relation clearly encompasses the previous examples. Namely, $\beta = 1/2$ corresponds to the distribution arrived at by Mott and Linfoot (1943), while $\beta = 1$ corresponds to that suggested by Grady and Kipp (1985).

Generality of the parameter β for a munitions-specific scaling equation is warranted for several reasons. Mott and Linfoot argued that when the fragment distribution was dominated by fragments of a size less than the case thickness, that $\beta = 1/3$ was probably more appropriate. For specific munitions systems a range of expansion strain rates will lead to statistical heterogeneity (a different size parameter at different positions along the munitions case). This breakup feature will broaden the distribution leading to smaller effective values of β. On the other hand, a degree of case scoring, or other processes, with the intention of biasing the distribution toward a unique size has the effect of increasing the distribution shape parameter β. (Note that as β approaches infinity (4.10) approaches a Heaviside function with all fragments the same size.)

4.1.2 Mott Release Waves and Survival Statistics

Mott's statistical interacting release waves theory of dynamic fragmentation finds application within the present survival statistics development. In the one-dimensional stretching ring or rod considered by Mott, (4.2) takes the form,

$$f(l) = h(l)\, e^{-\int_0^l h(l)dl}, \tag{4.11}$$

where the hazard function, $h(l)$, now provides the chance $h(l)\, dl$ of a fracture in the length interval l to $l + dl$. The likelihood of achieving a fracture within the neighborhood of an earlier fracture is governed for plastic fracture by the diffusive Mott wave propagating according to,

$$x = \sqrt{2Yt/\rho\dot{\varepsilon}}\,. \tag{4.12}$$

Thus, a point at distance l from an earlier fracture has the opportunity to fracture within a time, $t \propto l^2$ before being passed over by a propagating release wave. It is thus physically reasonable to select a hazard function of the form,

$$h(l) = \frac{3}{\lambda^2} l^2\,, \tag{4.13}$$

where λ will be the resulting distribution scale parameter ($\beta = 3$ in (4.9)).

Equation (4.10) then provides the fragment length probability density function for Mott plastic fracture,

$$f(l) = \frac{3}{\lambda^3} l^2 e^{-(l/\lambda)^3}\,, \tag{4.14}$$

and the cumulative fragment probability distribution,

$$F(l) = 1 - e^{-(l/\lambda)^3}\,. \tag{4.15}$$

In contrast, for Mott elastic fracture release waves propagate according to,

$$x = \sqrt{E/\rho}t \; . \tag{4.16}$$

Similar arguments would suggest the hazard function,

$$h\,(l) = \frac{2}{\lambda^2} l \; , \tag{4.17}$$

leading to the probability density function,

$$f\,(l) = \frac{2}{\lambda^2} l e^{-(l/\lambda)^2} \; , \tag{4.18}$$

and cumulative probability function,

$$F\,(l) = 1 - e^{-(l/\lambda)^2} \; . \tag{4.19}$$

Comparison of the various distributions are provided in Fig. 4.1. All curves are scaled to the expected fragment length. Length scales in each case for the Weibull distributions are adjusted, as the physical considerations leading to the respective hazard functions in (4.13) and (4.17) do not provide the characteristic length scale. For elastic fracture, the Mott analytic solution derived in the previous chapter (3.110) is very well represented by a Weibull distribution with Weibull shape parameter of $\beta = 2$ (4.18). The analytic solution for plastic fracture also obtained in the previous chapter in (3.120) is adequately, but less satisfactorily, represented by a Weibull distribution with $\beta = 3$ (4.14). It is interesting, but physically unmotivating, to note that with a Weibull parameter of $\beta = 3.4$ the plastic fracture analytic solution in Fig. 4.1 can be represented at least, as well, as the elastic fracture comparison.

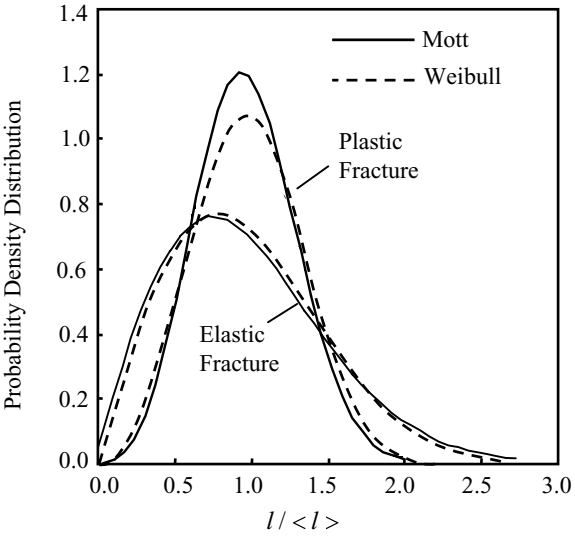

Fig. 4.1. Comparisons of Mott analytic solutions for both elastic and plastic fracture with Weibull distributions based on physically motivated hazard functions as described in the text

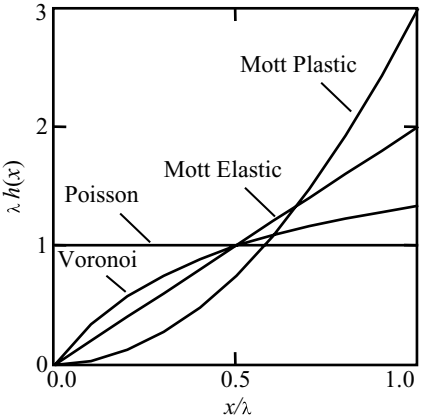

Fig. 4.2. Hazard functions for selected one-dimensional fragment size distributions

4.1.3 The Voronoi Hazard Function

It is instructive to examine the hazard function for the Voronoi fragment size distribution considered in Chap. 2. The one-dimensional Voronoi distribution in the form,

$$f(l) = \frac{4l}{\lambda^2} e^{-2l/\lambda} \,, \tag{4.20}$$

results from a hazard function of the form,

$$h(l) = \frac{2}{\lambda} \frac{2l/\lambda}{1 + 2l/\lambda} \,. \tag{4.21}$$

The Voronoi hazard function is compared with the constant Poisson hazard function and the two previous hazard functions derived for Mott plastic fracture and Mott elastic fracture in Fig. 4.2. The character of the Voronoi hazard function for higher dimensions (area or volume fragmentation) is qualitatively similar.

The Voronoi hazard function has physically attractive functional similarities to the hazard functions developed for Mott elastic and plastic fracture. Namely, a reduction in the probability of the smaller fragments, at least approximately accounting for the interaction and competition of nearby fractures during the fracture activation and growth process. For large fragments, however, the Voronoi hazard function takes on the same characteristics as the Poisson distribution of constant equal likelihood.

4.2 The Statistical Interaction of Fractures

The activation and subsequent stress release of fractures initiated as a consequence of the tensile stretching of a ductile metal shell is illustrated

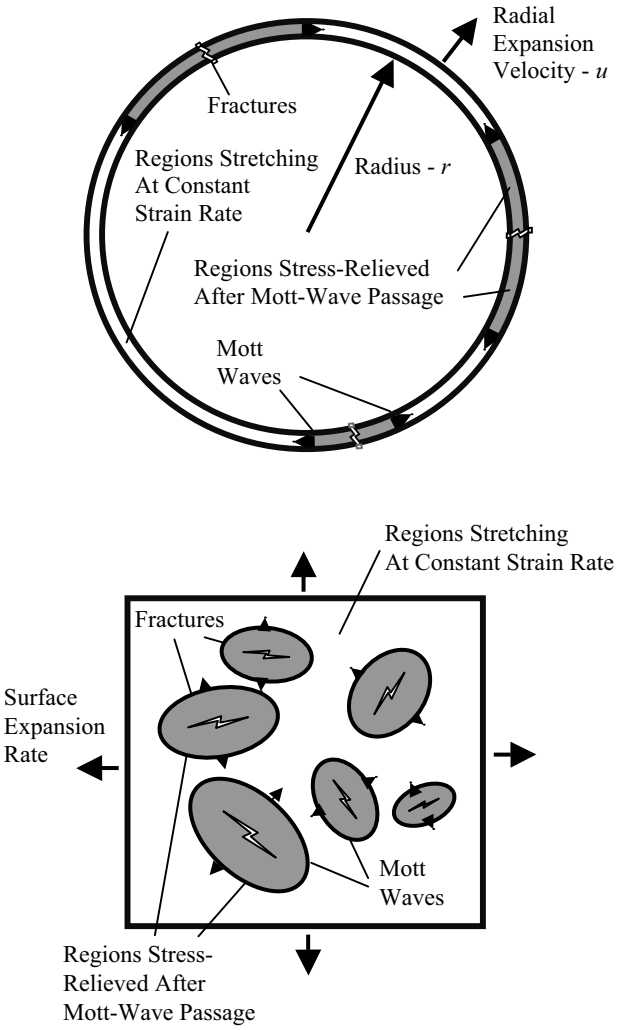

Fig. 4.3. Illustrates activation and subsequent stress release of multiple fractures in the dynamic expansion of ductile metal shells for the Mott cylinder (*upper*) and a biaxially expanding sheet

schematically in Fig. 4.3. The Mott cylinder considered previously illustrates the uniform expansion and one-dimensional (circumferential) fracture of a ring or cylinder. The biaxially stretching surface, on the other hand, depicts the two-dimensional (in-plane) fracture of the expanding surface.

In the Mott statistical theory of fragmentation a function $\lambda(\varepsilon)$ characterizes the rate of activation of fractures in the unruptured stretching plastic body. It is a material property which characterizes the initial or evolving defect structure of the material including interior and/or surface features. In

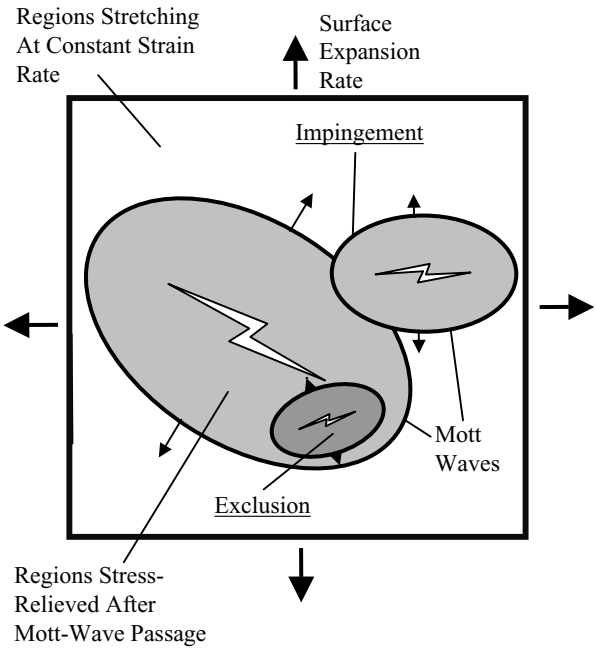

Fig. 4.4. Illustrates fracture activation exclusion and release wave impingement which must be accounted for in the statistical fragmentation theory

energy-limited fragmentation $\lambda(\varepsilon)$ also accounts for the fracture toughness or shear band energy which must be overcome to initiate a fracture as will be addressed in the next chapter. The material function $\lambda(\varepsilon)$ cannot, however, account for the interaction of multiple fractures through stress relief, or Mott, waves. Also, the fracture activation law does not exclude attempts to activate fractures within previously stress-relieved regions as illustrated in Fig. 4.4. The interaction of activated fractures and associated stress release regions is not explicitly treated in the theory developed by Mott.

Similarly, the stress release growth function $g(\varepsilon)$, which determines the distance or domain of the stress release region as a function of continued expansion or stretching ε after fracture activation, is developed from the physics of wave propagation after a single fracture has occurred at some point. It was modeled as either elastic fracture or diffusive plastic fracture in Chap. 3. It does not account for the behavior when the stress-release zones from two nearby fractures begin to interact.

Thus, early in the fracture process when the number of fractures and associated release domains are sufficiently diluted, such that the rate of fracture activation is sufficiently well represented by $\lambda(\varepsilon)$, and such that interactions between neighboring release zones are negligible, then the fraction of the region stress relieved by fracture is readily calculated from the superposition,

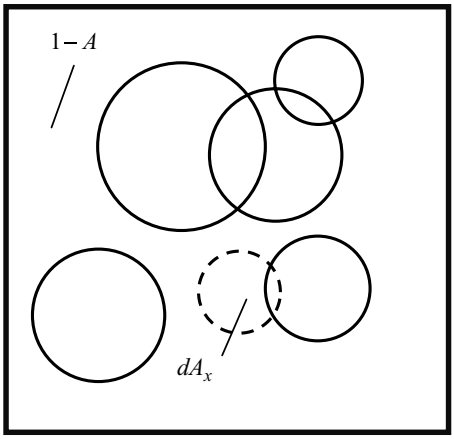

Fig. 4.5. The random placement of overlapping circles illustrates the statistical model accounting for exclusion and impingement developed by Johnson and Mehl (1939)

$$D_x(\varepsilon) = \int_0^{\varepsilon} 2g(\varepsilon - \eta)\lambda(\eta)d\eta \; . \tag{4.22}$$

As the stress release region becomes appreciable, however, (4.22) becomes increasingly in error (note that $D_x(\varepsilon)$ will eventually exceed unity). The interaction effects alluded to above, and not accounted for in (4.22) are collectively referred to as fracture domain impingement and exclusion, and are illustrated in Fig. 4.4.

4.2.1 Johnson–Mehl Treatment

A seminal study in the statistical theory of accounting for exclusion and impingement in kinetic processes of materials was put forth by Johnson and Mehl (1939). The essential idea is illustrated in Fig. 4.5 in which random size circles of area, dA_{xi}, are placed at random on a region of unit size. The total projected area of i circles placed on the region is then the sum,

$$A_x = \sum_i dA_{xi} \; . \tag{4.23}$$

The actual area covered by the circles (the area fraction due to the unit size of the region), because of overlap of the circles, is the union of the i circles,

$$A = \bigcup_i dA_{xi} \; , \tag{4.24}$$

such that $A < A_x$. In the random placement of an additional circle of area dA_x, as shown in the figure, the probability of any element of that circle falling

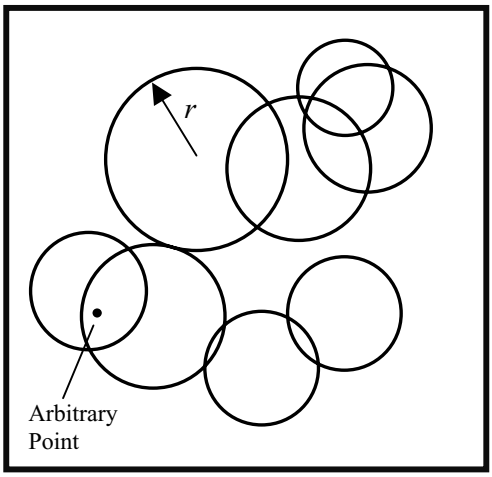

Fig. 4.6. The Getis and Jackson (1971) statistical model proceeds from the Poison probability of random circles covering an arbitrary point multiple times

outside of the area A is,

$$P(A) = 1 - A \ . \tag{4.25}$$

Consequently, the probable change in area A is just,

$$dA = P(A)dA_x = (1 - A)dA_x \ , \tag{4.26}$$

which integrates to,

$$A = 1 - e^{-A_x} \ . \tag{4.27}$$

4.2.2 Getis–Jackson Treatment

The statistical process for dealing with extinction and impingement in kinetic processes was interpreted by Getis and Jackson (1971) in another way. In Fig. 4.6, circles placed at random on the region are assumed to come from a distribution of circles with expected value in radius of $E(r^2)$. The projected fraction is then,

$$A_x = \pi E(r^2)n \ , \tag{4.28}$$

where, n is the average number of circle centers per unit area of the region. Random placement of the circle centers is a Poisson point process in which case the probability of k circles covering a particular point in the region is,

$$P(k) = \frac{A_x^k e^{-A_x}}{k!} \ . \tag{4.29}$$

The fraction of the region covered is then,

$$A = P(k \geq 1) = 1 - P(k = 0) \ , \tag{4.30}$$

or,

$$A = 1 - e^{-A_x} \ , \tag{4.31}$$

equivalent to the derivation of Johnson and Mehl (1939).

This statistical theory is used to account for the exclusion of fracture activation and the impingement of stress release regions in the present development of the Mott fragmentation theory and, accordingly, the area fraction of stress release regions at any expansion ε is,

$$D(\varepsilon) = 1 - e^{-D_x(\varepsilon)} \ , \tag{4.32}$$

where $D_x(\varepsilon)$ is provided by (4.22).

Although, not specifically pursued by Mott, application of the Johnson–Mehl or the Getis–Jackson statistical model to the Mott theory of the fragmentation of rapidly expanding ductile shells seems appropriate. The statistical model is particularly appropriate within the context of the Mott fragmentation model for the propagation of Mott stress release waves, which excludes communication of signals of any type to regions ahead of the release waves. In applications within metals with both elastic and plastic hardening properties applicability could probably be questioned. The approach is nonetheless physically attractive, leads to tractable analytic solutions for a number of features of the fracture process, and can be experimentally tested.

4.3 Length Distributions in the Fragmenting Mott Ring

The Mott fragmentation theory, when combined with the statistical treatment of extinction and impingement, leads to continuous analytic predictions of features of the fracture process such as number of fractures, fracture spacing, and cumulative strain, along with the time dependence of these features through the fracture process. A remarkable product of this theory is analytic relations for the statistical distributions for fragment size in the fragmentation event. Here we focus on the one-dimensional fragmentation event in which fragment size is unambiguously determined by the fragment length. An approach for determining size distributions in the two-dimensional fragmentation of an expanding area is pursued in a later chapter. These distribution relations for one-dimensional fragmentation were derived previously for several specific fracture activation and stress release growth laws in Chap. 3. Here the size distribution relation is developed in general terms. This development, when not buried in the algebra of a specific analysis, provides insight into the workings of the theoretical model.

First, the number density of fractures at any time, or strain ($\varepsilon = \dot{\varepsilon}t$), during the fracture process is given by,

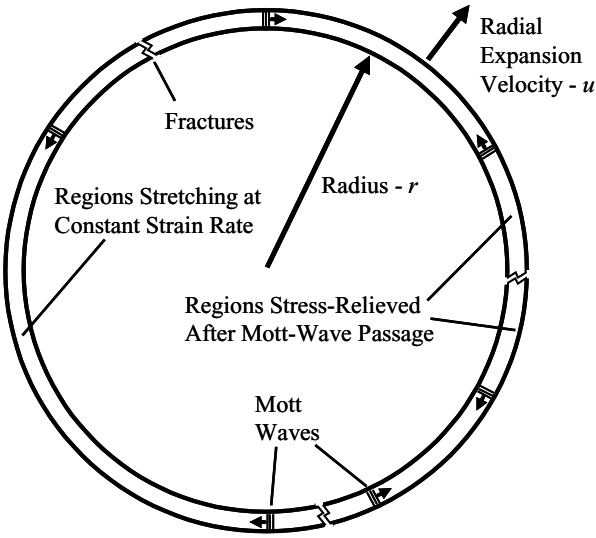

Fig. 4.7. Activation and arrest of Mott stress release waves from points of fracture

$$N(\varepsilon) = \int_0^{\varepsilon} (1 - D(\eta))\lambda(\eta)d\eta = \int_0^{\varepsilon} e^{-D_x(\eta)}\lambda(\eta)d\eta \,. \tag{4.33}$$

This fracture number relation is appropriate for one-dimensional fracture on the circumference of the Mott cylinder, as well as two-dimensional fracture of an expanding surface.

As previously noted, fracture on the Mott cylinder (ring) uniquely characterizes the size of fragments. Namely, they are the arc lengths of the regions between fractures. Random fracture activation on the surface, however, does not uniquely constrain fragment dimensions. Further assumptions concerning the extension and intersection of fractures are necessary, before assessment of statistical fragment size can be accomplished. Through the remainder of this section focus is strictly on the one-dimensional fragmentation problem.

When a fracture occurs at a point on the Mott cylinder, two Mott release waves are created and propagate away from the fracture as illustrated in Fig. 4.7. Therefore, ignoring exclusion and impingement, the number of Mott waves N activated at strain ε is,

$$N(\varepsilon) = 2\int_0^{\varepsilon} \lambda(\eta)\, d\eta \,. \tag{4.34}$$

Again, N is the Mott wave number, and not the fracture number, in the present analysis.

To account for the collision and arrest of active Mott waves as illustrated in the figure, and to account for attempted activation within zones of stress

release, (4.34) is multiplied by the exclusion and impingement factor $(1 - D)$,

$$N(\varepsilon) = 2(1 - D(\varepsilon)) \int_0^{\varepsilon} \lambda(\eta)\, d\eta = 2e^{-D_x(\varepsilon)} \int_0^{\varepsilon} \lambda(\eta)\, d\eta \,, \tag{4.35}$$

providing the number of active Mott waves at any strain ε. The rate of change of $N(\varepsilon)$ is then,

$$\frac{dN(\varepsilon)}{d\varepsilon} = 2e^{-D_x(\varepsilon)}\lambda(\varepsilon) - N(\varepsilon)\frac{dD_x(\varepsilon)}{d\varepsilon} \,, \tag{4.36}$$

which will be written as,

$$\frac{dN(\varepsilon)}{d\varepsilon} = I^+(\varepsilon) - N(\varepsilon)I^-(\varepsilon) \,. \tag{4.37}$$

The rate of activation of Mott waves is provided by $I^+(\varepsilon)$, while the fractional rate of active Mott waves arrested at strain ε is given by $I^-(\varepsilon)$.

The effort now will focus on determining the number of Mott waves which activated at some earlier strain η and arrested at later strain ε. These waves will have all propagated the same distance determined by the release domain growth law $g(\varepsilon - \eta)$. Therefore, let,

$$\delta N_o = I^+(\eta)\delta\eta \,, \tag{4.38}$$

specify the number of Mott waves activated at earlier strain η within increment $\delta\eta$. Further, let δN be the number of the original δN_o surviving at strain $\varepsilon > \eta$. Then the number arrested at strain ε within increment $d\varepsilon$ is just,

$$d(\delta N) = -\delta N I^-(\varepsilon)\, d\varepsilon \,. \tag{4.39}$$

Equations (4.36) and (4.37) provide $I^-(\varepsilon)$ and (4.39) integrates to,

$$\delta N = Ce^{-D_x(\varepsilon)} \,. \tag{4.40}$$

The constant of integration C is determined from the requirement $\delta N = \delta N_o$ at $\varepsilon = \eta$ and provides,

$$\delta N = I^+(\eta)e^{D_x(\eta) - D_x(\varepsilon)}\delta\eta \,. \tag{4.41}$$

Substituting from (4.39) finally yields,

$$d^2N = I^+(\eta)I^-(\varepsilon)e^{D_x(\eta) - D_x(\varepsilon)}d\eta d\varepsilon \,, \tag{4.42}$$

for the number of Mott waves activated at strain η and arrested at strain ε.

The change of integration variables,

$$u = \varepsilon + \eta \,,\; v = \varepsilon - \eta \,, \tag{4.43}$$

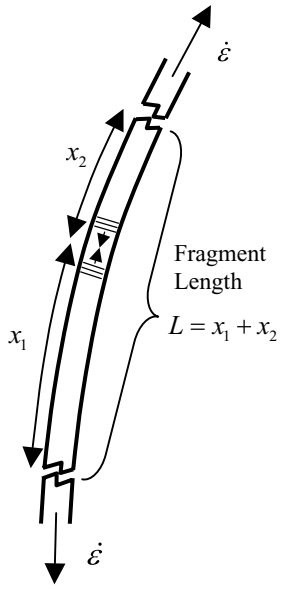

Fig. 4.8. Mott propagation distances combine in pairs to determine fragment lengths

and integration over u provides,

$$p(x) \propto \int\limits_{u=\varepsilon+\eta} I^{+}(\eta) I^{-}(\varepsilon) e^{D_x(\eta)-D_x(\varepsilon)} d\eta d\varepsilon \ , \tag{4.44}$$

where, $x = g(\varepsilon - \eta)$ is the distance of Mott wave propagation from activation to arrest and $p(x)$ is the statistical distribution in Mott propagation distances. Equation (4.44) does not, however, provide the distribution in fragment size. As shown in Fig. 4.8, Mott wave propagation distances combine in pairs to determine the length of a fragment. Thus the analytic expression for the statistical distribution in fragment lengths is,

$$f(x)dx = \int\limits_{\xi=x_1-x_2} p(x_1)p(x_2)\ dx_1 dx_2 \ , \tag{4.45}$$

where $p(x_1)$ and $p(x_2)$ are the distributions provided in (4.44). The change of variables,

$$x = x_1 + x_2 \ , \ \xi = x_1 - x_2 \ , \tag{4.46}$$

completes the integration in (4.45).

For the special Mott problem in which the activation rate $\lambda(\varepsilon) = \lambda_o$, a constant, and Mott wave propagate according to $g(\varepsilon) = \sqrt{2Y\varepsilon/\rho\dot{\varepsilon}^2}$, (4.45) provides the distribution,

$$f(x) = \frac{\beta^2}{4}\frac{1}{x_o}\left(\frac{x}{x_o}\right)^3 e^{-\frac{1}{4}(x/x_o)^3}\int_0^1 \left(1-y^2\right) e^{-\frac{3}{4}(x/x_o)^3 y^2} dy \,, \tag{4.47}$$

Derived in Chap. 3.

4.4 Distributions in Crack-Opening Displacement

The expanding Mott cylinder undergoes multiple fracture which is statistically random in both the position and the time of occurrence of the fractures. Following fracture, the fragment segments continue to expand outward and the crack-opening displacement at the points of fracture that separate the segments continues growing to accommodate the expansion and separation of the individual outwardly directed fragments. The dimension of the gaps between segments (the crack-opening displacement) and the statistical spread in the dimensions of these gaps at any time after fracture are the subject of the discussion and analysis in this section.

The issue of crack-opening displacement has application, for example, in assessing fracture gap spacing after breakup of an exploding cylinder through which detonation products will escape. Alternatively, at greater expansion, the same statistical issue will apply to the spacing of fragments and possible statistical interaction with an intercepting target.

The dynamics in the neighborhood of a single fracture is illustrated in Figs. 4.9 and 4.10. In Fig. 4.9 the conditions of a uniform velocity gradient corresponding to the stretching rate $\dot{\varepsilon}$ prior to fracture activation is depicted by the dashed line. After fracture Mott waves propagate away from the fracture separating regions in front of the waves and flowing plastically at stretching rate $\dot{\varepsilon}$, from rigid regions behind the waves moving at uniform velocity. The velocity profile at some time t after fracture is illustrated by the solid line shown in Fig. 4.9.

Opposing Mott waves are activated at neighboring fractures to the right and left of the fracture depicted in the figures. The collision of two opposing Mott waves from adjacent fractures concludes velocity gradients and plastic flow within the intervening mass segment. This segment continues to move at a constant velocity equal to the velocity at the position of the collision point of the Mott waves.

The segment to the left of the fracture moves away from the position of the initial fracture at a velocity $\Delta u_1 = x_1\dot{\varepsilon}$, while that to the right, at a velocity $\Delta u_2 = x_2\dot{\varepsilon}$, where x_1 and x_2 are the distances between the fracture point and the respective Mott wave collision points, as shown in Fig. 4.10. The crack-opening displacement is then,

$$w(t) = (x_1 + x_2)\dot{\varepsilon}t \,, \tag{4.48}$$

where t is the time after fracture.

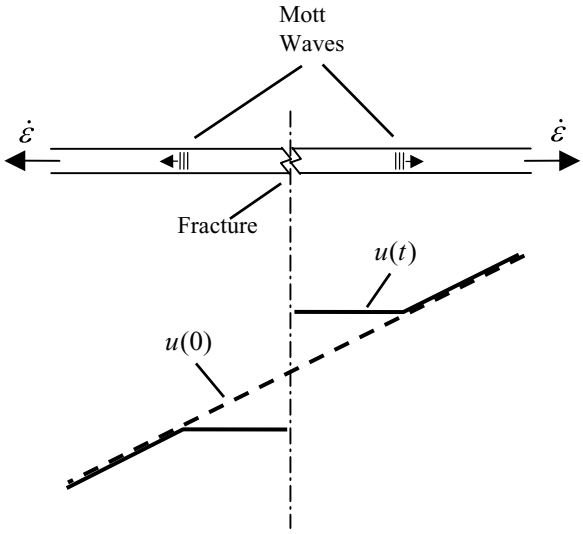

Fig. 4.9. Velocity profile in the stretching ring following fracture and determined by the Mott rigid-plastic wave solution

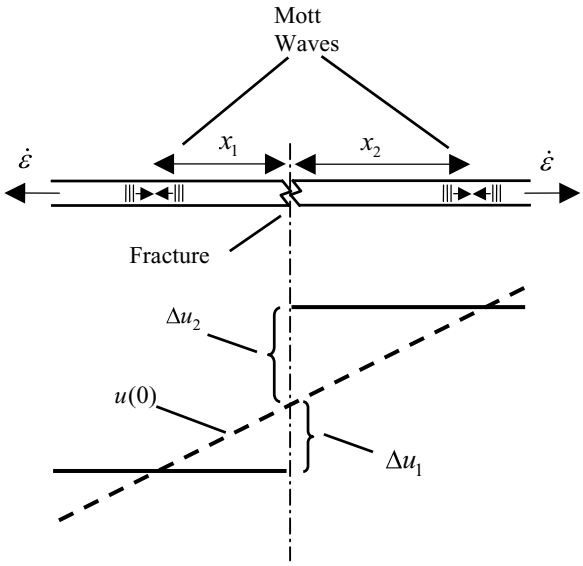

Fig. 4.10. Differential velocity of ring segments adjacent to fracture following completion of wave interaction

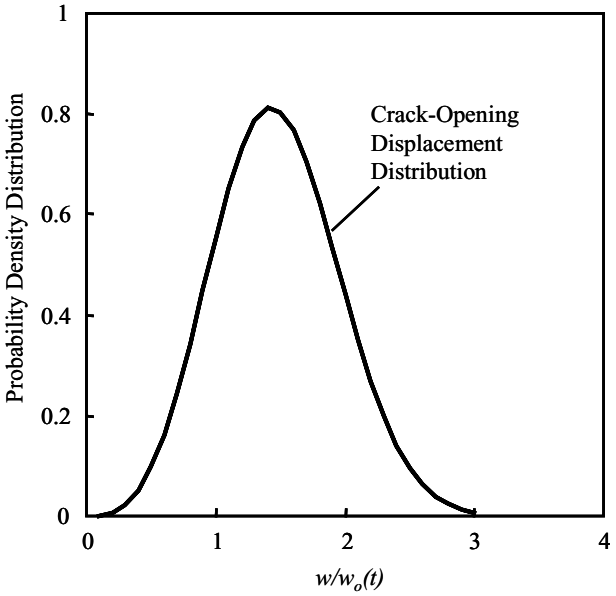

Fig. 4.11. Distribution in crack-opening displacement. Displacement is normalized by characteristic crack-opening displacement $w_o(t)$

There is a characteristic time t_c over which the statistical fracture process and interaction of propagating Mott waves proceeds. This characteristic time was derived from the Mott wave solution derived previously. The time after fracture in (4.48) is assumed to be sensibly larger than t_c.

At any time t there will be a statistical spread $f_c(w)$ in the crack-opening displacement $w(t)$ provided by (4.48). This comes about because the distances of stress release x_1 and x_2, determined by the propagation distances of Mott waves emanating from the fractures, are themselves random. These same distances, when interpreted as the propagation distances between two adjacent fractures, determine the length of the intervening fragment segment. They also uniquely determine the statistical distribution in fragment lengths for the one-dimensional Mott fragmentation problem as developed previously and provided in (4.47). Although, the distances x_1 and x_2 govern the crack-opening displacement in (4.48) are on opposite sides of the fracture, the statistical development of $f_c(w)$ is equivalent. Consequently, the distribution $f_c(w)$, shown in Fig. 4.11, and the fragment length distribution $f(x)$ from (4.47) are related according to,

$$f_c(w)dw = f(x)dx \ , \tag{4.49}$$

or,

$$f_c(w) = f_c(x(w))\frac{dx}{dw} \ . \tag{4.50}$$

The characteristic crack-opening displacement at time t is $w_o(t) = x_o\dot{\varepsilon}t$, where x_o is the characteristic fragment length scale.

The distribution in crack-opening displacement $f_c(w)$ is shown in Fig. 4.11. Displacement is normalized by the characteristic crack-opening displacement $w_o(t) = x_o\dot{\varepsilon}t$. Thus, fragment lengths and crack-opening displacement exhibit the same distribution in spread about the mean. Also, the distribution in crack-opening does not depend on the time after fracture.

4.5 Extended Solutions in Mott Waves

The inclusion of a transient boundary stress to model fracture resistance in the Mott fracture wave analysis has added a further dimension to both qualitative and quantitative understanding of the dynamic fracture process. This analysis determines the distance the rigid-plastic interface (Mott wave) must propagate to accommodate both crack-opening displacement and flux of energy to the fracture region to complete the fracture process. Hence, it provides an estimate of fracture spacing or fragment size when fracture energy principals control the growth and completion of dynamic fracture. The analysis further reveals that a characteristic time from fracture inception to fracture completion is determined by the rate at which momentum and energy can be fluxed into the fracture region. The dependence of this characteristic time on both material and kinematic properties is identified in the solution. This characteristic time determines in turn the additional strain accommodated by the body following onset of the fracture process.

4.5.1 Alternative Fracture Resistance Models

This analysis has to date, assumed a simple crack-opening displacement model that leads to tractable and readily solvable equations governing the dynamic fracture process. Namely, the assumption is that of a linearly decreasing resisting fracture stress with crack-opening displacement. This restricted crack opening resistance solution was developed in Chap. 3.

One can readily imagine other, possibly more realistic, models for the resisting fracture stress. The questions naturally arise as to the sensitivity of the calculated fracture properties to the assumed fracture resistance model and to what additional physical insights might be revealed by this further dimension in the fracture physics.

Other possible models are contrasted with the linear crack-opening displacement model in Fig 4.12. One might reasonable expect that a more brittle fracture process would be modeled by the concave downward resistance versus displacement curve in which a more abrupt drop in resisting stress occurs with increasing crack-opening displacement. In contrast, a more ductile fracture resistance would be more sensibly mirrored by the concave upward curve

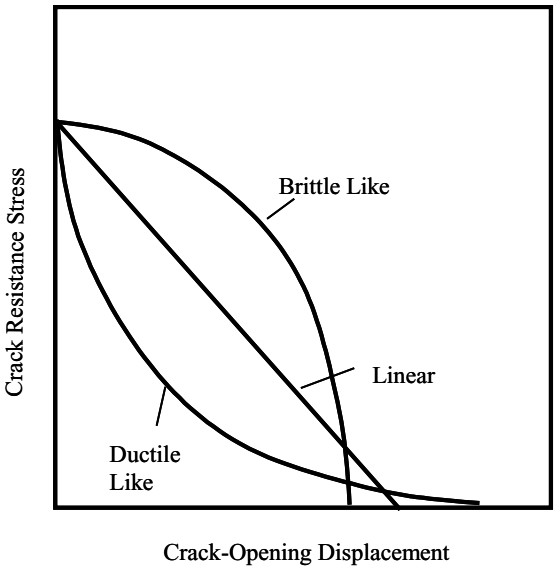

Fig. 4.12. Alternative crack-opening tensile stress versus displacement models

in which fracture resistance drops more rapidly, initially, but with a tendency to delay full fracture to somewhat larger crack-opening displacement.

A fuller spectrum of crack-opening resistance models including the three illustrated in Fig. 4.12 can be explored with a power-law softening model of the form for the tensile stress at the crack location $h = 0$,

$$\sigma(0) = Y_f \left(1 - \left(\frac{y}{y_c}\right)^{1/m}\right) , \tag{4.51}$$

where the range of valid values for the parameter m will be determined by the final solution but will encompass the range of crack opening behavior suggested in Fig. 4.12. The fracture energy Γ is then determined from the integral,

$$\Gamma = \int_0^{y_c} \sigma(0)\, dy . \tag{4.52}$$

Completing the integral provides,

$$\Gamma = \frac{1}{m+1} Y_f y_c . \tag{4.53}$$

The constant flow stress Y has been replaced with the symbol Y_f in the present analysis while y_c is the crack opening displacement at which stress in the fracture achieves zero.

The governing equations during crack opening become,

$$\rho\dot{\varepsilon}\frac{xdx}{dt} = Y_f\left(\frac{y}{y_c}\right)^{1/m} , \tag{4.54}$$

$$\frac{dy}{dt} = \dot{\varepsilon}x . \tag{4.55}$$

The following nondimensional variables are defined,

$$Y = y/y_c, \quad X = x/\sqrt{Y_f/\rho\dot{\varepsilon}^2}, \quad T = \dot{\varepsilon}t , \tag{4.56}$$

along with the single nondimensional constant,

$$\alpha = \frac{1}{y_c}\sqrt{\frac{Y_f}{\rho\dot{\varepsilon}^2}} . \tag{4.57}$$

The governing equations for the Mott fracture wave with general fracture resistance are then, in dimensionless form,

$$X\frac{dX}{dT} = Y^{1/m} , \tag{4.58}$$

$$\frac{dY}{dT} = \alpha X . \tag{4.59}$$

The governing equations are readily integrated through the following procedure. Let,

$$V = \frac{1}{2}\frac{dX^2}{dT} . \tag{4.60}$$

Equation (4.58) becomes,

$$Y = V^m . \tag{4.61}$$

Then,

$$\frac{dY}{dT} = \frac{dV^m}{dT} = \frac{V}{X}\frac{dV^m}{dX} , \tag{4.62}$$

and, from (4.59),

$$\frac{V}{X}\frac{dV^m}{dX} = \alpha X . \tag{4.63}$$

The differential expression,

$$mV^m dV = \alpha X^2 dX , \tag{4.64}$$

is then integrated providing,

$$\frac{m}{m+1}V^{m+1} = \frac{\alpha}{3}X^3 , \tag{4.65}$$

where the initial condition $V = 0$ at $X = 0$ has been employed. Continuing the solution yields,

$$V = X\frac{dX}{dT} = \left(\frac{m+1}{m}\right)^{\frac{1}{m+1}} \left(\frac{\alpha}{3}\right)^{\frac{1}{m+1}} X^{\frac{3}{m+1}} \ . \tag{4.66}$$

Variables are separable yielding the differential expression,

$$X^{\frac{m-2}{m+1}} dX = \left(\frac{m+1}{m}\right)^{\frac{1}{m+1}} \left(\frac{\alpha}{3}\right)^{\frac{1}{m+1}} dT \ . \tag{4.67}$$

Integrating with initial conditions $X = 0$ at $T = 0$ gives,

$$X = \left(\frac{2m-1}{m+1}\right)^{\frac{m}{2m-1}} \left(\frac{2m-1}{3m}\right)^{\frac{1}{2m-1}} \alpha^{\frac{1}{2m-1}} T^{\frac{m+1}{2m-1}} \ . \tag{4.68}$$

Substituting (4.68) into (4.59) and solving yields,

$$Y = \left(\frac{2m-1}{m+1}\right)^{\frac{m}{2m-1}} \left(\frac{2m-1}{3m}\right)^{\frac{2m}{2m-1}} \alpha^{\frac{2m}{2m-1}} T^{\frac{3m}{2m-1}} \ . \tag{4.69}$$

The dimensionless time to fracture T_f is calculated from (4.69) by setting $y = y_c$ or, equivalently, $Y = 1$,

$$T_f = \left(\frac{m+1}{2m-1}\right)^{1/3} \left(\frac{3m}{2m-1}\right)^{2/3} \left(\frac{1}{\alpha}\right)^{2/3} \ . \tag{4.70}$$

The distance traveled by the rigid-plastic boundary through substitution of T_f into (4.68) is,

$$X_f = \left(\frac{3m}{m+1}\frac{1}{\alpha}\right)^{1/3} \ . \tag{4.71}$$

At this point the fracture energy,

$$\Gamma = \frac{n}{n+1} Y_f y_c = \frac{1}{m+1} Y_f y_c \ . \tag{4.72}$$

is introduced into the solution. A further dimensionless constant β is defined through,

$$\alpha = \frac{1}{y_c}\sqrt{\frac{Y_f}{\rho\dot{\varepsilon}^2}} = \frac{Y_f}{(m+1)\,\Gamma}\sqrt{\frac{Y_f}{\rho\dot{\varepsilon}^2}} = \frac{1}{(m+1)\,\beta} \ , \tag{4.73}$$

where,

$$\beta = \frac{\Gamma/Y_f}{\sqrt{Y_f/\rho\dot{\varepsilon}^2}} \ . \tag{4.74}$$

The travel distance and fracture time then become,

$$X_f = (3m\beta)^{1/3} \ , \tag{4.75}$$

and,

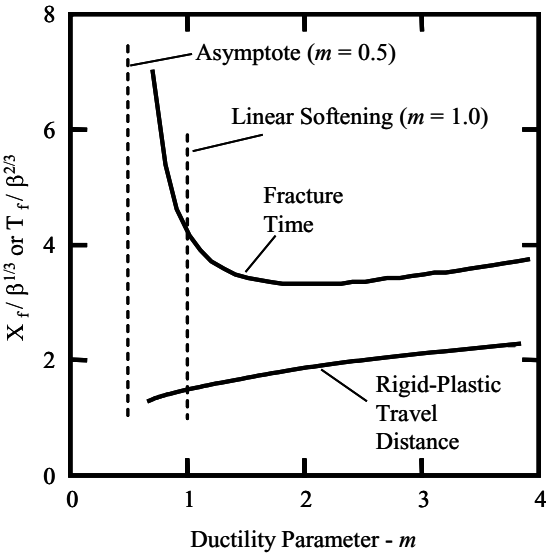

Fig. 4.13. A plot of the rigid–plastic boundary travel distance and fracture time as a function of the ductility parameter m

$$T_f = \frac{m+1}{2m-1}\,(3m\beta)^{2/3} = \frac{m+1}{2m-1}X_f^2\,. \tag{4.76}$$

The parameter m will be identified as a ductility parameter. (Increasing m leads to increasingly ductile fracture behavior according to the earlier introductory discussion.) Both travel distance of the rigid-plastic boundary and the time to fracture from (4.75) and (4.76) are plotted as a function of the parameter m in Fig. 4.13. The functional behavior of both offer insight into the processes of dynamic fracture of plastically stretching bodies.

The parameter X_f has previously been related to the natural spacing of fractures and fragment size [Kipp and Grady, 1985] with the linear softening model for crack opening displacement, $m = 1$, as discussed in Chap. 3. Equation (4.75) reveals that X_f is not independent of m, but increases modestly with m. Inferred fracture spacing is not sensitive to the parameter m, however, with variations in m from about 0.5 to 4 providing only a factor of two variation in spacing. Fracture spacing for linear softening would be nearly centered within this range.

The time from fracture inception to completion has more interesting character exhibiting, for a fixed fracture energy, a minimum with increasing fracture time toward both increasingly ductile-like (larger m), and brittle-like (smaller m) fracture. Toward the larger m, the increased crack-opening displacement to full separation y_c requires a corresponding increased in rigid plastic boundary travel distance and hence an increased fracture time. In contrast for smaller values of m the relatively small stress difference over

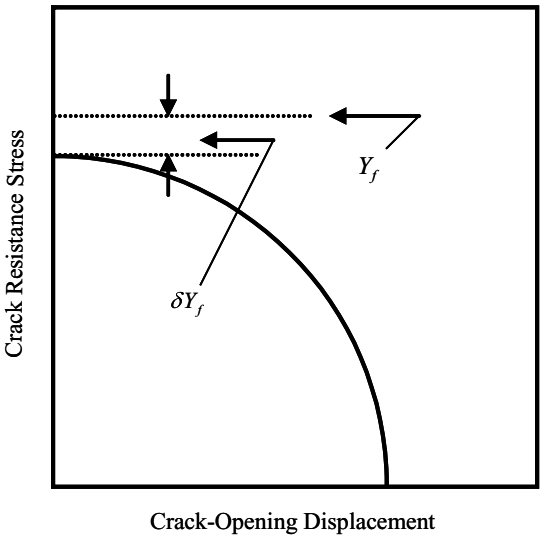

Fig. 4.14. Power-law softening crack-opening displacement model with initial perturbation of reduced crack-opening resistance of δY_f below floor stress Y_f

much of the crack-opening displacement before abrupt failure leads to slow acceleration and correspondingly increased fracture time.

It is also observed that for $m > 0.5$ the governing equations and subsequent motions based on power-law softening are self-starting. That is no perceptible perturbation is required to initiate onset of fracture growth. This is not the case for $m \leq 0.5$ as is reflected in Fig. 4.13, with fracture time asymptotically tending to infinity as m approaches 0.5 from above.

A perturbation can be introduced and its effects on the fracture dynamics explored by, for example, reducing the boundary stress at time zero as illustrated in Fig 4.14. Introducing a dimensionless perturbation parameter $\Delta = \delta Y_f / Y_f$ the governing equations equivalent to (4.58) and (4.59) are,

$$X \frac{dX}{dT} = \Delta + (1 - \Delta)\, Y^{1/m} \,, \tag{4.77}$$

$$\frac{dY}{dT} = \alpha X \,. \tag{4.78}$$

By similar methods the integral solution for motion of the rigid plastic interface is readily obtained for the linear softening model ($m = 1$) in the form,

$$T = \int_0^x \frac{X dX}{\sqrt{2\alpha\,(1 - \Delta)\, X^3/3 + \Delta^2}} \,. \tag{4.79}$$

Early and late time motions are readily understood without completing the integral. The early solution reduces to the form,

$$T = \int_0^x \frac{X dX}{\Delta} \ , \tag{4.80}$$

yielding the square root dependent motion $X \cong \sqrt{2\Delta T}$ originally obtained by Mott, but driven by the perturbation stress difference Δ. In contrast late time motion yield $X \cong \alpha T^2/6$, the solution of Kipp and Grady (1985) for linear softening crack-opening displacement.

Equating terms within the radical in (4.79) identifies the travel distance at which transition from early to late time motion occurs,

$$X \approx \left(\frac{3}{2}\frac{\Delta^2}{\alpha}\right)^{1/3} \ . \tag{4.81}$$

Comparison with the travel distance X_f at fracture, (4.71) shows that for modest perturbation amplitudes the solution and fracture properties are dominated by the late time motion.

The foregoing solutions, thus, provide additional physical insight into the fracture dynamics when variations in the crack-opening resistance is explored. Variations from nominally brittle behavior to quite ductile behavior influence both the time dependence of the fracture process as well as the characteristic distance of crack interaction.

4.5.2 Influence of a Strain Gradient on Fragmentation Size

Time dependent explosive detonation can lead to gradients in the expansion strain and a statistical difference in the strain to fracture of neighboring point on an expanding metal shell. This strain gradient will lead to an increase in the characteristic fracture spacing. An assessment of the influence of a strain gradient term on the characteristic fracture spacing is provided here base on the Mott wave interaction approach. The situation is illustrated in Fig. 4.15 where fracture has initiated at $x = 0$ and $t = 0$ while fracture at position x is delayed a time τ caused by a strain gradient term ε_x delaying achievement of the fracture strain. The objective will be to determine the minimum spacing for fracture one and fracture two allowed by the Mott wave interaction.

Fracture initiation at $x = 0$ reaches completion at $t = t_1$ while the Mott release wave originating from that fracture has propagated a distance $x_1 = x_f = \sqrt[3]{3\Gamma/\rho\dot{\varepsilon}^2}$ from the earlier energy based analysis of fracture spacing. A similar Mott release wave originating from fracture two, which initiates at a delayed time $\tau = \varepsilon_x x/\dot{\varepsilon}$, reaches a point x_2 at a time t_2 at fracture completion. The additional distance $x_2 - x_1$ traveled by a Mott release wave over the time $t_2 - t_1 = \tau$ determines the minimum fracture spacing x.

This distance,

$$x_2 - x_1 = \sqrt{\frac{2Yt_2}{\rho\dot{\varepsilon}}} - \sqrt{\frac{2Yt_1}{\rho\dot{\varepsilon}}} \ , \tag{4.82}$$

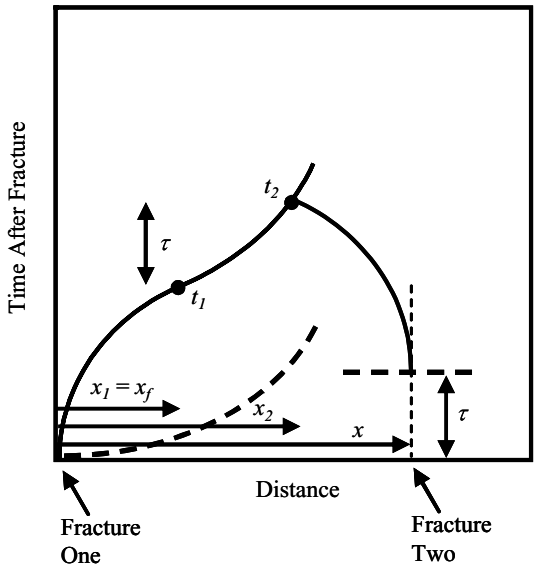

Fig. 4.15. Minimum fracture spacing of Mott fractures with separation in fracture initiation time due to strain gradient

readily leads to,

$$x = x_f \left(1 + \sqrt{1 + \frac{2Y\tau}{\rho \dot{\varepsilon} x_f^2}} \right) . \tag{4.83}$$

Replacing with $\tau = \varepsilon_x x / \dot{\varepsilon}$ yields an implicit expression for the fracture spacing in terms of the zero strain gradient fracture spacing and the magnitude of the strain gradient,

$$x = x_f \left(1 + \sqrt{1 + \frac{2Y\varepsilon_x x}{\rho \dot{\varepsilon}^2 x_f^2}} \right) . \tag{4.84}$$

This expression is readily solved for the fragment size dependence on the strain gradient,

$$x = 2x_f(1 + L\varepsilon_x) , \tag{4.85}$$

where the length scale,

$$L = \left(\frac{Y^3}{3\rho^2 \dot{\varepsilon}^4 \Gamma} \right)^{1/3} , \tag{4.86}$$

depends on both material and kinematic properties.

4.6 The Mott Fragmentation γ Parameter

In developing theoretical descriptions of matter, Mott was not inclined toward relations in which arbitrary material constants were inserted that could

be established only through curve fit to the data of interest. The Gumbel distribution Mott selected to describe the statistical activation of fractures has a single scale parameter, identified by him as γ, which, in addition to several known properties, determined the average fragment size. Mott expended some effort in identifying the underlying physical basis for γ and attempted to independently calculate its value.

Two approaches were pursued by Mott. In the first approach he proposed a fracture test through which γ could be independently assessed. Later he attempted to determine γ through analysis of the microscopic flaw structure governing statistical fracture. Both approaches are reviewed here.

4.6.1 Mott γ From Tensile Fracture Tests

The size, or spacing, length scale emerging from the statistical fragmentation theory of Mott is,

$$\mu = \sqrt{\frac{2Y}{\rho\dot{\varepsilon}^2}\frac{1}{\gamma}}\,, \tag{4.87}$$

where, γ is the scale parameter in the exponential hazard function,

$$\lambda(\varepsilon) = Ae^{\gamma\varepsilon}\,, \tag{4.88}$$

and the corresponding Gumbel probability density function,

$$f(\varepsilon) = Ae^{\gamma\varepsilon - \frac{A}{\gamma}e^{\gamma\varepsilon}}\,, \tag{4.89}$$

illustrated in Fig. 4.16. The standard deviation in strain to fracture from the Gumbel probability distribution is approximately $1.28/\gamma$.

Mott proposed that the statistical variation in strain to fracture from static tensile fracture could be used to calculate γ. Strain to fracture values for a 0.4% carbon steel from Mott's report are plotted in Fig. 4.17. From the calculated standard deviation for the scatter in strain to fracture for this data, a value of $\gamma = 88$ is arrived at.

Sensible properties for the same steel in an exploding cylinder fragmentation event would be $Y \cong 1$ GPa, $\rho \cong 8000$ kg/m^3, and $\dot{\varepsilon} \cong 5 \times 10^3$/s. These values in (4.87) lead to a calculated fracture spacing of $\mu \approx 1.1$ cm, a very reasonable estimate of the observed fragment size.

4.6.2 Mott γ From Microscopic Flaw Considerations

In the statistical development of fragmentation pursued by Mott (1943, 1947) it was recognized that some measure of the spread in strain to fracture was central in determining the characteristic spacing of fractures. In Mott's continuum development the parameter γ, related to the standard deviation in strain to failure in the Gumbel extreme value distribution, quantified this measure of spread in strain to fracture.

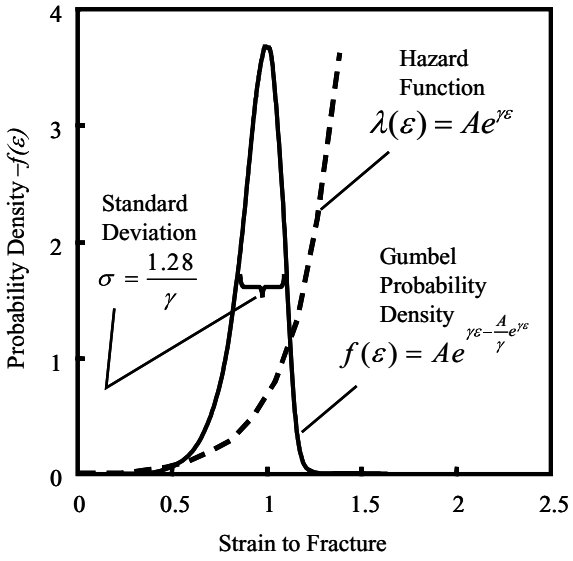

Fig. 4.16. Statistical characteristics of the exponential hazard function and the Gumbel probability density function

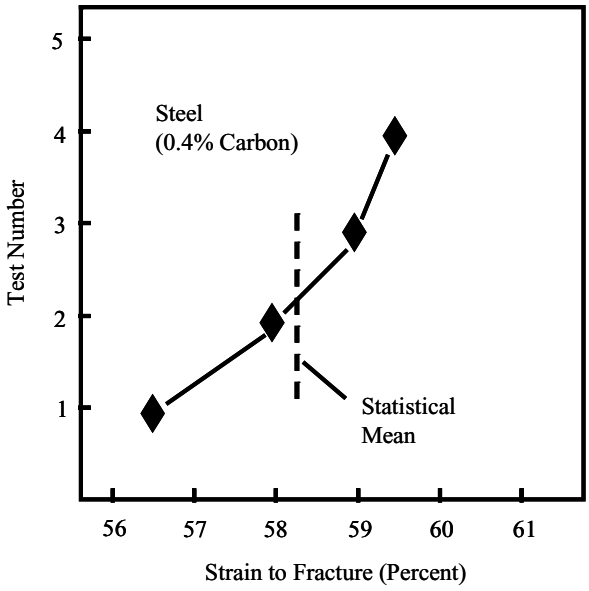

Fig. 4.17. Tensile strain-to-fracture data for a 0.4% carbon steel from the report of Mott (1943)

Mott was not satisfied with simply accepting γ as an empirical parameter in his theory. He pursued several efforts in deriving γ from other, more intrinsic, properties of the material, and attempted to uncover the underlying physics on several length scales. The previous subsection describes his estimates of γ based on statistical fracture data. He subsequently attempted to determine γ from microscopic fracture-producing flaw characteristics of the material.

Mott (1947) referred to the then recent theory of Griffith on the strength of brittle solids in which onset of fracture occurred when the stress load T achieved a critical condition of the form $T \sim A/c^{1/2}$. In this failure criterion c is the length of the responsible microcrack while A is a function of elastic and surface energy properties of the material. Mott noted that no comparable theory existed for ductile metals. He then proceeded by assuming fracture to begin at sites of weakness distributed throughout the material, and governed by a critical condition of the form,

$$T \sim A/c^n \ , \tag{4.90}$$

where again, c is a characteristic length scale of the fracture producing weaknesses and n is a number probably reasonably close to 1/2. Mott additionally assumed that the microcracks were Gaussian distributed in the microcrack length c and that the tension was governed by a hardening relation of the plastic strain of the form,

$$T = Y + H \ln(1 + \varepsilon) \ . \tag{4.91}$$

Through clever analysis Mott manipulated the Gaussian distribution into a form in which the parameter γ could be extracted,

$$\gamma \sim \frac{1}{n} \frac{H}{T_F} \frac{1}{(1 + \varepsilon_F)} \ . \tag{4.92}$$

In (4.92) H is the hardening parameter while T_F and ε_F the tension and plastic strain at fracture. Mott made quantitative predictions of fragment size and noted that trends inferred from (4.92) were consistent with observations then available.

4.6.3 Closing Observations of Mott

Mott's perception of the physical processes of ductile fracture in metals continued to mature over the remaining several years in which he found time to reflect on this problem. His most sophisticated thoughts are included in what appears to be his last writing focused on the issues of ductile fracture [Mott, 1948]. Mott suggested that cleavage fracture in metals was unlikely except at the fastest fracture velocities. By incorporating inertial energy into the Griffith energy balance he developed the first expression of the velocity of

a growing crack and noted a limiting velocity commensurate with the sound speed in the material. Applicability and limitations of the Mott crack velocity solution have been address by later workers [e.g., Freund, 1990; Lawn, 1993].

Mott also noted in the later work that the concept of intrinsic sites of weakness governing fracture in a ductile metal was probably not appropriate. Rather, ductile fracture required plastic strain and the accumulation of a local critical level of microscopic damage before onset of fracture at a point in the material. He cited several examples which clearly showed that a critical plastic strain criterion is inadequate and that the state of stress triaxiality under which the strain accumulates is essential to the fracture criterion. Mott was probably the first to recognize this central tenet of the ductile fracture process.

References

Freund, L. B. (1990), *Dynamic Fracture Mechanics*, Cambridge University Press.

Getis, A. and Jackson, P. H. (1971), The Expected Proportion of a Region Polluted by K Sources, *Geographical Analysis*, 3, 256–261.

Grady, D. E. and Kipp, M. E. (1985), Geometric Statistics and Dynamic Fragmentation, *J. Appl. Phys.*, 58, 3, 1210–1222.

Johnson, W. A. and Mehl, R. F. (1939), Reaction Kinetics in Processes of Nucleation and Growth, *Trans. AIMME*, 135, 414–458.

Kipp, M. E. and Grady, D. E. (1985), Dynamic Fracture Growth and Interaction in One-dimension, *J. Mech. Phys. Solids*, 33, 399–415.

Lawn, B. R. (1993), *Fracture of Brittle Solids – Second Edition*, Cambridge University Press.

Lineau, C. C. (1936), Random Fracture of a Brittle Solid, *J. Franklin Inst.*, 221, 485–494, 674–686, 769–787.

Mott, N. F. (1943), A Theory of the Fragmentation of Shells and Bombs, *Ministry of Supply AC4035*, May.

Mott, N. F. (1947), Fragmentation of Shell Cases, *Proc. Royal Soc.*, A189, 300–308, January.

Mott, N. F. (1948), Fracture of Metals: Theoretical Considerations, *Engineering*, 165, 16–18.

Mott, N. F. and Linfoot, E. H. (1943), A Theory of Fragmentation, *Ministry of Supply AC3348*.

5

Reconciling Mott-Statistical and Energy-Based Fragmentation

In earlier sections the statistical fragmentation theory of Mott was considered in some depth. An alternative fragmentation theory based on energy balance principals has also been pursued by the present author and others. As posed, the two theories appear to be based on strikingly different principals. In the present section attempts are pursued to understand and reconcile differences between the two theories. For the purpose of this reconciliation the essential features of both theories are summarized. This summary represents a condensation of same the material provided in the previous sections.

The present discussion will focus on the one-dimensional expanding ductile ring fragmentation as originally posed by Mott. To provide an experimental grounding for the theoretical comparisons the dynamic fragmenting ring data on uranium 6% niobium [Grady and Olsen, 2003], discussed in further detail later in this report, is used.

5.1 Mott Statistics-Based Fragmentation

As has been pursued here in some detail, three technical reports published within the first half of 1943 revealed the maturing of Mott's understanding of the dynamic fragmentation process and, in the last of these reports, a statistical theory of fragmentation emerged, which is still one of the leading theories available. The theory was published several years later in the open literature [Mott, 1947]. This development is summarized in the following subsections.

5.1.1 The Mott Cylinder

The Mott theory of fragmentation is most readily conceptualized by again considering the Mott cylinder (or ring) illustrated in Fig. 5.1. The Mott cylinder is an idealization of an expanding cylindrical shell whose outward motion is imparted by some radial impulse. Mott, in particular, focused on the natural fragmentation of exploding pipe bombs. The model is applicable to other

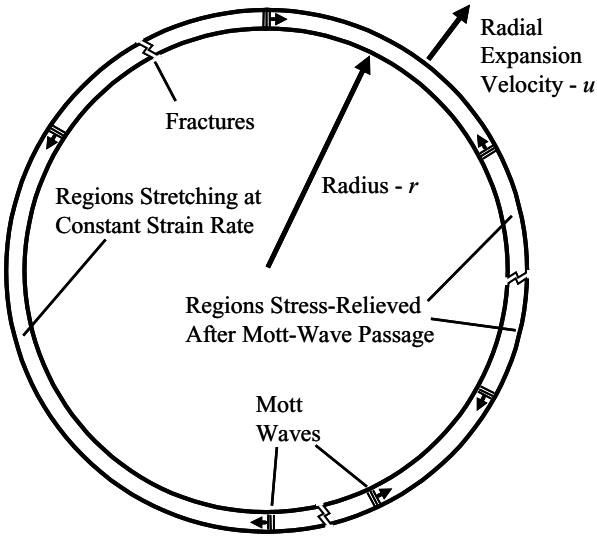

Fig. 5.1. Mott cylinder illustrating the one-dimensional activation and interaction of fractures leading to the statistical fragmentation of the body

test conditions such as the magnetically driven metal ring data considered in the present section.

An explosively-driven expanding metal cylinder is a decidedly multidimensional fragmentation event, and fragmentation of the Mott cylinder is only an approximation to this event. The theory attempts to capture the characteristic circumferential spacing of fractures and the statistical distribution in the spacing. It is not intended to account for the axial propagation and interaction of cracks within a finite length cylinder. The Mott cylinder is an expanding metal body with radial velocity u and radius r at the time when multiple fracture and break up of the cylinder proceeds. Just preceding break up, the cylinder body is in circumferential tension and undergoing uniform circumferential stretching at a rate given by the ratio $\dot{\varepsilon} = u/r$.

Mott proposed that fragmentation proceeded through the random spatial and temporal occurrence of fractures resulting in a distribution in fragment lengths. Release waves propagate away from the sites of fracture relieving the tension and precluding the possibility for further fracture within the regions encompassed by tension release waves. Fragmentation is complete when fracture-induced release waves subsume the entire cylinder.

Thus, within the model for dynamic fragmentation proposed by Mott, two physical issues need to be addressed. First, is the issue of when and where fractures occur on the Mott cylinder. Second, is the nature of propagation of tensile release waves (Mott waves) away from the sites of fracture. Here each issue will be addressed in turn.

5.1.2 Mott Fracture Activation

Mott put forth arguments that energy dissipation was not of consequence in the fracture process and proposed instead a statistical strain-to-fracture criterion. Mott assumed that fractures occurred at random, around the circumference of the cylinder at a frequency governed by a strain dependent hazard function $\lambda(\varepsilon)$ [e.g., Hahn and Shapiro, 1967], such that $\lambda(\varepsilon)d\varepsilon$ provided the statistical number of fractures occurring within a unit length of the cylinder circumference in the strain interval $d\varepsilon$. It is important to recognize that Mott considered $\lambda(\varepsilon)$ to be an independently measurable property of the material. An alternative and complementary application of the hazard function yields,

$$F(\varepsilon) = 1 - e^{-L\int \lambda(\varepsilon)d\varepsilon}, \tag{5.1}$$

for the cumulative probability of fracture failure in tensile test specimens of length L. Mott in fact used tensile test data on steels to estimate parameters in the function $\lambda(\varepsilon)$ as discussed in the preceding section.

Mott expected $\lambda(\varepsilon)$ to be a strongly increasing function of strain and suggested both an exponential and a power-law function. The former leads to Gumbel statistics, while the latter yields Weibull statistics. Relative differences between the two distributions were identified earlier in this report. Mott pursued the exponential hazard function. Here the two-parameter power-law hazard function,

$$\lambda(\varepsilon) = \frac{n}{\sigma}\left(\frac{\varepsilon}{\sigma}\right)^{n-1}, \tag{5.2}$$

will be used. For reasonably large n the parameter σ is the expected value of the strain to fracture of a unit length while σ/n is proportional to the standard deviation in the strain to fracture.

5.1.3 Mott Tension Release

Statistical fracture in the Mott cylinder can now be generally addressed. The tensile release function is,

$$D_x(\varepsilon) = \int_0^{\varepsilon} 2g(\varepsilon - \eta)\lambda(\eta)\, d\eta\,, \tag{5.3}$$

where $\lambda(\eta)d\eta$ is the statistical number of fractures activated on the Mott cylinder at a strain η within interval $d\eta$. The function $g(\varepsilon - \eta)$ is the distance traveled by a tensile stress release wave over the strain interval $\varepsilon - \eta$ for one fracture. (Since strain rate is assumed to be constant over the duration of the fracture process, strain and time are synonymous through $\varepsilon = \dot{\varepsilon}t$.)

In (5.3) $D_x(\varepsilon)$ is seen to provide the fraction of the Mott cylinder which has been encompassed by stress release waves emanating from sites of fracture at a current strain ε. The equation also determines the fraction of the cylinder

in which further fracture is precluded. A form of (5.3) was derived by Mott in the original 1943 report [Mott, 1943] and discussed in the previous several chapters.

An inspection of (5.3) reveals that the function $D_x(\varepsilon)$ will exceed unity at sufficiently large strain. This non-physical result is a consequence of not accounting for two factors in the fracture activation and stress wave propagation process. First, the fracture activation function $\lambda(\varepsilon)$ does not exclude the activation of further fractures within regions previously stress relieved. Second, the stress release function $g(\varepsilon)$ does not account for the impingement and the overlap of opposing release waves from separate neighboring fractures. Thus, (5.3) is only applicable for a dilute number of fractures early in the fracture and release process.

To account for fracture exclusion and wave impingement in the statistically random Mott model, a statistical method introduced by Johnson and Mehl (1939) discussed in the previous chapter is used. Exclusion and impingement is accounted for through the relation,

$$D(\varepsilon) = 1 - e^{-D_x(\varepsilon)} \,, \tag{5.4}$$

providing the fraction of the Mott cylinder $D(\varepsilon)$ encompassed by fracture stress release waves at any strain ε. $D(\varepsilon)$ and $D_x(\varepsilon)$ are equivalent at early times as they should be. The function $D(\varepsilon)$ does approach unity as ε becomes large.

5.1.4 Fracture Stress Release Function

A functional form of the stress release function $g(\varepsilon)$ must be specified. There are several possibilities. If the expanding Mott cylinder is elastic at the time of fracture, then a constant elastic release wave velocity governed by the elastic modulus is sensible. Mott, however, considered an expanding ductile metal cylinder and assumed a material on the tensile yield surface governed by a constant flow stress Y. Instantaneous fracture and rigid-ideally-plastic constitutive response leads to the stress release function,

$$g(\varepsilon) = \sqrt{\frac{2Y}{\rho \dot{\varepsilon}^2} \varepsilon} \,. \tag{5.5}$$

It was shown earlier that diffusion rather than wave propagation governs stress release under the assumed physical conditions.

5.1.5 Fracture Number Prediction

Given explicit forms for the fracture activation function from (5.2) and the stress release function from (5.5), statistical predictions of the number of fractures (and fragments) produced in the break-up of the Mott cylinder can be

determined. Accounting for the stress relieved fraction of the cylinder $D(\varepsilon)$, the number of fractures at a strain ε is given by,

$$N(\varepsilon) = \int_0^{\varepsilon} (1 - D(\eta))\lambda(\eta)\, d\eta \; . \tag{5.6}$$

Completing the integral in (5.3) and using (5.4) to obtain $D(\varepsilon)$, integration of (5.6) to infinite strain yields,

$$N = \beta_n \left(\frac{\rho \dot{\varepsilon}^2}{2\pi Y} \frac{n}{\sigma} \right)^{n/(2n+1)} \quad , \tag{5.7}$$

for the number of fractures per unit length, where the numerical constant is,

$$\beta_n = \left(\frac{2n}{2n+1} \right)^{1/(2n+1)} \left(\frac{1}{\sqrt{n}} \frac{\Gamma\left(n + 1/2\right)}{\Gamma\left(n\right)} \right)^{2n/(2n+1)} \Gamma\left(\frac{2n}{2n+1} \right) \; . \tag{5.8}$$

For reasonably large n the constant β_n approaches one in (5.7) and the power approaches one-half, leading to a linear dependence of fracture number on the expansion strain rate. The fracture number is determined by the standard deviation ($\simeq 1.283\, \sigma/n$) of the power-law fracture frequency function $\lambda(\varepsilon)$ as was noted by Mott. The statistical temporal history of fractures appearing on the Mott cylinder can be determined by retaining the strain dependence of the integral in (5.6).

5.1.6 Fracture Distribution Prediction

Additionally, the random placement of fractures on the Mott cylinder both in space and in time, as assumed in the Mott model, allows for calculation of the statistical distribution of fracture spacing (fragment lengths). This calculation was performed graphically by Mott and has been completed by analytic methods as shown in the previous section for the special case of $n = 1$ in the power-law fracture frequency function. The calculated analytic distribution in fracture spacing by this analytic method is,

$$f\left(x\right) = \frac{\beta^2}{4} \frac{1}{x_o} \left(\frac{x}{x_o} \right)^3 e^{-\frac{1}{4}(x/x_o)^3} \int_0^1 \left(1 - y^2\right) e^{-\frac{3}{4}(x/x_o)^3 y^2} dy \; , \tag{5.9}$$

where $\beta = 3\Gamma(2/3)$ and $x_o = (3\sigma Y/2\rho\dot{\varepsilon}^2)^{1/3}$. The sensitivity of the size distribution to the functional form of the fracture frequency function $\lambda(\varepsilon)$ is not known, but comparison of the analytic distribution from (5.9) and the graphical distribution of Mott suggests that this sensitivity is probably small. Both the analytic and the graphical distribution are again compared in Fig. 5.2.

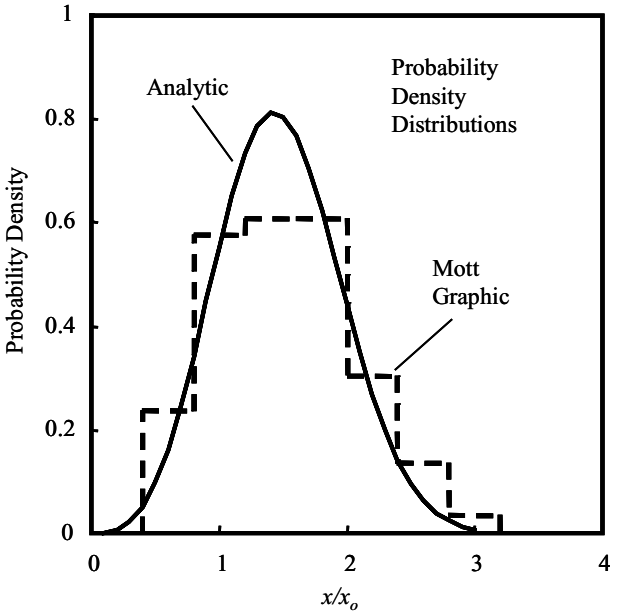

Fig. 5.2. Comparison of the graphic and the analytic solution for the Mott distribution of fragment lengths

In summary, the statistics-based theory of dynamic fragmentation developed in the seminal study of Mott provides a physically plausible and intellectually satisfying description of the fragmentation process. Within the one-dimensional model of the Mott cylinder the theory is fully predictive, providing the average fragment size and the distribution about the average, as well as the statistical temporal history of fracture and the strain-to-fracture.

5.2 Energy-Based Fragmentation

A theory of dynamic fragmentation based on markedly different initial assumptions has also been pursued [Grady et al., 1984; Kipp and Grady, 1985]. Again, the one-dimensional fracture and fragmentation on the Mott cylinder in Fig. 5.1 provides the model for consideration of the theory in the present context. The fundamental difference in the two theories is that Mott assumed energy dissipated in the fracture process was not of concern, and that fracture at a site on the cylinder would be effectively instantaneous. In contrast, energy dissipation and an associated fracture delay time lies at the heart of the energy-based fragmentation theory.

5.2.1 Fracture Calculation

Formulation of the energy-based fragmentation theory on the expanding ductile Mott cylinder proceeds by extending the stress release analysis developed by Mott to calculate the time history of plastic release waves (Mott waves) emanating from sites of fracture. The extension of the analysis has been pursued in Chaps. 3 and 4, and proceeds by considering, rather than instantaneous fracture, a fracture resistance which reduces from the flow stress Y to zero as a crack-opening-displacement parameter y goes from zero to some critical crack opening displacement y_c. An assumption of linear reduction of the fracture resistance then leads to a fracture energy dissipation $\Gamma = Y y_c/2$. The assumption of other functional forms for the reduction of fracture resistance (Chap. 4) does not markedly alter the value of Γ. Momentum balance for the rigid ideally plastic problem leads to the following differential expression for the position x of the Mott release wave [Kipp and Grady, 1985],

$$\rho\dot{\varepsilon}x\frac{dx}{dt} = \frac{Y^2}{2\Gamma}y \ , \tag{5.10}$$

while motion of the crack opening displacement gives,

$$\frac{dy}{dt} = \dot{\varepsilon}x \ . \tag{5.11}$$

The coupled equations are readily solved yielding,

$$x(t) = \frac{1}{12}\frac{Y^2}{\rho\Gamma}t^2 \ , \tag{5.12}$$

for the motion of the Mott release wave while crack opening over $0 \leq y \leq y_c$ is given by,

$$y(t) = \frac{1}{36}\frac{\dot{\varepsilon}Y^2}{\rho\Gamma}t^3 \ . \tag{5.13}$$

The time to fracture is determined by the time for the crack opening displacement to achieve y_c and is calculated to be,

$$t_c = \left(\frac{72\rho\Gamma^2}{Y^3\dot{\varepsilon}}\right)^{1/3} \ . \tag{5.14}$$

Over the time t_c the Mott release wave travels a distance from the site of fracture,

$$x_c = \left(\frac{3\Gamma}{\rho\dot{\varepsilon}^2}\right)^{1/3} \ . \tag{5.15}$$

5.2.2 Fragment Size and Fragmentation Toughness

The distance x_c over which the Mott release wave propagates determines the minimum spacing of separate fractures permitting fracture completion without interaction of release waves. The theory assumes that the nominal fragment length x_o is given by twice the distance x_c or,

$$x_o = 2x_c = \left(\frac{24\Gamma}{\rho\dot{\varepsilon}^2}\right)^{1/3} . \tag{5.16}$$

The fracture resistance Γ is considered to be a property of the material characterizing the dissipation in the fracture growth process. It is possible, under certain failure modes, to estimate the fracture resistance Γ from other material properties [Kipp and Grady, 1985]. Fracture toughness is the property commonly used to quantify the static (and dynamic) fracture resistance of metals. Thus, it is sensible in the present development to define a property with the dimensions of fracture toughness through the relation of linear elastic fracture mechanics relating fracture strain energy release and fracture toughness. Namely,

$$K_f = \sqrt{2E\Gamma} , \tag{5.17}$$

where E is the elastic modulus. The property K_f will be identified as the fragmentation toughness of the metal and will not presume any relationship to the clearly defined static fracture toughness K_c. Frequently, however, K_c is found to provide a very adequate first order estimate for the fragmentation toughness as will be shown in later chapters. The expression for the characteristic fracture spacing from (5.16) then becomes,

$$x_o = \left(\frac{\sqrt{12}K_f}{\rho c\dot{\varepsilon}}\right)^{2/3} . \tag{5.18}$$

The energy-based theory does not address the issue of the statistical distribution of fragment sizes. It is assumed that (5.18) provides an average fragment size and that the fragment number per unit length is provided by the inverse of (5.18), or,

$$N = \left(\frac{\rho c\dot{\varepsilon}}{\sqrt{12}K_f}\right)^{2/3} . \tag{5.19}$$

Thus, (5.19) provides the energy-based spatial fracture frequency prediction to be compared with (5.7) of the Mott statistical theory.

5.3 Comparisons of the Fragmentation Theories with Experiment

A range of diverse experimental fragmentation investigations could be used, and in fact has been used, to explore the predictive abilities of Mott's

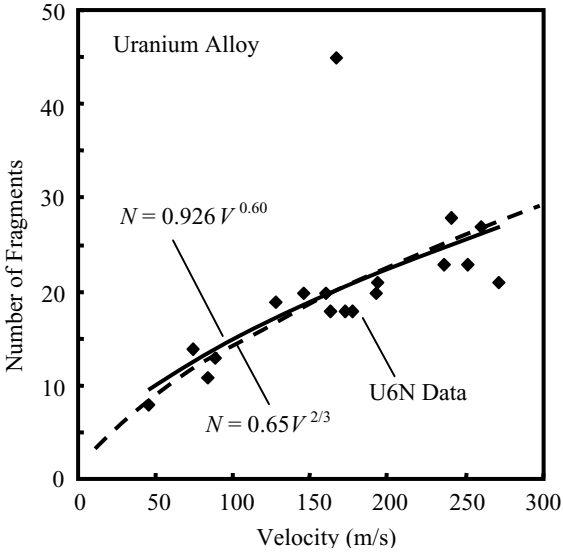

Fig. 5.3. Fragment number versus expansion velocity at fracture for U6Nb expanding ring fragmentation tests

statistics-based theory and the more recent energy-based fragmentation theory. Here, consideration will be restricted to a recent quite-thorough study of dynamic fragmentation of magnetically driven uranium-6%-niobium (U6Nb) metal rings with pertinent experimental data shown in Figs. 5.3 and 5.4. Further details on the experimental test method are provided in a later chapter. The experimental geometry nicely replicates the fragmentation model assumed by Mott and provides data directly comparable with the theoretical predictions.

5.3.1 Experimental Fragmentation Results

In the selected study U6Nb metal rings approximately 30 mm in diameter and with a 0.75 mm square cross section were accelerated by a pulsed magnetic field to radial velocities in the range of 50–300 m/s. Actual acceleration is provided by an aluminum pusher ring which accommodates most of the induced electric current. The aluminum ring is arrested prior to fragmentation allowing free flight of the U6Nb ring preceding break up. Additional details are provided in Chap. 8.

Radial velocity history of the U6Nb rings was measured with time-resolved velocity interferometry or VISAR [Barker and Hollenbach, 1972]. Measured deceleration of the freely expanding ring prior to fragmentation was used to calculate a tensile flow stress of nominally one GPa for the selected heat treated material. Fragmentation for the corresponding material occurred at an expansion of approximately 30%.

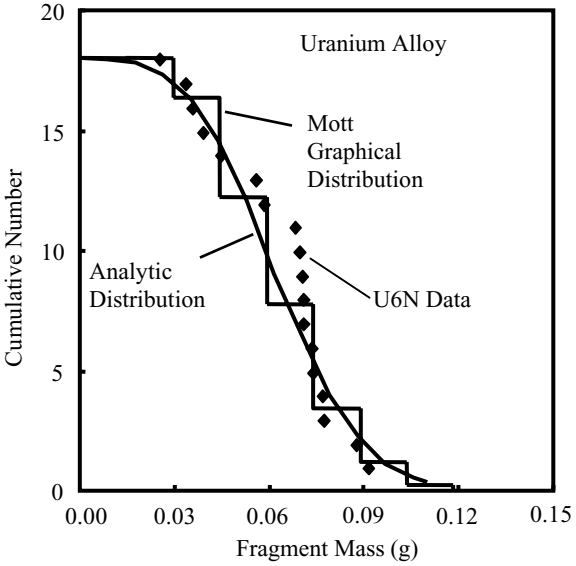

Fig. 5.4. Comparison of cumulative fragment distribution for one representative U6Nb expanding ring fragmentation test with the theoretical Mott fragment size distribution

In each test the number of fragments produced (equivalently, the number of fractures) was determined. Fragment number versus the expansion velocity at fragmentation are shown for the series of U6Nb expanding ring experiments in Fig. 5.3. The anomalous point high on the graph is the consequence of one test on a markedly differently heat treated U6Nb sample (discussed further in Chap. 8). A least squares fit, excluding the one anomalous point, provided the power law representation of the data shown in Fig. 5.3. In one representative test each fragment was separately weighed and the complementary cumulative fragment size distribution shown in Fig. 5.4 was obtained.

5.3.2 Comparison with the Mott Statistics-Based Theory

Weibull parameters σ and n are necessary in the Mott statistical theory to predict the fragment number dependence on velocity (or strain rate) and are not available for the U6Nb material tested. Hence, only sensibility of the experimental results can be examined. The observed experimental power law dependence of fragment number on expansion velocity is close to two-thirds and indicates that the Weibull parameter n in (5.7) is very close to unity. Assuming that $n = 1$, the second Weibull parameter is calculated to be $\sigma = 7.7 \times 10^{-5}$m. The standard deviation in strain to fracture calculated from (5.1) is approximately σ/L. Considering specimens of length one centimeter, the nominal length of fragments in the ring tests, a scatter in strain to fracture

of approximately 0.01 or about 3% of the observed 0.30 strain to fracture is calculated. Thus, the Weibull parameters within the Mott statistical theory for the fragmentation of U6Nb rings are quite plausible.

Prediction of the distribution in fracture spacing is also a facet of Mott's statistical theory. Comparison of both the graphic distribution generated by Mott and the analytic distribution from (5.9), both displayed in Fig. 5.2, are compared with the distribution determined experimentally in Fig. 5.4. The observed distribution and the theoretical distributions based on the Mott statistical fracture theory are also in reasonable accord.

5.3.3 Comparison with the Energy-Based Theory

The energy-based fragmentation theory directly predicts from (5.19) a two-thirds power dependence of fragment number on strain rate or, equivalently, the expansion velocity at fracture. A two-thirds power dependence curve is compared with the data and the experimental fit in Fig. 5.3 and shows sensible agreement with the data.

To further test the energy-based theory the fragmentation toughness is calculated through (5.19) for each experiment. This representation is shown in Fig. 5.5. A value of K_f in excess of $60\,\mathrm{MPa{\cdot}m^{1/2}}$ determined from the fragmentation data is remarkably close to a static fracture toughness of approximately 90–110 $\mathrm{MPa{\cdot}m^{1/2}}$ measured on similar U6Nb alloys.

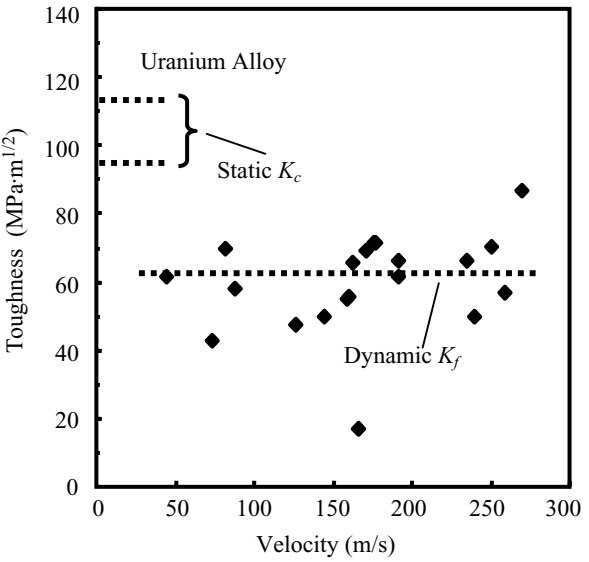

Fig. 5.5. Dynamic fragmentation toughness calculated through theoretical relation relating fragment number, expansion rate and material toughness. Comparison with static toughness data for U6Nb

Other features observed in the U6Nb ring fragmentation experiments also attest to the importance of energy dissipation and finite fracture time in the dynamic fracture process. Inspection of fragments revealed fully developed necking regions – a signature of fractures which were enveloped with tensile release (Mott) waves and fracture growth arrested before full fracture and separation was achieved.

5.3.4 Comments on the Mott Fracture Frequency Function

In the development of the Mott statistical fragmentation theory a statistical fracture frequency function was required. Mott discussed two very viable functional forms; the power law,

$$\lambda(\varepsilon) = \frac{n}{\sigma}\left(\frac{\varepsilon}{\sigma}\right)^{n-1} , \tag{5.20}$$

and the exponential law,

$$\lambda(\varepsilon) = Ae^{\gamma\varepsilon} . \tag{5.21}$$

The latter equation, written in a more common statistical form is,

$$\lambda\left(\varepsilon\right) = \frac{1}{\sigma}e^{(\varepsilon-\mu)/\sigma} , \tag{5.22}$$

where the correspondence to the Mott parameters, introduced in Chap. 3, $\sigma = 1/\gamma$ and $A = (1/\sigma)\exp(-\mu/\sigma)$, is made.

The power law leads to the Weibull extreme value cumulative probability of fracture function,

$$F\left(\varepsilon\right) = 1 - e^{-(\varepsilon/\sigma)^n} , \tag{5.23}$$

and probability density function,

$$f\left(\varepsilon\right) = \frac{n}{\sigma}\left(\frac{\varepsilon}{\sigma}\right)^{n-1} e^{-(\varepsilon/\sigma)^n} . \tag{5.24}$$

Correspondingly, the exponential law,

$$\lambda\left(\varepsilon\right) = \frac{1}{\sigma}e^{(\varepsilon-\mu)/\sigma}, \tag{5.25}$$

provides a Gumbel cumulative probability,

$$F(\varepsilon) = 1 - \exp\left(-e^{(1/\sigma)(\varepsilon-\mu)}\right) , \tag{5.26}$$

and probability density function,

$$f\left(\varepsilon\right) = \frac{1}{\sigma}\exp\left(\frac{1}{\sigma}\left(\varepsilon-\mu\right) - e^{(1/\sigma)(\varepsilon-\mu)}\right) . \tag{5.27}$$

Although, both extreme value representations of the statistical fracture frequency have two parameters, they are far from equivalent. The parameter σ in both is the distribution scale parameter. The Weibull representation also has a distribution shape parameter n, whereas the Gumbel distribution, in contrast, is lacking a shape parameter, but specifies instead the distribution location parameter μ. The Mott fragment number prediction based on a Gumbel fracture frequency representation is,

$$N = \frac{1}{\sqrt{\pi}} \sqrt{\frac{\rho \dot{\varepsilon}^2}{2Y\sigma}} \, . \tag{5.28}$$

The location parameter μ plays no role in the fragment number prediction either in terms of the fragment length scale or in the strain rate dependence. The parameter μ does govern the strain to fracture, however.

The fragment number prediction based on a Weibull representation is,

$$N = \beta_n \left(\frac{\rho \dot{\varepsilon}^2}{2\pi Y} \frac{n}{\sigma} \right)^{n/(2n+1)} , \tag{5.29}$$

and it is observed that the fragment number depends on both the distribution scale and shape parameter.

A location parameter could also be included in the power law fracture frequency and Weibull fracture probability by the replacement $\varepsilon \rightarrow \varepsilon - \mu$. The resulting distribution would then be a three parameter representation. Again, however, the location parameter would control only the strain to fracture and would not influence either the fragment length scale or the strain rate dependence. Equation (5.29) would remain the same.

As the shape parameter n in the Weibull distribution becomes large, the character of the two extreme value distributions becomes similar. The fragment number becomes dependent on the strain rate to the first power in both cases and the fragment size scale is determined solely by the distribution standard deviation (proportional to σ in both cases). As the standard deviation approaches zero both density distributions uniformly converge to a Dirac delta function.

Experimental data, however, suggest a two-thirds power strain rate dependence of fragment number in some cases (although not all). The U6Nb fragmenting ring data discussed here, for example, certainly supports such strain rate dependence. The Weibull fracture frequency representation (with shape parameter $n = 1$) supports this experimental observation. The Gumbel distribution does not.

5.4 Statistical and Energy-Based Theory of Fragmentation

Both Mott's statistical theory and the energy-based theory have features in accord with the results of the U6Nb expanding ring fragmentation experiments.

Frequency, and in particular, the statistical spread in spacing of fractures are consistent with predictions of the Mott theory. The favorable strain rate dependence and the very close agreement between static fracture toughness and the inferred dynamic toughness are, on the other hand, supportive of the energy-based theory. It would seem that a broader theory encompassing concepts from both the statistics-based and the energy-based approaches would be appropriate.

5.4.1 Merging of Theories

The statistical fragmentation theory of Mott is based on two functional properties characterizing response of the material in a dynamic fragmentation event. First, is a strain-dependent fracture activation function $\lambda(\varepsilon)$, which has been selected here as the power law form,

$$\lambda(\varepsilon) = \frac{n}{\sigma}\left(\frac{\varepsilon}{\sigma}\right)^{n-1} . \tag{5.30}$$

Second, is the diffusion-governed tensile stress release propagation function from sites of fracture,

$$g(\varepsilon) = \sqrt{\frac{2Y}{\rho\dot{\varepsilon}^2}\varepsilon} . \tag{5.31}$$

Together the Mott theory yields the spatial fracture frequency from (5.7),

$$N = \beta_n \left(\frac{\rho\dot{\varepsilon}^2}{2\pi Y}\frac{n}{\sigma}\right)^{n/(2n+1)} . \tag{5.32}$$

In contrast, the energy-based theory yields for the average spatial fracture frequency,

$$N = \left(\frac{\rho\dot{\varepsilon}^2}{24\Gamma}\right)^{1/3} . \tag{5.33}$$

The theories are equivalent, if the Weibull constants have the unique values,

$$n = 1 , \tag{5.34}$$

and,

$$\sigma = \beta_1^3 \frac{12}{\pi}\frac{\Gamma}{Y} \cong 5\frac{\Gamma}{Y} . \tag{5.35}$$

Thus, the requisites of the energy theory would uniquely constrain the Weibull parameters and the functional form of the fracture activation function of Mott's statistical theory. Equation (5.35) identifies a material-specific length scale σ and requires, through (5.30), that the fracture activation function be constrained to a constant $\lambda(\varepsilon) = \lambda_o = \sigma^{-1}$.

The fracture activation functions proposed by Mott, and as constrained by the energy theory, are illustrated in Figs. 5.6 and 5.7. The function $\lambda(\varepsilon)$ in

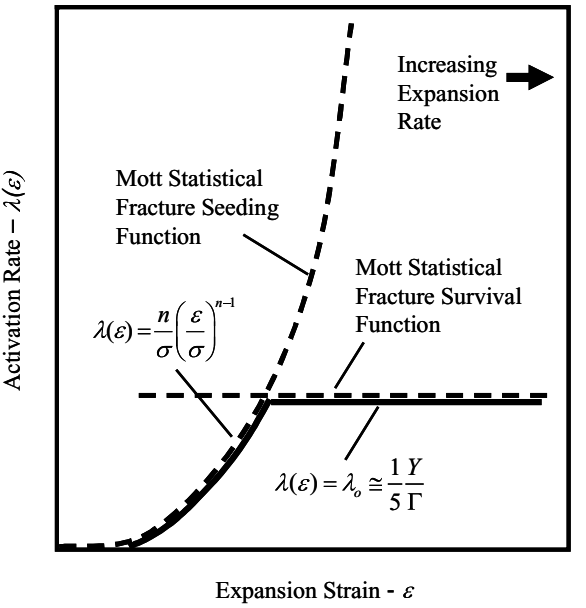

Fig. 5.6. Graphical interpretation of fracture functions in the merging of Mott statistics-based and energy-based fragmentation theories

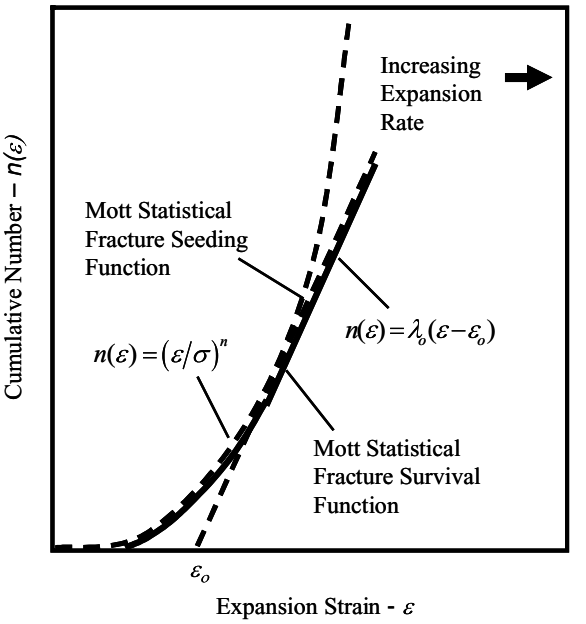

Fig. 5.7. Cumulative fracture seeding and survival functions in statistical energy-based theory of fragmentation

Fig. 5.6 specifies fracture activation frequency as increasing plastic strain ε is achieved. Thus, increasing expansion rates are required to achieve increasing levels of strain to fracture. Below the strain at which the two functions cross in Fig. 5.6, the lower rate of fracture activation is provided by the rapidly increasing power-law expression for $\lambda(\varepsilon)$. Above the cross-over strain the constant expression for $\lambda(\varepsilon) = \lambda_o$, inferred from energy considerations, provides the lesser rate of fracture activation.

From the Mott statistical development outlined earlier, the cumulative strain to fracture is calculated from the expression,

$$\varepsilon_f = \int_0^\infty (1 - D) d\eta \, . \tag{5.36}$$

It is readily shown that the cumulative strain to fracture is $\varepsilon_f = \alpha_n \dot{\varepsilon}^{2/(2n+1)}$ where α_n is a constant function of the material properties. The strain ε_f increases with the expansion rate $\dot{\varepsilon}$. Thus, the comparison indicates that, with increasing expansion rate, a strain to fracture which exceeds the cross-over strain is eventually achieved. Fragmentation and the frequency of fractures become governed by fracture energy dissipation properties above the cross-over strain.

This observation suggests a reinterpretation of the fracture activation functions. The rapidly increasing Mott power law function would, more appropriately, be the fracture seeding function. This function characterizes the perturbations and defects in the body leading to fracture (the seeds of fracture), but does not necessarily specify the fracture activation process itself. Above the cross-over strain the constant energy-based function provides the fracture survival rate. Below the cross-over strain the fracture seeding function limits the fracture activation and there is a one-to-one correspondence between fractures seeded and fractures that survive. Above the cross-over strain, however, many fractures are initiated, but energy requirements limit fracture survival and only a subset of fractures seeded achieve completion.

5.4.2 Strain to Fracture

In the statistical theory of Mott, both strain to fracture and fracture frequency are uniquely determined through the parameters σ and n in the power-law fracture activation function. The theory of Mott, however, cannot also account for the two-thirds power dependence of the average fragment number on strain rate predicted by the energy-based theory, and also observed in the U6Nb expanding ring experiments.

With the extended statistical energy-based theory, strain to fracture in addition to the statistical fragment size and strain-rate dependence features can be accounted for. Prediction is dependent on proper selection of the Mott fracture seeding function,

$$\lambda(\varepsilon) = \frac{n}{\sigma}\left(\frac{\varepsilon}{\sigma}\right)^{n-1} , \tag{5.37}$$

and the energy governed fracture survival function,

$$\lambda(\varepsilon) = \lambda_o , \tag{5.38}$$

where, λ_o has the unique material dependence specified in (5.35). The cumulative number $n(\varepsilon)$, or integral of the fracture seeding and fracture survival functions (the integral of (5.37) and (5.38)), are plotted in Fig. 5.7 (compare with Fig. 5.6). The new parameter revealed in Fig. 5.7 is the constant of integration ε_o of the fracture survival function. The Mott fracture function is determined by the solid segments of both of the functions shown in Fig. 5.7.

The theory has acquired an additional material parameter, but now supports the prediction of strain to fracture in addition to the statistical fracture frequency, spacing distribution, and associated strain-rate dependence. At fracture strain rates into the energy-governed fragmentation regime it is readily shown that the statistical strain to fracture from (5.36) is,

$$\varepsilon_f = \varepsilon_o + \alpha_1 \dot{\varepsilon}^{2/3} , \tag{5.39}$$

where, α_1 is calculated through (5.36) from the energy-based Mott fracture properties. Experimental support for a strain rate dependence of the strain to fracture is presented in Chap. 8.

This broader interpretation of fragmentation merges both the statistical principals of Mott and the fracture energy requirements of the energy-based theory. A wider set of properties characterizing the solid body of interest is required, however. The Mott seeding function characterizes the defect state of the body governing the strain-dependent nucleation of potential fractures. Weibull parameters in the two-parameter power law function serve this purpose in the present development. The Mott survival function incorporates the energy dissipation, or fragmentation toughness, properties of the material. Further material properties and supporting theory are needed to establish onset of the strain to fracture.

5.5 Computational Simulations of Ring Fragmentation

Partial support for the extended theory is provided by a one-dimensional computational simulation of the Mott fragmentation process performed by Kipp and Grady (1986). At that time it was recognized that interplay between dynamics of the fragmentation event and the population of flaws seeding the multiple fracture process could lead to conditions in which flaw structure controlled the extent of fragmentation on one hand while energy limitations controlled fragmentation on the other. A rationale for analytically merging the range of behaviors was not recognized, however.

The following computer simulations of dynamic fragmentation were performed to support experimental fragmenting ring studies performed at that time [Grady et al., 1984]. A one-dimensional finite difference wave code was used to calculate the response of an aluminum rod or wire 0.1 m in length and 1.0 mm in diameter stretching plastically at a flow stress $Y = 100$ MPa and at a uniform stretching rate $\dot{\varepsilon} = 10^4/\text{s}$. Fracture sites were introduced randomly in time according to a constant nucleation rate parameter $\lambda(\varepsilon) = \lambda_o$, and randomly placed within the length of the rod. The nucleation rate λ_o was the only parameter varied over the series of calculations. When fracture was nucleated at a computational cell, stress in that cell was relaxed from the flow stress Y to zero as the cell distended, such that the plastic fracture energy within that cell of $\Gamma = 20\,\text{kJ/m}^2$ was dissipated. The number of fragments produced as the nucleation rate λ_o was varied over approximately one order of magnitude was determined from the simulations and are shown in Fig. 5.8. Although, not directly duplicating the conditions of Fig. 5.7, the relationship is apparent.

At reduced nucleation rates every fracture nucleation site grows to full fracture. The number of fractures and the corresponding characteristic fragment size is, thus, governed fully by the flaw structure and the fracture nucleation (seeding) function. As the nucleation rate is increased the number of nucleated fracture sites which fail to grow to completion correspondingly increases. At

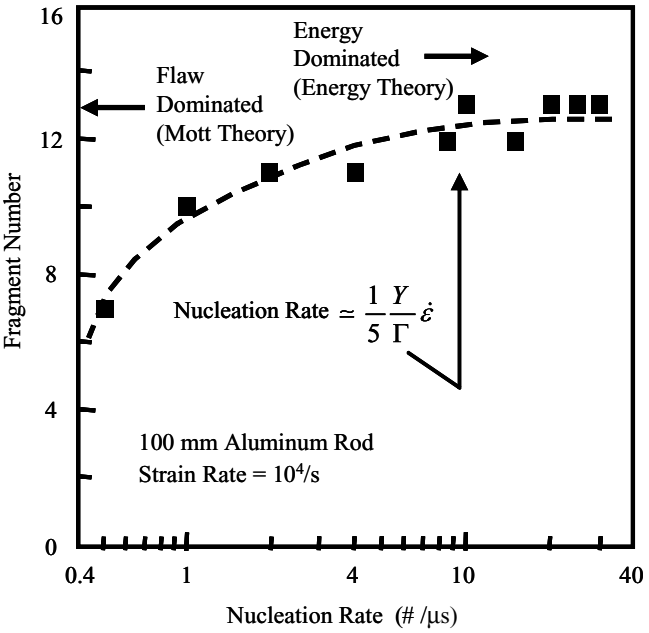

Fig. 5.8. Fragment number from computational simulations of a uniformly stretching aluminum rod [Kipp and Grady, 1986]

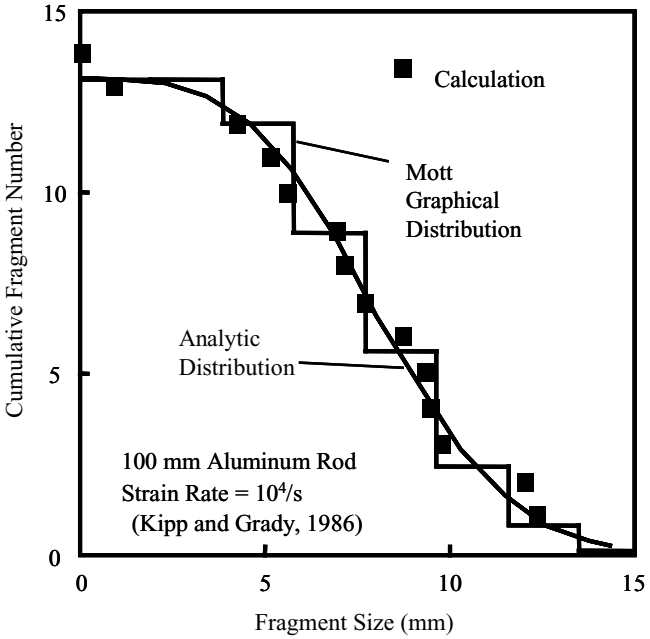

Fig. 5.9. Fragment distribution from computational simulation and comparisons with Mott statistical fragmentation theory

the highest nucleation rates the number of fragments becomes independent of the number of fracture sites nucleated and is determined strictly by the fracture energy Γ resisting fracture growth. The energy governed constant fracture survival rate, $\lambda_o \cong Y\dot{\varepsilon}/5\Gamma$, identified in Fig. 5.8, is sensibly consistent with the expected transition from flaw limited to energy-limited fragmentation.

A cumulative fragment length distribution from one computational simulation is compared with the predicted graphic and analytic Mott distribution in Fig. 5.9. The computational distribution is also fully consistent with the statistical theory.

5.6 Fracture Physics

Of the properties required to characterize the fragmentation response of an expanding metal cylinder, the fracture energy captured through the property Γ is probably the most apparent. That some degree of work must be expended, and some fracture energy overcome, in opening the cracks delineating the fragment boundaries produced in the fragmentation event is inherently reasonable. Less apparent are details of the deformation mechanisms occurring in the fracture growth and dissipation process. Plastic necking, adiabatic

shearing, and ductile fracture are all viable mechanisms. It is likely that all of the above mentioned mechanisms will contribute to some degree.

Considerably less intuitive are the material features responsible for onset of fracture; analytically expressed in this development by the Mott seeding function and quantified by the Weibull parameters in the power-law hazard function. In most events leading to the dynamic expansion and fragmentation of ductile metal rings and shells a degree of stable plastic stretching is accommodated before the fracture occurs. This deformation is most likely a consequence of stabilizing plastic hardening of the component metal. As plastic hardening saturates, however, continued stretching and thinning becomes inherently unstable and susceptible to perturbations in the deformation. Sources of these perturbations are far from certain. Granularity of the device metal is a reasonable source of deformation perturbations. Perturbations from metal granularity leading to fracture would suggest sensitivity of the fragmentation process (particularly the effective strain to fracture) to grain size and related material issues.

There are also convincing indications that surface features, either inherent or induced, play a role in the perturbations seeding fracture onset. Imperfections in metal-explosive interfaces leading to deformation perturbation as detonation-induced shock waves are coupled into the metal system are also suspect.

References

Barker, L. M. and Hollenbach, R. E. (1972), Velocity Interferometer for Measuring the Velocity of any Reflecting Surface, *J. Appl. Phys.*, 43, 4669–4680.

Grady, D. E. and Olsen, M. L. (2003), A Statistical and Energy Based Theory of Dynamic Fragmentation, *Int. J. Eng. Mech.*, 29, 293–306.

Grady, D. E., Kipp, M. E., and Benson, D. A. (1984), Energy and Statistical Effects in the Dynamic Fragmentation of Metal Rings, *Proceedings of the Conference of the Mechanical Properties of High Rates of Strain*, Oxford, 1984, Inst. Phys. Conf. Ser. No. 70, 315–320.

Hahn, G. J. and Shapiro, S. S. (1967), *Statistical Models in Engineering*, John Wiley & Sons, New York.

Johnson, W. A. and Mehl, R. F. (1939), Reaction Kinetics in Processes of Nucleation and Growth, *Trans. AIMME*, 135, 414–458.

Kipp, M. E. and Grady, D. E. (1985), Dynamic Fracture Growth and Interaction in One Dimension, *J. Mech. Phys. Solids* 33 (4), 399–415.

Kipp, M. E. and Grady, D. E. (1986), Random Flaw Nucleation and Interaction in One Dimension, *in Metallurgical Applications of Shock-Wave and High-Strain-Rate Phenomena*, L.E. Murr, K.P. Staudhammer, and M.A. Meyers, eds., Marcel Dekker, Inc., 781–791.

Mott, N. F. (1943), A Theory of the Fragmentation of Shells and Bombs, *Ministry of Supply* AC4035, May.

Mott, N. F. (1947), Fragmentation of Shell Cases, *Proc. Royal Soc.*, A189, 300–308, January.

6

Application to the Biaxial Fragmentation of Shells

Much of the development of a statistical energy-based theory of fragmentation of stretching ductile metals has been restricted to one-dimensional geometries such as expanding rings or, at best, a uniformly expanding cylinder where the theory is intended to describe the average and statistical spacing of axial fractures. In this chapter an analysis will be extended to describe the breakup of a biaxial expanding shell or membrane of ductile metal in which stretching rates in mutually orthogonal directions are each nonzero and are, in general, different. A specific case of interest, of course, is that of a stretching spherical shell segment in which the orthogonal stretching rates are the same.

In the development of the present two-dimensional fragmentation theory it will be assumed that at a point on the surface of the expanding shell orthogonal principal stretching directions can be determined and that fracture in the two principle directions are independent and governed by the conditions of the linear fragmentation theory developed in the earlier sections. This approach is illustrated in Fig. 6.1, where principal stretching directions on a surface are identified and a corresponding statistical distribution of fractures along the x and y stretching directions partition the surface into a statistical distribution of fragment areas.

6.1 The Fragment Size and Aspect Ratio Scales

Within the energy governed region of the linear statistical fragmentation theory a fracture activation rate, and a corresponding fracture spacing length scale, has been determined in the previous chapter based on a property of the material identified as the fragmentation toughness and the rate of stretching leading to fracture. The same relation will be used to determine the fracture spacing length scale in both orthogonal principal stretching directions. Namely,

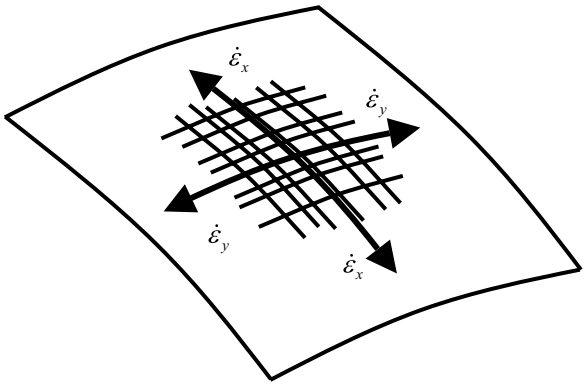

Fig. 6.1. Illustrates independent application of linear statistical fragmentation theory in orthogonal principal stretching directions to implement fragmentation of the surface at a point

$$x_o = \left(\frac{\sqrt{12} K_f}{\rho c \dot{\varepsilon}_x} \right)^{2/3} , \tag{6.1}$$

and,

$$y_o = \left(\frac{\sqrt{12} K_f}{\rho c \dot{\varepsilon}_y} \right)^{2/3} . \tag{6.2}$$

The fragment area scale is then determined from,

$$a_o = x_o y_o = \left(\frac{\sqrt{12} K_f}{\rho c \bar{\dot{\varepsilon}}} \right)^{4/3} , \tag{6.3}$$

where,

$$\bar{\dot{\varepsilon}} = \sqrt{\dot{\varepsilon}_x \dot{\varepsilon}_y} \, . \tag{6.4}$$

The nominal fragment aspect ratio is provided by,

$$r_o = x_o / y_o = \left(\dot{\varepsilon}_x / \dot{\varepsilon}_y \right)^{-2/3} . \tag{6.5}$$

Predictions of the fragment area scale based on (6.3) as a function of the stretching rate are shown in Fig. 6.2. The predicted curve is based on the equiaxial explosion driven expansion and fragmentation of a spherical shell segment of a common metal. The experimentally observed fracture fabric was in sensible qualitative and quantitative agreement with the predicted behavior. At typical stretching rates of a few times 10^3/s up to about 10^4/s for explosively loaded metal shells a fragment size scale on the order of a square centimeter or less, is predicted consistent with experimental observation. Increasing strain rate decreases this size scale. Increased toughness, on the other hand, is predicted to increase fragment size.

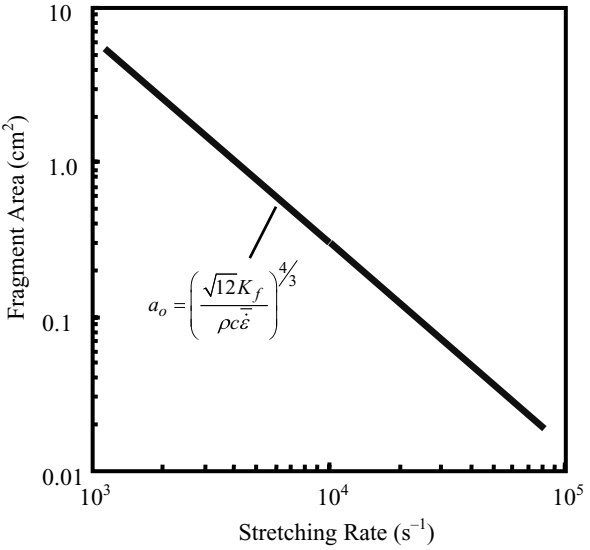

Fig. 6.2. Fragment area scale versus mean stretching rate based on energy determined characteristic fracture spacing and properties for equiaxial expansion of a metal

6.2 The Biaxial Fragment Distribution Properties

The dynamic fragmentation of a rapidly stretching metal shell involves a complexity of rapidly opening fissures and cracks that result in a multiplicity of separate fragments. Individual fragments continue on outward divergent paths at the velocity at which breakup occurred. Although the size scale determined previously adequately characterizes the number density and average size of these fragments, a statistical distribution in fragment size is clearly observed. The objective here will be to apply the linear statistical fragmentation theory to characterize the distribution in area fragment size observed experimentally.

In the linear theory, based on the Mott statistical premise, as constrained by the energy-based fracture spacing, a statistical distribution in fracture spacing was determined. The resulting distribution was found to satisfactorily describe linear fragmentation experiments such as the expanding ring studies. In the present development the assumption of independent statistical fracture in mutually orthogonal principal stretching directions is continued. The statistical size distribution to be pursued is as illustrated in Fig. 6.3. In either the x direction, or in the orthogonal y direction, the statistical spacing of fractures (lines) is governed by the linear Mott statistical distribution with independent length scales of x_o and y_o provided through (6.1) and (6.2), respectively. The statistical distribution in spacing in the x direction derived previously is,

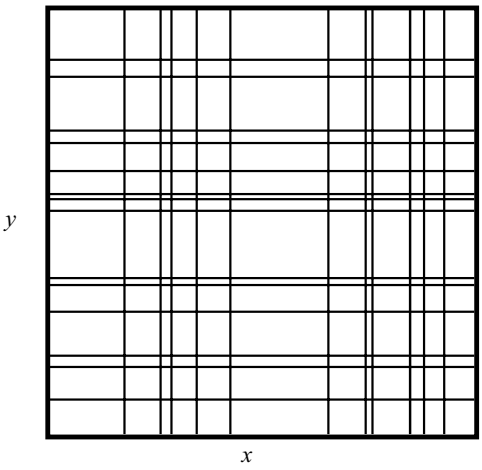

Fig. 6.3. Illustrates independent statistical distributions of fracture spacing in orthogonal x and y principal stretching directions. Areas determined by intersecting lines will model statistical distribution in fragment areas and fragment aspect rations

$$f\left(x\right) = \frac{\beta^2}{4}\frac{1}{x_o}\left(\frac{x}{x_o}\right)^3 e^{-\frac{1}{4}(x/x_o)^3}\int_0^1 \left(1-y^2\right) e^{-\frac{3}{4}(x/x_o)^3 y^2} dy \,, \tag{6.6}$$

where, $\beta = 3/\Gamma(2/3)$. An equivalent distribution applies to the spacing distribution in the y direction. With further analytic manipulation the integral in (6.6) can be expressed as an error function, if useful. The careful reader will note that the length scale x_0 in (6.6) is not precisely the expected value of the fragment size (see (3.121)). Uncertainties resulting from the assumptions leading to (6.1) and (6.2) provide allowance for this lack of rigor.

6.2.1 Fragment Area Distribution

The linear Mott distribution provided by (6.6) is not convenient for an analytic determination of the distribution in fragment areas provided by the overlap of horizontal and vertical lines as illustrated in Fig. 6.3. The approach pursued here will be to approximate the distribution from (6.6) with another more analytically tractable distribution. The distributions that will be tried are the Weibull distribution,

$$f(x) = \frac{n}{x_o}\left(\frac{x}{x_o}\right)^{n-1} e^{-(x/x_o)^n} \,, \tag{6.7}$$

and the gamma distribution,

$$f(x) = \frac{1}{x_o}\frac{n}{\Gamma(n)}\left(\frac{nx}{x_o}\right)^{n-1} e^{-nx/x_o} \,. \tag{6.8}$$

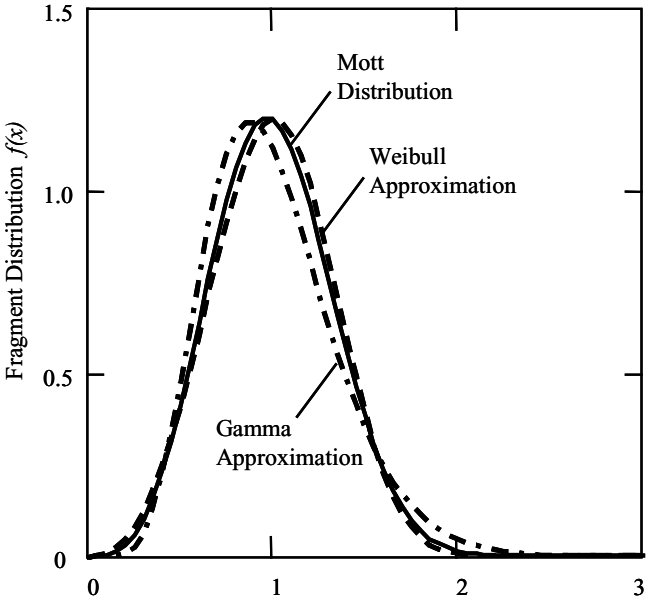

Fig. 6.4. Mott linear fragment size distribution compared with Weibull and Gamma distribution approximations

The Weibull and gamma distributions with the distribution parameter n adjusted to provide the optimum fit to the Mott distribution are compared with the Mott distribution from (6.6) in Fig. 6.4. Values of $n = 3.45$ for the Weibull distribution and $n = 8.0$ for the gamma distribution yielded the observed results. The Weibull distribution clearly provides the closer fit to the desired Mott distribution. Both Weibull and gamma distributions will be carried through the analysis in developing a fragment area distribution. Both are analytically tractable and both solutions provide a measure of sensitivity to the fit between the Mott distribution in (6.6) and either of the approximations in (6.7) and (6.8).

Working first with the Weibull distribution, an expression assessing the two-dimensional statistical partitioning of the surface in Fig. 6.3 is immediately written as a juxtaposition of (6.7) and the corresponding distribution in the y direction. Namely,

$$f(x,y) = \frac{n^2}{x_o y_o}\left(\frac{xy}{x_o y_o}\right)^{n-1} e^{-(x/x_o)^n} e^{-(y/y_o)^n} , \tag{6.9}$$

provides the probability density distribution for fragment areas of length x and width y. Equation (6.9) can be transformed to distribution over fragment area,

$$a = xy , \tag{6.10}$$

and aspect ratio,

$$r = x/y \; . \tag{6.11}$$

The differential invariant,

$$f(x,y)dxdy = g(a,r)\,dadr \; , \tag{6.12}$$

leads to,

$$dxdy = \left|\frac{\partial(x,y)}{\partial(a,r)}\right| dadr \; , \tag{6.13}$$

for the differential element through the transformation Jacobian [Buck, 1965]. Accordingly, the transformed probability density function is,

$$g(a,r) = f(x(a,r), y(a,r)) \left|\frac{\partial(x,y)}{\partial(a,r)}\right| \; . \tag{6.14}$$

Calculating the Jacobian through (6.10) and (6.11),

$$\left|\frac{\partial(x,y)}{\partial(a,r)}\right| = \frac{1}{2r} \; , \tag{6.15}$$

yields,

$$g(a,r) = \frac{1}{2}\frac{n^2}{(x_o y_o)^n}\frac{a^{n-1}}{r} e^{-\left(\frac{1}{x_o}\sqrt{ar}\right)^n} e^{-\left(\frac{1}{y_o}\sqrt{a/r}\right)^n} \; . \tag{6.16}$$

The distribution over fragment area is then written as the integral expression,

$$h(a) = \frac{n^2}{2a_o}\left(\frac{a}{a_o}\right)^{n-1} \int_0^\infty \frac{1}{r} e^{-\left(\sqrt{a/a_o}\right)^n \left[(r/r_o)^{n/2} + (r/r_o)^{-n/2}\right]} dr \; , \tag{6.17}$$

where, $a_o = x_o y_o$ and $r_o = x_o/y_o$. The substitution,

$$r = r_o e^{2\eta/n} \; , \tag{6.18}$$

provides,

$$h(a) = \frac{2n}{a_o}\left(\frac{a}{a_o}\right)^{n-1} \int_0^\infty e^{-2\left(\sqrt{a/a_o}\right)^n \cosh\eta} d\eta \; . \tag{6.19}$$

The integral is a modified Bessel function [Abramowitz and Stegun, 1954] yielding, for the area distribution, based on a Weibull approximation for the linear spacing distribution,

$$h(a) = \frac{2}{a_o}\left(\frac{a}{a_o}\right)^{n-1} K_o\left(2\left(\sqrt{a/a_o}\right)^n\right) \; . \tag{6.20}$$

A similar exercise using the gamma approximation provides,

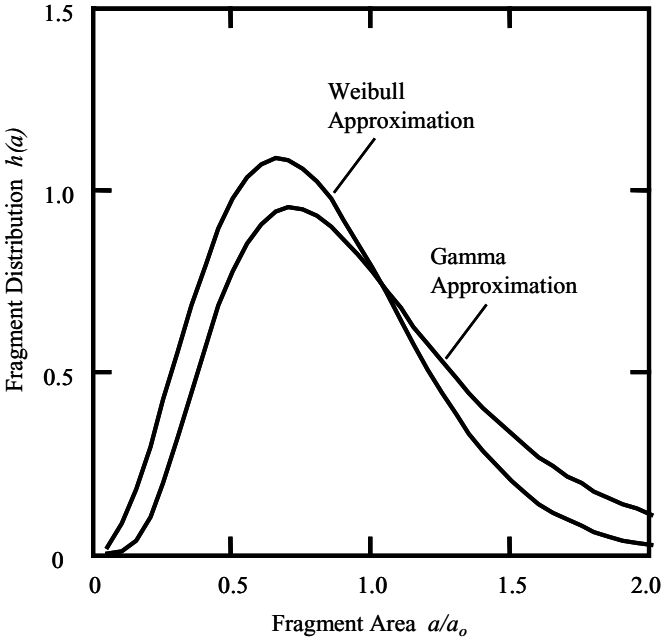

Fig. 6.5. Fragment area distributions base on Weibull and gamma distribution approximations to the Mott linear distribution

$$h(a) = \frac{2}{a_o}\left(\frac{n}{\Gamma(n)}\right)^2\left(\frac{n^2 a}{a_o}\right)^{n-1} K_o\left(2n\sqrt{a/a_o}\right) \ . \tag{6.21}$$

Area distributions resulting from the Weibull and the gamma distribution approximations to the linear Mott statistical fracture spacing distribution are shown in Fig. 6.5. The Weibull approximation provides a noticeably better fit to the linear distribution in Fig. 6.4 and is expected to provide the better representation of the area distribution based on the Mott theory.

Comparison of the Weibull approximation to the Mott area distribution based on random line partitioning of the area is compared with experimental results from the dynamic near-spherical expansion fragmentation of a metal shell in Fig. 6.6. The theoretical distribution reasonably represents the measured experimental distribution.

6.2.2 Fragment Linear Size Distribution

It is common in the experimental analysis and display of radiographic data of fragmentation of expanding metal surfaces to express the distribution in terms of a characteristic linear fragment size. For example, we will here identify the fragment size $s = a^{1/2}$, where a is the previous fragment area defined above.

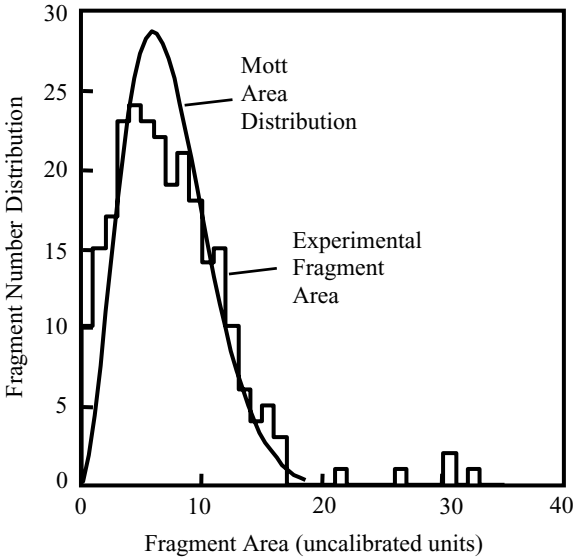

Fig. 6.6. A comparison of the theoretical distribution for fragment areas with experimental results

The statistical distribution in fragment size s is a straightforward transformation of the area distributions provided above. For completeness the appropriate statistical size distributions and their pictorial representation will be provided here. The appropriate transformation for (6.20), based on the Weibull approximation to the linear Mott distribution, leads to,

$$h(s) = \frac{4n}{s_o}\left(\frac{s}{s_o}\right)^{2n-1} K_o\left(2(s/s_o)^n\right) \ , \tag{6.22}$$

for the statistical size distribution. In contrast, (6.21) based on the gamma approximation provides,

$$h(s) = \frac{4}{s_o}\left(\frac{n^n}{\Gamma(n)}\right)^2\left(\frac{s}{s_o}\right)^{2n-1} K_o\left(2n(s/s_o)\right) \ . \tag{6.23}$$

Both size distributions are shown and compared in Fig. 6.7.

6.2.3 Fragment Aspect Ratio Distribution

The analysis pursued here also lends itself to a sensible assessment of the statistical distribution in fragment aspect ratio. Working with the distribution provided by the Weibull representation of the Mott distribution as written in (6.16), substitute the parameters $r_o = x_o/y_o$, $\xi = a/a_o$ and $\rho = r/r_o$. Integration over the fragment area variable is then written,

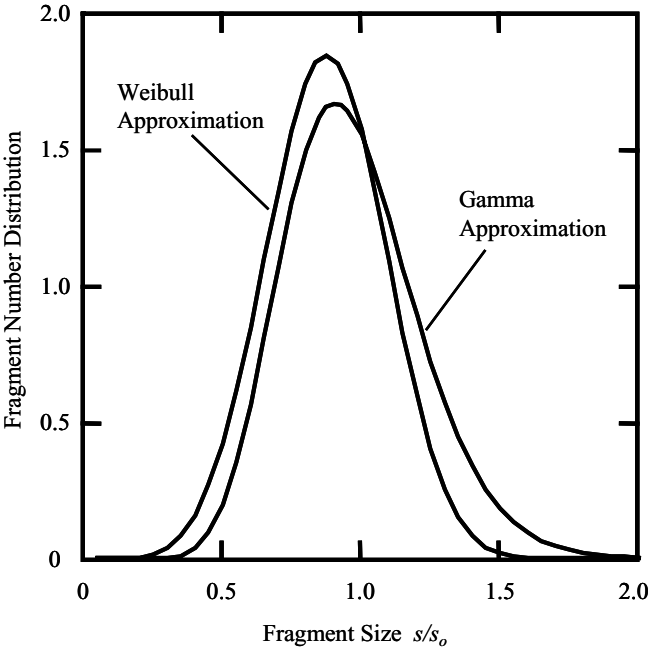

Fig. 6.7. Fragment size distributions base on Weibull and gamma distribution approximations to the Mott linear distribution

$$k(r) = \frac{1}{2}\frac{n^2}{r_o}\frac{1}{\rho}\int_0^\infty \xi^{n-1} e^{-(\rho^{n/2}+\rho^{-n/2})\xi^{n/2}} d\xi \ . \tag{6.24}$$

Equation (6.24) is readily integrated providing,

$$k(r) = \frac{n}{r_o}\frac{\rho^{n-1}}{(1+\rho^n)^2} \ . \tag{6.25}$$

The distribution over fragment aspect ratio with $n = 3.45$ is shown in Fig. 6.8. A similar distribution can be derived for the gamma distribution approximation to the Mott distribution.

6.3 Biaxial Strain to Failure Model

Neither the statistical fragmentation theory of Mott, nor the energy-based theory of fragmentation addresses the underlying deformation that a rapidly expanding metal shell can sustain before onset of fracture. Other physical considerations must be explored in pursuing a theory of the onset of fracture leading to the statistical fragmentation accompanying the disintegration of the expanding shell.

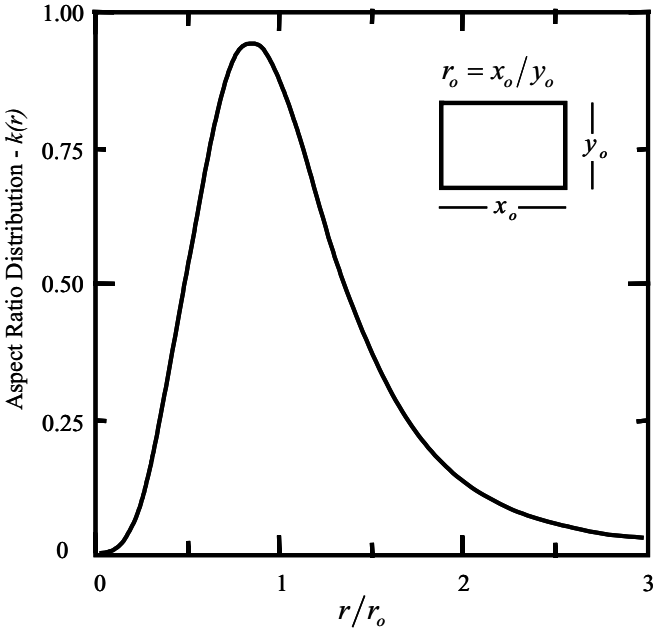

Fig. 6.8. Statistical distribution in fragment aspect ratio

As discussed earlier, Mott explored this issue on several levels. He pursued the ductile failure of steel tensile specimens in evaluating the critical gamma parameter in his relation for the prediction of fragment size. He also presaged the direction of much later work in forecasting the internal damage evolution through loss of cohesion in plastic straining metals and the dependence of this phenomenon on the local state of stress triaxiality.

The explosive impulsive load leads rapidly to the divergent plastic stretching and thinning of the metal shell. The onset of fracture is dependent on the thermo-plastic deformation properties and the geometry of the metal shell. The driving explosive pressure quickly diminishes to a negligible level and the outward divergent inertia of the body sustains the plastic deformation.

The latter comment, of course, introduces complicating considerations. The Gurney theory of explosive shell expansion [Gurney, 1943] assumes a sustained driving pressure reduced only by subsequent expansion of the accelerated shell. In energetic ideal explosives, however, much of the accelerating energy is imparted in the initial shock with rapid drop in the later driving pressure. Less ideal explosives, in contrast, will impart a larger fraction of the kinetic energy in late time push.

In any case both inertia and strain hardening of the plastic flow affect stability of the expanding and thinning shell. Sufficient inertia can lead to acceleration stresses which stabilize small perturbations in the thinning process [Romero 1991]. Inertial stabilization in this sense, however, does not appear

to play a significant role in governing the onset of fracture in the breakup of explosive driven shells.

Deformation hardening in the flow process appears paramount in stabilizing the plastic expansion and is the principal mechanism through which many materials sustain appreciable plastic deformation before rupture. The present dynamic expansion and rupture of metal shells have similarities to the extensive field of quasi-steady metal forming [e.g., Bartlat 1989]. The present application can be profitably studied through exploitation of this literature.

In essence plastic strain hardening stabilizes the thinning instabilities brought about by the reduction of in-plane tension caused by thinning of the stretching shell. While strain hardening dominates geometric softening (reduction in the tensile force due to the concomitant reduction in cross-sectional area), thinning through stable plastic expansion ensues. Saturation of strain hardening, however, ultimately leads to instability and rupture.

Plastic thinning instabilities are not unique to the dynamic environment. Within the physics introduced, namely rate independent strain hardening and geometric softening, the onset and subsequent growth of thinning instabilities would proceed the same on any time scale from static to rapid dynamic. Additional physical considerations markedly alter the dynamic event, however. These include the properties of material inertia and thermal conductivity in addition to rate sensitivity of the flow properties.

On the length scale of thinning instabilities, plastic dissipation in the dynamic event is effectively adiabatic. Plastic dissipation and the accompanying thermal softening will alter the effective stress versus strain behavior. Onset of instability would consequently occur earlier than in the corresponding static isothermal event. Adiabatic thermal softening would also localize the thinning instability growth process, markedly changing the character of the thinning and necking region. Unbounded thermal localization in the thinning region is constrained by local inertia, however.

The influence of adiabatic thermal softening on the onset of the tensile thinning instability is expected to be a second order effect. Thermal softening in the subsequent plastic flow during the growth of this instability under the appropriate loading conditions can profoundly alter the failure process, however. Along planes of maximum plastic shear (approximately 45 degrees with respect to the plane of the thinning shell) perturbations in the local temperature or deformation can lead to localized adiabatic shear deformation (adiabatic shear bands) within thin planar regions. Rupture of the expanding shell is then accommodated by the plastic shearing and separation of the body along the planes of adiabatic shear.

Adiabatic shear band failure, like fracture, is enhanced by inhomogeneities in the stress or deformation field. And also like fracture, adiabatic shear bands have a propensity for propagating from a site of initiation through the plane of shear rather than evolving homogeneously throughout that plane. Thus, shear bands depend sensitively on the nature of surface defects, which are the dominant source of stress and subsequent deformation inhomogeneity.

Thinning instability and adiabatic shear deformation can cooperate in a more complex serial failure process. Thinning instability can initiate when saturation of plastic strain hardening is overcome by the thinning geometric softening. Adiabatic deformation inhomogeneities brought about during growth of the thinning region can, in turn, trigger local adiabatic shear deformation and complete the failure process.

Plastic thinning instability and localization of adiabatic shear deformation are potential contributions to the processes of failure and rupture of dynamically expanding metal shells. Neither mechanism, however, is either complete, or necessary to the breakup process. Rupture ultimately requires the breaking of molecular bonds and the development of damage within the deforming material. In the fracture of metal this process has been shown to require a level of plastic deformation combined with a state of tensile stress triaxiality. This underlying physics has been noted from at least the early works of Mott [Mott, 1948] and has been addressed in considerable detail by later workers [e.g., Hancock and Mackenzie, 1976]. This feature of fracture is recognized, but will not be pursued in detail in the present development of a failure criterion.

6.3.1 Biaxial Strain Fracture Criterion

A theory and analytic model appropriate to the present dynamic fragmentation of biaxial expanding ductile shells is sought to predict the onset of fracture of a generally biaxial stretching sheet element of metal as illustrated in Fig. 6.9. Plastic stretching is brought about by an outward expansion velocity

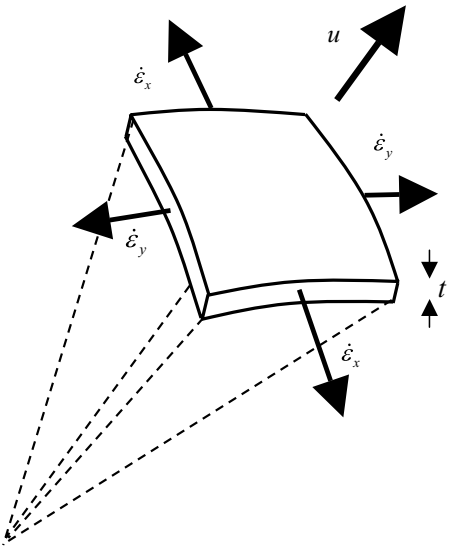

Fig. 6.9. Biaxial expanding element of metal plate with current thickness t due to imparted outward velocity u. Principal in-plane plastic stretching rates are identified

u imparted to the body. Current thickness of the element is t, while in-plane principal stretching rates are $\dot{\varepsilon}_x$ and $\dot{\varepsilon}_y$, respectively. Equivalent plastic strain rate in the element is provided through the relation,

$$\dot{\bar{\varepsilon}} = \sqrt{\frac{2}{9}\left[\left(\dot{\varepsilon}_x - \dot{\varepsilon}_y\right)^2 + \left(\dot{\varepsilon}_y - \dot{\varepsilon}_z\right)^2 + \left(\dot{\varepsilon}_z - \dot{\varepsilon}_x\right)^2\right]} \ . \tag{6.26}$$

Through-the-thickness stretching rate $\dot{\varepsilon}_z$ is related to the current thickness t of the element through the relation $\dot{\varepsilon}_z = \dot{t}/t$. The present problem is adequately addressed by considering motions characterized by the constant proportionality α of the in-plane stretching rates,

$$\alpha = \dot{\varepsilon}_y / \dot{\varepsilon}_x \ . \tag{6.27}$$

Special cases, of course, include spherical, or equiaxial, expansion ($\alpha = 1$), uniaxial cylindrical expansion ($\alpha = 0$), and the expanding ring ($\alpha = -1/2$).

Combining (6.26) and (6.27), along with the incompressibility condition,

$$\dot{\varepsilon}_x + \dot{\varepsilon}_y + \dot{\varepsilon}_z = 0 \ , \tag{6.28}$$

yields,

$$\dot{\bar{\varepsilon}} = -\sqrt{\frac{4}{3}\frac{(1 + \alpha + \alpha^2)}{(1+\alpha)^2}}\dot{\varepsilon}_z \ . \tag{6.29}$$

Equivalent plastic strain rates relative to the thinning rate and expansion rate as a function of α are illustrated in Fig. 6.10.

The plane stress ($\sigma_z = 0$), effective stress is provided by,

$$\bar{\sigma} = \sqrt{\sigma_x^2 + \sigma_y^2 - \sigma_x \sigma_y} \ , \tag{6.30}$$

where σ_x and σ_y are the in-plane principal stresses. In the present development stresses and strains are thickness averages through the sheet and only in-plane stresses are non-zero. For the corresponding proportional loading to the elastic limit,

$$\sigma_x = E\frac{1 + \alpha\nu}{1 - \nu^2}\varepsilon_x \ , \tag{6.31}$$

$$\sigma_y = E\frac{\alpha + \nu}{1 - \nu^2}\varepsilon_x \ , \tag{6.32}$$

where E is Young's modulus and ν is Poisson's ratio. The stress ratio is then,

$$\frac{\sigma_y}{\sigma_x} = \frac{\alpha + \nu}{1 + \alpha\nu} \ . \tag{6.33}$$

For a von Mises yield condition,

$$\sigma_x = \frac{Y}{\sqrt{1 - \beta + \beta^2}} \ , \tag{6.34}$$

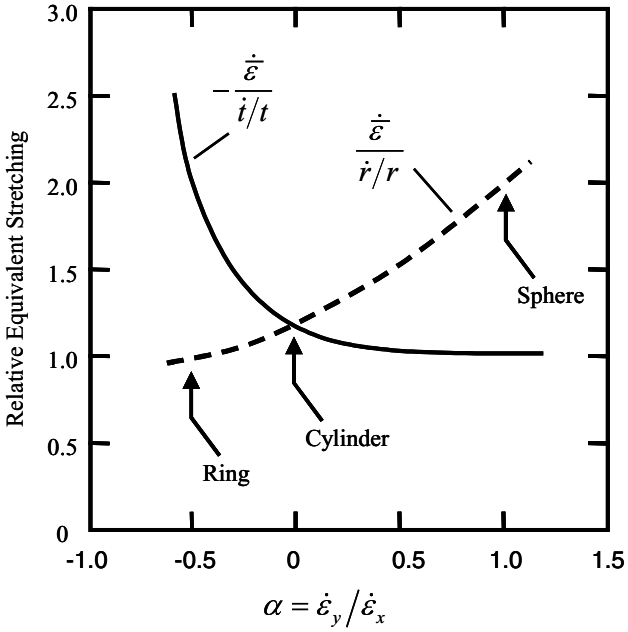

Fig. 6.10. The ratio of equivalent plastic stretching rate to the thinning rate is shown by the *solid curve*. The ratio to the expansion rate is provided by the broken curve. Values for expanding ring, expanding sphere and a uniaxial expanding cylinder geometries are identified

$$\sigma_y = \frac{\beta Y}{\sqrt{1-\beta+\beta^2}} \,, \tag{6.35}$$

where, Y is the yield stress and β is the stress ratio in (6.33). Equation (6.30) for a von Mises material gives $\bar{\sigma} = Y$.

A power-law hardening representation for the adiabatic effective stress versus strain behavior of the material of concern will be assumed of the form,

$$\bar{\sigma} = A\bar{\varepsilon}^n \,, \tag{6.36}$$

where both the coefficient A and the exponent n may, in general, depend on the biaxial proportionality parameter α. An effective in-plane tension T is provided by the product of the effective stress and the current thickness,

$$T = \bar{\sigma} t = A\bar{\varepsilon}^n t \,. \tag{6.37}$$

In the present model, onset of fracture is assumed to occur according to a maximum load instability criterion; namely, when the tension $T(\bar{\varepsilon})$ achieves a maximum under the proportional deformation loading. This instability criterion has been found to satisfactorily reproduce results of more detailed stability analyses [e.g., Romero, 1991]. The maximum of $T(\bar{\varepsilon})$ is identified from the differential,

$$dT = nA\bar{\varepsilon}^{n-1}td\bar{\varepsilon} + A\bar{\varepsilon}^n dt \ . \tag{6.38}$$

From (6.29),

$$\bar{\varepsilon} = -f(\alpha)\varepsilon_z \ , \tag{6.39}$$

where, $f(\alpha)$ is identified in the equation and,

$$d\bar{\varepsilon} = -f(\alpha)d\varepsilon_z = -f(\alpha)dt/t \ . \tag{6.40}$$

Combining (6.38) and (6.40), and equating the differential to zero, yields for the fracture criterion the critical effective fracture strain,

$$\bar{\varepsilon}_f = f(\alpha)n(\alpha) = \sqrt{\frac{4}{3}\frac{(1+\alpha+\alpha^2)}{(1+\alpha)^2}}n(\alpha) \ , \tag{6.41}$$

where the possible dependence of n on the biaxial proportionality parameter α is noted. Identifying through-the-thickness strain as $\varepsilon_z = \ln t/t_o$ thinning at fracture is,

$$\frac{t_f}{t_o} = e^{-n(\alpha)} \ . \tag{6.42}$$

Zero plastic volume strain for proportional loading of the familiar geometries requires that,

$$r_f t_f^{\kappa(\alpha)} = r_o t_o^{\kappa(\alpha)} \ , \tag{6.43}$$

where, $\kappa(\alpha) = 1/2,\ 1$, and 2 for an expanding sphere, uniaxial cylinder, and expanding ring geometry, respectively. The radial expansion at failure is then,

$$\frac{r_f}{r_o} = e^{\kappa(\alpha)n(\alpha)} \ . \tag{6.44}$$

In the absence of further data it is sensible to propose that the power-law hardening coefficient n in (6.36) be independent of the proportionality parameter α. The expanding ring data for U6Nb [Grady and Olsen, 2003] then provide a measure of the coefficient n for the dynamic expansion and fracture of the ductile uranium alloy. The data of Olsen indicate that $r_f/r_o \cong 1.3$ and (6.44) provides $n \simeq 0.13$.

Based on a power law hardening exponent of $n \simeq 0.13$ for the uranium alloy U6Nb, the through-the-thickness thinning, radial expansion, and equivalent plastic strain is shown in Fig. 6.11 as a function of the biaxial stretching parameter α. It is notable that both expansion and equivalent plastic strain reduce markedly as biaxial deformation approaches cylindrical, and then spherical, expansion.

Concerning the load maximum localization and fracture criterion, it has been noted [e.g., Storen and Rice, 1975; Needleman and Tvergaard, 1992] that only for $\alpha \leq 0$ is there a line of zero extension determining the orientation of the thinning localization. For $\alpha > 0$ a line of zero extension does not exist. Nonetheless, deformation localization when both in-plane principal strains are

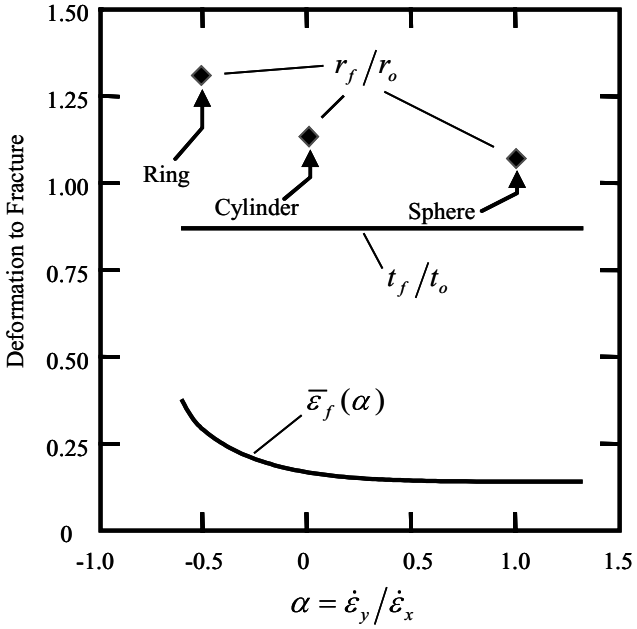

Fig. 6.11. Equivalent strain, thinning and radial expansion at fracture onset for U6Nb uranium alloy based on a power law hardening and load maximum model

positive is observed. Romero (1991) has demonstrated instability of the Levy-von Mises equations of a biaxial stretching ($\alpha = 0$) perfectly plastic plate, providing some justification of the load maximum criterion outlined here.

The power law hardening relation in (6.36) might be expected to depend on the biaxial load path α if deformation softening due to growth of microvoid damage in turn depended on the state of stress triaxiality [e.g., Mott, 1948; Hancock and MacKenzie, 1976]. Stress triaxiality equals $1/3$ for $\alpha = -1/2$ and $2/3$ for $\alpha = 1$. Additional test data would, of course, be needed to assess such load path dependence.

References

Abramowitz, M. and I. A. Stegun, eds. (1954), Handbook of Mathematical Function, No. 55, *National Bureau of Standards Applied Mathematics Series*, U. S. Government Printing Office.

Barlat, F. (1989), Forming Limit Diagrams – Predictions Based on Some Microstructural Aspects of Materials, in Form Limit Diagrams: Concepts, Methods and Applications, R. H. Wagner, K. S. Chang, S. P. Keeler, eds., The Minerals, Metals & Materials Society.

Buck, R. C. (1965), Advanced Calculus, McGraw-Hill, New York.

Grady, D. E. and Olsen, M. L. (2003), A Statistical and Energy Based Theory of Dynamic Fragmentation, *Int. J. Eng. Mech.*, 29, 293–306.

Gurney, R. W. (1943), The Initial Velocity of Fragments from Bombs, Shells and Grenades, Army Ballistic Research Laboratory Report BRL 405.

Hancock, J. W., and Mackenzie, A. C. (1976), On the Mechanisms of Ductile Failure in High-Strength Steels Subjected to Multi-Axial Stress States, *J. Mech. Phys. Solids*, 24, 147–169.

Needlemann, A., and V. Tvergaard (1992), Analysis of Plastic Flow Localization in Metals, *Applied Mechanics Review*, 45, s3–s18.

Mott, N. F. (1948), Fracture of Metals: Theoretical Considerations, *Engineering*, 165, 16–18.

Romero, L. A. (1991), The Stability of Stretching and Accelerating Plastic Sheets I & II, *J. Appl. Phys.* 69, 7474–7486, 7487–7499.

Storen, S. and J. R. Rice (1975), Localized Necking in Thin Sheets, *J. Mech. Phys. Solids*, 23, 421–441.

7

Scaling Relations for Fragmenting Shells

Mott (1943) recognized the need for scaling relations to allow designers the immediate ability to assess effects of parameter changes on the fragmentation characteristics of exploding bombs and warheads. Following extensive and insightful analysis, Mott arrived at the following scaling relations for the fragmentation of exploding cylindrical shells,

$$n\,(m)\,dm = Be^{-M/M_A}dm\ , \tag{7.1}$$

$$M_A = Ct^{5/6}d_2^{1/3}\,(1 + t/d_2)\ . \tag{7.2}$$

In Mott's notation (7.1) provides a statistical fragment size distribution with $n(m)dm$ being the number of fragments with mass between m and $m + dm$, while $M = m^{1/2}$ and M_A is a fragment size scale parameter dependent on the case inner diameter d_2 and case wall thickness t according to (7.2). In (7.1) and (7.2), B and C are constants dependent on explosive and metal properties of the specific system. The development of Mott's scaling relations is discussed later.

7.1 Fracture Model Based Scaling Relations

Here an alternative set of scaling relations for exploding munitions fragmentation is considered with the same intentions as Mott. This is undertaken for several reasons. First, additional physics of dynamic fragmentation has been explored since the seminal study of Mott, and efforts are taken to incorporate this science into the scaling relations. Further, a broader range of both explosives and of case metals and their metallurgical preparation are of current interest and the intention is to include material, as well as geometry properties, explicitly into the scaling relations.

One reasonable representation of appropriate scaling relations is presented here:

$$N(m) = N_o e^{-(m/\mu)^{\beta}} , \tag{7.3}$$

$$\frac{\mu}{\rho t^3} = a \left(\frac{r}{t}\right)^{2n/\alpha} \left(\frac{G t^{2-\alpha}}{\rho u^2}\right)^{n/\alpha} . \tag{7.4}$$

Equation (7.3) is the statistical fragment size distribution with $N(m)$ the cumulative number of fragments with masses greater than mass m, N_o is the total number of fragments, and μ is the distribution scale parameter characterizing the mean fragment size in the explosive event. The constant β is a reasonably constrained distribution shape parameter.

Equation (7.4) provides the distribution scale parameter μ in terms of geometric and kinematic properties of the exploding munitions. Briefly, a is a fragment aspect ratio parameter r and t are munitions case radius and thickness, G characterizes fracture resistance of the munitions case, while u is the effective expansion velocity of the case imparted by the explosive detonation. Exponent parameters, n and α, are physical constants. The above parameters will be discussed more fully in the following paragraphs.

7.1.1 Fragment Distribution Scaling Relation

We strive here for a physically based analytic description of the fragment size distribution resulting from an exploding munitions event. The method pursued complements and extends the approach pursued by Lineau (1936), and furthered in the works of Mott. It is in a sense quite general, encompassing the distributions proposed by Mott, as well as, later efforts. Features of survival statistics considered in Chap. 4 are applied.

Consider, a mass M broken into N_o fragments and, for the purpose of illustrating the theoretical development, consider the measure of this mass identified on a horizontal scale with mass units as shown in Fig. 7.1. N_o fragments are determined by $N_o - 1$ randomly placed breaks. At any break, consider the probability that the mass of the corresponding fragment is mass m within an interval dm. Couched within the framework of survival, or hazard, statistics [Hahn and Shapiro, 1967] this probability is,

$$f(m)\, dm = h(m)\, e^{-\int h(m) dm} dm , \tag{7.5}$$

where, $h(m)dm$ is the chance of a random break in the fragment mass interval m to $m + dm$ as described in Chap. 4.

The statistical fragment size distribution is constrained by specifying the functional dependence of $h(m)$ on the fragment mass m. This is done by either exploring additional physics specific to the fragmentation process, or by hypothesis to be tested by data, or alternative random fragmentation processes, such as the geometric methods pursued in Chap. 2.

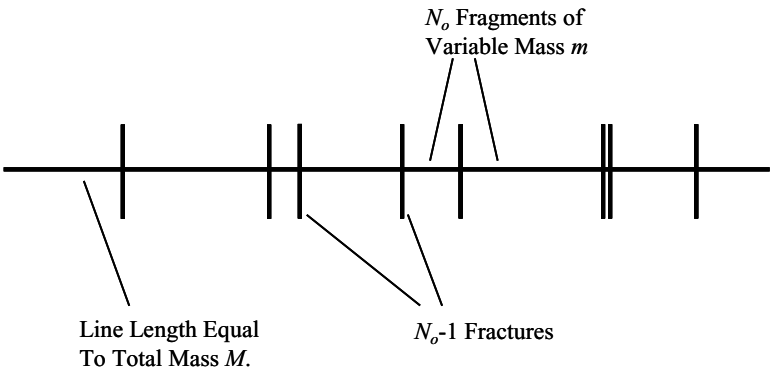

Fig. 7.1. Line of length corresponding to total mass M broken at random into N fragment length of variable mass m by N_o-1 fractures

The simplest assumption is $h\,(m) = h_o$, a constant. Thus $f(m)$ in (7.5) is,

$$f\,(m) = h_o e^{-h_o m}\,, \tag{7.6}$$

and the complementary cumulative fragment number distribution is,

$$N\,(m) = N_o e^{-m/\mu} dm\,, \tag{7.7}$$

where, $\mu = 1/h_o$ is the distribution scale parameter. The possible applicability of this distribution was suggested by Grady and Kipp (1985).

Mott and Linfoot (1943), following the theoretical work of Lineau (1936), assumed that a linear size measure x of the fragment dimension was a random variable and hence $h_o dx$ provided the chance of fracture determining a fragment of mass m. They considered the breakup of thin walled cylinders where fragment dimensions were large compared to the wall thickness. This suggests $x \sim m^{1/2}$ and $dx \sim m^{-1/2} dm/2$. Thus,

$$h\,(m) = \frac{1}{2\mu}\left(\frac{m}{\mu}\right)^{-1/2}\,, \tag{7.8}$$

is an appropriate hazard function and (7.5) becomes,

$$f\,(m) = \frac{1}{2\mu}\left(\frac{m}{\mu}\right)^{-1/2} e^{-(m/\mu)^{1/2}}\,, \tag{7.9}$$

and the corresponding complementary cumulative number distribution,

$$N\,(m) = N_o e^{-(m/\mu)^{1/2}}\,. \tag{7.10}$$

In the present development of fragmentation scaling relations we limit the functional dependence of $h(m)$ to,

$$h(m) = \frac{\beta}{\mu}\left(\frac{m}{\mu}\right)^{\beta-1} , \tag{7.11}$$

which, when integrated, leads to the size distribution scaling relation of the Weibull form,

$$N(m) = N_o e^{-(m/\mu)^{\beta}} . \tag{7.12}$$

This relation clearly encompasses the previous examples. Namely, $\beta = 1/2$ corresponds to the distribution arrived at by Mott and Linfoot (1943), while $\beta = 1$ corresponds to that suggested by Grady and Kipp (1985). Additionally, Mott's later physics based statistical fragmentation theory suggests values of β greater than unity.

Generality of the parameter β for a munitions-specific scaling equation is warranted for a number of reasons. Mott and Linfoot argued that when the fragment distribution was dominated by fragments of a size less than the case thickness that $\beta = 1/3$ was probably more appropriate. For a specific munition system a range of expansion strain rates will lead to statistical heterogeneity (a different size parameter at different positions along the munitions case). This breakup feature will broaden the distribution leading to smaller effective values of β. On the other hand, a degree of case scoring, or other processes, with the intention of biasing the distribution toward a unique size has the effect of increasing the distribution shape parameter β. As β approaches infinity, (7.12) approaches a Heaviside function.

In the complementary cumulative fragment number distribution, the total fragment number is not readily determined experimentally. It is not, however, a third distribution parameter but is constrained by the total mass of the distribution. The differential of the number distribution from (7.12) provides,

$$dN = N_o \frac{\beta}{\mu}\left(\frac{m}{\mu}\right)^{\beta-1} e^{-(m/\mu)^{\beta}} dm . \tag{7.13}$$

The mass differential is then,

$$dM = m dN = N_o \beta \left(\frac{m}{\mu}\right)^{\beta} e^{-(m/\mu)^{\beta}} dm . \tag{7.14}$$

Carrying out the integration it is readily shown that the total number and mass are related through,

$$N_o = \frac{M_o}{\mu \Gamma\left((1+\beta)/\beta\right)} . \tag{7.15}$$

7.1.2 Fragment Mass Scaling Relation

When fragments from the exploded cylindrical case retain portions of the inner and outer case surfaces, while length and width dimensions are sensibly

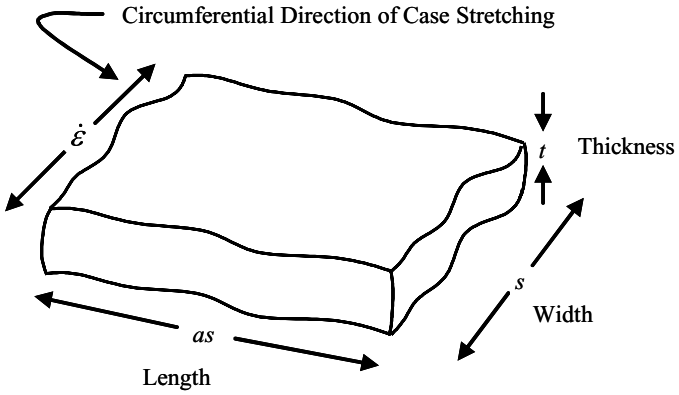

Fig. 7.2. Representative fragment identifying fragment thickness (and case wall thickness), fragment width, and fragment length, where a is the nominal fragment length-to-width aspect ratio

larger than the fragment (case) thickness t, as illustrated in Fig. 7.2, then the fragment mass scale parameter from the fragment distribution relation is related to a characteristic fracture spacing s through,

$$\mu = a\rho s^2 t \ . \tag{7.16}$$

In (7.16) fragment length is related to the fragment width s through an aspect ratio a, which may depend on details of the detonation and the case geometry.

If the distribution is dominated by fragments of dimension smaller than the case thickness then,

$$\mu = a\rho s^3 \ , \tag{7.17}$$

will be assumed. Equations (7.16) and (7.17) can be generally written,

$$\mu = a\rho t^3 \left(\frac{s}{t}\right)^n \ , \tag{7.18}$$

where $n = 2$ yields (7.16), while $n = 3$ gives (7.17). In this form the distribution size parameter μ is conveniently scaled to a cubic fragment of dimension equal to the case thickness t.

The nominal fracture spacing s will be written,

$$s = \left(\frac{G}{\rho \dot{\varepsilon}^2}\right)^{1/\alpha} \ , \tag{7.19}$$

where, the constant α ranges from $2 \leq \alpha \leq 3$ for the fragment spacing models considered. The constant G is case metal fracture resistance with dimensions of energy per unit area when $\alpha = 3$ and energy per unit volume when $\alpha = 2$. The dominant circumferential stretching rate is $\dot{\varepsilon} = u/r$. Substitution and rearrangement leads to the scaling relation provided previously,

$$\frac{\mu}{\rho t^3} = a \left(\frac{r}{t}\right)^{2n/\alpha} \left(\frac{G t^{2-\alpha}}{\rho u^2}\right)^{n/\alpha} . \tag{7.20}$$

In the dimensionless scaling relation for the size parameter μ, three effecting terms on the right hand side are noted. First is the aspect ratio a, which may in general depend on the size parameter μ. In the fragmentation of cylindrical cases, however, biaxiality of strain rate and the detonation contact sweep velocity are the principal physical conditions controlling a. An estimate of fragment aspect ratio in case fragmentation was provided by Mott (1943).

A measure of the munitions case curvilinearity (ratio of case radius to thickness) is included in the second term on the right. This term provides the geometric contribution to the stretching rate driving fragmentation.

The last term on the right includes the ratio of two energy densities (energy per unit volume). In the denominator is a measure of the expansion kinetic energy of the exploding munitions case. It is the product of the density and the square of the outward expansion velocity of the case metal at the time of breakup and fragmentation. It is reasonably estimated as the terminal expansion velocity of the munitions case brought about by the explosive acceleration. This velocity is readily calculated with current continuum computer codes. Alternatively, Gurney equations [e.g., Gurney, 1943; Jones et al., 1980] are quite adequate for calculating munitions case expansion velocities. The latter have the added benefit of explicitly revealing scaling behavior among explosive and munitions case properties.

In the numerator of the final term is a property G, which determines the fragmentation resistance of the munitions case metal. This fragmentation resistance depends on the model for fragmentation assumed to best describe the material response. The model may include material properties such as fracture or shear band toughness, yield stress, or properties characterizing failure from intrinsic or dynamic imperfects of the munitions case. The fragmentation energy may depend explicitly on the case thickness and directly affect the scaling of system performance.

Several models of the case fragmentation process have been pursued in the previous chapters leading to a measure of the fragmentation resistance G. The energy-based theory of dynamic fragmentation provides,

$$G = 48\Gamma , \tag{7.21}$$

or in terms of the fragmentation toughness,

$$G = 24 K_f^2 / \rho c^2 . \tag{7.22}$$

The observant analysis will note that the expressions above are a factor of two larger than the value of G resulting from (3.23). Equtions (7.21) and (7.22) result from a different formulation of the energy based fragment size theory [see Grady and Kipp, 1993; Kipp and Grady, 1995]. These expressions are used here to maintain consistency with the presentation of the same results

earlier [Grady, 1999; Reedal et al., 1999]. The parameter α in the size scaling relation is $\alpha = 3$, when (7.21) or (7.22) is applied.

The statistical fragmentation theory of Mott (1943) is also amenable to the present scaling relation formulation. In terms of the Mott γ factor the following expression for the fracture resistance can be determined,

$$G = 2\pi Y/\gamma \,, \tag{7.23}$$

where $\alpha = 2$ in (7.20).

7.2 The Mott Scaling Relations

Mott in 1943 developed two relations, which were intended for scaling exploding HE shells with respect to the statistical distribution in the sizes of metal fragments resulting from the explosion. They were, in his notation,

$$N\,(m)\,dm = Be^{-M/M_A}dM \,, \tag{7.24}$$

$$M_A = Ct^{5/6}d_2^{1/3}\,(1 + t/d_2) \ . \tag{7.25}$$

In (7.24) and (7.25), B and C are constants, while $M = m^{1/2}$, where m is a fragment mass. Cylinder dimensions are provided by d_2 and t. The geometry is illustrated in Fig. 7.3.

Equation (7.24) is a description of the statistical fragment size distribution, which is discussed in some detail in Chap. 2. Equation (7.25) provides a scaling relation (restricted to cylindrical geometries) for the characteristic fragment size. These relations continue to be used, frequently inappropriately, up to the present day.

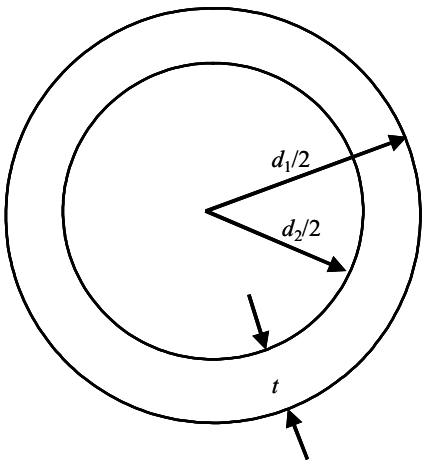

Fig. 7.3. Fragmenting cylinder geometry in the Mott scaling relations

Here we assess the second Mott scaling relation provided in (7.25). The size scale parameter M_A in the statistical fragment distribution from (7.24), has dimensions of $m^{1/2}$ and can be written,

$$M_A \propto \sqrt{\rho t s l} \,, \tag{7.26}$$

where, l and s are characteristic length and width of resulting fragments, while t is the through-the-case thickness of a fragment. Mott assumed initially, and later provided analytic support for, a constant proportionality between fragment length and width,

$$l \propto s \,, \tag{7.27}$$

and therefore,

$$M_A \propto \sqrt{\rho t s^2} \,. \tag{7.28}$$

Mott pursued two theories in establishing a predictive relation for the circumferential fracture spacing s and, through (7.28), the mean fragment size. First was a work transfer wherein a resisting work of fracture is equated to a driving kinetic energy in the expanding cylinder breakup. The second was the tensile strain activation of statistically distributed fracture sites. He clearly favored the second analytic pursuit and in later discussions offered arguments which downplayed applicability of the former.

It was, however, the former work balance calculation which led to the precise form of the oft quoted fragment size scaling rules of Mott. To calculate the characteristic fracture spacing s, Mott equated the work W required to open a single fracture with the stretching kinetic energy on both sides of the fracture. This calculation provided the following relation for the characteristic fragment width,

$$s = \left[\frac{24 r^2 W}{\rho u^2}\right]^{1/3} \,. \tag{7.29}$$

Combining material parameters into a constant of proportionality K (7.28) and (7.29) are solved for,

$$M_A = K r^{2/3} t^{1/2} u^{-2/3} \,. \tag{7.30}$$

The parameters r and t are values for the radius and thickness of the cylinder at the time of fracture. Since the product rt is proportional to the constant cross-sectioned area (volume) of the expanding cylindrical shell it is a reasonable approximation, as pointed out by Mott, to replace these geometry parameters with their initial values in (7.30).

The remaining step in developing the size scaling relation is to relate the velocity at breakup to dimensions of the cylinder. Mott defines the following ratio of the outer diameter d_1 and inner diameter d_2 of the cylindrical shell,

$$R = \frac{d_1^2 - d_2^2}{d_2^2} \,, \tag{7.31}$$

which is readily identified as proportional to the ratio of the cross-sectional area (or mass) of the metal shell to that of the contained explosive charge. For example,

$$R \propto M_g/C_g \,, \tag{7.32}$$

is the ratio of metal mass to explosive charge mass common to the Gurney analysis [Gurney, 1943; Jones et al., 1980] in cylindrical geometry. Mott proposed that the product,

$$Ru^2 = \text{constant} \,, \tag{7.33}$$

leading to the formula for the expansion velocity,

$$u = u_o d_2/\sqrt{d_1^2 - d_2^2} \,, \tag{7.34}$$

where u_o is considered to be a property only of the explosive-metal system. The property u_o will depend on the extent of expansion and is selected to correspond to the expansion at fragmentation. Mott attributed this velocity formula to a theoretical treatment of G. I. Taylor and reference an internal report in his presentation.

Equations (7.33) and (7.34) are recognized as a consequence of energy conservation arguments. Writing,

$$\frac{1}{2} M_g u^2 (r) + C_g U (r) = \text{ constant} \,, \tag{7.35}$$

where the first term is the kinetic energy of the expanding metal shell, while $U(r)$ is the specific compressional energy of the expanding explosive products. If the compressional energy $U(r)$ is identified as a material constant E at the initial cylinder radius $r = r_o$ then (7.35) leads to,

$$u (r) = \frac{\sqrt{2E}}{\sqrt{M_g/C_g}} \left(1 - \frac{U (r)}{E}\right) = u_o (r) \sqrt{C_g/M_g} \,, \tag{7.36}$$

where, r in $u_o(r)$ is the radius at which fracture occurs, and $u_o(r)$ is the explosive and metal specific u_o identified in (7.34).

Similarities of this analysis with concurrent work of Gurney (1943) are evident. Gurney, in fact, references the work of Taylor in the closing pages of his study. Mott and Taylor fail to account for kinetic energy of the expanding explosive products, a factor prominent in the development of Gurney.

Using $2r = (d_1 + d_2)/2$ and $2t = (d_1 - d_2)$ in (7.30) and combining with (7.34) leads to,

$$M_A = C t^{5/6} d_2^{1/3} (1 + t/d_2) \,, \tag{7.37}$$

for the geometric scaling law of Mott for the characteristic fragment size. The Mott constant C is dependent on case metal and explosive properties. It is readily calculated in terms of the properties introduced by Mott as,

$$C \propto \rho^{1/6} W^{1/3} u_o^{-2/3} \,, \tag{7.38}$$

where the proportionality constant requires knowledge of the fragment aspect ratio.

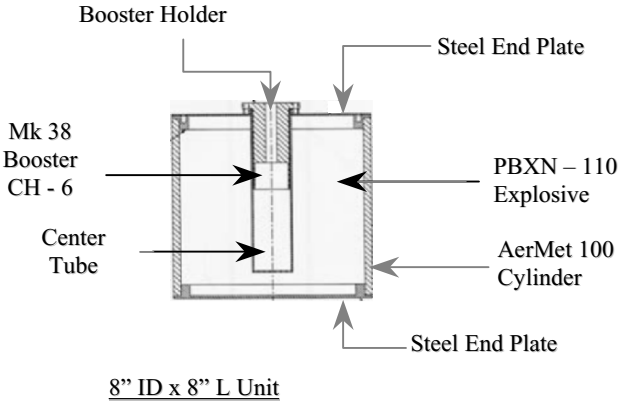

Fig. 7.4. Full Scale Representation of 8" ID × 8" L Unit

7.3 Application to Exploding Cylinder Fragmentation

Exploding steel cylinder tests appropriate for testing the scaling relation provided in (7.3) and (7.4) have been reported previously [Grady et al., 2001; Chhabildas et al., 2001]. Explosive fragmentation experiments were performed on both heat-treated and as-received AERMET-100 steel cylindrical shells. Three separate geometries were tested. A representative geometry is shown in Fig. 7.4. Two units of each geometry were tested – one each on heat-treated (ht) and as-received (ar) steel. Four tests were performed on right circular cylindrical shells with length equal to inner diameter. Replica scaling effects were investigated in this geometry, where tests were identified as full scale (FS) with length $\cong 20\,\text{cm}$, or half scale (HS) with length $\cong 10\,\text{cm}$. Wall thickness to inner radius ratio was $t/r = 0.08$.

Two additional tests were performed on thick-walled cylinders (TW), $t/r = 0.4$, with length equal to twice the inner diameter. These tests, when compared with half-scale tests, investigated strain rate scaling of fragmentation at a fixed inner diameter.

In these tests high-speed photography provided data for onset of fracture and explosive gas breakout. Flash radiography provided statistical velocity data on fragment ejecta. Soft recovery of fragments was pursued by capture in attapulgite/cellutex arresting media. Mass and dimension measurements on all collected fragments provided statistical data on fragment size and shape.

7.3.1 Fragment Distribution Data

Fragment distributions for the six experiments performed were determined. Cumulative distributions for the half- and full-scale tests on the heat treated material shown in Fig. 7.5 are representative. An analytic representation proposed as one of the two scaling relations of the form,

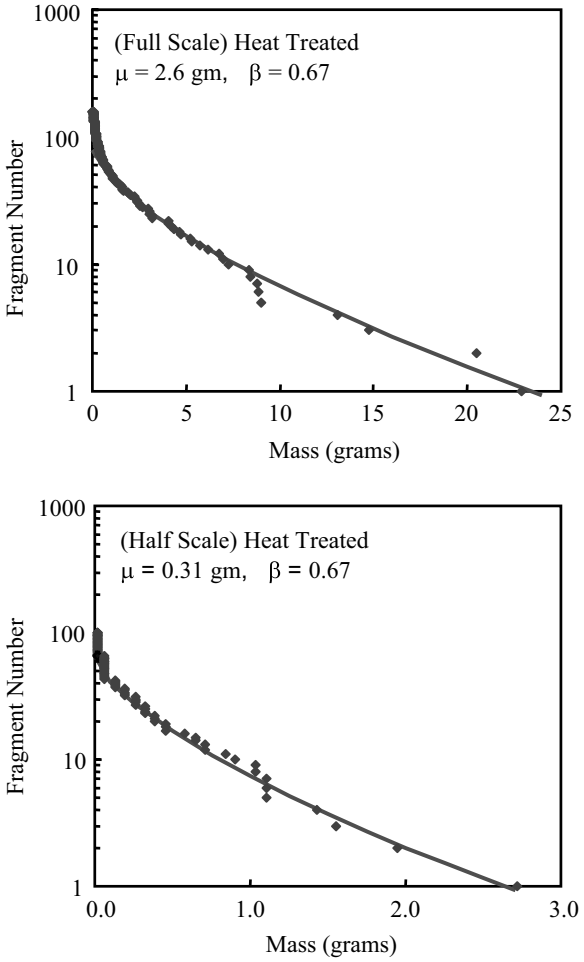

Fig. 7.5. Fragment distributions for AerMet 100 steel fragmentation tests

$$N(m) = N_o e^{-(m/\mu)^\beta} , \tag{7.39}$$

was fit to the fragment distribution data. Analytic curves are also shown in Fig. 7.5. Distribution parameters for the six experiments are provided in Table 7.1. Recall that the number parameter is not independent, but is constrained by the total recovered fragment mass M through the relation provided in (7.15).

7.3.2 Distribution Scale Parameter Data

Scale parameter μ for the four half-scale and full-scale experiments normalized by ρt^3(0.52 g (HS), 4.4 g (FS)) is plotted in Fig. 7.6. Tests on heat-treated steel

Table 7.1. Fragment Distribution Parameters

Parameter	HS(ht)	FS(ht)	HS(ar)	FS(ar)	TW(ht)	TW(ar)
Scale(μ)	0.31 g	2.6 g	0.70 g	5.2 g	5.0 g	7.5 g
Shape(β)	0.67	0.67	0.55	0.85	0.55	0.55
Num.(N_o)	66	79	42	88	76	69

HS = half scale, FS = full scale, TW = thick wall, ht = heat treated, ar = as received.

Material properties assumed for AERMET-100 steel: $Y = 1.5$ GPa, $K_f = 70$ MPa/m$^{1/2}$, $\rho = 7900$ kg/m^3, $c = 5000$ m/s, $\gamma = 80$

are clearly consistent with replica scaling. Distributions for tests on as-received steel do not as tightly constrain μ, but values here are also not inconsistent with replica scaling. Observations on scaling have implications on the several theories predicting the fragmentation resistance G in the scaling equations.

The energy-based theory based on a fracture toughness, K_f fragmentation resistance predicts,

$$G = 24\, K_c^2/\rho c^2 \ , \tag{7.40}$$

with exponent $\alpha = 3$. Mott's statistics-based theory, on the other hand, yields, with exponent $\alpha = 2$,

$$G = 2\pi Y/\gamma \ . \tag{7.41}$$

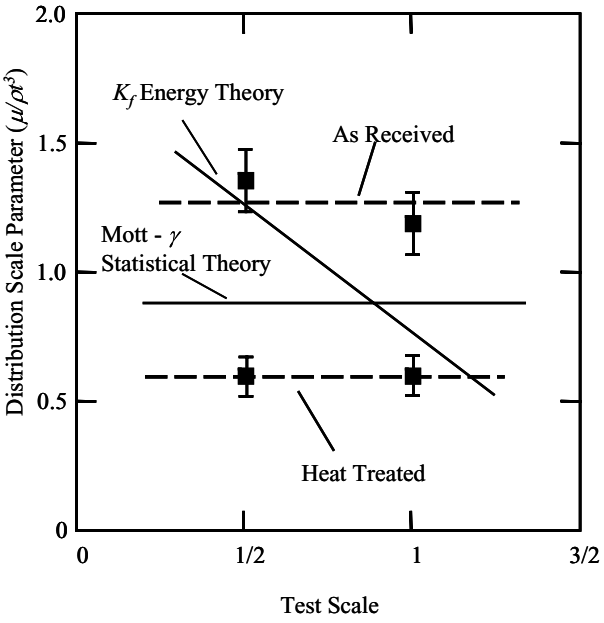

Fig. 7.6. Distribution scale parameter for cylinder fragmentation tests

Separate material properties for the two preparations of AERMET-100 steel were not available. Precise values are not critical to the present observations, however, and the very reasonable values used are included in Table 7.1. No attempt is made to account for the obvious difference in strength properties of heat-treated and as-received steels. An expansion velocity $u = 2000\,\mathrm{m/s}$ and an aspect ratio of $a = 1.5$ assumed are consistent with measured velocities and inspection of recovered fragments. Calculations of the scale parameter μ from the scaling equation based on either the K_f energy expression or the Mott statistical expression are compared with experiment in Fig. 7.6.

It is interesting that fracture resistances determined from Mott's statistical theory and the energy-based theory of Kipp and Grady provide equally reasonable quantitative predictions of the experimental fragment size scale μ. The Mott theory is consistent with the observed replica scaling, whereas the fracture toughness based theory is not. It is well known [e.g., Lawn and Wilshaw, 1975] that for ductile fracture in metals, yield stress and fracture toughness can be related through a process zone length scale. When this length scale approaches characteristic specimen dimensions (shell case thickness for example) size effects can be observed. Present replica scaling results for fragment size suggest that the effective toughness must depend on case thickness. Considering realities of the complex fracture mechanisms in expanding cylinder fragmentation including cooperative interaction of adiabatic shear banding along with shear and tensile fracture such dependence should probably not be surprising.

A further comparison is made with fragmentation data from the 4×4 half-scale (HS) cylinders and the 4×8 thick wall (TW) cylinders. Both units have the same inner diameter of 4 inches (the same charge diameter), but the substantial difference in wall thickness will lead to markedly different expansion velocities and fragmentation strain rates. Strain rate histories are calculated with the CTH continuum solid dynamics (CSD) wavecode. Maximum strain rates of approximately $1.1 \times 10^4/\mathrm{s}$ and $2.6 \times 10^4/\mathrm{s}$ are calculated for the TW units and HS units, respectively. Maximum strain rates occur at about 10–20 percent strain.

The size scale parameter μ for the respective tests is plotted as a function of the corresponding calculated maximum strain rate in Fig. 7.7. Again the data is compared with predictions based on Mott's statistical theory and the energy-based fragmentation toughness controlled theory. The same properties assumed for AERMET-100 steel provided in Table 7.1 were used.

As before both theories provide a reasonable absolute prediction of the size scale parameter. Dependence on strain rate of $\mu \sim \dot{\varepsilon}^3$ for the Mott theory, in contrast to $\mu \sim \dot{\varepsilon}^2$ for the K_f-energy theory, again appears to be in better agreement with the data. This agreement is certainly true for the heat-treated steel. It is less certain for the as-received steel.

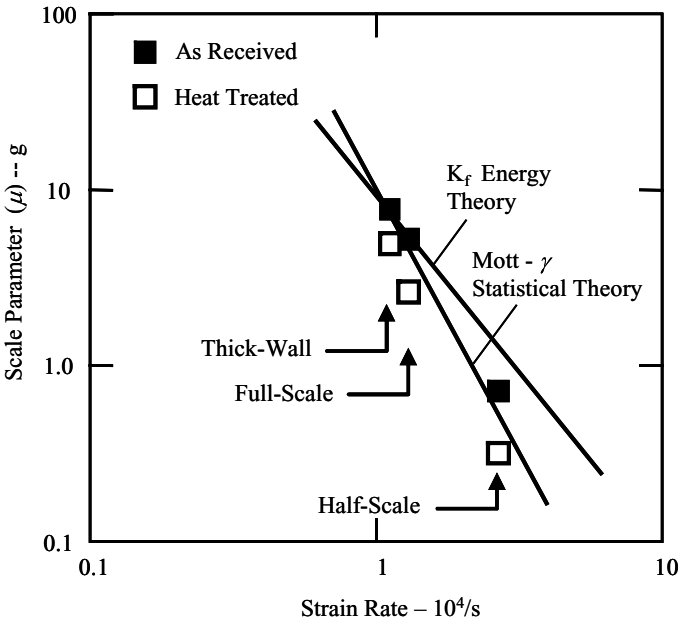

Fig. 7.7. Distribution scale parameter for cylinder fragmentation tests and dependence on expansion strain rate for the three test types

7.3.3 Distribution Shape Parameter Data

In the distribution representation,

$$N(m) = N_o e^{-(m/\mu)^\beta} , \tag{7.42}$$

was selected to describe the present fragment data. The shape parameter β provides a measure of the spread in fragment size.

For the present six experiments β was found to range over about $0.55 \leq \beta \leq 0.85$ with an average of 0.65. The initial baseline distribution proposed in the first of the Mott papers [Mott and Linfoot, 1943] required $\beta = 1/2$. It is noted that present experimental values are not significantly higher than the Mott baseline β and this distribution with $\beta = 1/2$ certainly has a long history of adequately quantifying munitions fragmentation data.

Nonetheless, it can be effectively argued that (7.42), with $\beta = 1/2$, is not the fundamental theoretical representation for natural fragmentation. These arguments are voiced earlier in this study and are probably supported most strongly by Mott's later theoretical efforts. The distribution shape parameters β from the distribution of the analytic form in (7.42) that were fit to the fragment number versus mass distribution data for the steel cylinder fragmentation tests are shown in Fig. 7.8. The parameter β ranges between 0.5 and 1.0 and shows no trend with the experimental parameters varied in the tests.

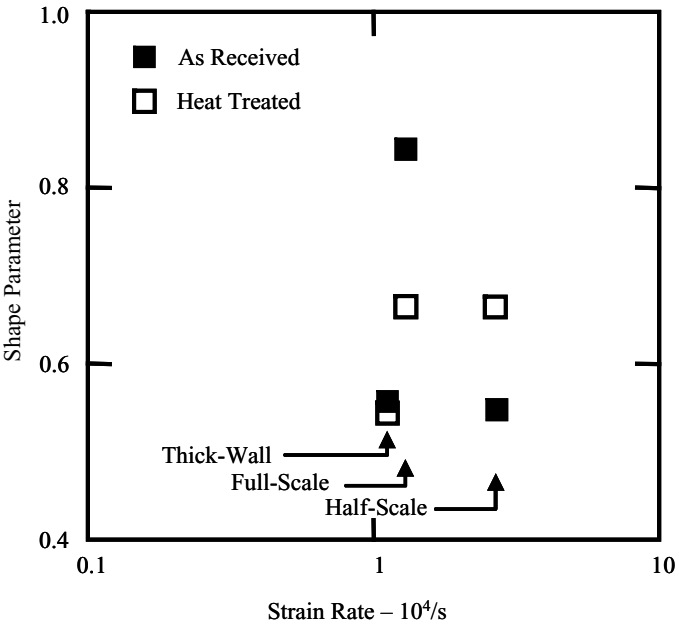

Fig. 7.8. Distribution shape parameter for cylinder fragmentation tests

Grady and Kipp (1985) have proposed (7.42) with $\beta = 1$ for the basis distribution. It has been suggested in the present report that this is the least biased distribution when no additional knowledge of the breakup physics is available. This distribution has been used within the CTH wavecode fragmentation model.

Accepting the Grady and Kipp distribution ($\beta = 1$) as the basis distribution for a statistically homogeneous event. In the present application statistical homogeneity implies that each and every point of the expanding cylinder fragments under the same driving strain rate. If this is not the case (which is always in practice) then the mean fragment size (and scale parameter μ) would vary with position and the distribution would be statistically heterogeneous. A distribution of the form of (7.42) with $\beta = 1$ would then apply at every point with μ a function of position. The heterogeneous distribution is formed from a superposition of each and every point distribution (a Poisson mixture as described in Chap. 2). To fit such a distribution with a single function of the form of (7.42) would require reduction of the shape parameter β to some value less than unity.

A CTH simulation on one of the right cylinder explosive fragmentation experiments [Kipp, 2001] provides the mass distribution over strain rate at

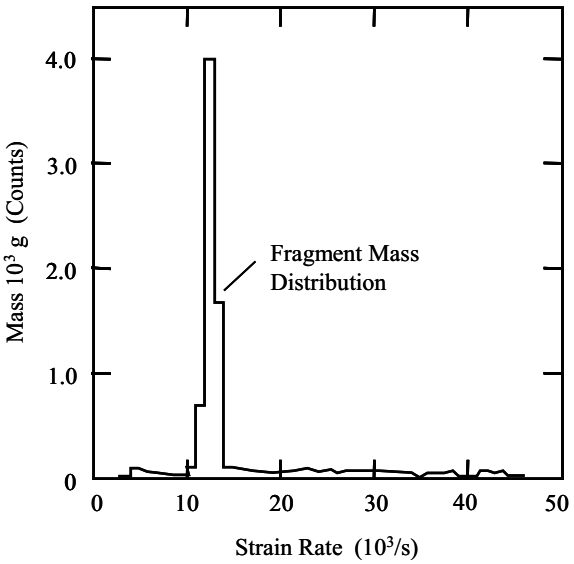

Fig. 7.9. The cylinder mass distribution over break up strain rate as determined from CTH wave code simulation

fragmentation shown in Fig. 7.9. The spread in strain rates was not sufficient to account for the observed reduction in the shape parameter β through statistical heterogeneity. It is suspected that not addressing the issue of aspect ratio of fragments may account in part for the present disagreements.

References

Chhabildas, L., Reinhart, W., Wilson, L. T., Reedal, D. R., Grady, D. E., Black, J. W. (2001), Fragmentation Properties of AerMet 100 Steel in Two Material Conditions in Proceedings 19^{th} International Symposium on Ballistics, Interlaken, Switzerland, May 7–11, I. R. Crewther, ed., 663–670.

Grady, D. E. (1999), Impact Failure and Fragmentation Properties of Tungsten Carbide, *Int. J. Impact Eng.* 23, 307–317.

Grady, D. E. and Kipp, M. E. (1985), Geometric Statistics and Dynamic Fragmentation, *J. Appl. Phys.*, 58, 3, 1210–1222.

Grady, D. E. and Kipp, M. E. (1993), Dynamic Fracture and Fragmentation in High-Pressure Shock Compression of Solids, J. R. Asay and M. Shahinpoor, eds., Springer-Verlag, New York, 265–322.

Grady, D. E., Wilson, L. T, Reedal, D. R., Kuhns, L. D., Kipp, M. E., Black, J. W. (2001), Comparing Alternative Approaches in the Scaling of Naturally Fragmenting Munitions in Proceedings 19^{th} International Symposium on Ballistics, Interlaken, Switzerland, May 7–11, I. R. Crewther, ed., 591–598.

Gurney, R. W. (1943), The Initial Velocity of Fragments from Bombs, Shells and Grenades, Army Ballistic Research Laboratory Report BRL 405.

Hahn, G. J. and Shapiro, S. S. (1967), *Statistical Models in Engineering*, John Wiley & Sons, New York.

Jones, G. E., Kennedy, J. E., and Bertholf, L. D. (1980), Ballistic Calculations of R. W. Gurney, *Am. J. Phys.*, 48, 264–269.

Kipp, M. E. and Grady, D. E. (1995), Experimental and Numerical Studies of High-Velocity Fragmentation in High-Pressure Shock Compression of Solids II, L. Davison, D. E. Grady and M. Shahinpoor, eds., Springer-Verlag, New York, 282–339.

Kipp, M. E. (2001), Private Communication.

Lawn, B. R., and Wilshaw, T. R. (1975), Fracture of Brittle Solids, Cambridge Univ. Press.

Lineau, C. C. (1936), Random Fracture of a Brittle Solid, *J. Franklin Inst.*, 221, 485–494, 674–686, 769–787.

Mott, N. F. and Linfoot, E. H. (1943), A Theory of Fragmentation, *Ministry of Supply*, AC3348.

Mott, N. F. (1943a), Fragmentation of H. E. Shells: A Theoretical Formula for the Distribution of Weights of Fragments, *Ministry of Supply*, AC3642, March.

Mott, N. F. (1943b), A Theory of the Fragmentation of Shells and Bombs, *Ministry of Supply*, AC4035, May.

Reedal, D., Wilson, L., Grady, D., Chhabildas, L., Reinhart, W. (1999), Impact and Explosion Induced Failure and Fragmentation Studies on Tungsten Carbide, Proceedings of the 15th U.S. Army Symposium on Solid Mechanics, Batelle Press, 569–585.

8

Experimental Fragmentation

A number of studies over the intervening years since Mott's seminal theoretical efforts in dynamic fragmentation have been undertaken which allow testing of his theories. Some were pursued specifically for that purpose. Others were undertaken for other applications, but nonetheless provide useful test data for examining aspects of the theory.

Selected experiment studies are examined in the present section and compared with the fragmentation theory of Mott. This selection is, of course, not exhaustive. We will show that many of the theoretical concepts introduced stand up well to experimental scrutiny. Certain mysteries remain unresolved, however, and provide the challenge for yet more advanced theoretical efforts in fragmentation.

8.1 Olsen Expanding Ring

The expanding ring experiment to test the dynamic deformation and failure properties of engineering metals has continued to be pursued at Lawrence Livermore National Laboratory (LLNL) [Gourdin, 1989; Gourdin et al., 1989]. Extended development of the ring method provided an effective technique for assessing the dynamic tensile strength and strain-to-fracture properties, as well as the statistical fracture and fragmentation characteristics of the material. Here, we focus on extensive dynamic data obtained with the technique on uranium-6%-niobium (U6Nb) metal [Olsen, 2000; Grady and Olsen, 2003]. Data for this study were examined in an earlier section. Here a more thorough examination of the test method and the experimental results is undertaken.

8.1.1 The Experimental Method

Expanding ring tests were performed on machined U6Nb rings subjected to selected metallurgical heat treatment. Test samples were rings 34.4 mm inner

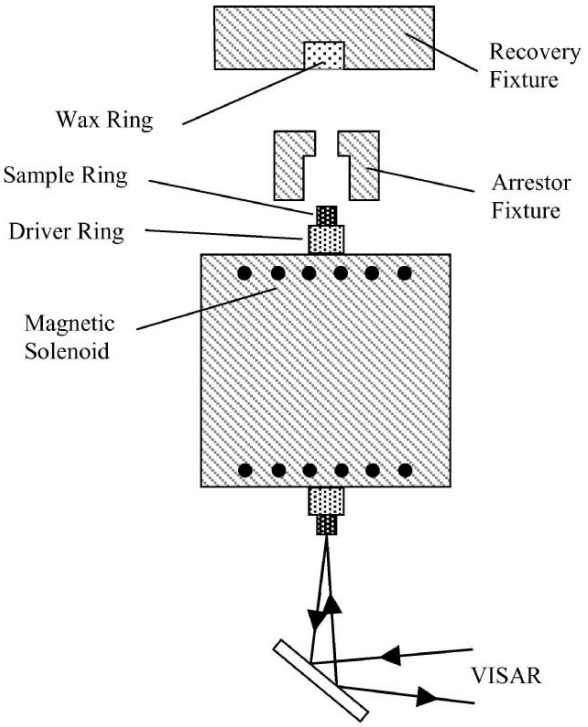

Fig. 8.1. Test configuration and diagnostics for expanding metal ring experiments are illustrated schematically

diameter and square cross section 0.76 mm on a side. The test configuration is illustrated schematically in Fig. 8.1.

The magnetic field excited by pulsing an electric current through a solenoid accelerates a metal driver ring and sample (U6Nb) ring radially outward. Expansion velocities ranging from about 100 to 300 m/s are achieved depending on the current amplitude. An arrestor fixture stops the driver permitting continued free flight of the sample ring. Velocity history of the ring is determined from time resolved velocity, or VISAR, measurements [Barker and Hollenbach, 1972] of the motion at one point on the ring. Free flight of the test ring is allowed through onset of fracture and fragmentation. Broken ring fragments are arrested and recovered within a stationary wax cavity in the experimental test fixture.

8.1.2 The Experimental Results

As noted, velocity histories of the U6Nb rings were measured with time-resolved velocity interferometry. Measured deceleration of the freely expanding ring prior to fragmentation, was used to calculate tensile flow stress of

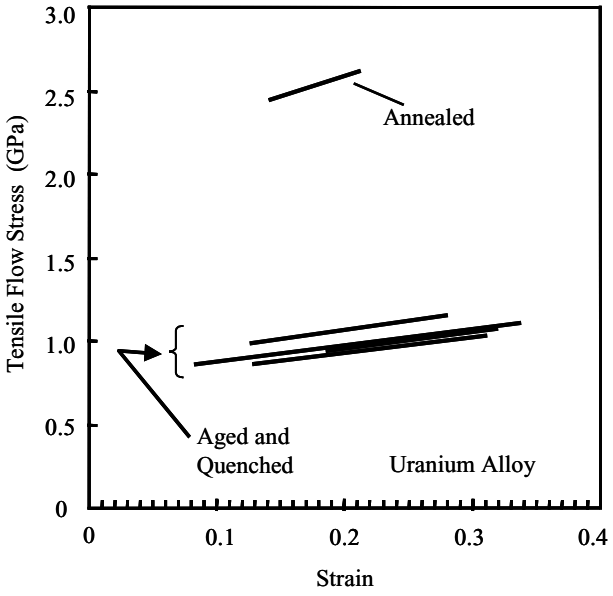

Fig. 8.2. Selected tensile stress versus strain to failure at an expansion rate of approximately $1.3 \times 10^4/\mathrm{s}$

the ring up to the time of fracture. Tensile stress, as a function of strain, for several aged and one annealed test sample is shown in Fig. 8.2. Strain rate during the free expansion deformation was approximately $1.3 \times 10^4/\mathrm{s}$. Tensile stress for the several aged samples was approximately 1.0 GPa to a fracture strain (increase in radius) of about 30%. On the other hand, the one annealed ring specimen exhibited a tensile flow stress of about 2.5 GPa and failed at a somewhat earlier 20% strain.

In each test the number of fragments produced (equivalently, the number of fractures) was determined. Fragment number versus the expansion velocity at fragmentation are shown for the series of U6Nb expanding ring experiments in Fig. 8.3. The anomalous point high on the graph is the one test on a markedly differently heat treated U6Nb sample identified as annealed in Fig. 8.2 and is discussed further, later in this section. A least squares fit, excluding the one anomalous point, provided the power law representation of the data shown in Fig. 8.3. Dynamic toughness data for the same data in Fig. 8.3, as calculated through the energy-based relation relating fragment number to toughness,

$$N = \left(\frac{\rho c \dot{\varepsilon}}{\sqrt{12} K_f} \right)^{2/3} , \tag{8.1}$$

are shown in Fig. 8.4.

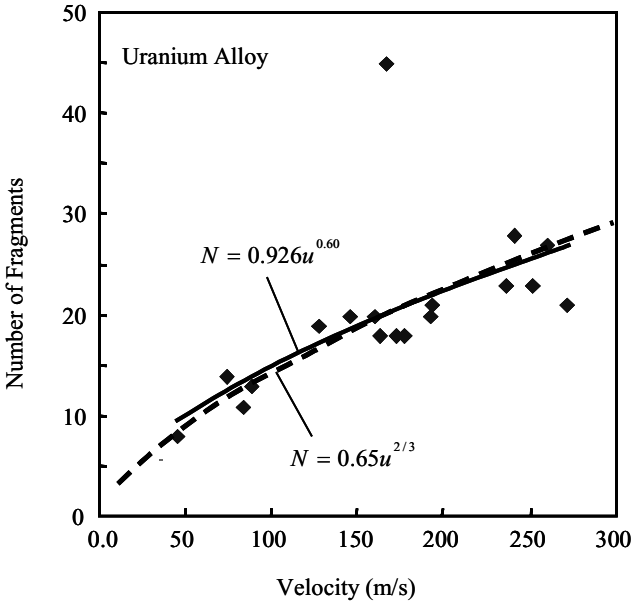

Fig. 8.3. Fragment number versus expansion velocity at fracture for U6Nb expanding ring fragmentation tests

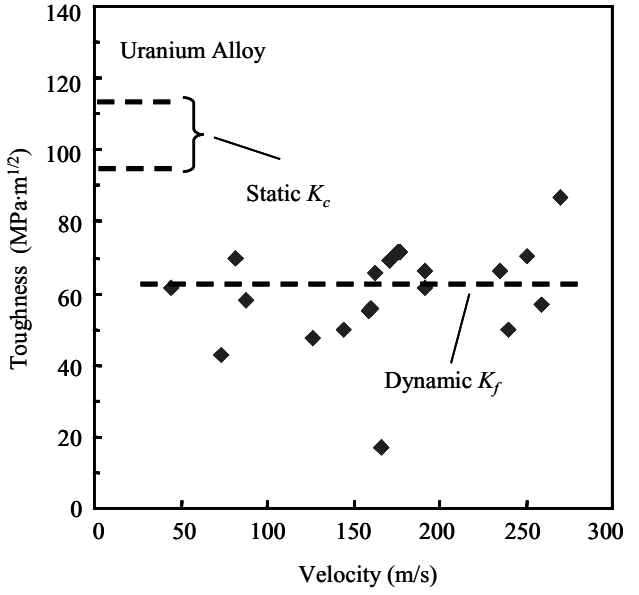

Fig. 8.4. Dynamic fragmentation toughness calculated through theoretical relation relating fragment number, expansion rate and material toughness

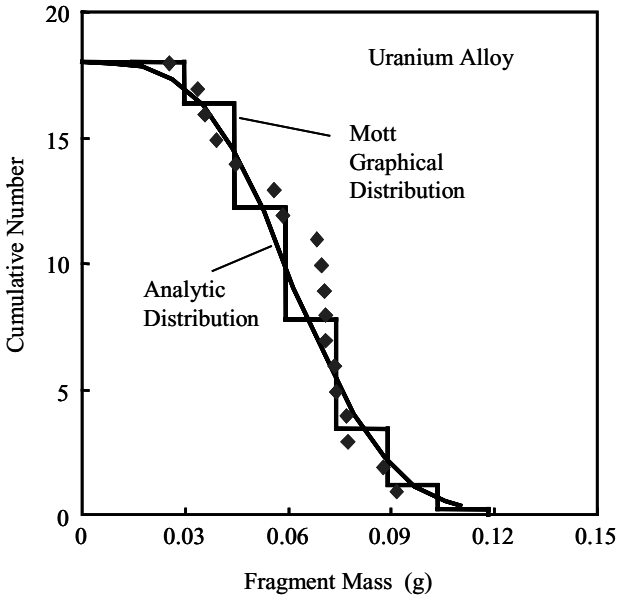

Fig. 8.5. Comparison of cumulative fragment distribution for one representative U6Nb expanding ring fragmentation test with the theoretical Mott fragment size distribution

In one representative test each fragment was separately weighed and the cumulative fragment size distribution shown in Fig. 8.5 was obtained. The data presented in Figs. 8.2 through 8.5 are also provided in Table 8.1.

8.1.3 Some Experimental Observations

The present study of dynamic fragmentation is afforded invaluable insight through a more in-depth examination of the expanding ring experimental fragmentation results. A metallographic image of a representative fracture is shown in Fig. 8.6. The outer deformed surface of the stretched ring exhibits an undulating, uneven surface characteristic of heterogeneous slip-line plasticity. The reduced area of the fracture surface points to a pre-fracture deformation localization through plastic necking. The failure process is completed through pervasive ductile extension fracture through the narrowest portion of the necking region. Arrested necking regions were also observed in a number of the recovered fragments.

Ductile deformation, through dimple plasticity, is clearly evident in the expanded image of the fracture surface shown in the upper fractograph in Fig. 8.7. The dimple morphology appears tri-modal. Dimple sizes range from 2–3 μm for the smallest up to 15–30 μm for the largest. Inclusions observed within larger dimples are probably fracture initiation sites. Dimple size may reflect local fracture speed in the failure process.

Table 8.1. Expanding ring fracture and fragmentation data

Test Number	Velocity at Failure (m/s)	Expansion at Failure (%)	Stress at Failure (GPa)	Number of Fragments	Cumulative Distribution Mass (g)	Num.
22	87.9	–	13	13	0.092	1
42	82.3	0.88	11	11	0.088	2
44	45.1	0.77	8	8	0.078	3
30	73.1	0.9	14	14	0.077	4
14	144.9	0.89	20	20	0.074	5
24	177.9	1.1	18	18	0.074	6
20	192.1	1.18	21	21	0.071	7
16	126.5	–	19	19	0.071	8
26	176.2	1.05	18	18	0.070	9
52	162.2	1.15	18	18	0.069	10
54	160.4	0.89	20	20	0.068	11
10	191.7	0.95	20	20	0.058	12
56	250.8	0.97	23	23	0.056	13
60	239.6	1.15	1.16	28	0.044	14
28	165.7	21	2.65	45	0.039	15
62	171.5	31.7	1.08	18	0.035	16
66	159.4	31.1	1.03	20	0.033	17
68	235.5	31.9	1.01	23	0.025	18
70	259.4	20.7	1.2	27		

The failure morphology shown in Fig. 8.6 and the expanded view of the fracture surface in the upper picture in Fig. 8.7 is illustrative of the fracture data examined in the present theoretical study. Data from these tests fall within the scatter of the curve shown in the fragment number plot in Fig. 8.3 even though these data represent materials subjected to several different aging treatments. All, however, were quenched from elevated temperature leaving the metal in the more ductile alpha phase. The modestly different aging treatments shows no apparent influence on either the fracture behavior or the fragmentation statistics.

The present fracture behavior of quenched U6Nb shows marked similarity to observations of spall fracture in U6Nb [Hixson, et al. 2000, and Zurek, et al. 2000]. Similarities extend to both the character of dimple plasticity on fracture surfaces and identification of carbide inclusion fracture initiation sites in higher resolution metallography. The similarity is not surprising in that strain rates at fracture in necking regions of the expanding ring tests exceed 10^4/s, approaching that of the spall experiments. Additionally, tensile stress triaxiality is amplified within necking regions again approaching conditions comparable to the spall experiment.

The anomalous data point observed in Figs. 8.2 through 8.4 corresponds, in contrast, to a sample in which the heat treatment left most of the metal in

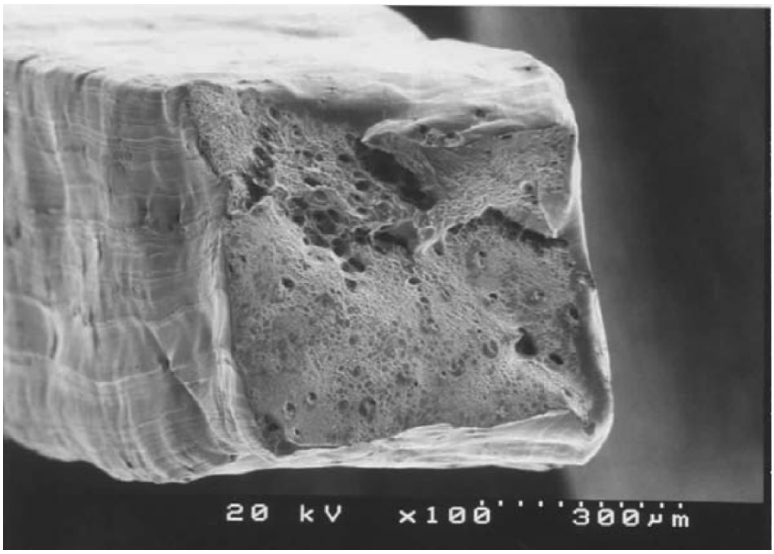

Fig. 8.6. Expanding ring dynamic fracture characteristics

the more brittle gamma phase. A corresponding fractograph of the fracture surface from the ring experiment on this sample is shown in the lower image of Fig. 8.7. The predominantly cleavage fracture character differs starkly from that of the more ductile fracture in the alpha phase material shown above (actually a variant α'' of the alpha phase, e.g., Addessio, et al. (2003)).

The expanding ring experiment is also unique, in providing a uniformly straining dynamic unconfined tension experiment, in which both tensile stress and plastic strain can be readily measured. Both stress and strain are determined in the present tests through velocity interferometry measurements of the radial velocity history. The effective measurement duration occurs from the time of decouple from the driving, current-carrying ring to the time of localization onset and failure. Strain and strain rate within this measurement period are provided by the velocity and displacement history. Stress is determined from the deceleration of free expansion through solution of the governing momentum equations.

Measured stress versus strain histories provided in Fig. 8.2 for selected experiments include several alpha phase materials subjected to different aging treatments and the one test on predominantly gamma phase metal. As previously stated, rings of the alpha phase materials achieve a dynamic flow stress of approximately 1.0 GPa before failing at expansions approaching 30% and higher. It should also be emphasized that failure in these materials proceeds first through deformation localization and ductile necking, and subsequently by extension fracture. Numerous arrested necking regions were observed in recovered fragments.

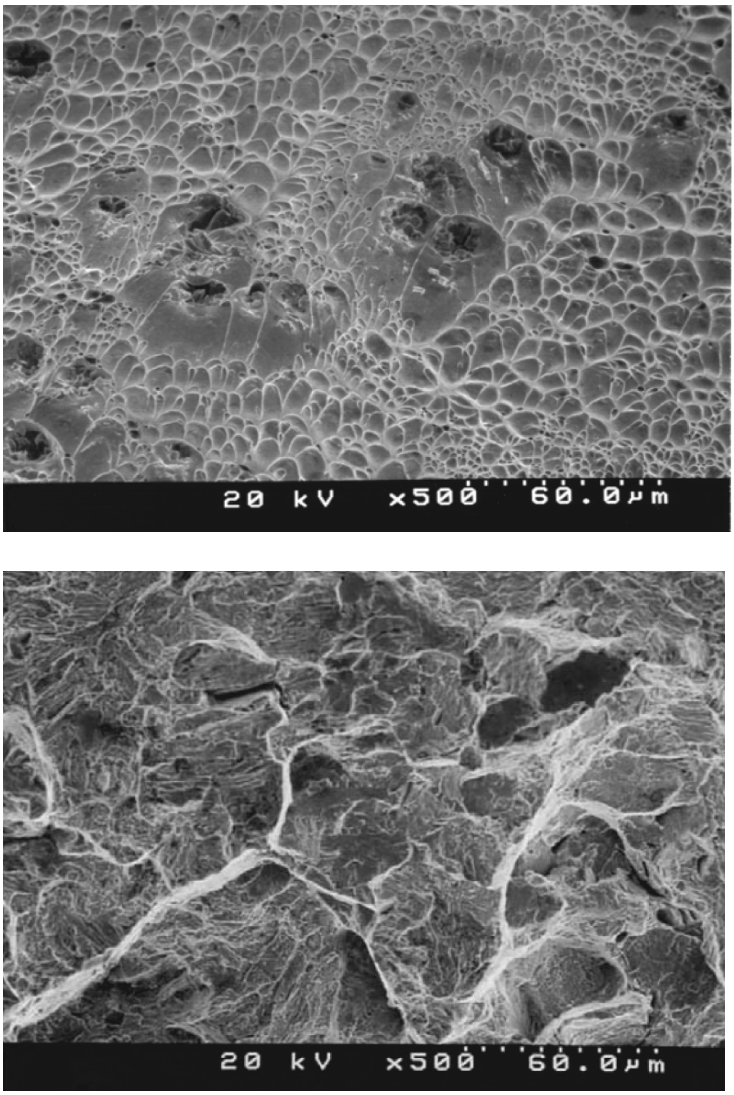

Fig. 8.7. Fractography of fracture surfaces for predominantly alpha phase (upper photo) and gamma phase (lower photo) U6Nb expanding ring samples

The test on the largely gamma phase U6Nb sample exhibited, in contrast, a dynamic flow stress well in excess of 2 GPa and a markedly reduced strain to failure (Fig. 8.2). Further evidence for the starkly more brittle character of dynamic fracture of U6Nb in this preparation is provided by the significantly reduced indications of ductile necking preceding extension fracture, clear indications of cleavage fracture as evident in Fig. 8.7, the larger number of fragments shown in Fig. 8.3 and the correspondingly

reduced fracture energy provided in Fig. 8.4. Although a static fracture toughness value for the present predominantly gamma phase metal was not available, an appreciable reduction from the alpha phase material would be expected.

A final comment on the comparison of the dynamic toughness inferred through the energy-based theory with the static fracture toughness in Fig. 8.5 is warranted. The reasonably close agreement between the dynamic and static values is remarkable and speaks strongly for an energy-controlled mechanism governing the characteristic fracture spacing and fragment number. On the other hand, one may question why they differ by almost a factor of two. First, there is a number of simplifying theoretical assumptions in the quantitative development of the energy theory which could readily account for the difference. But putting these explanations aside, there is an interesting material issue which could easily contribute to the difference. Dissipation resulting from the propagation of a through-going fracture in an engineering size sample of metal accounts for the observed fracture toughness of the material. Dissipation on the fracture surface is heterogeneous on some length scale, however dissipation at any point on the surface may exceed or be less than the average. The present metal rings with substantially less than a square millimeter cross section, combined with the statistical selectivity of weaker fracture sites, could lead to effectively lower dynamic fracture energy, as is observed. This possible material dependent difference would suggest something other than geometric scaling if the size of the test rings were varied. This complication has not been explored.

8.2 Grady and Benson Expanding Ring

The expanding ring fragmentation study on U6Nb metal described in the previous section nicely supports features of both Mott's statistical theory and the energy-based theory of dynamic fragmentation, and offers ideas for merging the two theories, as was pursued in Chap. 5. Here we will discuss earlier expanding ring tests of Grady and Benson (1983) in which the experimental results do not as tidily support the theoretical predictions. These experiments, in fact, motivated the experimental efforts of LLNL from which the reported study on U6Nb metal emerged. This previous work was in turn stimulated by even earlier experiments using explosives to drive expanding rings [Perrone, 1968; Hoggatt and Recht, 1969; Warnes et al., 1981] and magnetic loading methods [Walling and Forrestal, 1973].

8.2.1 The Experimental Method

The experimental method used in the study is described in detail in Grady and Benson (1983) with further analysis of the data provided in Grady

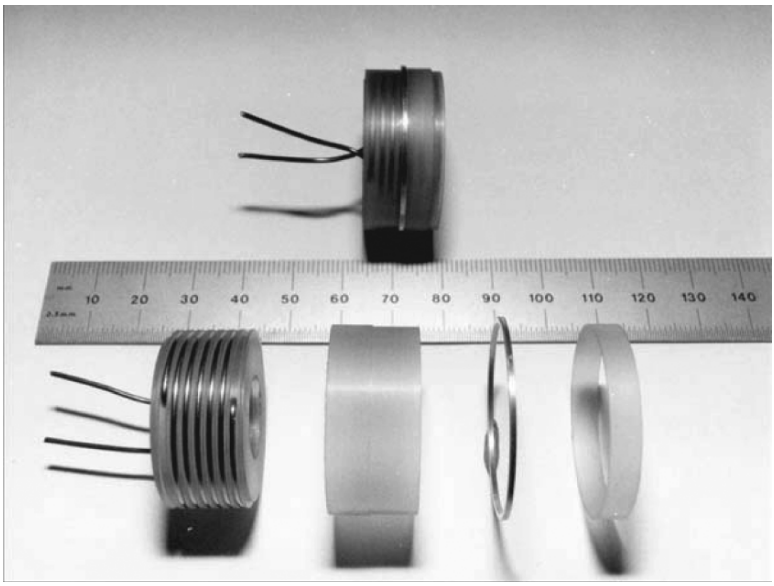

Fig. 8.8. Electromagnetic launch experiment illustrating assembled test (*top*) and assembly component parts (*bottom*) including, launching solenoid test ring and insulating plastic support pieces [Grady and Benson, 1983]

et al. (1984) and Kipp and Grady (1985, 1986). Briefly, a fast-discharge pulsed-power system was used to electromagnetically accelerate metal rings in a radially expanding geometry. The test assembly is illustrated in Fig. 8.8 in which the solonoidal coil carrying the driving current is sheathed with supporting, and insulating, plastic cylindrical sections and the test metal ring. The technique provided uniform radial acceleration of the ring to velocities of several hundred meters per second, although a slight figure-of-eight motion was imparted presumably due to the helicity of the driving coil. Another down side to the technique was an induced electric current in the test ring and the uncertain influence of inductive heating on the plastic flow and fracture properties of the metal. Estimates of heating are provided in the paper of Grady and Benson (1983).

Acceleration history and the velocity at fracture were measured with streak-camera methods. A variety of experiments were performed on aluminum and copper rings to assess the statistical fragmentation properties, including, the strain-to-fracture, the number and size statistics of fragments created, and details of the fracture process. Both the soft OFHC and the 1100-O aluminum selected for testing in the study fractured in dynamic tension through ductile necking followed by extension fracture at a late stage in the necking process. Representative fracture and arrested necking behavior in the dynamic tests are illustrated for the aluminum in Fig. 8.9. Static tension tests were also performed on comparable sized dog-bone shaped specimens.

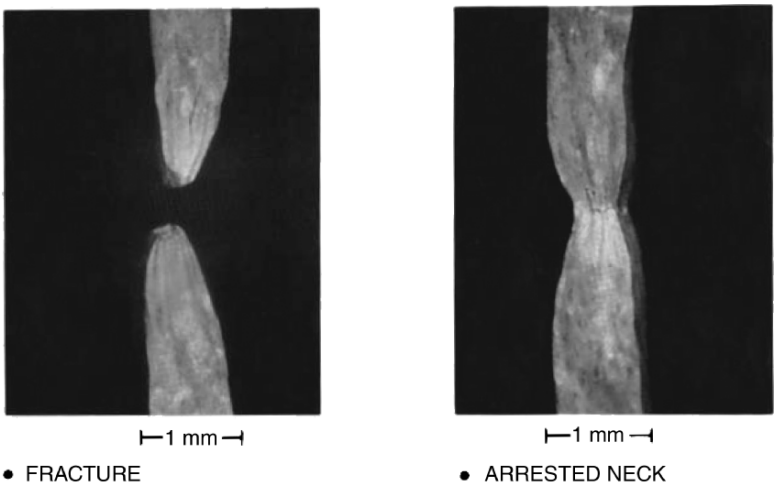

Fig. 8.9. Expanding ring fracture characteristics on 1100-O aluminum illustrating a completed fracture (*left*) and an arrested neck (*right*) [Grady and Benson, 1983]

8.2.2 Fragment Number Experiments

A series of fragmenting ring experiments was performed on 1100-O aluminum and soft OFHC copper, where the initial capacitor voltage was selected to vary the strain rate at the time of fracture. Velocities ranging from about 20 to 200 m/s were achieved which corresponded to strain rates from about 10^3/s to 10^4/s. At the lowest voltages it was not uncommon to recover markedly expanded, but unfractured rings. In these experiments, the number of fragments from each test were counted and correlated with the expansion velocity at fracture. These data are plotted in Fig. 8.10.

Clearly, fragment number data for ring fragmentation of these two ductile metals is better described by a linear dependence on expansion velocity. This behavior contrasts with the two-thirds power dependence observed for the U6Nb ring data. In searching for a possible experimental reason for the different behavior, electric current flow in the fragmenting aluminum and copper rings is a possible suspect. A pusher ring was used in the technique to fragment the U6Nb rings keeping residual electric currents to a minimum. Increasing currents at the higher driving velocities might be expected to influence breakup through excessive heating in the thinning fracture zones.

Ignoring this complication, the functional trend of the fragment number versus velocity for the soft aluminum and copper data is better captured with the earlier Mott statistical prediction of fragment number than with the energy-based prediction. Working with relations developed earlier, fragment number per unit length is provided by,

$$N = \sqrt{\frac{\rho\dot{\varepsilon}^2}{2\pi Y}\frac{n}{\sigma}}\,. \tag{8.2}$$

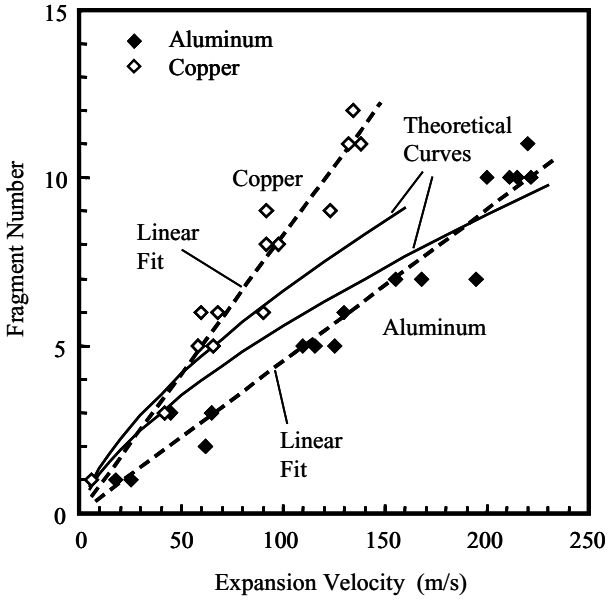

Fig. 8.10. Fragment number data for aluminum and copper ring tests. Curves are the least squares linear fits and predictions from energy-based fragmentation theory

Equation (8.2) is appropriate for sensibly large n, and N is determined by the statistical standard deviation in strain-to-fracture, ($\cong 1.28\sigma/n$) as well as the flow stress Y, metal density ρ and the expansion strain rate $\dot{\varepsilon}$. The ring is then predicted to break into a total number of fragments,

$$N_T = 2\pi RN = \left(\frac{2\pi\rho}{Y}\frac{n}{\sigma}\right)^{1/2} u \; . \tag{8.3}$$

A measure of the standard deviation in the strain-to-fracture is not known so a forward prediction of fragment number cannot be made. Linear fits to the data, shown in Fig. 8.10, can be made, however, and the necessary back calculation performed for the strain-to-fracture standard deviation calculated from (8.3). Values of 0.051 and 0.096 are obtained for copper and aluminum, respectively. The standard deviation in strain-to-fracture for copper is found to be about 12% of the measured static strain-to-fracture ($\simeq$0.4) and is not unreasonable. The calculated standard deviation in strain-to-fracture for aluminum is approximately equal to the static strain-to-fracture ($\simeq$0.1) and seems unreasonably large. Dynamic strains for this ductile aluminum are substantially larger, however, and considerations in the following subsection will show that this statistical failure measure is also sensible.

The corresponding total fragment number expression based on the fracture energy theory is,

$$N_T = 2\pi \left(\frac{\rho R}{24\Gamma} \right)^{1/3} u^{2/3} , \tag{8.4}$$

where Γ is the fracture energy. Equation (8.4) is clearly at odds with the functional dependence on the expansion velocity in Fig. 8.10. Nonetheless, predictions based on (8.4) are enlightening. The fracture energy Γ for the two metals was estimated from the measured static tensile flow stress at fracture and the deformation strain in the fracture zone inferred from the geometry of the neck and fracture deformation. Values of $\Gamma = 0.03$ MJ/m^2 for aluminum and $\Gamma = 0.07$ MJ/m^2 for copper were calculated and are probably reasonable within $\pm 50\%$. The values for Γ correspond to effective fracture toughness of 60 MPa·m$^{1/2}$ and 140 MPa·m$^{1/2}$ for aluminum and copper, respectively. Fragment number curves based on (8.4) are shown with the data in Fig. 8.10 and, although functionally wrong, the reasonable agreement in magnitude is encouraging. An interesting feature to ponder is the scale dependence of the energy-based relation (dependence on the ring radius R) in comparison to the scale independence of the Mott relation in (8.3). This scale dependence has not been explored in any of the previous ring studies.

A fascinating observation is provided by the plot shown in Fig. 8.11, where the fragment number data for both aluminum and copper are plotted as a function of the radial kinetic enrgy, $\rho u^2/2$. It is remarkable that the data are effectively collapsed in this plot. The curve is a best fit of the fragment number to the kinetic energy of the form $N_T = (T/\tau)^{1/2}$ with a value of $\tau = 64$ MJ/m^3. Both the statistical Mott and the energy-based relations for fragment number in (8.3) and (8.4) contain ρu^2 in the numerator. Overlay of the two data sets in Fig. 8.11 then requires that the corresponding governing fracture properties in either theory for the two materials scale to effect the invariance. This overlay of the data could certainly be fortuitous but it is certainly intriguing and warrants further study.

8.2.3 Fracture Strain Experiments

A further intriguing feature of the dynamic expanding ring experiments is plastic strain accumulated in the metal up to the point of fracture and fragmentation. In the work of Olsen (2000) in the previous section on U6Nb this strain was simply determined by the amount of expansion incurred at the point of fracture as determined through the VISAR velocity history measurements. In the present study strain to fracture was pursued in somewhat more depth.

Both of the ductile metals investigated in the present study exhibit substantial hardening in tension, and static strains-to-fracture of approximately 0.08 and 0.40 were measure for the ductile aluminum and copper, respectively. These static values provide a reference for examining the strains accumulated in the dynamic fracture process.

Before investigating the experimental results of the expanding ring tests of Grady and Benson (1983), it is instructive to examine the fracture strain

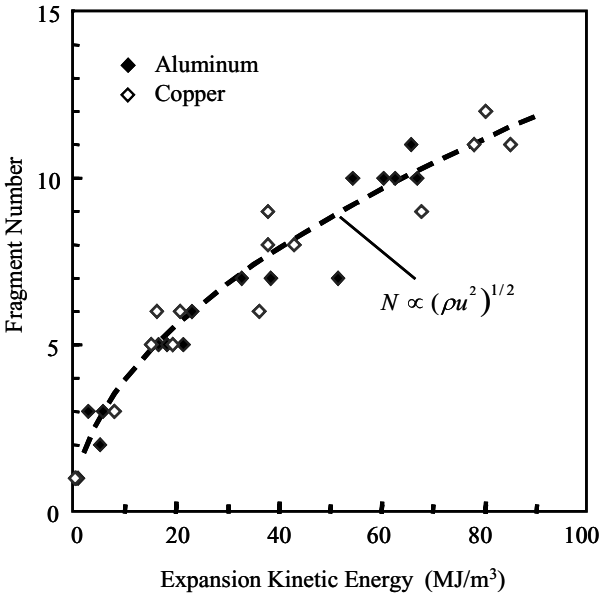

Fig. 8.11. Fragment number data plotted against expansion kinetic energy $\rho u^2/2$

behavior inferred from the several theories pursued here. Fracture in the Mott theory is characterized by a statistical strain-to-fracture and the cumulative strain-at-fracture completion is provided by the integral,

$$\varepsilon_f = \int_0^\infty (1 - D)\dot{\varepsilon} dt \ . \tag{8.5}$$

The factor of $1 - D$ accounts for the fraction of the length over which straining has arrested due to the propagation of Mott release waves from sites of fracture. This factor is provided by,

$$1 - D = e^{-\int \lambda(\varepsilon) d\varepsilon} \ . \tag{8.6}$$

A power law representation of $\lambda(\varepsilon)$, which has been pursued extensively in the present text, provides a Weibull description of the strain-to-fracture statistics. Alternatively, an exponential representation, and Gumbel statistics, as was pursued by Mott, could be used. Weibull statistics leads to a cumulative failure strain in (8.5) of,

$$\varepsilon_f = \alpha_n \left(\frac{\sigma^n}{\sqrt{2Y/\rho\dot{\varepsilon}^2}} \right)^{\frac{2}{2n+1}} \ . \tag{8.7}$$

For small values of the distribution shape parameter n the failure strain in (8.7) exhibits a more complex dependence on properties. (For $n = 1$ a dependence on strain rate of $\varepsilon_f \sim \dot{\varepsilon}^{2/3}$ is predicted.) However, for sensibly large n,

as is expected to be the case, (8.7) approaches $\varepsilon_f \cong \sigma$, and failure strain is effectively independent of the expansion rate, as well as other governing material properties. The Mott approach using Gumbel statistics leads immediately to a rate independent cumulative failure strain.

In the energy-based approach to fragmentation, the theory examines a representative fracture from fracture inception until completion. It was shown in Sect. 3 that, if the fracture resistance is characterized by a dissipation energy Γ, a time,

$$t_f = \left(\frac{72\rho\Gamma^2}{Y^3\dot{\varepsilon}}\right)^{1/3} , \tag{8.8}$$

is required for fracture completion and within this time a Mott release wave propagates a distance,

$$x_f = \left(\frac{3\Gamma}{\rho\dot{\varepsilon}^2}\right)^{1/3} , \tag{8.9}$$

from the fracture. Within this region a nominal strain,

$$\varepsilon_f = \varepsilon_{fo} + \int_0^{t_f} \dot{\varepsilon} dt , \tag{8.10}$$

is achieved, where ε_{fo} is the strain at fracture onset. Equation (8.10) yields,

$$\varepsilon_f = \varepsilon_{fo} + \left(\frac{72\rho\Gamma^2\dot{\varepsilon}^2}{Y^3}\right)^{1/3} , \tag{8.11}$$

and, if the onset of fracture strain ε_{fo} is independent of strain rate, a two-thirds power dependence on strain rate is expected, with a quantitative prediction provided by (8.11) if the material parameters governing Mott fragmentation are known.

There are various methods for assessing the fracture strain in the present expanding ring experiments and two of these methods are explored here. First, it was convenient to soft capture all of the fragments, measure the total length $L = \sum L_i$ of the fragments, and identify a fracture strain $\varepsilon_f = 1 - L/L_o$, where L_o is the initial circumferential length of the test ring. This strain measure is plotted as a function of expansion velocity in Fig. 8.12 for the same copper and aluminum fragmenting ring fragment number data shown in Figs. 8.10 and 8.11.

Curves through the data are based on (8.11) and values of Y and Γ determined from the static tension tests. Fracture onset strain ε_{fo} was selected to best fit the fracture data. This estimate of ε_{fo} is somewhat larger than the static tensile strain-to-fracture for the two metals. For contrast, the strain rate independent fracture strain intrinsic to the Mott theory is also illustrated.

The various comparisons in Fig. 8.12 certainly raise questions concerning the accumulation of strain up to and during the expanding ring breakup

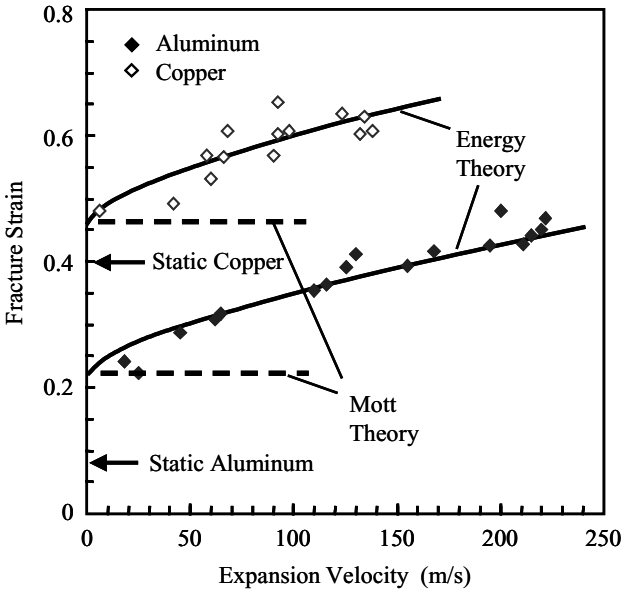

Fig. 8.12. Strain at fragmentation for aluminum and copper rings. Comparisons with energy-based and Mott theories are shown along with measured static strain-to-fracture

process. Intrinsic rate dependence during deformation leading up to the fracture process is certainly possible and could account for the observations within the context of the Mott statistical theory. Nevertheless, the reasonably close quantitative agreement of the measured excess strain with predictions based on the energy theory suggests that at least some of the features of the additional cumulative straining implied by the theory during the time-dependent fracture process are probably correct.

An alternative method for determining the strain-to-fracture in the ring experiments is to interrogate the accumulated strain in individual fragments. This can be done by both weighing each individual fragment and measuring its length. The extension, or fracture strain, corresponding to an individual fragment is provided by,

$$\frac{L}{L_o} = 1 + \varepsilon_f = \frac{L}{M}\frac{M_T}{2\pi R_o} \,, \tag{8.12}$$

where, L and M are the measured residual length and mass of the fragment, respectively, M_T the total mass of the ring, and $2\pi R_o$ the initial circumference of the ring. This approach was pursued in the earlier study [Grady and Benson, 1983], but was not reported in the publication of that study. Four fragments each were randomly selected from four separate tests conducted on the ductile aluminum at approximately the same expansion velocities (in the range of

310–350 m/s), and in which 12 to 13 fragments for each ring was achieved. (These were not the same experiments reported in Figs. 8.10–8.12.) Fragment extension determined through (8.12) is plotted against cumulative fragment number for the sixteen fragments in Fig. 8.13.

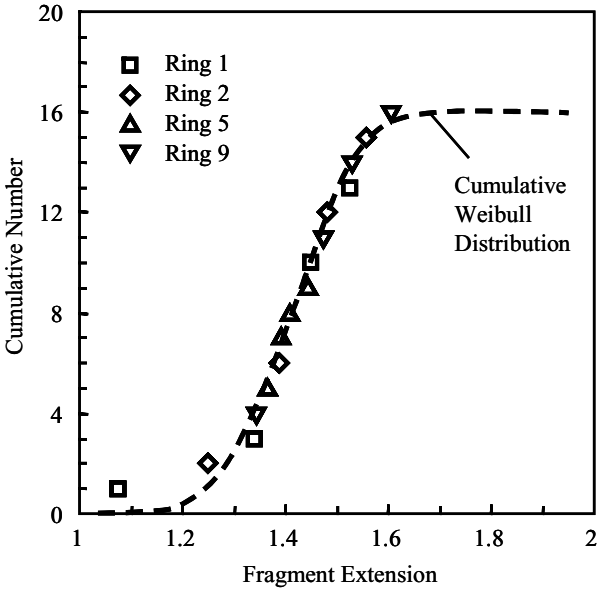

Fig. 8.13. Strain at fragmentation determined from the measured length and weight of individual aluminum fragments. A Weibull function is fit to the cumulative fragment number data

In this presentation of the data the recovered fragments showed a marked statistical spread in the strain-to-fracture. The distribution in Fig. 8.13 was fit to a cumulative Weibull distribution,

$$N(\varepsilon_f)/N_o = 1 - e^{-(\varepsilon_f/\sigma)^n} \ . \tag{8.13}$$

A best fit to the data provides a scale parameter $\sigma = 0.45$ and shape parameter of $n = 4.5$. A standard deviation in strain-to-fracture of approximately $1.28\sigma/n \cong 0.13$ is in reasonable agreement with the value of 0.096, previously back calculated from the fragment number data and the Mott relation in (8.3).

Thus, aspects of the Mott statistical theory are apparently playing a role in the breakup process. Namely, a statistical spread in the time, and strain, at which fractures achieve completion. This feature of the fracture process is further emphasized in the expanding tube experiments of Winter (1979) and the more recent tests of Vogler et al. (2003).

8.2.4 Fragment Size Statistics

Fragmentation of the expanding ring appears to be a random process. Both the breaks in the ring, as well as the well-defined necking regions constituting arrested fractures, appear to be statistically dispersed around the circumference of the ring. Fragments collected from any given test can vary in length by a factor of ten or more. This statistical fragmentation behavior was also noted in the expanding ring tests on U6Nb metal discussed in the previous subsection. Sensible agreement with the Mott treatment of the fragmentation statistics was found, although this was actually only quantified in the experimental study for one test.

The statistical distribution in fragment size (or length) was also explored in the present study. As in the case for fracture strain, there are different ways that the data can be displayed. For the one experiment on U6Nb a cumulative distribution in fragment size was presented. The number of fragments from that one test was too sparse to provide a meaningful density distribution.

In the present series of tests five experiment on 1100-O aluminum conducted at nominally the same expansion velocity, and in which 11 to 13 fragments each were produced, were combined and their collective density distribution was determined. A histogram of the fragment number versus mass is provided in Fig. 8.14. The mass intervals are 2.5 mg and, since aluminum density is approximately 2.7 mg/mm^3, each interval adds about one mm to the fragment length. The mode of the experimental distribution peaks somewhere in the range of 10–20 mg, and tails off for both larger and smaller fragments.

A best fit to the experimental data with both an exponential (Lineau) and an analytic Mott distribution is also shown in Fig. 8.14. The exponential distribution, as presented, is clearly at odds with the data. Note, however, that fragments at the small end of the distribution are within a factor of two to three times the initial cross section dimension of the metal ring (1 mm $\sim$ 2.7 mg). One might expect different physics to govern fracture at this length scale. Thus an exponential distribution with a tail off at the small fragment end due to this different physics might not be an unreasonable representation of the data.

The Mott distribution appears to be a better description of the data. Selecting rings with 11, 12 and 13 fragments probably unfairly broadens the distribution by about 10%. The several large fragments in the large end tail of the distribution are totally at odds with the Mott distribution, however.

Very distinct arrested necking regions such as shown in Fig. 8.9, were a conspicuous feature in the present expanding ring experiments. For the sake of interest a fragment size distribution for this same set of five tests was generated by also considering the well-defined necks as completed fractures. This distribution is provided in Fig. 8.15, and again compared with the Mott and the exponential Lineau theoretical representations of the data.

The Mott distribution does appear to capture the general trend of the experimental distribution. Again, however, it is not clear whether the decrease

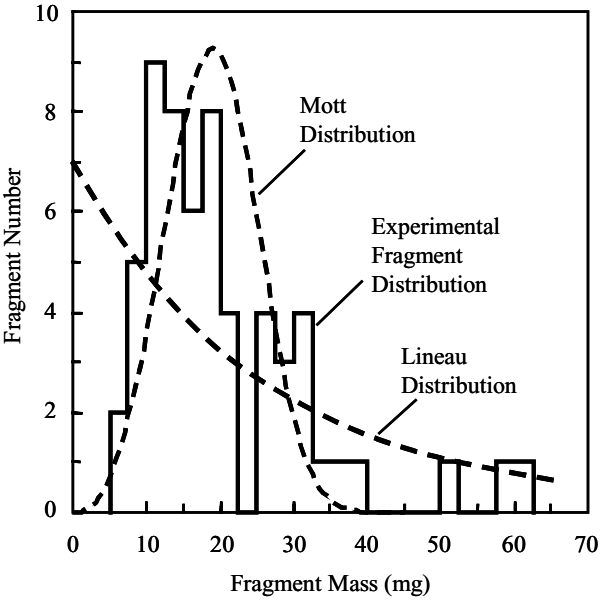

Fig. 8.14. A collective histogram of the fragments from five ring test on 1100-O aluminum in which 11 to 13 fragments were produced. The fragment mass in mg is approximately equal to the length in mm

in fragments at the small end of the distribution is due to the Mott interaction physics, or just due to the fact that fragment lengths are approaching the ring cross-section dimension. Also, as in the case of the fragment distribution in Fig. 8.14, there are several long segments of a size at odds with the Mott distribution.

It is also of interest to examine the fragment statistics over the wider range of expansion velocities achieved in the study. Representations of the fragment distributions such as shown in Fig. 8.14 become difficult, however, because of the limited number of fragments produced in some of the tests. One possible approach for examining the random nature of the fragmentation event is to pick a statistical measure in the spread of the fragments size, such as the standard deviation for each test, and compare this with the theoretically predicted standard deviation. This approach has been carried out for a limited number of the tests on 1100-O aluminum. For each ring fragmentation test the standard deviation is calculated and normalized by the average fragment size. This normalized standard deviation is plotted as a function of the number of fragments in each test in Fig. 8.16.

For comparison, the corresponding statistical measure is calculated for several of the theoretical distributions. The normalized standard deviation for the Lineau (exponential) distribution is unity. For some of the tests examined, the number of fragments produced was small (four in one – six in

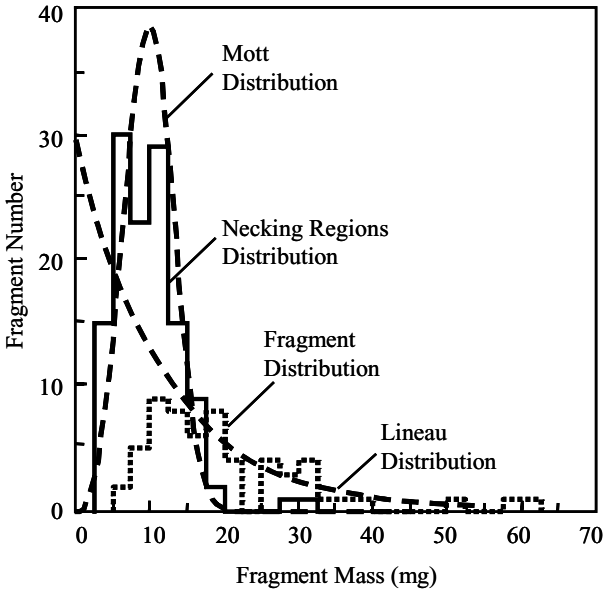

Fig. 8.15. A collective histogram for the same five ring test as the previous figure, where well defined arrested necks are also included in the partitioning of circumferential fragments

another). Consequently, it is sensible to calculate the same statistical parameter for the binomial distribution, which is equivalent to the Lineau distribution assumptions on a finite line length. The normalized standard deviation for the binomial distribution is also shown in Fig. 8.16. The normalized standard deviation of the Mott distribution ($\sim$0.321) is also shown in the Fig. 8.16.

Clearly, the experimental data are statistically tighter than predicted by a Lineau (or binomial) distribution. There is also a tendency for the standard deviation of the data to decrease with decreasing fragment number as suggested by the binomial distribution. The measured standard deviations are not, however, in agreement with the Mott distribution.

Usually it was an errant large fragment in the collection which markedly increased the experimental standard deviation, but not in every case. Nonetheless, the data disagree with the Mott prediction of the spread in fragment size by nearly a factor of two. So again, the present ring data suggest that the fragmentation process is more complex than the simpler theories predict.

8.3 Weisenberg and Sagartz Expanding Cylinder

An interesting experiment intermediate between the expanding ring tests discussed previously, and exploding cylinder tests considered in Sect. 7, was

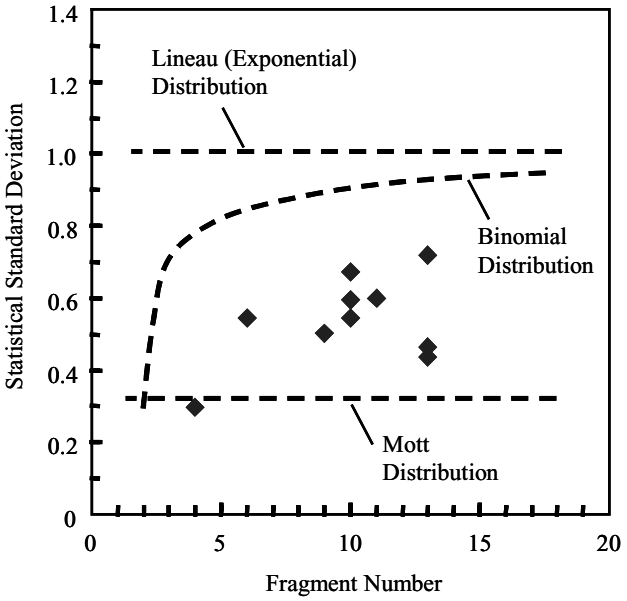

Fig. 8.16. Standard deviation normalized by the average fragment size plotted against the number of fragments produced in the test for the expanding ring fragmentation experiments on 1100-O aluminum

performed by Weisenberg and Sagartz (1977). In that study they used similar inductive methods powered by a large capacitor discharge system to rapidly expand and fracture thin cylinders of 6061-T6 aluminum. Current is carried by an internal copper conductor. The copper driver applies a radial driving pressure approaching 2 GPa for several microseconds accelerating the aluminum cylinder to its terminal radial velocity. Cylinders were 127 mm in diameter and 102 mm in length with a wall thickness of 1.27 mm. Dynamic fracture was observed photographically to occur at about 30% expansion strain and at a strain rate of approximately 10^4/s. This value is slightly below the approximately 40% strain in the 1100-O aluminum ring experiments in the previous section at a comparable strain rate.

During the deformation proceeding fracture, slip lines formed at angles of approximately 30° to the axis of the cylinder. Fracture then occurred along these slip lines and propagated until breakup was complete. Fragments from one test [Weisenberg and Sagartz, 1977] collected and displayed are shown in Fig. 8.17. The collection nicely illustrates the nature of the dynamic fracture process, including the tendency toward oblique fracture along plastic slip lines and arrested fractures due to unloading Mott waves. Details of the deformation processes leading to fracture are more readily observed in the high speed photograph of one cylinder test shown in Fig. 8.18.

Fig. 8.17. Fragments from one magnetic expanding cylinder test on 6061-T6 aluminum [Weisenberg and Sagartz, 1977]

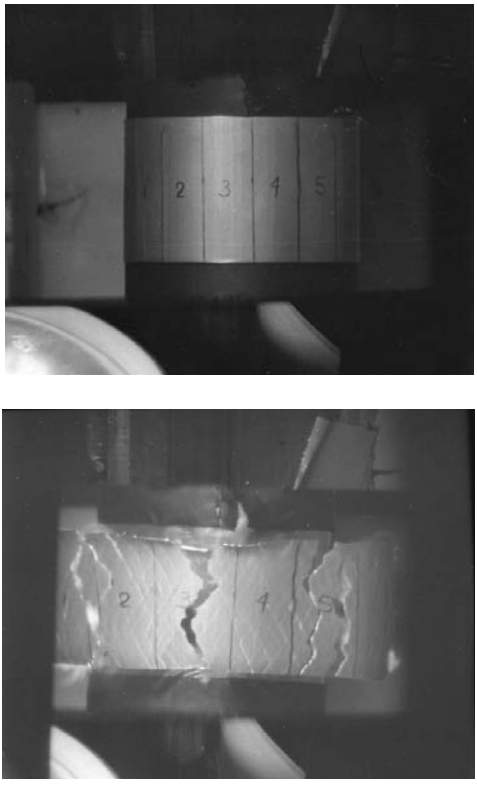

Fig. 8.18. High speed photograph illustrating deformation and fracture features in the expanding aluminum cylinder tests of Weisenberg and Sagartz (1977)

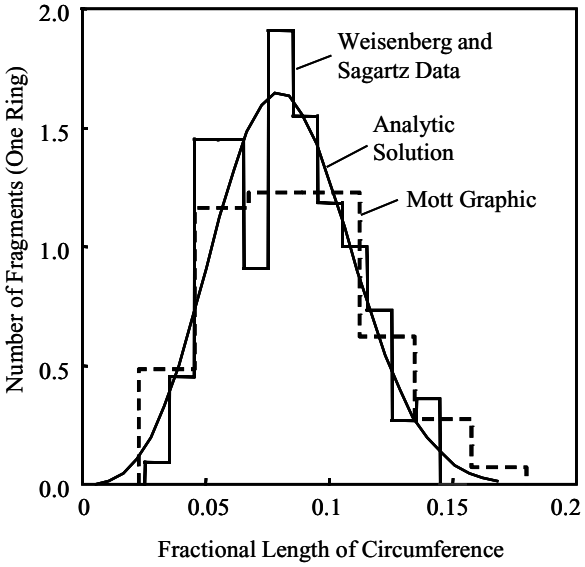

Fig. 8.19. Experimental fragment size data for expanding aluminum ring tests of Weisenberg and Sagartz (1977) and comparisons with statistical Mott theories

A total of 125 fragments were collected from 11 equivalent tests. All fragments were assigned an effective length by weight. Accordingly a histogram of the statistical size distribution for the aluminum cylinder data is provided in Fig. 8.19. In this figure the ordinate identifies the number of fragments normalized to a single ring which occurred within the corresponding fragment size (length) interval. The abscissa identified fragment size as a fraction of the original circumference of the ring.

Experimental fragment size data of Weisenberg and Sagartz (1977) in Fig. 8.19 are compared with both Mott's graphical distribution and the analytic distribution for plastic fracture developed previously in Sects. 3 and 4. Both distributions satisfactorily describe the relatively narrow spectrum of fragment lengths. It is straightforward to calculate the scatter in strain-to-fracture necessary within the Mott theory to account for the average fragment size displayed in the ring data. Using reasonable values of $Y = 300\,\mathrm{MPa}$ and $\rho = 2700\,\mathrm{kg/m^3}$ for 6061-T6 aluminum at an expansion strain rate of $10^4/\mathrm{s}$ a standard deviation in strain-to-fracture of about 0.25 is calculated from the Mott relation for fragment number. This estimated scatter in strain-to-fracture is probably not inconsistent with a nominal 0.3 strain-to-fracture determined in the experiments of Weisenberg and Sagartz (1977) although, it is somewhat larger than determined for 1100-O aluminum in the previous ring tests.

8.4 Winter's Expanding Cylinder

A further seminal experimental study of dynamic fragmentation performed in part to explore features of the Mott theory of fragmentation was conducted by Winter (1979). In that work thin cylinders (17 mm diameter and 1 mm wall thickness) of selected metals were loaded to fracture failure with a light gas gun. Metal cylinders were approximately half filled with an elastomeric material and nylon solid cylinder projectiles accelerated to velocities of several hundred meters per second were caused to enter the cylinder and strike the elastomeric material near the midpoint of the cylinder. Pressures brought about by the impact led to radial loading and plastic expansion of the metal cylinder. The intensity of the load and expansion speed of the cylinder was determined by the impact velocity of the nylon cylinder.

The test geometry and nature of the impact-induced deformation and subsequent failure are illustrated in Fig. 8.20. The cylinders experience rapid, relatively symmetric radial bulging at the waist. Radial velocity of the bulge extremum accelerates rapidly to a constant velocity and circumferential strain rates as determined from this velocity ranged from about 1×10^4/s to 4×10^4/s. Axial stretching rates within the bulge region were reported to be about one-third the circumferential strain rate.

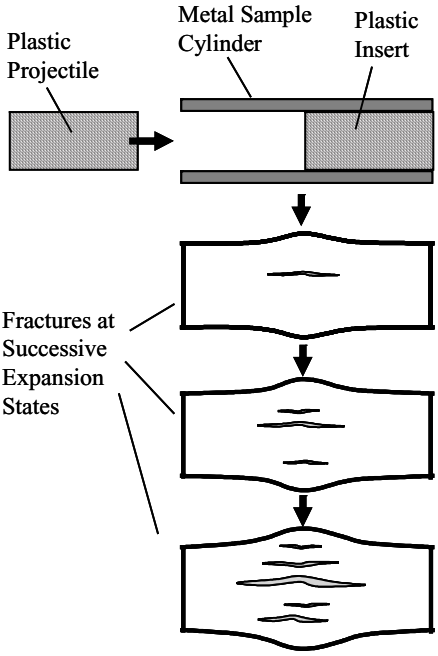

Fig. 8.20. Illustrated gun-accelerated-projectile technique for conducting dynamic expanding metal cylinder fracture experiments

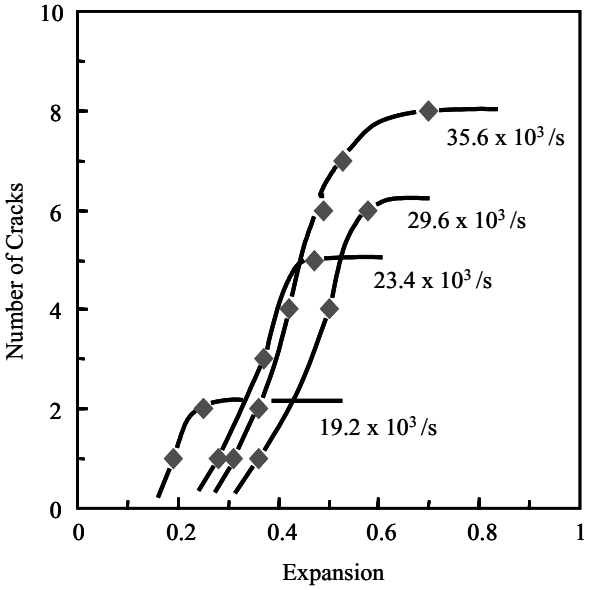

Fig. 8.21. Plot of fracture number as a function of cylinder expansion for the four experiments on naval brass of Winter (1979)

High-speed photography was the principal diagnostic providing deformation history as well as imaging inception and growth of axial fractures as dynamic deformation exceeded the failure limits of the material. Data are reported for aluminum, steel, copper, brass, and bronze. The more comprehensive study was that on naval brass. Metallurgical examination of fracture surfaces of recovered fragments revealed the shear fracture characteristics common to explosive fragmentation of metal shells.

Unique to this study was the effort to explore the temporal history of fracture inception. The multiple Kerr cell photographic images acquired at a rate of one every few microseconds (4 μs per frame was reported for the illustrated test on brass) provided a measure of the accumulation over time of the number of axial fractures participating in the failure process.

Results for the four tests on brass conducted by Winter (1979) at successively higher strain rates are shown in Fig. 8.21. Only fractures within the field of view imaged by the camera are included in this plot, which was approximately one-third of the cylinder.

This early study by Winter (1979) highlights a number of features unique to the failure of rapidly expanding ductile metal shells. The data focusing on the temporal history of fracture activation, is, however, absolutely unique and is central to the statistics-based fragmentation theory of Mott. Attention of the present efforts will address these data.

Each of the four tests on the brass cylinders shown in Fig. 8.21 illustrates the fact that the fractures responsible for cylinder failure do not all appear simultaneously but emerge statistically over time and expansion, in keeping with the statistical fracture criteria postulated by Mott. These data also illustrate that there is, in some sense, a measure of plastic strain incurred before fracture failure, although, a clear criteria for quantifying this strain-to-failure is less certain. Winter proposed a criteria based on a certain level of observable crack opening, which, from his plots of strain-to-failure, appears to correspond roughly to the cylinder expansion upon appearance of the last fracture. One might as readily propose strain-to-failure as the expansion upon appearance of the first fracture.

We will here also identify a strain-to-failure for the four experiments on naval brass for purposes of assessing the fragmentation theory of Mott. First, however, the theory will be pursued further to better understand the sense of strain-to-failure in Mott's statistics based theory. This pursuit will also reveal the coupling between the characteristic fracture spacing and the temporal occurrence of fractures necessitated by the theory of Mott and supported by the data of Winter.

In the earlier development of Mott's theory for ductile fracture in Chap. 3, the total number of fractures per unit circumferential length was provided through integration over all expansion $0 \leq \varepsilon < \infty$. Equally valid would be the expression providing the predicted number of fractures up to an expansion ε,

$$N(\varepsilon) = \frac{2n}{(2n+1)(a\sigma)^n} \int_0^y y^{\frac{2n}{2n+1}-1} e^{-y} dy \,, \tag{8.14}$$

where, $y = (a\varepsilon)^{(2n+1)/2}$ and with a provided in Sect. 3, where similar developments were pursued. The equation is readily integrated providing,

$$N(\varepsilon) = \beta_n \left(\frac{n}{\pi d^2 \sigma}\right)^{\frac{n}{2n+1}} G\left(\frac{2n}{2n+1}, y\right) \,, \tag{8.15}$$

where, β_n is the function of n provided in Chap. 3, and is sensibly unity for all n greater than one. The length scale $d = \left(2Y/\rho\dot{\varepsilon}^2\right)^{1/2}$and $G(\cdot, y)$ is the normalized gamma function, approaching unity as y approaches infinity.

A similar development can be put forth for the plastic strain accumulated through the cylinder expansion and fracture process. Early in the expansion before fracture initiates, expansion ε and the plastic strain ε_p are the same. When fractures initiate and Mott waves emanate from the points of fracture, regions encompassed by the waves will seize straining and the expansion and cumulative plastic strain will diverge. Analytically this is written,

$$\varepsilon_p(\varepsilon) = \int_0^\varepsilon (1 - D) d\varepsilon \,, \tag{8.16}$$

where, D is the fraction of circumference subsumed by Mott waves at expansion ε. This expression provides the integral,

$$\varepsilon_p(\varepsilon) = \frac{2}{(2n+1)a} \int_0^y y^{\frac{2}{2n+1}-1} e^{-y} dy \,, \tag{8.17}$$

with a and y the same as in the previous relations. Integration yields,

$$\varepsilon_p(\varepsilon) = \alpha_n \left(\frac{\sigma^n}{d}\right)^{\frac{2}{2n+1}} G\left(\frac{2}{2n+1}, y\right) \,, \tag{8.18}$$

where,

$$\alpha_n = \left(\frac{2}{2n+1}\right)^{\frac{2n-1}{2n+1}} \left[\frac{1}{\sqrt{\pi}} \frac{\Gamma(n+1/2)}{n\Gamma(n)}\right]^{\frac{2}{2n+1}} \Gamma\left(\frac{2}{2n+1}\right) \,, \tag{8.19}$$

is again close to unity for n greater than one.

Plots of the number of fractures and the cumulative plastic strain from (8.15) and (8.18) respectively, are shown in Fig. 8.22. The respective curves are normalized to σ and d equal to one, while $n = 7$ was chosen for illustration which corresponds to a standard deviation in the strain-to-fracture of $1.28\,\sigma/n$ or about 20%.

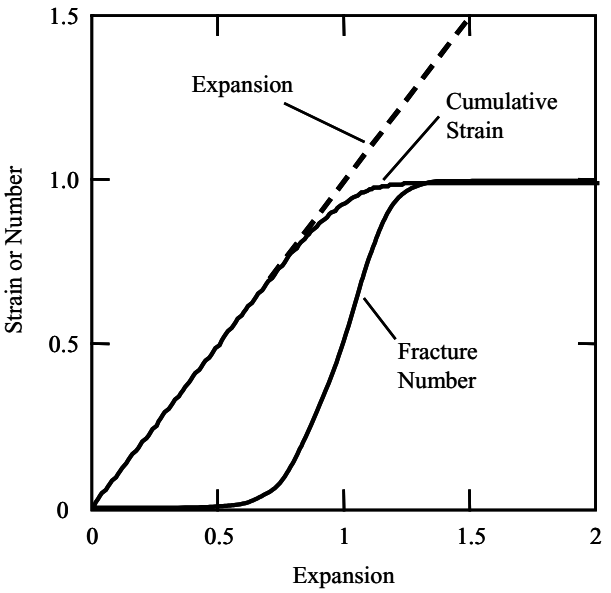

Fig. 8.22. Illustrates the temporal history of fragment number and cumulative plastic strain as a function of expansion

The plot illustrates the essential physics governing fragmentation in the Mott theory. Namely, the statistical spread in the strain-to-failure, governed by the parameter n when σ is fixed within a Weibull representation of the hazard function, determines both the characteristic fracture spacing (total fracture number) and the statistical temporal history of the appearance of fractures. Thus, within the Mott theory, the result of a certain characteristic fracture spacing requires a corresponding spread in the temporal occurrence of those fractures. The data of Winter (1979) for naval brass, in which both total fracture number and temporal history were measured, are therefore a unique and stringent test of the Mott theory.

In Fig. 8.22 the cumulative plastic strain is, according to the statistical Mott theory, observed to diverge smoothly from the cylinder expansion when fracture initiates and plateaus to a unique failure strain upon completion of the fracture process. The plot suggests that a reasonable observable estimate of the strain-to-failure is determined by the midpoint of the fracture number curve in the same plot. The data of Winter are consistent with this strain-to-failure interpretation.

Strain-to-failure by the above criteria as well as total fragment number for the four naval brass experiments of Winter (1979) are plotted as a function of expansion rate in Fig. 8.23. Assessing strain-to-failure from the midpoint of the number history curves in Fig. 8.21 reveals a degree of inconsistency in the data. Namely, the first (lowest expansion rate) and third test provide the lowest and the highest strain-to-failure, respectively, while the second and fourth are nominally the same. Error bars indicated in strain-to-failure are estimated from plotting uncertainties and photographic imaging frequency. These variations cannot be accounted for with Mott's statistics and perhaps relate to sensitivity of the dynamic fracture to preparation differences in individual

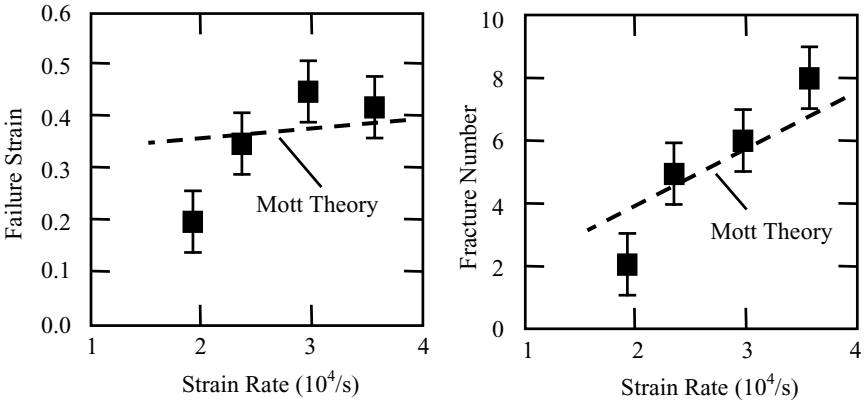

Fig. 8.23. Failure strain and fragment number from data of Winter (1979) on expanding naval brass cylinders. Curves represent the best fit with Mott fragmentation theory

cylinders (surface finish for example). In any case, these experimental variations in strain-to-failure are not captured in the theoretical representation to be described.

The fracture number data shown represent the fractures imaged by the photographic method over approximately a third of the circumference of the cylinder as described by Winter (1979). Error bars shown correspond to plus or minus one fracture.

Mott's theoretical equations for the total fracture number and the final strain-to-fracture ((8.15) and (8.18) for expansion approaching infinity) provided the best fit to the data in Fig. 8.23 by adjusting σ and n. The values were $n = 7$ and $\sigma = 0.18$ in S. I. units. A flow stress $Y = 300$ MPa and density $\rho = 8450\,\mathrm{kg/m^3}$ was used for the naval brass.

The statistical fracture number histories from (8.15) for the four experimental strain rates using the Mott parameters σ and n determined above from the final fracture number and plastic strain data for naval brass are shown in Fig. 8.24. Figures 8.23 and 8.24 clearly illustrate the coupling between final fracture spacing and the statistical appearance of fractures central to the theory of Mott. A comparison of the predicted histories of the fracture number in Fig. 8.24 with the experimental histories of Winter (1979) in Fig. 8.21 supports the Mott theoretical approach. Although the predicted curves cannot

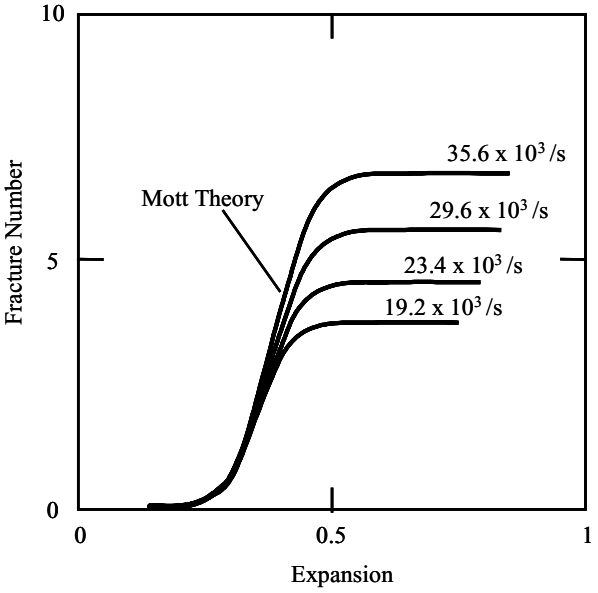

Fig. 8.24. Calculated fracture number history, or rate of fracture appearance, for the four naval brass experiments of Winter (1979) based on the Mott parameters n and σ selected to fit the fragment number and strain-to-fracture data

capture the scatter in translation of the several tests, the history of individual experimental tests is nicely reproduced by the theory.

8.5 Natural Fragmentation of an Exploding Cylinder

Smooth-walled explosively-loaded metal cylinders fragment without the aid of fragmentation enhancing techniques. In the natural fragmentation of exploding cylinders the statistical distribution in the size and velocity of fragments is determined thorough a complex interplay among explosive characteristics, geometry of the explosive-case system, and mechanical properties of the case metal. As noted in previous chapters, early attempts to introduce some scientific order to such violent event are attributed to Mott (1943, 1947, 1948), Taylor (1963), and Gurney (1943), among others. Chapter 7 of the present text is focused on issues of scaling of exploding cylinders. Literally thousand of arena tests of explosively-driven fragmenting cases in which various fragmentation data have been collected have been performed over the intervening decades.

In the present section discussion is focused on one study in which explosive and case metal were particularly well characterized, and quite thorough diagnostics were used to interrogate the explosive natural fragmentation event [Grady, and Hightower, 1992]. These results are considered in light of Mott's statistical and the energy-based predictions of fragmentation.

8.5.1 Natural Fragmentation Experiment

An explosive fragmentation experiment was performed on a 15.2 cm diameter smooth wall metal cylinder. The cylinder was 38.1 cm in length with a wall thickness of 5.7 mm. The cylinder was machined of 4140 steel and heat treated to a Rockwell hardness of 40 ($Y = 1.1$ GPa). The cylinder was filled with RX-35-AN explosive and the cylinder ends were confined. The explosive was center detonated at one end.

The insensitive high explosive RX-35-AN used in the present study has been calibrated through instrumented copper cylinder expansion experiments to provide expansion velocity data for purposes of establishing appropriate nonideal explosive equation-of-state parameters [Grady, 1990]. The measured expansion velocity data are scaled with appropriate Gurney relations to determine expansion velocity behavior for the steel cylinder experiment.

High speed front-lit photography using a CORDIN framing camera with 5 μs frame intervals was used to observe acceleration and breakup of the expanding cylinder. The opening of fractures and emergence of explosive gases were consistent with the 1.20–1.25 strain to fracture measured on recovered fragments. An expansion velocity of 1760–1830 m/s determined from the photographs compare well with the limiting Gurney velocity of about 1800 m/s calculated for this cylinder.

Multiple flash radiography was used to determine fragment velocity, trajectory and pattern for a 40° sector of the cylinder. Fragments from this sector were captured in fiberboard bundles which were placed approximately 6 meters from the event. From the bundles, 161 fragments were recovered which represents 90% of the weight of the 40° cylinder sector.

From the recovered fragments, it was observed that fracture was predominantly along elongated strips with the fracture parallel to the axis of the cylinder. A number of the fragments were 4 to 5 times longer than they were wide. Both tensile and shear fracture were observed from examination of fracture surfaces. Shear fracture appeared to be the dominant breakup mechanism. Fragment size statistics were determined from the recovered fragments for comparisons with the present fragmentation analysis.

8.5.2 Strain to Fracture

Within the fragmentation theories considered, it is necessary to establish the radial expansion velocity of the exploding cylinder at the moment of fracture to provide a measure of the strain rate at which breakup occurs. An early theory used to calculate the fracture strain of explosively expanding cylinders is due to Taylor (1963). Later improvements on Taylor's theory have been offered, however predicted fracture strains do not differ significantly from that of Taylor. Taylor's analysis led to a relation for the circumferential stress in the shell subjected to an internal pressure P given by $\sigma(y) = Y - P(1 - y/h)$ where Y is the yield stress in simple tension, h is the shell thickness and y *is* a coordinate through the thickness, $0 \leq y \leq h$. Thus $\sigma(0) = Y - P(\text{compression})$ at the inner surface and $\sigma(h) = Y(\text{tension})$ at the outer surface. The crossover point occurs at an interior point of the shell. Taylor assumed that failure occurs when the internal pressure within the expanding cylinder decreases to a value such that tension is just achieved at the inner surface.

It is common to assume ideal gas behavior for the explosive products and develop an expression for pressure versus expansion radius to calculate fracture strain with the Taylor method. The RX-35-AN explosive used in the present study was not suited to an ideal gas description of the explosive products, however. Instead, the velocity history data was used, through appropriate Gurney expressions, to calculate pressure versus radius behavior [Grady, 1990].

Through this method, an internal pressure of $P = Y = 1.1\,\text{GPa}$, corresponding to the yield stress of 4140 steel, is calculated at an expansion radius of $R/R_o = 1.24$. This fracture strain calculated through the Taylor criterion is compared with through-the-thickness measurements on a number of fragments recovered from the natural fragmentation experiment on the 4140 steel cylinder in Fig. 8.25. The comparison is reasonably consistent with the Taylor prediction.

Also shown is a best fit to the data of a Mott statistical strain to fracture function of the Gumbel type. The distribution curve required a mode,

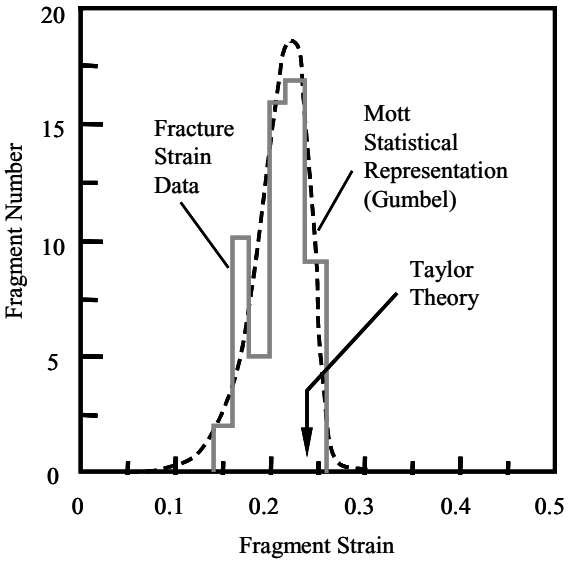

Fig. 8.25. Strain to fracture data from thickness measurements of individual fragments. Comparison with prediction of Taylor theory and a best fit to a Mott strain to fracture statistical distribution (Gumbel distribution)

$\mu = 0.22$, and scale parameter, $\sigma = 0.025$. (The standard deviation is 1.283 σ whereas the Mott gamma parameter is $\gamma = 1/\sigma$).

The analyses of Gurney were then applied to determine the radial expansion velocity at the predicted fracture strain [Grady, 1990]. For the present experiment an expansion velocity of 1530 m/s was calculated. This value will be used in the subsequent fragmentation analysis to establish the strain rate at the time of fragmentation of $\dot{\varepsilon} \approx 1.6 \times 10^4/\text{s}$.

8.5.3 Fragment Size

Calculations of fragment size will be based on the several theoretical approaches considered in some detail in the earlier chapters. The statistics-based theory of Mott was found to provide a characteristic fracture spacing relation dependent on the current flow stress and circumferential strain rate, and on the spread in the strain to fracture (Mott's γ property) according to,

$$s = \sqrt{\frac{2Y}{\rho\dot{\varepsilon}^2}\frac{1}{\gamma}}\,, \tag{8.20}$$

Alternatively, an energy theory of fragmentation based on an extension of Mott's fracture interaction analysis [Kipp and Grady, 1985] including a fracture resistance property, leads to a circumferential fracture spacing of,

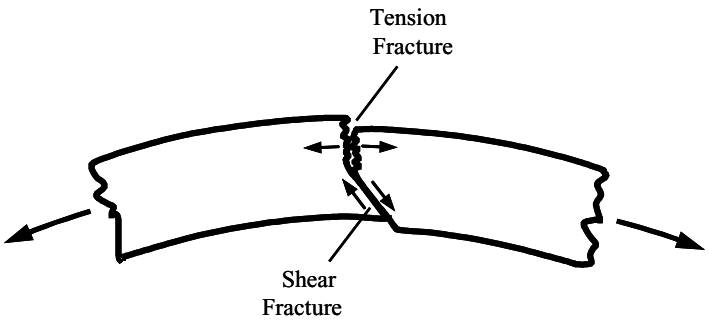

Fig. 8.26. Mechanisms of tension and shear fracture observed 4140 steel cylinder fragmentation

$$s = \left(\frac{24\Gamma}{\rho \dot{\varepsilon}^2} \right)^{1/3} , \tag{8.21}$$

where Γ is the fracture energy dissipated, and the work required, to compete the single fracture process. Comparisons of the present natural fragmentation data will be made with the several predictions of fracture spacing provided in (8.20) and (8.21).

8.5.4 Fragmentation Energy

Calculation of the nominal circumferential fracture spacing from (8.21) requires knowledge of the fragmentation energy Γ. The fragmentation energy is a material and mechanism dependent property which is determined through experimental measurements and models of the fracture dissipation process. There are two predominant modes of fracture in the breakup of an expanding metal shell which are illustrated in Fig. 8.26. The first is tensile fracture where failure proceeds by the opening of mode I cracks. Fracture dissipation is governed by the material fracture toughness K_c, and an estimate of the fragmentation energy is provided by,

$$\Gamma = \frac{K_c^2}{2E} , \tag{8.22}$$

where E is the elastic modulus of the material. Here it is assume that the static fracture toughness K_c provides a reasonable measure of the fragmentation toughness K_f. Material properties for the 4140 steel tested in the present study are provided in Table 8.2, and provide a fragmentation energy of $\Gamma \approx 16\,\mathrm{kJ/m^2}$ for tensile fracture.

In explosively-expanding cylinders, shear fracture preceded by localized adiabatic shear banding on the planes of fracture is also an important mode of failure. In determining the fragmentation energy associated with shear fracture, we will assume that the energy is principally accounted for by dissipation

Table 8.2. 4140 Steel Properties

ρ	(kg/m^3)	7870
Hardness	(HRC)	~ 40
E	(GPa)	200
K_c	(MN/m$^{3/2}$)	80
Y	(GPa)	1.1
χ	(m^2/s)	1.5×10^{-5}
c	(J/kg K°)	450
α	($K^{\circ -1}$)	7.5×10^{-4}
Γ Tensile	(kJ/m^2)	16
Γ Shear	(kJ/m^2)	19

in the adiabatic shear banding process. Grady and Kipp (1987) have analyzed the energy dissipated in adiabatic shear banding and have arrived at the expression,

$$\Gamma = \frac{\rho c}{\alpha} \left(\frac{9\rho^3 c^2 \chi^3}{Y^3 \alpha^2 \dot{\gamma}} \right)^{1/4} . \tag{8.23}$$

In (8.4), $\dot{\gamma}$ is the shear strain rate and is approximately equal to the circumferential stretching rate in the present application ($\approx 1.6 \times 10^4$/s). The new material properties include the specific heat c, the thermal diffusion coefficient χ, and the thermal softening coefficient α. From properties provided in Table 8.2 a fragmentation energy of $\Gamma \approx 19\,\mathrm{kJ/m^2}$ is obtained for shear fracture, which is remarkably close to that calculated for toughness governed tensile fracture.

Whether tensile or shear fracture dominated in the present fragmentation test on 4140 steel was not clear. Metallography on explosively fractured specimens indicated that this steel had a strong tendency to shear band and fracture along shear banded planes. There was also observation of fracture on planes oriented at approximately 45° to the shell surface, a further indication of shear dominated fracture. The close numerical values for the tensile and shear fragmentation energies will lead to similar predictions of circumferential fracture spacing, however. This similarity in magnitude of the two energy values is still not understood.

8.5.5 Distribution in Fracture Spacing and Comparison with Predictions

The present study is focused on predicting the circumferential fragmentation intensity. It does not consider axial breakup of the longitudinal strips. To make a statistical comparison of the fragment size data with the present analysis, the following reduction of the data was performed: Every fragment was weighed and the length of every fragment was measured. An effective rectangle was assumed for a fragment such that the mass is given by $m = \rho wtl$ where ρ is

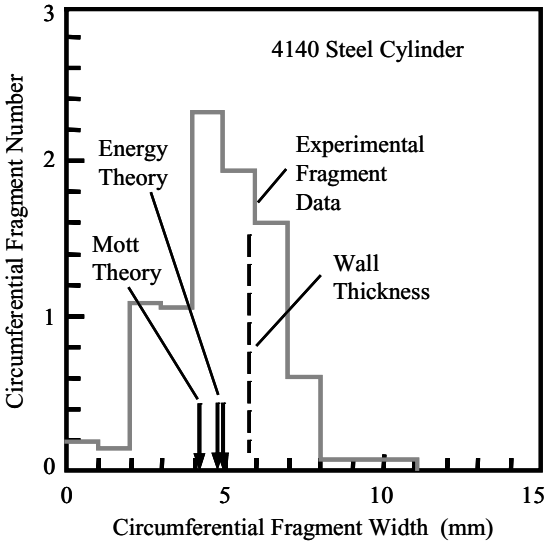

Fig. 8.27. Number histogram of the 161 fragments from the natural fragmentation of the 4140 steel cylinder and comparisons with predictions of circumferential fracture spacing

the density and w, t and l are the width, thickness and length, respectively. A circumferential fragment width was then calculated for each fragment from $w = m/\rho tl$ where m and l are the measured values and t is the initial wall thickness of the cylinder. The width w then provides an effective average measure of fracture spacing for that fragment in terms of the initial cylinder dimensions. A fragment of length l was then considered to be a fraction of a strip of length L, given by $n = l/L$, where L is the length of the cylinder. Through this method, a number versus circumferential width distribution was determined for the fracture spacing data.

The experimental circumferential fragment number data are plotted as a number histogram in Fig. 8.27. The same data are plotted as a cumulative number distribution in Fig. 8.28. The number data on the ordinate has been scaled from the 40 degree sector to a full cylinder. Initial wall thickness of the cylinder is identified in each figure for reference.

Predictions of the nominal fracture spacing based on the energy governed expression from (8.21) using both the tensile fracture energy ($\sim$16 kJ/m^2) and the shear band enhance fracture energy ($\sim$19 kJ/m^2) are identified in the figures. Specifically, the values are $s = 4.6$ mm (tension) and $s = 4.9$ mm (shear) referenced to initial circumferential dimensions. Predictions are slightly smaller than reported in Grady and Hightower (1992) because of a slightly different method of calculating the strain rate.

Fracture spacing predictions based on the Mott statistical theory through (8.20) additionally requires the γ property characterizing the statistical strain to fracture material behavior. Mott provided several methods for estimating γ. Here the statistical spread in fracture strain reported in Fig. 8.25 for the present fragmentation test will be used to determine γ. A value of $\gamma = 40$ calculated earlier in this section combined with the flow stress and density values from Table 8.2 yield a fracture spacing of 4.2 mm.

It is readily observed that all of the predicted values for fracture spacing are in sensible agreement with each other and the measured data. The 10% to 90% spread in fragment number ranges over about 3 mm and 7 mm easily spanning the predicted values. The close agreement between the energy-based prediction and Mott's statistics based prediction is intriguing and not fully understood. As discussed in Chap. 5, where the two theories are compared, the present agreement in predictions occurs in the regime of energy controlled fragmentation where Mott statistics is expected to characterizes the statistical fracture activation rather than the fracture survival and completion processes. This comparison also apparently carries over to the statistical variation in circumferential stretching, and corresponding fragment thickness strain, in the energy governed dynamic breakup process. Almost obscured in the data in Fig. 8.28 is a fit of the cumulative distribution with the Mott statistical fracture spacing distribution developed in Chap. 3. Again the agreement is surprisingly good. Disconcerting, however, is the observation that fracture

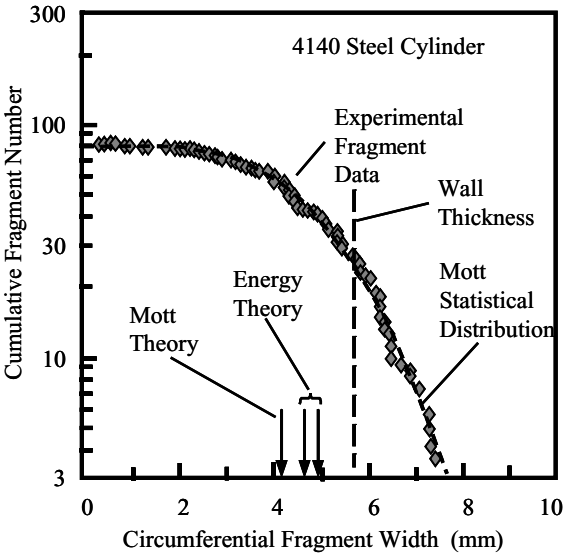

Fig. 8.28. Cumulative fragment number plot and comparisons with predicted fragment size and distribution

spacing in the present test span the thickness of the cylinder case bringing into question issues of thin case versus thick case behavior.

8.6 Tube Fragmentation Tests of Vogler and Coworkers

The seminal techniques developed by Winter (1979) have been revisited and extended in the dynamic fragmentation study of Vogler et al. (2003). Much of the early observations of Winter are supported in this extended investigation. Additionally, new results are reported due in part to the different materials studied and a broader range of diagnostic techniques.

8.6.1 Experimental Methods

Two well characterized metals were examined in this experimental study. The first was a heat treated AerMet 100 steel that has received considerable attention in fragmenting munitions applications [Wilson et al., 2001; Chhabildas et al., 2001]. Scaling studies of cylinder fragmentation performed on this steel are discussed in Chap. 7. The second is a highly ductile alloy of uranium, U6Nb, discussed in an early section in the present chapter.

The experimental test technique replicates much of that developed by Winter (1979). The test metals are produced in tubes 50.8 mm in length, 12.7 mm in inner diameter and with several tube wall thicknesses. Controlled inner loading is produced through a gas gun acceleration and insertion of a solid cylinder lexan projectile 25.4 mm in length striking an identical stationary lexan cylinder at the center point of the metal tube as previously illustrated in Fig. 8.20. The impact pressure and subsequent outward motion leads to dynamic budging of the metal cylinder causing in turn, rapid plastic straining, multiply dynamic fracture, and statistical fragmentation of the test metal.

Various diagnostic techniques were used to interrogate the dynamic failure and fragmentation process. High-speed photography provided detailed measurement of the expansion history along with the temporal evolution of dynamic fracture activation and propagation. Time resolved velocity interferometery or VISAR [Barker and Hollenbach, 1972] provided detailed expansion velocity history including initial shock intensity. PVDF pressure gages were mounted interior to measure impact generated pressure amplitude and quantitative pressure history of the cylinder loading function. Lastly, soft recovery methods captured fragment debris for post test evaluation and metallography.

8.6.2 Experimental Results

Results representative of the study are shown from high speed photographic imaging of the dynamic tests in Fig. 8.29. The images on the left are for a heat-treated AerMet tube with a 3 mm wall thickness. Comparable images for

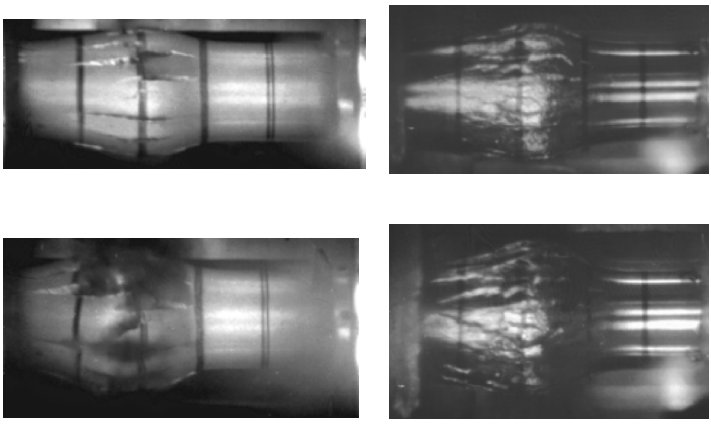

Fig. 8.29. The images on the left are for heat treated AerMet 100 steel at 15.4 µs and 23.4 µs after impact. Images on the right are for U6Nb uranium 18.3 µs and 25.1 µs after impact. Impact velocities were 1.92 km/s for steel and 1.86 km/s for uranium, respective

an experiment on a U6Nb tube are shown on the right. Timing of the images after impact are provided in the figure caption.

Initial expansion of the tube is visually homogeneous and cracking is not observed until some time after impact. For the one AerMet tube, fracture was first perceived at 10.4 µs after impact. This first observation corresponds to a circumferential strain at the maximum bulge of 18%. Comparable strains determined from the deformed thickness of collected fragments ranged over about 9% and 16%. Strains determined from the observation of first fracture on three U6Nb experiments were 12%, 21% and 24%, respectively. Strains inferred from fragments collected ranged over about 15% to 23%. Such scatter in strain to fracture should not be surprising and is consistent with similar results in the study of Winter.

After fractures become visible in the photographic imaging, their number increases rapidly. In the AerMet 100 experiment shown in the left of Fig. 8.29 a maximum of seven cracks were visible at 15.4 µs after impact. That number decreased, however, as the axially propagating cracks intersected and coalesced. The velocity of the principle cracks could be measured. Growth was not steady, especially immediately after activation, but measured velocities ranged from about 0.54 to 1.7 km/s. This crack speed compares with a Rayleigh wave speed for steel of 2.84 km/s.

The VISAR velocity profile measurements for comparable tests on AerMet steel and U6Nb uranium are shown in Fig. 8.30. The three VISAR locations are illustrated in the inset, and recorded radial motion at 5 mm intervals along the tube axis. Reverberation of the loading shock wave through the wall thickness is clearly observed as the radial acceleration proceeds. Maximum

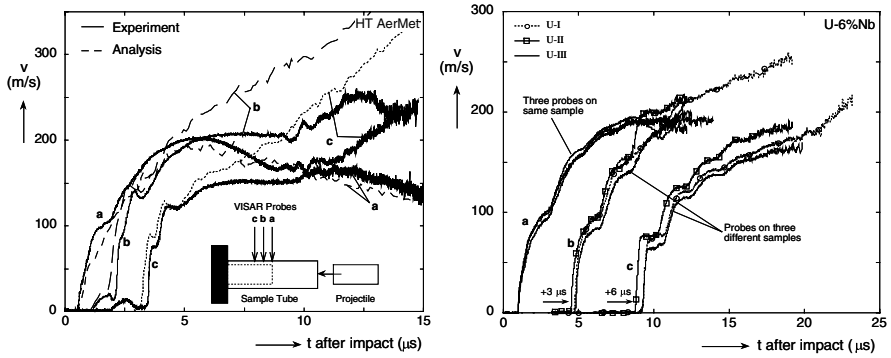

Fig. 8.30. Velocity measurements with VISAR for AerMet 100 steel (*left*) and U6Nb uranium (*right*) are shown as solid curves. CTH computational simulations are the broken curves compared with the measured data

radial velocity is achieved near the VISAR location b and is about 10% of the projectile impact velocity.

Computational simulations of the dynamic event were performed using the Sandia National Laboratories CTH shock physics code [Bell et al., 2000]. A Mie-Gruneisen equation of state model and von Mises ideal plasticity strength model were used for the participating materials. A Johnson-Cook fracture model [Johnson and Cook, 1983] was employed to determine fracture onset in the test metals. Simulations are compared with the measured velocity data in Fig. 8.30. Agreement with the data is reasonable although significant divergence at later time is observed. This discrepancy is attributed to both overly simplistic metal strength models, and to motion irregularities brought about by the statistical fracture and fragmentation process.

In selected tests under comparable impact conditions fragments from the dynamic event were soft recovered, counted and weighed. Fragment distribution data for one heat treated AerMet steel specimen and three U6Nb specimens are shown in Fig. 8.31. Cumulative fragment number is provided on the ordinate while cumulative fragment mass fraction (fraction of total tube mass) is shown on the abscissa. A representative fragment from each metal is also shown in the figure.

Typically a large section of the tubular specimen nearest the projectile insertion end remained intact. For the AerMet steel test provided in Fig. 8.31 this section was 48% of the whole tube mass. For the AerMet steel test fourteen fragments with mass greater that one gram were recovered. These fragments constituted the steeper portion of the distribution curve in Fig. 8.31. Thirteen smaller fragments were also recovered and complete the smaller particle shallow portion of the distribution curve. Steel fragments were generally elongated as the photograph illustrates in Fig. 8.31. Shear fracture at approximately 45 degrees to the surface normal was the rule. Fragments also exhibited crack steps and arrested fractures.

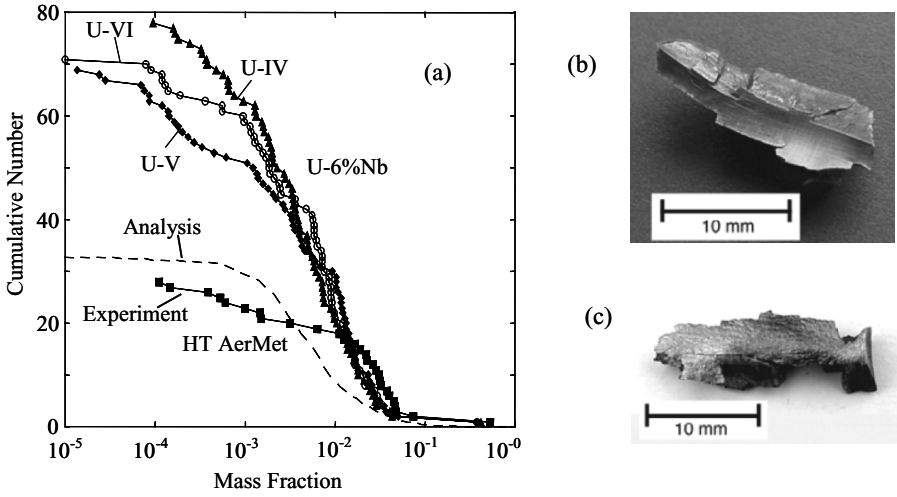

Fig. 8.31. Cumulative fragment number distributions versus fragment mass fraction for steel and uranium tube fragmentation tests. Representative recovered fragments for (**b**) heat treated AerMet 100 steel and (**c**) U6Nb uranium are also shown

The fragment mass distribution trend for U6Nb uranium, also shown in Fig. 8.31, is similar to that of steel but with markedly more fragments. Fragments were significantly more jagged and irregular, and tended to be more equi-dimensional. Significant deformation-induced surface roughening was also noted on the uranium fragments.

Fragment distributions for both the heat treated AerMet steel and U6Nb uranium were adequately fit to a bilinear distribution of the form,

$$N(m) = N_o^l e^{-m/\mu_l} + N_o^s e^{-m/\mu_s} \ . \tag{8.24}$$

Argument for the application of a bilinear mixture distribution are considered in Chap. 2 and have been discussed in earlier studies [Grady and Kipp, 1985; Odintsov, 1992]. Since large fragments dominate the distribution, the fitted distribution parameter μ_l was used along with the circumferential strain rate determined from VISAR or high-speed photography in the relation,

$$K_f = \sqrt{\frac{\rho c^2 \dot{\varepsilon}^2 \mu_l}{24}} \ , \tag{8.25}$$

to provide a measure of the effective fragmentation toughness under the present test conditions. For two AerMet heat-treated steel experiments strain rate at fracture of 5×10^4/s was determined and toughness values of 62 and 71 MPa $\mathrm{m}^{1/2}$ were obtained. For four U6Nb uranium tests the measured distributions provided toughness values of $49, 55, 58$ and $61\,\mathrm{MPa\ m}^{1/2}$. These values are remarkably close to the fragmentation toughness determined from expanding ring experiments on U6Nb discussed earlier in the present chapter.

8.6.3 Summary

The present extension of the expanding tube test technique initially explored by Winter (1979) is shown to provide a valuable method for investigating the phenomena of dynamic fracture and fragmentation. Additionally, barring the stochastic nature of dynamic fracture, the test method is found to be very reproducible, especially in the initial expansion phase of the tube. The method is quite amenable to the combined use of VISAR, high-speed photography and soft-recovery diagnostics.

The steel and uranium metals studied in the present investigation exhibit strikingly different fracture and fragmentation characteristics. Some of these features are not yet well understood. The outwardly more brittle fracture appearance and more abundant fragmentation of the uranium alloy was not expected but may relate to the propensity for this metal to undergo adiabatic shear failure.

The sensible agreement of the fragmentation toughness determined in the expanding tube method with other dynamic methods and with static fracture toughness values is encouraging. This agreement should be viewed with caution, however, as some of the assumptions important to the model are not realized in the expanding tube test. Nonetheless, the reasonable agreement among the different test methods suggest that the model must capture some of the physics reasonably well and should continue as a useful engineering tool.

8.7 Steel Cylinder Fragmentation of Mock and Holt

An instructive study of metal fragmentation is provided by the experimental investigation of Mock and Holt (1983) into the explosive-driven fragmentation of iron and steel cylindrical shells. In that study explosive loading was performed on the more ductile Armco iron and on HF-1 steel subjected to several heat treatments producing markedly more brittle response. Thick-walled test cylinders provided large numbers of fragments, and well-constrained fragment distributions. The study also included a detailed examination of fragment morphology and provided a classification scheme for the sorting of fragments. Both distributions and fragment classification provide unique data for testing statistical theories and examine the physical processes governing dynamic fracture over several ferrous metals with different fracture characteristics.

8.7.1 Experimental Methods

Explosive fragmentation tests were performed on metal open-end cylindrical shells approximately 20 cm in length, 7.5 cm in inner diameter and 2 cm in wall thickness. The explosive was cast-in-place composition B explosive which

was detonated at one end and extended well beyond each end of the metal cylinder.

The first metal was as-received Armco iron. The second, was an HF-1 steel heat treated to a tempered martensite state. The third, was also HF-1 steel heat treated to a more brittle cementite and pearlite structure. Six fragmentation tests, two on each metal, were performed. Fragments were soft captured in sawdust and extracted with magnetic methods. Over 99% of the original cylinder mass was recovered on all tests. Over 1400 fragments weighing more that 1 gr (0.065 g) were collected from the Armco iron tests and contributed to the data analysis. Similarly, over 10,000 and 12,000 fragments, respectively, were collected for the two heat treatments of HF-1 steels.

8.7.2 Fragment Distributions

Cumulative fragment number greater than mass m versus fragment mass is plotted in Fig. 8.32 for both experiments on Armco iron. Separate symbols are not used to distinguish between the two tests because they overlay within the statistical scatter. One curve in the figure represents the distribution of all (total) of the fragments collected. The other curve identifies the distribution of specific type 1 fragments which will be described shortly.

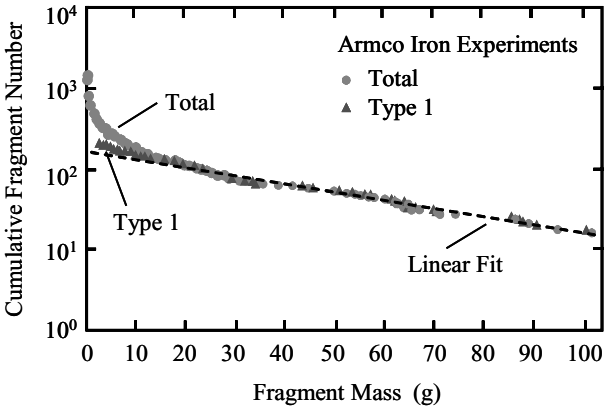

Fig. 8.32. Fragment mass distributions for Armco iron exploding cylinder tests [Mock and Holt, 1983]

In Fig. 8.33 similar fragment distributions are shown for the total number of fragments for the first (heat treatment A) and second (heat treatment B) preparations for the HF-1 steel. Again, two tests were performed on each heat treatment, so the two curves represent the resulting distributions for approximately 21,000 and 25,000 fragments, respectively.

It was pointed out by Mock and Holt (1983) that the distributions in Figs. 8.32 and 8.33 for the total number of fragments were well described

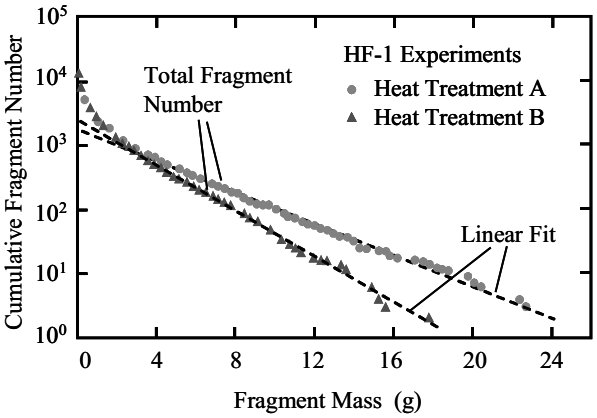

Fig. 8.33. Fragment mass distributions for HF-1 steel exploding cylinder tests [Mock and Holt, 1983]

with a linear curve in these semi logarithmic plots with the exception of the upturn associated with the smaller fragment end of the distribution. These curves would correspond to $\beta = 1$ for the general scaling relation suggested in Chap. 7. Grady and Kipp (1985) have shown that the data of Mock and Holt are very well described by a bilinear exponential, or Poisson mixture, distribution as described in Chap. 2.

8.7.3 Fragment Morphology

A further feature of the study of Mock and Holt (1983) was the classification of fragments according to the shape and the mode of fracture governing the fragment separation process. The author's noted that attempts to type sort fragments resulting from exploding munitions events goes back to at least the early reports of Mott. Several of these reports by Mott do in fact examine the shape and fracture surface features of collected fragments, and comment on the several fracture processes possibly responsible. In Fig. 8.34 sketches from the report of Mott are reproduce and illustrate the classification of fragments observed by him. He suggested that failure probably initiated on the inner surface of the munition cylinder as shear rupture, transitioned to extension fracture at some interior point, and culminated at the cylinder outer surface. In his observations, fragments of type 1–4 were commonest with occasional fragment of type 5. He also pointed out that for mild steel and carbon steel, through-going shear rupture was frequently observed as illustrated in his lower sketch in Fig. 8.34.

Mock and Holt (1983) found the more extensive fragment classification scheme shown in Fig. 8.34 more appropriate to the Armco iron and HF-1 steel cylinder tests performed by them. This method suggested four principle fragment types comprised of type 1 fragments (including both inner and

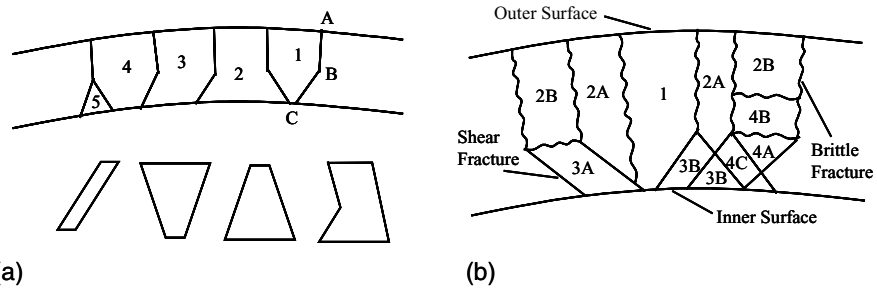

Fig. 8.34. Classification schemes for fragment type resulting from exploding munitions fragmentation. (**a**) Original sketches of Mott (1943). (**b**) Fragmentation classification of Mock and Holt (1983)

outer cylinder surfaces), type 2 (outer cylinder surface only), type 3 (inner cylinder surface only), and type 4 (no cylinder surface). Fragments were further subtyped according to the shear or extension character of the fracture surfaces.

Sorting of the fragments according to this scheme was carried out for the tests performed. It was shown that for the more ductile Armco iron fragments of type 1 (both inner and outer fragment surface) constituted very close to 80% of the total cylinder mass. The authors further showed that the distribution for only the type 1 fragments for the Armco iron tests plotted linear on a semi logarithmic cumulative number versus mass graph over the full range of the data as illustrated in Fig. 8.32. Fragments of the remaining type contributed to the small mass upturn adequately described by a bilinear exponential distribution. Behavior is reminiscent of the cylinder tests of Odintsov (1992) discussed in Chap. 2.

Sorting of fragments from tests on HF-1 steel, on the other hand, resulted in less than 5% of the mass of type 1 fragments. A complex mix of fragments of type 2 through type 4 constituted the preponderance of the fragment mass distribution.

A final noteworthy observation in the tests of Mock and Holt were correlations among static strength properties of the several metals and features of the fragmentation results. Armco iron provided a tensile strength of approximately 300 MPa and a permanent elongation to fracture of 34%. In contrast, the two heat treatments of HF-1 steels, A and B, respectively, exhibited 1100 MPa and 880 MPa tensile strengths and elongations to fracture of 3% and 1%. Some variations in properties with respect to orientation relative to rolling direction were noted, however.

For comparison, expected fragment mass for the fragment distributions for Armco iron and for the HF-1 steel with heat treatments A and B were $\mu = 41\,\mathrm{g}$, $3.6\,\mathrm{g}$ and $2.5\,\mathrm{g}$ respectively, based on a linear exponential description of the linear portion of the respective distributions. Estimating a circumferential strain rate from Gurney considerations of approximately $10^4/\mathrm{s}$ the

respective mass scale parameters in (8.25) of the previous section yield fragmentation toughness values of $K_f = 185, 55$, and 45 MPa $m^{1/2}$, respectively for the three metals.

Type 1 fragments which were large enough to include both inner and outer surfaces of the original cylinder were examined to infer other feature of the dynamic fracture event. These included all of the type 1 fragments from each of the HF-1 steel experiments (approximately 25 to 50 fragments per test) and a comparable representative number from the Armco iron tests. A permanent dynamic strain to fracture was estimated from the change in thickness relative to the initial cylinder wall thickness. These engineering strain values were 0.34 and 0.36 for the two Armco iron tests, 0.11 and 0.12 for HF-1 steel heat treatment A, and 0.12 and 0.14 for heat treatment B.

Lastly the authors showed that the extent of shear fracture through the thickness before transition to the more brittle extension fracture behavior was dependent on the metal properties. For Armco iron shear fracture proceeded through nearly one-half (approximately 45%) of the cylinder wall thickness before transitioning to extension fracture. For the two HF-1 steels this shear fracture distance was reduced to about 25% and 20% of the wall thickness for heat treatments A and B, respectively.

References

Addesssio, F.L., Zuo, Q.H., Mason, T.A. (2003) Model for High-Strain-Rate Deformation of Uranium-Niobium Alloys, *J. Appl. Phys.*, 93, 12, 9644–9654.

Barker, L.M., and Hollenbach, R.E. (1972) Velocity Interferometer for Measuring the Velocity of any Reflecting Surface, *J. Appl. Phys.*, 43, 4669–4680.

Bell, R.L., Baer, M.R., Brannon, R.M., Elrick, M.G., Hertel, E.S., Silling, S.A., Taylor, P.A. (2000) CTH User's Manual and Input Instructions, Version 4.00, Sandia National Laboratories Tech. Rept., April.

Chhabildas, L.C., Reinhart, W., Wilson, L.T., Reedal, D.R., Grady, D.E., Black, J.W. (2001) Fragmentation Properties of AerMet 100 Steel in Two Material Conditions in Proceedings 19^{th} International Symposium on Ballistics, Interlaken, Switzerland, May 7–11, I.R. Crewther, ed., 663–670.

Gourdine, W.H. (1989) *J. Appl. Phys.*, 65, 411.

Gourdine, W.H., Weinland, S.L., Boling, R.M. (1989) *Rev. Sci. Inst.*, 60, 427.

Grady, D.E. (1990) Natural Fragmentation of Conventional Warheads, Sandia National Laboratories Technical Report SAND90–0254, May 1990.

Grady, D.E. and Benson (1983) Fragmentation of Metal Rings by Electromagnetic Loading, *Experimental Mechanic*, 23, 393–400.

Grady, D.E. and Kipp, M.E. (1985) Geometric Statistics and Dynamic Fragmentation, *J. Appl. Phys.*, 58, 3, 1210–1222.

Grady, D.E. and Kipp, M.E. (1987) The Growth of Unstable Thermoplastic Shear with Applications to Steady-Wave Shock Compression in Solids, *J. Mech. Phys. Solids* 35, (1), 95–118.

Grady, D.E. and Hightower, M.M. (1992) Natural Fragmentation of Exploding Cylinders, in Shock-Wave and High-Strain-Rate Phenomena in Materials, and K.P. Staudhammer, eds., Marcel Dekker, Inc., 713–721.

Grady, D.E. and Olsen, M.L. (2003) A Statistics and Energy Based Theory of Dynamic Fragmentation, *In. J. Impact Eng.*, 29, 293–306.

Gurney, R.W. (1943) The Initial Velocity of Fragments from Bombs, Shells and Grenades, Army Ballistic Research Laboratory Report BRL 405.

Hixson, R.S., Vorthman, J.E., Zurek, A.K. Anderson, W.W., Tonks, D.L. (2000) Spall Response of U-NB (6%) Alloy, in Shock Compression of Condensed Matter, – 1999, edited by M.D. Furnish, L.C. Chhabildas, R.S. Hixson, *Am. Inst. Physics*, New York, pp. 489–492.

Hogatt, C.R. and Recht, R.F. (1969) Stress Strain Data Obtained at High Rates Using an Expanding Ring, *Experimental Mechanic*, 9, 441–448.

Johnson, G.R. and Cook, W.H. (1983) A Constitutive Model and Data for Metals Subjected to Large Strains, High Strain Rates and High Temperatures, Proceedings Seventh International Symposium on ballistics, The Hague, The Netherlands.

Kipp, M.E. and Grady, D.E. (1985) Dynamic Fracture Growth and Interaction in One Dimension, *J. Mech. Phys. Solids* 33 (4), 399–415.

Kipp, M.E. and Grady, D.E. (1986) Random Flaw Nucleation and Interaction in One Dimension in Metallurgical Applications of Shock-Wave and High-Strain-Rate Phenomena, L.E. Murr, K.P. Staudhammer, and M.A. Meyers, eds., Marcel Dekker, Inc., 781–791.

Mock, W. and Holt, W.H. (1983) Fragmentation Behavior of Armco Iron and HF-1 Steel Explosive Filled Cylinders, *J. Appl. Phys.*, 54, 2344–2351.

Mott, N.F. (1943) Fragmentation of H.E. Shells: A Theoretical Formula for the Distribution of Weights of Fragments, *Ministry of Supply*, AC3642, March.

Mott, N.F. (1943) A Theory of the Fragmentation of Shells and Bombs, *Ministry of Supply*, AC4035, May.

Mott, N.F. (1947) Fragmentation of Shell Cases, *Proc. Royal Soc.*, A189, 300–308, January.

Mott, N.F. (1948) Fracture of Metals: Theoretical Considerations, *Engineering*, 165, 16–18.

Odintsov, V.A. (1992) Hyper Exponential Spectra of Exponential Fracture, *Mechanics of Solids*, (Meckhanika Tverdogo Tela), 27, 5, 42–48.

Olsen, M.L. (2000) Private Communication.

Perrone, N. (1968) On the Use of the Ring Test for Determining Rate-Sensitive Material Constants, *Experimental Mechanic*, 8, 232–236.

Taylor, G.I. (1963) Scientific Papers of G.I. Taylor, Volume III, No. 44, Cambridge University Press.

Vogler, T.J., Thornhill, T.F., Reinhart, W.D., Chhabildas, L.C., Grady, D.E., Wilson, L.T., Hurricane, O.A., Sunwoo, A. (2003) Fragmentation of Materials in Expanding Tube Experiments, *Int. J. Impact Eng.*, 29, 735–746.

Walling, H.C. and Forrestal, M.J. (1973) Elastic Plastic Expansion of 6061-T6 Aluminum Rings, *J. AIAA*, 11, 1196.

Warnes, R.H., Duffy, T.A., Karpp, T.A., Carden, A.E. (1981) An Improved Technique for Determining Dynamic Material Properties Using the Expanding Ring, *in Shock Waves and High-Strain-Rate Phenomena*, M.A. Meyers and L.E. Murr, eds., Plenum, 47.

Weisenberg, D.L., and Sagartz, M.J. (1977) Dynamic Fracture of 6061-T6 Aluminum Cylinders, *J. Appl. Mech.*, 44, 643.

Wilson, L.T., Reedal, D.R., Kipp, M.E., Martinez, R.R., Grady, D.E. (2001) Comparison of Calculation and Experimental Results of Fragmenting Cylinder Experiments, in Shock Waves and High Strain Rate Phenomena, K.P. Staudhammer, M.A. Meyers, L.E. Murr, eds., Elevier, pp. 561–570.

Winter, R.E. (1979) Measurement of Fracture Strain at High Strain Rates, *Inst. Phys. Conf. Ser.* 47, 81–89.

Zurek, A.K., Hixson, R.S., Anderson, W.W., Vorthman, J.E., Gray, G.T., Tonks, D.L. (2000) Elastic Response of U-Nb (6%) Alloy, Proceedings 6th International Conference on Mechanical and Physical Behaviour of Materials under Dynamic Loading, Sept. 25–29, EDP Sciences, 677–682.

Part II

Transcription and Facsimiles of Reports of N.F. Mott

Preface by Sam Ellis

The copies of these papers were released by the Science and Technology Division of the Defence Ordnance Safety Group (DOSG) DOSG is the UK Ministry of Defence's focal point for Ordnance, Munitions, and Explosives (OME) Safety. It is a support group within the joint Defence Procurement Agency/Defence Logistics Agency Technical Enabling Service work stream. The organization contains a mix of military and civilian staff with science, engineering, and safety management expertise. It provides independent safety advice and assessment, interpretation of tests and trials, development of OME design standards, and qualification of energetic materials throughout the Ministry of Defence.

DOSG was formed in 2000 by merging the Ordnance Board, the Chief Inspectorate Naval Ordnance, the Explosives Storage and Transport Committee support group, and some of the Aircraft Weapons Advisory Committees. The work of all these bodies depended on fragmentation models – from basic models for single warheads to complex models for stacks of munitions and buildings – and the Science and Technology division provides advice not only on the application of models but trials management and data analysis to allow development and verification of these models. It also maintains a comprehensive library of technical documents that dates back to the 1920's with the majority of them from the Ordnance Board archives.

The Ordnance Board has a history going back nearly 600 years to the Office of Ordnance (1414–1597). As with most organizations minor changes were made to the name over the years, for example it was known as the Board of Ordnance between 1597 and 1855 and the Ordnance Committee between 1915 and 1938. It was finally designated the Ordnance Board when together with the Research, Design and Inspection Departments, and the Royal Ordnance Factories, it came under the administration of the Ministry of Supply in July 1939. The organization's remit extended beyond safety and it dealt with all requests for development of new or improvement of existing armament stores. The Board, when it formally met to review publications, comprised some 20 senior military officers, the heads of other major organizations (such

as the Chief Inspector Naval Ordnance, the Superintendent of the Research Department, the Director of the National Physical Laboratory, and the Director of Scientific Research at the Ministry of Supply) plus some 20 associate members including a number of distinguished scientists and engineers with 9 of them being Fellows of the Royal Society.

Mott's wartime work produced six classified papers on fragmentation, in 1943 and 1944, for the Fragmentation Panel of the Static Detonation Committee of the Advisory Council of Scientific Research and Technical Development of the Ministry of Supply. An unclassified paper describing some of the findings was published in the Proceedings of the Royal Society in 1947. Despite the fact that an enormous effort has been, and is still being, expended on developing models for fragmentation Mott's fundamental work is still being used both directly and indirectly. Although he did not work directly for the Ordnance Board the continuing importance of this work lead to Mott being formally made an Associate Member of the Ordnance Board in January 1985.

Yours sincerely
Sam Ellis

Biographies of Sir Nevill Francis Mott

Nevill Francis Mott was born in Leeds, U.K., on September 30th, 1905. His parents, Charles Francis Mott and Lilian Mary (née) Reynolds, met when working under J.J. Thomson in the Cavendish Laboratory; his great grandfather was Sir John Richardson, the arctic explorer. He was educated at Clifton College, Bristol and St. John's College, Cambridge, where he studied mathematics and theoretical physics. He started research in Cambridge under R.H. Fowler, in Copenhagen under Niels Bohr and in Göttingen under Max Born, and spent a year as a lecturer at Manchester with W.L. Bragg before accepting a lectureship at Cambridge. Here he worked on collision theory and nuclear problems in Rutherford's laboratory. In 1933 he went to the chair of theoretical physics at Bristol, and under the influence of H. W. Skinner and H. Jones turned to the properties of metals and semiconductors. Work during his Bristol period before the war included a theory of transition metals, of rectification, hardness of alloys (with Nabarro) and of the photographic latent image (with Gurney). After a period of military research in London during the war, he became head of the Bristol physics department, publishing papers on low-temperature oxidation (with Cabrera) and the metal-insulator transition.

In 1954 he was appointed Cavendish Professor of Physics, a post which he held till 1971, serving on numerous government and university committees. The research for which he was awarded the Nobel Prize began about 1965. Some of his main books are "The Theory of Atomic Collisions" (with H.S.W. Massey), "Electronic Processes in Ionic Crystals" (with R.W. Gurney) and "Electronic Processes in Non-Crystalline Materials" (with E.A. Davis).

Outside research in physics he has taken a leading part in the reform of science education in the United Kingdom and is still active on committees about educational problems. He was chairman of a Pugwash meeting in Cambridge in 1965. He was chairman of the board and is now president of Taylor & Francis Ltd., scientific publishers since 1798. He was Master of his Cambridge college (Gonville and Caius) from 1959–66. He was President of

the International Union of Physics from 1951 to 1957, and holds more than twenty honorary degrees, including Doctor of Technology at Linkoping.

In 1930 he married Ruth Eleanor Horder. They have two daughters and three grandchildren, Emma, Edmund and Cecily Crampin.

For the last ten years he has lived in a village, Aspley Guise, next door to his son-in-law and family. During this period he has written an autobiography "A Life in Science" (Taylor and Francis, London, 1986), which provides a fascinating history of the time and events. He also edited a book with several authors on a religion-science interface "Can Scientists Believe?" (James and James, London), together with many scientific papers, mainly in the last 3 years on high-temperature superconductors.

From Nobel Lectures, Physics 1971–1980, Editor Stig Lundqvist, World Scientific Publishing Co., Singapore, 1992.

This autobiography/biography was written at the time of the award and later published in the book series Les Prix Nobel/Nobel Lectures. The information is sometimes updated with an addendum submitted by the Laureate. To cite this document, always state the source as shown above.

Sir Nevill F. Mott died on August 8, 1996.

1

A Theory of Fragmentation

N.F. Mott and E.H. Linfoot

(January 1943), Ministry of Supply, A.C.3348

Summary. A tentative theory is given to account for the mean fragment sizes of certain types of bomb and shell, and for the relative numbers of large and small fragments.

1.1 The Mean Fragment Size

The theory given here is applicable only to casings which expand plastically before rupture. This may not be the case for brittle materials such as cast iron.

We consider first fragmentation of the type occurring in the 3.7 inch A.A. shell. The larger fragments appear from inspection to be formed as shown in Fig. 1.1, which represents a section through part of the casing. Cracks start on the inside, at such points as A_1, A_2, $A_3 \ldots$ and spread outwards to B_1, B_2, B_3. This type of break-up has been discussed in Report No. 2232 from the Dept. of Metallurgy of the University of Sheffield, Ref. A.C. 3098. The widths of typical fragments are of the order 1 cm; the length, parallel to the axis of the shell, is considerably greater.

At the moment of rupture, let r be the radius of the shell casing, t its thickness and V the velocity with which it is moving outwards. We suppose that rupture takes place when work-hardening has proceeded to such an extent that a crack will propagate itself with the expenditure of less energy than further plastic flow. Suppose that the casing then splits along two lines distant a apart; the cracks are represented by AB, A′B′ in Fig. 1.2, which, like Fig. 1.1, represents a cross section through the shell casing. A splinter of cross section ABB′A′ is then flying outwards with velocity V. The top surface AB of the fragment will have, in addition to the large outward velocity V, a velocity at right angles to it of amount $\frac{1}{2}V\alpha$, where $\alpha = a/r$. Similarly the bottom surface A′B′ will have a downward velocity of the same amount. Referred to axes moving with the fragment, the metal will have kinetic energy, per unit length parallel to the axis of the shell, equal to

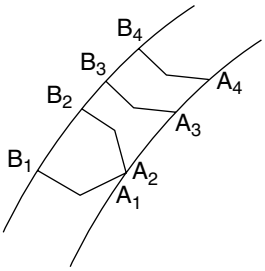

Fig. 1.1.

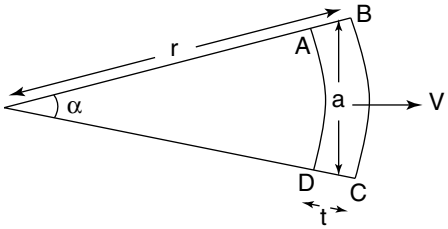

Fig. 1.2.

$$\frac{1}{2}\rho t\, V^2 \int_{(-1/2)\alpha}^{(1/2)\alpha} r\theta^2 d\theta = \frac{1}{24}\rho t r \alpha^3 V^2$$

where ρ is the density of the metal. Since $r\alpha = a$, this becomes

$$\frac{1}{24} t V^2 \rho a^3 / r^2 \tag{1.1}$$

We now make the assumption that if the energy (1.1) is great enough to form a new crack through the fragment, it will do so, and the fragment will break into two. If W is the energy per unit area required to form a crack, the energy required for this is Wt. Thus no fragment will be formed with thickness a greater than that given by equating Wt to (1.1), which gives

$$a = \left[\frac{24\, r^2 W}{\rho V^2}\right]^{1/3} \tag{1.2}$$

For W we may take a value given by impact tests; according to Southwell (Trans. Manchester Assoc. of Engineers, 1937) this ranges from 70 to 800 ft/lbs. per sq. inch. We should take a value appropriate to the metal at the moment of rupture, i.e. *after* plastic deformation, when it will be very brittle. We therefore take the lower value, 70 ft/lbs. It is realised that the energy of rupture is not, in practice, proportional to the area, so our value will be very approximate. Moreover heating of the metal during its expansion may have an effect. Fortunately, since W occurs as $W^{1/3}$, the value of a is not very sensitive

to the value of W. A measurement of the rupture energy for cold-worked H.E. steel would be of interest[1].

For r we take 2.2 inches, and for V, the velocity of the fragments, 2500 ft/sec. We obtain for a

$$a = 0.55 \text{ inches}$$

in good agreement with the observed value.

For steels where fracture is due to shear we have no information from which the magnitude of W can be estimated.

We have not been able to find a theory to account for the average *length* of the splinters in this type of shell. For shells or bombs which bulge out in the middle before breaking up, the dimension parallel to the axis might be determined by the same mechanism, r being the radius of curvature of an axial section of the casing.

We may use formula (1.2) to compare the mean fragment sizes of bombs with different charge-weight ratios, sizes etc., Since, however, we have no theory of what determines the lengths of the splinters from a shell, we confine ourselves to a bomb which, at the moment of bursting, is roughly spherical. Then we can take the mean weight of a fragment to be proportional to $\rho a^2 t$, and thus to

$$\rho^{1/3}\ r^{4/3}\ W^{2/3}\ V^{-4/3} t$$

If r_o, t_o refer to the bomb before expansion, and r, the radius at the moment of burst is equal to εr_o, then $t = t_o/\varepsilon^2$, so that the mean fragment weight is proportional to

$$r_o^{4/3} \rho^{1/3} t_o\ W^{2/3} / V^{4/3}\ \varepsilon^{2/3} \tag{1.3}$$

If we keep the charge constant and vary the thickness t_o, we expect for heavy casings that V^2 will be proportional to $1/t_o$; thus the average weight of fragment is proportional to $t_o^{5/3}$ if ε is constant; actually, however, thick cased shells expand further than thin ones before breaking up, so we expect a rather less rapid variation with t_o than this.

1.2 Distribution of Fragment Weights

It was pointed out to the present authors by Dr. L.L. Welch (private communication dated 24th Sept. 1941) that the distributions of fragments from two such different projectiles as the 3″ U.P. (initial fragment velocity 4500 ft/sec.) and the 3.7″ A.A. shell (fragment velocity about 2500 ft/sec) can be fitted approximately to the same law. This law is the following: if $N(m)\,dm$ is the number of fragments with weights between m and $m + dm$, then

[1] It is of interest to compare the much smaller rupture energy for a brittle substance such as quartz, which from experiments on grinding sand appears to be of the order 61 ft/lbs. per sq. ft. (Martin, Trans. Ceramic Society, 23, 61, 1923).

$$N(m)dm = Ce^{-M/M_o}\, dM \tag{1.4}$$

where $M = m^{1/3}$ and C and M_o are constants. For the shell and the U.P., M_o has respectively the values (in (ounces)$^{1/3}$)

	3.7″ shell	3″ U.P.
M_o	0.33	0.15

The agreement is shown below:

	Shell		U.P.	
oz.	obs.	calc.	obs.	calc.
1/50 – 1/25	not	recovered	570	528
1/25 – 1/4	452	454	751	793
1/4 – 1/2	131	129	93	101
1/2 – 4	193	181	64	56
4 – 8	5	13	0	0
>8	1	5		

The total number of fragments is CM_o and the total weight $6M_o{}^4C$, so the average weight is $6M_o{}^3$, or 0.21 ounces for the 3.7 inch shell. The distribution is very skew, however, so that there are a large number of fragments with weights considerably greater than the average.

This observed distribution law suggested a theoretical explanation along the following lines: $m^{1/3}$ is proportional to the mean linear dimension of a fragment, and if this is written x, it suggests that the number of fragments with lengths between x and $x + dx$ is given by

$$Ce^{-x/x_o}\, dx$$

Such a formula can be derived for a rod or line broken up at random in one dimension only. Consider a line AB of length l, cut at random into $n + 1$ pieces; each cut is independent of the positions of all the others and is equally likely to be at any point between A and B. Consider then any interval ξ of the line. The average number of cuts that it contained is $n\xi/l$ and the chance that it does not contain one at all is

$$e^{-n\xi/l}$$

Consider then any one cut, and let us calculate the chance that the next cut to the right is in an interval dx at a distance x; this is

$$e^{-nx/l}\, \frac{ndx}{l}$$

Thus the number intervals of lengths between x and $x + dx$ is

$$\frac{l}{x_o^2}\, e^{-x/x_o}\, dx, \quad x_o = \frac{l}{n} \tag{1.5}$$

This immediately suggests that (1.4) is a three dimensional analogue of (1.5). We might expect that if a solid is broken up "at random", e.g. by planes cut at random through it, the distribution of fragment weights will be given, at any rate approximately, by (1.4). Unfortunately we have been unable to prove this; a mathematical discussion is given in Sect. 3.

Inspection shows, however, that for the $3.7''$ shell fragments of weight greater than about half an ounce usually have part of the original inner and outer surfaces on them; thus we should expect that, for the heavier fragments at any rate a distribution law of the type

$$N dm = C e^{-\alpha m^{1/2}}\, d(m^{1/2}) \tag{1.6}$$

would give a better fit than (1.4). It was in fact found that for this shell and for the $4.7''$ A.A. shell and $3''$ U.P., either formula (1.4) or (1.6) would give an equally good agreement for fragments of medium size, and that (1.6) was somewhat better for the largest fragments.

For a detailed comparison with experiment, Dr. Paymans results with model bombs are the most suitable, because they include an analysis of fragments down to one milligram. We should expect to get the most exact fit with (1.6), and the greatest divergence from (1.4), for very thin casings. Figure 1.3 shows the fragmentation of a model bomb with casing of thickness $0.018''$ filled with tetryl (W. Payman, Fragmentation Report IV, R.C. 276). The quantity ν, of which the logarithm is plotted as ordinate, is the number of fragments between two given weights m_1 and m_2, divided by the interval $({m_2}^{1/2} - {m_1}^{1/2})$, or $m_2^{1/3} - m_1^{1/3}$, according to the method of plotting; the abscissae are the mean of the extreme masses, namely $\frac{1}{2}({m_1}^{1/2} + m_2^{1/2})$ or $\frac{1}{2}(m_1^{1/3} + m_2^{1/3})$. It will be seen that the fit with formula (1.6) is much better than with formula (1.4). The weights are here in grammes.

Figure 1.4 shows what happens for a much thicker casing 0.3 inches thick. It will be seen that formula (1.6) gives fair agreement for the larger fragments, but that there are too many very small ones. This is to be expected, because small fragments will be broken off the ends or edges of the large ones.

The slopes of all these curves, plotted according to formula (1.6), give what seems to us the best indication of the mean linear size. The quantity a of formula (1.2) might be equated to $1/\alpha\sqrt{t}$.

We have not, however, attempted at this stage to compare formulae such as (1.3) with the mean fragment weight of any bomb or shell, because our theory is incomplete, as it does not account for the length of splinters from shells, but only for their breadth, and for bombs which do not give long splinters we have not been able to find experimental information about mean weights

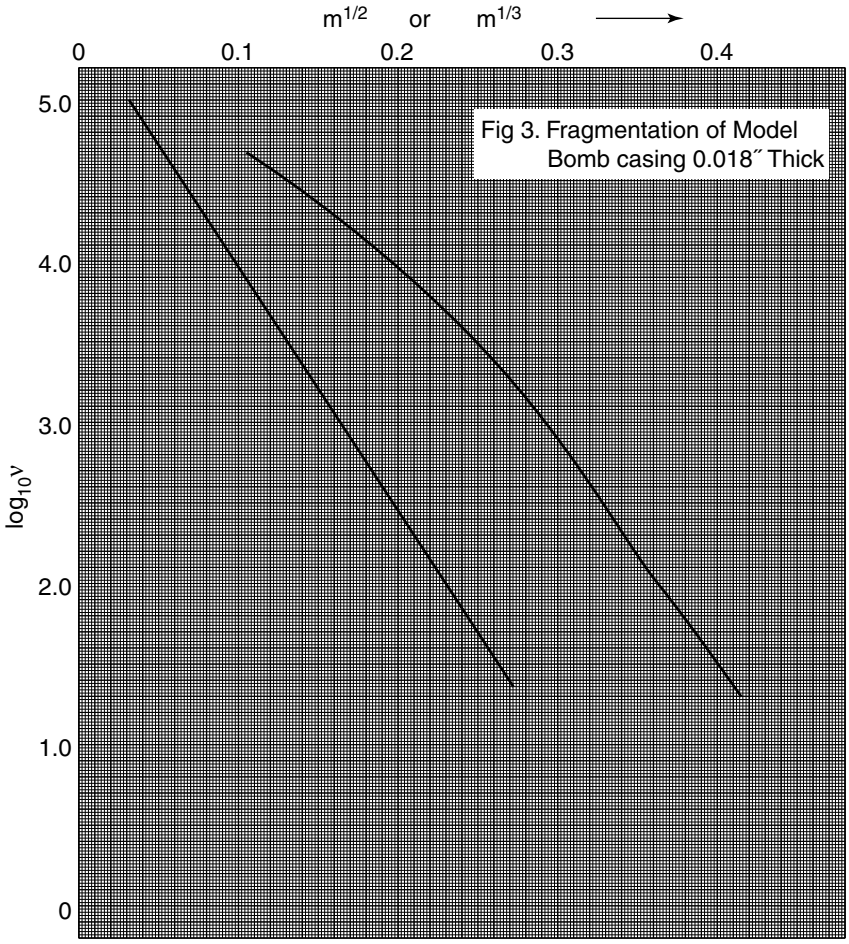

Fig. 1.3.

and speeds. Further, a direct comparison with theory would only be possible where most fragments are projected under the same conditions, e.g. from a long cylinder detonated from one end, or a spherical bomb detonated in the middle.

1.3 Mathematical Discussion of the Distribution Law for Fragment Sizes

Distribution laws of the types (1.4) and (1.6) have been proposed in a number of papers for the weights or diameters of mineral particles after crushing, of

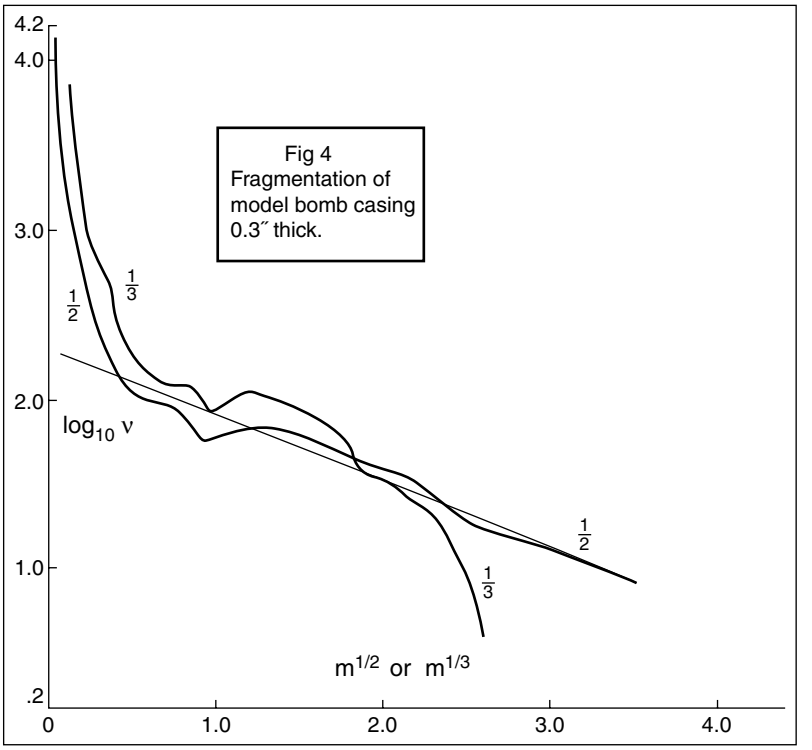

Fig. 1.4.

sand particles and so on[2]. We do not know of any attempt to derive mathematically the two or three dimensional formulae.

We discuss first the case where a thin sheet is broken up into rectangular fragments by two sets of parallel lines. The analysis will be appropriate if a shell casing is broken up by cracks parallel to the axis at an average distance, say, x_o apart, and the lengths have an average value y_o independent of the breadth and are distributed according to the usual law. According to our assumptions, the number with breadths between x and $x + dx$ is proportional to $\exp(-x/x_o)dx$, and the number with lengths between y and $y + dy$ proportional to $\exp(-y/y_o)dy$. Thus the number per unit area with area greater than a^2 is given by

$$\frac{1}{(x_o y_o)^2} \iint \exp\left[-\frac{x}{x_o} - \frac{y}{y_o}\right] dxdy$$

where the integration is for all positive values of xy for which $xy > a^2$. Integrating with respect to y we obtain

[2] cf. Lienau. J. Franklin Inst. 1935, p. 485, where other references are given.

$$\frac{1}{x_o^2 y}\int_0^\infty \exp\left[-\frac{x}{x_o}-\frac{a^2}{xy_o}\right]dx$$

Putting $x = a\sqrt{\frac{x_o}{y_o}}e^\theta$, the integral becomes

$$\frac{1}{x_o y_o} z \int_0^\infty e^{-z\cosh\theta}\cosh\theta d\theta$$

where

$$z = \frac{2a}{\sqrt{x_o y_o}}$$

This is equal to

$$-\frac{z}{x_o y_o}K_1(z)$$

Differentiating with respect to a, we find for the number of fragments for which a lies between a and $a + da$

$$\frac{2}{(x_o y_o)^{3/2}}\ zK_o(z)da$$

for large z this behaves like

$$\left(\frac{1}{2}\pi z\right)^{1/2} e^{-z}$$

and for small z like

$$z\log z$$

The function $\log(zK_o(z))$ is plotted against z in Fig. 1.5; it will be seen that it is nearly linear except for small z.

If a thin shell casing is broken up at random, and a denotes the square root of the area, and νda the number of fragments such that a lies between a and $a + da$, then a plot of $\log\nu$ against a should give a closer approximation to a straight line than Fig. 1.5. The proof is as follows:

We must first define what we mean by "at random". We suppose that the sheet is cut by a large number of straight lines, of which the directions are random. Consider any one of these lines; then we may take it that a length L of this line is cut by L/x_o other lines, and that the number of intervals of length between x and $x + dx$ is $Ldxe^{-x/x_o}/x_o^2$. Also that $L\sin\theta d\theta/2x_o$ of these lines make an angle with it between θ and $\theta + d\theta (0 \le \theta \le \pi)$.

If the fragments were all of the same shape, then we should have $\nu = \exp(-a/a_o)$ exactly. They are, however, much more nearly all the same shape than when the sheet is cut up by two parallel sets of lines, as was assumed above. Then, if one side of a fragment is very small, there is no particular

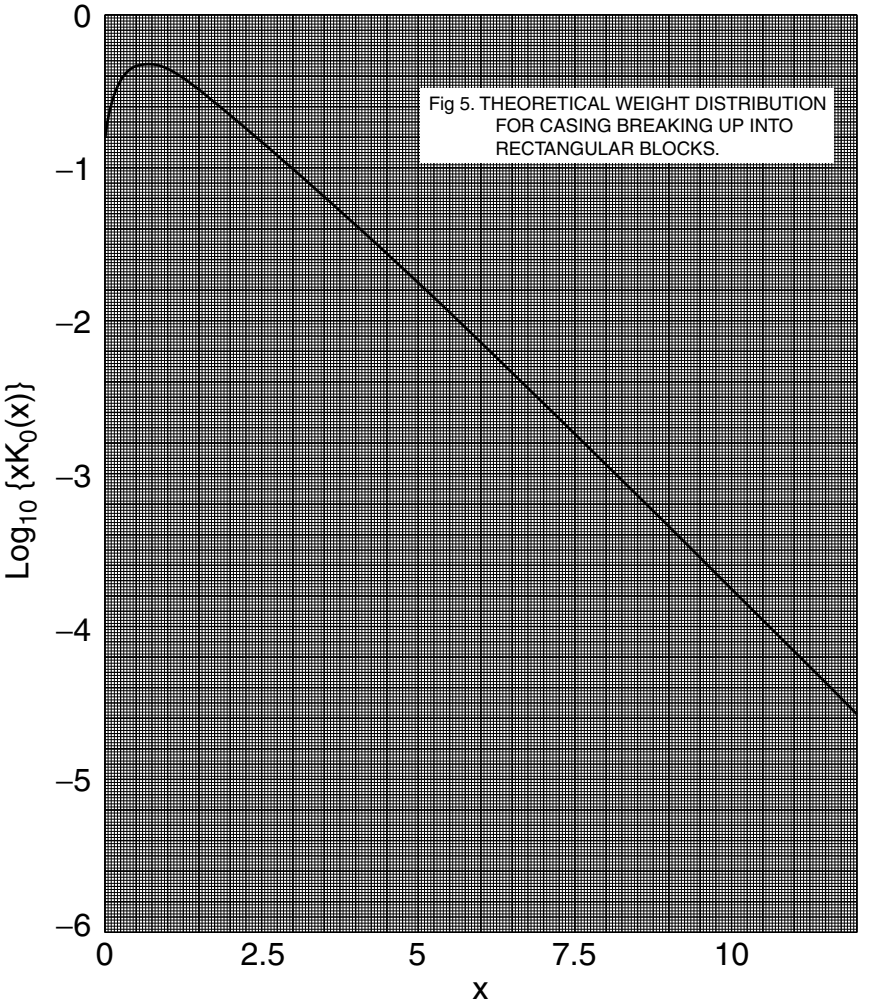

Fig. 1.5.

likelihood that the other one is. On the other, with random fragmentation, any very small interval a on one of the lines cutting the sheet is probably one side of a small triangle of area of the order a^2. Thus we have more very small fragments than with the above distribution. A similar argument shows that we should have more very large ones. Thus if $\log \nu$ is plotted against a, a straighter line should be obtained than that shown in Fig. 1.5.

We can prove that ν tends to a constant non-zero value as $a \to 0$. The very small fragments will nearly all be triangles. If θ, ϕ are the two angles of one of these triangles adjacent to a side of base x the area is

$$\frac{1}{2}x^2/(\cot\theta+\cot\phi)$$

Thus the number of fragments with area less than a^2 is proportional to

$$\iiint e^{-x/x_o}\ \sin\theta\ \sin\phi\ dx\,d\theta\ d\phi$$

the integral being over all values of x, θ, ϕ such that

$$\frac{1}{2}x^2 < a^2(\cot\theta+\cot\phi)$$

The integral becomes, on integrating with respect to x,

$$\int_0^{\pi}\int_0^{\pi-\theta} x_o\left\{1-e^{-\frac{a}{x_o}[2(\cot\theta+\cot\phi)]^{1/2}}\right\}\ \sin\theta\ d\theta\ \sin\phi\ d\phi$$

The first term in the expansion of this function in ascending powers of a is

$$a\iint\sqrt{2(\cot\theta+\cot\phi)}\ \sin\theta\ \sin\phi\,d\theta\,d\phi$$

which does not vanish. Thus $\nu(a)$ tends to a constant value as a tends to zero.

Facsimiles of N.F. Mott: A Theory of Fragmentation

UNCLASSIFIED 7/11/90 Copy No. (14)

~~SECRET~~

A.C. 3348
SD/FP.67

MINISTRY OF SUPPLY

A.C. 3348
SD/FP.67

ADVISORY COUNCIL ON SCIENTIFIC RESEARCH
AND TECHNICAL DEVELOPMENT

FRAGMENTATION PANEL OF THE
STATIC DETONATION COMMITTEE.

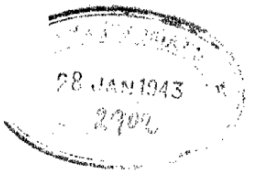

A theory of fragmentation

by

N.F. Mott and E.H. Linfoot

Extra-mural Research No. F72/80

Communicated by C.E.R.S.D.

January 11th, 1943.

MHH.

A THEORY OF FRAGMENTATION

CONFIDENTIAL

by
N. F. MOTT and E.H. LINFOOT,
Bristol University Extra-Mural Group.

SUMMARY. A tentative theory is given to account for the mean fragment sizes of certain types of bomb and shell, and for the relative numbers of large and small fragments.

1. THE MEAN FRAGMENT SIZE. The theory given here is applicable only to casings which expand plastically before rupture. This may not be the case for brittle materials such as cast iron.

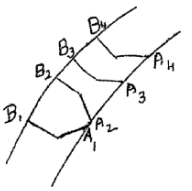

Fig. 1

We consider first fragmentation of the type occurring in the 3.7 inch A.A.shell. The larger fragments appear from inspection to be formed as shown in fig. 1, which represents a section through part of the casing. Cracks start on the inside, at such points as A_1, A_2, A_3 .... and spread outwards to B_1, B_2, B_3. This type of break-up has been discussed in Report No. 2232 from the Dept. of Metallurgy of the University of Sheffield, Ref. A.C.3098. The widths of typical fragments are of the order 1 cm; the length, parallel to the axis of the shell, is considerably greater.

At the moment of rupture, let r be the radius of the shell casing, t its thickness and V the velocity with which it is moving outwards. We suppose that rupture takes place when work-hardening has proceeded to such an extent that a crack will propagate itself with the expenditure of less energy than further plastic flow. Suppose that the casing then splits along two lines distant a apart; the cracks are represented by AB, A'B' in fig. 2, which, like fig. 1, represents a cross section through the shell casing. A splinter of cross section ABB'A' is then flying outwards with velocity V. The top surface AB of the fragment will have, in addition to the large outward velocity V, a velocity at right angles to it of amount $\frac{1}{2}V\alpha$, where $\alpha = a/r$. Similarly the bottom surface A'B' will have a downward velocity of the same amount. Referred to axes moving with the fragment, the metal will have kinetic energy, per unit length parallel to the axis of the shell, equal to

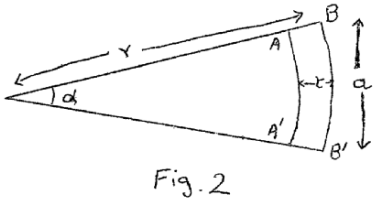

Fig. 2

$$\tfrac{1}{2}\rho t V^2 \int_{-\frac{1}{2}\alpha}^{\frac{1}{2}\alpha} r\theta^2\, d\theta = \tfrac{1}{24}\rho t r \alpha^3 V^2$$

where ρ is the density of the metal. Since $r\alpha = a$, this becomes

$$\tfrac{1}{24} t V^2 \rho a^3 / r^2 \qquad (1)$$

We now make the assumption that if the energy (1) is great enough to form a new crack through the fragment, it will do so, and the fragment will break into two. If W is the energy per unit area required to form a crack, the energy required for this is Wt. Thus no fragment will be formed with thickness a greater than that given by equating Wt to (1), which gives

$$a = \left[\frac{24 r^2 W}{\rho V^2}\right]^{\frac{1}{3}} \qquad (2)$$

For W we may take a value given by impact tests; according to Southwell (Trans. Manchester Assoc. of Engineers, 1937) this ranges from 70 to 800 ft/lbs. per sq. inch. We should take a value appropriate to the metal at the moment of rupture, i.e. after plastic deformation, when it will be very brittle. We therefore take the lower value, 70 ft/lbs. It is realised that the energy of rupture is not, in practice, proportion-

al to the area, so our value will be very approximate. Moreover heating of the metal during its expansion may have an effect. Fortunately, since W occurs as $W^{1/3}$, the value of a is not very sensitive to the value of W. A measurement of the rupture energy for cold-worked H.E. steel would be of interest*.

* It is of interest to compare the much smaller rupture energy for a brittle substance such as quartz, which from experiments on grinding sand appears to be of the order 61 ft/lbs.per sq. ft. (Martin, Trans. Ceramic Society, 23, 61, 1923).

For r we take 2.2 inches, and for V, the velocity of the fragments, 2500 ft/sec. We obtain for a

$$a = 0.55 \text{ inches}$$

in good agreement with the observed value.

For steels where fracture is due to shear we have no information from which the magnitude of W can be estimated.

We have not been able to find a theory to account for the average length of the splinters in this type of shell. For shells or bombs which bulge out in the middle before breaking up, the dimension parallel to the axis might be determined by the same mechanism, r being the radius of curvature of an axial section of the casing.

We may use formula (2) to compare the mean fragment sizes of bombs with different charge-weight ratios, sizes etc., Since, however, we have no theory of what determines the lengths of the splinters from a shell, we confine ourselves to a bomb which, at the moment of bursting, is roughly spherical. Then we can take the mean weight of a fragment to be proportional to $\rho a^2 t$, and thus to

$$\rho^{\frac{1}{3}} r^{\frac{4}{3}} W^{\frac{2}{3}} V^{-\frac{4}{3}} t$$

If r_0, t_0 refer to the bomb before expansion, and r, the radius at the moment of burst is equal to εr_0, then $t = t_0/\varepsilon^2$, so that the mean fragment weight is proportional to

$$r_0^{\frac{4}{3}} \rho^{\frac{1}{3}} t_0 W^{\frac{2}{3}} / V^{\frac{4}{3}} \varepsilon^{\frac{2}{3}} \qquad (3)$$

If we keep the charge constant and vary the thickness t_0, we expect for heavy casings that V^2 will be proportional to $1/t_0$; thus the average weight of fragment is proportional to $t_0^{5/3}$ if ε is constant; actually, however, thick cased shells expand further than thin ones before breaking up, so we expect a rather less rapid variation with t_0 than this.

2. DISTRIBUTION OF FRAGMENT WEIGHTS.

It was pointed out to the present authors by Dr. D.L.Welch (private communication dated 24th Sept.1941) that the distributions of fragments from two such different projectiles as the 5" U.P. (initial fragment velocity 4500 ft/sec.) and the 3.7" A.A.shell (fragment velocity about 2500 ft/sec) can be fitted approximately to the same law. This law is the following : if N(m)dm is the number of fragments with weights between m and m + dm, then

$$N(m)\, dm = C e^{-M/m_0}\, dM \qquad (4)$$

where $M = m^{1/3}$ and C and M_0 are constants. For the shell and the U.P., M_0 has respectively the values (in $(\text{ounces})^{1/3}$)

	3.7" shell	5" U.P.
M_0	0.33	0.15

The agreement is shown below :-

oz.	Shell obs.	Shell calc.	U.P. obs.	U.P. calc.
1/50 - 1/25	not recovered		570	528
1/25 - 1/4	452	454	751	793
1/4 - ½	131	129	93	101
½ - 4	193	181	64	56
4 - 8	5	13	0	0
> 8	1	5		

The total number of fragments is CM_0 and the total weight $6M_0^4C$, so the average weight is $6M_0^3$, or 0.21 ounces for the 3.7 inch shell. The distribution is very skew, however, so that there are a large number of fragments with weights considerably greater than the average.

This observed distribution law suggested a theoretical explanation along the following lines : $m^{1/3}$ is proportional to the mean linear dimension of a fragment, and if this is written x, it suggests that the number of fragments with lengths between x and x + dx is given by

$$C e^{-x/x_0} dx$$

Such a formula can be derived for a rod or line broken up at random in one dimension only. Consider a line AB of length ℓ, cut at random into n + 1 pieces; each cut is independent of the positions of all the others and is equally likely to be at any point between A and B. Consider then any interval ξ of the line. The average number of cuts that it contained is $n\xi/\ell$ and the chance that it does not contain one at all is

$$e^{-n\xi/\ell}$$

Consider then any one cut, and let us calculate the chance that the next cut to the right is in an interval dx at a distance x; this is

$$e^{-nx/\ell} \frac{n dx}{\ell}$$

Thus the number intervals of lengths between x and x + dx is

$$\frac{\ell}{x_0^2} e^{-x/x_0} dx \quad , \quad x_0 = \frac{\ell}{n} \qquad (5)$$

This immediately suggests that (4) is a three dimensional analogue of (5). We might expect that if a solid is broken up "at random", e.g. by planes cut at random through it, the distribution of fragment weights will be given, at any rate approximately, by (4). Unfortunately we have been unable to prove this; a mathematical discussion is given in Section 3.

Inspection shows, however, that for the 3.7" shell fragments of weight greater than about half an ounce usually have part of the original inner and outer surfaces on them; thus we should expect that, for the heavier fragments at any rate a distribution law of the type

$$Ndm = C e^{-\alpha m^{\frac{1}{2}}} d(m^{\frac{1}{2}}) \qquad (6)$$

would give a better fit than (4). It was in fact found that for this shell and for the 4.7" A.A. shell and 3" U.P., either formula (4) or (6) would give an equally good agreement for fragments of medium size, and that (6) was somewhat better for the largest fragments.

For a detailed comparison with experiment, Dr. Payman's results with model bombs are the most suitable, because they include an analysis of fragments down to one milligram. We should expect to get the most exact fit with (6), and the greatest divergence from (4), for very thin casings. Fig. 3 shows the fragmentation of a model bomb with casing of thickness 0.018" filled with tetryl (W. Payman, Fragmentation Report IV, R.C.276). The quantity v, of which the logarithm is plotted as ordinate, is the number of fragments between two given weights m_1 and m_2, divided by the interval $(m_2^{\frac{1}{2}} - m_1^{\frac{1}{2}})$, or $m_2^{\frac{1}{3}} - m_1^{\frac{1}{3}}$, according to the method of plotting; the abscissae are the mean of the extreme masses, namely $\frac{1}{2}(m_1^{\frac{1}{2}} + m_2^{\frac{1}{2}})$ or $\frac{1}{2}(m_1^{\frac{1}{3}} + m_2^{\frac{1}{3}})$. It will be seen that the fit with formula (6) is much better than with formula (4). The weights are here in grammes.

Fig. 4 shows what happens for a much thicker casing 0.3 inches thick. It will be seen that formula (6) gives fair agreement for the larger fragments, but that there are too many very small ones. This is to be expected, because small fragments will be broken off the ends or edges of the large ones.

The slopes of all these curves, plotted according to formula (6), give what seems to us the best indication of the mean linear size. The quantity a of formula (2) might be equated to $1/\alpha\sqrt{t}$.

We have not, however, attempted at this stage to compare formulae such as (3) with the mean fragment weight of any bomb or shell, because our theory is incomplete, as it does not account for the length of splinters from shells, but only for their breadth, and for bombs which do not give long splinters we have not been able to find experimental information about mean weights and speeds. Further, a direct comparison with theory would only be possible where most fragments are projected under the same conditions, e.g. from a long cylinder detonated from one end, or a spherical bomb detonated in the middle.

5. MATHEMATICAL DISCUSSION OF THE DISTRIBUTION LAW FOR FRAGMENT SIZES.

Distribution laws of the types (4) and (6) have been proposed in a number of papers for the weights or diameters of mineral particles after crushing, of sand particles and so on*. We do not know of any attempt to derive mathematically the two or three dimensional formulae.

* cf. Lienau. J. Franklin Inst. 1935, p.485, where other references are given.

We discuss first the case where a thin sheet is broken up into rectangular fragments by two sets of parallel lines. The analysis will be appropriate if a shell casing is broken up by cracks parallel to the axis at an average distance, say, x_0 apart, and the lengths have an average value y_0 independent of the breadth and are distributed according to the usual law. According to our assumptions, the number with breadths between x and $x + dx$ is proportional to $\exp(-x/x_0)dx$, and the number with lengths between y and $y + dy$ proportional to $\exp(-y/y_0)dy$. Thus the number per unit area with area greater than a^2 is given by

$$\frac{1}{(x_0 y_0)^2} \iint \exp\left[-\frac{x}{x_0} - \frac{y}{y_0}\right] dx\, dy$$

where the integration is for all positive values of xy for which $xy > a^2$. Integrating with respect to y we obtain

$$\frac{1}{x_0^2 y} \int_0^\infty \exp\left[-\frac{x}{x_0} - \frac{a^2}{x y_0}\right] dx$$

Putting $x = a\sqrt{\frac{x_0}{y_0}}\, e^\theta$, the integral becomes

$$\frac{1}{x_0 y_0} z \int_0^\infty e^{-z\cosh\theta} \cosh\theta\, d\theta$$

where $z = \frac{2a}{\sqrt{x_0 y_0}}$

This is equal to $-\frac{z}{x_0 y_0} K_1(z)$

Differentiating with respect to a, we find for the number of fragments for which a lies between a and $a + da$

$$\frac{2}{(x_0 y_0)^{3/2}}\, z K_0(z)\, da$$

for large z this behaves like

$$\left(\tfrac{1}{2}\pi z\right)^{\frac{1}{2}} e^{-z}$$

and for small z like

$$z \log z$$

The function $\log(z K_0(z))$ is plotted against z in fig. 5; it will be seen that it is nearly linear except for small z.

If a thin shell casing is broken up at random, and $\underline{a}$ denotes the square root of the area, and νda the number of fragments such that a line between a and $a + da$, then a plot of $\log \nu$ against a should give a closer approximation to a straight line than fig. 5. The proof is as follows :

We must first define what we mean by "at random". We suppose that the sheet is cut by a large number of straight lines, of which the directions are random. Consider any one of these lines; then we may take it that a length L of this line is cut by L/x_0 other lines, and that the number of intervals of length between x and $x + dx$ is $L\,dx\, e^{-x/x_0}/x_0^2$. Also that $L \sin\theta\, d\theta/2x_0$ of these lines make an angle with it between θ and $\theta + d\theta$ $(0 \leq \theta \leq \pi)$.

If the fragments were all of the same shape, then we should have $\nu = \exp(-a/a_0)$ exactly. They are, however, much more nearly all the same shape than when the sheet is cut up by two parallel sets of lines, as was assumed above. Then, if one side of a fragment is very small, there is no particular likelihood that the other one is. On the other, with random fragmentation, any very small interval $\underline{a}$ on one of the lines cutting the sheet is probably one side of a small triangle of area of the order a^2. Thus we have more very small fragments than with the above distribution. A similar argument shows that we should have more very large ones. Thus if $\log \nu$ is plotted against $\underline{a}$, a straighter line should be obtained than that shown in fig. 7.

We can prove that ν tends to a constant non-zero value as $a \to 0$. The very small fragments will nearly all be triangles. If θ, ϕ are the two angles of one of these triangles adjacent to a side of base $\underline{x}$ the area is

$$\tfrac{1}{2} x^2 / (\cot\theta + \cot\phi)$$

Thus the number of fragments with area less than a^2 is proportional to

$$\iiint e^{-x/x_0} \sin\theta \sin\phi \, dx\, d\theta\, d\phi$$

the integral being over all values of x, θ, ϕ such that

$$\tfrac{1}{2} x^2 < a^2 (\cot\theta + \cot\phi)$$

The integral becomes, on integrating with respect to x,

$$\int_0^{\pi} \int_0^{\pi-\theta} x_0 \left\{1 - e^{-\frac{a}{x_0}\left[2(\cot\theta + \cot\phi)\right]^{\frac{1}{2}}}\right\} \sin\theta\, d\theta \sin\phi\, d\phi$$

The first term in the expansion of this function in ascending powers of a is

$$a \iint \sqrt{2(\cot\theta + \cot\phi)} \sin\theta \sin\phi \, d\theta\, d\phi$$

which does not vanish. Thus $\nu(a)$ tends to a constant value as $\underline{a}$ tends to zero.

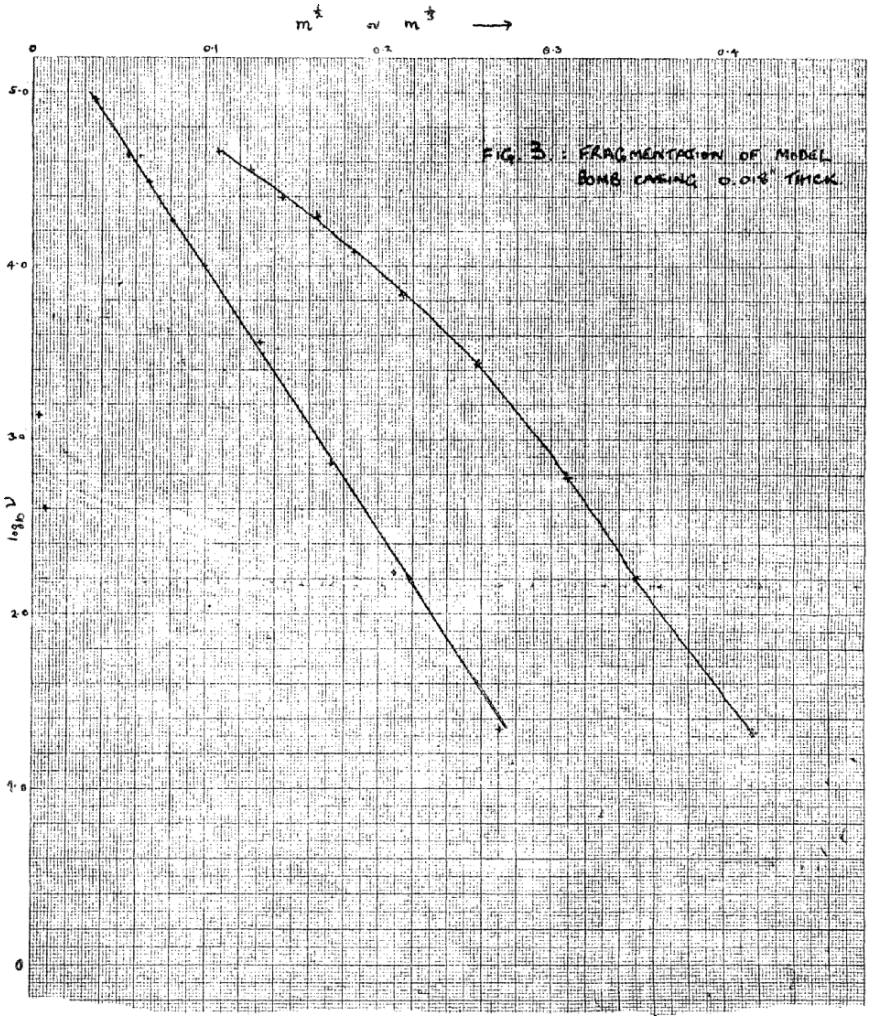
$m^{\frac{1}{4}}$ or $m^{\frac{1}{3}}$ ⟶
0
0·1
0·2
0·3
0·4
5·0
4·0
3·0
2·0
1·0
0
$\log_{10} N$
FIG. 3. FRAGMENTATION OF MODEL BOMB CASING 0.018" THICK.

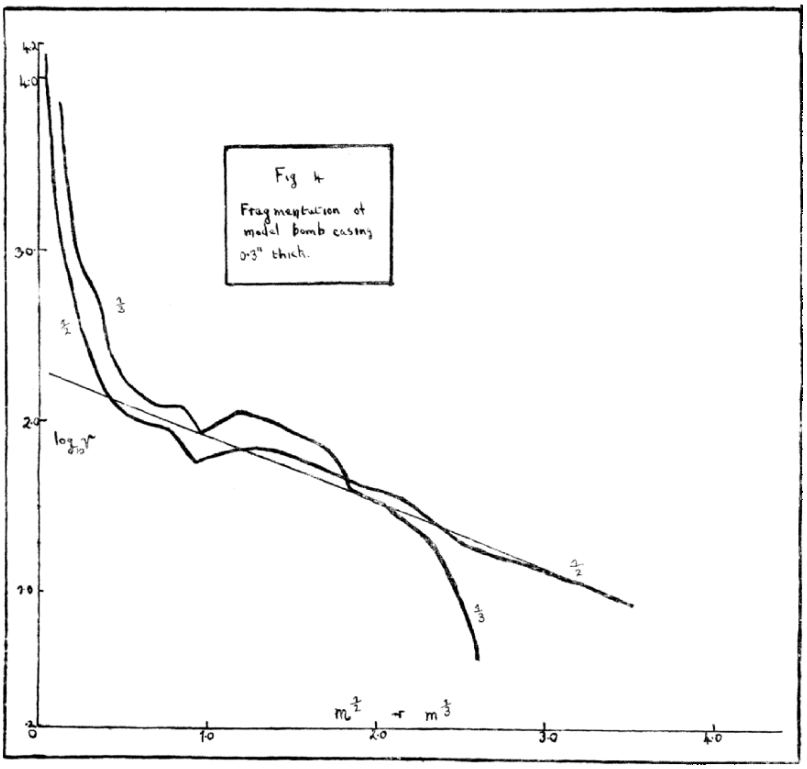
Fig 4
Fragmentation of
metal bomb casing
·3" thick.
50
40
30
20
10
0
10
20
30
40
log N
m^1/2 + m^1/3

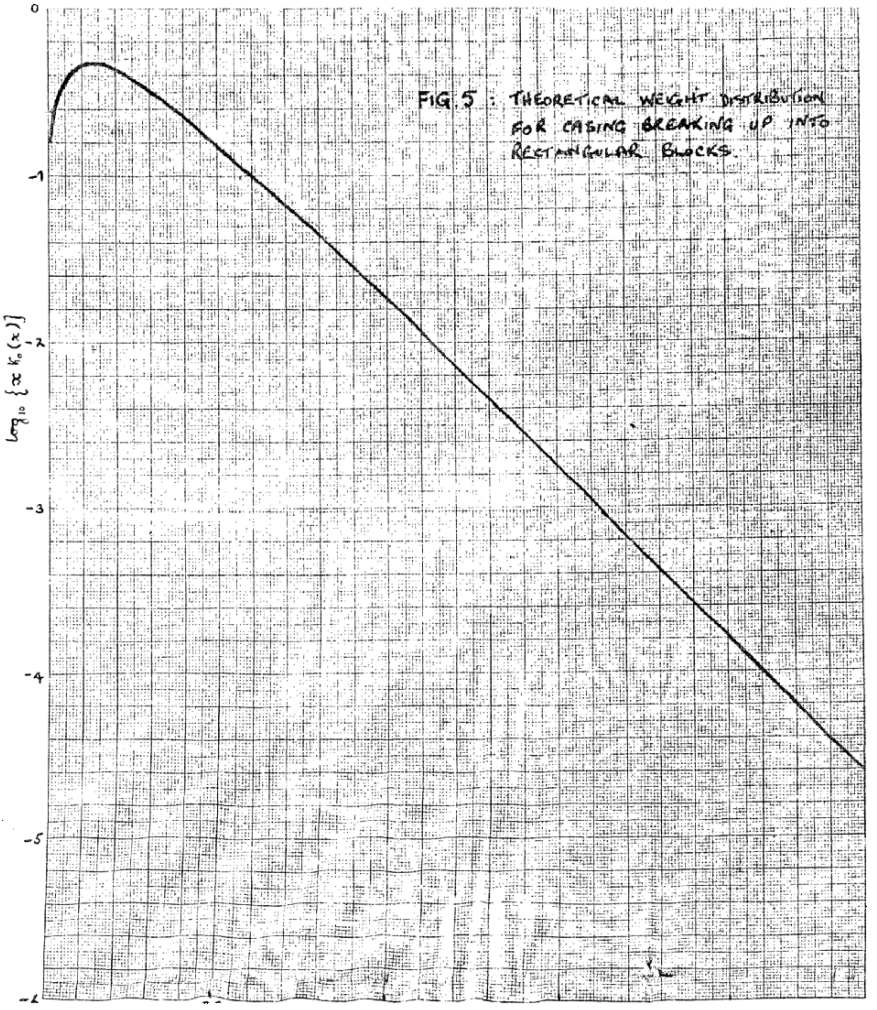
FIG 5 : THEORETICAL WEIGHT DISTRIBUTION FOR CASING BREAKING UP INTO RECTANGULAR BLOCKS.
0
-1
-2
-3
-4
-5
-6
$\log_{10}\{\propto \psi_0(x)\}$

2

Fragmentation of H.E. Shells: a Theoretical Formula for the Distribution of Weights of Fragments

N.F. Mott

(March 1943) Ministry of Supply, A.C. 3642

Summary. It is suggested, following earlier theoretical work, that for all cylindrical shells and bombs the number of fragments of weights between m and $m + dm$ will be given by the formula

$$B\, e^{-M/M_A} dM, \quad M = m^{1/2}\,,$$

where M_A is given in terms of the dimensions of the casing by

$$M_A = Ct^{5/6} d_2^{1/3} \left(1 + \frac{t}{d_2}\right)$$

and where t is the thickness and d_2 the internal diameter of the casing in inches. Comparison with observed fragmentation of service weapons gives

$$\begin{aligned} C &= 0.30 \text{ (TNT)} \\ &= 0.325 \text{ (Amatol 50/50)} \end{aligned}$$

2.1 Purpose of Report

In a recent report on this subject (D.S.R. extra-mural report F. 72/80, A.C.3348), two facts about fragmentation of shells were pointed out:

(a) On the basis of certain hypotheses about the method of break-up, it was shown that no fragment could be formed from the cylindrical part of the casing with breadth greater than

$$\left[\frac{24r^2W}{\rho V^2}\right]^{1/3} \tag{2.1}$$

where r is the radius of the shell casing and V its velocity, both at the moment of break-up, ρ is the density of the steel and W the energy per unit area required to rupture it. Taking reasonable values of W, a value of the breadth was obtained of the order observed ($\frac{1}{2}$ inch for the $3.7''$ shell). No theory was given to account for the lengths of the fragments.

(b) It was pointed out that the fragment distribution for many projectiles fits the formula

$$B\, e^{-M/M_A} dm \quad M = m^{1/2} \tag{2.2}$$

for the number of fragments with weights between m and $m + dm$, the fit breaking down for very small fragments. It was shown that formulae of this type could be derived mathematically for a sheet breaking up at random, and that

$$M_A/\sqrt{\rho t} \tag{2.3}$$

would give a measure of the average linear dimension of the fragments, where t is the thickness of the shell casing at the moment of break-up.

In this report we suggest that the ratio of (2.1) to (2.3) should be the same for all shells. This might be the case if the average ratio of length to breadth of fragments were the same for all shells; so that the length would be a constant multiple of formula (2.1). We have no experimental evidence to show whether this is so.

It is realised, also, that the derivation of formula (2.1), which gives an upper limit to the breadth, is incompatible with a random break-up. Nevertheless it seems reasonable to equate the length (2.3) which describes the fragment distribution actually observed with a multiple of the length (2.1) obtained from theory.

It must also be pointed out that the theory on which formulae (2.1) and (2.2) are based applies only to the cylindrical part of the casing; in the 3.7″ shell, for instance, about 1/5th of the metal is in the base. We should therefore expect only rather approximate agreement between the theory and the observed results.

Assuming, however, that (2.1) and (2.3) are proportional and that W, ρ are the same for all shells, we obtain

$$M_A = K r^{2/3} t^{1/2} / V^{2/3}$$

where K is a constant, r and t refer to the casing at the moment of break-up; since however rt remains constant during the expansion, the error in taking them to apply to the case before expansion will be small.

We assume V^2 to be proportional, not to the charge-weight ratio of the whole shell, but to the charge-weight ratio of a cross-section of it. The amount of metal in the base of the shell will obviously not affect the velocity of most of the fragments. If d_1, d_2 are the outer and inner diameters then

$$R = \frac{{d_1}^2 - {d_2}^2}{{d_2}^2}$$

gives the ratio (by volume) of metal to charge. We assume that

$$RV^2 = \text{const.}$$

where the constant depends only on the type of explosive.

Taking r equal to $1/4(d_1 + d_2)$, this gives

$$M_A = (d_1 + d_2)(d_1 - d_2)^{5/6} {d_2}^{-2/3} \quad x \text{ const.}$$

which may be written

$$M_A = Ct^{5/6} {d_2}^{1/3} \left(1 + \frac{t}{d_2}\right)$$

where t is the thickness of the casing, d_2 is its internal diameter, and C a constant.

The purpose of this report is to see to what extent this formula is in agreement with the facts for standard shells.

For most shells the case thickness increases towards the base; we have taken the value in the middle of the shell the values were obtained from drawings in the possession of the Ordnance Board. We have found M_A by plotting as ordinates the number of fragments in each weight category m_1 to m_2 say, which we write $n(m)\ \Delta m$, divided by the interval $\Delta M = {m_2}^{1/2} - {m_1}^{1/2}$. The abscissa are the quantity $\frac{1}{2}(m_1^{1/2} + m_2^{1/2})$. In many cases an excellent straight line is obtained; for some of the thicker casings the agreement was less good, and then a line was drawn to fit for fragments of medium weight. The plots are shown in Fig. 2.1.

2.2 Projectiles Considered

(a) *The standard 3″ U.P. filled TNT.* The fragmentation has been investigated by Dr. Payman (D.S.R. extra-mural report AC. 3133, 2.12.42). The fit with formula (2.2) is excellent. Ordnance Board give the thickness of the case as between 0.25 and 0.30 inches; Paymen, however, states that the charge-weight ratio of a cross-section is 0.5. Taking the sp. gravity of TNT to be 1.42 and of steel to be 7.8, this gives $t = 0.25$.

We thus take

$$M_A = 0.134, \quad d_2 = 2.5, \quad t = 0.25$$

(b) Payman has also fragmented a U.P. with thick sides, so that

$$t = 0.5'' \quad d_1 = 3.25'' \quad d_2 = 2.25''$$

The fit with formula (2.2) is not so good; we find

$$M_A = 0.265 \pm 0.015$$

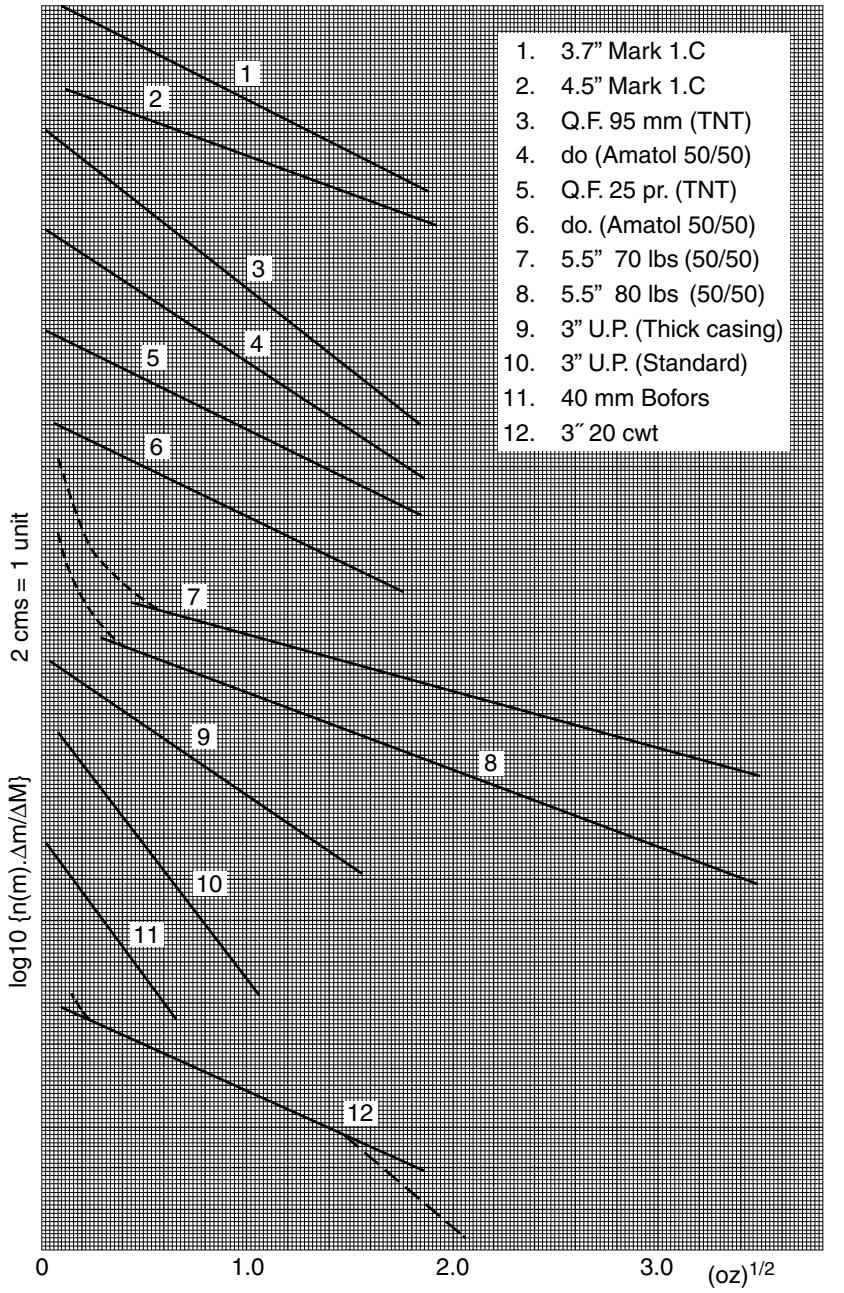
1. 3.7" Mark 1.C
2. 4.5" Mark 1.C
3. Q.F. 95 mm (TNT)
4. do (Amatol 50/50)
5. Q.F. 25 pr. (TNT)
6. do. (Amatol 50/50)
7. 5.5" 70 lbs (50/50)
8. 5.5" 80 lbs (50/50)
9. 3" U.P. (Thick casing)
10. 3" U.P. (Standard)
11. 40 mm Bofors
12. 3˝ 20 cwt
1
2
3
4
5
6
7
8
9
10
11
12
2 cms = 1 unit
log10 {n(m).Δm/ΔM}
0
1.0
2.0
3.0
(oz)1/2

Fig. 2.1.

(c) *Shell, H.E., O.F. 95 mm. TK and SP (25 lbs).* This is a high capacity projectile with charge-weight ratio equal to 12.5%. The dimensions are

$$d_1 = 3.69'' \quad t = 0.45'' - 0.40''$$

The thickness is fairly constant along the length of the shell. The fragmentation with TNT and 50/50 Amatol are given in O.B. Proc. 21099 and the fit with formula (2.2) is excellent, giving

TNT	Amatol\50/50
$M_A = 0.23$	0.26

(d) *Shell, H.E., B.L., 5.5″ 70 lb. and 80 lb.* The fragmentation with Amatol 50/50 is given in O.B. Proc. 21051, and gives

	70 *lb.*	80 *lb.*
M_A	0.64	0.46 ± 0.03
t	0.95	*c.* 0.62

The thickness of the case of the 80 lb. projectile varies between 0.4″ at the nose and 1.0″ at the base. That of the 70 lb. is more nearly constant. The agreement between formula (2.2) and the fragmentation observed is not very good for the 80 lb. weapon, which is not surprising in view of the shape.

(e) *3.7″ and 4.5″ shells, H.E.* The fragmentation with TNT fillings are taken from Dr. Welch's report, quoted from O.B. Proc. 19226. The agreement with the theoretical formula is good. The values are:

	3.7″	4.5″
M_A	0.36	0.49
t	0.58–0.63	0.875

(f) *25 pdr. Shell H.E.* The calibre is 3.435″ and thickness 0.65″. The fragmentation with TNT and Amatol 50/50 is given in O.B. Proc. 21099, the agreement with formula (2.2) being fair. We estimate for M_A

TNT	Amatol 50/50
0.35 ± 0.03	0.38 ± 0.02

(g) *3″ shell H.E., filling TNT.* The thickness; is 0.65″. The fragmentation has been investigated in Dr. Payman's Laboratory (D.S.R. extra-mural reports 72/174, A.C. 3011 and 3515 dated 14.11.42 and 17.1.43), with and

without smoke box and with two exploders. This shell has the smallest charge-weight ratio (defined for a cross-section of the shell) of any investigated. The agreement between the fragmentation observed and formula (2.2) is very poor. M_A is about 0.4 ± 0.1 for the standard shell. The fragmentation is stated to be incomplete and variable owing to an insufficient exploder.

2.3 Bofors 40 mm. Filled TNT

The calibre is $1.56''$ and the thickness $0.24''$. The fragmentation has been investigated in Dr. Payman's Laboratory (extra-mural reports D.S.R.F. 72/174, A.C. 3432 dated 30.1.43). The material is a load-steel alloys, and the charge compressed TNT. The fragment velocity was also determined and was 630 m/sec. The fragmentation did not fit well with formula (2.2) and the number of fragments obtained was small. We find

$$M_A = 0.135 \pm 0.015$$

2.3.1 Results

These are shown in Table 2.1; the projectiles are classified in order of the ratio R, which gives the ratios of the volumes occupied by metal and explosive in a cross-section. The velocities of the shell fragments are also shown, assuming RV^2 to be constant and the $3.7''$ shell to give a fragment velocity of 2500 ft/sec. In P.D.E. report 1942/67 it is stated that the fragment velocity of the U.P. is 4500 ft/sec., instead of the 4200 shown here. If this is correct these velocities should be raised proportionally.

Within the limits of the considerable uncertainties in the date – particularly in the thickness of the casing, the ratio

$$C = M_A / t^{5/6} {d_2}^{1/3} \left(1 + \frac{t}{d_2}\right)$$

remains remarkably constant for the two types of explosive.

According to the P.D.E. report quoted above, substituting Amatol 50/50 for TNT in the U.P. degrades the velocity from 4500 to 4000. Since according to the theory

$$M_A \propto 1/V^{2/3}$$

the values of the constant should be in the ratio $(4500/4000)^{2/3} = 1.08$ for the two explosives[1]. We therefore set

[1] This ratio is in fair agreement with that found for the two 95 mm. shells, where the values of M_A are in the ratio 1–1.2.

Table 2.1.

Projectile	Filling	Metal/charge ratio (volumes) R	V ft./sec	d_1 inches	d_2 inches	t inches	M_A (obs.)	$M_A/t^{5/6}d_2^{1/3}(1+\frac{t}{d_2})$ TNT	$M_A/t^{5/6}d_2^{1/3}(1+\frac{t}{d_2})$ Amatol 50/50
3″ U.P.	TNT	0.42	4200	3.0	2.5	0.25	0.134	0.28	
95 mm shell	TNT	0.69	3200	3.7	2.85	0.425±.025	0.23	0.29 ±.01	
95 mm shell	50/50	0.69	2950	3.7	2.85	0.425±.025	0.26		0.325±.015
5.5″ shell 80 lb	50/50	0.72	2900	5.5	4.2	c. 0.62	0.46±0.03		0.365±.025
Bofors 40 mm	TNT	1.08	2610	1.56	1.08	0.24	0.135 ± 0.015	0.32–0.39	
U.P. (thick case)	TNT	1.09	2610	3.25	2.25	0.50	0.255 ± 0.015	0.28 ± .015	
3.7″ shell	TNT	1.18	2500	3.7	2.5	0.6 ± 0.02	0.36	0.32 ± .015	
5.5″ shell 70 lb	50/50	1.33	2400	5.5	3.6	0.95	0.64		0.34
4.5″ shell	TNT	1.57	2200	4.5	2.8	0.875	0.49	0.29	
25 pr. shell	TNT	1.57	2200	3.435	2.135	0.65	0.35 ± 0.03	0.29 ± .025	
25 pr. shell	50/50	1.57	1800	3.435	2.135	0.65	0.38 ± 0.02		0.32 ± .015
3″ shell	TNT	2.12	1800	3.0	1.7	0.65	0.4 ± 0.1	0.26–0.43	

$$C = 0.30 \text{ (TNT)}$$
$$= 0.325 \text{ (Amatel 50/50)}$$

These values can then be used to work out M_A for any shell.

For reference we give the formula from which the fragment velocities are calculated, based on the assumptions above: these are

$$V = V_o \frac{d_2}{\sqrt{d_1^2 - d_2^2}} \tag{2.4}$$

where

$$V_o = 2750 \text{ (TNT)}$$
$$2450 \text{ (Amatel 50/50)}$$

It is of interest to compare the velocities given by Taylor's[2] theory of the expansion of long cylindrical cased charge of TNT. Taking the specific gravities of TNT and steel to be 1.42 and 7.8, the velocities of the casing after expanding by various amounts are given by the above formula (2.4) with the following values of V_o.

Percentage expansion	11	30	67
V_o (ft/sec.)	2000	2200	2500

[2] G.I. Taylor. A theoretical analysis of the explosion of a cylindrical bomb detonated at one end. Ministry of Home Security, Civil Defence Research Commitee, RC.193.

Facsimiles of N.F. Mott: Fragmentation of H.E. Shells a Theoretical Formula for the Distribution of Weights of Fragments

UNCLASSIFIED

Copy No. (14)

A.C.3642
SD/FP.85

7/11/90

MINISTRY OF SUPPLY

A.C.3642
SD/FP.85

ADVISORY COUNCIL ON SCIENTIFIC RESEARCH
AND TECHNICAL DEVELOPMENT

FRAGMENTATION PANEL OF THE STATIC DETONATION COMMITTEE

Fragmentation of H.E. shells; a theoretical formula
for the distribution of weights of fragments

Communicated by Professor N.F. Mott, M.A., F.R.S.

A.O.R.G. Memorandum No.24
T.87/NFM.

March 12th, 1943.

T87/NFM
SECRET

A.O.E.G. MEMORANDUM NO.34

Fragmentation of H.E. Shells; a theoretical formula for the distribution of weights of fragments

SUMMARY

It is suggested, following earlier theoretical work, that for all cylindrical shells and bombs the number of fragments of weights between m and m + dm will be given by the formula

$$B e^{-M/M_A}\, dM, \qquad M = m^{\frac{1}{2}},$$

where M_A is given in terms of the dimensions of the casing by

$$M_A = C t^{\frac{5}{6}} d_2^{\frac{1}{3}} \left(1 + \frac{t}{d_2}\right)$$

and where t is the thickness and d_2 the internal diameter of the casing in inches. Comparison with observed fragmentation of service weapons gives

C = 0.30 (TNT)
= 0.325 (Amatol 50/50)

1. PURPOSE OF REPORT

In a recent report on this subject (D.S.R. extra-mural report F.72/80, A.C.3348), two facts about fragmentation of shells were pointed out :

(a) On the basis of certain hypotheses about the method of break-up, it was shown that no fragment could be formed from the cylindrical part of the casing with breadth greater than

$$\left[\frac{24 r^2 W}{\rho V^2}\right]^{\frac{1}{3}} \qquad (1)$$

where r is the radius of the shell casing and V its velocity, both at the moment of break-up, ρ is the density of the steel and W the energy per unit area required to rupture it. Taking reasonable values of W, a value of the breadth was obtained of the order observed ($\frac{1}{2}$ inch for the 3.7" shell). No theory was given to account for the lengths of the fragments.

(b) It was pointed out that the fragment distribution for many projectiles fits the formula

$$B e^{-M/M_A}\, dM \qquad M = m^{\frac{1}{2}} \qquad (2)$$

for the number of fragments with weights between m and m + dm, the fit breaking down for very small fragments. It was shown that formulae of this type could be derived mathematically for a sheet breaking up at random, and that

$$M_A / \sqrt{\rho t} \qquad (3)$$

would give a measure of the average linear dimension of the fragments, where t is the thickness of the shell casing at the moment of break-up.

In this report we suggest that the ratio of (1) to (3) should be the same for all shells. This might be the case if the average ratio of length to breadth of fragments were the same for all shells; so that the length would be a constant multiple of formula (1). We have no experimental evidence to show whether this is so.

It is realised, also, that the derivation of formula (1), which gives an upper limit to the breadth, is incompatible with a random break-up. Nevertheless it seems reasonable to equate the length (3) which describes the fragment distribution actually observed with a multiple of the length (1) obtained from theory.

It must also be pointed out that the theory on which formulae (1) and (2) are based applies only to the cylindrical part of the casing; in the 3.7" shell, for instance, about 1/5th of the metal is in the base. We should therefore expect only rather approximate agreement between the theory and the observed results.

Assuming, however, that (1) and (3) are proportional and that W, ρ are the same for all shells, we obtain

$$M_A = K r^{\frac{2}{3}} t^{\frac{1}{2}} / V^{\frac{2}{3}}$$

where K is a constant, r and t refer to the casing at the moment of break-up; since however rt remains constant during the expansion, the error in taking them to apply to the case before expansion will be small.

We assume V^2 to be proportional, not to the charge-weight ratio of the whole shell, but to the charge-weight ratio of a cross-section of it. The amount of metal in the base of the shell will obviously not affect the velocity of most of the fragments. If d_1, d_2 are the outer and inner diameters then

$$R = \frac{d_1^2 - d_2^2}{d_2^2}$$

gives the ratio (by volume) of metal to charge. We assume that

$$RV^2 = \text{const.}$$

where the constant depends only on the type of explosive.

Taking r equal to $1/4(d_1 + d_2)$, this gives

$$M_A = (d_1 + d_2)\,(d_1 - d_2)^{5/6}\, d_2^{-\frac{2}{3}} \times \text{const.}$$

which may be written

$$M_A = C t^{\frac{5}{6}}\, d_2^{\frac{1}{3}} \left(1 + \frac{t}{d_2}\right)$$

where t is the thickness of the casing, d_2 is its internal diameter, and C a constant.

The purpose of this report is to see to what extent this formula is in agreement with the facts for standard shells.

For most shells the case thickness increases towards the base; we have taken the value in the middle of the shell the values were obtained from drawings in the possession of the Ordnance Board. We have found M_A by plotting as ordinates the number of fragments in each weight category m_1 to m_2 say, which we write n(m) Δm, divided by the interval $\Delta M = m_2^{\frac{1}{2}} - m_1^{\frac{1}{2}}$. The ordinates are the quantity $\frac{1}{2}(m_1^{\frac{1}{2}} + m_2^{\frac{1}{2}})$. In many cases an excellent straight line is obtained; for some of the thicker casings the agreement was less good, and then a line was drawn to fit for fragments of medium weight. The plots are shown in fig. 1.

2. PROJECTILES CONSIDERED

(a) The standard 3" U.P. filled TNT. The fragmentation has been investigated by Dr. Payman (D.S.R. extra-mural report AC.3135, 2.13.42). The fit with formula (2) is excellent. Ordnance Board give the thickness of the case as between 0.25 and 0.30 inches; Payman, however, states that the charge-weight ratio of a cross-section is 0.5. Taking the sp. gravity of TNT to be 1.42 and of steel to be 7.8, this gives t = 0.25.

We thus take

$$M_A = 0.134, \quad d_2 = 2.5, \quad t = 0.25$$

(b) Payman has also fragmented a U.P. with thick sides, so that

$$t = 0.5" \qquad d_1 = 3.25" \quad d_2 = 2.25"$$

The fit with formula (2) is not so good; we find

$$M_A = 0.265 \pm 0.015$$

(c) Shell, H.E., Q.F. 95 mm. TK and SP (25 lbs).

This is a high capacity projectile with charge-weight ratio equal to 12.5%. The dimensions are

$$d_i = 3.69" \qquad t = 0.45" - 0.40"$$

The thickness is fairly constant along the length of the shell. The fragmentation with TNT and 50/50 Amatol are given in O.B.Proc.21099 and the fit with formula (2) is excellent, giving

	TNT	Amatol 50/50
M_A	0.23	0.26

(d) Shell, H.E., B.L., 5.5" 70 lb. and 80 lb.

The fragmentation with Amatol 50/50 is given in O.B.Proc.21051, and gives

	70 lb.	80 lb.
M_A	0.64	0.46 ± 0.03
t	0.95	c. 0.62

The thickness of the case of the 80 lb. projectile varies between 0.4" at the nose and 1.0" at the base. That of the 70 lb. is more nearly constant. The agreement between formula (2) and the fragmentation observed is not very good for the 80 lb. weapon, which is not surprising in view of the shape.

(e) 3.7" and 4.5" shells, H.E.

The fragmentation with TNT fillings are taken from Dr. Welch's report, quoted from O.B.Proc.19226. The agreement with the theoretical formula is good. The values are :

	3.7"	4.5"
M_A	0.56	0.49
t	0.58 - 0.63	0.875

(f) 25 pdr. Shell, H.E.

The calibre is 3.435" and thickness 0.65". The fragmentation with TNT and Amatol 50/50 is given in O.B.Proc.21099, the agreement with formula (2) being fair. We estimate for M_A

TNT	Amatol 50/50
0.35 ± 0.03	0.38 ± 0.02

(g) 3" shell H.E., filling TNT

The thickness is 0.65". The fragmentation has been investigated in Dr. Payman's Laboratory (D.S.R. extra-mural reports 73/174, A.C.3011 and 3515 dated 14.11.42 and 17.1.43), with and without smoke box and with two exploders. This shell has the smallest charge-weight ratio (defined for a cross-section of the shell) of any investigated. The agreement between the fragmentation observed and formula (2) is very poor. M_A is about 0.4 ± 0.1 for the standard shell. The fragmentation is stated to be incomplete and variable owing to an insufficient exploder.

8. BOFORS 40 mm. FILLED TNT

The calibre is 1.56" and the thickness 0.24". The fragmentation has been investigated in Dr. Payman's Laboratory (extra-mural reports D.S.R. F.73/174, A.C. 3432 dated 30.1.43). The material is a lead-steel alloy and the charge compressed TNT. The fragment velocity was also determined and was 630 m/sec. The fragmentation did fit well with formula (2) and the number of fragments obtained was small. We find

$$M_A = 0.135 \pm 0.015$$

RESULTS

These are shown in Table I; the projectiles are classified in order of the ratio R, which gives the ratios of the volumes occupied by metal

and explosive in a cross-section. The velocities of the shell fragments are also shown, assuming RV^2 to be constant and the 3.7"shell to give a fragment velocity of 2500 ft/sec. In P.D.E. report 1942/67 it is stated that the fragment velocity of the U.P. is 4500 ft/sec., instead of the 4200 shown here. If this is correct these velocities should be raised proportionally.

Within the limits of the considerable uncertainties in the data - particularly in the thickness of the casing, the ratio

$$C = M_A / t^{5/6} d_2^{1/3} \left(1 + \frac{t}{d_2}\right)$$

remains remarkably constant for the two types of explosive.

According to the P.D.E. report quoted above, substituting Amatol 50/50 for TNT in the U.P. degrades the velocity from 4500 to 4000. Since according to the theory

$$M_A \propto 1/V^{2/3}$$

the values of the constant should be in the ratio $(4500/4000)^{2/3} = 1.08$ for the two explosives*. We therefore set

$$\begin{aligned} C &= 0.30 \quad \text{(TNT)} \\ &= 0.325 \quad \text{(Amatol 50/50)} \end{aligned}$$

Those values can then be used to work out M_A for any shell.

For reference we give the formula from which the fragment velocities are calculated, based on the assumptions above : these are

$$V = V_o \frac{d_2}{\sqrt{d_1^2 - d_2^2}} \qquad (4)$$

where

$$\begin{aligned} V_o &= 2750 \quad \text{(TNT)} \\ &\quad 2450 \quad \text{(Amatol 50/50)} \end{aligned}$$

It is of interest to compare the velocities given by Taylor's** theory of the expansion of long cylindrical cased charge of TNT. Taking the specific gravities of TNT and steel to be 1.42 and 7.8, the velocities of the casing after expanding by various amounts are given by the above formula (4) with the following values of V_o.

Percentage expansion	11	30	67
V_o (ft/sec.)	2000	2200	2500

---

* This ratio is in fair agreement with that found for the two 95 mm. shells, where the values of M_A are in the ratio 1 - 1.2.

** G.I. Taylor. A theoretical analysis of the explosion of a cylindrical bomb detonated at one end. Ministry of Home Security, Civil Defence Research Committee, RC.193.

Table I

Projectile	Filling	Metal/charge ratio (volumes) R	V ft./sec	d_1 inches	d_2 inches	t inches	M_A (obs.)	$M_A/t^{5/6} d_2^{1/3}(1+\frac{t}{d_2})$	
								TNT	Amatol 50/50
3" U.P.	TNT	0·42	4200	3·0	2·5	0·25	0·134	0·28	
95 mm shell	TNT	0·69	3200	3·7	2·85	0·425 ± ·025	0·23	0·29 ± ·01	
"	50/50	"	2950	"	"	"	0·26		0·325 ± ·015
5·5" shell 80 lbs.	50/50	0·72	2900	5·5	4·2	c. 0·62	0·46 ± 0·03		0·365 ± ·025
Bofors 40 mm	TNT	1·08	2610	1·56	1·08	0·24	0·135 ± 0·015	0·32 – 0·39	
U.P. (thick case)	TNT	1·09	2610	3·25	2·25	0·50	0·255 ± 0·015	0·28 ± ·015	
3·7" shell	TNT	1·18	2500	3·7	2·5	0·6 ± 0·02	0·36	0·32 ± ·015	
5·5" shell 70 lbs.	50/50	1·33	2400	5·5	3·6	0·95	0·64		0·34
4·5" shell	TNT	1·57	2200	4·5	2·8	0·875	0·49	0·29	
25 pr. shell	TNT	1·57	2200	3·435	2·135	0·65	0·35 ± 0·03	0·29 ± ·025	
"	50/50	"	1800	"	"	"	0·38 ± 0·02		0·32 ± ·015
3" shell	TNT	2·12	1800	3·0	1·7	0·65	0·4 ± 0·1	0·26 – 0·43	

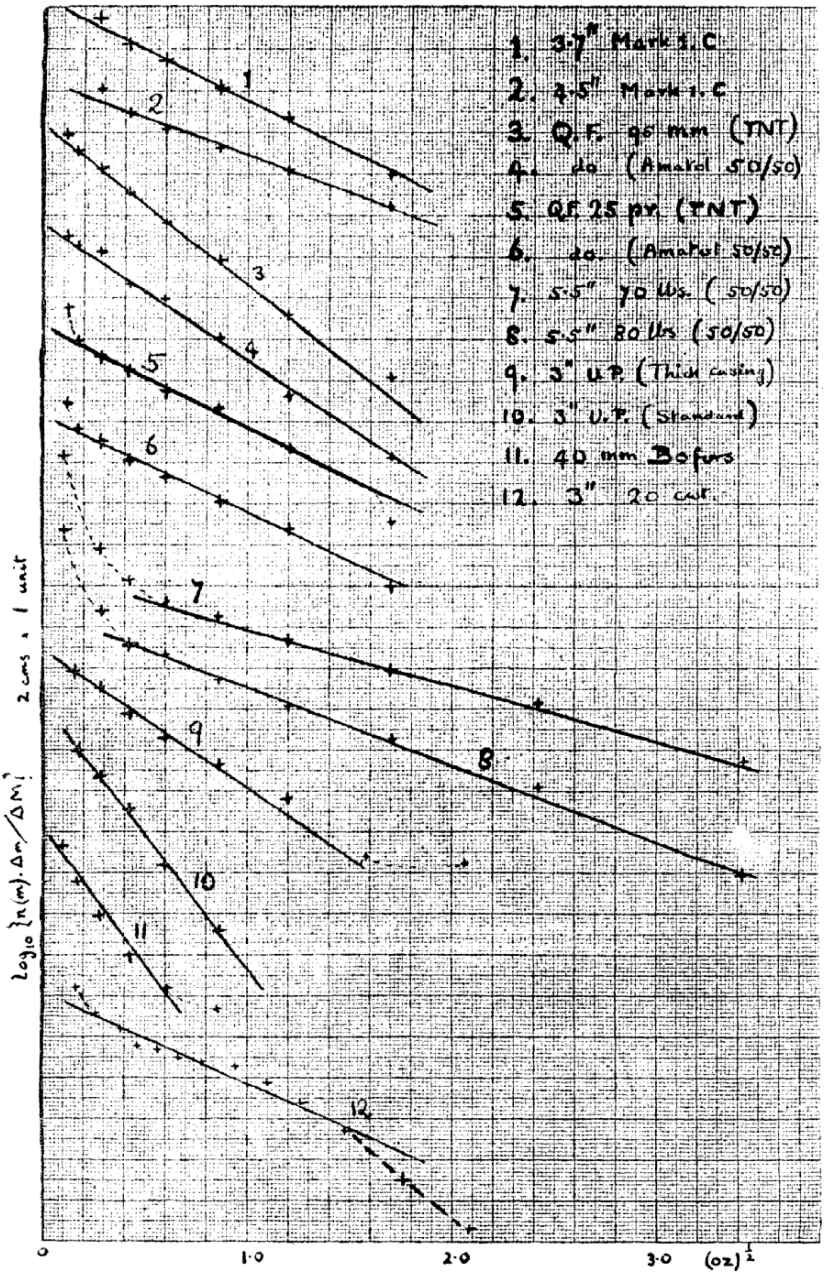
1. 3·7" Mark 1. C
2. 3·5" Mark 1. C
3. Q.F. 95 mm (TNT)
4. do (Amatol 50/50)
5. QF 25 pr. (TNT)
6. do (Amatol 50/50)
7. 5·5" 70 lbs. (50/50)
8. 5·5" 80 lbs (50/50)
9. 3" U.P. (Thick casing)
10. 3" U.P. (Standard)
11. 40 mm Bofors
12. 3" 20 cwt.
2 cms = 1 unit
$\log_{10}\{n(m).\Delta m/\Delta M\}$
0
1·0
2·0
3·0
$(oz)^{\frac{1}{2}}$

3

A Theory of the Fragmentation of Shells and Bombs

N.F. Mott

(May 1943), Ministry of Supply, A.C.4035

Summary. In a recent report on this subject[1], a tentative theory was put forward to account for the sizes of the fragments obtained from steel projectiles. In a further note[2], the theory was compared with the observed fragmentation of service shells. In this report an attempt is made to extend and to improve the theory, as far as is possible without a satisfactory theory of rupture in metals, which does not exist at present.

Before discussing the theory of fragmentation in Part II of this paper we shall give in Part I a summary of the information available about the velocities, weights and shapes of fragments and the mechanisms by which the explosive transfers its energy to them. We shall confine ourselves as far as possible to cylindrical projectiles of uniform diameter, both internal and external; shells with conical cavities are obviously less suitable for the deduction of theoretical conclusions. The rocket head is particularly suitable from this point of view, as is also the German 88 mm shell, and a special British 3.7″ shell recently fragmented by C.S.A.R., Millersford.

PART I

3.1 Expansion of the Casing

It is well known that steel casings expand considerably before rupture; this can be seen most clearly by examining the larger fragments which contain part of the inner and outer surfaces; the case has become thinner by an amount which varies very little from one fragment to another[3]. The present author has examined fragments from the following projectiles which have a uniform case

[1] A Theory of Fragmentation, by N.F. Mott and E.H. Linfoot, D.S.R. Extra-Rural Report A.C. 3348

[2] A.O.R.G. Memo. No. 24. "Fragmentation of H.E. Shells; a theoretical formula for the distribution of weights of fragments"

[3] Report R.C. 282 from Dept. of Metallurgy, University of Sheffield.

thickness: A German 88 mm shell, a special British 3.7″ shell with cylindrical cavity, and three rocket shells fragmented in the Safety in Mines Research Station, Buxton. The filling was TNT in each case; the results are as follows:

Table 3.1.

Type of Shell	Carbon content of shell %	External diameter (mm)	Thickness of Casing (mm)	Thickness of Fragment (mm)	Extension %
German AA 88 mm	0.7	88	15	11.8	27
British A.A. 3.7″ (cylindrical cavity)	0.4–0.5	94	16.5	12.8	30
Service A.A. rocket head	0.4–0.5	85	6.75	4.5	50
Thick cased rocket head	0.4–0.5	85	12.8	9	42
Thick cased rocket head	0.15	85	12.8	8.5	50

Further evidence is available from photographic records of the explosions of model bombs obtained at the Safety in Mines Research Station, Buxton[4]). According to these, model bombs 2″ in dia. with mild steel casings filled with tetryl expanded by the following amounts before breaking up:

Thickness of case (inches)	Expansion (%)
0.125	67
0.30	100

The result obtained that the thicker cased bomb expands further may however be due to end effects; it is not confirmed by the two rocket heads in Table 3.1.

3.2 Fragment Velocities

A theoretical treatment of the expansion of the casing of a long cylindrical cased charge of TNT has been given by G.I. Taylor[5]. Apart from the unknown end effect at the base of the shell, his results should be applicable to the nose-fuzed projectiles considered here.

According to Taylor the velocity of the casing can be expressed by the following formula:

$$V = V_o\, d_2 / \sqrt{d_1^2 - d_2^2} \tag{3.1}$$

[4] Report R.C. 236 from the Safety in Mines Research Station.
[5] Report to M. of H. S. No. R.C. 193.

where d_1, d_2 are the external and internal diameters of the casing before expansion, and V_o is given for different degrees of expansion in Table 3.2 Actual velocities calculated for certain shells are also given:

Table 3.2.

	Velocities in ft/sec				
% Expansion	11	30	67	124	200
V_o	2000	2400	2700	3000	3100
V (88 mm shell)	1750	2100	2400	2700	2800
V (3″ U.P.)	2750	3300	3700	4100	4250

These figures neglect the work done in deforming the case; assuming a constant[6] resistance to elongation T_o (poundals/sq.ft) and a density ρ for the steel, a short calculation gives for the reduction in velocity due to this cause

$$\delta V = \frac{T_o}{\rho V} \log(1 + \varepsilon) \tag{3.2}$$

Assuming T_o to be 30 tons/sq.in., we obtain the following values:

Table 3.3.

% Expansion	11	30	67	124	200
V (88 mm shell)	1700	2000	2300	2500	2550

The work done against the plastic forces does not decrease the fragment velocity appreciably, except perhaps for projectiles of very low charge-weight ratio (A.P. shells). The work done in rupturing the case is probably quite negligible.

It cannot be assumed that the fragments are projected from the shell with the velocity of the casing at the moment of break-up; the following observations show this:

(1) According to (unpublished) results obtained at Buxton, model bombs of similar dimensions made of steel and cast iron give fragments of about the same velocity. The cast iron gives very fine fragmentation and probably breaks up without plastic expansion.
(2) By grooving the charge, controlled fragments can be obtained of a desired size from U.P. casings. These fragments do not show thinning, but have

[6] In steels the resistance is, of course, not constant, but increases somewhat as the metal hardens.

the original thickness of the case. The case must therefore have broken before expansion. Nevertheless the velocity of the fragments is appreciably the same as for the normal shell without a grooved charge (unpublished results with model bomb).

Both these results show that the explosive must continue to exert pressure on the fragments after break-up, and up to about 20 or 30% expansion the pressure cannot depend much on whether the case has broken or not.

Evidence about fragment velocities is contradictory; at Buxton all fragments from a given model bomb are found to have approximately the same speed, except for a few very small ones of high velocity, probably acquired from the expanding gases after break-up; at Millersford, on the other hand, whilst most of the fragments from shells of the 88 mm or 3.7″ type have fragments with speeds in the range 2000−2500 ft/sec., there are a considerable number with much lower speeds down to 1000 ft/sec., and thus with speeds less than the calculated velocity of the casing before breakup. The origin of these is unexplained.

Photographic measurements of the velocity with which the casing of a model bomb expands have been made at Buxton; surprisingly enough, the velocity of the case comes out in one case to be *greater* than that of the fragments[7].

In view of these contradictory results we shall take theoretical values for the velocities of the casing, calculated as in Table 3.3; these agree at any rate as regards order of magnitude with observed fragment velocities.

3.3 Types of Fragmentation Observed

The cross sections of the large fragments from a cylindrical shell are usually of one or other of the types shown in Fig. 3.1; on the outside of the case (along AB) the rupture is brittle, with shear rupture from B to C. Types 1 and 4 are the commonest, with small pieces of triangular cross section frequently shearing off (as in type 5 in Fig. 3.1).

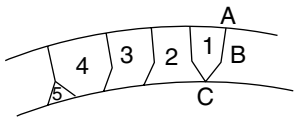

Fig. 3.1.

In some casings the rupture is by shear only, fragments of the types shown in Fig. 3.2 being observed. This has been observed both for mild steel and

[7] cf. Reference [4]; values given on pp. 2 and 5 for a model bomb with 0.018″ casing.

Fig. 3.2.

carbon steel casings. In the theories of part II we have limited ourselves to rupture which is at least partly brittle.

Fragments are commonly five to ten times as long as they are wide.

3.4 Weights of Fragments

The most usual classification is by weighing. The present writer has pointed out[8] that for many shells and bombs the weight distribution satisfies the following formula; the number of fragments with weights between m and $m + dm$ is equal to

$$Ce^{-M/M_A}dM, \qquad M = m^{1/2} \tag{3.3}$$

where C, M_A are constants. Since C depends on the total weight of the casing, the fineness of the fragmentation is given by a single parameter M_A. Apart from any theoretical significance of formula (3.3), it provides a convenient practical method of comparing the fragmentation of different projectiles.

Using ${M_A}^2$ as a measure of the mean fragment weight, the following factors appear to affect it in the following ways:

1. *Type of Steel*: there is little evidence that the tensile strength or yield point affects the fragmentation, but the carbon content certainly does. Thus two similar projectiles, the German 88 mm and the British 5.7″ shell give the following values of M_A:

	Diameter (mm)	Thickness (mm)	Steel, carbon %	M_A (ounce)$^{1/2}$
88 mm shell	88	15	0.7	0.19
3.7″ shell	94	16.5	0.4–5	0.36

   Also 3.25″ rocket heads of carbon (0.4%) and mild steels, thickness 0.5 gave the following values of M_A:

Carbon	0.30 (ounce)$^{1/2}$
Mild steel	0.33

2. *Calibre of shell*: for given charge-weight a big shell undoubtedly gives bigger fragments. For example, values of M_A for a large and for a small shell of similar capacities are (U.B. Proc. 21099 and 21051)

[8] Reference [1].

	M_A
95 mm shell Amatol 50/50	0.26
5.5″ (80 lb. shell) (140 mm Amatol 50/50	0.46

3. *Charge-weight ratio*: this affects both the thickness of the casing and its velocity at the moment of break-up. That the velocity at the moment of break-up has a profound influence on the fragmentation is shown by two facts:
   (a) That a 250 lb. bomb fragmented in water gives only about a quarter as many fragments as when exploded in air[9].
   (b) The well known gross fragmentation of that part of an H.E. shell with direct acting fuze which is in contact with the ground at the moment of explosion; large pieces can be picked from the crater.

   Apart from its influence on the velocity, a thin casing will of course give thinner fragments than a thick one. Whether it affects the other dimensions will be discussed below.

   Values of M_A for two otherwise similar rocket heads with thicknesses 0.265″ and 0.5″ are [2]

Thickness	0.263″	0.5″
M_A	0.134	0.255 (ounce)$^{1/2}$

The velocity of expansion could be altered at will without affecting the size or thickness of the casing by putting a lead covering round the outside of the shell. Experiments to determine the effect of this or the fragmentation would be of great interest. The pressure distribution within the case would also be altered (cf. Sect. 3.11).

3.5 Dimensions of Fragments

The primary process in fragmentation must be splitting parallel to the axis of the shell, with subsequent rupture at the ends, and production of secondary fragments of type 5 in Fig. 3.1. Assuming that cracking (e.g. along BC in Fig. 3.3) precedes shear rupture (e.g. along CD), the first task of any theory of fragmentation must be to account for the distance AB in Fig. 3.3 between the edges of the average fragment. The observed distributions of the breadth AB are shown in Figs. I and II at the end of this paper[10]. It is of course true

[9] Compilation of data on Trials on Explosive Effects of Aircraft Bombs. R.D. Woolwich, 1938

[10] In this report Mott included hand drawn sketches within the text identified as Arabic numbered figures as well as graphs appended at the end of the text identified as Roman numbered figures. The four graphs are identified as Figs. I, II, III and IV in this transcription. This identification agrees with the original with the exception of the present Fig. IV. Further author's notes will attempt to clarify this apparent miss-numbering in the original.

that the length AB often varies considerably along the length of a fragment, and a visual estimate of the mean breadth is subject to error; nevertheless the general shape of the curves is significant. We plot against fragment breadth not the total number of fragments, but the total length of all fragments (placed end to end) in each category.

The following points will be noted:

(a) The rather sharp cut-off for large breadths.
(b) The much narrower fragments obtained with the German 88 mm shell (0.7% carbon steel) than with the British 3.7″ shell or thick cased rocket head, (0.45% steel but similar diameter and casing thickness).
(c) The narrower fragments obtained with the thin cased (high capacity) rocket head than with the thick cased projectiles of similar steel.

The lengths of fragments from the German 88 mm shell are shown in Fig. III; the curve does not show the same cut-off at high values. In Fig. IV we show the length distribution for fragments of different breadths; there is obviously a rough correlation, broad fragments being longer[11]. The average length of fragments in different categories is given in Table 3.4.

Table 3.4.

	Lengths in mm							
Breadth (mm)	2−3	4	5	6	7	8	9	10
Thick-cased U.P. (carbon steel)		39	39	56	44	37	50	36
Thick-cased U.P. (mild steel)		34	35	33	36	47	58	54
Service U.P.			27	30	28	29		
German 88 mm	5.5	10	14.8		21.7			

Evidence for correlation between breadth and length is not marked except for the German shell. For the British shells a ratio of length to breadth of the order 5 seems to be normal, for the German shell a somewhat smaller value.

3.6 Weight Distribution of Fragments

The formula (3.3) was derived by the author[1] on the assumption of some sort of random break-up; Figs. 3.1 to 3.3 show however that neither the break-up parallel or perpendicular to the axis can be considered random as would be

[11] Although Mott refers to Figs. III and IV discussion in this paragraph is clearly covered by the data in Fig. III.

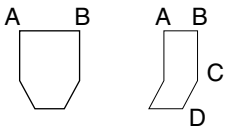

Fig. 3.3.

the case if the breadths were distributed according to the law: number of fragments with breadths between a and $a + da$ is preportional to $\exp(-a/a_o)da$. It therefore seems worth while to attempt a derivation of (3.3) from different assumptions.

Let us assume:

(a) that the casing is broken into strips and that the number of strips with breadths between x and $x + dx$ is

$$Cx \ \exp(-x/x_o)\, dx \tag{3.4}$$

This does not represent the facts exactly, but gives a nearer approximation than the random fracture.

(b) that each strip is broken up according to the same law, and that the average length of fragment is proportional to the thickness x of the strip. Thus from a strip of length l the number of fragments of length between y and $y + dy$ is

$$ye^{-y/px}\ l\, dy/(px)^3 \tag{3.5}$$

where p is a factor (of the order 5).

Then the number of fragments of area greater than a^2 is

$$\frac{Cl}{p^3} \int\limits_{xy\,>a^2} \int \frac{y}{x^2} \left[\exp\left(-\frac{x}{x_o} - \frac{y}{px}\right)\right] dx\, dy$$

This reduces to

$$\text{const}\, \lambda \int\limits_0^\infty \left(1 + \frac{1}{z^2}\right)\ \exp\left(-\lambda z - \frac{1}{z^2}\right)\, dz, \quad \lambda = a/x_o\ p^{1/2}$$

and thus the number of fragments with area such that $a(= \sqrt{\text{area}})$ lies between a and $a + da$ is

$$\text{const}\ f(\lambda) d\lambda$$

where

$$f(\lambda) = \int\limits_0^\infty \left\{\left(1 + \frac{1}{z^2}\right) - \lambda\left(z + \frac{1}{z}\right)\right\} \exp\left(-\lambda z - \frac{1}{z^2}\right) dz \tag{3.6}$$

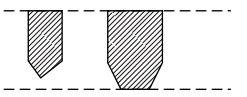

Fig. 3.4.

This function is plotted logarithmically in Fig. V over all values of λ from 0 to 10, i.e. over a range of $\log_{10} f$ equal to 3, which is about the range over which the fragment distribution is usually plotted. It will be seen that the deviation from a straight line is not very large[12].

Weight distributions of actual fragments are likely to deviate from this theoretical curve for the following reason : the narrower fragments frequently break as shown in Fig. 3.4, thus having a smaller depth than they should. Moreover the removal of the triangular pieces from the base of the smaller fragments will obviously make a greater proportional difference to their weight. This will result in a shift of the whole upper part of the curve in Fig. V somewhat to the left. On the other hand, on reaching the weight categories of the small triangular fragments, a large number of new fragments appear which are not included in the analysis given above. Thus the curve should appear as the dotted curve in Fig. V, which is very similar to those observed.

PART II

THEORY OF THE MEAN FRAGMENT SIZE

3.7 Dependence on Velocity

We consider that the fragmentation will be determined by the properties of the casing at the moment of break-up, and will not depend, for instance, on the pressures to which the case has been subjected during the expansion. The factors that may be of importance are thus

(a) Properties of the steel at the moment of rupture − for example the true ultimate tensile strength rather than the yield point.
(b) The rate of increase of plastic strain; this is equal to V/r, where V is the velocity of the case and r its radius.
(c) The thickness of the casing.
(d) The pressure of the explosive at the moment of break-up; according to Taylor's calculations this is from 60–25 tons/sq. in. for casings that break up after a 25 to 50% expansion; this is much less than the initial pressure, which is of the order 1000 tons/sq. in.

[12] A Fig. V does not appear in the original graphs however discussions in this paragraph clearly refer to the upper plot in the present Fig. IV.

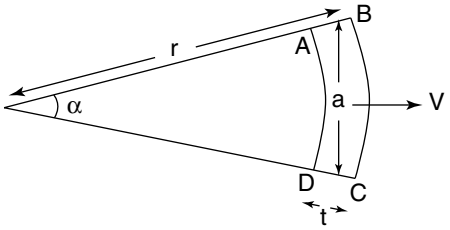

Fig. 3.5.

The theory which we shall develop suggests that (c) and (d) are of minor importance in determining the breadths and lengths of fragments. As in the author's previous report, we take the point of view that it is the kinetic energy of the case which tears it to pieces; the fragmentation would be almost the same if the expanding explosive could be miraculously removed just before the case broke up, leaving it to fly into pieces under its own momentum.

In the author's previous report[1] the following derivation of the fragment breadth was given. Suppose that ABCD in Fig. 3.5 is the cross section of a fragment which has just broken along BA, CD. The fragment is still in a state of plastic flow, the rate of increase of plastic strain being V/r. The kinetic energy of this flow of metal is

$$\frac{1}{2}\rho t\, V^2 \int_{-\frac{1}{2}\alpha}^{\frac{1}{2}\alpha} r\theta^2 d\theta = \frac{1}{24} V^2\, t\rho a^3/r^2$$

It was argued that if this were greater than the energy Wt required to rupture the metal, the fragment would split in half. Thus the value

$$a = \left[\frac{24r^2W}{\rho V^2}\right]^{1/3} \tag{3.7}$$

would give an upper limit to the possible breadth of a fragment.

Agreement with observation, i.e. values of a of the order 1 cm, was obtained with values of W given by the notched bar impact test for a brittle steel, i.e. 40 ft/lbs. per sq. inch.[13] Since W occurs only as $W^{1/3}$, the values obtained are not very sensitive to W.

[13] Measurements were made at the N.P.L. of the Izod value of test pieces cut from a 3.7″ H. E. shell casing which had been extended 20% in the direction originally circumferential to the shell, to represent the state of the steel at the moment of rupture; values obtained for specimens with the usual 10 × 8 mm section at the notch were, for the energy absorbed to fracture

5.0 5.9 5.0 ft. lbs.

This gives 45 ft. lbs/sq. inch. (Ref. Eng. Dept/OYY/RE/B. 104 A, 5.3.43).

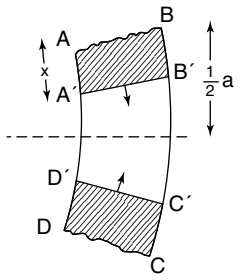

Fig. 3.6.

Equation (3.7) will certainly give a lower limit to the maximum fragment breadth, if W is the true fracture energy under the conditions existing in an H.E. shell. It is doubtful however if this bears any relation to the energy expended in the notched bar test, most of which is probably due to plastic deformation of the metal in the neighbourhood of the notch until the formation of a true crack of atomic width at its apex, leading to brittle rupture. The actual work necessary to separate two planes of atoms in a metal is of course much less, of the order 10^{-3} ft. lbs/sq. inch.

We shall therefore attempt a theory of fragmentation based on the assumption that the energy of fracture is negligible. In addition we shall make the following assumption: fracture can start at any one of a number of places on the surface or in the body of the casing, and once started will rapidly spread across it. During the initial stages of the expansion, it is very unlikely (or even impossible) that a crack will start anywhere; as the expansion increases the chance of a crack forming in any part of the case increases. We introduce a function $f(s)\,ds\,dx$, which gives the chance that a crack will form on a length dx of the circumference of the casing as the strain increases from s to $s + ds$. We may take $f(s)$ to be zero up to a certain value of s (the rupture point), or we may assume a very rapid increase of $f(s)$ in the neighbourhood of the rupture point. We shall find that the form of $f(s)$ determines the mean fragment size.

As before we consider a fragment that has just broken along the lines AB, CD (Fig. 3.6), and ask whether it is likely to break again. As soon as a fracture has formed along AB, for instance, the metal in the neighbourhood of AB will stop flowing. A boundary A′B′ between the part of the metal which is still in plastic flow and the metal which has stopped flowing will move downwards with a velocity that can be calculated. It will soon reach the boundary C′D′ moving upwards from the lower crack; when this has happened, no further crack can form. For a fragment of average width, therefore, the chance of a new crack forming before A′B′ and C′D′ meet each other must be small. This chance can be calculated by comparing the function $f(s)$, giving the rate of formation of cracks, with the time available before the surfaces join.

The velocity with which the surface A′B′ moves can be determined as follows, if we assume that this is small compared with the velocity of sound in steel: Let a be the breadth of the fragment, x the breadth of the part that has stopped flowing, and T_o the stress required to cause plastic flow. The velocity upwards of all material above A′B′ is then

$$\frac{V}{r}\left(\frac{1}{2}a - x\right)$$

Therefore the equation of motion of the block ABB′A′ is

$$T_o = -\rho x \frac{d}{dt}\left\{\left(\frac{1}{2}a - x\right)\frac{V}{r}\right\}$$

which gives

$$T_o = \frac{\rho V}{r} x \frac{dx}{dt} \tag{3.8}$$

Thus

$$\frac{1}{2}x^2/t = rT_o/\rho V \ , \tag{3.9}$$

and the time which the fragment takes to stop expanding is

$$a^2\rho V/8\,T_o r \ ,$$

which is of order 10^{-6} secs. if $a \sim 7$ mm The increase in the strain s of the material during this time is of the order 10^{-2}.

From (3.9) we find

$$\dot{x} = T_o r/\rho V x \sim 6 \times 10^4/x \text{ cm/sec}$$

so the velocity, except for very thin fragments, is considerably less than that of sound in steel (5×10^5 cm/sec.).

We have now to make some assumption about the function $f(s)$. We could assume alternatively that.

(a) $f(s)$ is zero up to a definite value s_o (the rupture point) and is then constant and equal to f_o, say.
(b) $f(s)$ is zero up to s_o, and then increases, as $c(s - s_o)^n$ say.
(c) $f(s)$ is never zero, but increases rapidly in the neighbourhood of the rupture point, as $Ae^{\gamma s}$ say.

The hypothesis (c) is the most attractive, for reasons that will be given in the next section; but they all lead to somewhat similar conclusions about the fragmentation.

An idea of the order of magnitude of the constants involved can be obtained from the behaviour of steel in tensile tests, if we make the assumption that the behaviour in static tests is similar to that at high rates of strain. In tensile tests, steels nearly always fracture after necking; the reduction of area thus

gives a measure of the strain at which fracture occurs. Specimens prepared from one sample of carbon steel show a certain seatter in the measured values of the reduction of area; thus, if a steel fractures on the average for a reduction of area of 50%, individual specimens will show values between 49 and 51 approximately. The following, for instance, are values[14] for a normalised 0.4% carbon steel:

$$58 \quad 56\frac{1}{2} \quad 59\frac{1}{2} \quad 59 \quad \text{per cent}$$

Now according to our assumptions, the chance that a specimen of length l will fracture before the strain reaches a value s is

$$1 - \exp\left[l \int_0^s f(s)ds\right] \tag{3.10}$$

In case (a) this gives

$$1 - \exp\left[-f_o l(s - s_o)\right] \tag{3.11}$$

and in case (c), to a sufficient approximation

$$1 - \exp\left[-\frac{lA}{\gamma} e^{\gamma s}\right] \tag{3.12}$$

Suppose that we assume that an increase in s by Δs increases the chance that fracture has taken place from 10 to 90%. Then we find from (3.11) and (3.12)

$$f_o l = 2.2/\Delta s \quad \text{(case a)}$$
$$\gamma = 3.1/\Delta s \quad \text{(case c)}$$

In case (a) it is not clear what value of l should be taken, since the maximum strain only occurs at the neck. In case (c), however, l does not occur in the formula for γ; if, in accordance with the experimental values given above, we take $\Delta s = 0.02$, we obtain

$$\gamma = 155$$

A plot of the functions (3.11) and (3.12), showing the chance that a fracture has occurred when the strain (reduction in area) is s, is given in Fig. VI for $l f_o = 100$ and for $\gamma = 150$. The origin of s for curve (c) is arbitrary[15].

Experiments on the extent to which the reduction in area at the breaking point fluctuates from specimen to specimen, carried out for a sufficiently large sample, would shed light on the nature of the function $f(s)$.

With any of these form of $f(s)$, an estimate of the order of magnitude of the breadth a can be made as follows: At each crack, after a time t, a breadth

[14] N.P.L. Report to A.R. Committee, Paper 4755

[15] A Fig. VI does not appear in the original graphs however discussions in this paragraph refer to the lower curves plotted in the present Fig. IV.

$$2\left(\frac{2T_o r}{V\rho}\right)^{1/2} t^{1/2}$$

has stopped expanding and is thus "safe" from cracking. Since the strain increases as Vt/r, when the strain has increased by Δs after the formation of a given crack, a breadth round it equal to

$$\beta(\Delta s)^{1/2}, \quad \beta = 2^{3/2}\left(\frac{T_o}{\rho}\right)^{1/2} \frac{r}{V}$$

is "safe" also. If we neglect the overlapping of "safe" areas, a proportion

$$\beta \int^{s} f(s')\sqrt{s - s'}\, ds'$$

is safe when the strain is s. When this approaches unity, the break up is complete. Thus a, the average breadth, is given as regards its order of magnitude, by eliminating s between

$$\beta \int^{s} f(s')\sqrt{s - s'}\, ds' \simeq 1 \tag{3.13}$$

$$\int^{s} f(s')\, ds' \simeq 1/a$$

With the forms for $f(s)$ suggested above we obtain the following:

(a) Equations (3.13) lead to

$$a = \left(\frac{2}{3}\right)^{2/3} f_o^{-1/3}\, 2\sqrt{\frac{T_o}{\rho}}\left(\frac{r}{V}\right)^{2/3}$$

This gives the same power of (r/V) as the author's previous theory, and with $f_o = 100\,\mathrm{cm}^{-1}$, values of a of the order 0.5 cm

(b) Equation (3.13) give

$$a = (n+1)\left[\frac{\Gamma(n+1)\Gamma\left(\frac{3}{2}\right)}{\Gamma\left(n+\frac{5}{2}\right)}\right]^{1-\frac{1}{2n+3}} C^{\frac{-1}{2n+3}}\, \beta^{1-\frac{1}{2n+3}}$$

It will be seen that the fragment size is proportional to $(r/V)^{1-\frac{1}{2n+3}}$ and thus to some power of r/V between 1 and 2/3.

(c) With $f(s) = Ae^{\gamma s}$, the (3.13) give us

$$A\beta e^{\gamma s} \int_0^{\infty'} e^{-\gamma s'} s^{1/2}\, ds' = 1$$

$$Ae^{\gamma s} \int_0^{\infty} e^{-\gamma s'}\, ds' = 1/a$$

and hence

$$a = \sqrt{\frac{2\pi T_o}{\rho}} \frac{1}{V} \frac{1}{\gamma^{1/2}}$$

With $\gamma = 100, T_o = 60$ tons/sq. inch, this gives 0.7 cm for a normal shall of the calibres considered here.

It will be seen that a is now proportional to r/V.

Our formulae suggest, then, that the mean width of fragment will be proportional to

$$\text{const. } (r/V)^s,$$

where s lies between 2/3 and 1, the constant will depend on the nature of the steel; it may depend on the thickness of the case and pressure of the explosive, but consideration of the next section suggests that it will not.

We have not been able to find an analytical expression for the number of fragments with breadth between a and $a + da$, but our equations for the break-up enable a distribution to be found graphically. We limit ourselves to the form (c) for $f(s)$. The theory is at present one-dimensional; we are considering the division of a line (a circumference of the shell.) by random fracture. Let l be the length of this line; then as before where each crack is formed, a space on each side of it equal to

$$\left(\frac{2T_o}{\rho}\right)^{1/2} \frac{r}{V} (\Delta s)^{1/2}$$

is safe from further cracking when s has increased by Δs. If N is the number of cracks already formed then the rate of increase of N is given by

$$\frac{dN}{dS} = Aple^{\gamma S}$$

where p the proportion of the line where cracks can still form. The first crack will form, on the average, when

$$Ale^{\gamma s}/\gamma = 1$$

If the value of s given by this equation be denoted by s_o, and a new variable σ defined by

$$\sigma = \gamma(s - s_o) \ ,$$

then the rate of increase in the number of cracks is given by the equation

$$\frac{dN}{d\sigma} = pe^{\sigma}$$

Also, if a crack is formed when $\sigma = \sigma_1$, the region round it where subsequent cracking is impossible is at any subsequent instant

Table 3.5. Values of γ deduced from observed distributions of fragment breadths

	88 mm shell	3.7″ shell	Rocket head* (thick case)	Rocket head (thin case)
x_o (cm) observed	0.37	0.56	0.44	0.31
$2r$ (cm)	11.4	12.2	12.8	12.8
V (cm/sec)	64,000	63,000	76,000	110,000
$\gamma = \frac{2T_o}{\rho}\left(\frac{r}{Vx_o}\right)^2$	230	105	125	124

* The values of x_o for 0.15 and 0.45% carbon are about the same.

$$2x_o(\sigma - \sigma_1)^{1/2} \tag{3.14}$$

where

$$x_o = \left(\frac{2T_o}{\rho\gamma}\right)^{1/2} \frac{r}{V}$$

A line drawn on paper can now be cut at random, using playing cards or dice. Initially σ is supposed to be zero; after each successive cut is made σ is supposed to increase by $d\sigma$ where

$$d\sigma = 1/pe^{\sigma}$$

After each new cut is made, the "safe" region round all cuts made earlier must be increased according to formula (3.14). Any arbitrary value of the ratio l/x_o may be taken. We took $l/x_o = 20$. The line is repeatedly cut until the whole region is "safe" from further cracking. The lengths of all intervals are then measured and recorded, and the process repeated a number of times until enough data are obtained to draw a histogram, in which the numbers of "fragments" (i.e. intervals) are plotted against their lengths. The results are shown in Fig. II(c)[16]. The similarity to the distributions of fragment breadths observed in Figs. I and II (a) and (b) is satisfactory.

By comparing Fig. V with the observed fragment distributions and especially the values of their upper limits, we have estimated in Table 3.5 the value of x_o for the projectiles investigated[17]. The values are not correct to more than $\pm 10\%$.

From these values we have attempted to deduce γ. For this we require the radius of the shell at the moment of break-up (r), the velocity of the casing and the true ultimate tensile strength, T_o. The two former quantities are deduced from the values given in Part I. To deduce T_o from a tensile test we require the stress at the moment of rupture at the base of the neck, which

[16] This theoretical curve is an inset identified by Mott as "(c) Theory" in the graph provided in the present Fig. II.

[17] Again Fig. V refer to the curves provided in the upper plot in the present Fig. IV.

is of course considerably greater that the U.T.S. given in engineering tables. For steels the following values are given by Korber and Rohland, (Mitt. d. K. Wilhelm Inst. f. Eisenforschung, 5 (1924) 55).

Carbon	Reduction in Area	True Ultimate Stress	
(%)	(%)	kg/mm^2	tons/sq.inch
0.13	70	78	51
0.25	63	80	52
0.45	57	82	53
0.55	50	87	57

These will probably be somewhat higher for high rates of strain;[18] we have thus assumed

$$\begin{aligned} T_o &= 80\,\text{tons/sq. inch} \\ &= 100 \quad '' \qquad '' \end{aligned}$$

for British (0.45% carbon) and German (0.7% carbon) shell steels respectively.

For the values of γ we cannot claim an accuracy greater than $\pm 30\%$; within these limits the British shells (0.45% carbon) show the same value, which is of the order expected. The German shell shows a higher value, which we assume to be due to the higher carbon content of the steel.

3.8 Dependence on Thickness and Pressure

We have seen that the hypothesis

$$f(s) = Ae^{\gamma s} \qquad \gamma \sim 100$$

fits the facts well both for the fragmentation of shells and for the consistency of the rupture point, and seems a priori more likely than the other hypotheses. We have now to consider the following points:

(a) Is γ likely to depend on the thickness of the casing, or the pressure of the gases at the moment of rupture?
(b) Why is γ larger for steels with high carbon content?
(c) Can we deduce a factor γ of this order from any known property of the metal?

It has not at present been possible to answer point (b); to the others an answer can be given:

Let us make the following assumptions about fracture in ductile metals:

[18] cf. G.I. Taylor, Stress Strain Relationship on Impact. Civil Defence Research Committee. R.C. 36.

(i) Cracks can start at a limited number of points or regions in the metal of which we assume that there are n per unit volume.
(ii) Cracks will start at these points, on the average, when the strain has increased to a value s_1
(iii) The strains at which cracks will form at the individual points of weakness show a certain scatter about the value s_1; it is natural to represent this scatter by a Gaussian distribution. We thus assume that the number of points per cm^3 at which a crack will form as the strain increases from s to $s + ds$ is

$$\frac{n}{s_2\sqrt{2\pi}} \exp\left[\frac{-(s-s_1)^2}{s_2^2}\right] ds \ ,$$

For a tensile specimen of cross sectional area A, this gives us for our function $f\,(s)$

$$f(s) = \frac{nA}{s_2\sqrt{2\pi}} \exp\left[\frac{-(s-s_1)^2}{s_2^2}\right] cm^{-1} \tag{3.15}$$

We are interested only in the tail end of this curve where $f(s)$ first becomes appreciable; let us then define the rupture point s_o as the strain for which one crack per cm is expected, so that

$$\int^{s_o} f(s)ds = 1 \ , \tag{3.16}$$

and write

$$s = s_o + s'$$

Then we obtain from (3.15)

$$f(s) \simeq \frac{nA}{s_2\sqrt{2\pi}} \exp\left[\frac{-(s_1-s_o)^2}{s_2}\right] e^{\gamma s'}$$

with

$$\gamma = 2(s_1 - s_o)/{s_2}^2 \tag{3.17}$$

Also from (3.16)

$$\frac{nAs_2}{2\sqrt{2\pi}(s_1-s_o)} \exp\left[\frac{-(s_1-s_o)^2}{s_2}\right] = 1 \ ,$$

whence

$$\left(\frac{s_1-s_o}{s_2}\right)^2 = \log_e\left[\frac{nAs_2}{2\sqrt{2\pi}(s_1-s_o)}\right] \tag{3.18}$$

Hence from (3.17) we obtain finally

$$\gamma = 2\log_e\left[\frac{nAs_2}{2\sqrt{2\pi}(s_1-s_o)}\right]/(s_1-s_o) \tag{3.19}$$

Since n comes within the logarithm, its exact value is not important. For a number of reasons we expect the distance between the points where rupture can start to be of the order 10^{-4} to 10^{-5} cm. This is for instance the distance between the slip bands[19] in a metal, the "dislocations" in G.I. Taylor's theory of slip,[20] or the "crystallites" whose existence has been suggested in cold worked metals.[21] We thus take n of the order 10^{15}; the other terms within the square bracket are negligible in comparison and we obtain

$$\begin{aligned} \gamma &= 2\log_e 10^{15}/(s_1 - s_o) \\ &= 69/(s_1 - s_o) \end{aligned} \tag{3.20}$$

From formulae (3.19), (3.20) we deduce:

(a) That γ is practically independent of the cross section of the specimen, and thus of the thickness of the shell casing.
(b) That γ is practically independent of the pressure of the explosive at the moment of rupture, because (cf. footnote 12) the pressure must vanish at the outside surface, and if the formation of cracks were confined to a small layer near the surface only, it would not affect γ appreciably.
(c) The properties of the steel affect the value of γ only through the value of $s_1 - s_o$, and if s_1 is of the order unity, as is not unlikely, values of γ in agreement with observation are obtained.

3.9 Lengths of Fragments

Up till this section we have discussed only the breadths of fragments, believing that splitting parallel to the axis is the primary process in fragmentation. We have now to discuss the factor determining their lengths.

Observation on fragments of marks cut on the surface of the case shows that shell casings do not stretch parallel to their axis; we must therefore look for an explanation of rupture at the ends of the fragments different from that given for the longitudinal cracks.

If cracks start at A and B and spread to the right, and from C and D and spread to the left, then as Professor Andrew[22] has pointed out, when the cracks bounding two fragments meet, there will be a tendency to split, as at E. According however to the hypothesis on which this paper is based, a split like this is only likely to take place if the steel between the cracks A

[19] cf. for example, Orowan, Nature, 147, 452 (1941) or the beautiful photographs of worked steel obtained with the electron microscope by Heidonreich and Peck, J. Applied Physics, 14, 24 (1943).
[20] Proc. Roy. Soc. A. 145, 362 (1934).
[21] Smith and Wood. Proc. Roy. Soc. A. 178, 93 (1941).
[22] Report R.C. 342 from the Dept. of Metallurgy of the University of Sheffield (31.8.42).

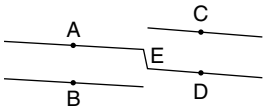

Fig. 3.7.

and B has already stopped flowing before the crack D reaches it; otherwise the crack D will be unaware of the presence of the cracks A and B and will penetrate between them. If however plastic flow has stopped, the different directions in which the two fragments are moving will, we consider, lead to their separation.

Let u be the velocity with which each crack extends. As soon as a crack has formed, the region spreads in which flow has stopped, so that after a time t its width a is given by

$$a = 2\left(\frac{2rT_o}{\rho V}\right)^{1/2} t^{1/2}$$

Thus a crack starting at 0 in Fig. 3.8 and which has spread to a length 2b is surrounded by a region bounded by two parabolas, in which plastic flow has stopped; the breadth PQ of this region is

$$2\left[\frac{2rT_o b}{\rho V u}\right]^{1/2}$$

As a rough criterion for the condition that the region between two cracks should be no longer in flow, we write a, the width of the crack, equal to half this;

$$a = \left[\frac{2rT_o b}{\rho V u}\right]^{1/2}$$

Thus the ratio, length to breadth, is equal to

$$\frac{2b}{a} = \left[\frac{\rho V u a}{rT_o}\right] \tag{3.21}$$

According to (3.14), a for the average fragment is proportional to r/V; we obtain

$$\frac{2b}{a} = 2\sqrt{\frac{\pi\rho}{2T_o}}\,\frac{u}{\gamma^{1/2}} \tag{3.22}$$

With $T_o = 60\,\text{tons/sq. inch} = 9 \times 10^9$ c.g.s. units, $\rho = 8, \gamma = 100$, this gives

$$2b/a = 0.7 \times 10^{-5} u$$

If we equate u to the velocity of sound in steel, 5×10^5 cm/sec., we obtain

$$2b/a \simeq 3.5$$

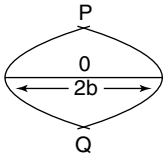

Fig. 3.8.

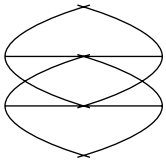

Fig. 3.9.

Fig. 3.10.

in fair agreement with experiment. The hypothesis that cracks spread with the speed of sound is not unlikely to be correct, if the atomic cohesion only has to be overcome, and no plastic deformation is involved.

Formula (3.18) suggests that the length/breadth ratio of the average fragment is independent of the calibre of capacity of the projectile, but will be less for the German high carbon steel (large γ) than for the British steel. These conclusions seem to be born out by the figures of Table 3.4.

3.10 Shape of Cross Section of Fragments

We have already remarked on the types of rupture observed, and pointed out that the type of rupture shown in Fig. 3.10 is usual, with a brittle crack on the outside of the casing and shear rupture at 45° on the inside. In this section we attempt an explanation of this double type of rupture. For this purpose we calculate the stresses in the case during plastic expansion.

According to G.I. Taylor's calculations, the pressure at various stages in the expansion of a long cylindrical cased charge are given by the following figures, where r is the radius of the inner surface of the case and r_o its initial value:

At the moment of break-up, therefore, the pressure is of the same order as the yield stress, and both will be of comparable importance in determining the stresses in the material for thick casings.

Table 3.6.

r/r_o	1.0	1.05	1.1	1.3	1.54	2.4
pressure dynes/ $cm^2 \times 10^{-9}$	150	49	25	8.4	4.0	2.0
pressure tons/ sq. in.	1000	320	160	55	26	13

In a cylindrical tube subject to an internal pressure just great enough to cause flow, the stresses have been worked out.[23] The radial and tangential stresses are, at distance r from the axis

$$S_r = -T_o \log \frac{b}{r}$$
$$S_t = T_o \left(1 - \log \frac{b}{r}\right)$$

where b, a are the external and internal radii; the pressure necessary to cause flow is

$$T_o \log \frac{b}{a}$$

Here $T_o = 2\ S_o/\sqrt{3}$ where S_o is the shearing stress. If p is the actual pressure of the gases, we have an additional pressure at the surface

$$p - T_o \log \frac{b}{a}$$

giving a hydrostatic pressure at a distance r from the axis equal to

$$\left(p - T_o \log \frac{b}{a}\right) \frac{a}{b-a} \left(\frac{b}{r} - 1\right)$$

The stresses can thus be resolved into

(1) A tangential stress T_o
(2) A hydrostatic pressure equal to

$$\left(p - T_o \log \frac{b}{a}\right) \frac{a(b-r)}{(b-a)r} + T_o \log \frac{b}{r}\ ,$$

which vanishes at the outside surface and reaches the value p at the inner surface.

Now it is known that hydrostatic pressure makes fracture more difficult, while having little effect on the resistance to glide. For nonplastic materials, where fracture starts from a microscopic crack, the following account of the

[23] Nadai, Plasticity, McGraw Hill Book Co., p. 188:

effect of hydrostatic pressure has been given by A.A. Griffiths in a well-known paper.[24] Suppose elliptical cracks are acted on by a stress T and a hydrostatic pressure P; the angle made by the plane of any crack to the normal to T is denoted by θ, and θ is distributed over all values Fig. 3.11. Then T will be great enough to cause cracks to spread under the following conditions:

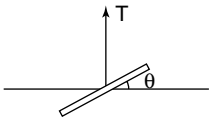

Fig. 3.11.

(a) $4p < 3T$ If this condition is fulfilled, cracks for which $\theta = 0$ will be the first to spread, where T reaches a value $k + p$, where k depends on the elastic constants and surface tension of the metal, and the dimensions of the crack.

(b) $4p > 3T$ Under these conditions cracks for which $\theta = 0$ will not be the first to spread, but those for which

$$\cos 2\theta = \frac{1}{2}\frac{T}{2p - T}$$

At the critical pressure given by $4p = 3T$, this gives $\theta = 45°$.

In plastic materials it is probable that the high tensile stress T near the apex of a crack will cause cracks to form in crystal grains near to it. As the apex of the crack travels inwards, if a point is reached where $4p$ exceeds $3T$, the crack should abruptly change its direction by 45°. This is just what is observed.

Since T is certainly greater than T_o, an necessary condition for such a change of direction will be

$$\frac{4}{3}p > T_o$$

where p is the pressure exerted by the explosive. For casings that break up at 30 and 50% expansions respectively, the calculated values of $4p/3$ are 73 and 35 tons per sq. inch, which are of the same order as T_o, though they are somewhat less than the values that we have assumed to hold for the metal at high rates of strain.

For this reason we put forward the above explanation somewhat tentatively.

[24] Proc. Int. Congress for Applied Mechanics. Delft (1924), p. 55.

3.11 Comparison with Observed Fragmentation of Service Projectiles

In this memorandum we have reached the following conclusions:
For a given type of steel

(a) The ratio of length to breadth of fragments is constant.
(b) The average fragment area is proportional to $(r/V)^{2s}$, where s lies between 2/3 and 1, probably nearer the latter value.
(c) The weight distribution is given approximately by formula (3.3)

We may thus equate M_A of formula (3.3) to

$$\text{const } t^{1/2}(r/V)^s$$

where the value of the constant depends on the properties of the steel, or, making use of formula (3.1) for the velocity

$$M_A = \text{const } t^{5/6} {d_2}^{1/3} \left(1 + \frac{t}{d_2}\right) \qquad s = \frac{2}{3}$$

$$M_A = \text{const } t {d_2}^{1/2} \left(1 + \frac{t}{d_2}\right) \qquad s = 1$$

where the constant depends on the type of explosive and steel, d_2 is the internal diameter and t the thickness of the casing. The first of these formulae has already been compared with experiment in 2), in which M_A was determined for a number of service weapons.

Comparison with fragmentation of observed projectiles should show whether $s = 1$ or $s = 2/3$ or some intermediate value gives the best fit. Ursell[25] has determined the best value of M_A for three model bombs fragmented by Payman,[26] with thicknesses 0.018, 0.125 and 0.3 inches (diameter 2″). He comes to the conclusion that M_A is proportional to $1/V^{1.2}$. The casings of these bombs were of mild steel and gave shear fracture, and so are not directly comparable with our theory. Unfortunately the range of values of r and v available in British shells of carbon steel for which detailed information is available is not great enough to allow any certain conclusion to be drawn.

Observed values of M_A for a number of projectiles filled with TNT are shown in Table 3.7; we have limited ourselves to those with a reasonably cylindrical cross section. It looks as though $s = 1$ gave rather a better fit than $s = 2/3$.

[25] A.W.A.S. Report No. 46; Ministry of Supply No. A.C. 3817
[26] loc. cit.,

Table 3.7.

Projectile	d_1 inches	t inches	M_A $(\text{oz})^{1/2}$ observed	$\frac{M_A}{t^{5/6}d_2^{1/3}\left(1+\frac{t}{d_2}\right)}$	$\frac{M_A}{td_2^{1/2}\left(1+\frac{t}{d_2}\right)}$
$3''$ U.P.	3.25	0.265	0.134	0.265	0.27
95 mm shell	3.7	0.425	0.23	0.29	0.26
U.P. (thick cased)	3.5	0.50	0.30	0.32	0.29
$3.7''$ shell	3.7	0.60	0.36	0.32	$0.275 \pm .015$
25 pr. shell	3.43	0.65	0.35 ± 0.03	$0.29 \pm .025$	$0.245 \pm .02$

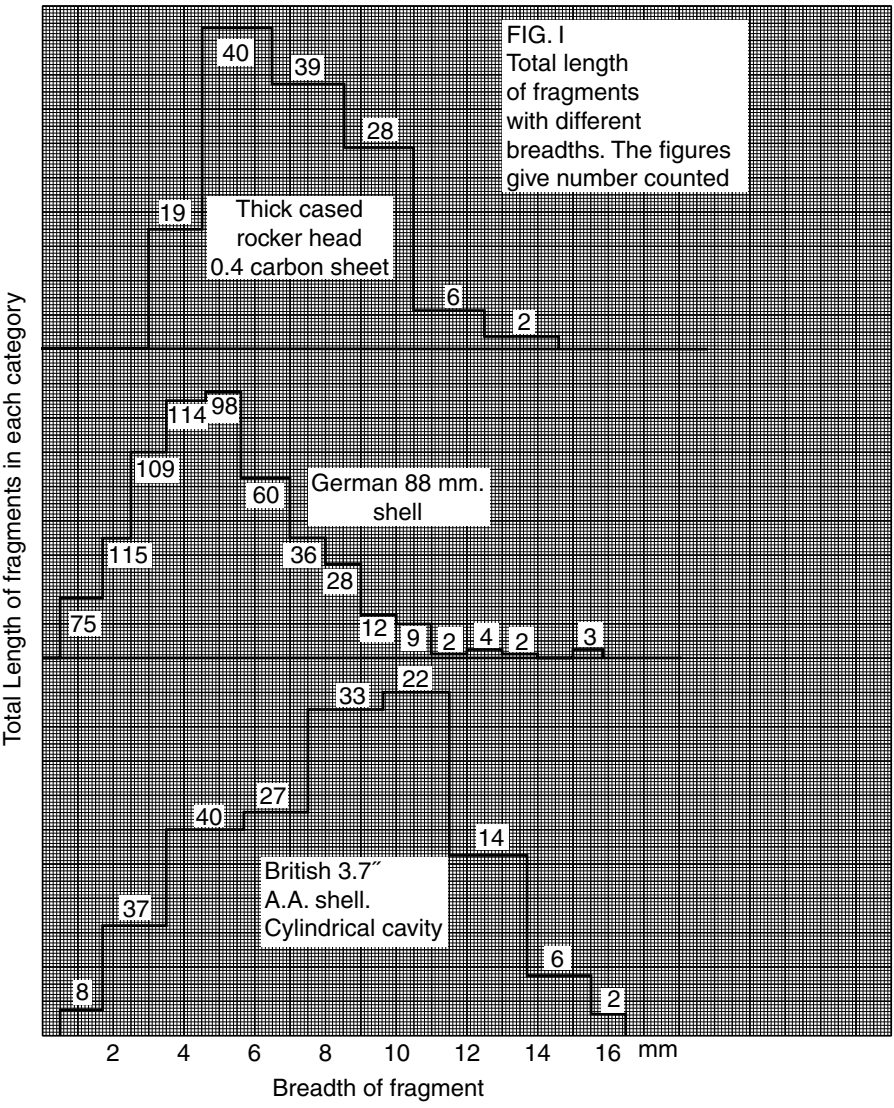
FIG. I
Total length
of fragments
with different
breadths. The figures
give number counted
Thick cased
rocker head
0.4 carbon sheet
German 88 mm.
shell
British 3.7″
A.A. shell.
Cylindrical cavity
40
39
28
19
6
2
114
98
109
60
115
36
28
75
12
9
2
4
2
3
33
22
27
40
14
37
6
8
2
4
6
8
10
12
14
16
mm
Total Length of fragments in each category
Breadth of fragment

Fig. I.

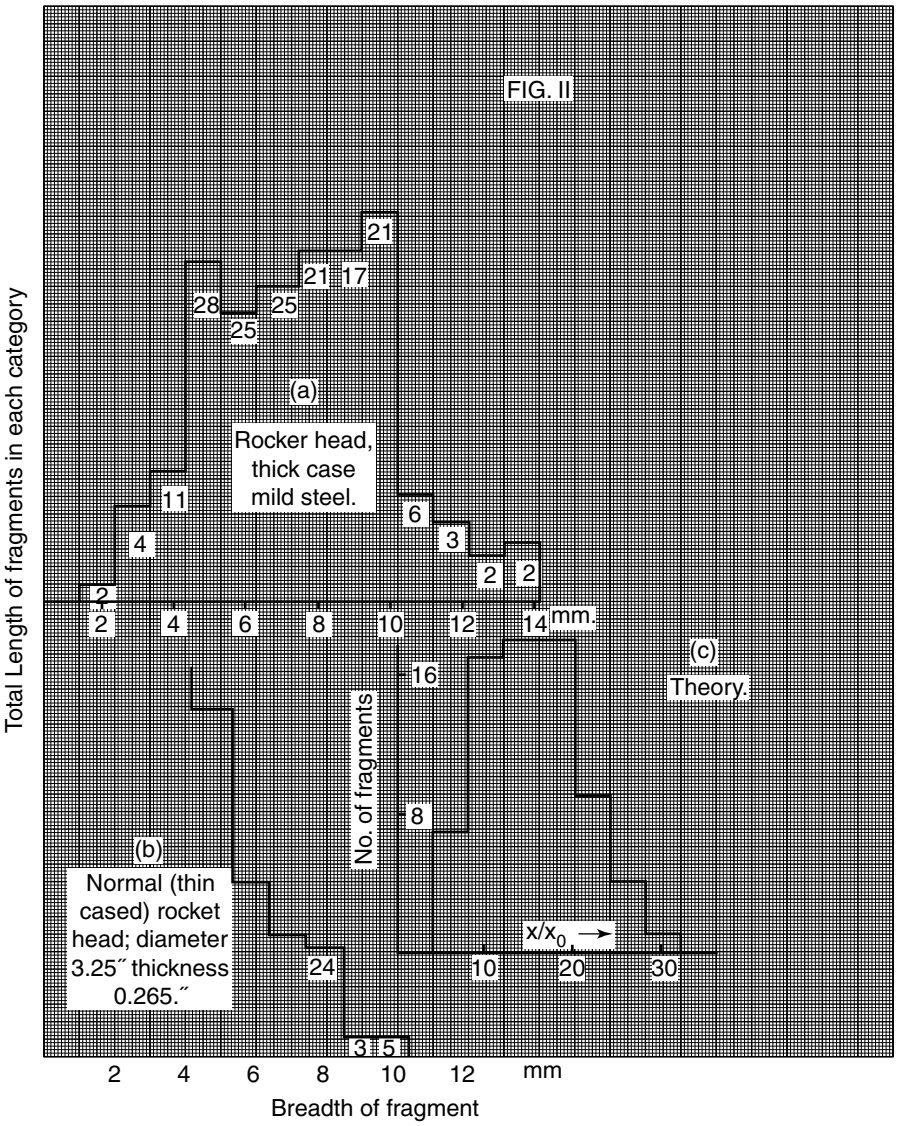
FIG. II
Total Length of fragments in each category
No. of fragments
Breadth of fragment
mm
(a)
Rocker head, thick case mild steel.
(b)
Normal (thin cased) rocket head; diameter 3.25″ thickness 0.265.″
(c)
Theory.
x/x0 →
21
21 17
28
25
25
11
4
2
2
6
3
2
2
16
8
24
3 5
2 4 6 8 10 12 14 mm.
10 20 30

Fig. II.

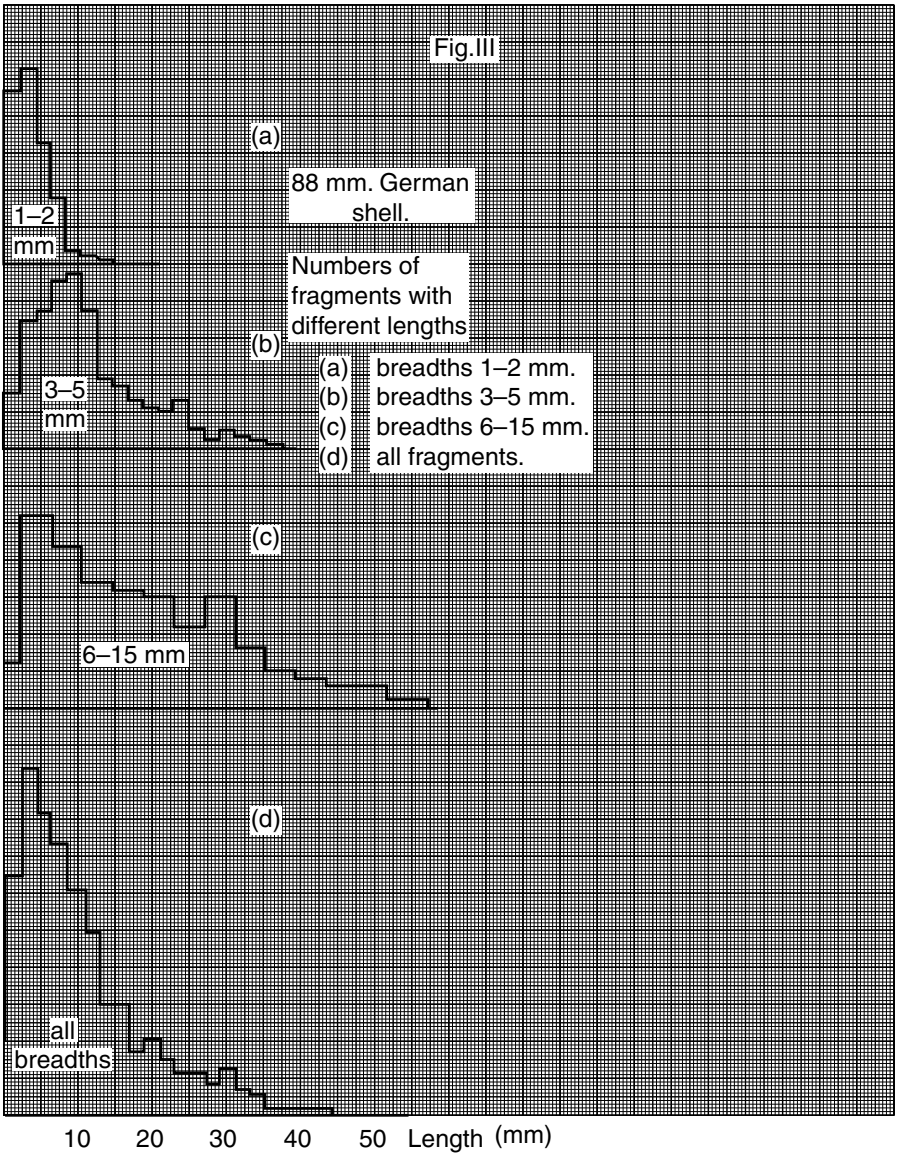
Fig.III
(a)
88 mm. German shell.
1–2 mm
Numbers of fragments with different lengths
(b)
(a) breadths 1–2 mm.
(b) breadths 3–5 mm.
(c) breadths 6–15 mm.
(d) all fragments.
3–5 mm
(c)
6–15 mm
(d)
all breadths
10
20
30
40
50
Length (mm)

Fig. III.

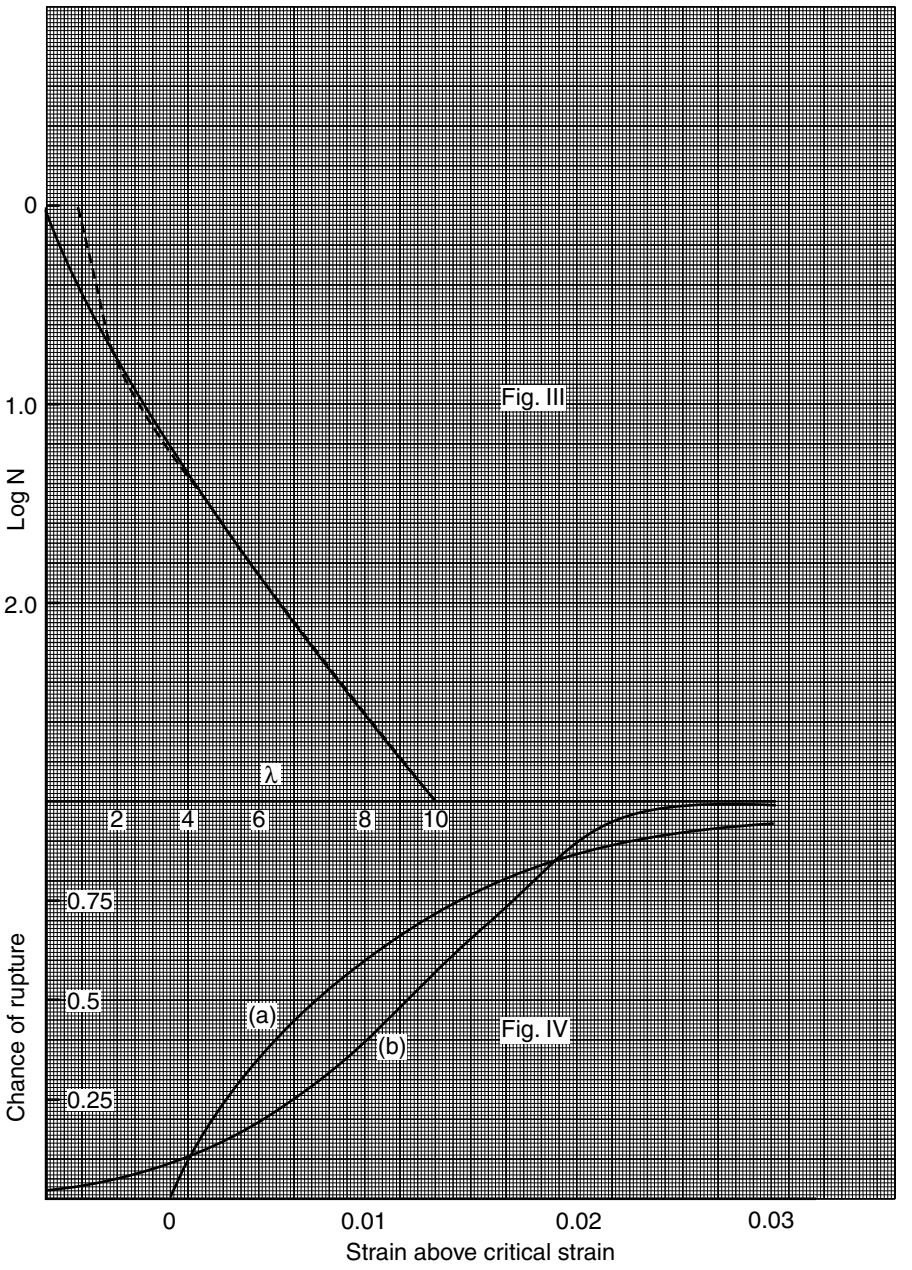
0
1.0
2.0
Log N
Fig. III
λ
2
4
6
8
10
0.75
0.5
0.25
Chance of rupture
(a)
(b)
Fig. IV
0
0.01
0.02
0.03
Strain above critical strain

Fig. IV.

Facsimiles of N.F. Mott: A Theory of the Fragmentation of Shells and Bombs

UNCLASSIFIED
~~SECRET~~ 7/11/90.9

Copy No. (14)

A.C.4035
SD/FP.106

MINISTRY OF SUPPLY

ADVISORY COUNCIL ON SCIENTIFIC RESEARCH
AND TECHNICAL DEVELOPMENT

FRAGMENTATION PANEL OF THE
STATIC DETONATION COMMITTEE

A theory of the fragmentation of shells and bombs

by

Professor N.F. Mott

Received May 27th, 1943.

E.G.

A.C.4035
SD/FP.106

A THEORY OF THE FRAGMENTATION OF SHELLS AND BOMBS.

By N. F. MOTT.

1. In a recent report on this subject[1], a tentative theory was put forward to account for the sizes of the fragments obtained from steel projectiles. In a further note[2], the theory was compared with the observed fragmentation of service shells. In this report an attempt is made to extend and to improve the theory, as far as is possible without a satisfactory theory of rupture in metals, which does not exist at present.

Before discussing the theory of fragmentation in Part II of this paper we shall give in Part I a summary of the information available about the velocities, weights and shapes of fragments and the mechanisms by which the explosive transfers its energy to them. We shall confine ourselves as far as possible to cylindrical projectiles of uniform diameter, both internal and external; shells with conical cavities are obviously less suitable for the deduction of theoretical conclusions. The rocket head is particularly suitable from this point of view, as is also the German 88 mm. shell, and a special British 3.7" shell recently fragmented by C.S.A.R., Millersford.

PART I

2. EXPANSION OF THE CASING

It is well known that steel casings expand considerably before rupture; this can be seen most clearly by examining the larger fragments which contain part of the inner and outer surfaces; the case has become thinner by an amount which varies very little from one fragment to another[3]. The present author has examined fragments from the following projectiles which have a uniform case thickness : A German 88 mm. shell, a special British 3.7" shell with cylindrical cavity, and three rocket shells fragmented in the Safety in Mines Research Station, Buxton. The filling was TNT in each case; the results are as follows :

TABLE I

Type of shell	Carbon content of shell %	External diameter (mm)	Thickness of Basing (mm)	Thickness of Fragment (mm)	Extension %
German AA 88 mm.	0.7	88	15	11.8	27
British A.A. 3.7" (cylindrical cavity)	0.4 - 0.5	94	16.5	12.8	30
Service A.A. rocket head	"	85	6.75	4.5	50
Thick cased rocket head	"	85	12.8	9	42
"	0.15	85	12.8	8.5	50

Further evidence is available from photographic records of the explosions of model bombs obtained at the Safety in Mines Research Station, Buxton[4].

1) A Theory of Fragmentation, by N.F.Mott and E.H.Linfoot, D.S.R. Extra-Mural Report A.C. 3348.

2) A.O.R.G. Memo. No. 24. "Fragmentation of H.E. Shells; a theoretical formula for the distribution of weights of fragments".

3) Report R.C. 282 from Dept. of Metallurgy, University of Sheffield.

4) Report R.C.236 from the Safety in Mines Research Station.

According to these, model bombs 2" in dia. with mild steel casings filled with tetryl expanded by the following amounts before breaking up :

Thickness of case (inches)	Expansion (%)
0.125	67
0.30	100

The result obtained that the thicker cased bomb expands further may however be due to end effects; it is not confirmed by the two rocket heads in Table I.

3. FRAGMENT VELOCITIES

A theoretical treatment of the expansion of the casing of a long cylindrical cased charge of TNT has been given by G.I. Taylor[5]. Apart from the unknown end effect at the base of the shell, his results should be applicable to the nose-fuzed projectiles considered here.

According to Taylor the velocity of the casing can be expressed by the following formula :

$$V = V_0 \, d_2 / \sqrt{d_1^2 - d_2^2} \qquad (1)$$

where d_1, d_2 are the external and internal diameters of the casing before expansion, and V_0 is given for different degrees of expansion in Table II Actual velocities calculated for certain shells are also given :

TABLE II
Velocities in ft/sec.

% expansion	11	30	67	124	200
V_0	2000	2400	2700	3000	3100
V(88 mm. shell)	1750	2100	2400	2700	2800
V (5" U.P)	2750	3500	3700	4100	4250

These figures neglect the work done in deforming the case; assuming a constant* resistance to elongation T_0 (poundals/sq.ft) and a density ρ for the steel, a short calculation gives for the reduction in velocity due to this cause

$$\delta V = \frac{T_0}{\rho V} \log (1+\varepsilon) \qquad (2)$$

Assuming T_0 to be 30 tons/sq.in., we obtain the following values :

TABLE III

% expansion	11	30	67	124	200
V (88 mm. shell)	1700	2000	2300	2500	2550

The work done against the plastic forces does not decrease the fragment velocity appreciably, except perhaps for projectiles of very low charge-weight ratio (A.P. shells). The work done in rupturing the case is probably quite negligible.

It cannot be assumed that the fragments are projected from the shell with the velocity of the casing at the moment of break-up; the following observations show this :

(1) According to (unpublished) results obtained at Buxton, model bombs of similar dimensions made of steel and cast iron give fragments of about the same velocity. The cast iron gives very fine fragmentation and probably breaks up without plastic expansion.

(2) By grooving the charge, controlled fragments can be obtained of a

5) Report to M. of H. S. No. R.C. 193.

* In steels the resistance is, of course, not constant, but increases somewhat as the metal hardens.

desired size from U.P. casings. These fragments do not show thinning, but have the original thickness of the case. The case must therefore have broken before expansion. Nevertheless the velocity of the fragments is appreciably the same as for the normal shell without a grooved charge (unpublished results with model bomb.)

Both these results show that the explosive must continue to exert pressure on the fragments after break-up, and up to about 20 or 30% expansion the pressure cannot depend much on whether the case has broken or not.

Evidence about fragment velocities is contradictory; at Buxton all fragments from a given model bomb are found to have approximately the same speed, except for a few very small ones of high velocity, probably acquired from the expanding gases after break-up; at Millersford, on the other hand, whilst most of the fragments from shells of the 88 mm or 3.7" type have fragments with speeds in the range 2000-2500 ft/sec., there are a considerable number with much lower speeds down to 1000 ft/sec., and thus with speeds less than the calculated velocity of the casing before break-up. The origin of these is unexplained.

Photographic measurements of the velocity with which the casing of a model bomb expands have been made at Buxton; surprisingly enough, the velocity of the case comes out in one case to be <u>greater</u> than that of the fragments*.

In view of these contradictory results we shall take theoretical values for the velocities of the casing, calculated as in Table III; these agree at any rate as regards order of magnitude with observed fragment velocities.

4. TYPES OF FRAGMENTATION OBSERVED

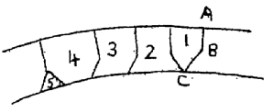

Fig. 1

The cross sections of the large fragments from a cylindrical shell are usually of one or other of the types shown in fig.1; on the outside of the case (along AB) the rupture is brittle, with shear rupture from B to C. Types 1 and 4 are the commonest, with small pieces of triangular cross section frequently shearing off (as in type 5 in fig.1).

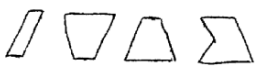

Fig. 2

In some casings the rupture is by shear only, fragments of the types shown in fig. 2 being observed. This has been observed both for mild steel and carbon steel casings. In the theories of Part II we have limited ourselves to rupture which is at least partly brittle.

Fragments are commonly five to ten times as long as they are wide.

5. WEIGHTS OF FRAGMENTS

The most usual classification is by weighing. The present writer has pointed out** that for many shells and bombs the weight distribution satisfies the following formula; the number of fragments with weights between m and m + dm is equal to

$$C e^{-M/M_A} \, dM , \qquad M = m^{1/2} \qquad (3)$$

---

* cf. Reference 4); values given on pp. 2 and 5 for a model bomb with 0.018" casing.

** Reference 1).

where C, M_A are constants. Since C depends on the total weight of the casing, the fineness of the fragmentation is given by a single parameter M_A. Apart from any theoretical significance of formula (3), it provides a convenient practical method of comparing the fragmentation of different projectiles.

Using M_A^2 as a measure of the mean fragment weight, the following factors appear to affect it in the following ways :

1. Type of Steel : there is little evidence that the tensile strength or yield point affects the fragmentation, but the carbon content certainly does. Thus two similar projectiles, the German 88 mm. and the British 3.7" shell give the following values of M_A :

	Diameter (mm)	Thickness (mm)	Steel, carbon %	M_A (ounce)$^{\frac{1}{2}}$
88 mm. shell	88	15	0.7	0.19
3.7" "	94	16.5	0.4-5	0.36

Also 3.25" rocket heads of carbon (0.4%) and mild steels, thickness 0.5 gave the following values of M_A :

Carbon	0.30 (ounce)$^{\frac{1}{2}}$
Mild steel	0.33

2. Calibre of shell : for given charge-weight a big shell undoubtedly gives bigger fragments. For example, values of M_A for a large and for a small shell of similar capacities are (U.B.Proc. 21099 and 21051)

		M_A
95 mm. shell	Amatol 50/50	0.26
5.5" (80 lb. shell)	(140 mm. Amatol 50/50	0.46

3. Charge-weight ratio : this affects both the thickness of the casing and its velocity at the moment of break-up. That the velocity at the moment of break-up has a profound influence on the fragmentation is shown by two facts :

(a) That a 250 lb. bomb fragmented in water gives only about a quarter as many fragments as when exploded in air 6).

(b) The well known gross fragmentation of that part of an H.E.shell with direct acting fuze which is in contact with the ground at the moment of explosion; large pieces can be picked from the crater.

Apart from its influence on the velocity, a thin casing will of course give thinner fragments than a thick one. Whether it affects the other dimensions will be discussed below.

Values of M_A for two otherwise similar rocket heads with thicknesses 0.265" and 0.5" are (Reference 2))

Thickness	0.265"	0.5"
M_A	0.134	0.255 (ounce)$^{\frac{1}{2}}$

The velocity of expansion could be altered at will without affecting the size or thickness of the casing by putting a lead covering round the outside of the shell. Experiments to determine the effect of this on the fragmentation would be of great interest. The pressure distribution within the case would also be altered (cf. 11).

6. DIMENSIONS OF FRAGMENTS

The primary process in fragmentation must be splitting parallel to the axis of the shell, with subsequent rupture at the ends, and production of secondary fragments of type 5 in fig. 1. Assuming that cracking

---

6) Compilation of data on Trials on Explosive Effects of Aircraft Bombs, R.D. Woolwich, 1938.

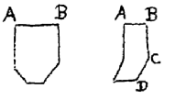

Fig. 3

(e.g. along BC in fig. 3) precedes shear rupture (e.g. along CD), the first task of any theory of fragmentation must be to account for the distance AB in fig. 3 between the edges of the average fragment. The observed distributions of the breadth AB are shown in figs. I and II at the end of this paper. It is of course true that the length AB often varies considerably along the length of a fragment, and a visual estimate of the mean breadth is subject to error; nevertheless the general shape of the curves is significant. We plot against fragment breadth not the total number of fragments, but the total length of all fragments (placed end to end) in each category.

The following points will be noted :

(a) The rather sharp cut-off for large breadths.

(b) The much narrower fragments obtained with the German 88 mm. shell (0.7% carbon steel) than with the British 3.7" shell or thick cased rocket head, (0.45% steel but similar diameter and casing thickness).

(c) The narrower fragments obtained with the thin cased (high capacity) rocket head than with the thick cased projectiles of similar steel.

The lengths of fragments from the German 88 mm. shell are shown in fig. III; the curve does not show the same cut-off at high values. In fig. IV we show the length distribution for fragments of different breadths; there is obviously a rough correlation, broad fragments being longer. The average length of fragments in different categories is given in Table IV.

TABLE IV
Lenghts in mm.

Breadth (mm.)	2 - 3	4	5	6	7	8	9	10
Thick-cased U.P. (carbon steel)		39	39	56	44	37	50	36
Thick-cased U.P. (mild steel)		34	35	33	36	47	58	54
Service U.P.			27	30	28	29		
German 88 mm.	5.5	10	14.8			21.7		

Evidence for correlation between breadth and length is not marked except for the German shell. For the British shells a ratio of length to breadth of the order 5 seems to be normal, for the German shell a somewhat smaller value.

7. WEIGHT DISTRIBUTION OF FRAGMENTS

The formula (3) was derived[1] by the author on the assumption of some sort of random break-up; figs. 1 to 3 show however that neither the break-up parallel or perpendicular to the axis can be considered random as would be the case if the breadths were distributed according to the law : number of fragments with breadths between a and a + da is proportional to $\exp(-a/a_0)da$. It therefore seems worth while to attempt a derivation of (3) from different assumptions.

Let us assume :

(a) that the casing is broken into strips and that the number of strips with breadths between x and x + dx is

$$C\, x \exp\left(-x/x_0\right) dx \qquad (4)$$

This does not represent the facts exactly, but gives a nearer approximation than the random fracture.

(b) that each strip is broken up according to the same law, and that the average length of fragment is proportional to the thickness x of the strip. Thus from a strip of length ℓ the number of fragments of length between y and y + dy is

$$y\, e^{-y/px}\, \ell\, dy/(px)^3 \qquad (5)$$

where p is a factor (of the order 5).

Then the number of fragments of area greater than a^2 is

$$\frac{C\ell}{p^3} \iint_{xy>a^2} \frac{y}{x^2} \left[\exp\left(-\frac{x}{x_0} - \frac{y}{px}\right)\right] dx\, dy$$

This reduces to

$$\text{const}\ \lambda \int_0^\infty \left(1+\tfrac{1}{z^2}\right) \exp\left(-\lambda z - \tfrac{1}{z^2}\right) dz, \qquad \lambda = a/x_0 p^{\frac{1}{2}}$$

and thus the number of fragments with area such that a(= $\sqrt{\text{area}}$) lies between a and a + ds is

$$\text{const}\ f(\lambda)\, d\lambda$$

where

$$f(\lambda) = \int_0^\infty \left\{\left(1+\tfrac{1}{z^2}\right) - \lambda\left(z+\tfrac{1}{z}\right)\right\} \exp\left(-\lambda z - \tfrac{1}{z^2}\right) dz \qquad (6)$$

This function is plotted logarithmically in fig. V over all values of λ from 0 to 10, i.e. over a range of $\log_{10} f$ equal to 3, which is about the range over which the fragment distribution is usually plotted. It will be seen that the deviation from a straight line is not very large.

Weight distributions of actual fragments are likely to deviate from this theoretical curve for the following reason : the narrower fragments frequently break as shown in fig. 4, thus having a smaller depth than they should. Moreover the removal of the triangular pieces from the base of the smaller fragments will obviously make a greater proportional difference to their weight. This will result in a shift of the whole upper part of the curve in fig. 5 somewhat to the left. On the other hand, on reaching the weight categories of the small triangular fragments, a large number of new fragments appear which are not included in the analysis given above. Thus the curve should appear as the dotted curve in fig. V, which is very similar to those observed.

Fig. 4

PART II

THEORY OF THE MEAN FRAGMENT SIZE

8. DEPENDENCE ON VELOCITY

We consider that the fragmentation will be determined by the properties of the casing at the moment of break-up, and will not depend, for instance, on the pressures to which the case has been subjected during the expansion. The factors that may be of importance are thus

(a) Properties of the steel at the moment of rupture - for example the true ultimate tensile strength rather than the yield point.

(b) The rate of increase of plastic strain; this is equal to V/r, where V is the velocity of the case and r its radius.

(c) The thickness of the casing.

(d) The pressure of the explosive at the moment of break-up; according to Taylor's calculations this is from 60 - 25 tons/sq. in. for casings that break up after a 25 to 50% expansion; this is much less than the initial pressure, which is of the order 1000 tons/sq. in.

The theory which we shall develop suggests that (c) and (d) are of minor importance in determining the breadths and lengths of fragments. As in the author's previous report, we take the point of view that it is the kinetic energy of the case which tears it to pieces; the fragmentation would be almost the same if the expanding explosive could be miraculously removed just before the case broke up, leaving it to fly into pieces under its own momentum.

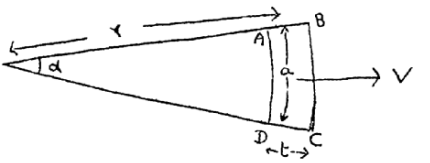

Fig. 5

In the author's previous report[1] the following derivation of the fragment breadth was given. Suppose that ABCD in fig. 5 is the cross section of a fragment which has just broken along BA, CD. The fragment is still in a state of plastic flow, the rate of increase of plastic strain being V/r. The kinetic energy of this flow of metal is

$$\tfrac{1}{2}\rho t V^2 \int_{-\frac{1}{2}\alpha}^{\frac{1}{2}\alpha} r\theta^2 \, d\theta = \tfrac{1}{24} V^2 t \rho a^3 / r^2$$

It was argued that if this were greater than the energy Wt required to rupture the metal, the fragment would split in half. Thus the value

$$a = \left[\frac{24 r^2 W}{\rho V^2} \right]^{1/3} \qquad (7)$$

would give an upper limit to the possible breadth of a fragment.

Agreement with observation, i.e. values of a of the order 1 cm., was obtained with values of W given by the notched bar impact test for a brittle steel, i.e. 40 ft/lbs. per sq. inch*. Since W occurs only as $W^{1/3}$, the values obtained are not very sensitive to W.

Equation (7) will certainly give a lower limit to the maximum fragment breadth, if W is the true fracture energy under the conditions existing in an H.E. shell. It is doubtful however if this bears any relation to the energy expended in the notched bar test, most of which is probably due to plastic deformation of the metal in the neighbourhood of the notch until the formation of a true crack of atomic width at its apex, leading to brittle rupture. The actual work necessary to separate two planes of atoms in a metal is of course much less, of the order 10^{-3} ft.lbs/sq.inch.

We shall therefore attempt a theory of fragmentation based on the assumption that the energy of fracture is negligible. In addition we shall make the following assumption : fracture can start at any one of a number of places on the surface or in the body of the casing, and once started will rapidly spread across it. During the initial stages of the expansion, it is very unlikely (or even impossible) that a crack will start anywhere; as the expansion increases the chance of a crack forming in any

---

* Measurements were made at the N.P.L. of the Izod value of test pieces cut from a 3.7" H.E. shell casing which had been extended 20% in the direction originally circumferential to the shell, to represent the state of the steel at the moment of rupture; values obtained for specimens with the usual 10 x 8 mm. section at the notch were, for the energy absorbed to fracture

5.0 5.9 5.0 ft. lbs.

This gives 43 ft.lbs/sq. inch. (Ref. Eng. Dept/OYY/RE/B.104 A, 5.3.43).

part of the case increases. We introduce a function f(s)ds dx, which gives the chance that a crack will form on a length dx of the circumference of the casing as the strain increases from s to s + ds. We may take f(s) to be zero up to a certain value of s (the rupture point), or we may assume a very rapid increase of f(s) in the neighbourhood of the rupture point. We shall find that the form of f(s) determines the mean fragment size.

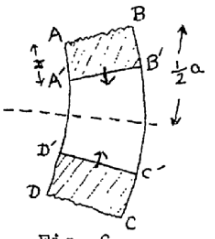

Fig. 6

As before we consider a fragment that has just broken along the lines AB,CD (fig.6), and ask whether it is likely to break again. As soon as a fracture has formed along AB, for instance, the metal in the neighbourhood of AB will stop flowing. A boundary A'B' between the part of the metal which is still in plastic flow and the metal which has stopped flowing will move downwards with a velocity that can be calculated. It will soon reach the boundary C'D' moving upwards from the lower crack; when this has happened, no further crack can form. For a fragment of average width, therefore, the chance of a new crack forming before A'B' and C'D' meet each other must be small. This chance can be calculated by comparing the function f(s), giving the rate of formation of cracks, with the time available before the surfaces join.

The velocity with which the surface A'B' moves can be determined as follows, if we assume that this is small compared with the velocity of sound in steel : Let a be the breadth of the fragment, x the breadth of the part that has stopped flowing, and T_0 the stress required to cause plastic flow. The velocity upwards of all material above A'B' is then

$$\frac{V}{\gamma}\left(\tfrac{1}{2}a - x\right)$$

Therefore the equation of motion of the block ABB'A' is

$$T_0 = -\rho x \frac{d}{dt}\left\{\left(\tfrac{1}{2}a - x\right)\frac{V}{\gamma}\right\}$$

which gives

$$T_0 = \frac{\rho V}{\gamma} x \frac{dx}{dt} \qquad (8)$$

Thus

$$\tfrac{1}{2}x^2/t = \gamma T_0/\rho V, \qquad (9)$$

and the time which the fragment takes to stop expanding is

$$a^2\rho V/8 T_0 \gamma,$$

which is of order 10^{-6} secs. if a ~ 7 mm. The increase in the strain s of the material during this time is of the order 10^{-2}.

From equation (9) we find

$$\dot{x} = T_0\gamma/\rho V x \sim 6 \times 10^4/x \quad \text{cm/sec}$$

so the velocity, except for very thin fragments, is considerably less than that of sound in steel (5×10^5 cm/sec.)

We have now to make some assumption about the function f(s). We could assume alternatively that

(a) f(s) is zero up to a definite value s_0 (the rupture point) and is then constant and equal to f_0, say.

(b) f(s) is zero up to s_0, and then increases, as $c(s - s_0)^n$ say.

(c) f(s) is never zero, but increases rapidly in the neighbourhood of the rupture point, as $Ae^{\gamma s}$ say.

The hypothesis (c) is the most attractive, for reasons that will be given in the next section; but they all lead to somewhat similar conclusions about the fragmentation.

An idea of the order of magnitude of the constants involved can be obtained from the behaviour of steel in tensile tests, if we make the assumption that the behaviour in static tests is similar to that at high rates of strain. In tensile tests, steels nearly always fracture after necking; the reduction of area thus gives a measure of the strain at which fracture occurs. Specimens prepared from one sample of carbon steel show a certain scatter in the measured values of the reduction of area; thus, if a steel fractures on the average for a reduction of area of 50%, individual specimens will show values between 49 and 51 approximately. The following, for instance, are values* for a normalised 0.4% carbon steel :

58 $\quad 56\frac{1}{2} \quad 59\frac{1}{2} \quad$ 59 per cent

Now according to our assumptions, the chance that a specimen of length ℓ will fracture before the strain reaches a value s is

$$1 - \exp\left[\ell \int_0^s f(s)\, ds\right] \tag{10}$$

In case (a) this gives

$$1 - \exp\left[-f_0 \ell\, (s - s_0)\right] \tag{11}$$

and, in case (c), to a sufficient approximation

$$1 - \exp\left[-\frac{\ell A}{\gamma} e^{\gamma s}\right] \tag{12}$$

Suppose that we assume that an increase in s by Δs increases the chance that fracture has taken place from 10 to 90%. Then we find from (11) and (12)

$$f_0 \ell = 2 \cdot 2/\Delta s \qquad \text{(case a)}$$

$$\gamma = 3 \cdot 1/\Delta s \qquad \text{(case c)}$$

In case (a) it is not clear what value of ℓ should be taken, since the maximum strain only occurs at the neck. In case (c), however, ℓ does not occur in the formula for γ; if, in accordance with the experimental values given above, we take $\Delta s = 0.02$, we obtain

$$\gamma = 155$$

A plot of the functions (11) and (12), showing the chance that a fracture has occurred when the strain (reduction in area) is s, is given in fig. VI for $\ell f_0 = 100$ and for $\gamma = 150$. The origin of s for curve (c) is arbitrary.

Experiments on the extent to which the reduction in area at the breaking point fluctuates from specimen to specimen, carried out for a sufficienrly large sample, would shed light on the nature of the function f(s).

With any of these forms of f(s), an estimate of the order of magnitude of the breadth a can be made as follows : At each crack, after a time t, a breadth

$$2\left(\frac{2T_0 r}{V\rho}\right)^{\frac{1}{2}} t^{\frac{1}{2}}$$

gas stopped expanding and is thus 'safe' from cracking. Since the strain increases as Vt/r, when the strain has increased by Δs after the formation of a given crack, a breadth round it equal to

$$\beta (\Delta s)^{\frac{1}{2}}, \qquad \beta = 2^{3/2} \left(\frac{T_0}{\rho}\right)^{\frac{1}{2}} \frac{r}{V}$$

---

* N.P.L. Report to A.R. Committee, Paper 4755

is "safe" also. If we neglect the overlapping of "safe" areas, a proportion

$$\beta \int_0^s f(s') \sqrt{s - s'}\, ds'$$

is safe when the strain is s. When this approaches unity, the break up is complete. Thus a, the average breadth, is given as regards its order of magnitude, by eliminating s between

$$\beta \int_0^s f(s') \sqrt{s - s'}\, ds' \simeq 1 \qquad (13)$$
$$\int_0^s f(s')\, ds' \simeq 1/a$$

With the forms for f(s) suggested above we obtain the following :

(a) Equations (13) lead to

$$a = \left(\frac{2}{3}\right)^{2/3} f_0^{-1/3}\, 2 \sqrt{\frac{T_0}{\rho}} \left(\frac{r}{V}\right)^{2/3}$$

This gives the same power of (r/V) as the author's previous theory, and with $f_0 = 100$ cm^{-1}, values of a of the order 0.5 cm.

(b) Equations (13) give

$$a = (n+1) \left[\frac{\Gamma(n+1)\,\Gamma\left(\frac{3}{2}\right)}{\Gamma\left(n+\frac{5}{2}\right)}\right]^{1-\frac{1}{2n+3}} C^{\frac{n+1}{2n+3}}\, \beta^{1-\frac{1}{2n+3}}$$

It will be seen that the fragment size is proportional to $(r/V)^{1-\frac{1}{2n+3}}$ and thus to some power of r/V between 1 and 2/3.

(c) With $f(s) = A e^{\gamma s}$, the equations (13) give us

$$A\beta e^{\gamma s} \int_0^\infty e^{-\gamma s'} s'^{\frac{1}{2}}\, ds' = 1$$
$$A e^{\gamma s} \int_0^\infty e^{-\gamma s'}\, ds' = 1/a$$

and hence

$$a = \sqrt{\frac{2\pi T_0}{\rho}}\, \frac{1}{V}\, \frac{1}{\gamma^{\frac{1}{2}}}$$

With $\gamma = 100$, $T_0 = 60$ tons/sq. inch, this gives 0.7 cm. for a normal shell of the calibres considered here.

It will be seen that a is now proportional to r/V.

Our formulae suggest, then, that the mean width of fragment will be proportional to

$$\text{const.}\ (r/V)^s,$$

where s lies between 2/3 and 1; the constant will depend on the nature of the steel; it may depend on the thickness of the case and pressure of the explosive, but consideration of the next section suggests that it will not.

We have not been able to find an analytical expression for the number of fragments with breadths between a and a + da, but our equations for the break-up enable a distribution to be found graphically. We limit ourselves to the form (c) for f(s). The theory is at present one-dimensional; we are considering the division of a line (a circumference of the shell) by random fracture. Let ℓ be the length of this line; then as before when each crack is formed, a space on each side of it equal to

$$\left(\frac{2T_0}{\rho}\right)^{\frac{1}{2}} \frac{\gamma}{V} (\Delta s)^{\frac{1}{2}}$$

is safe from further cracking when s has increased by Δs. If N is the number of cracks already formed, then the rate of increase of N is given by

$$\frac{dN}{ds} = A p \ell e^{\gamma s}$$

where p is the proportion of the line where cracks can still form. The first crack will form, on the average, when

$$A \ell e^{\gamma s}/\gamma = 1$$

If the value of s given by this equation be denoted by s_0, and a new variable σ defined by

$$\sigma = \gamma(s - s_0),$$

then the rate of increase in the number of cracks is given by the equation

$$\frac{dN}{d\sigma} = p e^{\sigma}$$

Also, if a crack is formed when $\sigma = \sigma_1$, the region round it where subsequent cracking is impossible is at any subsequent instant

$$2 x_0 (\sigma - \sigma_1)^{1/2} \qquad (14)$$

where

$$x_0 = \left(\frac{2T_0}{\rho\gamma}\right)^{\frac{1}{2}} \frac{\gamma}{V}$$

A line drawn on paper can now be cut at random, using playing cards or dice. Initially σ is supposed to be zero; after each successive cut is made σ is supposed to increase by $d\sigma$ where

$$d\sigma = 1/p e^{\sigma}$$

After each new cut is made, the "safe" region round all cuts made earlier must be increased according to formula (14). Any arbitrary value of the ratio ℓ/x_0 may be taken. We took $\ell/x_0 = 20$. The line is repeatedly cut until the whole region is "safe" from further cracking. The lengths of all intervals are then measured and recorded, and the process repeated a number of times until enough data are obtained to draw a histogram, in which the numbers of "fragments" (i.e. intervals) are plotted against their lengths. The results are shown in fig. II(c). The similarity to the distributions of fragment breadths observed in figs. I and II (a) and (b) is satisfactory.

By comparing fig. V with the observed fragment distributions and especially the values of their upper limits, we have estimated in Table V the value of x_0 for the projectiles investigated. The values are not correct to more than ± 10%.

From these values we have attempted to deduce γ. For this we require the radius of the shell at the moment of break-up (r), the velocity of the casing and the true ultimate tensile strength, T_0. The two former quantities are deduced from the values given in Part I. To deduce T_0 from a tensile test we require the stress at the moment of rupture at the base of the neck, which is of course considerably greater that the U.T.S. given in engineering tables. For steels the following values are given by Korber and Rohland, (Mitt. d. K. Wilhelm Inst. f. Eisenforschung, 5 (1924) 55).

Carbon (%)	Reduction in area (%)	True ultimate stress kg/mm²	tons/sq.inch
0.13	70	78	51
0.25	63	80	52
0.45	57	82	53
0.55	50	87	57

These will probably be somewhat higher for high rates of strain*; we have thus assumed

T_0 = 80 tons/sq. inch
= 100 " "

for British (0.45% carbon) and German (0.7% carbon) shell steels respectively.

---

* cf. G. I. Taylor, Stress Strain Relationship on Impact. Civil Defence Research Committee. R.C. 36.

TABLE V

Values of γ deduced from observed distributions of fragment breadths

	88 mm shell	3.7" shell	Rocket head* (thick case)	Rocket head (thin case)
x_0 (cm) observed	0.37	0.56	0.44	0.31
2r (cm)	11.4	12.2	12.8	12.8
V (cm/sec)	64,000	63,000	76,000	110,000
$\gamma = \frac{2T_0}{\rho}\left(\frac{r}{Vx_0}\right)^2$	230	105	125	124

For the values of γ we cannot claim an accuracy greater than $\pm$ 30%; within these limits the British shells (0.45% carbon) show the same value, which is of the order expected. The German shell shows a higher value, which we assume to be due to the higher carbon content of the steel.

9. DEPENDENCE ON THICKNESS AND PRESSURE

We have seen that the hypothesis

$$f(s) = A e^{\gamma s} \qquad \gamma \sim 100$$

fits the facts well both for the fragmentation of shells and for the consistency of the rupture point, and seems a priori more likely than the other hypotheses. We have now to consider the following points :

(a) Is γ likely to depend on the thickness of the casing, or the pressure of the gases at the moment of rupture?

(b) Why is γ larger for steels with high carbon content?

(c) Can we deduce a factor γ of this order from any known property of the metal?

It has not at present been possible to answer point (b); to the others an answer can be given :

Let us make the following assumptions about fracture in ductile metals :

(i) Cracks can start at a limited number of points or regions in the metal of which we assume that there are n per unit volume.

(ii) Cracks will start at these points, on the average, when the strain has increased to a value S_1

(iii) The strains at which cracks will form at the individual points of weakness show a certain scatter about the value S_1 ; it is natural to represent this scatter by a Gaussian distribution. We thus assume that the number of points per cm^3 at which a crack will form as the strain increases from s to s + ds is

$$\frac{n}{S_2\sqrt{2\pi}} \exp\left[-\frac{(s-S_1)^2}{S_2^2}\right] ds .$$

For a tensile specimen of cross sectional area A, this gives us for our function f(s)

$$f(s) = \frac{nA}{S_2\sqrt{2\pi}} \exp\left[-\frac{(s-S_1)^2}{S_2^2}\right] \quad cm^{-1} \qquad (15)$$

* The values of x_0 for 0.15 and 0.45% carbon are about the same.

We are interested only in the tail end of this curve where f(s) first becomes appreciable; let us then define the rupture point s_o as the strain for which one crack per cm. is expected, so that

$$\int_0^{s_o} f(s)\, ds = 1, \tag{16}$$

and write

$$s = s_o + s'$$

Then we obtain from (15)

$$f(s) \simeq \frac{n A}{s_2 \sqrt{2\pi}} \exp\left[-\left(\frac{s_1 - s_o}{s_2}\right)^2\right] e^{\gamma s'}$$

with

$$\gamma = 2(s_1 - s_o)/s_2^2 \tag{17}$$

Also from (16)

$$\frac{n A s_2}{2\sqrt{2\pi}(s_1 - s_o)} \exp\left[-\left(\frac{s_1 - s_o}{s_2}\right)^2\right] = 1,$$

whence

$$\left(\frac{s_1 - s_o}{s_2}\right)^2 = \log_e \left[\frac{n A s_2}{2\sqrt{2\pi}(s_1 - s_o)}\right] \tag{18}$$

Hence from (17) we obtain finally

$$\gamma = 2 \log_e \left[\frac{n A s_2}{2\sqrt{2\pi}(s_1 - s_o)}\right] \Big/ (s_1 - s_o) \tag{19}$$

Since n comes within the logarithm, its exact value is not important. For a number of reasons we expect the distance between the points where rupture can start to be of the order 10^{-4} to 10^{-5} cm. This is for instance the distance between the slip bands* in a metal, the "dislocations" in G.I. Taylor's theory of slip**, or the "crystallites" whose existence has been suggested in cold worked metals***. We thus take n of the order 10^{15}; the other terms within the square bracket are negligible in comparison and we obtain

$$\gamma = 2 \log_e 10^{15} / (s_1 - s_o) = 69/(s_1 - s_o) \tag{20}$$

From formulae (19), (20) we deduce :

(a) That γ is practically independent of the cross section of the specimen, and thus of the thickness of the shell casing.

(b) That γ is practically independent of the pressure of the explosive at the moment of rupture, because (cf. § 12) the pressure must vanish at the outside surface, and if the formation of cracks were confined to a small layer near the surface only, it would not affect γ appreciably.

(c) The properties of the steel affect the value of γ only through the value of $s_2 - s_o$, and if s_1 is of the order unity, as is not unlikely, values of γ in agreement with observation are obtained.

---

* cf. for example, Orowan, Nature, 147, 452 (1941) or the beautiful photographs of worked steel obtained with the electron microscope by Heidenreich and Peck, J. Applied Physics, 14, 24 (1943).

** Proc. Roy. Soc. A. 145, 362 (1934).

*** Smith and Wood. Proc. Roy. Soc. A. 178, 93 (1941).

10. LENGTHS OF FRAGMENTS

Up till this section we have discussed only the breadths of fragments, believing that splitting parallel to the axis is the primary process in fragmentation. We have now to discuss the factor determining their lengths.

Observation on fragments of marks cut on the surface of the case shows that shell casings do not stretch parallel to their axis; we must therefore look for an explanation of rupture at the ends of the fragments different from that given for the longitudinal cracks.

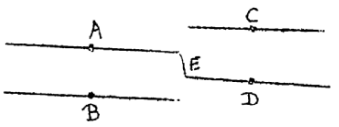

FIG. 7

If cracks start at A and B and spread to the right, and from C and D and spread to the left, then as Professor Andrew* has pointed out, when the cracks bounding two fragments meet, there will be a tendency to split, as at E. According however to the hypothesis on which this paper is based, a split like this is only likely to take place if the steel between the cracks A and B has already stopped flowing before the crack D reaches it; otherwise the crack D will be unaware of the presence of the cracks A and B and will penetrate between them. If however plastic flow has stopped, the different directions in which the two fragments are moving will, we consider, lead to their separation.

Let u be the velocity with which each crack extends. As soon as a crack has formed, the region spreads in which flow has stopped, so that after a time t its width a is given by

$$a = 2\left(\frac{2\gamma T_0}{\rho V}\right)^{\frac{1}{2}} t^{\frac{1}{2}}$$

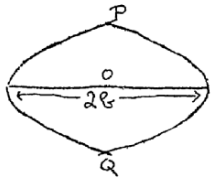

Fig. 8

Thus a crack starting at O in fig. 8 and which has spread to a length 2b is surrounded by a region bounded by two parabolas, in which plastic flow has stopped; the breadth PQ of this region is

$$2\left[\frac{2\gamma T_0 b}{\rho V u}\right]^{\frac{1}{2}}$$

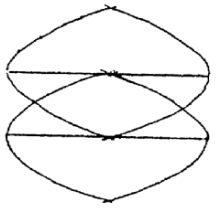

Fig. 9

As a rough criterion for the condition that the region between two cracks should be no longer in flow, we write a, the width of the crack, equal to half this;

$$a = \left[\frac{2\gamma T_0 b}{\rho V u}\right]^{\frac{1}{2}}$$

Thus the ratio, length to breadth, is equal to

$$\frac{2b}{a} = \frac{\rho V u a}{\gamma T_0} \qquad (21)$$

According to equation (14), a for the average fragment is proportional to r/V; we obtain

$$\frac{2b}{a} = 2\sqrt{\frac{\pi\rho}{2T_0}}\ \frac{u}{\gamma^{\frac{1}{2}}} \qquad (22)$$

With T_0 = 60 tons/sq. inch = 9 x 10^9 c.g.s. units, ρ = 8, γ = 100, this gives

$$2b/a = 0.7 \times 10^{-5}\, u$$

---

* Report R.C. 342 from the Dept. of Metallurgy of the University of Sheffield (31.8.42).

If we equate u to the velocity of sound in steel, 5×10^5 cm/sec., we obtain

$$2b/a \simeq 3.5$$

in fair agreement with experiment. The hypothesis that cracks spread with the speed of sound is not unlikely to be correct, if the atomic cohesion only has to be overcome, and no plastic deformation is involved.

Formula (18) suggests that the length/breadth ratio of the average fragment is independent of the calibre or capacity of the projectile, but will be less for the German high carbon steel (large γ) than for the British steel. These conclusions seem to be born out by the figures of Table IV.

11. SHAPE OF CROSS SECTION OF FRAGMENTS

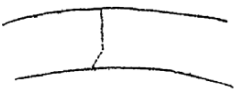

Fig. 10

We have already remarked on the types of rupture observed, and pointed out that the type of rupture shown in fig. 10 is usual, with a brittle crack on the outside of the casing and shear rupture at 45° on the inside. In this section we attempt an explanation of this double type of rupture. For this purpose we calculate the stresses in the case during plastic expansion.

According to G.I. Taylor's calculations, the pressure at various stages in the expansion of a long cylindrical cased charge are given by the following figures, where r is the radius of the inner surface of the case and r_0 its initial value :

TABLE VI

r/ro	1.0	1.05	1.1	1.3	1.54	2.4
pressure dynes/ $cm^2 \times 10^{-9}$	150	49	25	8.4	4.0	2.0
pressure tons/ sq. in.	1000	320	160	55	26	13

At the moment of break-up, therefore, the pressure is of the same order as the yield stress, and both will be of comparable importance in determining the stresses in the material for thick casings.

In a cylindrical tube subject to an internal pressure just great enough to cause flow, the stresses have been worked out*. The radial and tangential stresses are, at distance r from the axis

$$S_r = -T_0 \log \frac{b}{r}$$

$$S_t = T_0 \left(1 - \log \frac{b}{r}\right)$$

where b, a are the external and internal radii; the pressure necessary to cause flow is

$$T_0 \log \frac{b}{a}$$

Here $T_0 = 2 S_0/\sqrt{3}$ where S_0 is the shearing stress. If p is the actual pressure of the gases, we have an additional pressure at the surface

$$p - T_0 \log \frac{b}{a}$$

giving a hydrostatic pressure at a distance r from the axis equal to

$$\left(p - T_0 \log \frac{b}{a}\right) \frac{a}{b-a} \left(\frac{b}{r} - 1\right)$$

* Nadai, Plasticity, McGraw Hill Book Co., p.188.

The stresses can thus be resolved into

(1) A tangential stress T_o
(2) A hydrostatic pressure equal to

$$\left(p - T_o \log \frac{\rho}{a}\right) \frac{a(\rho - r)}{(\rho - a)r} + T_o \log \frac{\rho}{r} ,$$

which vanishes at the outside surface and reaches the value p at the inner surface.

Now it is known that hydrostatic pressure makes fracture more difficult, while having little effect on the resistance to glide. For non-plastic materials, where fracture starts from a microscopic crack, the following account of the effect of hydrostatic pressure has been given by A.A.Griffiths in a well-known paper*. Suppose elliptical cracks are acted on by a stress T and a hydrostatic pressure P; the angle made by the plane of any crack to the normal to T is denoted by θ, and θ is distributed over all values. Then T will be great enough to cause cracks to spread under the following conditions :

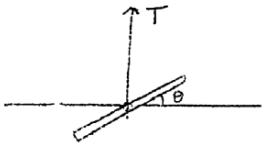

Fig. 11

(a) $4p < 3T$ If this condition is fulfilled, cracks for which $\theta = 0$ will be the first to spread, where T reaches a value $K + p$, where K depends on the elastic constants and surface tension of the metal, and the dimensions of the crack.

(b) $4p > 3T$ Under these conditions cracks for which $\theta = 0$ will not be the first to spread, but those for which

$$\cos 2\theta = \frac{1}{2} \frac{T}{2p - T}$$

At the critical pressure given by $4p = 3T$, this gives $\theta = 45^o$.

In plastic materials it is probable that the high tensile stress T near the apex of a crack will cause cracks to form in crystal grains near to it. As the apex of the crack travels inwards, if a point is reached where $4p$ exceeds $3T$, the crack should abruptly change its direction by 45^o. This is just what is observed.

Since T is certainly greater than T_o, a necessary condition for such a change of direction will be $\frac{4}{3}p > T_o$

where p is the pressure exerted by the explosive. For casings that break up at 30 and 50% expansions respectively, the calculated values of $4p/3$ are 73 and 35 tons per sq. inch, which are of the same order as T_o, though they are somewhat less than the values that we have assumed to hold for the metal at high rates of strain.

For this reason we put forward the above explanation somewhat tentatively.

12. COMPARISON WITH OBSERVED FRAGMENTATION OF SERVICE PROJECTILES.

In this memorandum we have reached the following conclusions :

For a given type of steel

(a) The ratio of length to breadth of fragments is constant.

(b) The average fragment area is proportional to $(r/V)^{2s}$, where s lies between 2/3 and 1, probably nearer the latter value.

(c) The weight distribution is given approximately by formula (3)

* Proc. Int. Congress for Applied Mechanics. Delft (1924), p.55.

We may thus equate M_A of formula (3) to

$$\text{const } t^{\frac{1}{2}} \left(\frac{r}{V}\right)^s$$

where the value of the constant depends on the properties of the steel, or, making use of formula (1) for the velocity

$$M_A = \text{const } t^{5/6} d_2^{\frac{1}{3}} \left(1 + \frac{t}{d_2}\right) \qquad s = \frac{2}{3}$$

$$M_A = \text{const } t\, d_2^{\frac{1}{2}} \left(1 + \frac{t}{d_2}\right) \qquad s = 1$$

where the constant depends on the type of explosive and steel, d_2 is the internal diameter and t the thickness of the casing. The first of these formulae has already been compared with experiment in 2), in which M_A was determined for a number of service weapons.

Comparison with fragmentation of observed projectiles should show whether s = 1 or s = 2/3 or some intermediate value gives the best fit. Ursell* has determined the best value of M_A for three model bombs fragmented by Payman **, with thicknesses 0.018, 0.125 and 0.3 inches (diameter 2"). He comes to the conclusion that M_A is proportional to $1/V^{1.2}$. The casings of these bombs were of mild steel and gave shear fracture, and so are not directly comparable with our theory. Unfortunately the range of values of r and V available in British shells of carbon steel for which detailed information is available is not great enough to allow any certain conclusion to be drawn.

Observed values of M_A for a number of projectiles filled with TNT are shown in Table VII; we have limited ourselves to those with a reasonably cylindrical cross section. It looks as though s = 1 gave rather a better fit than s = 2/3.

---

* A.W.A.S, Report No. 46; Ministry of Supply No. A.C.3817

** loc. cit.,

TABLE VII

Projectile	d_1 inches	t inches	$M_A(oz)^{\frac{1}{3}}$ observed	$\frac{M_A}{t^{5/6} d_2^{\frac{1}{3}}\left(1+\frac{t}{d_2}\right)}$	$\frac{M_A}{t d_2^{\frac{1}{2}}\left(1+\frac{t}{d_2}\right)}$
3" U.P.	3.25	0.265	0.134	0.265	0.27
95 mm.shell	3.7	0.425	0.23	0.29	0.26
U.P.(thick cased)	3. 5	0.50	0.30	0.32	0.29
3.7" shell	3.7	0.60	0.36	0.32	$0.275 \pm .015$
25 pr. shell	3.43	0.65	0.35 ± 0.03	$0.29 \pm .025$	$0.245 \pm .02$

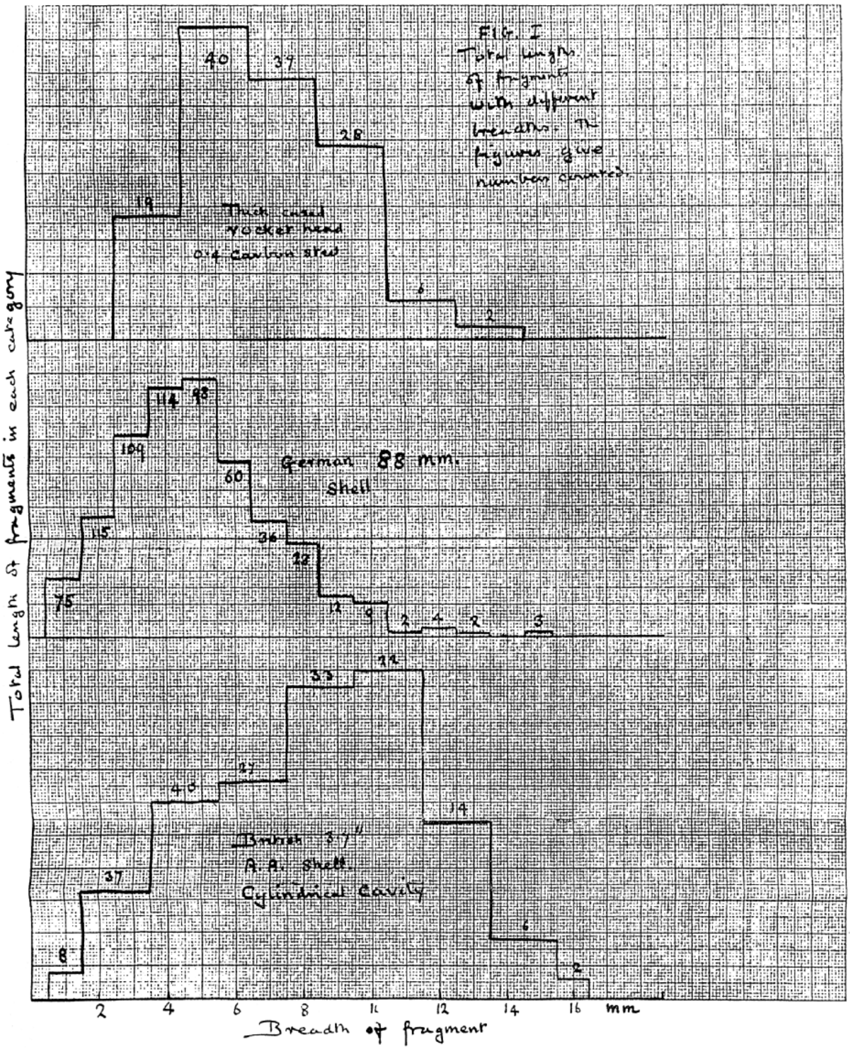
FIG. I
Total lengths of fragments with different breadths. The figures give number counted.
Thick cased rocket head
0·4 Carbon steel
German 88 mm. Shell
British 3.7" A.A. Shell. Cylindrical Cavity
Total length of fragments in each category
Breadth of fragment
2
4
6
8
11
12
14
16
mm
40
37
28
19
6
2
114
98
109
60
115
36
22
75
12
9
2
4
2
3
33
42
46
27
37
14
8
6
2

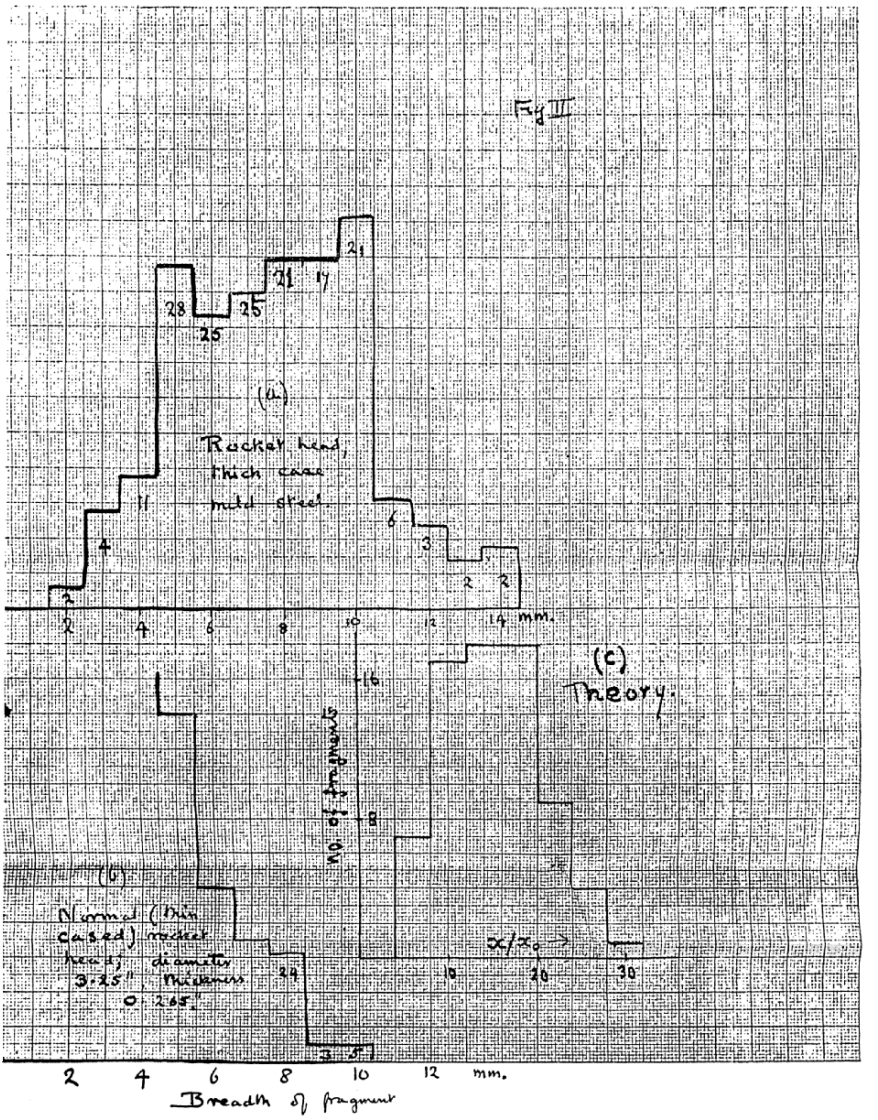
Fig III
(a)
Rocker head, thick case mild steel.
28
25
25
21
17
24
11
4
2
6
3
2
2
2
4
6
8
10
12
14
mm.
(c)
Theory.
No. of fragments
16
8
(b)
Normal (thin cased) rocker head 3·25" diameter thickness 0·265"
29
3
5
10
20
30
x/x₀
2
4
6
8
10
12
mm.
Breadth of fragment

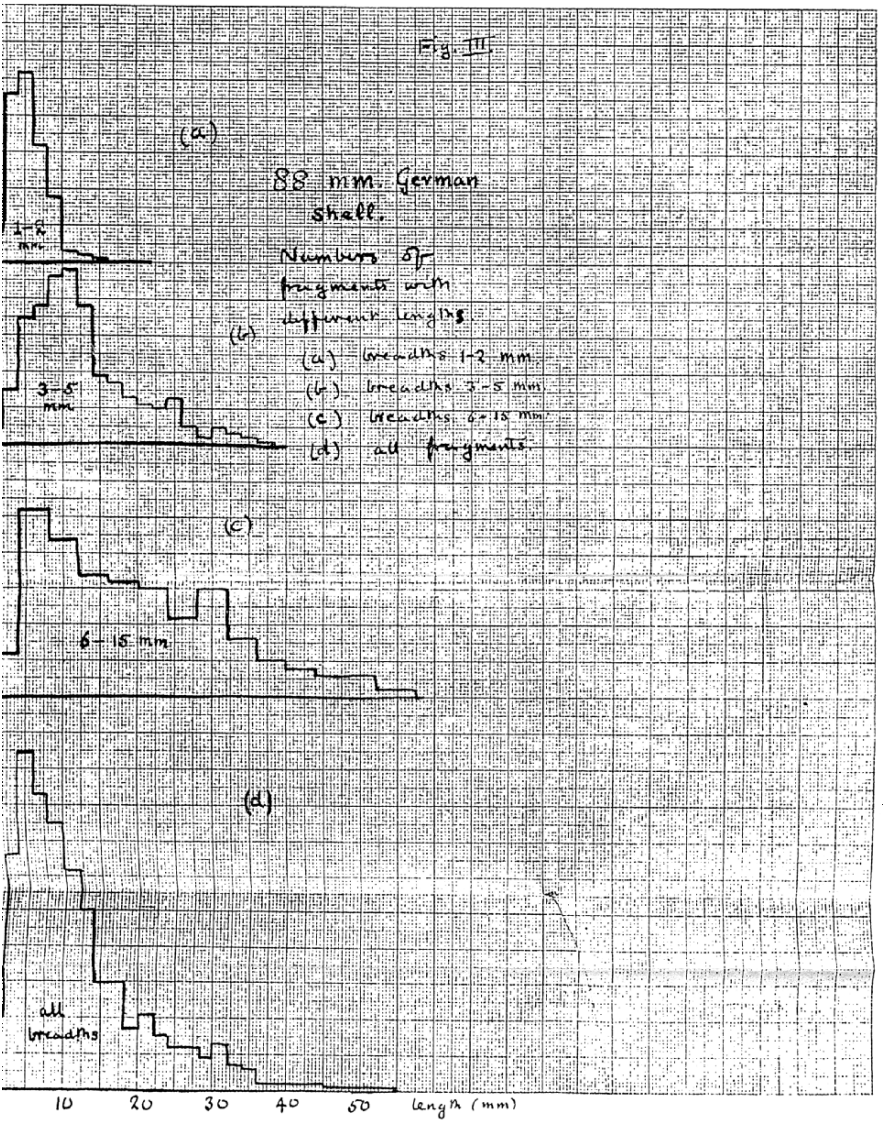
Fig. III
(a)
88 mm. German shell.
Number of fragments with different lengths
(a) breadths 1-2 mm.
(b) breadths 3-5 mm.
(c) breadths 6-15 mm.
(d) all fragments.
1-2 mm
(b)
3-5 mm
(c)
6-15 mm
(d)
all breadths
10
20
30
40
50
length (mm)

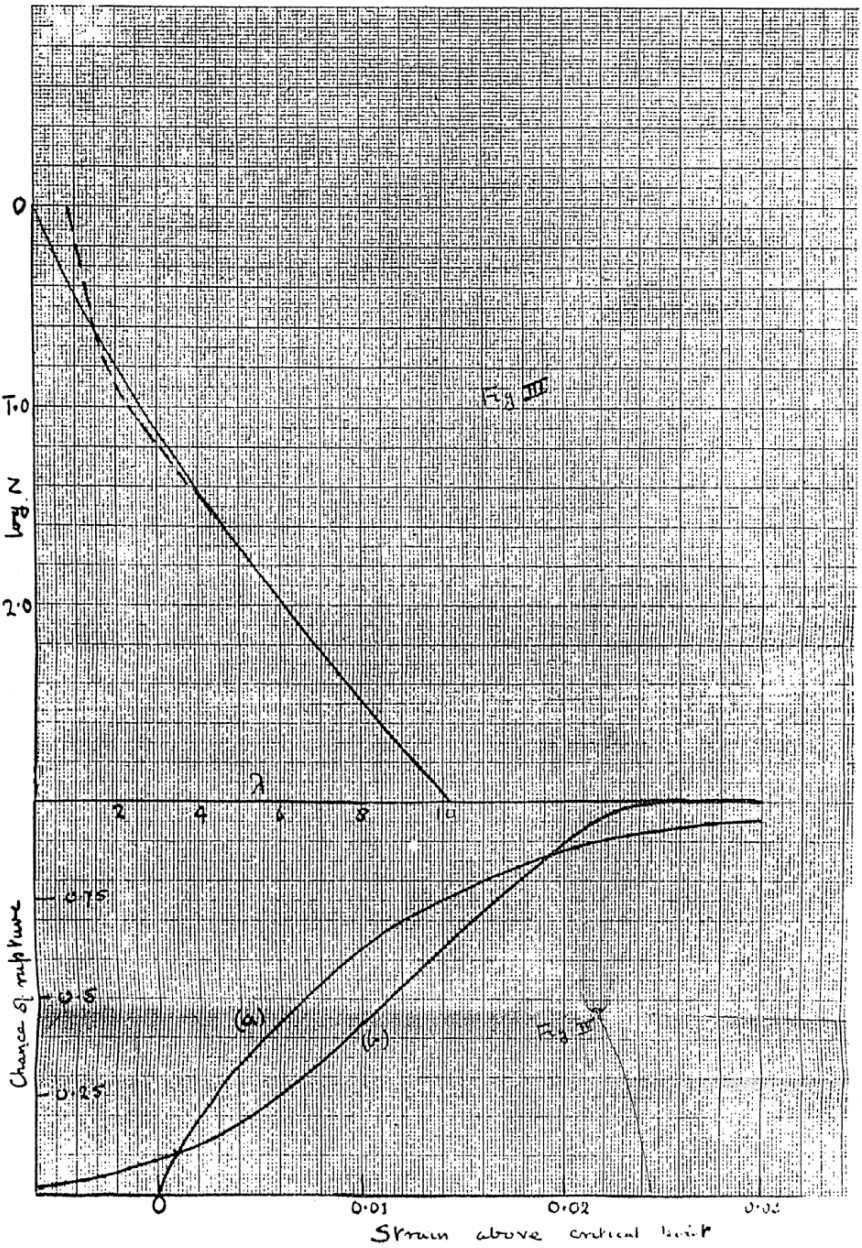
0
1·0
log N
2·0
λ
2
4
6
8
10
Fig III
Chance of multiple
0·75
0·5
0·25
(a)
(b)
Fig IV
0
0·01
0·02
0·03
Strain above critical limit

4

Fragmentation of Shell Casings and the Theory of Rupture in Metals

N.F. Mott

(August, 1943), Ministry of Supply, A.C.4613

Summary. In para. 2 the Griffith theory of rupture in brittle materials is reviewed; in paras. 3 and 4 the information available about the stress strain curves of metals at high rates of strain is reviewed, and it is suggested that the increase in the yield point of steel of a given composition is independent of the degree of cold work. A correlation is also suggested between the variations of yield point with temperature and with rate of strain. In para. 5 the evidence is discussed for the hypothesis that metals in a given state of plastic strain will fracture when the maximum principal stress reaches a given value. It is shown that the fracture stress of steel is either independent of strain or increases slowly with it. The fracture stress appears to increase with rate of strain, by about the same amount as the yield point. In para. 6 it is pointed out that two well-defined types of rupture occur, brittle and shear; the condition for the occurrence of either is discussed. Para. 7 applies the conclusions reached to certain phenomena observed in the rupture of bomb and shell casings. Para. 8 discusses the evidence that the rupture stress increases with rate of strain. Para. 9 discusses the scatter observed in the values of the reduction in area obtained in tensile tests; this scatter was assumed in a previous report on fragmentation to be responsible for the average size of fragments. It is shown that a numerical estimate of the order of magnitude of this scatter, and of its dependence on the properties of the steel, can be made using very general assumptions about the mechanism of rupture. It appears probable that the magnitudes of the scatter will be the same for shear rupture as for brittle rupture.

FRAGMENTATION AND RUPTURE OF METALS

4.1 Purpose of Report

In a recent report[1] the present author has given a theory of fragmentation which attempts to account for the size of fragments from a bomb or shell of given dimensions and filling. The purpose of the present report is:

[1] A Theory of the fragmentation of shells and bombs. M. of S. Extra-Mural Report A.C.4035.

(a) To extend the theory and in particular to attempt to account for the differences in fragmentation shown by high and low carbon steels.
(b) To review the information available about fracture of ductile metals; it is probable that the study of fragmentation can throw considerable light on the processes involved, which may be useful in other fields, such as that of armour piercing projectiles.

4.2 Fracture of Non-Ductile Materials; the Theory of A.A. Griffith

While no molecular theory exists to account for fracture in ductible materials, for non-ductile materials such as glass the accepted theory is that due to Griffith[2]. Griffith explains the discrepancy of 100 to 1000 between the observed and the theoretical tensile strength of materials such as glass or rocksalt by postulating the existence of surface cracks, which weaken the specimen; considerable experimental evidence exists in support of this hypothesis. Griffith has given a quantitative theory of the weakening effect of certain types of crack, based on Inglis' solution of the equations determining the stresses round an elliptical cavity. He gives a condition that a crack of width $2c$ and length, perpendicular to the plane of the paper, large compared with c should spread when subjected to a stress P. This condition is

$$P = \sqrt{\frac{2E\sigma}{\pi c}} \tag{4.1}$$

where E is Young's modulus and σ the surface tension. The formula is obtained by treating the cross-section of the crack as an ellipse of zero eccentricity, and assuming that Hooke's law is valid up to the apex of the crack. A formula differing from (4.1) by a factor 0.8 has been derived by Orowan[3] on rather similar assumptions.

Griffith has also considered the behaviour of cracks under biaxial stresses. A material is supposed to be subject to stresses P, Q as shown, and P is greater than Q. It is also supposed to contain cracks oriented at all angles θ to the normal to P. As P is increased certain of the cracks will begin to spread and the material will fracture. The question at issue is, which crack will begin to spread first, and how does the critical value of P depend on Q?

According to Griffith, two cases may be distinguished:

(a) $3P + Q > 0$. In this case cracks for which $\theta = 0$ spread first and the critical value K of P, given by (4.1) above, is independent of Q.
(b) $3P + Q < 0$. In this case rupture takes place when

[2] A.A. Griffith. Trans. Roy. Soc. 221, 180 (1920).
II. Int. Congress Applied Mechanics, Delft, p. 55 (1924).
[3] E. Orowan. Zs. f. Kristallographie, 89, 327 (1934).

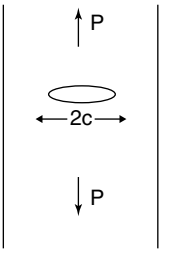

Fig. 4.1.

$$(P-Q)^2 + 8K(P+Q) = 0 \tag{4.2}$$

at an angle θ given by

$$\cos 2\theta = -\frac{1}{2}\frac{P-Q}{P+Q}$$

Two interesting cases arise:

(i) Compressive stress, $P = 0, Q = -T$. Then $Q = 8\,K$, so rupture takes place at 8 times the stress necessary under tension, and at an angle θ equal to 30°.

(ii) Hydrostatic pressure. Owing to the two dimensional nature of the Griffith theory, we shall have to make the assumption that stresses perpendicular to the plane of the paper in Fig. 4.2 do not affect the stress for rupture. With this assumption, if the specimen is subjected to a hydrostatic pressure p, we may write $p = -Q$. If $p < 3P$, rupture is determined by the maximum principal stress, at a value independent of p.

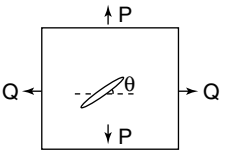

Fig. 4.2.

If a specimen is initially under tensile stress T, for example from a spring, and both spring and specimen are immersed in a hydrostatic pressure p, the maximum tensile stress is $T - p$. In a recent paper[4] Bridgman has called $P(= T - p)$ the net stress and T the true stress, which is perhaps unfortunate since P is actually the stress in the material.

[4] P.W. Bridgman. ORSD Report 1347, "Plastic Deformation of Steel under High Pressure".

Since the tensile strength of a material such as glass is determined by the size of the largest of a comparatively small number of random surface cracks, we should expect a large fluctuation in the strength of specimens prepared in the same way. Some values of the fluctuation have been given by Holland and Turner of the Dept. of Glass Technology, University of Sheffield[5]. The bending stresses of flat drawn sheets of thickness 0.27 cm with sides mechanically ground and polished showed, when 25 specimens were tested, coefficients of variation of from 8 to 18%.

4.3 Plastic Flow and Strain Hardening in Metals

In this report we shall deal always with the true stress, which we shall denote by P, and not the engineering stress, which is the product of P and the reduction of area of the specimen, at the base of the neck if necking has commenced. It is obvious that P, not the engineering stress, determines fracture phenomena in the metal.

The following relation between strain s and true stress P has been given by Bridgman (loc. cit.,) and by Hollomon[6]

$$P = P_1 + P_2 \quad \log_e \frac{A_o}{A} \tag{4.3}$$

where A_1, A_o, are the area and initial area of the specimen, so that

$$s = (A_o - A)/A$$

Bridgman's investigations were carried out under high hydrostatic pressure which is almost without effect on the stress-strain curve but enables the strain to be carried to much higher values without rupture. Hollomon investigates two steels with different carbon and nickel contents. For a given steel he finds a wide variety of values of P_1 depending on the heat treatment, but a fairly constant value of P_2, as follows:

Composition of steel		P_2
C	Ni	(1000 p.s.i)
0.44	0	73
0.19	1.83	73
0.20	0	55

The formula is not satisfactory near the yield point of the unworked metal

[5] A. J. Holland and W.E.S. Turner. Effect of Width on the Breaking Stress of Sheet Glass. Proc. Soc. Glass Technology, (1956), vol. 20, p. 72.

[6] U.S.A. Ordnance Dept. Report No. 630/7. "Tensile Properties of Steel". Oct. 17 (1942).

4.4 Yield at High Rates of Strain

For a discussion of fragmentation we require information about the yield point, at high rates of strain, of steels at the rupture point. Little evidence exists about this, most investigations being confined to the beginning of the stress-strain curve. We therefore attempt a theoretical estimate of the increase in yield stress to be expected.

At rates of strain of the order $500\,\mathrm{sec}^{-1}$ the tensile yield strength of low tensile steels is about doubled[7]; for instance, that of a medium carbon steel increased from 18 to 28 tons and a mild steel by about the same amount. On the other hand the tensile strength of hard steels is scarcely affected. In compressive tests at high striking velocities the actual rate of yield is not known, but must be much higher. It is found[8] that a variety of steels with yield points between 18 and 72 tons/sq. inch showed approximately the same increase of yield point, about 35 tons/sq. inch. Between 1,600 and 2,500 ft/sec. the striking velocity has no effect on the yield point[9].

According to a theory put forward by Becker[10], it is not unexpected that the absolute values of the yield points of steels should increase by the same amount. According to Becker, the "dislocations" responsible for plastic flow will move under a stress P with velocity

$$v = C \exp\left[-\frac{(P_o - P)^2 V}{2GkT}\right] \tag{4.4}$$

Here P_o is the stress required to move them at the absolute zero of temperature, T the absolute temperature, G the shear modulus and V a volume determined by the thickness of the disloction zone. If λ is the distance between dislocations and a the interatomic distance, then the rate of shear is av/λ^2. C/a should be of the order of the period of atomic vibrations, namely 10^{-12} sec^{-1}; thus for the rate of shear we obtain

$$\frac{ds}{dt} = \left(\frac{a}{\lambda}\right)^2 \times 10^{12} \exp\left[-\frac{(P_o - P)^2\ V}{2GkT}\right] .$$

Expressing P in terms of ds/dt we find

$$P = P_o - \sqrt{\frac{2GkT}{V}}\left[2\log_e\left(\frac{a}{\lambda}10^6\right) - \log\left(\frac{ds}{dt}\right)\right]^{1/2} . \tag{4.5}$$

[7] The determination of static and dynamic yield stresses by a ball method, by R.M. Davies, M. of S. Extra-Mural Report A.C.1228. Brown and Vincent, Proc. Inst. Mech. Engineers, vol. 145, p. 126 (1941).

[8] D.S.I.R. Road Research Lab. Report MOS/172/ACW. Nov. (1942).

[9] Road Research Labortory Report, MOS/33/ACW. Nov. 1941.

[10] R. Becker. Zs. f. Physik, 26, 919 (1925); E. Orowan, Proc. Phys. Soc. 52, 19 (1940).

For a constant, just observable, rate of strain, this gives the well-known relation between yield point and temperature[11]

$$P = P_o - A\sqrt{T} \tag{4.6}$$

We might expect that V would be a property of the material but not of the internal strains. This may not be true of λ, but as a/λ comes within a logarithm, its exact value does not much matter. Taking $\lambda/a = 100$, (4.5) gives us[12]

$$P = P_o - B\sqrt{T}\left[8.0 - \log_{10}\left(\frac{ds}{dt}\right)\right]^{1/2}, \tag{4.7}$$

where ds/dt is the rate of strain in $\sec^{-1}$ and B does not depend on the degree of cold work of the material.

The suggestion made here, that the term in the stress sensitive to rates and temperature is independent of cold work, agrees qualitatively with the fact that the increase of yield point shown by steels of widely different yield points is about the same. More exact verification can be obtained from the dependence of the yield point on temperature. The values are from H.W. Russell[13]. It will be seen that, for a given material the change of yield point with temperature depends little on the heat treatment or cold work[14].

For carbon steel, assuming that the yield point is that for which $ds/dt = 10^{-3}\,\sec^{-1}$, comparing these values with (4.7) gives

$$\sqrt{1}1(\sqrt{3}00 - \sqrt{7}0)B = 70$$

which gives

$$B = 2.35 \times 10^3\,\text{lbs/sq. in.}$$

Thus at room temperature the yield stress is related to the rate of strain by the equation

[11] See, for instance, Orowan, Zs. f. Physik, 89, 605 (1934) for Zn and Cd crystals.

[12] Perhaps the term in this equation most open to doubt is that due to our choice of a/λ, namely, 8.0. According to this equation, the whole stress-strain curve of a metal should remain unchanged if temperature and rate of strain are changed in such a way that

$$T[8 - \log_{10}(ds/dt)]$$

remains constant. Some confirmation of this hypothesis is given by some results on copper due to Nadai (J. Applied Mech. vol, 8, p. A77 (1941)). He finds that the U.T.S. was equal to 30,000 lbs/sq.inch for the following values of T and ds/dt

T (degrees K)	300	473	673	873
$\log_{10}(ds/dt)$	-3.5	1.5	3	4
$10^{-3}x\ T[8 - \log_{10}(ds/dt)]$	3.45	3.1	3.4	3.5

[13] Symposium in the Effect of Temperature in the Properties of Metals. Am. Soc. for Testing Materials and Am. Soc. Mech. Engineers, (1931), p. 658.

[14] These data and discussion in the following several paragraphs refer to Table 4.1.

Table 4.1.

Metal	Yield point (1000 lbs/sq.in) Room temp.	Liquid air.	Difference
Cold-rolled copper	43.3	50.4	7.1
Annealed copper	12.7	18.3	5.6
Annealed 0.4 carbon steel	45.8	114.1	68.3
Treated 0.4 carbon steel	76.9	150.2	73.3
Annealed 3 p. c. nickel steel	57.0	110.0	53.0
Treated 3 p. c. nickel steel	76.4	132.0	55.6

$$P = P_o - 41 \times 10^3 \sqrt{8.0 - \log_{10}\left(\frac{ds}{dt}\right)} \text{ lbs/sq.inch} \tag{4.8}$$

Taking as before $ds/dt = 10^{-3}$ for static tests, we obtain the following values of the increment in the yield stress for a 0.4 carbon steel *with any degree of cold work*

ds/dt ($\sec^{-1}$)	1	10^2	10^3	10^4
Increase in yield stress (1000 lbs/sq. inch)	20	36	44	54

The values are of the order observed.

For copper, according to the values of Table 4[15], the increase in yield point with lowered temperature is only about 1/10th of the value observed for steel. We should thus expect an increase at high rates of strain of the order 4000 lbs/sq. inch.

4.5 Fracture in Ductile Metals

A ductile metal specimen under tension extends a certain amount and then fractures, the reduction of area at the neck at fracture being a well reproducible quantity with a small coefficient of variation. Fracture, when it takes place, cannot be determined by *surface* cracks, because

(a) Surface conditions are found not to affect the strain at which rupture occurs.
(b) Rupture is observed to begin at the centre of tensile specimens.

It has therefore been suggested on several sides that a metal, in a given state of plastic strain, will fracture when the greatest principal stress reaches

[15] Reference to Table 4.1 was clearly intended here.

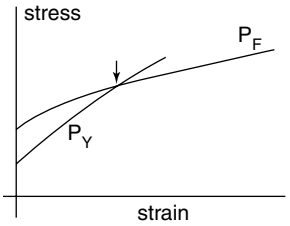

Fig. 4.3.

a critical value P_F, called in the literature the "Technical tensile strength" (German "Reissfestigkeit"). When a metal is strained under tension, P_F will change in some unknown way with strain, and the yield stress P_Y will increase according to the usual stress-strain curve (e.g. (4.3)). When the two curves cross the metal fractures.

We shall in this report assume that such a rupture stress P_F exists, and that it is independent of the components of principal stress other than the maximum. Not much evidence exists for this assumption; if fracture took place according to the Griffith theory starting from *internal* cracks, formed by the cold work, then the two dimensional theory of para. 2 suggests that the stress for fracture should be independent of the other components. Difficulties in applying the Griffith theory to ductile materials, however, are:

(i) The Griffith theory is based on the existence of high concentrations of stress at the apex of a crack; it is difficult to see how such high concentrations can exist in a ductile material[16].
(ii) The stresses inside a cold-worked metal are certainly very unhomogeneous; if the cracks were formed initially in regions of high local stress, the stress there would be quite different from the applied stress.

On the experimental side, Bridgman (loc. cit.,) has recently made some measurements of the stress-strain curves of steel under high pressure ($13,000\,\mathrm{kg/cm^2}$). He finds, as was to be expected, that much higher strains, up to values of A_o/A equal to 10 could be obtained without rupture; for if T is the applied stress, $\frac{1}{2}T$ is the shear stress and $T-p$ is the maximum principal stress. He finds that rupture occurs at a value of $T-p$ (called by him the "net" stress), which is, roughly, independent of pressure. This may mean that the rupture stress P_F is independent of the other components of stress *and* of the degree of strain; or if P_F increases with strain (cold work), then it must increase also with pressure. Unfortunately Bridgman did not carry out the experiment of extending the specimen under pressure past the rupture point, then reducing the pressure and determing the rupture stress.

[16] An interesting discussion of the way in which cracks may spread in ductile materials has been given by Orowan, Proc. Int. Congreee of Physics, London (1934), vol. II, p. 81.

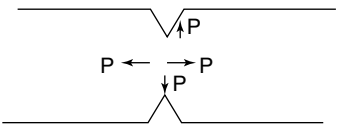

Fig. 4.4.

An extensive investigation of the tensile strengths of notched bars has been made by Ludwig and Kunze[17], with a view to determining the true stress for rupture. The idea of this work is to extrapolate the ultimate strength (maximum load divided by initial core area of notch) of notched specimens to the case of vanishing notch angle and vanishing core area. It is assumed that the high stresses at the edge of the notch are relieved by plastic flow, which is not however sufficient to affect the state of cold work in the interior of the core. The stress is thus assumed to be uniform throughout the core; and since further plastic flow is impossible, the stress distribution in the core must correspond to a negative pressure. The rupture stresses obtained in this way will correspond to this limiting case, and be valid for uniaxial stresses only if the rupture stress depends on the maximum stress component only.

For some reason which is not clear, Kunze calculates the stress in the core of the notch from the elastic Poisson contraction, which can scarcely be justified, since by hypothesis plastic deformation takes place at the apex. The stress could be calculated directly by dividing the tension by the area.

Kunze gives curve of fracture stress P_F against plastic strain (the specimens being strained before the notch was made). Kunze's curve of P_F first rises[18] with increasing strain, and then drops. We believe that this drop does not actually exist, and was obtained owing to the failure of the hardened metal to relieve the abnormal stress concentrations in the neighbourhood of the notch[19]. Any rapid fall of P_F near the normal rupture point is precluded by Bridgman's result quoted above.

Some values of the true ultimate tensile stress for some metals are given below for reference (from Ludwig, Bestimmung d. Reissfestigkeit aus Gleichmassigen Dehnung, Z. f. Metallkunde, 18, 269 (1926))[20].

[17] Described in a number of papers; for a review see "Kohasionsfestigkeit" by W. Kunze, Mit. d. deutschen Material prufungsanstalten, Sonderheft, 20, p.1 (1932). See also a critical review of this work by D.J. McAdam, J. of Applied Mechanics, vol. 8, p. 155 A, (1941).

[18] For single crystals of zinc and certain other materials, e.g. W, Te, NaCl, there is a considerable rise of P_F with plastic strain, c.f. Kristalplastizitat, Schmid and Boas, p. 175.

[19] This drop has also been criticised by McAdam on different grounds.

[20] Reference here is to Table 4.2.

Table 4.2.

Material	Yield Stress*	True U.T.S.*
Al (pure)	4.0	24.6
Cu (pure)	4.2	53.0
Ni (pure)	10.5	128.7
Steel (0.08% C)	21.6	87
Steel (0.13% C)	26.2	93.1
Steel (0.2% C, 2.9 Ni. annealed)	46.3	100.8
Steel (0.45% C rolled)	41.0	104.0

*Tensile stresses in kg/mm^2 (to convert to tons/sq. inch multiply by 0.64).

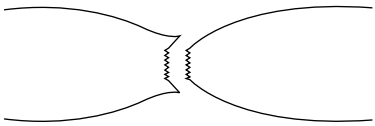

Fig. 4.5.

4.6 Brittle and Shear Rupture

These two types of rupture can, and usually do, occur in the same tensile specimen. Brittle rupture occurs perpendicular to the direction of the principal stress, and the material in the neighbourhood of the fracture does not show especially heavy cold work; shear rupture takes place at 45° to it, and the material is heavy strained round it.

Shear rupture occurs in the following circumstances:

(a) Cup and cone fracture, usual in tensile tests on ductile metals. Fracture is known to start in the middle of the specimen, where a brittle rupture is obtained; shear rupture occurs at the edges.
(b) According to Bridgman's experiments tensile rupture under high hydrostatic pressure is entirely by shear; a cone or series of cones marks the fractured surface (Fig. 4.6).
(c) Under pure shear metals will normally fail by shear fracture, as shown by the behaviour of sheet metal when cut by scissors.
(d) Shell and bomb casings which show plastic expansion before fracture, break up as shown in Fig. 4.7. With shells brittle rupture occurs on the outside of the shell case, shear rupture inside; with bombs (higher rates of strain than in shells) shear rupture alone is frequently observed.

We suggest that, for a metal with a given degree of cold work, there exists a critical shear stress S_R at which shear rupture will occur. This will normally be greater than the shear stress for yield; but the facts listed under (c) and (d) above suggest that if S_R and yield stress are plotted against strain, the curves will ultimately cross, if brittle fracture has been prevented. In the tensile test

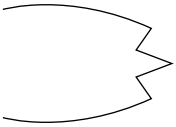

Fig. 4.6.

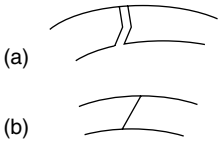

Fig. 4.7.

giving cup and cone fracture, when the brittle fracture has occurred in the centre of the test piece, the stresses near the surface will be raised to a high value giving a high rate of strain. We must deduce from the occurrence of the cup and cone fracture that, when the shear stress S_R is reached, the material prefers to rupture by shear, even though the tensile stress exceeds the critical value P_F. This is a rather surprising result.

We have at present no idea why, at a certain critical shear stress, shear should become unstable in this way.

4.7 Rupture of Bomb Casings

The stress distribution within a bomb casing has been discussed in the author's previous report (A.C.4035). It consists of:

(a) A uniform[21] tangential stress equal to the yield stress of the metal at the strain and rate of flow concerned.
(b) A hydrostatic pressure decreasing from that of the explosive gases at the inner surface to zero at the outer.

Interesting experiments on the break-up of thick cased cylindrical bombs have been made by Porter (ARD, Swamsea). These bombs broke by shear rupture; it was found possible to fit together the fragments, showing that break-up took place after a very definite expansion. For bombs of different case thickness it was found that rupture took place at the same percentage elongation of the *inner* surface. This suggests that shear fracture starts at the inner surface. This is natural, because the shear stress is (slightly) greatest there, owing to the greater strain hardening. Porter also found that the strains

[21] If the case is thick, the strain will not be exactly uniform, because the strain will be greater at the inside surface, since the expansion of the inner circumference is greater than that of the outer.

reached at the inner surface were much greater than those obtainable in static tests. This is not surprising, because rupture in brittle static tests will be determined by brittle fracture, a process which cannot take place at the high pressures at the inner surface, where the resultant tangential stress is reduced and may be negative.

We suppose that the condition for shear rupture is that the shear stress at the inside of the case reaches the critical value S_R before the tensile stress at the outside reaches P_F.

For casings that fracture, as in Fig. 4.9(a), there is evidence that for some shells at any rate the cracks start from the outside sometime before normal break-up, and penetrate slowly through the case[22]. The evidence is as follows.

(a) Porter[23] has shown from work on bombs with grooves on the outer surface that, when the pieces are fitted together, they appear as in Fig. 4.8.
(b) A metallographic and X-ray examination[24] of fragments from a British $3.7''$ shell shows much greater elongation of the crystal grains near the inner surface than the outer. The effect, however, was not observed with a fragment from a German shell (0.7 carbon as compared with 0.4)

Fig. 4.8.

The explanation of this effect must be the following: fracture starts at the outer surface when the tensile stress reaches the critical value P_F. In the more ductile metals the crack cannot spread into the region where the tensile stress is below P_F; in other words, the stress is not appreciably enhanced near the vertex of the crack. This fact speaks against the Griffith mechanism, according to which a large crack of macroscopic dimensions would spread under the influence of a very small stress.

A difference of this type between the behaviours of brittle and tough steels seems to be shown by notched bar impact tests. The facts quoted are given in the discussion of Notched Bar Impact Testing, Trans. Menchester Assoc. of Engineers (1937).

Figure 4.9(a) shows a notched specimen and Figs. 4.9(b) and (c) the type of load-deflection curve that can be obtained for brittle and tough steels respectively, when the specimen is bent statically; the area under the curve is the work done to fracture, which agrees well with the work done in impact tests. We interpret these curves as follows:

[22] Reference to Fig. 4.7(a) is apparently intended here.
[23] Controlled Fragmentation on Anti-Personnel Bombs, AC.1241, October, (1941).
[24] N.P.L. Investigation Ref. G.C. 774, June (1943).

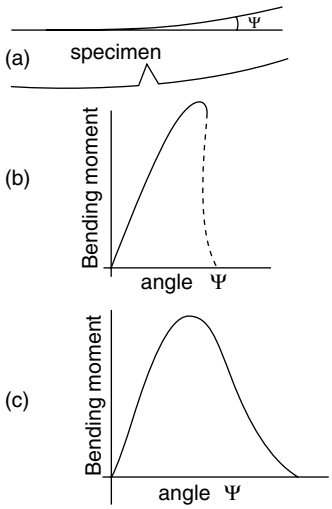

Fig. 4.9.

In the rising parts of the curve, plastic deformation is taking place at the base of the crack, until the rupture point is reached at the surface, because, as in Fig. 4.3, the curve for P_F crosses the curve for the yield point. Since, however, the stress at the base of the crack is not uniaxial, the shear stress is less than half the maximum tensile stress, and a crack will start for a smaller plastic strain than in the normal tensile test.

In steels of the type shown in Fig. 4.9b, the rapid drop in the curve shows that a crack, once started, will go right across the specimen, although the upper part (Fig. 4.9a) has not been appreciably strained. The propagation of the crack appears to require no further energy[25]. In impact tests it is stated that as soon as the crack started to traverse the body of the specimen, it did so with explosive suddenness (loc. cit. p.151). For metals showing curves of type (c), on the other hand, it is clear that the crack cannot propagate itself into the unhardened material until further bending with work hardening has taken place.

4.8 Thinning of Fragments; Dependence of Rupture Stress on Rate of Strain

The thinning observed in bomb and shell fragments is usually of the order 30 to 50%, and thus the plastic strain is not much less than that obtained in static tests. In casings that break by brittle rupture from the outside, we have seen in the last section that there is some uncertainty as to when cracking begins;

[25] The calculated energy required to separate two rows of atoms is quite negligible.

for casings that break by shear rupture, on the other hand, the observed expansion shows that the outer surface can expand by 50% without brittle fracture; in other words, that the strain at which fracture occurs under simple uniaxial stress is at any rate not decreased by a high rate of shear.

This is also in agreement with results obtained in high speed tensile tests. For instance, Clark and Datwyler (Am. Soc. Testing Materials, (1941),) using a rate of strain of the order 10^2, find the following values of the reduction in area at fracture:

	Yield Point (lbs.)		Max. load		R. in A.	
	Static	Dynamic	Static	Dynamic	Static	Dynamic
Cold-rolled steel (composition not stated)	265	352	280	360	48	50.7
18–8 Cr. Ni Alloy steel	303	371	385	466	69	54
Brass (cold-rolled)	138	192	177	202	44	50
Aluminium	50	76	59	79	69	75

It will be seen that, in spite of the considerable increase of yield point with rate of strain, the reduction in area changes in either direction, by a small factor only.

If P_F, the fracture stress, is independent of strain, then by (4.3) rupture occurs when

$$P_1 + P_2 \log \frac{A_o}{A} = P_F \ ,$$

i.e. when

$$\frac{A_o}{A} = e^{(P_F - P_1)/P_2}$$

Since P_2 is roughly independent of rate of strain and of the order 70,000 lbs/sq. in., while P_1 is increased by about 60,000, we see that, if P_F is independent of rate of strain, fracture should occur for a very small reduction in area or none at all. Since this is contrary to the observed facts, it follows that

EITHER P_F decreases rapidly with increasing strain,
OR P_F increases with rate of strain by about the same amount as the yield stress P_o.

We have seen that the first hypothesis (that of Kunze) is not compatible with Bridgman's results, that under pressure a very high degree of plastic deformation can be achieved in a *tensile* test. We are thus driven to the second conclusion, that the rupture stress of a material *increases* with rate

of strain[26]. This result, that the rupture stress increases with rate of strain is somewhat unexpected. Similar evidence does not exist for the dependence on temperature, where for steels the reduction in area drops considerably at liquid air temperature. Thus for an annealed carbon steel H.W. Russell (loc. cit.,) gives a drop from 49 to 7.1%, suggesting that the rupture stress does not increase with the yield stress.

4.9 Coefficient of Dispersion of Rupture Points

In the author's previous paper on fragmentation, it was suggested that the strain (reduction of area) at which a metal fractures in tensile tests is a quantity which shows a certain scatter about a mean value. It was suggested that, per unit volume of metal, the chance that a crack would start as the strain increased from s to $s + ds$ could be represented by a function of the form

$$Ce^{\gamma s}\, ds$$

With this assumption, the average size of fragments could be calculated and it was deduced that γ should have the values

γ	$\simeq$	110	Low and medium (0.4) carbon steel.
	$\simeq$	230	0.7% carbon steel.

So high a value gives a dispersion of the rupture points of about 1%.

An examination[27] of the fragment weights from service bombs and shells shows that, for medium carbon steels, the fragmentation does not depend on whether the rupture is brittle (starting from the outer surface) or by shear. Thus γ must be roughly the same for either type of rupture.

In this section, then, we attempt a derivation of γ from the most general hypotheses; the method is an improvement of that given in para. 9 of AC. 4035.

We have seen (para. 2) that in glass, where the fracture stress is determined by the largest of a comparatively small number of Griffith cracks, the values of the tensile stress show a large scatter (10%). In metals we shall assume that rupture, whether brittle or shear, starts at one of a much larger number of "singular points" of unspecified nature, distributed throughout the

[26] The rise in temperature due to the work done against the resistance of the steel to shear is not sufficient to affect the properties greatly. Using formula (4.3) for the stress-strain relation, with $P_1 = 52$ tons/sq. inch (for high rates of strain) and $P_2 = 33$ tons/sq.inch, we calculate for a 50% increase of radius that the rise of temperature should be 19° C. This will give a change in P_o of the order 2 tons/sq. inch.

[27] A.O.R.G. Memo. No. 113 (Aug. 1943).

volume. Let N be the number of such points per unit volume; we may safely assume $N^{-1/3}$ to be of the order $10^{-3} - 10^{-5}$ cm. since distances of this order always occur in any analysis of the structure of the "real" crystal. It is not, of course, suggested that the same type of centre is responsible for both types of rupture.

Let c be some parameter specifying the size of the "singular points". For instance, if they were Griffith cracks, $2c$ would be the width of a crack (Fig. 4.1). We shall assume that the values of c are distributed at random about some mean value c_o according to the Gaussian distribution function; thus the number of points for which c lies between c and $c + dc$ is

$$B\,dc\,\exp\left[-\frac{(c-c_o)^2}{2\tau^2}\right] \tag{4.9}$$

where

$$B\int_0^\infty \exp\left[-\frac{(c-c_o)^2}{2\tau^2}\right] dc = N$$

We may expect the distribution to be fairly wide about the mean value; as a guess we shall put $2\tau^2 = c_o^2$. Then clearly

$$B = N/c_o \;\times\; \text{factor of order unity}$$

Consider a tensile specimen of unit volume; then the largest "crack", or singular point, is the one that will cause rupture. The chance that for this "crack" the size parameter c will exceed the value c is

$$A\int_c^\infty \exp\left[-\frac{(c-c_o)^2}{c_o^2}\right] dc \tag{4.10}$$

If we put this equal to unity we obtain an expression for the size of crack c_R actually responsible for rupture.

For values c in the neighbourhood of c_R we write

$$\frac{c-c_R}{c_R} = x\,,$$

so that, neglecting terms in x^2

$$\frac{(c-c_o)^2}{c_o^2} = \frac{(c_R-c_o)^2}{c_o^2} + \frac{2xc_R(c_R-c_o)}{c_o^2}$$

Thus (4.10) becomes

$$\frac{c_o^2 B}{2(c_R-c_o)}\exp\left[-\frac{(c_R-c_o^2}{c_o^2}\right]\exp\left[-\frac{2x(c_R-c_o)c_R}{c_o^2}\right] \tag{4.11}$$

When x vanishes this must be unity, which gives for C_R

$$\left(\frac{c_R - c_o}{c_o}\right)^2 = \log_e \frac{c_o^2 B}{2\,(c_R - c_o)}$$

Since $B \sim N/c_o$, and N is a very large number $(10^9 - 10^{15})$, we may write

$$\frac{c_R - c_o}{c_o} \simeq \sqrt{\log_e N} = \theta \,, \tag{4.12}$$

Also, the chance that the greatest crack is greater than c may from (4.11) be written $e^{\beta x}$

$$\begin{aligned}\beta &= \frac{2(c_R - c_o)c_R}{c_o^2} \\ &= 2\theta(1+\theta)\end{aligned}$$

by (4.12).

Now let us assume the following relation between c, the size of the singular points, and P, the strain to rupture them

$$P = \text{const}/c^n \,.$$

Thus if the points were Griffith cracks we should have by formula (4.1) $n = 1/2$. Thus in the neighbourhood of the rupture point

$$\begin{aligned}\Delta P/P_F &= -n\Delta c/c_R \\ &= -nx\end{aligned}$$

Also let us assume the stress-strain relation (4.3), namely

$$P = P_1 + P_2 \log(1+s) \,,$$

so that

$$\Delta P = P_2 \frac{\Delta s}{1+s}$$

It follows that

$$\beta x = -\frac{\beta \Delta P}{P_F n} = -\frac{P_2 \beta \Delta s}{P_F n(1+s_R)}$$

where s_R is the strain at rupture. It follows that our parameter γ is given by

$$\begin{aligned}\gamma &= \frac{P_2}{nP_F}\frac{\beta}{1+s_R} \\ &= \frac{2}{n}\frac{P_2}{P_F}\frac{\theta(1+\theta)}{1+s_R}\end{aligned}$$

It will be seen that, in this formula, the only unknown quantities are n and θ; also that as θ^2 is equal to $\log N$, the values does not depend much on

the choice of N, the number of singular points per unit volume. We thus have reason to believe that γ might be of the same order, at any rate, for brittle and shear rupture.

Taking $N = 10^{15}$, and $n = 1/2$, as for Griffith cracks, we find $\theta = 5.85$ and

$$\gamma = 160\, P_2/P_F(1 + s_R)$$

Some values for the other constants have been deduced from some curves given by Korber and Rohland (loc. cit.,)

		Reduction in area R	True U.T.S.	P_2	γ (calc.)
Iron		.83	54	34	20
Steel	0.1 C	.70	70	42	42
	0.13 C	.70	78	45	40
	0.25 C	.63	80	45	53
	0.45 C	.57	82	38	67
	0.55 C	.50	87	39	69

The values of γ are somewhat too low, but in view of the very crude state of the theory the agreement may be considered satisfactory. The rise in γ with increasing carbon content is in agreement with observation.

Facsimiles of N.F. Mott: Fragmentation of Shell Casings and the Theory of Rupture in Metals

UNCLASSIFIED
~~SECRET~~ 7/11/90 .J.

Copy No. 14

A.C.4613
SD/FP.139

MINISTRY OF SUPPLY

ADVISORY COUNCIL ON SCIENTIFIC RESEARCH
AND TECHNICAL DEVELOPMENT

FRAGMENTATION PANEL OF THE
STATIC DETONATION COMMITTEE

Fragmentation of shell casings and the theory of rupture in metals

by

N.F. Mott

Received August 19th, 1943.

PIB

A.C.4613
SD/FP.139

FRAGMENTATION OF SHELL CASINGS AND THE THEORY OF RUPTURE IN METALS

By N. F. MOTT.

SUMMARY

In para. 2 the Griffith theory of rupture in brittle materials is reviewed; in paras. 3 and 4 the information available about the stress-strain curves of metals at high rates of strain is reviewed, and it is suggested that the increase in the yield point of steel of a given composition is independent of the degree of cold work. A correlation is also suggested between the variations of yield point with temperature and with rate of strain. In para. 5 the evidence is discussed for the hypothesis that metals in a given state of plastic strain will fracture when the maximum principal stress reaches a given value. It is shown that the fracture stress of steel is either independent of strain or increases slowly with it. The fracture stress appears to increase with rate of strain, by about the same amount as the yield point. In para. 6 it is pointed out that two well-defined types of rupture occur, brittle and shear; the condition for the occurrence of either is discussed. Para. 7 applies the conclusions reached to certain phenomena observed in the rupture of bomb and shell casings. Para 8 discusses the evidence that the rupture stress increases with rate of strain. Para. 9 discusses the scatter observed in the values of the reduction in area obtained in tensile tests; this scatter was assumed in a previous report on fragmentation to be responsible for the average size of fragments. It is shown that a numerical estimate of the order of magnitude of this scatter, and of its dependence on the properties of the steel, can be made using very general assumptions about the mechanism of rupture. It appears probable that the magnitudes of the scatter will be the same for shear rupture as for brittle rupture.

FRAGMENTATION AND RUPTURE OF METALS

1. PURPOSE OF REPORT

In a recent report* the present author has given a theory of fragmentation which attempts to account for the size of fragments from a bomb or shell of given dimensions and filling. The purpose of the present report is :

(a) To extend the theory and in particular to attempt to account for the differences in fragmentation shown by high and low carbon steels.

(b) To review the information available about fracture of ductile metals; it is probable that the study of fragmentation can throw considerable light on the processes involved, which may be useful in other fields, such as that of armour piercing projectiles.

2. FRACTURE OF NON-DUCTILE MATERIALS; THE THEORY OF A.A. GRIFFITH

While no molecular theory exists to account for fracture in ductile materials, for non-ductile materials such as glass the accepted theory is that due to Griffith**. Griffith explains the discrepancy of 100 to 1000 between the observed and the theoretical tensile strength of materials such as glass or rocksalt by postulating the existence of surface cracks, which weaken the specimen; considerable experimental evidence exists in support of this hypothesis. Griffith has given a quantitative theory of the weakening effect of certain types of crack, based on Inglis' solution of the equations determining the stresses round

---

* A Theory of the fragmentation of shells and bombs. M. of S. Extra-Mural Report A.C.4035.

** A.A. Griffith. Trans. Roy. Soc. 221, 180 (1920).
II. Int. Congress Applied Mechanics, Delft, p.55 (1924).

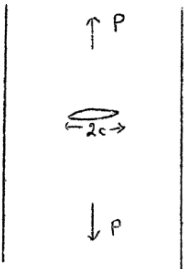

Fig.1

an elliptical cavity. He gives a condition that a crack of width $2c$ and length, perpendicular to the plane of the paper, large compared with c should spread when subjected to a stress P. This condition is

$$P = \sqrt{\frac{2E\sigma}{\pi c}} \qquad (1)$$

where E is Young's modulus and σ the surface tension. The formula is obtained by treating the cross-section of the crack as an ellipse of zero eccentricity, and assuming that Hooke's law is valid up to the apex of the crack. A formula differing from (1) by a factor 0.8 has been derived by Orowan* on rather similar assumptions

Griffith has also considered the behaviour of cracks under biaxial stresses. A material is supposed to be subject to stresses P, Q as shown, and P is greater than Q. It is also supposed to contain cracks oriented at all angles θ to the normal to P. As P is increased certain of the cracks will begin to spread and the material will fracture. The question at issue is, which crack will begin to spread first, and how does the critical value of P depend on Q?

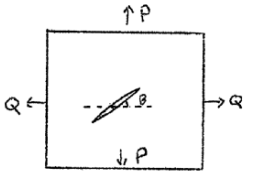

Fig.2

According to Griffith, two cases may be distinguished :

(a) $3P + Q > 0$. In this case cracks for which $\theta = 0$ spread first and the critical value K of P, given by eqn. (1) above, is independent of Q.

(b) $3P + Q < 0$. In this case rupture takes place when

$$(P - Q)^2 + 8K(P + Q) = 0 \qquad (2)$$

at an angle θ given by

$$\cos 2\theta = -\tfrac{1}{2}\,\frac{P - Q}{P + Q}$$

Two interesting cases arise :

(i) Compressive stress, $P = 0$, $Q = -T$. Then $Q = 8K$, so rupture takes place at 8 times the stress necessary under tension, and at an angle θ equal to 30°.

(ii) Hydrostatic pressure. Owing to the two dimensional nature of the Griffith theory, we shall have to make the assumption that stresses perpendicular to the plane of the paper in fig. 2 do not affect the stress for rupture. With this assumption, if the specimen is subjected to a hydrostatic pressure p, we may write $p = -Q$. If $p < 3P$, rupture is determined by the maximum principal stress, at a value independent of p.

If a specimen is initially under tensile stress T, for example from a spring, and both spring and specimen are immersed in a hydrostatic pressure p, the maximum tensile stress is $T - p$. In a recent paper** Bridgman has called $P(= T - p)$ the net stress and T the true stress, which is perhaps unfortunate since P is actually the stress in the material.

---

* E. Orowan. Zs. f. Kristallographie, 89, 327 (1934).

** P.W. Bridgman. ORSD Report 1347, "Plastic Deformation of Steel under High Pressure".

Since the tensile strength of a material such as glass is determined by the size of the largest of a comparatively small number of random surface cracks, we should expect a large fluctuation in the strength of specimens prepared in the same way. Some values of the fluctuation have been given by Holland and Turner of the Dept. of Glass Technology, University of Sheffield*. The bending stresses of flat drawn sheets of thickness 0.27 cm. with sides mechanically ground and polished showed, when 25 specimens were tested, coefficients of variation of from 8 to 18%.

3. PLASTIC FLOW AND STRAIN HARDENING IN METALS

In this report we shall deal always with the true stress, which we shall denote by P, and not the engineering stress, which is the product of P and the reduction of area of the specimen, at the base of the neck if necking has commenced. It is obvious that P, not the engineering stress, determines fracture phenomena in the metal.

The following relation between strain s and true stress P has been given by Bridgman (loc. cit.,) and by Hollomon**

$$P = P_1 + P_2 \log_e \frac{A_o}{A} \qquad (3)$$

where A_1, A_o are the area and initial area of the specimen, so that

$$s = (A_o - A)/A$$

Bridgman's investigations were carried out under high hydrostatic pressure which is almost without effect on the stress-strain curve but enables the strain to be carried to much higher values without rupture. Hollomon investigates two steels with different carbon and nickel contents. For a given steel he finds a wide variety of values of P_1 depending on the heat treatment, but a fairly constant value of P_2, as follows :

Composition of steel		P_2
C	Ni	(1000 p.s.i)
0.44	0	73
0.19	1.83	73
0.20	0	55

The formula is not satisfactory near the yield point of the unworked metal

4. YIELD AT HIGH RATES OF STRAIN

For a discussion of fragmentation we require information about the yield point, at high rates of strain, of steels at the rupture point. Little evidence exists about this, most investigations being confined to the beginning of the stress-strain curve. We therefore attempt a theoretical estimate of the increase in yield stress to be expected.

At rates of strain of the order 500 sec^{-1} the tensile yield strength of low tensile steels is about doubled***; for instance, that of a medium carbon steel increased from 16 to 28 tons and a mild steel by about the same amount. On the other hand the tensile strength of hard steels is scarcely affected. In compressive tests at high striking velocities the actual rate of yield is not known, but must be much higher. It is found†

* A.J.Holland and W.E.S.Turner. Effect of Width on the Breaking Stress of Sheet Glass. Proc.Soc.Glass Technology,(1956), vol.20, p.72.

** U.S.A. Ordnance Dept. Report No.630/7. "Tensile Properties of Steel". Oct. 17 (1942).

*** The determination of static and dynamic yield stresses by a ball method, by R.M.Davies, M. of S. Extra-Mural Report A.C.1228. Brown and Vincent, Proc. Inst. Mech. Engineers, vol.145, p.126 (1941).

† D.S.I.R. Road Research Lab. Report MOS/172/ACW. Nov. (1942).

that a variety of steels with yield points between 18 and 72 tons/sq.inch showed approximately the same increase of yield point, about 35 tons/sq. inch. Between 1,600 and 2,500 ft/sec. the striking velocity has no effect on the yield point*.

According to a theory put forward by Becker**, it is not unexpected that the absolute values of the yield points of steels should increase by the same amount. According to Becker, the "dislocations" responsible for plastic flow will move under a stress P with velocity

$$v = C \exp\left[-\frac{(P_o - P)^2 V}{2GkT}\right] \qquad (4)$$

Here P_o is the stress required to move them at the absolute zero of temperature, T the absolute temperature, G the shear modulus and V a volume determined by the thickness of the dislocation zone. If λ is the distance between dislocations and a the interatomic distance, then the rate of shear is av/λ^2. C/a should be of the order of the period of atomic vibrations, namely 10^{-12} sec^{-1}; thus for the rate of shear we obtain

$$\frac{ds}{dt} = \left(\frac{a}{\lambda}\right)^2 \times 10^{12} \exp\left[-\frac{(P_o-P)^2 V}{2GkT}\right].$$

Expressing P in terms of $\frac{ds}{dt}$ we find

$$P = P_o - \sqrt{\frac{2GkT}{V}}\left[2\log_e\left(\frac{a}{\lambda}10^6\right) - \log\left(\frac{ds}{dt}\right)\right]^{\frac{1}{2}}. \qquad (5)$$

For a constant, just observable, rate of strain, this gives the well-known relation between yield point and temperature

$$P = P_o - A\sqrt{T} \qquad *** \qquad (6)$$

We might expect that V would be a property of the material but not of the internal strains. This may not be true of λ, but as a/λ comes within a logarithm, its exact value does not much matter. Taking $\lambda/a = 100$, eqn. (5) gives us ****

$$P = P_o - B\sqrt{T}\left[8.0 - \log_{10}\left(\frac{ds}{dt}\right)\right]^{\frac{1}{2}}, \qquad (7)$$

where ds/dt is the rate of strain in sec^{-1} and B does not depend on the degree of cold work of the material.

---

* Road Research Laboratory Report, MOS/33/ACW. Nov. 1941.

** R. Becker, Zs. f. Physik, 26, 919 (1925); E. Orowan, Proc. Phys.Soc. 52, 19 (1940).

*** See, for instance, Orowan, Zs. f. Physik, 89, 605 (1934) for Zn and Cd crystals.

**** Perhaps the term in this equation most open to doubt is that due to our choice of a/λ, namely, 8.0. According to this equation, the whole stress-strain curve of a metal should remain unchanged if temperature and rate of strain are changed in such a way that

$$T\left[8 - \log_{10}(ds/dt)\right]$$

remains constant. Some confirmation of this hypothesis is given by some results on copper due to Nadai (J. Applied Mech. vol, 8, p.A77 (1941)). He finds that the U.T.S. was equal to 30,000 lbs/sq.inch for the following values of T and ds/dt

T (degrees K)	300	473	673	873
$\log_{10}(ds/dt)$	-3.5	1.5	3	4
$10^{-3} \times T\left[8 - \log_{10}(ds/dt)\right]$	3.45	3.1	3.4	3.5

The suggestion made here, that the term in the stress sensitive to rates and temperature is independent of cold work, agrees qualitatively with the fact that the increase of yield point shown by steels of widely different yield points is about the same. More exact verification can be obtained from the dependence of the yield point on temperature. The values are from H.W. Russell*. It will be seen that, for a given material the change of yield point with temperature depends little on the heat treatment or cold work.

TABLE I

Metal	Yield point (1000 lbs/sq.in) Room temp.	Liquid air.	Difference
Cold-rolled copper	43.3	50.4	7.1
Annealed copper	12.7	18.3	5.6
Annealed 0.4 carbon steel	45.8	114.1	68.3
Treated " " "	76.9	150.2	73.3
Annealed 3 p.c. nickel steel	57.0	110.0	53.0
Treated " " "	76.4	132.0	55.6

For carbon steel, assuming that the yield point is that for which $ds/dt = 10^{-3}$ sec^{-1}, comparing these values with (7) gives

$$\sqrt{11}\,(\sqrt{300} - \sqrt{70})\,B = 70$$

which gives

$$B = 2.35 \times 10^3 \text{ lbs/sq. in.}$$

Thus at room temperature the yield stress is related to the rate of strain by the equation

$$P = P_0 - 41 \times 10^3 \sqrt{8.0 - \log_{10}\left(\frac{ds}{dt}\right)} \text{ lbs/sq.inch} \quad (8)$$

Taking as before $ds/dt = 10^{-3}$ for static tests, we obtain the following values of the increment in the yield stress for a 0.4 carbon steel with any degree of cold work

ds/dt (sec^{-1})	1	10^2	10^3	10^4
Increase in yield stress (1000 lbs/sq. inch)	20	36	44	54

The values are of the order observed.

For copper, according to the values of Table 4, the increase in yield point with lowered temperature is only about 1/10th of the value observed for steel. We should thus expect an increase at high rates of strain of the order 4000 lbs/sq. inch.

5. FRACTURE IN DUCTILE METALS

A ductile metal specimen under tension extends a certain amount and then fractures, the reduction of area at the neck at fracture being a well reproducible quantity with a small coefficient of variation. Fracture, when it takes place, cannot be determined by surface cracks, because
(a) Surface conditions are found not to affect the strain at which rupture occurs.
(b) Rupture is observed to begin at the centre of tensile specimens.

It has therefore been suggested on several sides that a metal, in a given state of plastic strain, will fracture when the greatest principal stress reaches a critical value P_F, called in the literature the

* Symposium in the Effect of Temperature in the Properties of Metals. Am. Soc. for Testing Materials and Am. Soc. Mech. Engineers, (1931), p.658.

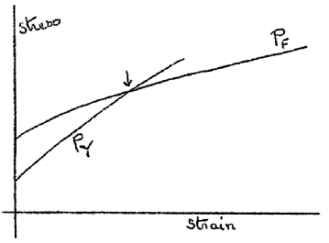

Fig. 3

"Technical tensile strength" (German "Reissfestigkeit"). When a metal is strained under tension, P_F will change in some unknown way with strain, and the yield stress P_Y will increase according to the usual stress-strain curve (e.g. eqn.(3)). When the two curves cross the metal fractures.

We shall in this report assume that such a rupture stress P_F exists, and that it is independent of the components of principal stress other than the maximum. Not much evidence exists for this assumption; if fracture took place according to the Griffith theory starting from internal cracks, formed by the cold work, then the two dimensional theory of para. 2 suggests that the stress for fracture should be independent of the other components. Difficulties in applying the Griffith theory to ductile materials, however, are :

(i) The Griffith theory is based on the existence of high concentrations of stress at the apex of a crack; it is difficult to see how such high concentrations can exist in a ductile material*.

(ii) The stresses inside a cold-worked metal are certainly very unhomogeneous; if the cracks were formed initially in regions of high local stress, the stress there would be quite different from the applied stress.

On the experimental side, Bridgman (loc. cit.,) has recently made some measurements of the stress-strain curves of steel under high pressure (13,000 kg/cm²). He finds, as was to be expected, that much higher strains, up to values of A_o/A equal to 10, could be obtained without rupture; for if T is the applied stress, $\frac{1}{2}T$ is the shear stress and $T - p$ is the maximum principal stress. He finds that rupture occurs at a value of $T - p$ (called by him the "net" stress), which is, roughly, independent of pressure. This may mean that the rupture stress P_F is independent of the other components of stress and of the degree of strain; or if P_F increases with strain (cold work), then it must increase also with pressure. Unfortunately Bridgman did not carry out the experiment of extending the specimen under pressure past the rupture point, then reducing the pressure and determing the rupture stress.

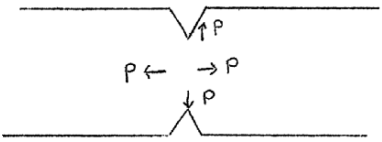

Fig. 4

An extensive investigation of the tensile strengths of notched bars has been made by Ludwig and Kunze**, with a view to determining the true stress for rupture. The idea of this work is to extrapolate the ultimate strength (maximum load divided by initial core area of notch) of notched specimens to the case of vanishing notch angle and vanishing core area. It is assumed that the high stresses at the edge of the notch are relieved by plastic flow, which is not however sufficient to affect the state of cold work in the interior of the core. The stress is thus assumed to be uniform throughout the core; and since further plastic flow is impossible, the stress distribution in the core must correspond to a negative pressure. The rupture stresses obtained in this way will correspond to this limiting case, and be valid for uniaxial stresses only if the rupture stress depends on the maximum stress component only.

For some reason which is not clear, Kunze calculates the stress in the core of the notch from the elastic Poisson contraction, which can scarcely be justified, since by hypothesis plastic deformation takes place at the apex. The stress could be calculated directly by dividing the tension by the area.

---

* An interesting discussion of the way in which cracks may spread in ductile materials has been given by Orowan, Proc. Int. Congreee of Physics, London (1934), vol. II, p. 81.

** Described in a number of papers; for a review see "Kohasionsfestigkeit" by W. Kunze, Mit. d. deutschen Material prufungsanstalten, Sonderheft, 20, p. 1 (1932). See also a critical review of this work by D. J. McAdam, J. of Applied Mechanics, vol. 8, p. 155 A, (1941).

Kunze gives curve of fracture stress P_F against plastic strain (the specimens being strained before the notch was made). Kunze's curve of P_F first rises* with increasing strain, and then drops. We believe that this drop does not actually exist, and was obtained owing to the failure of the hardened metal to relieve the abnormal stress concentrations in the neighbourhood of the notch**. Any rapid fall of P_F near the normal rupture point is precluded by Bridgman's result quoted above.

Some values of the true ultimate tensile stress for some metals are given below for reference (from Ludwig, Bestimmung d. Reissfestigkeit aus Gleichmassigen Dehnung, Z. f. Metallkunde, 18, 269 (1926)).

TABLE II

Material	Yield Stress	True U.T.S.
Al (pure)	4.0	24.6
Cu (pure)	4.2	53.0
Ni (pure)	10.5	128.7
Steel (0.08% C)	21.6	87
" (0.13% C)	26.2	93.1
" (0.2% C, 2.9 Ni. annealed)	46.3	100.8
" (0.45% C rolled)	41.0	104.0

Tensile stresses in kg/mm² (to convert to tons/sq. inch multiply by 0.64).

6. BRITTLE AND SHEAR RUPTURE

These two types of rupture can, and usually do, occur in the same tensile specimen. Brittle rupture occurs perpendicular to the direction of the principal stress, and the material in the neighbourhood of the fracture does not show especially heavy cold work; shear rupture takes place at 45° to it, and the material is heavy strained round it.

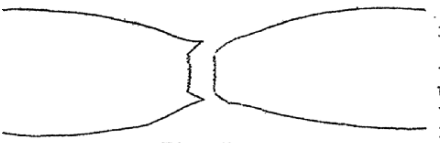

Fig. 5

Shear rupture occurs in the following circumstances :
(a) Cup and cone fracture, usual in tensile tests on ductile metals. Fracture is known to start in the middle of the specimen, where a brittle rupture is obtained; shear rupture occurs at the edges.

(b) According to Bridgman's experiments tensile rupture under high hydrostatic pressure is entirely by shear; a cone or series of cones marks the fractured surface (fig. 6).

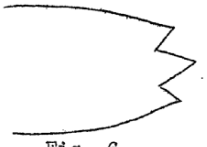

Fig. 6

(c) Under pure shear metals will normally fail by shear fracture, as shown by the behaviour of sheet metal when cut by scissors.

(d) Shell and bomb casings which show plastic expansion before fracture, break up as shown in fig. 7. With shells brittle rupture occurs on the outside of the shell case, shear rupture inside; with bombs (higher rates of strain than in shells) shear rupture alone is frequently observed.

We suggest that, for a metal with a given degree of cold work, there exists a critical shear stress S_R at which shear rupture will occur

---

* For single crystals of zinc and certain other materials, e.g. W, Te, NaCl, there is a considerable rise of P_F with plastic strain, c.f. Kristalplastizitat, Schmid and Boas, p.175.

** This drop has also been criticised by McAdam on different grounds.

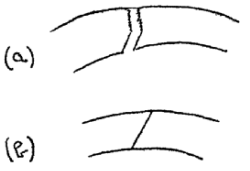

Fig. 7

This will normally be greater than the shear stress for yield; but the facts listed under (c) and (d) above suggest that if S_R and yield stress are plotted against strain, the curves will ultimately cross, if brittle fracture has been prevented. In the tensile test giving cup and cone fracture, when the brittle fracture has occurred in the centre of the test piece, the stresses near the surface will be raised to a high value giving a high rate of strain. We must deduce from the occurrence of the cup and cone fracture that, when the shear stress S_R is reached, the material prefers to rupture by shear, even though the tensile stress exceeds the critical value P_F. This is a rather surprising result.

We have at present no idea why, at a certain critical shear stress, shear should become unstable in this way.

7. RUPTURE OF BOMB CASINGS

The stress distribution within a bomb casing has been discussed in the author's previous report (A.C.4035). It consists of :

(a) A uniform* tangential stress equal to the yield stress of the metal at the strain and rate of flow concerned.

(b) A hydrostatic pressure decreasing from that of the explosive gases at the inner surface to zero at the outer.

Interesting experiments on the break-up of thick cased cylindrical bombs have been made by Porter (ARD, Swansea). These bombs broke by shear rupture; it was found possible to fit together the fragments, showing that break-up took place after a very definite expansion. For bombs of different case thickness it was found that rupture took place at the same percentage elongation of the inner surface. This suggests that shear fracture starts at the inner surface. This is natural, because the shear stress is (slightly) greatest there, owing to the greater strain hardening. Porter also found that the strains reached at the inner surface were much greater than those obtainable in static tests. This is not surprising, because rupture in brittle static tests will be determined by brittle fracture, a process which cannot take place at the high pressures at the inner surface, where the resultant tangential stress is reduced and may be negative.

We suppose that the condition for shear rupture is that the shear stress at the inside of the case reaches the critical value S_R before the tensile stress at the outside reaches P_F.

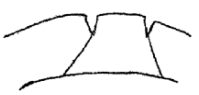

Fig. 8

For casings that fracture, as in fig. 9 (a), there is evidence that for some shells at any rate the cracks start from the outside sometime before normal break-up, and penetrate slowly through the case. The evidence is as follows .

(a) Porter** has shown from work on bombs with grooves on the outer surface that, when the pieces are fitted together, they appear as in fig. 8.

---

* If the case is thick, the strain will not be exactly uniform, because the strain will be greater at the inside surface, since the expansion of the inner circumference is greater than that of the outer.

** Controlled Fragmentation on Anti-Personnel Bombs, AC.1241, October, (1941).

(b) A metallographic and X-ray examination* of fragments from a British 3.7" shell shows much greater elongation of the crystal grains near the inner surface than the outer. The effect, however, was not observed with a fragment from a German shell (0.7 carbon as compared with 0.4)

The explanation of this effect must be the following : fracture starts at the outer surface when the tensile stress reaches the critical value P_F. In the more ductile metals the crack cannot spread into the region where the tensile stress is below P_F; in other words, the stress is not appreciably enhanced near the vertex of the crack. This fact speaks against the Griffith mechanism, according to which a large crack of macroscopic dimensions would spread under the influence of a very small stress.

A difference of this type between the behaviours of brittle and tough steels seems to be shown by notched bar impact tests. The facts quoted are given in the discussion of Notched Bar Impact Testing, Trans. Manchester Assoc. of Engineers (1937).

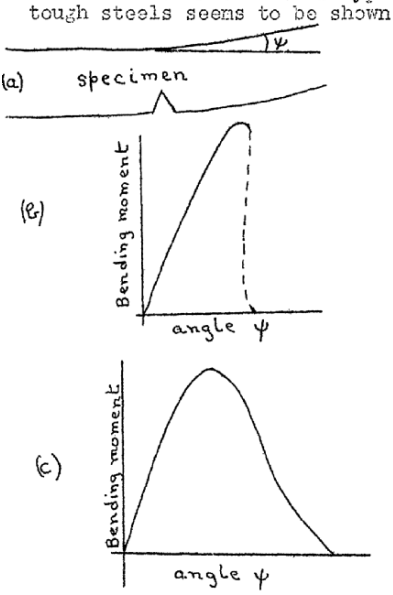

Fig. 9

Fig. 9(a) shows a notched specimen and figs. 9(b) and (c) the type of load-deflection curve that can be obtained for brittle and tough steels respectively, when the specimen is bent statically; the area under the curve is the work done to fracture, which agrees well with the work done in impact tests. We interpret these curves as follows :

In the rising parts of the curve, plastic deformation is taking place at the base of the crack, until the rupture point is reached at the surface, because, as in fig. 3, the curve for P_F crosses the curve for the yield point. Since, however, the stress at the base of the crack is not uniaxial, the shear stress is less than half the maximum tensile stress, and a crack will start for a smaller plastic strain than in the normal tensile test.

In steels of the type shown in fig. 9(b), the rapid drop in the curve shows that a crack, once started, will go right across the specimen, although the upper part (fig. 9(a)) has not been appreciably strained. The propagation of the crack appears to require no further energy**. In impact tests it is stated that as soon as the crack started to traverse the body of the specimen, it did so with explosive suddenness (loc. cit. p.151). For metals showing curves of type (c), on the other hand, it is clear that the crack cannot propagate itself into the unhardened material until further bending with work hardening has taken place.

8. THINNING OF FRAGMENTS; DEPENDENCE OF RUPTURE STRESS ON RATE OF STRAIN

The thinning observed in bomb and shell fragments is usually of the order 30 to 50%, and thus the plastic strain is not much less than that obtained in static tests. In casings that break by brittle rupture from the outside, we have seen in the last section that there is some uncertainty as to when cracking begins; for casings that break by shear rupture, on the other hand, the observed expansion shows that the outer surface can expand by 50% without brittle fracture; in other words, that

* N.P.L. Investigation Ref. G.C.774, June (1943).

** The calculated energy required to separate two rows of atoms is quite negligible.

the strain at which fracture occurs under simple uniaxial stress is at any rate not decreased by a high rate of shear.

This is also in agreement with results obtained in high speed tensile tests. For instance, Clark and Datwyler (Am. Soc. Testing Materials, (1941),) using a rate of strain of the order 10^2, find the following values of the reduction in area at fracture :

	Yield Point (lbs.)		Max. load		R. in A.	
	Static	Dynamic	Static	Dynamic	Static	Dynamic
Cold-rolled steel (composition not stated)	265	352	280	360	48	50.7
18-8 Cr.Ni Alloy steel	303	371	385	466	69	54
Brass (cold-rolled)	138	192	177	202	44	50
Aluminium	50	76	59	79	69	75

It will be seen that, in spite of the considerable increase of yield point with rate of strain, the reduction in area changes in either direction, by a small factor only.

If P_F, the fracture stress, is independent of strain, then by eqn. (3) rupture occurs when

$$P_1 + P_2 \log \frac{A_o}{A} = P_F ,$$

i.e. when $$\frac{A_o}{A} = e^{(P_F - P_1)/P_2}$$

Since P_2 is roughly independent of rate of strain and of the order 70,000 lbs/sq. in., while P_1 is increased by about 60,000, we see that, if P_F is independent of rate of strain, fracture should occur for a very small reduction in area or none at all. Since this is contrary to the observed facts, it follows that

EITHER P_F decreases rapidly with increasing strain,

OR P_F increases with rate of strain by about the same amount as the yield stress P_o.

We have seen that the first hypothesis (that of Kunze) is not compatible with Bridgman's results, that under pressure a very high degree of plastic deformation can be achieved in a tensile test. We are thus driven to the second conclusion, that the rupture stress of a material increases with rate of strain*. This result, that the rupture stress increases with rate of strain is somewhat unexpected. Similar evidence does not exist for the dependence on temperature, where for steels the reduction in area drops considerably at liquid air temperature. Thus for an annealed carbon steel H.W. Russell (loc. cit.,) gives a drop from 49 to 7.1%, suggesting that the rupture stress does not increase with the yield stress.

9. COEFFICIENT OF DISPERSION OF RUPTURE POINTS

In the author's previous paper on fragmentation, it was suggested that the strain (reduction of area) at which a metal fractures in tensile tests is a quantity which shows a certain scatter about a mean value. It was suggested that, per unit volume of metal, the chance that a crack would start as the strain increased from s to s + ds could be

---

* The rise in temperature due to the work done against the resistance of the steel to shear is not sufficient to affect the properties greatly. Using formula (3) for the stress-strain relation, with P_1 = 52 tons/sq. inch (for high rates of strain) and P_2 = 33 tons/sq.inch, we calculate for a 50% increase of radius that the rise of temperature should be 19° C. This will give a change in P_o of the order 2 tons/sq. inch.

represented by a function of the form

$$C e^{\gamma s} ds$$

With this assumption, the average size of fragments could be calculated, and it was deduced that γ should have the values

$\gamma \simeq 110$ Low and medium (0.4)carbon steel.
$\simeq 230$ 0.7% carbon steel.

So high a value gives a dispersion of the rupture points of about 1%.

An examination* of the fragment weights from service bombs and shells shows that, for medium carbon steels, the fragmentation does not depend on whether the rupture is brittle (starting from the outer surface) or by shear. Thus γ must be roughly the same for either type of rupture.

In this section, then,we attempt a derivation of γ from the most general hypotheses; the method is an improvement of that given in para. 9 of AC.4035.

We have seen (para. 2) that in glass, where the fracture stress is determined by the largest of a comparatively small number of Griffith cracks, the values of the tensile stress show a large scatter (10%). In metals we shall assume that rupture, whether brittle or shear, starts at one of a much larger number of "singular points" of unspecified nature, distributed throughout the volume. Let N be the number of such points per unit volume; we may safely assume $N^{-1/3}$ to be of the order 10^{-3} - 10^{-5} cm. since distances of this order always occur in any analysis of the structure of the "real" crystal. It is not, of course, suggested that the same type of centre is responsible for both types of rupture.

Let c be some parameter specifying the size of the "singular points". For instance, if they were Griffith cracks, 2c would be the width of a crack (fig. 1). We shall assume that the values of c are distributed at random about some mean value c_0 according to the Gaussian distribution function; thus the number of points for which c lies between c and c + dc is

$$B\, dc\, \exp\left[-\frac{(c-c_0)^2}{2\tau^2}\right] \qquad (9)$$

where

$$B \int_0^\infty \exp\left[-\frac{(c-c_0)^2}{2\tau^2}\right] dc = N$$

We may expect the distribution to be fairly wide about the mean value; as a guess we shall put $2\tau^2 = c_0^2$ Then clearly

$$B = N/c_0 \times \text{factor of order unity}$$

Consider a tensile specimen of unit volume; then the largest "crack", or singular point, is the one that will cause rupture. The chance that for this "crack" the size/c will exceed the value c is

$$A \int_c^\infty \exp\left[-\frac{(c-c_0)^2}{c_0^2}\right] dc \qquad (10)$$

If we put this equal to unity we obtain an expression for the size of crack c_R actually responsible for rupture,

For values c in the neighbourhood of c_R we write

$$\frac{c-c_R}{c_R} = x,$$

so that, neglecting terms in x^2

$$\frac{(c-c_0)^2}{c_0^2} = \frac{(c_R-c_0)^2}{c_0^2} + \frac{2x\,c_R(c_R-c_0)}{c_0^2}$$

Thus (10) becomes

$$\frac{c_0^2 B}{2(c_R-c_0)} \exp\left[-\frac{(c_R-c_0)^2}{c_0^2}\right] \exp\left[-\frac{2x(c_R-c_0)c_R}{c_0^2}\right] \qquad (11)$$

* A.O.R.G. Memo. No.113 (Aug.1943).

When x vanishes this must be unity, which gives for c_R

$$\left(\frac{c_R - c_o}{c_o}\right)^2 = \log_e \frac{c_o^2 B}{2(c_R - c_o)}$$

Since $B \sim N/c_o$, and N is a very large number $(10^9 - 10^{15})$, we may write

$$\frac{c_R - c_o}{c_o} \simeq \sqrt{\log_e N} = \theta, \qquad \text{say (12)}$$

Also, the chance that the greatest crack is greater than c may from (11) be written

$$e^{\beta x}$$

$$\beta = \frac{2(c_R - c_o)c_R}{c_o^2}$$

by (12). $$= 2\theta(1+\theta)$$

Now let us assume the following relation between c, the size of the singular points, and P, the strain to rupture them

$$P = \text{const}/\, c^n .$$

Thus if the points were Griffith cracks we should have by formula (1) n = 1/2. Thus in the neighbourhood of the rupture point

$$\Delta P/P_F = -n\,\Delta c/c_R = -n x$$

Also let us assume the stress-strain relation (3), namely

$$P = P_1 + P_2 \log(1 + s),$$

so that

$$\Delta P = P_2 \frac{\Delta s}{1+s}$$

It follows that

$$\beta x = -\frac{\beta \Delta P}{P_F n} = -\frac{P_2 \beta \Delta s}{P_F n (1+s_R)}$$

where s_R is the strain at rupture. It follows that our parameter γ is given by

$$\gamma = \frac{P_2}{n P_F}\frac{\beta}{1+s_R} = \frac{2}{n}\frac{P_2}{P_F}\frac{\theta(1+\theta)}{1+s_R}$$

It will be seen that, in this formula, the only unknown quantities are n and θ; also that as θ^2 is equal to log N, the values does not depend much on the choice of N, the number of singular points per unit volume. We thus have reason to believe that γ might be of the same order, at any rate, for brittle and shear rupture.

Taking $N = 10^{15}$, and n = 1/2, as for Griffith cracks, we find $\theta = 5.85$ and

$$\gamma = 160\, P_2/P_F(1 + s_R)$$

Some values for the other constants have been deduced from some curves given by Korber and Rohland (loc.cit.,)

	Reduction in area R	True U.T.S.	P_2	γ (calc.)
Iron	.83	54	34	20
Steel 0.1 C	.70	70	42	42
0.13 C	.70	78	45	40
0.25 C	.63	80	45	53
0.45 C	.57	82	38	67
0.55 C	.50	87	39	69

The values of γ are somewhat too low, but in view of the very crude state of the theory the agreement may be considered satisfactory. The rise in γ with increasing carbon content is in agreement with observation.

5

A Theory of Fragmentation: Application to Wire Wound Bombs such as the American 20 lb, F.

N.F. Mott

(May, 1944), Ministry of Supply, A.C.6338

Summary. A theory of fragmentation of bomb and shell casings of ductile materials proposed by the present author in earlier reports is applied to the break-up of the helically wound coil of steel strip that forms part of the casing of this bomb. For this strip the break-up is one dimensional, and it is possible to formulate the theory in a much more exact form than for a solid case. The theory is restated in a form applicable to this bomb, and it is suggested that experiments with model bombs of this type would yield information of a fundamental nature about fracture of metals.

Distribution List

The initial distribution of copies was as follows:

Nos. 1–8	Ministry of Supply, S.R.7, for distribution as follows: (1) British Central Scientific Office, Washington (for U.S. Army, Navy and British Missions in Washington) (2) Office of Scientific Research and Development, U.S.A. (3) Inspector General, Ottawa, Canada (4) National Research Council, Canada (5) Australian Scientific Research Liaison Office (6) S.R.7 Technical Records. This copy is available on loan to South Africa and New Zealand, if required. (7) Dr. C. Zener, Watertown Arsenal (8) Dr. R.W. Gurney, Aberdeen Proving Ground
Nos. 9–51	Secretary, Fragmentation Panel of Static Detonation Committee
No. 52	Commandant, Military College of Science
No. 53	Royal Naval College
No. 54	C.S.P.D.E.
No. 55	D.S.R. (Admiralty)
Nos. 56–58	C.S.A.R. (Attention:- S.C.R., S.B.R., S.A.E.)
Nos. 59–60	U.S. Embassy (Attention:- Mr. Bennett Archambault)
No. 61	Brigadier Mackenzie
Nos. 62–63	Aberdeen Proving Ground (Attention:- Mr. R.H. Kent)

No. 64 A.R.D. Library
Nos. 65–66 Theoretical Research Branch Files

Further copies of this report can be obtained from Armament Research Department, (Branch for Theoretical Research), Fort Halstead, Sevanoaks, Kent.

5.1 Introduction

In several recent papers, [1–4], the present author has attempted a theory of the break-up of cylindrical bomb and shell cases of steel or other ductile materials. An exact mathematical theory can at present be given only for cases giving fragments of which the dimensions parallel to the axis of the cylinder are predetermined, either by grooves or for cases formed by wrapping wire or steel strip helically about thin inner tube. The theory is then able to make predictions about the lengths of the fragments of ring or strip that will be formed.

It would be extremely difficult to extend this one dimensional theory to the two dimensional break-up of a solid steel case in any rigorous way; in the author's reports on the subject a number of arbitrary assumptions were made, which do in fact give a fairly satisfactory method of estimating fragment weights of service bombs and shells. In the last section of this report these assumptions are reviewed.

The American 20 lb. fragmentation bomb has a helically wrapped coil of drawn steel strip around a thin inner tube. The fragmentation has been determined in [5], and fragments of strip of the form shown in Fig. 5.1 are obtained. The cross section, originally square, becomes rectangular owing to plastic extension, and fracture is by shear, fragments up to 1 inch long being obtained. There is no necking. The bomb is therefore ideally suited to the application of theory.

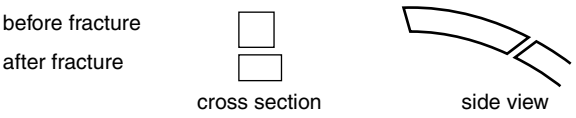

Fig. 5.1.

In this report the theory is restated so as to apply to this bomb, mainly in the hope that it will be possible to do experiments on model bombs of this type. From such experiments information of considerable value about the mechanism of fracture in metals could be obtained.

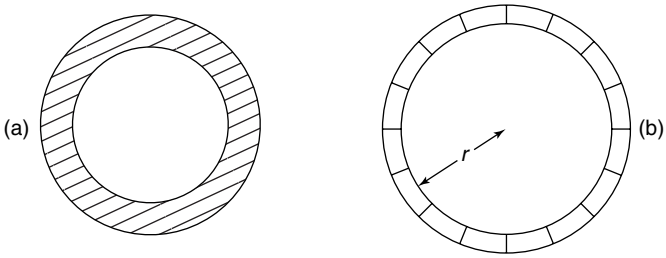

Fig. 5.2.

5.2 Mathematical Theory of Fragmentation

The problem can be stated in the following way: a ring (or helix) of some ductile material such as steel (Fig. 5.2a) is set in motion by the pressure of a detonating explosive acting on its inner surface, or by the pressure of a liner acted on by the explosive, and after a given amount of plastic flow it breaks up (Fig. 5.2b). We require to find the average length of fragment, and the distribution of fragment lengths.

The problem was solved in [2] by making the following assumptions about the process of fracture:

(a) That a crack, having once started, propagates itself instantaneously across the ring.

(b) That fracture does not take place at a definite value of the strain, but that there is a certain small scatter about a mean value. It was assumed that, as the strain increased from a value s to a value $s + ds$, the probability of a fracture occurring per unit length of specimen would be

$$Ae^{\gamma s}ds \tag{5.1}$$

The constants A and γ may depend on the area of the cross section of the specimen as well as on its composition and on the rate of strain[1]. The

[1] Using formula (5.1), the chance that the specimen of length l breaks before a strain s is reached is

$$p = 1 - \exp\left\{-\frac{A}{\gamma}e^{ys}\right\}$$

The average strain for fracture, s, is given by

$$\begin{aligned} s_o &= \int_0^\infty s\,\frac{dp}{ds}\,ds \\ &= \frac{1}{\gamma}\left\{\log_e\left(\frac{\gamma}{A}\right) + e\right\} \end{aligned}$$

where

$$\varepsilon = \int_{-\infty}^{\infty} x\; e^x \exp(-e^{-x})\; dx = -0.577$$

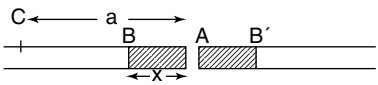

Fig. 5.3.

validity of these assumptions, and the numerical values of the constants, is discussed in para. 3.

If r is the radius of the case and V its velocity outwards, the rate of strain is V/r. We shall assume this to be constant while the case is breaking up; in other words, that the whole process is over before V/r has changed much. With this assumption, the problem is the same as that of calculating the break-up of an infinite length of straight wire in which the rate of strain is everywhere equal to V/r.

Suppose that such a wire breaks at a point A (Fig. 5.3). At a time t after fracture occurs a length x on each side of the fracture will be free from stress. Our first problem is to calculate the relation between x and t. This was done by the author [2] by an approximate method in which the velocity of sound in steel was taken to be large compared with all velocities concerned. The calculation is as follows: we take an arbitrary point C on the strip distant a from A, and axes of reference through C. Then relative to C the velocity of the stress-free region AB is

$$\frac{V}{r}\ (a-x)$$

If ρ is the density of the steel and Y its flow stress in tension at the moment just before fracture for the rates of strain concerned, then the equation of motion of AB is

$$Y = -\rho x \frac{d}{dt}\left\{(a-x)\frac{V}{r}\right\}$$

which gives, on integrating,

$$x^2/t = 2rY/\rho V \tag{5.2}$$

Lee [9] has given an exact solution for the motion of the boundary B based on the recently developed theory of plastic waves. He finds that it moves with the velocity c of sound in steel for a distance $2Yr/\rho cV$, then with one-third of this velocity for an equal distance, then with one-fifth of the velocity and so on. For distances exceeding $2Yr/\rho\ cV$, the two solutions give almost identical

The root-mean-square of the scatter about this value is

$$\left\{\int (s-s_o)^2 \frac{dp}{ds} ds\right\} = 1.28/\gamma$$

results (Fig. 5.7 of Dr. Lee's report)[2]. The results to be discussed below for the American 20 1b. bomb suggest that for steel the solution (5.2) should be adequate, though this may not be the case for other materials.

Using (5.1) and (5.2), the distribution of fragment lengths can be found as follows: Consider a length l of the wire. Suppose a crack forms at a given value of s; then when s has increased by Δs, by (5.2) a space on each side of it equal to

$$\frac{r}{V}\left(\frac{2Y}{\rho}\right)^{1/2}(\Delta s)^{1/2}$$

is safe from further cracking. If N is the number of fractures already formed, then by (5.1) the rate of increase of N is given by

$$\frac{dN}{ds} = Aple^{\gamma s}$$

where p is the proportion of the line where cracks can still form. It is convenient to introduce a new variable $\sigma = \gamma s$.

Then

$$\frac{dN}{d\sigma} = \frac{Ap}{\gamma} le^{\sigma} \tag{5.3}$$

and, if a fracture forms at a strain σ_1, the region round it on each side which is safe from cracking is at any subsequent value of σ

$$x_o(\sigma - \sigma_1)^{1/2} \tag{5.4}$$

where

$$x_o = (2Y/\rho\gamma)^{1/2} r/V \tag{5.5}$$

The distribution of fragment lengths was now found experimentally. A line was drawn on paper about 10 inches long and x_o taken to be $\frac{1}{2}$ in., it was assumed that a ratio of l/x_o of 20 would give approximately the same distribution as an infinite ratio. The first fracture could be taken to occur for a value σ_o of σ so that

$$\frac{Al}{\gamma} e^{\sigma_o} = 1 \ ,$$

and successive fractures after unit increments of dN , i.e. increments d of σ equal to

$$d\sigma = 1/pe^{(\sigma - \sigma_o)}$$

After each fracture was made, at a random position, the length round it and round previous fractures where plastic flow had stopped was marked off and the process repeated until fragmentation was complete. It was then repeated with a new line, until sufficient fragments were obtained to draw a histrogram. This is shown in Fig. 5.5.

[2] E. H. Lee reproduces this solution in his later review article on plastic wave propagation; see 1967 reference to Lee in Part I.

We see, therefore, that most of the fragments will have lengths between x_o and $2x_o$ where x_o is given by (5.5).

It will be seen that the distribution is very unlike the Poisson distribution function $ce^{-x/x_o}dx$, which would give the numbers of fragments with lengths between x and $x + dx$ for purely random fracture.

The changes made by the use of Lee's more accurate solution for the release of stress after a fracture will be small if $2Yr/\rho\, cV$ is less than x_o and thus if

$$\gamma < \frac{1}{2}\frac{E}{Y} \sim 100$$

where E is Young's modulus.

Comparison with experiment for the American 20 lb. F. bomb, at any rate, suggests that this is the case.

5.3 The Value of γ

Formula (5.5) shows the way in which the average fragment length depends on the velocity and radius of the case at the moment of break-up (as r/V) and also on the constants Y and ρ of the material of the case. We now have to discuss how γ will depend on the material and cross section of the wire.

A tentative theory of the constant γ was given by the author in [4] and [6]. As so little is known of the fundamental cause of fracture in ductile metals the theory was based on a number of assumptions which may or may not be correct. In this report we shall make assumptions as general as possible in order to obtain

(a) The dependence of γ on the cross section of the specimen
(b) The dependence on the stress-strain curve

We assume that fracture starts at one of a number of weak places within the material; and that, per unit volume, the number of these which will start a fracture when the maximum principal stress is between S and $S + dS$ is

$$Ae^{cS}dS$$

Reasons for expecting the exponential form are given in the references quoted. Fracture for a specimen of volume V will normally take place when

$$\int_0^S AV \exp(cS)\, dS = 1$$

If we therefore set

$$(VA/c) \exp(cS_1) = 1 \tag{5.6}$$

the chance that fracture will take place when S is in the range dS is

$$\exp\left[c\left(S - S_1\right)\right] dS/c$$

If the relationship between stress and strain is of the form

$$S = f\left(s\right) \ ,$$

then the chance that a fracture will occur when s increases by ds is

$$\exp\left[cf'\left(s_1\right)\left(s - s_1\right)\right] f'\left(s\right) ds/c$$

and thus we have for γ

$$\gamma = cf'\left(s_1\right)$$

where s_1 is the average strain for fracture. If the stress-strain curve is of the form suggested by Bridgman and others

$$f\left(s\right) = P_1 + P_2 \log\left(1 + s\right) \ , \tag{5.7}$$

we have

$$\gamma = CP_2/\left(1 + s_1\right) \tag{5.8}$$

It will be seen that the only term in (5.8) which depends on the volume is s_1. A short calculation using (5.6) shows that

$$V\frac{dy}{dV} = \frac{1}{1 + s_1}$$

and since γ itself is probably equal to 10 at least, and $1 + s$ of the order 2, we see that the variation with volume is likely to be of the form

$$y \sim 10 + \frac{1}{2}\log_e V \qquad \text{(V in c.c.)}$$

so that the dependence on V is small.[3]

Formula (5.7) also enables a comparison to be made between the dispersion of R. of A. to be expected in the brittle fracture of a ring or helix round a bomb,

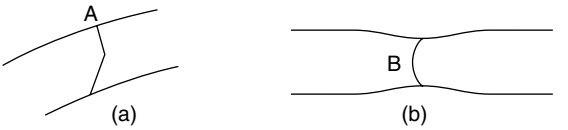

Fig. 5.4.

and in the tensile test of a material. In the former fracture will begin at A on the outside of the shell case (Fig. 5.4a) where the stress is purely radial;

[3] For a comparable treatment of brittle materials compare [11].

in the latter it will begin on the axis of the specimen in a region of triaxial stress (B in Fig. 5.4b). According to current ideas [6] the maximum principal stress determines fracture, and the effect of radial stress in the neck is to enable a larger longitudinal stress to exist without causing flow. Thus, owing to the necking, the longitudinal stress on the axis increases more rapidly with strain than it should according to formula (5.7). γ will therefore be larger (dispersion smaller) in tensile tests than bombs. According to the analyses in a neck given by Bridgman [10], however, the stress on the axis of a necked specimen is likely to be not more than 30 per cent greater than the mean stress across the neck, and thus, unless P_2 is much smaller for high rates of strain than in tensile tests (less work-hardening) we expect a change of γ only of this order. The dispersion of the reduction of area in tensile tests will thus give us the order of magnitude of γ.

It must be pointed out that the theory of fragmentation given here is only applicable if a crack, once it has started on the outside of the specimen, travels at once right through it. It has been pointed out in [4] and [6] that this will happen in some steels of a notch brittle type and not in others.

There is no theoretical reason to believe that γ will have the same value when fracture is by shear as when it is of brittle type. It is by shear in the bomb considered below. The dispersion of the stress or strain at fracture in static tension tests would give an independent value of γ for shear fracture.

5.4 Comparison with the Fragmentation of the American 20 lb. F. Bomb

Fracture with this bomb is by shear and there is no necking.

Figure 5.5 shows the experimental length distribution fitted to the theoretical, a value of x_o of 0.44 in. giving the best fit.

γ was calculated from formula (5.5) to be equal to 12, using the above value of x_o and the following values of the other constants

$$V = 2,000 \text{ ft./sec.}$$
$$Y = 100 \text{ tons/sq. in.}$$
$$r = 2.07 \text{ inches.}$$

V, since it refers to the velocity at the moment of break-up, has been taken slightly smaller than the observed fragment velocity 2890 ft./sec.

Y, the stress at fracture at this high rate of strain might be anything between, say, 80 and 150 tons/sq. in.; the value of γ obtained may thus be in error by up to 50 per cent.

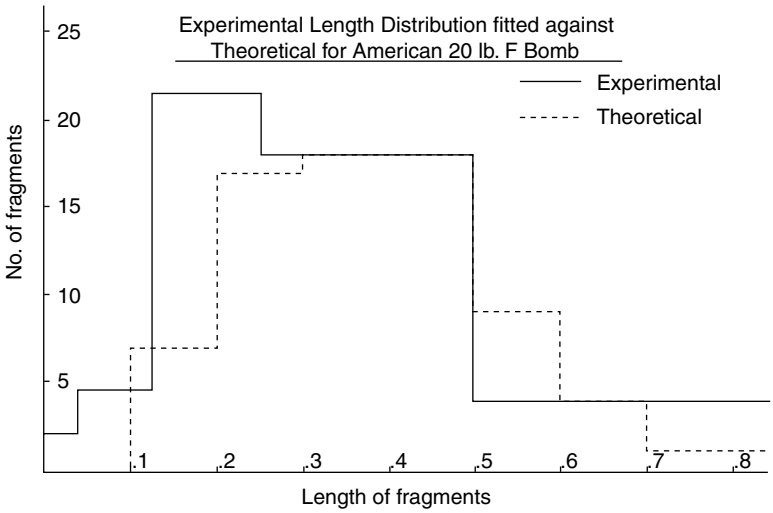

Fig. 5.5.

5.5 Suggestions for Experimental Work

The first prediction of the theory that needs to be verified is that for given V and r the cross section of the wire makes little difference to the fragment length, but that for very thin wire a small increase in the fragment length will occur. This could be tested by winding casings of cylindrical model bombs with wires of different thicknesses, keeping the total weight of casing constant. It might be best to wind thick and thin wire round the same bomb.

Secondly, measurements should be made of the dependence of the fragment length on composition of the steel strip.

Finally, the theoretical result that for given wire the fragment length is proportional to r/V should be tested by using model bombs of different diameters and charge-weight ratios.

It would also be of interest to try to determine γ from the dispersion in the values of the reduction in area at which fracture occurs in tensile or torsion tests; as shown above, values obtained by this method should be only slightly greater than for bomb casings.

5.6 Connection of the Theory with the Fragmentation of a Solid Casing

Certain features of the theory can obviously be extended to the break-up of a solid cylindrical casing; thus the same general arguments show that the lengths and breadths of fragments should depend only on the value of r/V at the moment of break-up and on the properties of the steel at that moment,

and that they will be independent of the thickness of the case except insofar as this affects V.

Values of γ deduced from the steel strip of the American 20 lb. F bomb are considerably smaller than those deduced for solid cases, assuming that the breadth of each fragment is the same as it would be for a thin strip [2]. It is probable that this assumption is not correct.

The considerations of this paper do no affect the attempts made in a number of reports (2 and 3) to develop a semi-empirical set of rules for the prediction of the fragmentation of service bombs and shells. The above considerations show that the average fragment weight must be proportional to

$$t(r/V)^s \tag{5.9}$$

where t is the thickness of the case and s a constant, for which the values 2 and 4/3 have been tried. Some reasons were given in [2] for considering $s = 2$ the most probable value, but $s = 4/3$ gave a rather better fit. Since V is the velocity of the case at the moment of break-up, not the observed fragment velocity, its value was calculated from G.I. Taylor's theory of the expansion of the case of a long cylindrical bomb.

In the reports quoted the formula

$$e^{-M/M_A} \qquad M = m^{1/2} \tag{5.10}$$

was used for the proportion of fragments with weight greater than m. A formula of this type frequently represents the weights of solids broken up at random; however it is doubtful whether it can be said to have any theoretical justification for the fragmentation of shell casings, since the one dimensional break-up discussed in para. 2 does not give a Poisson distribution. Actually an alternative formula due to Payman [7] gives a rather better fit. According to this formula the proportion by weight of the case that fragments into pieces greater than m is

$$e^{-\alpha m} \tag{5.11}$$

Either formula can be combined with (5.6) by equating the average weight,

$$M_A^2 \text{ or } 1/\alpha \quad \text{to} \quad \text{const. } t(r/V)^s$$

the constant being supposed to depend on the properties of the steel only.

References

[1] A Theory of Fragmentation by N.F. Mott and E.H. Linfoot, D.S.R. Extra-mural Report A.C. 3348.
[2] A Theory of Fragmentation of Shells and Bombs by N.F. Mott, A.C. 4035.
[3] Fragmentation of Service Bombs and Shells, A.O.R.G. Memo. No. 113.
[4] Fragmentation of Shell Casings and the Theory of Rupture in Metals, A.C. 4613.

[5] Fragmentation of American 20 lb. F. bomb, Type M. 41, A.R.D. Explosives Report 363/43, A.C. 5105.
[6] The Theory of Fracture in Ductile Metals by N.F. Mott, A.R.D. Theoretical Research Report No. 4/43.
[7] Cased Charges XXI by W. Payman, A.C. 4604, SP/FP. 137, R.C. 388.
[8] Analysis of the Expansion of a Cylindrical Bomb Casing by G.I. Taylor, R.C. 197.
[9] E.H. Lee. A.R.D. Theoretical Research Report No. 6/43.
[10] Tensile Tosts on Steel under High Pressure by P.W. Bridgman. R.D.R.C. Armor and Ordnance Report A. 218, S.R. 7/43/1025.
[11] A statistical theory of the Brittle Strength of Real Crystals by T. Kontorova and J. Frenkel. J. Tech. Physics U.S.S.R. Vol. 11, p. 174, 1941 (translated by S.R. 7, Technical Records No. 13).

Facsimiles of N.F. Mott: A Theory of Fragmentation: Application to Wire Wound Bombs such as the American 20 lb, F.

UNCLASSIFIED ~~RESTRICTED~~ ~~SECRET~~ E13 7/11/90

Copy No. 2

A.C.6338
SD/FP.240

MINISTRY OF SUPPLY

ADVISORY COUNCIL ON SCIENTIFIC RESEARCH AND TECHNICAL DEVELOPMENT

FRAGMENTATION PANEL OF THE STATIC DETONATION COMMITTEE

A theory of fragmentation.
Application to wire wound bombs such as the American 20 lb. F.

by

N.F. Mott

Communicated by C.S.A.R.

Theoretical Research Report No.8/44.
January, 1944.

Received
May 17th, 1944.

MHH.

~~SECRET~~ RESTRICTED (Grade reduced from Lord No 5)

Armament Research Department

THEORETICAL RESEARCH REPORT NO. 8/44

A Theory of Fragmentation

Application to wire wound bombs such as the American 20 lb. F.

by

M.F. Mott

Branch for Theoretical Research,
Fort Halstead, Kent.

January, 1944.
Copy No. 25

Summary

A theory of fragmentation of bomb and shell casings of ductile materials proposed by the present author in earlier reports is applied to the break-up of the helically wound coil of steel strip that forms part of the casing of this bomb. For this strip the break-up is one dimensional, and it is possible to formulate the theory in a much more exact form than for a solid case. The theory is restated in a form applicable to this bomb, and it is suggested that experiments with model bombs of this type would yield information of a fundamental nature about fracture of metals.

Distribution List

The initial distribution of copies was as follows:-

Nos.1-8 Ministry of Supply, S.R.7, for distribution as follows:
- (1) British Central Scientific Office, Washington (for U.S. Army, Navy and British Missions in Washington)
- (2) Office of Scientific Research and Development, U.S.A.
- (3) Inspector General, Ottawa, Canada
- (4) National Research Council, Canada
- (5) Australian Scientific Research Liaison Office
- (6) S.R.7 Technical Records. This copy is available on loan to South Africa and New Zealand, if required.
- (7) Dr. C. Zener, Watertown Arsenal
- (8) Dr. R.W. Gurney, Aberdeen Proving Ground

Nos.9-51 Secretary, Fragmentation Panel of Static Detonation Committee

No.52 Commandant, Military College of Science

No.53 Royal Naval College

No.54 C.S.P.D.E.

No.55 D.S.R. (Admiralty)

Nos.56-58 C.S.A.R. (Attention:- S.C.R., S.B.R., S.A.E.)

Nos.59-60 U.S. Embassy (Attention:- Mr. Bennett Archambault)

No.61 Brigadier Mackenzie

Nos.62-63 Aberdeen Proving Ground (Attention:- Mr. R.H. Kent)

No.64 A.R.D. Library

Nos.65-66 Theoretical Research Branch Files

Further copies of this report can be obtained from

Armament Research Department,
(Branch for Theoretical Research),
Fort Halstead,
Sevenoaks, Kent.

Introduction

In several recent papers, refs.1 - 4, the present author has attempted a theory of the break-up of cylindrical bomb and shell cases of steel or other ductile materials. An exact mathematical theory can at present be given only for cases giving fragments of which the dimensions parallel to the axis of the cylinder are predetermined, either by grooves or for cases formed by wrapping wire or steel strip helically about thin inner tube. The theory is then able to make predictions about the lengths of the fragments of ring or strip that will be formed.

It would be extremely difficult to extend this one dimensional theory to the two dimensional break-up of a solid steel case in any rigorous way; in the author's reports on the subject a number of arbitrary assumptions were made, which do in fact give a fairly satisfactory method of estimating fragment weights of service bombs and shells. In the last section of this report these assumptions are reviewed.

The American 20 lb. fragmentation bomb has a helically wrapped coil of drawn steel strip around a thin inner tube. The fragmentation has been determined in ref.5, and fragments of strip of the form shown in Fig.1 are obtained. The cross section, originally square, becomes rectangular owing to plastic extension, and fracture

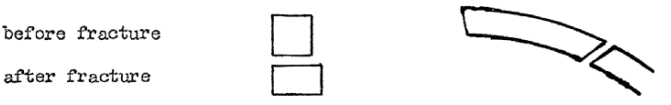

Fig.1

is by shear, fragments up to 1 inch long being obtained. There is no necking. The bomb is therefore ideally suited to the application of theory.

In this report the theory is restated so as to apply to this bomb, mainly in the hope that it will be possible to do experiments on model bombs of this type. From such experiments information of considerable value about the mechanism of fracture in metals could be obtained.

2. Mathematical Theory of Fragmentation

The problem can be stated in the following way:

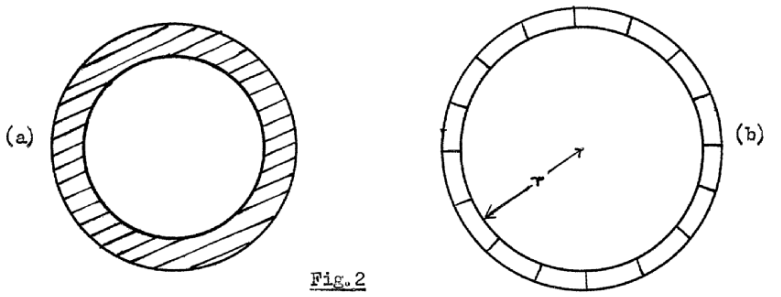

Fig.2

a ring (or helix) of some ductile material such as steel (Fig.2a) is set in motion by the pressure of a detonating explosive acting on its inner surface, or by the pressure of a liner acted on by the explosive, and after a given amount of plastic flow it breaks up (Fig.2b). We require to find the average length of fragment, and the distribution of fragment lengths.

The problem was solved in ref.2 by making the following assumptions about the process of fracture:

(a) That a crack, having once started, propagates itself instantaneously across the ring.

(b) That fracture does not take place at a definite value of the strain, but that there is a certain small scatter about a mean value. It was assumed that, as the strain increased from a value s to a value s + ds, the probability of a fracture occurring per unit length of specimen would be

$$Ae^{\gamma s}\ ds \qquad (1)$$

The constants A and γ may depend on the area of the cross section of the specimen as well as on its composition and on the rate of strain.* The validity of these assumptions, and the numerical values of the constants, is discussed in para. 3.

If r is the radius of the case and V its velocity outwards, the rate of strain is V/r. We shall assume this to be constant while the case is breaking up; in other words, that the whole process is over before V/r has changed much. With this assumption, the problem is the same as that of calculating the break-up of an infinite length of straight wire in which the rate of strain is everywhere equal to V/r.

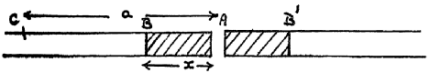

Fig. 3

Suppose that such a wire breaks at a point A (Fig. 3). At a time t after fracture occurs a length x on each side of the fracture will be free from stress. Our first problem is to calculate the relation between x and t. This was done by the author (ref. 2) by an approximate method in which the velocity of sound in steel was taken to be large compared with all velocities concerned. The calculation is as follows: we take an arbitrary point C on the strip distant a from A, and axes of reference through C. Then relative to C the velocity of the stress-free region AB is

$$\frac{V}{r}\ (a - x)$$

If ρ is the density of the steel and Y its flow stress in tension at the moment just before fracture for the rates of strain concerned, then the equation of motion of AB is

$$Y = -\rho x \frac{d}{dt}\left\{(a - x)\frac{V}{r}\right\}$$

which gives, on integrating,

$$x^2/t = 2\,r\,Y/\rho V \qquad (2)$$

---

* Using formula (1), the chance that the specimen of length l breaks before a strain s is reached is

$$p = 1 - \exp\left\{-\frac{A}{\gamma}\,e^{\gamma s}\right\}$$

The average strain for fracture, s_0, is given by

$$s_0 = \int_0^\infty s\,\frac{dp}{ds}\,ds = \frac{1}{\gamma}\left\{\log_e\left(\frac{\gamma}{A}\right) + e\right\}$$

where

$$e = \int_{-\infty}^{\infty} x\,e^{x}\exp\left(-e^{-x}\right)dx = -0.577$$

The root-mean-square of the scatter about this value is

$$\left\{\int (s - s_0)^2\,\frac{dp}{ds}\,ds\right\} = 1.28/\gamma$$

Lee (ref.9) has given an exact solution for the motion of the boundary B based on the recently developed theory of plastic waves. He finds that it moves with the velocity c of sound in steel for a distance $2Yr/\rho cV$, then with one-third of this velocity for an equal distance, then with one-fifth of the velocity and so on. For distances exceeding $2Yr/\rho cV$, the two solutions give almost identical results (fig.7 of Dr. Lee's report). The results to be discussed below for the American 20 lb. bomb suggest that for steel the solution (2) should be adequate, though this may not be the case for other materials.

Using equations (1) and (2), the distribution of fragment lengths can be found as follows: Consider a length ℓ of the wire. Suppose a crack forms at a given value of s; then when s has increased by Δs, by (2) a space on each side of it equal to

$$\frac{r}{V}\left(\frac{2Y}{\rho}\right)^{\frac{1}{2}} (\Delta s)^{\frac{1}{2}}$$

is safe from further cracking. If N is the number of fractures already formed, then by (1) the rate of increase of N is given by

$$\frac{dN}{ds} = A\, p\, \ell\, e^{ys}$$

where p is the proportion of the line where cracks can still form. It is convenient to introduce a new variable $\sigma = ys$.

Then

$$\frac{dN}{d\sigma} = \frac{Ap}{y}\, \ell\, e^{\sigma} \qquad (3)$$

and, if a fracture forms at a strain σ_1, the region round it on each side which is safe from cracking is at any subsequent value of σ

$$x_0\, (\sigma - \sigma_1)^{\frac{1}{2}} \qquad (4)$$

where

$$x_0 = (2Y/\rho y)^{\frac{1}{2}}\, r/V \qquad (5)$$

The distribution of fragment lengths was now found experimentally. A line was drawn on paper about 10 inches long and x_0 taken to be $\frac{1}{2}$ in., it was assumed that a ratio of ℓ/x_0 of 20 would give approximately the same distribution as an infinite ratio. The first fracture could be taken to occur for a value σ_0 of σ so that

$$\frac{A\ell}{y}\, e^{\sigma_0} = 1,$$

and successive fractures after unit increments of dN, i.e. increments $d\sigma$ of σ equal to

$$d\sigma = 1/pe^{(\sigma - \sigma_0)}$$

After each fracture was made, at a random position, the length round it and round previous fractures where plastic flow had stopped was marked off and the process repeated until fragmentation was complete. It was then repeated with a new line, until sufficient fragments were obtained to draw a histrogram. This is shown in Fig.5.

We see, therefore, that most of the fragments will have lengths between x_0 and $2x_0$ where x_0 is given by (5).

It will be seen that the distribution is very unlike the Poisson distribution function $ce^{-x/x_0}\, dx$, which would give the numbers of fragments with lengths between x and $x + dx$ for purely random fracture.

The changes made by the use of Lee's more accurate solution for the release of stress after a fracture will be small if $2Yr/\rho cV$ is less than x_0 and thus if

$$\gamma < \tfrac{1}{2}\frac{E}{Y} \sim 100$$

where E is Young's modulus.

Comparison with experiment for the American 20 lb. F. bomb, at any rate, suggests that this is the case.

3. The value of γ

Formula (5) shows the way in which the average fragment length depends on the velocity and radius of the case at the moment of breaking (as r/γ), and also on the constants Y and ρ of the material of the case. We have now to discuss how γ will depend on the material and cross section of the wire.

A tentative theory of the constant γ was given by the author in refs. 4 and 6. As so little is known of the fundamental cause of fracture in ductile metals the theory was based on a number of assumptions which may or may not be correct. In this report we shall make assumptions as general as possible in order to obtain

(a) The dependence of γ on the cross section of the specimen.

(b) The dependence on the stress-strain curve.

We assume that fracture starts at one of a number of weak planes within the material; and that, per unit volume, the number of these which will start a fracture when the maximum principal stress is between S and S + dS is

$$Ae^{cS}\, dS$$

Reasons for expecting the exponential form are given in the references quoted. Fracture for a specimen of volume V will normally take place when

$$\int_0^S AV \exp(cS)\, dS = 1$$

If we therefore set

$$(VA/c)\exp(cS_1) = 1 \qquad (6)$$

the chance that fracture will take place when S is in the range dS is

$$\exp(c(S-S_1))\, dS/c$$

If the relation between stress and strain is of the form

$$S = f(s),$$

then the chance that a fracture will occur when s increases by ds is

$$\exp\left\{c f'(s_1)(s - s_1)\right\} f'(s)\, ds/c$$

and thus we have for γ

$$\gamma = cf'(s_1)$$

where s_1 is the average strain for fracture. If the stress-strain curve is of the form suggested by Bridgman and others,

$$f(s) = F_1 + F_2 \log(1 + s), \qquad (7)$$

we have

$$\gamma = cF_2/(1 + s_1), \qquad (8)$$

It will be seen that the only term in (8) which depends on the wall is s_1. A short calculation using (6) shows that

$$V\frac{d\gamma}{dV} = \frac{\gamma}{1 + s_1}$$

and since γ itself is probably equal to 10 at least, and $1 + s$ of the order 2. we see that the variation with volume is likely to be of the form

$$\gamma \sim 10 + \tfrac{1}{2} \log_e V \qquad (V \text{ in c.c.})$$

so that the dependence on volume is small.*

Formula (7) also enables a comparison to be made between the dispersion of R. of A. to be expected in the brittle fracture of a ring or helix round a bomb,

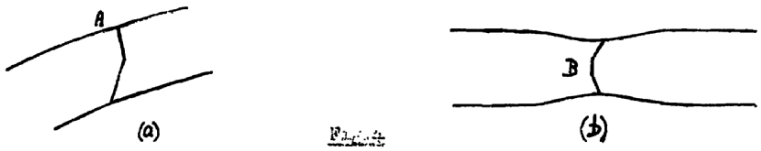

Fig.4

and in the tensile test of a material. In the former fracture will begin at A on the outside of the shell case (Fig.4(a)) where the stress is purely radial; in the latter it will begin on the axis of the specimen in a region of triaxial stress (B in Fig.4(b)). According to current ideas (Ref. 5) the maximum principal stress determines fracture, and the effect of the radial stress in the neck is to enable a larger longitudinal stress to exist without causing flow. Thus, owing to the necking, the longitudinal stress on the axis increases more rapidly with strain than it should according to formula (7). γ will therefore be larger (dispersion smaller) in tensile tests than in bombs. According to the analysis of the stresses in a neck given by Bridgman (Ref. 10), however, the stress on the axis of a necked specimen is likely to be not more than 30 per cent. greater than the mean stress across the neck, and thus, unless P_2 is much smaller for high rates of strain than in tensile tests (less work-hardening) we expect a change of γ only of this order. The dispersion of the reduction of area in tensile tests will thus give us the order of magnitude of γ.

It must be pointed out that the theory of fragmentation given here is only applicable if a crack, once it has started on the outside of the specimen, travels at once right through it. It has been pointed out in refs. (4) and (6) that this will happen in some steels of a notch brittle type and not in others.

There is no theoretical reason to believe that γ will have the same value when fracture is by shear as when it is of brittle type. It is by shear in the bomb considered below. The dispersion of the stress or strain at fracture in static torsion tests would give an independent value of γ for shear fracture.

4. Comparison with the fragmentation of the American 20 lb. F. bomb

Fracture with this bomb is by shear and there is no necking.

Fig(5) shows the experimental length distribution fitted to the theoretical, a value of x_0 of 0.44 in. giving the best fit.

γ was calculated from formula (5) to be equal to 12, using the above value of x_0 and the following values of the other constants

V = 2,800 ft./sec.

T = 100 tons/sq.in.

ρ = 2.07 inches.

---

* For a comparable treatment of brittle materials, compare ref.11.

V, since it refers to the velocity at the moment of break-up, has been taken slightly smaller than the observed fragment velocity 2890 ft./sec..

Y, the stress at fracture at this high rate of strain might be anything between, say, 80 and 150 tons/sq.in.; the value of y obtained may thus be in error by up to 50 per cent..

5. Suggestions for experimental work

The first prediction of the theory that needs to be verified is that for given V and r the cross section of the wire makes little difference to the fragment length, but that for very thin wire a small increase in the fragment length will occur. This could be tested by winding casings of cylindrical model bombs with wires of different thicknesses, keeping the total weight of casing constant. It might be best to wind thick and thin wire round the same bomb.

Secondly, measurements should be made of the dependence of the fragment length on composition of the steel strip.

Finally, the theoretical result that for given wire the fragment length is proportional to r/V should be tested by using model bombs of different diameters and charge-weight ratios.

It would also be of interest to try to determine γ from the dispersion in the values of the reduction in area at which fracture occurs in tensile or torsion tests; as shown above, values obtained by this method should be only slightly greater than for bomb casings.

6. Connection of the theory with the fragmentation of a solid casing

Certain features of the theory can obviously be extended to the break-up of a solid cylindrical casing; thus the same general arguments show that the lengths and breadths of fragments should depend only on the value of r/V at the moment of break-up and on the properties of the steel at that moment, and that they will be independent of the thickness of the case except insofar as this affects V.

Values of y deduced from the steel strip of the American 20 lb. F bomb are considerably smaller than those deduced for solid cases, assuming that the breadth of each fragment is the same as it would be for a thin strip (ref. 2). It is probable that this assumption is not correct.

The considerations of this paper do not affect the attempts made in a number of reports (2 and 3) to develop a semi-empirical set of rules for the prediction of the fragmentation of service bombs and shells. The above considerations show that the average fragment weight must be proportional to

$$t(r/V)^s \qquad (9)$$

where t is the thickness of the case and s a constant, for which the values 2 and 4/3 have been tried. Some reasons were given in ref. 2 for considering s = 2 the most probable value, but s = 4/3 gave a rather better fit. Since V is the velocity of the case at the moment of break-up, not the observed fragment velocity, its value was calculated from G.I. Taylor's theory of the expansion of the case of a long cylindrical bomb.

In the reports quoted the formula

$$e^{-M/M_A} \qquad M = m^{\frac{1}{2}} \qquad (10)$$

was used for the proportion of fragments with weight greater than m. A formula of this type frequently represents the weights of solids broken up at random; however it is doubtful whether it can be said to have any theoretical justification for the fragmentation of shell casings, since the one dimensional break-up discussed in para.2 does not give a Poisson distribution. Actually an alternative formula due to Payman (ref.7) gives a rather better fit. According to this formula the proportion by weight of the case that fragments into pieces greater than m is

$$e^{-\alpha m} \qquad (11)$$

Either formula can be combined with (6) by equating the average weight,

$$M^2_A \text{ or } 1/a \quad \text{to} \quad \text{const. } t(r/V)^{\delta}$$

the constant being supposed to depend on the properties of the steel only.

Fig. 5

Experimental Length Distribution fitted against Theoretical for American 20 lb. F Bomb

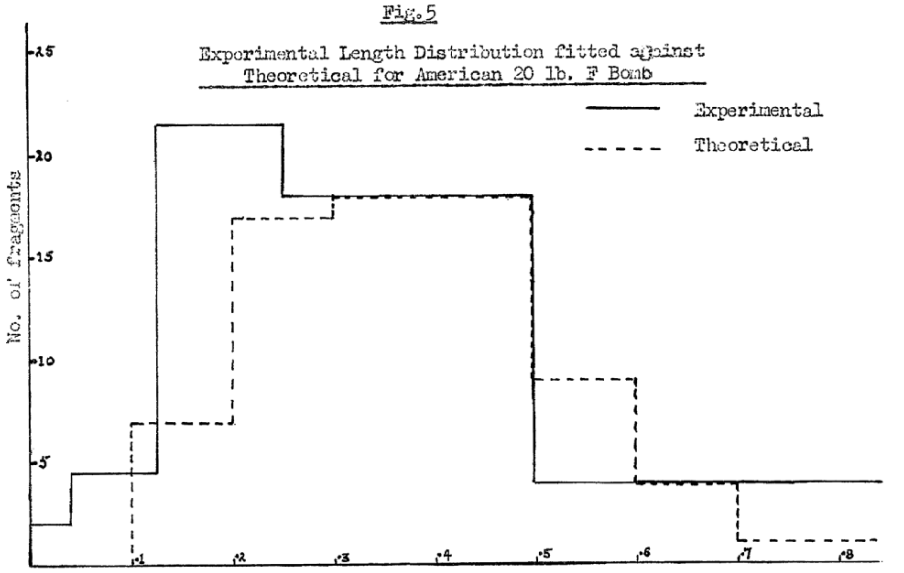

References

(1) A Theory of Fragmentation by N.F. Mott and E.H. Linfoot, D.S.R. Extra-mural Report A.C.3348.

(2) A Theory of Fragmentation of Shells and Bombs by N.F. Mott, A.C.4035.

(3) Fragmentation of Service Bombs and Shells, A.C.R.C. Memo. No113.

(4) Fragmentation of Shell Casings and the Theory of Rupture in Metals. A.C.4613.

(5) Fragmentation of American 20 lb. F bomb, Type M.41, A.R.D. Explosives Report 363/43, A.C.5105.

(6) The Theory of Fracture in Ductile Metals by N.F. Mott, A.R.D. Theoretical Research Report No. 4/43.

(7) Cased Charges XXI by W. Payman, A.C.4604, SP/TP.137, R.C.388

(8) Analysis of the Expansion of a Cylindrical Bomb Casing by G.I. Taylor, R.C.197.

(9) E.H. Lee. A.R.D. Theoretical Research Report No.6/43.

(10) Tensile Tests on Steel under High Pressure by P.W. Bridgman. N.D.R.C. Armor and Ordnance Report A.218, S.R.7/43/1025.

(11) A statistical theory of the Brittle Strength of Real Crystals by T. Kontorova and J. Frenkel. J. Tech. Physics U.S.S.R. Vol.11, p.174, 1941 (translated by S.R.7, Technical Records No.13).

6

Fragmentation of Service Projectiles

N.F. Mott, J.H. Wilkinson, and T.H. Wise

(December, 1944), Ministry of Supply, A.C.6338

Summary. In previous reports, formulae have been given by means of which the fragment weight distribution could be deduced from the design of the shell. The derivation of these formulæ can be divided into two parts, as follows:

(1) It is assumed that the distance between fractures on the surface of the shell casing depends only on the rate of strain at the moment of fracture, and thus on r/v, where r is the radius and v the velocity of the case at this moment.
(2) The theory of plastic waves is used to deduce what function of r/v this distance should be, and a formula for the average weight is thereby deduced.

An attempt at a rigorous application of the plastic wave theory can only be made for wire-wound or ring bombs, where the one dimensional break-up of a long strip has to be considered. For solid casings, therefore, in this report the assumption (1) above is maintained, and the best function of r/v to fit the experimental data is determined empirically. The investigation confirms a theoretical formula already given, formula (6.8) of this report, as giving, satisfactorily, the fragment weight distribution of Service shells.

In order to test the dependence of fragment weight distribution on r/v, values had to be estimated for the velocity of the case. It is suggested that this is to be associated with the mode of the curve plotting number of fragments against velocity.

Distribution List

The initial distribution of copies was as follows:

Nos. 1–10 Ministry of Supply, S.R. 7, for distribution as follows:

(1)	British Central Scientific Office, Washington, (for U.S. Army, Navy and British Missions in Washington)
(2)	Office of Scientific Research and Development, U.S.A.
(3)	National Research Council, Canada
(5)–(6)	Canadian Military Headquarters
(7)	Australian Scientific Research and Development

(8)	New Zealand Government Offices
(9)–(10)	S.R. 7 Technical Records (These copies are available on loan to South Africa and New Zealand, if required)
Nos. 11–60	Secretary, Scientific Advisory Council (Attention: Fragmentation Panel)
Nos. 61–62	Secretary, Ordnance Board
No. 63	Military College of Science
No. 64	Royal Naval College
No. 65	D.S.R. (Admiralty)
No. 66	A.O.R.G.
No. 67	C.S.P.D.E.
Nos. 68–69	C.S.A.R. (Attention: S.S.R. (A), S.A.E.)
Nos. 70–71	U.S. Embassy (Attention: Mr. Bennett Archambault)
Nos. 72–73	U.S. Embassy (Attention: Naval Attaché)
No. 74	Brigadier Mackenzie
No. 75	Aberdeen Proving Ground (Attention: Mr. R.H. Kent)
Nos. 76–77	Ordnance Technical Division (Attention: Dr. Marston Morse)
No. 78	Dr. Payman
No. 79	Professor L. Rosenhead (P.D.E.)
No. 80	A.R.D. Library
No. 81	Explosives Branch Records Section
Nos. 82–83	Theoretical Research Branch Files

Further copies can be obtained from Armament Research Department, (Branch for Theoretical Research), Fort Halstead, Sevenoaks, Kent.

6.1 Introduction

A series of reports has been issued, dealing with the theory of the break-up of shell and bomb casings. The aim of such theories is to attempt to predict the fragment weight distribution in terms of the design of the projectile, type of explosive and properties of the steel case. In [1], a fairly complete theory was given for a long cylindrical wire-wound bomb; the theory predicts the length distribution of the fragments of the wire casing in terms of one unknown parameter depending on the steel, and seems in fair accord with the small amount of experimental evidence available. Earlier attempts to obtain a theory of the break-up of solid casings contain some arbitrary assumptions, and it seems worth while to re-examine the experimental data from a partly theoretical, partly empirical point of view.

The assumptions made in this report are as follows:

(a) The fragment weight distribution is taken to be given by either Payman's formula [2] or that due to Welch, as modified by Mott and Linfoot [3]. These are to be regarded as empirical. The formulae are

(i) The proportion p by weight of the case breaking into fragments greater than w is given by

$$\log_{10} p = -cw \tag{6.1}$$

(ii) The number of fragments in any random sample with weights between w and $w + dw$ is

$$B \exp(-M/M_A) dM \qquad M = w^{1/2} \tag{6.2}$$

Either $1/c$ or M_A^2 may be regarded as proportional to the *average fragment weight* and it is the purpose of this report to relate this to the design of the projectile.

Consider now the fragmentation of a very long cylindrical case. We make the following assumptions:

(i) After the usual plastic expansion, fracture occurs on any circumference of the cylinder when the external radius is r and velocity of the outside of the casing v_c, and all the cracks which ultimately lead to fracture occur during a time interval so short that r does not change appreciably.
(ii) Fracture starts from the outside of the casing.

Neither assumption is necessarily true in general; the considerable and fairly uniform thinning of fragments, suggests that (i) is often valid. (ii) may not be the case when fracture is by shear, but is probably correct if fracture is partly tensile; the hoop stress is a maximum on the outside of the case.

If these assumptions are valid, the distance between cracks must depend only on the rate of strain of the metal on the surface of the case at the moment of fracture, and also on the properties of the metal. The rate of strain is equal to v_c/r. Thus the area of the external surface of a typical fragment must be a function of r/v_c. The weight of the average fragment, divided by the thickness t, will therefore be a function of r/v_c. Thus, if we take M_A^2 as our measure of the average weight, we may write

$$M_A/\sqrt{t} = f(r/v_c) \tag{6.3}$$

We shall make a further assumption, namely, that for a given steel the percentage expansion before fracture is constant. Then, in (6.3), we may take r and t to refer to the dimensions of the case before detonation.

In this report, we examine the fragmentation of Service projectiles in relation to (6.3). We plot $\log(M_A/\sqrt{t})$ against $\log(r/v_c)$. The possibility of obtaining a smooth curve depends upon the following two assumptions:

(1) The steels of which Service projectiles are made can be taken as having the same composition and mechanical properties.
(2) The different shapes of the projectiles, i.e. the ratio of length to breadth and the tapering at the ends are not important in determining fragmentation.

The results are shown in Figs. 6.5 and 6.7, and a similar plot for $\log ct$ in Fig. 6.6. The scatter about the straight line is doubtless due to differences in shell steel and shape, and also to different degrees of break-up in the collecting media used, when this has not been allowed for (points 4, 8, 9, 10). More detailed discussion of these curves will be given in para. 3.

In these curves, M_A is determined from the observed data by the method of [4], which gives a unique value; the values taken are shown in Appendix II. The thickness (t) and external diameter (d_o) were measured in each case on the cylindrical portion of the projectile, except for the 250 and 500 lb. S.A.P. bombs, the 40 lb. G.P. bomb and the 20 lb. F. bomb. In these cases, mean values were taken. Again, the values assumed are given in Appendix II; manufacturing tolerances may be an additional cause of scatter.

The chief difficulty is to make an estimate of v_c, the velocity of the case at the moment of break-up. The position with regard to this is discussed in the next section.

6.2 Velocity of the Casing

According to theoretical calculations, for a long cylindrical casing filled with a given explosive, and if the speed of reaction in the detonation wave is assumed infinite, the velocity of the case, after a given expansion, will depend only on the charge-weight ratio. Also, after an expansion of from 30 to 50 per cent., at which the case normally breaks, the case will have attained nearly its final velocity. Flash photographs taken in the United States confirm that the silhouette of the case before rupture is approximately straight.

Since shell casings break after a fairly well defined expansion, one would expect all the fragments from a long thin casing to have the same velocity. For Service projectiles, however, the fragment velocities show a wide spread. Whether or not this is due to end effects, is not clear. Some assumption must therefore be made about the relation between the casing velocity to be used in formula (6.3) and the observed fragment velocities.

In Figs. 6.1, 6.2 and 6.3, we have plotted the results of a number of measurements of fragment velocity by C.S.A.R. in the following manner: the ordinates are the number of fragments with velocities between 250 n and 250 $(n + 1)$ ft./sec. (n being integral); the abscissæ are 250 $(n + \frac{1}{2})$. It is found that these curves usually contain a number of peaks; the peak corresponding to the greatest velocity is usually the highest. The velocity of the top of this peak we denote by v_c, and make the *assumption* that this corresponds to the casing velocity that a long tube of the same dimensions would have.

There is some indeterminacy in the estimation of v_c from the available experimental evidence; the range within which we consider that it can be fixed is shown on the curves 1–4. We have assumed that the peaks are to be drawn as symmetrically as possible; if this were not done, the choice of v_c would be somewhat more arbitrary.

In Fig. 6.4, v_c is plotted against $\sqrt{(E/c)}$, where E/c, the charge-weight ratio, is defined by

$$E/c = \frac{\rho_E}{\rho_s} \frac{d_1^2}{d_o^2 - {d_1}^2} \tag{6.4}$$

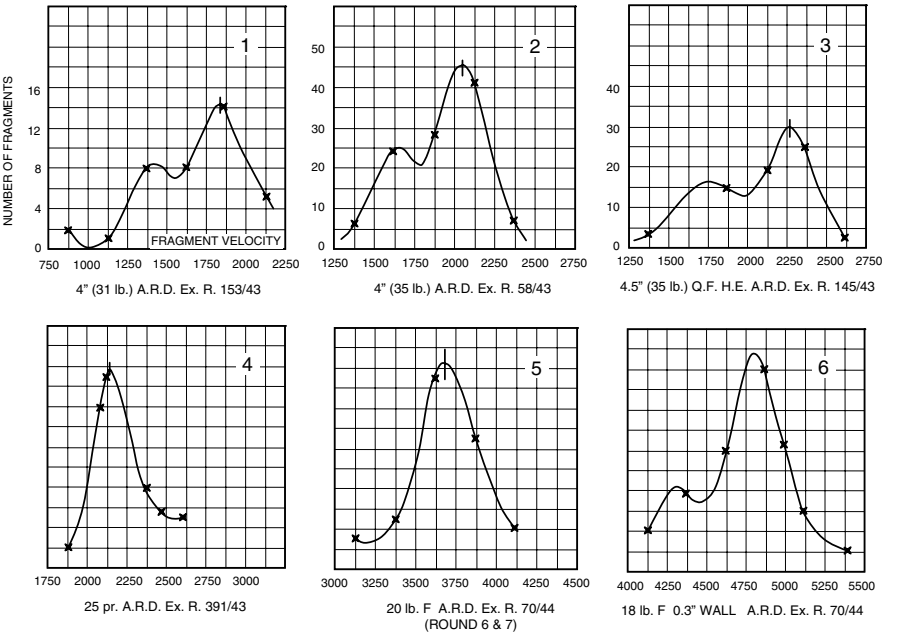
NUMBER OF FRAGMENTS
1
FRAGMENT VELOCITY
4" (31 lb.) A.R.D. Ex. R. 153/43
2
4" (35 lb.) A.R.D. Ex. R. 58/43
3
4.5" (35 lb.) Q.F. H.E. A.R.D. Ex. R. 145/43
4
25 pr. A.R.D. Ex. R. 391/43
5
20 lb. F A.R.D. Ex. R. 70/44
(ROUND 6 & 7)
6
18 lb. F 0.3" WALL A.R.D. Ex. R. 70/44

Fig. 6.1.

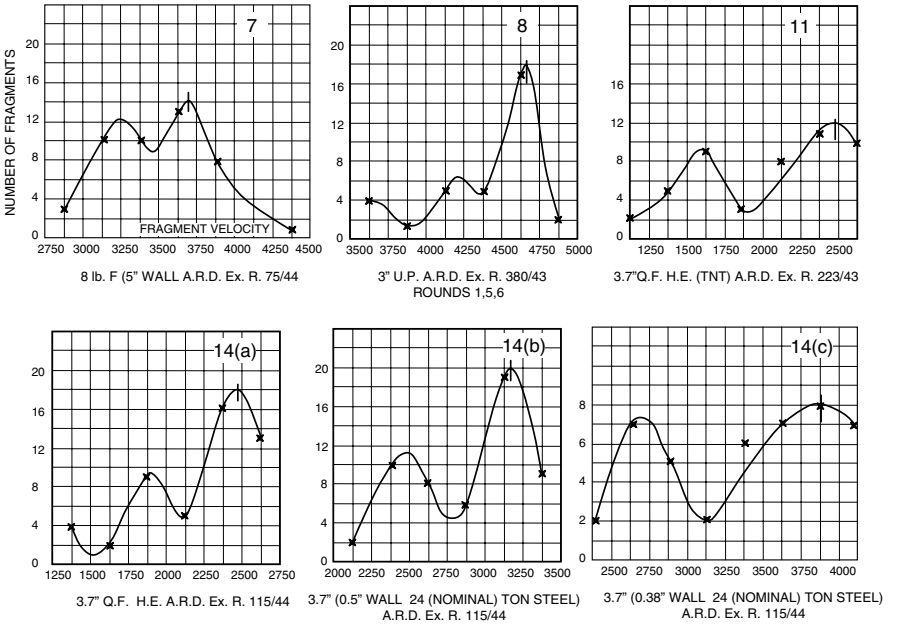
NUMBER OF FRAGMENTS
7
FRAGMENT VELOCITY
8 lb. F (5" WALL A.R.D. Ex. R. 75/44
8
3" U.P. A.R.D. Ex. R. 380/43
ROUNDS 1,5,6
11
3.7"Q.F. H.E. (TNT) A.R.D. Ex. R. 223/43
14(a)
3.7" Q.F. H.E. A.R.D. Ex. R. 115/44
14(b)
3.7" (0.5" WALL 24 (NOMINAL) TON STEEL)
A.R.D. Ex. R. 115/44
14(c)
3.7" (0.38" WALL 24 (NOMINAL) TON STEEL)
A.R.D. Ex. R. 115/44

Fig. 6.2.

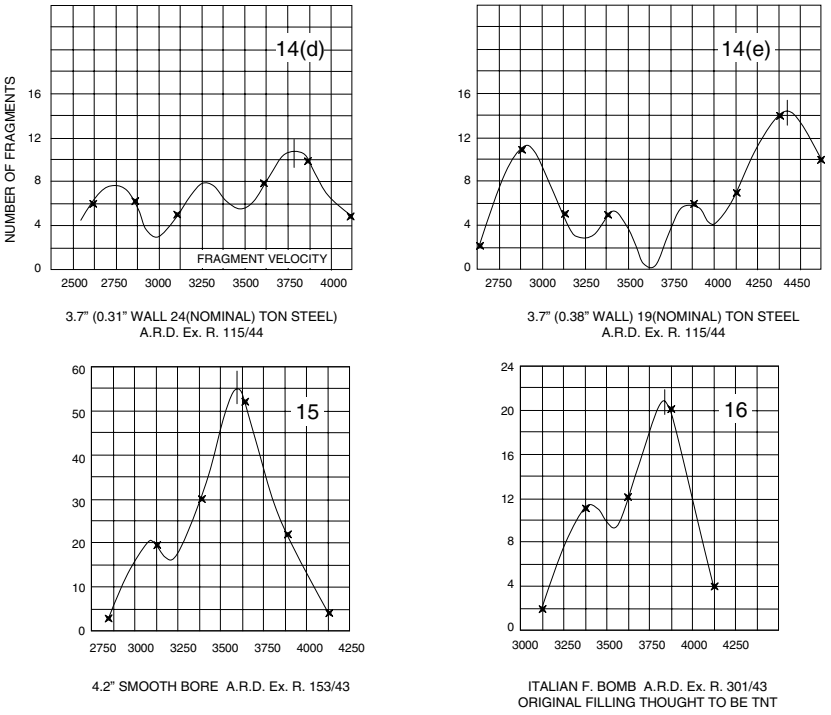
14(d)
NUMBER OF FRAGMENTS
FRAGMENT VELOCITY
3.7" (0.31" WALL 24(NOMINAL) TON STEEL)
A.R.D. Ex. R. 115/44
14(e)
3.7" (0.38" WALL) 19(NOMINAL) TON STEEL
A.R.D. Ex. R. 115/44
15
4.2" SMOOTH BORE A.R.D. Ex. R. 153/43
16
ITALIAN F. BOMB A.R.D. Ex. R. 301/43
ORIGINAL FILLING THOUGHT TO BE TNT

Fig. 6.3.

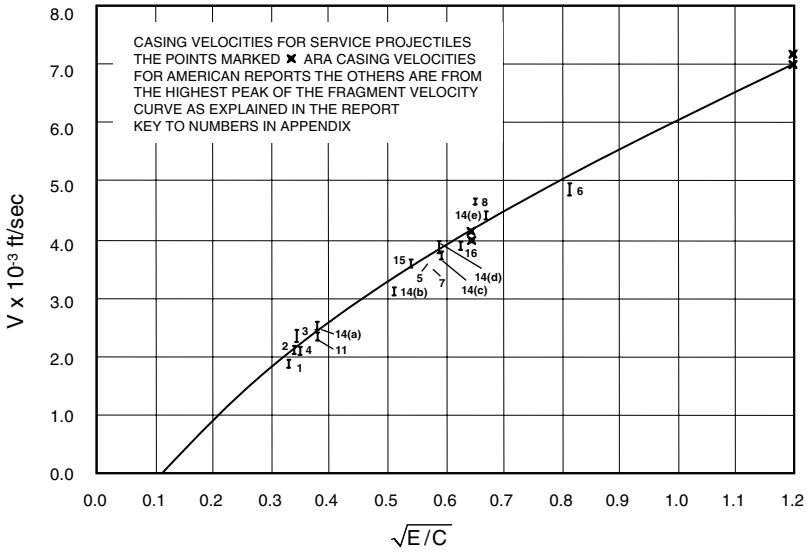
CASING VELOCITIES FOR SERVICE PROJECTILES
THE POINTS MARKED ✖ ARA CASING VELOCITIES
FOR AMERICAN REPORTS THE OTHERS ARE FROM
THE HIGHEST PEAK OF THE FRAGMENT VELOCITY
CURVE AS EXPLAINED IN THE REPORT
KEY TO NUMBERS IN APPENDIX
V x 10-3 ft/sec
√E/C

Fig. 6.4.

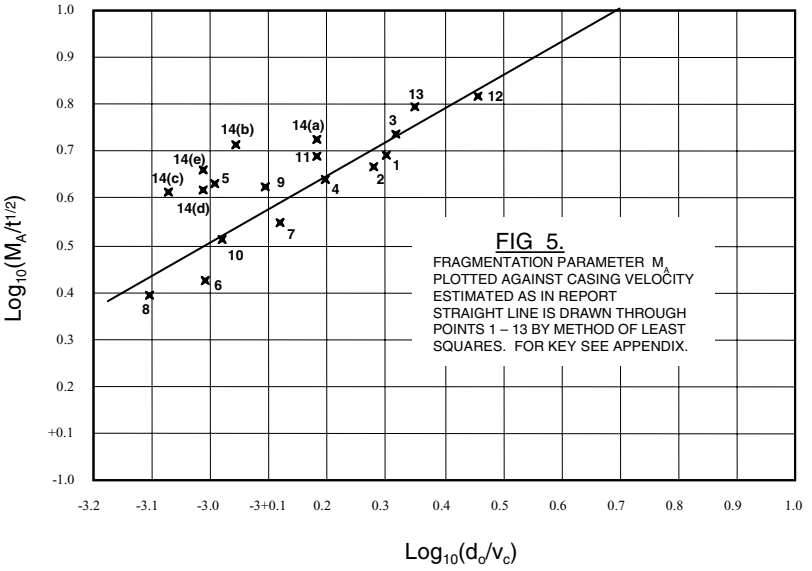
1.0
0.9
0.8
0.7
0.6
0.5
0.4
0.3
0.2
+0.1
-1.0
-3.2
-3.1
-3.0
-3+0.1
0.2
0.3
0.4
0.5
0.6
0.7
0.8
0.9
1.0
Log10(MA/t1/2)
Log10(do/vc)
13
12
14(b)
14(a)
3
14(e)
11
14(c)
5
1
9
2
4
14(d)
7
10
6
8
FIG 5.
FRAGMENTATION PARAMETER MA
PLOTTED AGAINST CASING VELOCITY
ESTIMATED AS IN REPORT
STRAIGHT LINE IS DRAWN THROUGH
POINTS 1 – 13 BY METHOD OF LEAST
SQUARES. FOR KEY SEE APPENDIX.

Fig. 6.5.

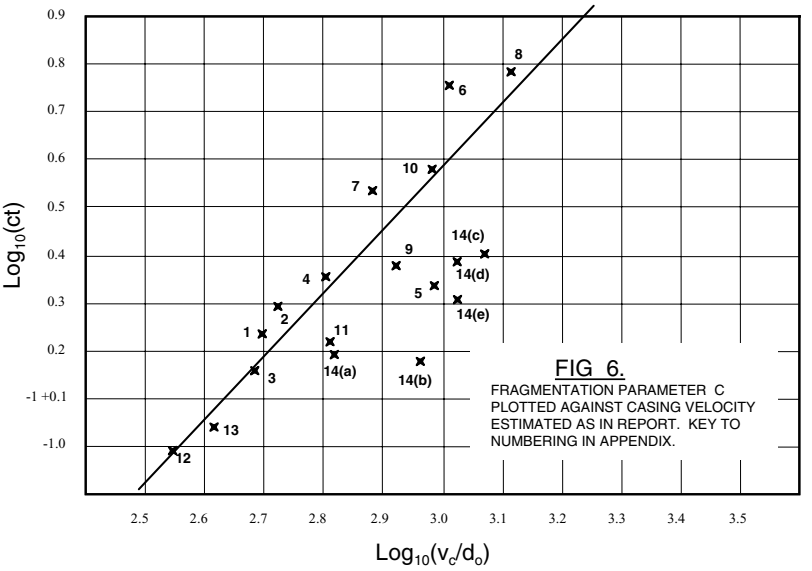
0.9
0.8
0.7
0.6
0.5
0.4
0.3
0.2
-1 +0.1
-1.0
2.5
2.6
2.7
2.8
2.9
3.0
3.1
3.2
3.3
3.4
3.5
Log10(ct)
Log10(vc/do)
8
6
10
7
14(c)
9
14(d)
4
5
14(e)
2
1
11
14(a)
3
14(b)
13
12
FIG 6.
FRAGMENTATION PARAMETER C
PLOTTED AGAINST CASING VELOCITY
ESTIMATED AS IN REPORT. KEY TO
NUMBERING IN APPENDIX.

Fig. 6.6.

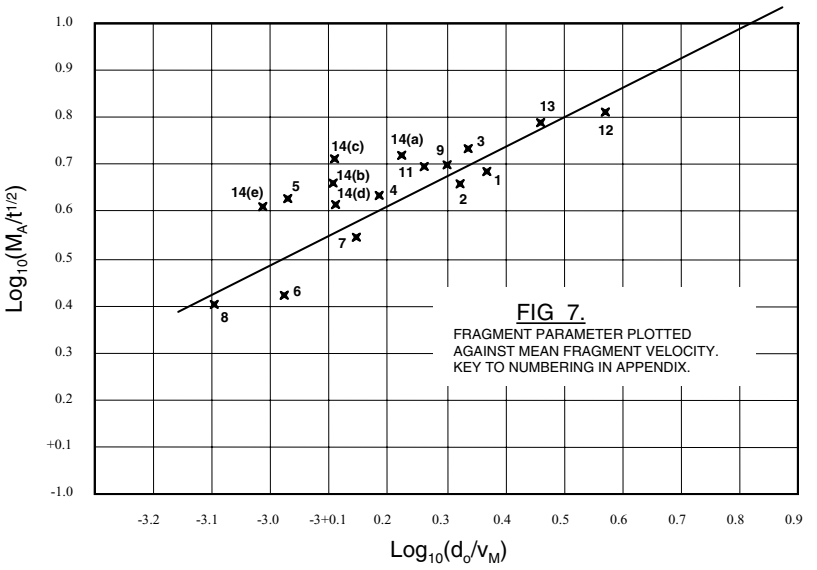

Fig. 6.7.

where d_1, d_o are the internal and external diameters and ρ_s, ρ_E the densities of steel and of T.N.T. which was the filling in all the projectiles considered here. For the bombs previously mentioned, whose shapes differed considerably from that of a cylinder, a mean value of E/c was obtained by measuring the internal and external diameters at a number of points along the casing and evaluating by means of Simpson's rule. On the same curve, we have plotted two values for the casing velocity obtained by flash photography (O.S.R.D. reports). They appear to lie on the same curve, thus confirming our hypothesis that the casing velocity is to be identified with the high velocity peak for the fragments.

This curve has been extrapolated to zero velocity at that value of $\sqrt{(E/c)}$ for which the energy of the explosive would be just sufficient to expand the case by 100 per cent., assuming an average resistance to yield during the expansion of 50 tons/sq. inch.

6.3 Fragment Weight Distribution

In Figs. 6.5 and 6.6, we have plotted $\log(M_A/\sqrt{t})$ and $\log(ct)$ against $\log(d_o/v_c)$, v_c being determined from the *curve* of Fig. 6.4. The points lie reasonably well on a curve, approximately a straight line if trials with 3.7 in. shell with thin walls are excluded.

If the wide spread of fragment velocities comes from the end effects, then, since some of the fragments come from the ends, it might be considered more

logical to take log (d_o/v_M) as abscissæ, where v_M is the mean velocity. For the series of 3.7 in. shells, the difference between v_c and v_M is abnormally large. A plot with these abscissæ is shown in Fig. 6.3; the points for the 3.7 in. shell appear to be a little closer to the others but these shell still seem to give abnormally coarse fragmentation.

Straight lines fitted to these (excluding the 3.7 in. shells), by the method of least squares, give the following:

$$\frac{M_A}{\sqrt{t}} = 50.7 \left(\frac{d_o}{v_c}\right)^{0.739} \tag{6.5}$$

$$ct = 2.89 \times 10^{-5} \left(\frac{v_c}{d_o}\right)^{1.337} \tag{6.6}$$

$$\frac{M_A}{\sqrt{t}} = 22.6 \left(\frac{d_o}{v_M}\right)^{0.623} \tag{6.7}$$

Formula (6.5) can be used to predict M_A if v_c is read off the curve of Fig. 6.4.

References

[1] Theory of the Fragmentation of the M. 41 Wire-Wound Bomb. A.R.D. Theoretical Research Report 8/44.
[2] S.M.R.B., Buxton. Cased Charges XXI. Empirical relationships for use in comparing results of fragmentation trials. II. Weight distribution of fragments (A.O.4604; SD/FP.137).
[3] A Theory of Fragmentation by Mott and Linfoot. D.S.R. Extra-Mural Report, A.C.3348.
[4] Effect of carbon-content of steel on the fragmentation of shell. A.R.D. Theoretical Research Report 23/44 (A.C.6998; SD/FP.281).

APPENDIX I

References of papers from which velocities were taken.

	Projectile	v_c (f.s.)	v_M (f.s.)	Reference
1.	4 in. (31 lb.) shell	2000	1680	A.R.D. Expl. Report 153/43
2.	4 in. (35 lb.) shell	2100	1890	A.R.D. Expl. Report 58/43
3.	4.5 in. Q.F. H.E. shell	2110	2020	A.R.D. Expl. Report 145/43
4.	25 pr. shell	2180	2250	A.R.D. Expl. Report 391/43
5.	20 lb. F bomb	3770	3620	A.R.D. Expl. Report 70/44 (rds. 6 & 7)
6.	18 lb. F bomb (0.3 in. wall)	5090	4770	A.R.D. Expl. Report 75/44
7.	18 lb. F bomb (0.5 in. wall)	3770	3540	A.R.D. Expl. Report 75/44
8.	3 in. U.P.	4150	3940	A.R.D. Expl. Report 380/43 (rds. 1,5,6)
9.	40 lb. G.P. bomb Mk.I	3950	–	–
10.	95 mm.	3510	–	–
11.	3.7 in. shell	2410	2020	A.R.D. Expl. Report 223/43
12.	500 lb. S.A.F. bomb (tail initiated)	4000	3030*	A.R.D. Expl. Report 73/44
13.	250 lb. S.A.P. bomb (tail initiated)	4000	3070*	A.R.D. Expl. Report 73/44
14.	(a) 3.7 in. Q.F. H.E.	2410	2210	A.R.D. Expl. Report 115/44
	(b) 3.7 in. (0.5 in. wall 24 ton steel)	3310	2850	A.R.D. Expl. Report 115/44
	(c) 3.7. in. (0.38 in. wall 24 ton steel)	3780	3370	A.R.D. Expl. Report 115/44
	(d) 3.7 in. (0.38 in. wall 19 ton steel)	3780	3370	A.R.D. Expl. Report 115/44
	(e) 3.7 in. (0.31 in. wall 24 ton steel)	4300	3790	A.R.D. Expl. Report 115/44
15.	Italian F bomb (wire wound)	–	–	A.R.D. Expl. Report 301/43
16.	4.2 in. smooth bore	–	–	A.R.D. Expl. Report 17/44
	Flash photographs for casing velocities			S.R.7 44/1440

*Average of all velocities given in reference quoted.

All these projectiles were filled T.N.T. (The original filling of the Italian F bomb was not known for certain, but was thought to have been T.N.T.). The 250 lb. S.A.P. bomb was filled T.N.T./Beeswax 93/7. Values of v_M from reports quoted, values of v_c taken from the curve in Fig. 6.4.

APPENDIX II

References of papers giving fragment weight distributions; d_o and t are taken from drawings; values for the actual shells fragmented may differ slightly. M_A and c are calculated by the shortened methods given in A.R.D. Theoretical Research Report 23/44 (A.C. 6998; SD/FP. 281) and S.M.R.B. Buxton. Cased Charges XXV, Application to Service shell of a simplified method of assessing fragmentation cell tests. (A.C. 5392; SD/FP. 190). M_A may thus differ from values given in the reports.

	Projectile	M_A	c	$t^{1/2}$ $(\text{in.})^{1/2}$	d_o (in.)	Collecting Medium	Reference
1.	4 in. (31 lb.) shell (Rds. 1, 3, 5)	0.432	0.216	0.89	3.95	Strawboard	A.R.D. Exp. Rep. 153/43
2.	4 in. (35 lb.) shell (Rds. 7, 8, 9)	0.413	0.248	0.89	4.00	Strawboard	A.R.D. Exp. Rep. 58/43
3.	4.5 in. shell (Rds. 1, 2, 3)	0.492	0.172	0.91	4.43	Strawboard	A.R.D. Exp. Rep. 145/43
4.	25 pr. shell	0.350	0.342	0.81	3.43	Sawdust	SD/FP.218 (Buxton report)
5.	20 lb. F bomb	0.258	0.590	0.61	3.90	Strawboard	A.R.D. Exp. Rep. 70/44
6.	18 lb. F bomb (0.3 in. wall)	0.145	1.914	0.55	5.00	Strawboard	A.R.D. Exp. Rep. 75/44
7.	18 lb. F bomb (0.5 in. wall)	0.247	0.683	0.71	5.00	Strawboard	A.R.D. Exp. Rep. 75/44
8.	3 in. U.P.	0.128	2.30	0.52	3.25	Sawdust	SD/FP. 190 (Buxton report)
9.	40 lb. G.P. bomb	0.290	0.502	0.69	4.94	Sand	O.B. Proc. 1598
10.	95 mm. shell	0.212	0.900	0.65	3.70	Sand	O.B. Proc. 21099
11.	3.7 in. shell	0.396	0.256	0.81	3.70	Strawboard	A.R.D. Exp. Rep. 223/43
12.	500 lb. S.A.P. bomb (tail initiated)	0.651	0.097	1.00	11.35	Strawboard	A.R.D. Exp. Rep. 73/43
13.	250 lb. S.A.P. bomb (tail initiated)	0.544	0.143	0.87	9.00	Strawboard	A.R.D. Exp. Rep. 73/43
14.	(a) 3.7 in. Service	0.421	0.240	0.81	3.7	Strawboard	A.R.D. Exp. Rep. 115/44
	(b) 3.7 in. C	0.365	0.308	0.71	3.7	Strawboard	A.R.D. Exp. Rep. 115/44
	(c) 3.7 in. B	0.281	0.537	0.62	3.7	Strawboard	A.R.D. Exp. Rep. 115/44
	(d) 3.7 in. A	0.253	0.653	0.62	3.7	Strawboard	A.R.D. Exp. Rep. 115/44
	(e) 3.7 in. D	0.228	0.816	0.56	3.7	Strawboard	A.R.D. Exp. Rep. 115/44

APPENDIX III

In the following table we compare values of M_A obtained by various methods. Column 1 contains the values given in Appendix II as determined from trials; Column 2 contains corresponding values calculated from (6.5) of this report, using the data of Appendices I and II; Column 3 contains values obtained by using the formula

$$M_A = 0.3\, t^{5/6} d_2^{1/3} (1 + t/d_2) \tag{6.8}$$

where t is the thickness and d_2 the internal diameter of the projectile. For completeness, we give, in Column 4, the values of M_A obtained from (6.7) of this report. This equation is, however, not so useful as (6.5) or (6.8) above, which both predict M_A from a knowledge of the dimensions of the projectile, whereas (6.7) requires a knowledge of trial velocities.

Projectile (see Appendix II)	M_A			
	Column 1	Column 2	Column 3	Column 4
1	0.432	0.453	0.440	0.463
2	0.413	0.441	0.440	0.435
3	0.492	0.484	0.469	0.454
4	0.350	0.348	0.355	0.322
5	0.258	0.192	0.216	0.195
6	0.145	0.167	0.194	0.173
7	0.247	0.267	0.303	0.269
8	0.128	0.134	0.154	0.141
9	0.290	0.250	0.287	–
10	0.212	0.208	0.238	–
11	0.396	0.342	0.359	0.361
12	0.651	0.665	0.699	0.696
13	0.544	0.487	0.512	0.520
14(a)	0.421	0.342	0.359	0.341
(b)	0.365	0.237	0.280	0.255
(c)	0.281	0.188	0.219	0.201
(d)	0.253	0.188	0.219	0.201
(e)	0.228	0.154	0.183	0.169

Facsimiles of N.F. Mott: Fragmentation of Service Projectiles

Ministry of Supply
Armament Research Department

THEORETICAL RESEARCH REPORT NO. 37/44

Fragmentation of Service Projectiles

by

N.F. Mott, J.H. Wilkinson and T.H. Wise

Branch for Theoretical Research,
Fort Halstead, Kent.

Copy No. 46
December, 1944

Summary

In previous reports, formulae have been given by means of which the fragment weight distribution could be deduced from the design of the shell. The derivation of these formulae can be divided into two parts, as follows:

(1) It is assumed that the distance between fractures on the surface of the shell casing depends only on the rate of strain at the moment of fracture, and thus on r/v, where r is the radius and v the velocity of the case at this moment.

(2) The theory of plastic waves is used to deduce what function of r/v this distance should be, and a formula for the average weight is thereby deduced.

An attempt at a rigorous application of the plastic wave theory can only be made for wire-wound or ring bombs, where the one dimensional break-up of a long strip has to be considered. For solid casings, therefore, in this report the assumption (1) above is maintained, and the best function of r/v to fit the experimental data is determined empirically. The investigation confirms a theoretical formula already given, formula (8) of this report, as giving, satisfactorily, the fragment weight distribution of Service shells.

In order to test the dependence of fragment weight distribution on r/v, values had to be estimated for the velocity of the case. It is suggested that this is to be associated with the mode of the curve plotting number of fragments against velocity.

Distribution List

The initial distribution of copies was as follows:

Nos.1-10 Ministry of Supply, S.R.7, for distribution as follows:

(1) British Central Scientific Office, Washington, (for U.S. Army, Navy and British Missions in Washington)
(2) Office of Scientific Research and Development, U.S.A.
(3) National Research Council, Canada
(5)-(6) Canadian Military Headquarters
(7) Australian Scientific Research and Development
(8) New Zealand Government Offices
(9)-(10) S.R.7 Technical Records
(These copies are available on loan to South Africa and New Zealand, if required)

Nos.11-60 Secretary, Scientific Advisory Council (Attention: Fragmentation Panel)

Nos.61-62 Secretary, Ordnance Board

No.63 Military College of Science

No.64 Royal Naval College

No.65 D.S.R. (Admiralty)

No.66 A.O.R.G.

No.67 C.S.P.D.E.

Nos.68-69 C.S.A.R. (Attention: S.S.R.(A), S.A.E.)

Nos.70-71 U.S. Embassy (Attention: Mr. Bennett Archambault)

Nos.72-73 U.S. Embassy (Attention: Naval Attaché)

No.74 Brigadier Mackenzie

No.75 Aberdeen Proving Ground (Attention: Mr. R.H. Kent)

Nos.76-77 Ordnance Technical Division (Attention: Dr. Marston Morse)

No.78 Dr. Payman

No.79 Professor L. Rosenhead (P.D.E.)

No.80 A.R.D. Library

No.81 Explosives Branch Records Section

Nos.82-83 Theoretical Research Branch Files

Further copies can be obtained from

Armament Research Department,
(Branch for Theoretical Research),
Fort Halstead,
Sevenoaks, Kent.

1. Introduction

A series of reports has been issued, dealing with the theory of the break-up of shell and bomb casings. The aim of such theories is to attempt to predict the fragment weight distribution in terms of the design of the projectile, type of explosive and properties of the steel case. In Ref.1, a fairly complete theory was given for a long cylindrical wire-wound bomb; the theory predicts the length distribution of the fragments of the wire casing in terms of one unknown parameter depending on the steel, and seems in fair accord with the small amount of experimental evidence available. Earlier attempts to obtain a theory of the break-up of solid casings contain some arbitrary assumptions, and it seems worth while to re-examine the experimental data from a partly theoretical, partly empirical point of view.

The assumptions made in this report are as follows:

(a) The fragment weight distribution is taken to be given by either Payman's formula (Ref.2) or that due to Welch, as modified by Mott and Linfoot (Ref.3). These are to be regarded as empirical. The formulae are

(i) The proportion p by weight of the case breaking into fragments greater than w is given by

$$\log_{10} p = -c w \qquad \ldots\ldots\ldots\ldots\ldots\ldots\ldots\ldots (1)$$

(ii) The number of fragments in any random sample with weights between w and w + dw is

$$B \exp(-M/M_A)\, dM \qquad M = w^{\frac{1}{2}} \qquad \ldots\ldots\ldots\ldots\ldots (2)$$

Either $1/c$ or M_A^2 may be regarded as proportional to the average fragment weight and it is the purpose of this report to relate this to the design of the projectile.

Consider now the fragmentation of a very long cylindrical case. We make the following assumptions:

(i) After the usual plastic expansion, fracture occurs on any circumference of the cylinder when the external radius is r and velocity of the outside of the casing v_c, and all the cracks which ultimately lead to fracture occur during a time interval so short that r does not change appreciably.

(ii) Fracture starts from the outside of the casing.

Neither assumption is necessarily true in general; the considerable and fairly uniform thinning of fragments, suggests that (i) is often valid. (ii) may not be the case when fracture is by shear, but is probably correct if fracture is partly tensile; the hoop stress is a maximum on the outside of the case.

If these assumptions are valid, the distance between cracks must depend only on the rate of strain of the metal on the surface of the case at the moment of fracture, and also on the properties of the metal. The rate of strain is equal to v_c/r Thus the area of the external surface of a typical fragment must be a function of r/v_c. The weight of the average fragment, divided by the thickness t, will therefore be a function of r/v_c. Thus, if we take M_A^2 as our measure of the average weight, we may write

$$M_A/\sqrt{t} = f(r/v_c) \qquad \ldots\ldots\ldots\ldots\ldots\ldots\ldots\ldots (3)$$

We shall make a further assumption, namely, that for a given steel the percentage expansion before fracture is constant. Then, in (3), we may take r and t to refer to the dimensions of the case before detonation.

In this report, we examine the fragmentation of Service projectiles in relation to equation (3). We plot $\log(M_A/\sqrt{t})$ against $\log(r/v_c)$. The possibility of obtaining a smooth curve depends upon the following two assumptions:

(1) The steels of which Service projectiles are made can be taken as having the same composition and mechanical properties.

(2) The different shapes of the projectiles, i.e. the ratio of length to breadth and the tapering at the ends are not important in determining fragmentation.

The results are shown in Figs.5 and 7, and a similar plot for log ct in Fig.6. The scatter about the straight line is doubtless due to differences in shell steel and shape, and also to different degrees of break-up in the collecting media used, when this has not been allowed for (points 4, 8, 9, 10). More detailed discussion of these curves will be given in para.3.

In these curves, M_A is determined from the observed data by the method of Ref.4, which gives a unique value; the values taken are shown in Appendix II. The thickness (t) and external diameter (d_o) were measured in each case on the cylindrical portion of the projectile, except for the 250 and 500 lb. S.A.P. bombs, the 40 lb. G.P. bomb and the 20 lb. F. bomb. In these cases, mean values were taken. Again, the values assumed are given in Appendix II; manufacturing tolerances may be an additional cause of scatter.

The chief difficulty is to make an estimate of v_c, the velocity of the case at the moment of break-up. The position with regard to this is discussed in the next section.

2. Velocity of the casing

According to theoretical calculations, for a long cylindrical casing filled with a given explosive, and if the speed of reaction in the detonation wave is assumed infinite, the velocity of the case, after a given expansion, will depend only on the charge-weight ratio. Also, after an expansion of from 30 to 50 per cent., at which the case normally breaks, the case will have attained nearly its final velocity. Flash photographs taken in the United States confirm that the silhouette of the case before rupture is approximately straight.

Since shell casings break after a fairly well defined expansion, one would expect all the fragments from a long thin casing to have the same velocity. For Service projectiles, however, the fragment velocities show a wide spread. Whether or not this is due to end effects, is not clear. Some assumption must therefore be made about the relation between the casing velocity to be used in formula (3) and the observed fragment velocities.

In Figs.1,2 and 3, we have plotted the results of a number of measurements of fragment velocity by C.S.A.R. in the following manner: the ordinates are the number of fragments with velocities between 250 n and 250 (n + 1) ft./sec. (n being integral); the abscissae are 250 $(n + \frac{1}{2})$. It is found that these curves usually contain a number of peaks; the peak corresponding to the greatest velocity is usually the highest. The velocity of the top of this peak we denote by v_c, and make the assumption that this corresponds to the casing velocity that a long tube of the same dimensions would have.

There is some indeterminacy in the estimation of v_c from the available experimental evidence; the range within which we consider that it can be fixed is shown on the curves 1 - 4. We have assumed that the peaks are to be drawn as symmetrically as possible; if this were not done, the choice of v_c would be somewhat more arbitrary.

In Fig.4, v_c is plotted against $\sqrt{(E/c)}$, where E/c, the charge-weight ratio, is defined by

$$E/c = \frac{\rho_E}{\rho_s} \frac{d_1^2}{d_o^2 - d_1^2} \qquad \ldots\ldots\ldots\ldots\ldots\ldots\ldots\ldots\ldots (4)$$

where d_1, d_o are the internal and external diameters and ρ_s, ρ_E the densities of steel and of T.N.T. which was the filling in all the projectiles considered here. For the bombs previously mentioned, whose shapes differed considerably from that of a cylinder, a mean value of E/c was obtained by measuring the internal and

external diameters at a number of points along the casing and evaluating by means of Simpson's rule. On the same curve, we have plotted two values for the casing velocity obtained by flash photography (C.S.R.D. reports). They appear to lie on the same curve, thus confirming our hypothesis that the casing velocity is to be identified with the high velocity peak for the fragments.

This curve has been extrapolated to zero velocity at that value of $\sqrt{(E/c)}$ for which the energy of the explosive would be just sufficient to expand the case by 100 per cent., assuming an average resistance to yield during the expansion of 50 tons/sq.inch.

3. Fragment weight distribution

In Figs.5 and 6, we have plotted $\log(M_A/\sqrt{t})$ and $\log(ct)$ against $\log(d_o/v_c)$, v_c being determined from the curve of Fig.4. The points lie reasonably well on a curve, approximately a straight line if trials with 3.7 in. shell with thin walls are excluded.

If the wide spread of fragment velocities comes from the end effects, then, since some of the fragments come from the ends, it might be considered more logical to take $\log(d_o/v_M)$ as abscissæ, where v_M is the mean velocity. For the series of 3.7 in. shells, the difference between v_c and v_M is abnormally large. A plot with these abscissæ is shown in Fig.3; the points for the 3.7 in. shell appear to be a little closer to the others but these shell still seem to give abnormally coarse fragmentation.

Straight lines fitted to these (excluding the 3.7 in. shells), by the method of least squares, give the following:

$$\frac{M_A}{\sqrt{t}} = 50.7 \left(\frac{d_o}{v_c}\right)^{0.739} \quad \ldots\ldots (5)$$

$$ct = 2.89 \times 10^{-5} \left(\frac{v_c}{d_c}\right)^{1.377} \quad \ldots\ldots (6)$$

$$\frac{M_A}{\sqrt{t}} = 22.6 \left(\frac{d_o}{v_M}\right)^{0.623} \quad \ldots\ldots (7)$$

Formula (5) can be used to predict M_A if v_c is read off the curve of Fig.4.

References

1. Theory of the Fragmentation of the M.41 Wire-Wound Bomb. A.R.D. Theoretical Research Report 8/44.

2. S.M.R.B., Buxton. Cased Charges XXI. Empirical relationships for use in comparing results of fragmentation trials. II. Weight distribution of fragments (A.C.4604; SD/ME.137)

3. A Theory of Fragmentation, by Mott and Linfoot. D.S.R. Extra-Mural Report, A.C.3348

4. Effect of carbon-content of steel on the fragmentation of shell. A.R.D. Theoretical Research Report 23/44 (A.C.6998; SD/FP.281).

APPENDIX I

References of papers from which velocities were taken.

	Projectile	v_G (f.s.)	v_M (f.s.)	Reference
1.	4 in. (31 lb.) shell	2000	1680	A.R.D. Expl. Report 153/43
2.	4 in. (35 lb.) shell	2100	1890	" " " 58/43
3.	4.5 in. Q.F. H.E. shell	2110	2020	" " " 145/43
4.	25 pr. shell	2180	2250	" " " 392/43
5.	20 lb. F bomb	3770	3620	" " " 70/44 (rds.6 & 7)
6.	18 lb. F bomb (0.3 in. wall)	5090	4770	" " " 75/44
7.	18 lb. F bomb (0.5 in. wall)	3770	3540	" " " 75/44
8.	3 in. U.P.	4150	3940	" " " 380/43 (rds.1,5,6)
9.	40 lb. G.P. bomb Mk.I	3950	-	-
10.	95 mm.	3510	-	-
11.	3.7 in. shell	2410	2020	A.R.D. Expl. Report 223/43
12.	500 lb. S.A.P. bomb (tail initiated)	4000	3030*	" " " 73/44
13.	250 lb. S.A.P. bomb (tail initiated)	4000	3070*	" " " 73/44
14.	(a) 3.7 in. Q.F. H.E.	2410	2210	" " " 115/44
	(b) 3.7 in. (0.5 in. wall 24 ton steel)	3310	2850	" " " 115/44
	(c) 3.7 in. (0.38 in. wall 24 ton steel)	3780	3370	" " " 115/44
	(d) 3.7 in. (0.38 in. wall 19 ton steel)	3780	3370	" " " 115/44
	(e) 3.7 in. (0.31 in. wall 24 ton steel)	4300	3790	" " " 115/44
15.	Italian F bomb (wire wound)	-	-	" " " 301/43
16.	4.2 in. smooth bore	-	-	" " " 17/44
	Flash photographs for casing velocities			S.R.7 44/1440

* Average of all velocities given in reference quoted.

All these projectiles were filled T.N.T. (The original filling of the Italian F bomb was not known for certain, but was thought to have been T.N.T.). The 250 lb. S.A.P. bomb was filled T.N.T./Beeswax 93/7. Values of v_M from reports quoted, values of v_G taken from the curve in Fig.4.

APPENDIX II

References of papers giving fragment weight distributions; d_o and t are taken from drawings; values for the actual shells fragmented may differ slightly. M_A and c are calculated by the shortened methods given in A.R.D. Theoretical Research Report 23/44 (A.C.6998; SD/FP.281) and S.M.R.B. Buxton. Cased Charges XXV, Application to Service shell of a simplified method of assessing fragmentation cell tests. (A.C.5392; SD/FP.190). M_A may thus differ from values given in the reports.

	Projectile	M_A	c	$t^{\frac{1}{2}}$ (in.)$^{\frac{1}{2}}$	d_o (in.)	Collecting Medium	Reference
1.	4 in. (31 lb.) shell (Rds. 1, 3, 5)	0.432	0.216	0.89	3.95	Strawboard	A.R.D.Exp.Rep. 153/43
2.	4 in. (35 lb.) shell (Rds. 7, 8, 9)	0.413	0.248	0.89	4.00	"	" " " 58/43
3.	4.5 in. shell (Rds. 1, 2, 3)	0.492	0.172	0.91	4.43	"	" " " 145/43
4.	25 pr. shell	0.350	0.342	0.81	3.43	Sawdust	SD/FP.218 (Buxton report)
5.	20 lb. F bomb	0.258	0.590	0.61	3.90	Strawboard	A.R.D.Exp.Rep. 70/44
6.	18 lb. F bomb (0.3 in. wall)	0.145	1.914	0.55	5.00	"	" " " 75/44
7.	18 lb. F bomb (0.5 in. wall)	0.247	0.683	0.71	5.00	"	" " " 75/44
8.	3 in. U.P.	0.128	2.30	0.52	3.25	Sawdust	SD/FP.190 (Buxton report)
9.	40 lb. G.P. bomb	0.290	0.502	0.69	4.94	Sand	O.B.Proc.1598
10.	95 mm. shell	0.212	0.900	0.65	3.70	"	O.B.Proc.21099
11.	3.7 in. shell	0.396	0.256	0.81	3.70	Strawboard	A.R.D.Exp.Rep. 223/43
12.	500 lb. S.A.P. bomb (tail initiated)	0.651	0.097	1.00	11.35	"	" " " 73/43
13.	250 lb. S.A.P. bomb (tail initiated)	0.544	0.143	0.87	9.00	"	" " " 73/43
14.	(a) 3.7 in. Service	0.421	0.240	0.81	3.7	"	" " " 115/44
	(b) 3.7 in. C	0.365	0.308	0.71	3.7	"	" " " 115/44
	(c) 3.7 in. B	0.281	0.537	0.62	3.7	"	" " " 115/44
	(d) 3.7 in. A	0.253	0.653	0.62	3.7	"	" " " 115/44
	(e) 3.7 in. D	0.228	0.816	0.56	3.7	"	" " " 115/44

APPENDIX III

In the following table we compare values of M_A obtained by various methods. Column 1 contains the values given in Appendix II as determined from trials; Column 2 contains corresponding values calculated from equation (5) of this report, using the data of Appendices I and II; Column 3 contains values obtained by using the formula

$$M_A = 0.3\, t^{5/6}\, d_2^{\frac{1}{3}}\, (1 + t/d_2) \quad \ldots\ldots\ldots\ldots\ldots\ldots (8)$$

where t is the thickness and d_2 the internal diameter of the projectile. For completeness, we give, in Column 4, the values of M_A obtained from equation (7) of this report. This equation is, however, not so useful as (5) or (8) above, which both predict M_A from a knowledge of the dimensions of the projectile, whereas equation (7) requires a knowledge of trial velocities.

Projectile (see Appendix II)	M_A			
	Column 1	Column 2	Column 3	Column 4
1	0.432	0.453	0.440	0.463
2	0.413	0.441	0.440	0.435
3	0.492	0.484	0.469	0.454
4	0.350	0.348	0.355	0.322
5	0.258	0.192	0.216	0.195
6	0.145	0.167	0.194	0.173
7	0.247	0.267	0.303	0.269
8	0.128	0.134	0.154	0.141
9	0.290	0.250	0.287	-
10	0.212	0.208	0.238	-
11	0.396	0.342	0.359	0.361
12	0.651	0.665	0.699	0.696
13	0.544	0.487	0.512	0.520
14(a)	0.421	0.342	0.359	0.341
(b)	0.365	0.237	0.280	0.255
(c)	0.281	0.188	0.219	0.201
(d)	0.253	0.188	0.219	0.201
(e)	0.228	0.154	0.183	0.169

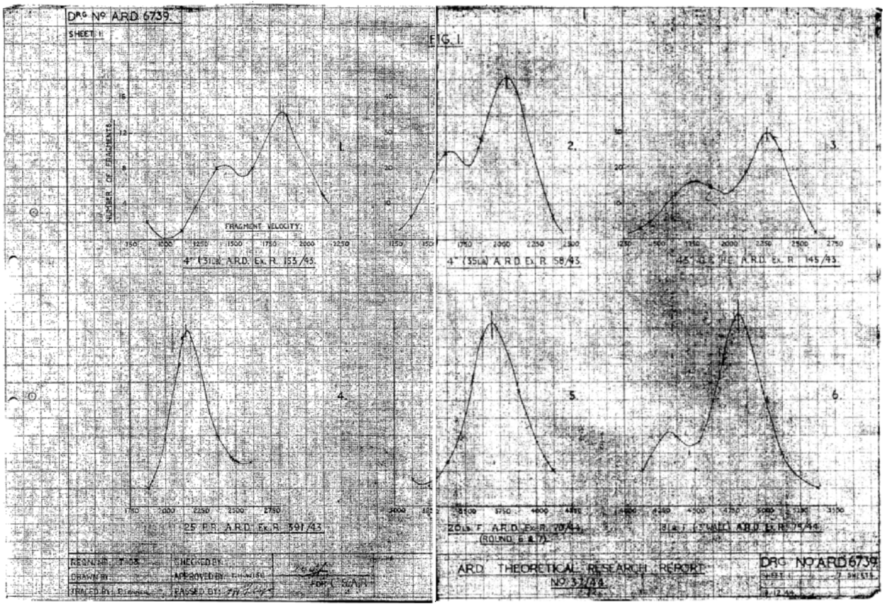
DRG NO ARD 6739
SHEET 1
FIG. 1.
NUMBER OF FRAGMENTS.
FRAGMENT VELOCITY.
4" (35LB) A.R.D. Ex. R. 153/43.
4" (35LB) A.R.D. Ex. R. 58/43.
25 P.R. A.R.D. Ex. R. 391/43.
A.R.D. THEORETICAL RESEARCH REPORT
NO 37/44.
DRG NO ARD 6739

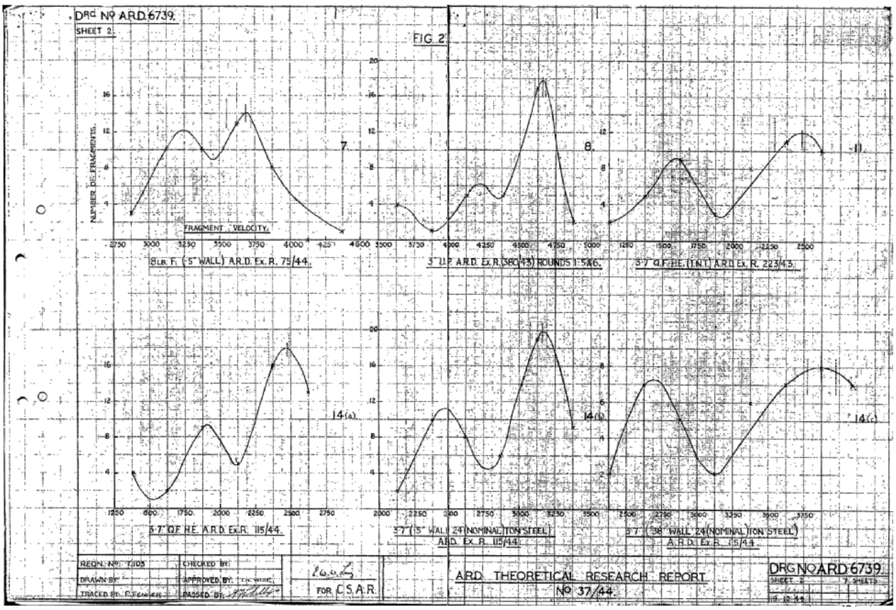
DRG NO ARD 6739.
SHEET 2.
FIG. 2.
NUMBER OF FRAGMENTS.
FRAGMENT VELOCITY.
A.R.D. Ex. R. 223/43.
3·7" Q.F. H.E. A.R.D. Ex.R. 115/44.
A.R.D. Ex. R. 115/44.
A.R.D. Ex. R. 15/44.
FOR C.S.A.R.
A.R.D. THEORETICAL RESEARCH REPORT
NO 37/44.
DRG NO ARD 6739.

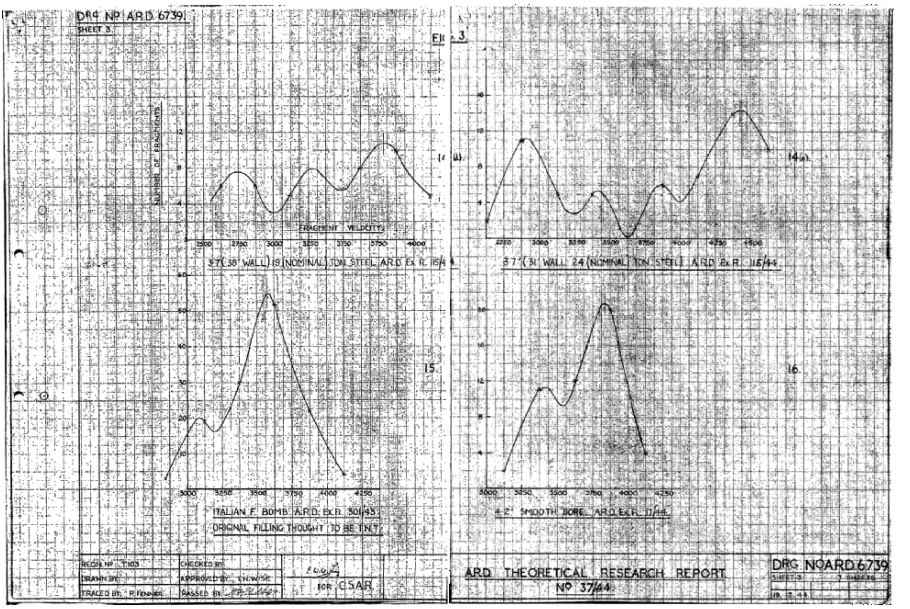
DRG Nº ARD 6739
SHEET 3
FIG. 3
NUMBER OF FRAGMENTS
FRAGMENT VELOCITY
37 (L.58" WALL) 19 (NOMINAL) TON STEEL ARD EX R. 154
37 (3¼ WALL 24 (NOMINAL TON STEEL) ARD EX R. 116/44
ITALIAN F. BOMB ARD EXR 501/45
ORGINL FILLING THOUGHT TO BE TNT
4.2" SMOOTH BORE ARD EX R. 17/44
ARD THEORETICAL RESEARCH REPORT
Nº 37/44
DRG Nº ARD 6739

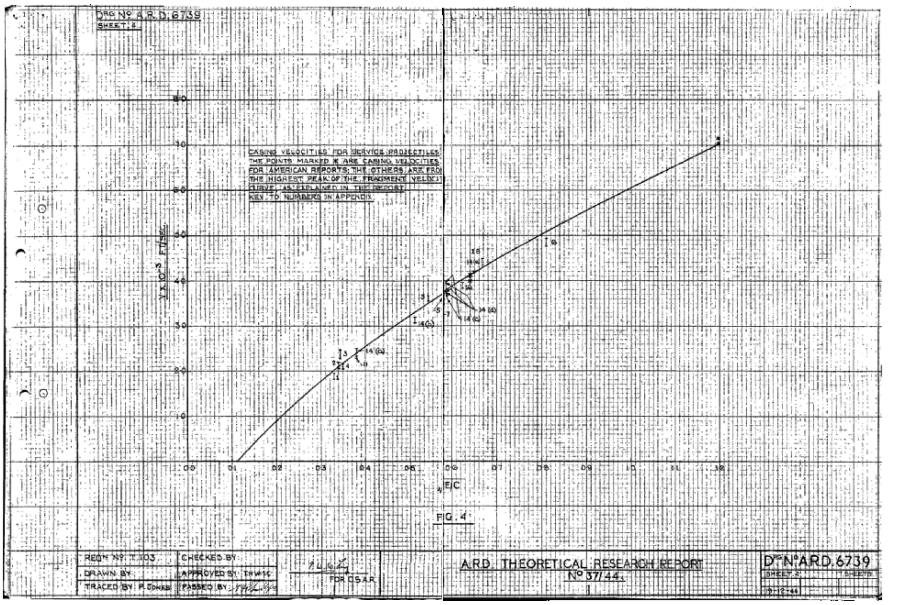
DRG Nº A.R.D. 6739
SHEET 8
CASING VELOCITIES FOR SERVICE PROJECTILES
THE POINTS MARKED X ARE CASING VELOCITIES
FOR AMERICAN REPORTS, THE OTHERS ARE FOR
THE HIGHEST PEAK OF THE FRAGMENT VELOCITY
CURVE. AS SET LAWS IN THIS REPORT.
KEY TO NUMBERS IN APPENDIX
FIG. 4
ARD THEORETICAL RESEARCH REPORT
Nº 37/44.
Dº Nº ARD 6739

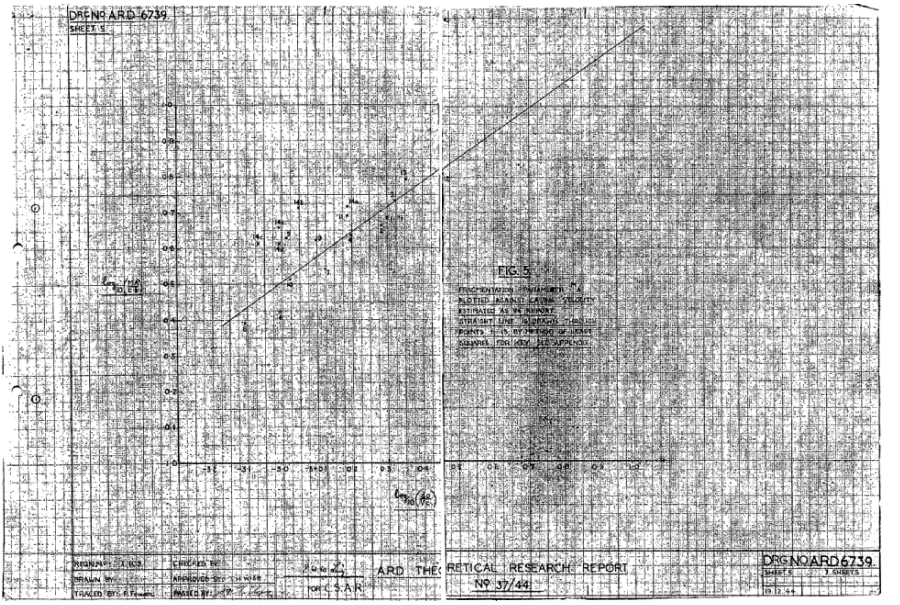
DRG No A.R.D. 6739
SHEET 5
FIG. 5.
ARD THEORETICAL RESEARCH REPORT
No 37/44
DRG NO ARD 6739

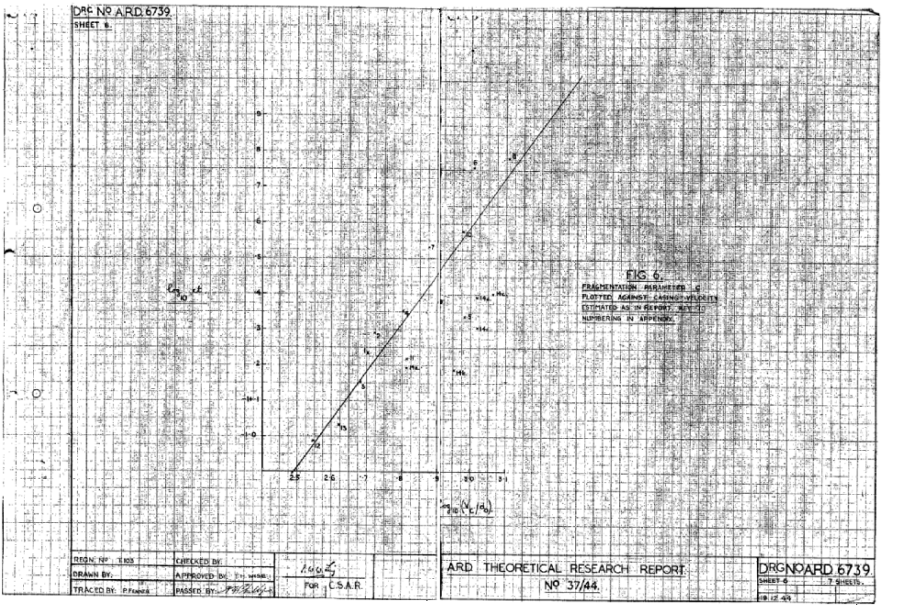
DRG No A.R.D. 6739
SHEET 6.
FIG. 6.
ARD THEORETICAL RESEARCH REPORT
No 37/44.
DRG NO ARD 6739

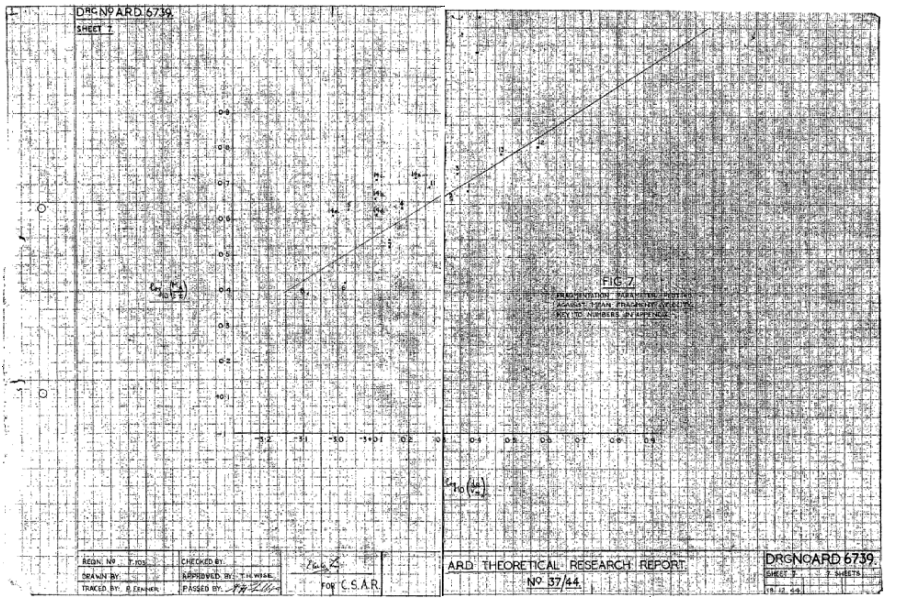
DRG Nº ARD 6739
SHEET 7
FIG 7
ARD THEORETICAL RESEARCH REPORT
Nº 37/44
DRG Nº ARD 6739
SHEET 7
DRAWN BY
TRACED BY: R ZENNER
CHECKED BY
APPROVED BY: T.H. WISE
PASSED BY
FOR C.S.A.R.